

FANS

DESIGN AND OPERATION OF CENTRIFUGAL, AXIAL-FLOW
AND CROSS-FLOW FANS

BY

Dr.-Ing. BRUNO ECK

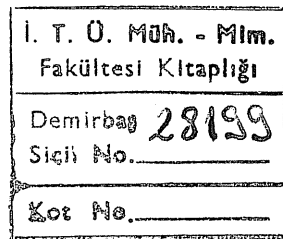
First English Edition

Translated and Edited by

Dr. RAM S. AZAD

and

Dr. DAVID R. SCOTT



PERGAMON PRESS

OXFORD NEW YORK TORONTO
SYDNEY BRAUNSCHWEIG

Pergamon Press Ltd., Headington Hill Hall, Oxford
Pergamon Press Inc., Maxwell House, Fairview Park, Elmsford,
New York 10523
Pergamon of Canada Ltd., 207 Queen's Quay West, Toronto 1
Pergamon Press (Aust.) Pty. Ltd., 19a Boundary Street,
Rushcutters Bay, N.S.W. 2011, Australia
Vieweg & Sohn GmbH, Burgplatz 1, Braunschweig

Copyright © 1973 B. Eck

*All Rights Reserved. No part of this publication may be
reproduced, stored in a retrieval system, or transmitted, in any
form or by any means, electronic, mechanical, photocopying,
recording or otherwise, without the prior permission of
Pergamon Press Ltd.*

First English edition 1973

Library of Congress Catalog Card No. 72-137613

Printed in Germany

ISBN 0 08 015872 2

CONTENTS

<i>Author's Preface to the First English Edition</i>	XIII
<i>Foreword to the First English Edition</i>	XV
<i>From the Preface to the Fourth German Edition</i>	XVII
<i>From the Preface to the Third German Edition</i>	XVIII
<i>From the Preface to the Second German Edition</i>	XIX

PART A. CENTRIFUGAL FANS

CHAPTER I.	ELEMENTARY STREAMLINE THEORY	3
	1. Fundamental Equations	3
	2. Radial Entry	10
	3. Reaction Effect	12
	Total Reaction Effect	14
	4. Characteristics in the Case of an Infinite Number of Blades	15
	5. Fundamental Problems	20
	6. The Effects of Compression	20
CHAPTER II.	CALCULATION OF FLOW IN BLADE PASSAGES	22
	7. Velocity Distribution in the Blade Passage	22
	8. Forces Perpendicular to the Direction of Flow	23
	9. Forces in the Direction of Flow	24
	10. Relative Circulation	26
	11. Straight Blades	27
	12. Equal Velocity Distribution in the Blade Passage	28
	13. Equal Pressure Distribution in the Blade Passage	28
	14. Calculation of Velocity and Pressure Distributions in an Arbitrary Blade Passage	29
CHAPTER III.	INFLUENCE OF A FINITE NUMBER OF BLADES	31
	15. Fundamentals	31
	16. Graphical Determination of the Reduction in Output	33
	17. Approximate Calculation According to Stodola	36
	18. Precise Analytical Determination of the Reduction in Output	37
	Velocity Coefficient with High-efficiency Fans	41
	19. Influence of the Reaction Effects	42
	20. Visualisation of the Actual Flow at the Blade	43
	21. Number of Blades	51
CHAPTER IV.	SHAPE OF THE BLADE TIP	52
	22. Inactive Blade	52
	23. Study of the Thickness of a Blade	55
CHAPTER V.	DIMENSIONLESS CHARACTERISTICS	57
	24. Coefficients	57
	25. Optimum Curves	62

	26. Other Coefficients	64
	27. Basic Formulae	67
	28. Review of the Characteristics of Different Types of Fan	69
CHAPTER VI.	LOSSES	72
	29. Impeller Friction Losses	72
	30. Impeller Losses	75
	31. Shock Losses	78
	(a) Impeller Entrance Loss	78
	(b) Guide Vanes Loss	79
	32. Clearance Losses	80
	33. Diffuser Losses	83
	34. Bearing Losses	83
	35. Efficiency	84
	(a) Hydraulic Efficiency	84
	(b) Volumetric Efficiency	84
	(c) Mechanical Efficiency	84
	(d) Total Efficiency	85
	(e) Change of Total Efficiency owing to a Variation in Mechanical Losses Produced by Variation in Speed	85
	36. Hydraulic Efficiency by Thermal Assessment	86
CHAPTER VII.	THE DESIGN OF IMPELLERS	89
	37. Introduction	89
	38. Optimum Entry Breadth b_1	89
	39. Optimum Inlet Diameter and Blade Angle at Entry	92
	40. Influence of the Curvature of the Entrance upon the Optimum Blade Angle	95
	41. Calculation of the Optimum Blade Angle in the Case of Pre-rotation	97
	42. Tapered or Parallel Impeller Shrouds	98
	43. Determination of the Blade Shape	99
	(a) Straight Blade	99
	(b) Circular Arc Blade	100
	(c) Determination of the Blade Passage	100
	(d) Graphical Determination of the Blade Form	102
CHAPTER VIII.	OPERATING CHARACTERISTICS OF CENTRIFUGAL FANS	107
	44. Theoretical Characteristics as a Reference	107
	45. Influence of a Finite Number of Blades upon the Characteristic	108
	46. Effects of Friction on the Characteristic	108
	(a) Friction in the Blade Passage	108
	(b) Shock Losses	109
	47. Variation of the Breadth/Diameter Ratio	111
	Gap Pressure Characteristic	113
	48. The Effects of Reduced Volume-flow on the Fan Characteristic	113
	49. Pressure Coefficients in the Case of Radial Impellers	116
CHAPTER IX.	THE MAIN TYPES OF CENTRIFUGAL FAN	117
	50. High-performance Fans	117
	Blade Profiles	124
	Conclusions	126
	51. Centrifugal Fans with Values of Static Regain above Unity	127
	52. The Design of Fans for the Transport of Dust-laden Gases	132
	53. Double-entry Fan	137
	54. Design of the Multivane Impeller (Sirocco Runner)	139
	(a) Impeller Width	140
	(b) Blade Shape	141
	(c) Number of Blades	142
	(d) Reaction Effect	143
	(e) Detailed Study	144

CONTENTS

vii

	(f) Blades with Accelerating Blade Passages	146
	(g) Experimental Values Obtained with Multivane Impellers	151
	55. Radial Impeller with an Axial Pre-runner	153
CHAPTER X.	CROSS-FLOW FANS. DOUBLE PASSAGE THROUGH CASCADE FANS	156
	56. History of the Development of the Cross-flow Fan	156
	57. General Principles of Double Passage through Radial Blading	158
	(a) Reaction Effect ω	163
	(b) Selection of the Diameter Ratio and of the Blade Angle	163
	58. Vortex Motions within the Impeller	164
	59. Vortex Control	166
	The Flow in the Impeller at Zero Delivery	170
	60. Arrangement of the Diffusers of Cross-flow Fans	170
	61. Theoretical and Actual Characteristics	172
	62. Characteristics, Efficiency, Evaluation, Applications	173
	(a) Applications	175
	(b) Cross-flow Multivane Impeller	178
	63. Cross-flow in Impellers without Casing	178
	64. Oscillating Blade Impeller	182
CHAPTER XI.	GUIDE ARRANGEMENTS	185
	65. Guide Blades	185
	66. Interchange Action	187
	67. Spiral Housing	189
	(a) Fundamentals	189
	(b) Construction of Volute without Considering Friction	190
	α) Parallel side walls	190
	β) Parallel side walls which are wider than the impeller	191
	γ) Tapering side walls	193
	δ) Rectangular cross-section	194
	ϵ) Circular cross-section	195
	ζ) Inner volute	196
	η) Axial volute	197
	θ) Helix volute	197
	i) Volute casing for axial-flow fans	199
	κ) Helix-formed construction of volute casings	199
	λ) Subdivided volute casing	200
	μ) Volute casing with an adjustable tongue	202
	ν) Volute casing with a number of discharge points	202
	ξ) Graphical methods	205
	(c) Precise Method	205
	(d) Approximate Method	207
	68. The Influence of Friction in Volute on the Total Energy Conversion	208
	69. Reduction of Rotational Flow owing to Friction in Annular Spaces and Stationary Guide Vanes	211
	70. Effect of Small Changes on the Behaviour of Volute	214
	71. The Dimensions of the Lip	216
	72. The Distribution of Pressure and Force in the Volute Casing	217
	73. Losses in the Volute Casing	217
	74. Diffusers for Improving the Performance of Volute Casings	219
	75. Discharge Filters	220
PART B. THEORY AND CALCULATION OF AXIAL-FLOW FANS		
CHAPTER XII.	CALCULATION OF THE NORMAL AXIAL-FLOW FAN	225
	76. General Remarks	225
	77. Simple Relationships of Cascade Flow	226
	(a) Stationary Cascade	226

(b) Adjustable Cascade	228
(c) The Four Main Cases of Axial-flow Fan	230
78. Reaction Effect of Moving Cascade	233
79. Calculation by the Aerofoil Theory	234
80. Influence of Reynolds Numbers. Advantage of Profiling	237
81. Behaviour of Boundary Layer in Axial-flow Fans	240
82. Calculation without Considering the Aerofoil Friction	242
83. Generally Applicable Relationships	243
84. Calculation taking Friction into Account	245
85. The Efficiency as a Function of Dimensionless Quantities	248
86. Efficiency of Freely Discharging Axial-flow Fans	251
87. Reduced Output owing to Boundary-layer Effects	256
88. Geometry of the Circular Arc Blade	257
89. The Most Favourable Blade Pitch according to Zweifel	260
90. Cascade Calculations according to Weinig	263
91. Increase of Outlet Angles in Profiling	265
92. Minimum Hub Diameter	265
93. Vortex Core Formation	266
94. Effect of Tip Clearance	268
95. Calculation and Construction of Guide Wheels	269
96. Comparison between Constructions with Upstream Guide Wheel and Downstream Guide Wheel	271
97. Upstream Guide Blades with Constant Outlet Angle (Cylindrical Blade)	272
98. Radial Pressure Distribution in Axial-flow Fans	275
99. Diffuser Losses	276
(a) General Relationships	277
(b) Diffuser Losses as Proportion of Total Loss	277
(c) Influence of Hub Discharge at Equal Passage Widths	278
100. The Shape of Diffusers	279
101. When Does It Pay to Use a Guide Arrangement?	281
102. Layout of Multistage Axial-flow Fans	283
103. Practical Design Calculation. Review of the Calculation Procedure	284
104. Examples of Calculation	285
105. Behaviour of an Axial-flow Fan away from the Best Operating Point	288
106. Characteristic and Part Characteristic of Axial-flow Fans	290
107. Preliminary Calculation of the Operating Characteristics in Blade Setting	293
108. Test Results of Axial-flow Fans	294
109. Irregular Inlet-flow Conditions	299
110. Axial-flow Fans with Variable Pressure Drop	302
111. Open-running Axial-flow Fans	303
 CHAPTER XIII. MERIDIONALLY ACCELERATED AXIAL-FLOW FANS	308
112. General Outline	308
113. Constant-pressure Fans	312
114. Meridionally Accelerated High-pressure Fan	313
 CHAPTER XIV. CONTRA-ROTATING AXIAL-FLOW FANS	316
115. Design and Test Values	316
 PART C. GENERAL PROBLEMS RELATING TO BLOWERS	
 CHAPTER XV. REGULATION OF BLOWERS	323
116. General Principles	323
117. Adjustable Inlet Guide Vanes	325
118. Adjustable Blade Tips	333
119. The Adjustable Disc	333
120. Adjustable Guide Devices	336

CONTENTS

ix

121. Control of Rotation	337
122. Self-adjustment by Characteristic	338
123. Mechanical and Hydraulic Speed Adjustment	339
124. Gears	342
125. Relationship due to the Speed Variation	343
126. Logarithmic Representation of the Characteristics	345
CHAPTER XVI. FANS AND DRIVING MACHINES	
127. General Principles	347
128. Drive by Electric Motors	348
129. Steam-turbine Drive	354
130. Determination of Characteristic at Constant Setting of the Prime Mover	355
131. Starting an Electric Motor for Direct Drive	357
CHAPTER XVII. OPERATING BEHAVIOUR OF A FAN	
132. The Operating Point of the Fan	362
Safety Allowances in Fan Design	363
133. Speed Control or Throttle Control?	364
134. Unstable Operating Parts of the Individual Blower	365
135. Satisfactory and Unsatisfactory Operations at Unstable Range	366
136. Several Fans Working Together	367
(a) Determination of the Resultant Characteristic in a Parallel Arrangement	368
(b) Fans Arranged in Series	370
(c) Instability, Oscillation	370
(d) Two Identical Circuits Working in Parallel and Joined by Cross-connection	371
(e) Double-inlet Fans	375
137. Performance of One or Several Fans Connected to Any Duct System	375
(a) System Characteristic in Duct Branches	375
(b) Characteristic Field of the Equivalent Orifice	379
(c) Variation of the Fan Characteristics by Throttling	379
(d) Resistance and Fan as Parts of a System of Ducts	381
(e) Bypass Duct for Starting and Controlling Fans	383
(f) Fans and Resistances in Various Combinations	385
(g) Ducting Systems with Cross-connections	387
(h) The Leaking Duct	389
(i) Additional Load of a Duct System by Constant Positive Pressure or Negative Pressure	390
(k) Ventilating a Space with Return Air	393
(l) Two Fans with Variable Resistance Working Together	394
(m) Design with Fluctuating Resistances	395
(n) Closed Ducting System	396
(o) Fan Characteristic at Various Densities	396
(p) The Effect of Density Variation on the System Line	398
(q) Experimental Determination of the Duct Characteristic	400
138. Electrical Methods for Determining the System Characteristics	402
PART D. SPECIAL PROBLEMS, SPECIAL USES	
CHAPTER XVIII. MINE VENTILATION AND BOILER FANS	
139. Blowers for Mine Ventilation	409
140. Boiler Fans	419
Wear	423
Design and Regulation of Boiler Fans	425
CHAPTER XIX. TYPICAL APPLICATIONS	
141. Impeller for Air Circulation	431
142. Free-running Radial Impellers without Casing	433

143. Load Relief of a Fan by Rising Hot Air, Effect of Wind, Effect of Travel Drive	435
Cooling Towers	436
144. Ventilation by Momentum Drive, Tunnel Ventilation	438
145. Suction Effect of Wind Passing Duct Openings (Roof Ventilators and Similar)	441
146. Elevator Blowers, Blowers for Pneumatic Transport of Material	445
Fans for Highly Corrosive Materials	448
147. Miniature Fans	449
148. Super-chargers	452

PART E. CONSTRUCTIONAL SHAPES AND CONSTRUCTIONAL FEATURES OF FANS

CHAPTER XX. SURVEY	457
149. General Aspects for Shaping of Radial-flow Fans	457
150. Form of Axial-flow Fans	467
151. Important Constructional Details	472
152. Air-cooled Bearings for Hot-gas Blowers	478

PART F. SOUND GENERATION AND SOUND ATTENUATION OF FAN INSTALLATIONS

CHAPTER XXI. SOUND GENERATION BY FANS	485
<i>(Treatise by B. Regenscheit)</i>	
153. Dependency of Radiated Sound Power on the Peripheral Speed	485
154. Dependency of Sound Level on the Aerodynamic Factors of the Fan	486
(a) Dependency on Efficiency	486
(b) Dependency on Flow Volume and Pressure	486
155. Fan Noise as a Function of Frequency	487
156. Some Remarks on Sound Generation	490
157. Derivation of a Reference Quantity for the Sound Power	496
CHAPTER XXII. SOUND INSULATION OF FANS AND AIR-HANDLING INSTALLATIONS	499
<i>(By E. Goehlich, Dipl.-Ing. Dortmund)</i>	
158. Basic Concepts	499
159. Logarithmic Ratio Number. Sound Level	500
160. Damage through Noise	504
161. Noise Abatement Regulations, Criteria Curves	505
162. A Few Theoretical Basic Principles	509
163. Direct and Reverberant Sound Fields	511
164. Sound Insulation Elements	512
165. Sound Absorption	516
166. The Resonance Silencer	522
167. Reflection Silencer	523
168. Interference Silencers	523
169. Noise Absorption	523
170. Sound-absorbing Hood	524
171. Sound-absorbing Lagging of Pipes and Ducts	524
172. Sound-absorbing Room Lining	525
173. Flexible Mounting of Machines	525
174. Isolation of Fan Vibration	527
175. Noise Reduction Devices in Fans	528
176. Assessing the Necessary Attenuation of Noise	530
Choice and Layout of Sound-attenuating Components	531
177. Examples of Design	535
178. Gas Turbines, Blast Furnace Blowers, Turbo-compressors, High-pressure Blowers	538
179. Induced Draught by Injection	539
180. Future Prospects	540

CONTENTS

XI

PART G. CALCULATIONS OF STRENGTH

CHAPTER XXIII. SHORT REVIEW	543
181. Basic Principles	543

PART H. EXPERIMENTAL TESTING OF FANS

EXPERIMENTAL TESTING OF FANS	553
CHAPTER XXIV. GENERAL ASPECTS	554
182. Outline of Test Circuit for Fan Testings	554
183. Sources of Error in Pressure Measurements	559
(a) Unequal Pressure Distribution in the Duct Cross-section	559
(b) Unequal Pressure Distribution along the Duct without Longitudinal Vortices	562
(c) Pressure Measurement of Rotational Flow	563
(d) Magnitude of Error	565
184. Reassessment	567
185. Test Equipment	568
CHAPTER XXV. MEASUREMENTS AND THEIR SOURCES OF ERROR	573
186. Pressure Curve for the Different Measuring Methods	573
187. Mechanical Power Measurements	577
188. Electrical Power Measurement	578
The Efficiency	580
189. Examples of an Acceptance Test	581
(a) Test Arrangement	581
(b) Description of Measurements Carried Out and Their Evaluation	581
(c) Test Equipment Used	584
<i>Author Index</i>	587
<i>Subject Index</i>	589

AUTHOR'S PREFACE TO THE FIRST ENGLISH EDITION

IT IS a pleasant task to write a preface to the English translation of my book on fans, particularly as this field has taken a new turn over the last decade. Before this time the radial-flow fan was one of the least efficient fluid-moving machines. Nowadays the reverse is true, and the change has been brought about by scientific research. In the past aerofoil theory had been successful when applied to axial-flow fans but not to radial-flow fans. The situation has changed owing to the development of boundary-layer theory and its application to radial-flow fans.

At the same time as fresh progress in the design of the radial-flow fans was taking place, the long-forgotten cross-flow fan was newly discovered. Of especial importance in the new development of this particular fan was the decisive effect of a free whirl unknown up to that time.

Thus theoretical advances have opened up very interesting possibilities for the development of new fans, and both engineers and research men should devote their full attention to this branch of turbo-machines.

BRUNO ECK

FOREWORD TO THE FIRST ENGLISH EDITION

DR. BRUNO ECK has said in the preface to the second edition of his well-known textbook on fan engineering that "The fan has been the stepchild of technology". By this he means that firms have been left to develop their own designs without assistance from research institutions and the Government and, in consequence, little real information has been published.

In England the situation is such that no authoritative textbook on fan engineering exists.

The editors recognised this and, as a result, the present translation of Dr. Eck's book into English has just been completed. The expert advisers of the publishers, after a survey of the international literature, unanimously endorsed our selection of Eck's book.

The book gives the fundamental fluid dynamics of turbo-machinery and applies this to fans. It continues with experimental investigations of fans and includes a comprehensive account of all work done in this field. Both theoretical and empirical results are then applied to problems of design. All applications of fans are dealt with in considerable detail. Some sixty pages of the present edition are devoted to the important subject of noise generation and its control in fans.

The book reveals many gaps in existing knowledge and presents a challenge to both engineers and research workers in the field.

It is agreed by leading experts that the days of "cut-and-try" in fan design are over and that fundamental investigations involving the development of advanced measurement techniques are essential.

Our own survey of the literature shows that two institutes, one in Germany and one in Russia, have developed such techniques, which are adapted to the direct measurement of fluid flow between the blades of the rotating impeller.

Thus all components of the velocity triangle may be measured directly without relying on dubious assumptions.

The validity of existing theories of fan design may now be tested experimentally for the first time.

It appears that no work of a comparable nature is being done in this country. From the point of view of developing what in Great Britain is a comparatively backward industry, it seems to us essential that effort and finance be devoted to this field. It is noteworthy that, on the Continent, where fan technology is considerably in advance of our own, many universities have a chair of Turbo-machinery.

The book should be of interest to students, teachers, practising engineers, designers, and research workers, and indeed anyone concerned with the design or application of fans.

We are indebted to many collaborators without whose help the completion of this work would not have been possible. In particular, we wish to name Mr. Daly of Woods of Colchester, and Mr. Janicki and Dr. Chrenko of the National College for their generous and unstinted assistance.

Our grateful acknowledgments are due also to Woods of Colchester for their financial help and encouragement.

R.S. AZAD
D.R. SCOTT

FROM THE PREFACE TO THE FOURTH GERMAN EDITION

THE continuously progressive development of fan technology made it necessary to prepare a completely revised and enlarged version of the third edition. The technology of fan engineering was given an unexpected impetus when the construction of high-efficiency blowers (1952) with 90% efficiencies became practicable and the effects of this change are still far from complete.

As far as high-efficiency blowers are concerned, the latest improvements seem to have reached the maximum possible limits. Some new types have achieved a volumetric capacity equal to that of axial-flow fans at efficiencies as high as over 80% although the dimensions are remarkably small. The new performances of multi-blade blowers are noteworthy: they are widely used in certain applications on account of their silence in operation and small sizes. New types of application for cross-flow fans have become available and it is now possible to explain the theory and construction of these unconventional fans to some extent.

I have created a new and comprehensive system of classifying characteristics for all types of fan.

In the field of automatic control of centrifugal as well as axial-flow fans, progress has been achieved.

It is, however—as previously—still very difficult to adjust fans to given operating conditions. Many fans are wrongly selected. Investigation into this difficult problem by research is indispensable, as otherwise it will not be possible to take advantage of the high efficiency now obtainable with new types of fan.

In the meantime the demand for noise reduction of fans and adjacent installations becomes more and more urgent. For certain applications these requirements are even more imperative than high efficiencies. It became essential to improve the treatment of the subject of fan technology by dealing with acoustic problems. Messrs. B. Regenscheit and E. Goehlich undertook to deal with this fairly new subject; we are grateful for their contribution.

Thanks are due to Baurat Dipl.-Ing. Niermeyer, Berlin, who carefully checked this new edition, and to the publishers Springer-Verlag for the presentation of this book, especially for the very great number of new illustrations.

*Cologne,
July 1961*

BRUNO ECK

FROM THE PREFACE TO THE THIRD GERMAN EDITION

ALTHOUGH the second edition was sold out very quickly, preparation of the third edition was completed only recently. In the meantime considerable progress has been made in the development of fans. The progressive improvement of the centrifugal fan led to a reassessment. The result is that it deservedly regained its former lead. With regard to quality the centrifugal fan is superior to the axial-flow fan. There has been noteworthy progress in controls. Attention has been given to the new development of meridian accelerated constructions in axial-flow fans. One may predict the development of cross-flow fans.

A few years ago fans were the least efficient when compared with other types of turbo-machine.

Nowadays the increase in the efficiency of fans is such that they can rank with the best of other turbo-machines, i.e. pumps, compressors, and turbines.

The comparatively rapid development of new types of fan emphasises problems which had been previously ignored. To take complete advantage of the newest types of fan it is imperative to match them with operating conditions more effectively than hitherto. This entails many practical difficulties. In addition to methods of measurement, drive problems, and automatic control, selection of the motive power becomes more important than ever before. Special treatment of these subjects in the text was therefore unavoidable. The purchaser of fans should be aware of these problems and recognise that many of them remain unsolved.

*Cologne,
September 1956*

BRUNO ECK

FROM THE PREFACE TO THE SECOND GERMAN EDITION

THE rapid developments which are taking place in the field of fan engineering have shown the need for a thorough revision and enlargement of the first edition.

The improvements in fan efficiencies achieved in the last few years are remarkable. At the same time it seems that centrifugal fans have been able to regain the lead from the axial-flow fan. For a long time the axial-flow fan was ahead previously on account of its particular construction. Nowadays there are small low-pressure centrifugal fans on the market with a total efficiency of 89 % at a brake horsepower of 2 kW. If one recalls that more than 1 million kW fan power is installed in Germany alone, one can assess the importance which such an increase in efficiency represents.

The fan has been the stepchild of technology in the past. Its development received scientific attention only when there were prospects of military application. Owing to these circumstances only a few firms were engaged in developmental and research work at their own expense. The firms were reluctant to publish their findings. Since it was difficult to ascertain the progress made, the author was forced to put more emphasis on his own research work.

A review of fan technology must deal with attempts to increase efficiency, but the vast field of applications, viz. ventilation of buildings, ships, etc., must not be overlooked. With these the prime consideration is the construction of noiseless fans, an aim which is not always compatible with highest efficiency. Thus it happens that many types of construction remain on the market despite low efficiencies, as they fulfil a very real demand. In addition there are many applications, e.g. plant engineering where small equipment is required, best fixing conditions, etc.; these prevail over other considerations. A fan with the highest efficiency does not always satisfy these conditions. Frequently, however, remarkable improvements have been achieved. Constructions with high-pressure characteristics are superior in the field. The existing possibilities can best be exemplified by the fact that the pressure characteristic of cross-flow blowers is about sixty times greater than that of axial-flow impellers.

*Cologne,
February 1952*

BRUNO ECK

PART A

CENTRIFUGAL FANS

CHAPTER I

ELEMENTARY STREAMLINE THEORY

1. FUNDAMENTAL EQUATIONS

We shall consider firstly an ideal impeller with backward-curved blades. An ideal impeller is defined as an impeller having an infinite number of blades, so that all friction loss is eliminated, and the relative motion of the air will be in the same direction as the actual blade. Furthermore, the thickness of the blades is considered to be infinitely small. At the point of entry indicated by diameter d_1 the angle of the blade to the tangent of the circumference is β_1 , while at the point of discharge the corresponding angle is β_2 .

This arrangement, although very different from practice, is a very useful basis for discussion. Streamline theories are, however, absolutely essential for comparisons and often very useful in other connections. The above assumptions are made in Euler's turbine theory which will be given in more detailed discussion in a later chapter.

We shall assume that the impeller revolves with a peripheral velocity u_2 and that the air enters the impeller in a radial direction, so that its entry into the blade passages is tangential to their direction. This type of air entry we shall call *shock-free*. The assumption that the impeller has an infinite number of blades implies that, on exit from the impeller, a fluid has a relative velocity which is in the same direction as the tangent at the tip of the blades, whereas in actual fact, i.e. when a finite number of blades is considered, the fluid has a relative velocity whose direction varies from that of the tangent at the tip of the blades and has an angle that is different from the geometrical outlet angle.

In actual cases under consideration air does not enter in a truly radial direction but at an angle α_1 to the circumference, as seen by a standing observer, due to the pre-rotation imposed upon the air in the direction of the rotary movement of the impeller. It is in this sense we employ the term peripheral component c_{1u} .

Figure 1 shows typical velocity diagrams for entry and exit with designations customarily employed in turbine construction. The student should study the construction and meaning of the different quantities thereon so that they become very familiar. As a simple guide the student should memorise the following sentence: *the vector sum of the relative velocity and the peripheral velocity gives the absolute velocity*.

With a flow through such an impeller the first question to be asked is: how great is the turning moment required to produce such a flow? The theorem of momentum in mechanics supplies us with the necessary information. When it is applied in our case, the significant point is that the resultant torque is given by the difference between the outgoing and incoming moments of momentums. Let us consider the torque expressed by $q c_u r$, where q is the mass flow per second through a circular disc, c_u is the circumferential

or peripheral velocity of the air, and r is the radius. One can write

$$M = q (r_2 c_{2u} - r_1 c_{1u}). \quad (1)$$

In this expression, q is taken outside the brackets because it has a constant value at inlet and outlet. Should one require to study this point further, full information can be obtained from the literature under the heading of "Continuity Equation".

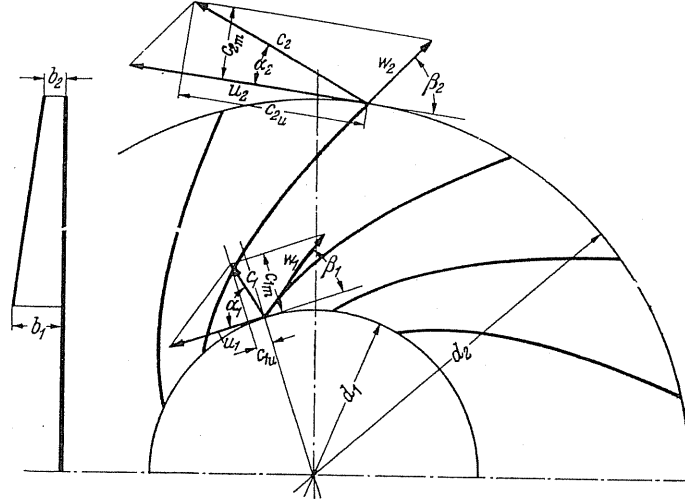


FIG. 1. Impeller with backward-curved blades and other details.

Furthermore, one may ask: what is the amount of energy supplied in relation to the output? As we are considering a frictionless flow through the impeller, the external energy supplied to the fluid is converted into pressure energy: energy transformation is considered as being perfect and therefore losses have not been considered, so that the energy supplied is the same as the energy at discharge. If one considers the mass flow per second q to consist of solid particles which are raised through a height H in one second, the rate of working or power due to the displacement is given by Hqg . If the impeller rotates with an angular velocity ω radians/sec, then the power is $L = M\omega$. We write

$$L = M\omega = H_{th\infty} qg = q\omega [r_2 c_{2u} - r_1 c_{1u}] = q [u_2 c_{2u} - u_1 c_{1u}],$$

and from this,

$$H_{th\infty} = \frac{1}{g} [u_2 c_{2u} - u_1 c_{1u}]; \quad (2)$$

by radial entry ($c_{1u} = 0$), therefore,

$$M = q r_2 c_{2u}; \quad H_{th\infty} = \frac{1}{g} u_2 c_{2u}. \quad (3)$$

In the case of fluids and gases, the meaning of the term "height of lift" is identical with "pressure head"; its relation to pressure in excess of atmospheric is given by

$$\Delta p = \gamma H \quad (4)$$

(γ density of a liquid or gas).

In fan design we put the pressure in excess of atmospheric Δp in place of H , so that we now write

$$\Delta p_{\text{th}\infty} = \frac{\gamma}{g} [u_2 c_{2u} - u_1 c_{1u}] = \varrho [u_2 c_{2u} - u_1 c_{1u}], \quad (5)$$

$$\Delta p_{\text{th}\infty} = \varrho u_2 c_{2u} \quad (\text{radial entry}). \quad (6)$$

The output of a fan can be directly compared to the lifting of water by a pump. One can introduce an expression for G , the weight of air drawn into a fan per second and raised to a pressure head $H = \Delta p/\gamma$. Therefore the output is

$$L = GH = V\gamma H = V\Delta p, \quad (7)$$

that is, the theoretical output of a fan is the product of the volume of air passing through the fan each second and the total pressure.

One must note that the total pressure is designated by Δp . Starting with the difference of the static pressure Δp_{stat} one gets the total energy by adding the variation in kinetic energy between entry and exit:

$$\Delta p_{\text{tot}} = \Delta p_{\text{stat}} + \frac{\varrho}{2} (c_a^2 - c_e^2).$$

In this case the effects of compression have been neglected but, in the case of high pressures the effects of compression must be taken into account. If we note that a small element of the pressure head gives

$$dH = \frac{dp}{\gamma} = v dp,$$

the total pressure is given by integration as

$$H = \int v dp.$$

The integral is dependent on whether changes are isothermal, isentropic, or polytropic. Isentropic changes in fans serve as a standard of reference:

$$H_s = \frac{\kappa}{\kappa - 1} \frac{p_1}{\gamma_1} \left[\left(\frac{p_2}{p_1} \right)^{(\kappa-1)/\kappa} - 1 \right] = \frac{\kappa}{\kappa - 1} RT_1 \left[\left(\frac{p_2}{p_1} \right)^{(\kappa-1)/\kappa} - 1 \right].$$

By putting

$$\frac{p_2}{p_1} = \frac{p_1 + \Delta p}{p_1} = 1 + \frac{\Delta p}{p_1}$$

and expanding in terms of $(\Delta p/p_1)$, this expression becomes

$$H_s = \frac{\Delta p}{\gamma_1} \left[1 - \frac{1}{2 \cdot 8} \frac{\Delta p}{p_1} + \frac{1}{4 \cdot 9} \left(\frac{\Delta p}{p_1} \right)^2 - + \dots \right]. \quad (8)$$

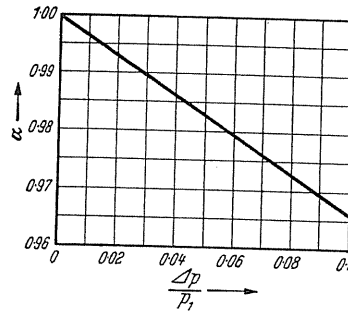


FIG. 2.

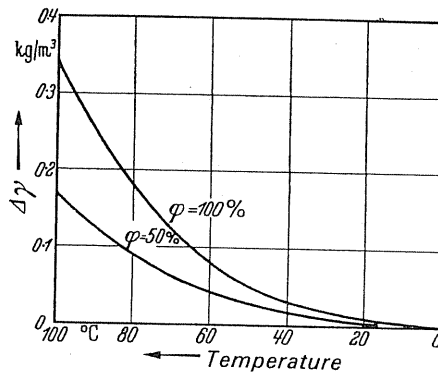


FIG. 3. Percentage decrease of density of moist air with falling temperature.

Considering only the linear term we get:

$$H_s = \frac{\Delta p}{\gamma_1} \left[1 - \frac{1}{2.8} \frac{\Delta p}{p_1} \right] = \frac{\Delta p}{\gamma_1} \alpha.$$

Figure 2 shows the relationship of

$$\left(1 - \frac{1}{2.8} \frac{\Delta p}{p_1} \right) \text{ to } \left(\frac{\Delta p}{p_1} \right).$$

If 100 mm WG is used in the above calculation one will incur an error of 0.5%.

Table 1 shows the difference between isentropic and isothermal compression.

TABLE 1

Δp	100	200	400	1000	2000
α isentrop	0.996	0.993	0.986	0.966	0.96
α isotherm	0.995	0.99	0.98	0.952	0.942

For air one can take $\gamma/g = \frac{1}{8}$ so that the equation of discharge for jets is reduced to

$$c = 4 \sqrt{\Delta p \text{ (mm WG)}}.$$

Determination of density. In the practice of fan design, density is the only physical property of gases and vapours that receives attention. The density γ is derived from the general gas equation

$$pv = p/\gamma = RT \quad \text{or} \quad \gamma = \frac{p}{RT}.$$

The absolute pressure p is obtained from the gauge pressure Δp , giving $p = p_a + \Delta p$ (p_a = atmospheric pressure) and the temperature $T = t + 273$. For the determination of gas constants for mixtures one can find simplified calculations in various handbooks (e.g. by Dubbel or Hütte).

Atmospheric air is almost always moist, and one should remember that moist air is always *lighter* than dry air. In the case of higher temperatures to which moist air might be subjected, the decrease of density becomes important. Figure 3 shows the reduction of density for air of 50% and 100% humidity in relation to the temperature.

Equation (2) (or (5)) is the main equation of the Euler theory of turbines. This states that the *pressure head* H is:

1. Independent of the density. That means that the *pressure head* in the case of water or air is the same. (One can recall a similarity that is found in mechanics, i.e. all bodies falling in a vacuum have the same rate of fall.)

2. With equal peripheral speeds, H or Δp is dependent only on the component c_u .

3. Because $\Delta p = \gamma H$, we can state the following: if the same impeller at the same peripheral speed is used first for air of density γ_L and then for any gas of density γ_G , we would get

$$\Delta p_L = \gamma_L H; \quad \Delta p_G = \gamma_G H.$$

From above

$$\frac{\Delta p_L}{\Delta p_G} = \frac{\gamma_L}{\gamma_G},$$

i.e. the pressures obtained are in the same ratio as their densities.

4. If the density changes with temperature, we apply the main gas equation

$$\Delta p = H\gamma = H \frac{p}{RT}.$$

With constant absolute pressure p and similar pressure head, the pressure difference varies with

$$\frac{\Delta p_{(T_1)}}{\Delta p_{(T_2)}} = \frac{\gamma_{(T_1)}}{\gamma_{(T_2)}} = \frac{T_2}{T_1}, \quad (9)$$

i.e. the pressure difference is inversely proportional to the absolute temperature.

Fan specifically designed for hot gas when used to handle cold air. One can be almost certain that at some time during its operation a fan specified for duty with hot gases or industrial gases will be required to operate with normal cold air. This situation arises in testing a fan on the test-bed or when it is temporarily installed to establish an industrial rating.

Such a case would also arise when a fan is operating on an electric furnace which has just been commissioned and the fan must start off at a temperature significantly lower than the operational temperature. What is the change in pressure and efficiency of the fan under this new condition?

Providing the external controls remain unchanged, the velocity triangles of the fan will remain the same. This means that the volume flow will be the same in both cases, but the pressure changes according to the equation

$$\Delta p = H\gamma = \frac{Hp}{RT},$$

so that the power $L = (V \Delta p / \eta)$ is inversely proportional to the absolute temperature.

Example

A fan designed specifically for duty with hot air at temperature of 500°C will, on initial start up, be operating with cold air at a temperature of 15°C. What will be the change in pressure and output?

$$\text{From } L = \frac{V \Delta p}{\eta} = \frac{VHp}{\eta RT}$$

($V = \text{const}$; $H = \text{const}$; $p = \text{const}$; $R = \text{const}$),

$$\frac{L_1}{L_2} = \frac{\Delta p_1}{\Delta p_2} = \frac{T_2}{T_1} = \frac{273 + 500}{273 + 15} = \frac{773}{288} = 2.68.$$

This means that there has been an increase in output of about 168%. In especially large installations it is often impossible to supply oversized motors so as to cater for these occasional duties: so the general aim is to reduce the output of the fan by some means of throttling. This method of volume control applies to centrifugal fans only, as will be shown in a later chapter.

Through a slight modification of eqn. (5) we obtain another form which is just as informative. In both velocity triangles shown in Fig. 4, we now apply the cosine law, so that

$$w_1^2 = c_1^2 + u_1^2 - 2c_1 u_1 \cos \alpha_1 = c_1^2 + u_1^2 - 2u_1 c_{1u},$$

and

$$w_2^2 = c_2^2 + u_2^2 - 2c_2 u_2 \cos \alpha_2 = c_2^2 + u_2^2 - 2u_2 c_{2u},$$

hence

$$u_1 c_1 \cos \alpha_1 = u_1 c_{1u} = \frac{1}{2} [c_1^2 + u_1^2 - w_1^2],$$

$$u_2 c_2 \cos \alpha_2 = u_2 c_{2u} = \frac{1}{2} [c_2^2 + u_2^2 - w_2^2].$$

By substituting these values in the main equation (5), we get

$$\Delta p = \frac{\gamma}{2g} [c_2^2 - c_1^2] + \frac{\gamma}{2g} [u_2^2 - u_1^2] + \frac{\gamma}{2g} [w_1^2 - w_2^2]. \quad (10)$$

Before we can interpret this equation let us consider Fig. 5 which shows a fan with extremely narrow blade passages, whose entry and exit openings are closed filled with air which is itself rotating. The passage is so narrow that any relative motion is impossible. Thus the air is, so to speak, rotating as a solid body and exerting a centrifugal force. To

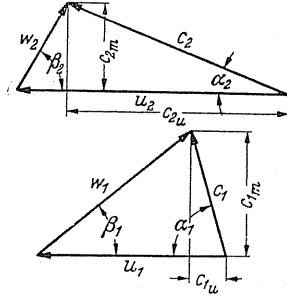


FIG. 4. Velocity triangles for backward-curved blades.

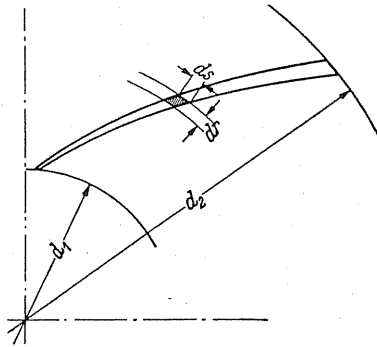


FIG. 5.

calculate this excess in pressure due to the centrifugal force we take an element $ds dr$. This element exerts a centrifugal force:

$$dZ = dr ds b \frac{\gamma}{g} r \omega^2, \quad (a)$$

where b is the width perpendicular to the paper.

This force causes a pressure increase dp on the outside which operates on the surface $ds b$:

$$dZ = dp ds b. \quad (b)$$

By equating expressions (a) and (b),

$$dp = \frac{\gamma}{g} r \omega^2 dr.$$

Integrating from the inner radius r_1 to the outer radius r_2 , we get the total pressure difference,

$$\begin{aligned} \Delta p &= \int_{r_1}^{r_2} dp = \frac{\gamma}{g} \omega^2 \int_{r_1}^{r_2} r dr = \frac{\gamma}{g} \omega^2 \left[\frac{r_2^2}{2} - \frac{r_1^2}{2} \right] \\ \Delta p &= \frac{\gamma}{2g} [u_2^2 - u_1^2]. \end{aligned} \quad (11)$$

With this statement eqn. (10) acquires meaning. The pressure increase is divided into three terms:

(a) The first term $(\gamma/2g) [c_2^2 - c_1^2]$ means an increase in kinetic energy. This increase in kinetic energy is available for conversion in the machine itself and not in the impeller. This means that, according to the Bernoulli equation, providing the transformation is free from loss, a recovery of static pressure is achieved through *retardation in the leading passages*, volute, etc. It follows that if the *conversion takes place without loss*, static pressure $(\gamma/2g) [c_2^2 - c_1^2]$ is produced.

(b) The term $(\gamma/2g) [u_2^2 - u_1^2]$ means that a change in static pressure is accomplished in the impeller due to centrifugal force acting on the fluid. *When* the peripheral velocities u_1 and u_2 are unequal, as in the case of centrifugal fans, the fluid flows radially: as it tends towards the blade tip, it obtains an increasing centrifugal effect. Emphasis must be given to this particular term because direct losses are in no way connected to it. *In axial-flow fans this term is missing because $u_2 = u_1$. Therefore with this term missing it follows that, all things being equal, the pure pressure increase with radial-flow fans will be higher than in the case of axial-flow fans.*

(c) The third term is a change in kinetic energy due to the retardation of the fluid flow relative to the impeller, so that $w_1 > w_2$; this term, therefore, represents a conversion of kinetic energy into potential energy within the impeller itself. This conversion into static pressure, subject to no losses, occurring during transformation, is given by Bernoulli's equation as

$$\frac{\gamma}{2g} [w_1^2 - w_2^2].$$

2. RADIAL ENTRY

In general, when air enters an impeller it has no peripheral component. Such a component must first be produced⁽¹⁾ through inlet vanes. If these vanes are not available then the air enters radially, and according to eqn. (6)

$$\Delta p_{th\infty} = \frac{\gamma}{g} u_2 c_{2u} = \rho u_2 c_{2u}.$$

A further simplification is possible. If one substitutes a coefficient τ for the ratio c_{2u}/u_2 , then by this means c_{2u} is replaced and the pressure can be expressed in terms of the peripheral component u_2 ,

$$\Delta p_{th\infty} = \frac{\gamma}{g} u_2^2 \frac{c_{2u}}{u_2} = \frac{\gamma}{g} u_2^2 \tau. \quad (12)$$

The dimensionless coefficient τ is dependent only on the angle of the velocity triangle. From Fig. 4 through the application of the sine-rule we obtain $c_2 = u_2 [\sin \beta_2 / \sin (\alpha_2 + \beta_2)]$;

¹ The air rotation at the entry could be caused by using double bending in the suction line.

this is introduced in

$$c_{2u} = c_2 \cos \alpha_2 = \frac{\sin \beta_2 \cos \alpha_2}{\sin (\alpha_2 + \beta_2)} u_2$$

and we get

$$\tau = \frac{c_{2u}}{u_2} = \frac{\sin \beta_2 \cos \alpha_2}{\sin \alpha_2 \cos \beta_2 + \cos \alpha_2 \sin \beta_2} = \frac{\tan \beta_2}{\tan \alpha_2 + \tan \beta_2}; \quad (13)$$

therefore τ represents a function of the blade angle β_2 and the outlet angle α_2 of the absolute velocity.

In Fig. 6 the value of $\tau = c_{2u}/u_2$ is shown as a function of α_2 for different angles of β_2 . With the use of Fig. 6, if the peripheral velocity is given, the increase in pressure of a frictionless impeller having an infinite number of blades can be determined.

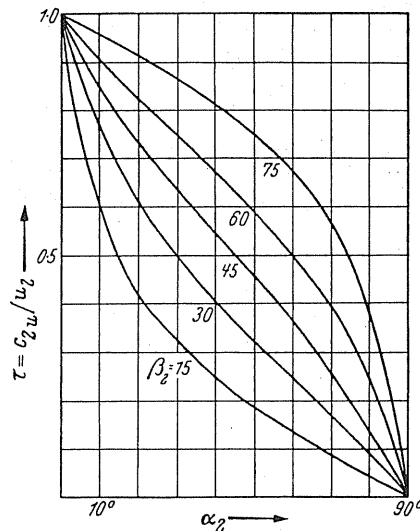


FIG. 6. c_{2u} divided by u_2 plotted against α_2 .

Example

What is the pressure increase with a blade angle $\beta_2 = 60^\circ$, $\alpha_2 = 20^\circ$, if the peripheral velocity $u_2 = 80$ m/sec? From Fig. 6 we obtain the value of τ as being 0.82 and inserting this value in eqn. (12) we get

$$\Delta p_{th\infty} = \tau \frac{\gamma}{g} u_2^2 = 0.82 \times \frac{1}{8} \times 80^2 = 656 \text{ mm WG.}$$

Entry rotation. The question is often asked whether action upon air begins before the blade entry. Some observers believe that a slight pre-rotation occurs, while others claim that the question is still open to doubt. For this question let us establish an answer based upon well-defined scientific principles—namely, a certain pre-rotation must essentially exist by virtue of the mechanism of energy transfer. This is indicated by the fact that energy transfer from blades to air is only possible when the absolute flow is not stationary. This non-stationary flow is brought about by the periodic rotation of the working blades. Thus

if the flow is not stationary it cannot be steady at the blade, but it can extend itself so as to be steady in the suction chamber. Although this means that a fundamental pre-rotation does exist it is so slight that it is virtually impossible to measure.

3. REACTION EFFECT

For the proper assessment of the performance of a fan it is important to know what the magnitude of the static pressure behind the impeller actually is and what pressure must still be recovered by the conversion of the velocity, i.e. conversion of kinetic energy into pressure.

In eqn. (10) the term $(\rho/2) [u_2^2 - u_1^2] + (\rho/2) [w_1^2 - w_2^2]$ represents the pressure behind the impeller, the so-called *gap pressure*, while the term $(\rho/2) [c_2^2 - c_1^2]$ is the conversion term for determining the degree of static pressure recovered in the diffuser or guide passages. As has already been emphasised, considerable losses are connected with the process to which this term relates, and one should strive to maintain its value at as low a level as possible, otherwise the ratio $(\Delta p_{\text{stat th}\infty} / \Delta p_{\text{tot th}\infty})$ may become large. This ratio is called the 'reaction effect'. At this point we shall introduce the letter r . From eqn. (10)

$$\Delta p_{\text{stat th}\infty} = \frac{\rho}{2} [u_2^2 - u_1^2] + \frac{\rho}{2} [w_1^2 - w_2^2] = \frac{\rho}{2} [u_2^2 - w_2^2 + w_1^2 - u_1^2]$$

with $c_{1u} = 0$ we obtain from Fig. 4,

$$w_1^2 - u_1^2 = c_1^2,$$

$$\Delta p_{\text{stat th}\infty} = \frac{\rho}{2} [u_2^2 - w_2^2 + c_1^2].$$

By considering eqn. (6), we then get

$$r = \frac{\Delta p_{\text{stat th}\infty}}{\Delta p_{\text{tot th}\infty}} = \frac{u_2^2 - w_2^2 + c_1^2}{2 u_2 c_{2u}}.$$

To simplify the problem we assume that $c_1 = c_{1m} = c_{2m}$, which is reasonable with average fan dimensions. This assumption is only correct with axial impellers, but in the case of radial impellers it produces a good average value.

From this we get

$$r = \frac{u_2^2 - w_2^2 + c_{2m}^2}{2 u_2 c_{2u}} = \frac{u_2^2 - (u_2 - c_{2u})^2}{2 u_2 c_{2u}},$$

since

$$w_2^2 - c_{2m}^2 = (u_2 - c_{2u})^2,$$

thus

$$r = \frac{-c_{2u}^2 + 2 u_2 c_{2u}}{2 u_2 c_{2u}} = 1 - \frac{1}{2} \frac{c_{2u}}{u_2}. \quad (14)$$

We get a clear picture of the reaction effect r as well as of the total pressure Δp in the case of different blade angles from the following considerations. If we compare impellers having similar peripheral velocity, equal diameters and blade widths, which give equal volumes, then c_{2m} is constant. Now for different blade angles velocity triangles similar to those shown in Fig. 7 are obtained. By relating $\Delta p_{th\infty} = (\gamma/g) c_{2u} u_2$ to the velocity pres-

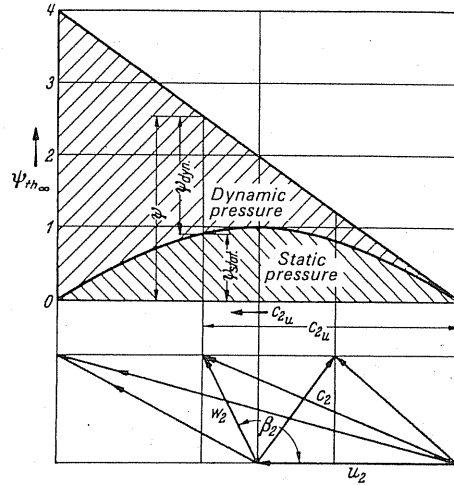


FIG. 7. Dynamic and static pressure for various blade angles.

sure $(\gamma/2g) u_2^2$ due to peripheral velocity a significant coefficient can be introduced. The peripheral velocity pressure, since it is easily envisaged, is used as a basis of comparison. This new coefficient is called the pressure coefficient, which we introduce as

$$\psi_{th\infty} = \frac{\Delta p_{th\infty}}{(\gamma/2g) u_2^2} = 2 \frac{c_{2u}}{u_2} = 2\tau \quad (15)$$

and plot $\psi_{th\infty}$ as well as $\psi_{stat th\infty}$ against the velocity triangles, so that immediately above the end point of c_{2u} each corresponding value of $\psi_{th\infty}$ and $\psi_{stat th\infty}$ can be found. The static pressure $\Delta p_{stat th\infty} = r \Delta p_{th\infty}$ is also expressed by a pressure coefficient

$$\psi_{stat th\infty} = \frac{\Delta p_{stat th\infty}}{(\gamma/2g) u_2^2}.$$

Figure 7 shows that with increasing blade angles β_2 pressure $\Delta p_{th\infty}$ increases, i.e. $\psi_{th\infty}$ increases, while the reaction effect ($\psi_{stat th\infty}/\psi_{th\infty}$) decreases. With large blade angles β_2 one gets a high total pressure, but, as the angles have increased, the proportion of the static pressure existing behind the blades has decreased, which means that there is an increasing proportion of kinetic energy that must be transformed into pressure. The absolute value of the static pressure is given by the product

$$\psi_{stat th\infty} = \psi_{th\infty} r = 2\tau \left[1 - \frac{\tau}{2} \right] = 2\tau - \tau^2 = 2 \frac{c_{2u}}{u_2} - \left(\frac{c_{2u}}{u_2} \right)^2 \quad (16)$$

since

$$c_{2u}/u_2 = \psi_{th\infty}/2,$$

$$\psi_{stat\ th\infty} = \psi_{th\infty} \left(\frac{1 - \psi_{th\infty}}{4} \right),$$

which gives

$$\psi_{th\infty} = 4(1 - r).$$

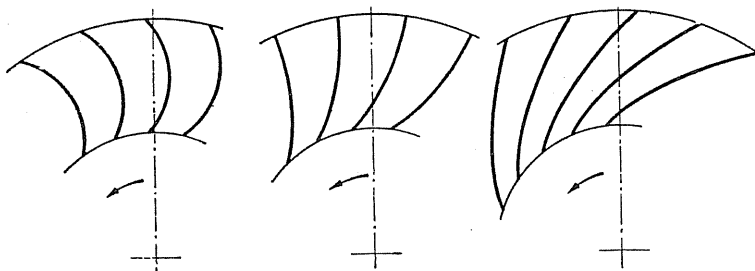


FIG. 8. Diagrams of forward-curved, radial-tipped, and backward-curved blades.

The graph of $\psi_{stat\ th\infty}$ is a parabola which cuts the abscissa at $c_{2u} = 0$ and $c_{2u} = 2u_2$, the highest value being 1 when $c_{2u} = u_2$. When the blade angle is 90° , i.e. radial tip blades, the pressure is divided equally, one half being comprised of the static pressure and the other being the velocity pressure. At the point where $c_{2u} = 2u_2$, then $\psi_{stat\ th\infty} = 0$ and $\psi_{th\infty} = 4$, which means, of course, that this is the point where the highest total pressure exists yet the static pressure portion is zero. The impeller has only produced kinetic energy. A centrifugal impeller with these characteristics is called an *action impeller*, while centrifugal impellers in which the static pressure increases in the impeller are called *reaction impellers*. Most fans work on the reaction principle.

The form of the blades is fundamentally changed depending on the blade angle β_2 which has significant influence on the conversion of energy. These blade forms are:

- (a) *Backward-curved*,
- (b) *Radial*,
- (c) *Forward-curved*.

They are schematically represented in Fig. 8 for identical blade entry angles and number of blades. The entry profile in all cases is identical because in the case of equal volumes and rotational speeds it is necessary to have identical angles. In the construction of fans all three forms of blades are employed.

TOTAL REACTION EFFECT

The previously derived reaction effect is an extremely useful factor for the fan designer. It is indispensable in the comparison of different impellers. Nevertheless, it deals with a definite characteristic of the inner processes of a fan impeller which is not apparent on

the outside. This means that its value is of interest to the fan designer or engineer only. The fan user hardly ever interests himself in this factor, but is more concerned with the total performance of a fan. Therefore it is more significant to know the comparative value of the dynamic in relation to the total pressure. Many applications require, for instance, a very large cross-sectional area. This means that it would be of little use to employ a high-velocity fan, and may be a high-performance fan, to exhaust the system because the effect of losses is to reduce this high velocity. Such characteristics of a fan become more clearly grasped if one considers an open-suction fan, as shown in Fig. 1, in which a pressure network is produced by joining a system to the discharge side of the fan. The build-up of pressure (i.e. stagnation pressure) measured at the fan outlet is the *fan total pressure*, whilst the *static pressure* measurement at this point indicates the *static pressure in excess of atmospheric pressure*. With this procedure the necessity of an intake duct is dispensed with, while the discharge cross-sectional area, which is an extremely important factor in fan construction, comes to the fore. The above characteristic of a fan should become apparent if one defines the total reaction effect

$$r_{\text{tot}} = \frac{\Delta p_{\text{stat}}}{\Delta p_{\text{tot}}}.$$

From the relationship

$$\Delta p_{\text{tot}} - \Delta p_{\text{stat}} = \frac{\rho}{2} c^2$$

the meaning of discharge velocity now becomes clear. For most applications it is desirable that r_{tot} should, if possible, be large.

4. CHARACTERISTICS IN THE CASE OF AN INFINITE NUMBER OF BLADES

For the application of a fan it is of interest to know how the pressure is dependent upon the volume. In the case of identical peripheral velocities the volume is proportional to the meridian component c_{2m} . According to the equation

$$V = c_{2m} \pi d_2 b_2, \quad (17)$$

c_{2m} can only change in accordance with the method shown in Fig. 9; the apex of the velocity triangle adjusts itself on the *side* of the angle β_2 , so that the direction of the relative

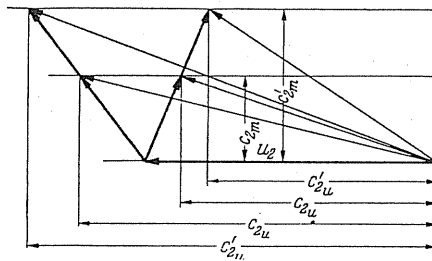


FIG. 9. Velocity triangles for various outputs.

velocity before and after is fixed by means of the exit angle β_2 . If c_{2m} increases, then c_{2u} changes, and it is obvious that in the case of backward-curved blades c_{2u} gets smaller; while with forward-curved blades with increasing c_{2m} the value of c_{2u} increases. An easy calculation gives the numerical relationship

$$\frac{c_{2m}}{u_2 - c_{2u}} = \tan \beta_2. \quad (17a)$$

From this

$$c_{2u} = u_2 - \frac{c_{2m}}{\tan \beta_2},$$

and by substituting

$$\Delta p_{th\infty} = \rho u_2 c_{2u},$$

we get

$$\Delta p_{th\infty} = \rho u_2^2 - \rho \frac{u_2}{\tan \beta_2} c_{2m}.$$

From eqn. (17) we have

$$c_{2m} = \frac{V}{\pi d_2 b_2},$$

and now we get

$$\Delta p_{th\infty} = \rho u_2^2 - V \rho \frac{u^2}{\pi d_2 b_2 \tan \beta_2}, \quad (18)$$

which means the relation

$$\Delta p_{th\infty} = f(V)$$

is a straight line, whose slope is fixed by the angle β_2 , other conditions remaining the same. (Figure 10 shows the result.)

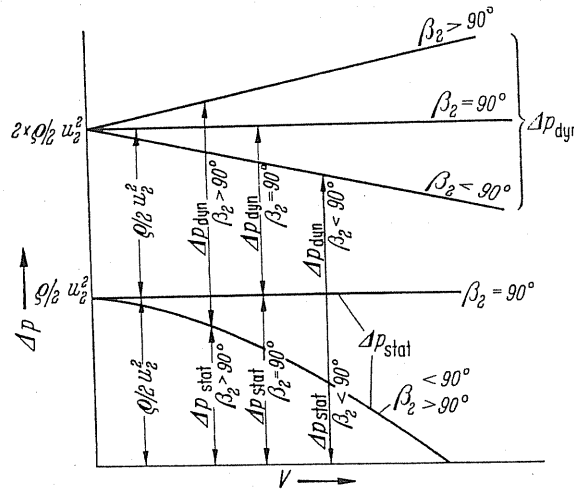


FIG. 10. Theoretical characteristics for a fan with an infinite number of blades and a loss-free stream at various blade angles.

Explanation of Fig.10: *Forward-curved blades*, the pressure increases as the volume increases; *Radial blades*, pressure remains constant as the volume increases; *Backward-curved blades*, the pressure decreases as the volume increases.

It is also a comparatively simple matter to calculate the power requirements (without consideration of losses). The stated performance is given by the expression

$$L = \gamma HV = \Delta p V = \rho u_2^2 V - V^2 \rho \frac{u_2}{\pi d_2 b_2 \tan \beta_2}. \quad (19)$$

The relationship $L = f(V)$ is a parabola, but in the case of $\beta_2 = 90^\circ$ it becomes a straight line, sloping upwards. For backward-curved blades $\beta_2 < 90^\circ$ the parabola lies below this straight line, and for forward-curved blades $\beta_2 > 90^\circ$ it lies above it, as shown in Fig.11.

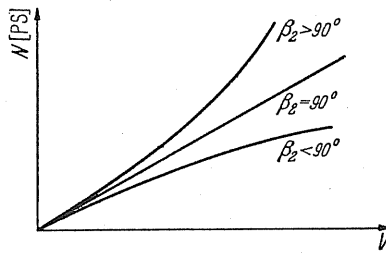


FIG.11. Output curves for various blade angles.

From eqn. (7) the actual air power is given in m kg/sec by the expression

$$L = V [\text{m}^3/\text{sec}] \Delta p [\text{kg}/\text{m}^2].$$

This form of output calculation is simple for fans because V and Δp are usually known. The input horse-power to the impeller is given by, using η_{tot} (the total efficiency),

$$N_{\text{shaft}} = \frac{L}{75\eta_{\text{tot}}} = \frac{\Delta p V}{75\eta_{\text{tot}}} \quad [\text{h.p.}] \quad (20)$$

From this, if the volume or weight (e.g. of steam) is known, then the energy requirements can be obtained in the following dimensions:

$$L = \frac{HG}{\eta} = \frac{\Delta p V}{\eta} \quad [\text{kg m/sec}], \quad (21)$$

$$N = \frac{HG}{75\eta} = \frac{\Delta p V}{75\eta} \quad [\text{h.p.}], \quad (22)$$

$$N = \frac{HG}{102\eta} = \frac{\Delta p V}{102\eta} \quad [\text{kW}]. \quad (23)$$

For a constant angular velocity N is proportional to M , since $N = M\omega$. This means that the energy requirement curves are also identical with the torque curves if the corresponding scales are changed.

Characteristic of static pressure developed in the impeller gap. The question arises of how the gap pressure varies with the delivered volume, i.e. what static pressure is available at the exit of the impeller. To determine this we use eqn. (14) and assuming that $c_1 = c_{2m}$, we will obtain an average value,

$$\Delta p_{\text{stat th}\infty} = \frac{\rho}{2} [u_2^2 - w_2^2 + c_{2m}^2].$$

From Fig. 4, $w_2 = c_{2m}/\sin \beta_2$. After inserting this value we have

$$\Delta p_{\text{stat th}\infty} = \frac{\rho}{2} \left[u_2^2 - \frac{c_{2m}^2}{\tan^2 \beta_2} \right] = \frac{\rho}{2} \left[u_2^2 - \frac{V^2}{\pi^2 d_2^2 b_2^2 \tan^2 \beta_2} \right].$$

The function $\Delta p_{\text{stat}} = f(V)$ is also represented by a *parabola*. There is no difference for identical values of β_2 between backward- and forward-curved blades since the expression involves $\tan^2 \beta_2$. When $\beta_2 = 90^\circ$, the curve becomes a straight line as shown in Fig. 10, because $\Delta p_{\text{stat th}\infty} = (\rho/2)u_2^2$.

The equations for the characteristics become clearly understood when the coefficients ψ , φ , λ defined later are used in them. If one employs these quantities in eqns. (18) and (19) instead of Δp , V , and L , the following equations are obtained:

$$\begin{aligned} \psi_{\text{th}\infty} &= 2 - \frac{\varphi}{2} \frac{d_2}{b_2 \tan \beta_2}, \\ \psi_{\text{stat th}\infty} &= 1 - \varphi^2 \frac{d_2^2}{16b_2^2 \tan^2 \beta_2}, \\ \lambda &= \frac{2}{\eta} \left(\varphi - \varphi^2 \frac{d_2}{4b_2 \tan \beta_2} \right). \end{aligned}$$

Taking $\tan \beta_2 = c_{2m}/(u_2 - c_{2u})$ from eqn. (17a) and knowing that $\psi_{\text{th}\infty} = 2c_{2u}/u_2$ we have

$$\tan \beta_2 = \frac{c_{2m}}{u_2} \frac{1}{1 - \psi_{\text{th}\infty}/2}.$$

For the case where $c_{2m} = c_{1m}$, which is a reasonable assumption,

$$u_1/u_2 = d_1/d_2 \quad \text{and} \quad c_{1m} = u_1 \tan \beta_1,$$

we obtain

$$\tan \beta_2 = \frac{d_1}{d_2} \tan \beta_1 \frac{1}{1 - \psi_{\text{th}\infty}/2}.$$

One can also combine the velocity triangles and characteristics, to which Stepanoff⁽²⁾ first drew attention. It is only necessary to make the velocity triangle dimensionless and then to turn the diagram through an angle of 90° . We divide c_{2u} and c_{2m} by u_2 respectively to obtain the ratios c_{2u}/u_2 for the ordinate and c_{2m}/u_2 for the abscissa. Because

$$c_{2u}/u_2 = \frac{\psi_{\text{th}\infty}}{2} = \frac{gH_{\text{th}\infty}}{u_2^2} = \frac{\Delta p_{\text{th}\infty}}{\rho u_2^2},$$

² Stepanoff, A. J., *Turboblowers*, New York, John Wiley, 1955.

the ordinate represents the theoretical increase in pressure in dimensionless terms, while c_{2m}/u_2 represents a ratio of the volumes. The velocity diagram ABC is now a right-angled triangle expressed in dimensionless quantities. With respect to a finite number of blades, point C' , which lies directly beneath C , represents the theoretical pressure head without losses. AC' , therefore, is the simultaneous characteristic in non-dimensional terms. The points D and D' give the best possible theoretical intake volume.

For the very important case of a fan having a free intake, i.e. a system which is only loaded on the delivery side, the static pressure behind the impeller is

$$\Delta p_{\text{stat th } \infty} = \Delta p_{\text{th } \infty} - \frac{\rho}{2} c_2^2.$$

The reaction effect will be:

$$r = 1 - \frac{\rho}{2} c_2^2 \frac{1}{\Delta p_{\text{th } \infty}}.$$

If we consider

$$c_2^2 = c_{2m}^2 + c_{2u}^2 \quad \text{and} \quad \Delta p_{\text{th } \infty} = \rho u_2 c_{2u},$$

then we get

$$r = 1 - \frac{(c_{2m}/u_2)^2 + (c_{2u}/u_2)^2}{2(c_{2u}/u_2)}.$$

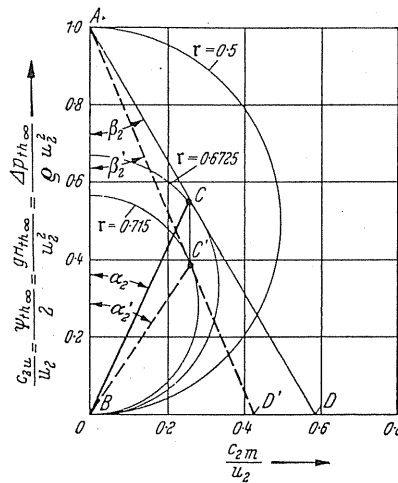


FIG. 12. Combination of velocity triangles and characteristics according to Stepanoff.

The curves $r = \text{constant}$ according to this equation are shown in Fig. 12 as simple semicircles of radius $1 - r$. With the construction of these semicircles the reaction effect can immediately be seen. For instance, we find at point C the value is 0.6725 and at point C' the value is 0.715, so that it can be seen at once that, in the case of finite blades, there is an increase in the reaction effect.

5. FUNDAMENTAL PROBLEMS

With the aid of the previously derived equations the main fundamental problems can be readily solved.

(1) Given α_2 and β_2 , it is required to find the theoretical increase in pressure head $H_{th\infty}$ in the case of an infinite number of blades. The solution may be obtained from eqns. (3) and (13):

$$u_2 = \sqrt{gH_{th\infty} \left(1 + \frac{\tan \alpha_2}{\tan \beta_2} \right)}. \quad (24)$$

(2) Given c_{2m} and β_2 , $H_{th\infty}$ can be calculated from equation (17):

$$u_2 = \frac{c_{2m}}{2} \cot \beta_2 + \sqrt{\left(\frac{c_{2m}}{2} \cot \beta_2 \right)^2 + gH_{th\infty}}. \quad (25)$$

(3) Given c_{2u}/u_2 , $H_{th\infty}$ can be calculated from eqn. (3):

$$\begin{aligned} H_{th\infty} &= \frac{1}{g} u_2 c_{2u} = \frac{1}{g} u_2^2 \frac{c_{2u}}{u_2}, \\ u_2 &= \sqrt{\frac{2H_{th\infty}}{c_{2u}/u_2}}. \end{aligned} \quad (26)$$

6. THE EFFECTS OF COMPRESSION

With higher velocities there are higher pressures; gases change their densities noticeably and therefore their volumes. So far we have tacitly neglected this factor, but it is necessary to find out up to what limit this simplification is valid.

We start from the well-known differential equation for the velocity of sound:⁽³⁾

$$a = \sqrt{\frac{dp}{d\rho}},$$

where a is the velocity of sound, p the pressure, and ρ the density of medium.

If we express this

$$a = \sqrt{\frac{\Delta p}{\Delta \rho}},$$

then for the purposes of illustration Δp is considered as the dynamic pressure, $\Delta p = (\rho/2)c^2$, of a velocity c .

The change in density expressed as a proportion of the original density is given by

$$\frac{\Delta \rho}{\rho} = \frac{\Delta p}{p} = \frac{1}{2} \left(\frac{c}{a} \right)^2.$$

³ Eck, B., *Technische Strömungslehre*, 7th edn., Berlin/Göttingen/Heidelberg, Springer, 1966.

This relation satisfies our original question because a change of density is proportional to the change of force. Accordingly the pressure on the blades will change so that we can expect to have corresponding errors in our calculations.

The errors are shown in the measurement if one calculates the dynamic pressure according to the equation $\Delta p \approx (\rho/2)c^2$. The exact value is given by

$$\Delta p = \frac{\rho}{2} c^2 \left[1 + \frac{1}{4} \left(\frac{c}{a} \right)^2 \right].$$

From this the error is

$$\frac{\Delta [\Delta p]}{\Delta p} = \frac{1}{4} \left(\frac{c}{a} \right)^2.$$

The percentage errors, arising from this formula, which were previously neglected, are given in Table 2 for different velocities.

TABLE 2

m/sec	50	100	150	200
$\frac{\Delta \rho}{\rho} \times 100$	1.21	4.8	11.65	20.8
$\frac{\Delta [\Delta p]}{\Delta p} \times 100$	0.605	2.4	5.825	10.4

The table demonstrates the validity of ignoring the effects of compression. For example, the error is 2.5% for 100 m/sec, and 10% for 200 m/sec.

In conclusion, the effect of compressibility is negligible for all practical purposes provided the velocity at any point within the fan is below 100 m/sec.

It must be borne in mind that in accordance with the calculation of performance shown in Fig. 2, the compressibility effect must receive prior consideration.

CHAPTER II

CALCULATION OF FLOW IN BLADE PASSAGES

7. VELOCITY DISTRIBUTION IN THE BLADE PASSAGE

At this stage we will consider the influence of a finite number of blades. This is important because we are now dealing with conditions differing widely from the previous assumption of an infinite number of blades with each blade extending towards infinity in length and breadth.

In the case of a finite number of blade passages, a variation of velocity perpendicular to the flow must exist. This arises from the following argument. By means of the blades, pressure forces are transferred to the air in a peripheral direction. According to Bernoulli's equation, pressure differences could only be effected in a flowing medium provided that a velocity gradient exists. In the case of non-rotating flows, this follows from Bernoulli's equation $\Delta p = (c_2^2 - c_1^2) \gamma / 2g$; accordingly $c_2 > c_1$, if $\Delta p > 0$. The converse is also true.

The point now arises as to how we can explain the difference between pressure and velocity changes in respect to rotating flow.

In the following we shall consider simultaneously the blade passages of backward- and forward-curved blades, and investigate the equilibrium condition of an element whose length in the direction of flow is ds and width is dn perpendicular to the flow (Figs. 13 and 14). The dimension perpendicular to the plane of the page is designated by b , i.e. the axial blade length.

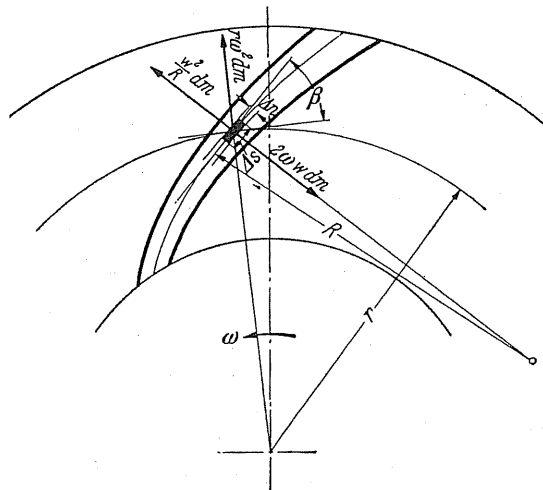


FIG. 13. Forces in a narrow blade passage in the case of backward-curved blades.

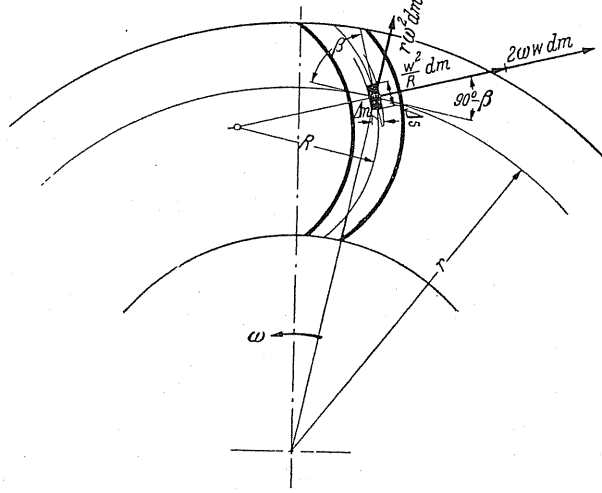


FIG. 14. Forces in a narrow blade passage in the case of forward-curved blades.

8. FORCES PERPENDICULAR TO THE DIRECTION OF FLOW

The curvature of the passage with radius of curvature R produces a centrifugal force $(w^2/R) dm$ perpendicular to the blade passage, while a centrifugal force $r \omega^2 dm$ in the direction of the impeller radius is caused by the total rotation of the impeller. Only the component $r \omega^2 \cos \beta dm$ of this force acts normal to the direction of flow. Finally, the Coriolis force acts in addition. This force always appears if a body is guided in a rotating path, and moves along this path with a relative velocity w . In this case a guiding pressure $2\omega w dm$ acts normal to the direction of flow. The resultant of all these forces produces a pressure change Δp perpendicular to the direction of flow. Figures 13 and 14 illustrate these forces in magnitude and direction in the case of backward- and forward-curved blades respectively.

For backward-curved blades these forces yield

$$\frac{\partial p}{\partial n} \Delta n \Delta s b = \Delta n \Delta s b \frac{\gamma}{g} \left[\frac{w^2}{R} + r \omega^2 \cos \beta - 2\omega w \right],$$

and for forward-curved blades,

$$\frac{\partial p}{\partial n} \Delta n \Delta s b = \Delta n \Delta s b \frac{\gamma}{g} \left[\frac{w^2}{R} + r \omega^2 \cos \beta + 2\omega w \right].$$

From the above it is possible to calculate the pressure gradient $\partial p / \partial n$ perpendicular to the relative direction of flow.

Accordingly the pressure gradient is as follows:

(1) Backward-curved blades:

$$\frac{\partial p}{\partial n} = \frac{\gamma}{g} \left[\frac{w^2}{R} + r \omega^2 \cos \beta - 2\omega w \right], \quad (27)$$

(2) Forward-curved blades:

$$\frac{\partial p}{\partial n} = \frac{\gamma}{g} \left[\frac{w^2}{R} + r \omega^2 \cos \beta + 2\omega w \right]. \quad (28)$$

9. FORCES IN THE DIRECTION OF FLOW

The forces acting in the direction of flow are a component of the centrifugal force $r \omega^2 dm \sin \beta$ and a pressure force which originates from a possible variation of pressure in the direction of flow. The sum of both forces produces an acceleration according to the Newtonian equation

$$\frac{\gamma}{g} b \, dn \, ds \frac{dw}{dt} = -dn \, b \frac{\partial p}{\partial s} ds + \frac{\gamma}{g} ds \, dn \, b \, r \omega^2 \sin \beta.$$

It is well known that

$$\frac{dw}{dt} = \frac{\partial w}{\partial s} \frac{ds}{dt} = \frac{\partial w}{\partial s} w,$$

so by substituting this in the preceding equation,

$$\frac{\gamma}{g} w \frac{\partial w}{\partial s} = -\frac{\partial p}{\partial s} + \frac{\gamma}{g} r \omega^2 \sin \beta,$$

and so

$$\frac{\gamma}{g} w \, dw = -dp + \frac{\gamma}{g} r \omega^2 \sin \beta \, ds.$$

From Fig. 13 we can state $\sin \beta \, ds = dr$ which gives

$$\frac{\gamma}{g} w \, dw - \frac{\gamma}{g} r \omega^2 \, dr + dp = 0.$$

Thus after integration we get

$$\frac{w^2}{2g} + \frac{p}{\gamma} - \frac{u^2}{2g} = H' = \text{const}, \quad (29)$$

which is the energy equation of the relative flow. This equation is very similar to Bernoulli's equation, with the exception that $(u^2/2g)$ is an additional term.

It will be noticed that this relationship can also be directly derived from the main equation. Both the latter terms indicate the static pressure difference $p_2 - p_1$, so that the following equation is true:

$$p_2 - p_1 = \frac{\gamma}{2g} [u_2^2 - u_1^2] + \frac{\gamma}{2g} [w_1^2 - w_2^2].$$

If we rearrange the terms so that each side has terms designated by the same suffix, we get

$$\frac{w_2^2}{2g} + \frac{p_2}{\gamma} - \frac{u_2^2}{2g} = \frac{w_1^2}{2g} + \frac{p_1}{\gamma} - \frac{u_1^2}{2g} = H' = \text{const.}$$

Equation (29) is, in effect, the Bernoulli equation as applied to the case of a rotating flow. Accordingly, for a stream filament, the value H' is a constant. If we neglect friction, the neighbouring stream filaments have no other forms of energy, because the tangential stresses which could result in such differences are non-existent. This means that $\partial H' / \partial n = 0$. After differentiation of eqn. (29) we get

$$\frac{\partial H'}{\partial n} = \frac{w}{g} \frac{\partial w}{\partial n} + \frac{1}{\gamma} \frac{\partial p}{\partial n} - \frac{u}{g} \frac{\partial u}{\partial n} = 0,$$

from which

$$\frac{\partial p}{\partial n} = \frac{\gamma}{g} \left[u \frac{\partial u}{\partial n} - w \frac{\partial w}{\partial n} \right].$$

If we substitute $u = r \omega$ and $dn = dr / \cos \beta$, we get

$$\frac{\partial p}{\partial n} = \frac{\gamma}{g} \left[r \omega^2 \cos \beta - w \frac{\partial w}{\partial n} \right];$$

comparing this result with eqn. (27) for backward-curved blades,

$$\frac{\partial p}{\partial n} = \frac{\gamma}{g} \left[\frac{w^2}{R} + r \omega^2 \cos \beta - 2\omega w \right],$$

and eqn. (28) for forward-curved blades,

$$\frac{\partial p}{\partial n} = \frac{\gamma}{g} \left[\frac{w^2}{R} + r \omega^2 \cos \beta + 2\omega w \right],$$

we obtain for backward-curved blades

$$\frac{\partial w}{\partial n} = 2\omega - \frac{w}{R} \quad (30)$$

and for forward-curved blades

$$\frac{\partial w}{\partial n} = - \left[2\omega + \frac{w}{R} \right]. \quad (31)$$

Equations (30) and (31) represent the differential equations of the relative rotating flow, and it should be noted that *they constitute the basis for a more detailed study of flow.*

However, before use can be made of these equations we must examine yet another characteristic of the relative rotating flow.

10. RELATIVE CIRCULATION

For a finite number of blades, the assumption of frictionless flow introduces a motion which is known as "relative circulation". The clearest way to observe this motion is to consider the blade passages being completely sealed as shown in Fig. 15. Because the passage walls do not exercise any frictional forces, rotation of the air and consequently tangential stresses are neglected. During rotation of the impeller, displacement of the air will follow a circular path, so that an apparent rotation, called "relative rotation", will be seen by an observer travelling with the impeller. The stream filaments of the motion are shown in Fig. 15. On the leading edge of the blade the air flows radially inwards and on the trailing edge outwards, thus creating a circulation within the blade passages. If the passages are opened so that a definite volume flows through, the main flow is superimposed upon the relative circulation, the superimposed flow increases the velocity at the trailing edge of the blade and reduces it at the leading edge as indicated by Fig. 16. Because the relative circulation remains independent of the volume, according to its magnitude, a significantly changed picture of the flow will be expected.

A particular case arises when the volume flow is reduced and the subsequent reduction of the velocity at the leading edge of the blade (i.e. pressure side) is equal to the flow velocity at this point. Consequently the flow at the leading edge comes to a halt: a further

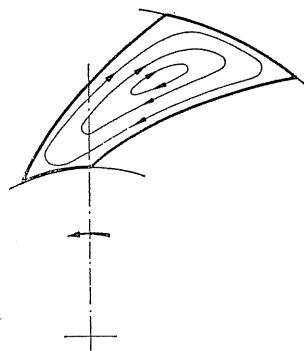


FIG. 15. Relative circulation in an enclosed blade passage.

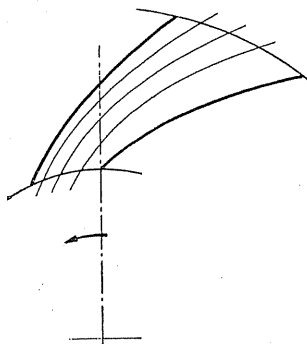


FIG. 16. Relative flow in an open blade passage.

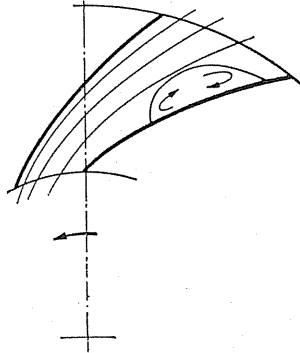


FIG. 17. Relative flow where vortices appear in the blade passages.

reduction in volume will result in a reversal of flow. Figure 17 illustrates this case. *Therefore in the case of frictionless flow there is an optimum volume flow for each blade passage below which the flow at the leading edge of the blade "reverses".* These phenomena were first studied by Kucharski.⁽¹⁾

11. STRAIGHT BLADES

In some cases, eqn. (30) furnishes the required values in a very simple manner. Kucharski has demonstrated that a rotating passage bounded by straight blades (not curved ones) is comparatively easy to deal with. In this particular case the radius of curvature R is infinite, so that eqn. (30) simplifies to

$$\frac{\partial w}{\partial n} = 2\omega; \quad \partial w = \partial n \, 2\omega.$$

The solution of this equation is

$$w = w' + 2n \, \omega,$$

where w' is the velocity at the leading edge of the blade, and n is the perpendicular distance to the next blade. The velocity increases linearly with the distance n , as Fig. 18 shows, so

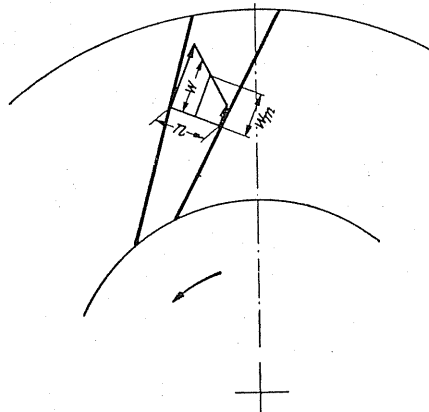


FIG. 18. Distribution of velocity between straight blades.

¹ Kucharski, W., *Strömungen einer reibungsfreien Flüssigkeit*, Munich, Oldenbourg, 1918.

that the velocity has its lowest value at the leading edge of the blade. One can easily calculate the volume flow at which the velocity is zero at this point. This means that $w' = 0$; and $w_{\max} = 2n\omega$, so that average velocity $w_m = n\omega$. Thus the case now arises of a volume flow below $V = n^2 \omega b$ when a reversal of flow will begin at the leading edge of the blade.

It is accepted that identical behaviour is displayed in the case of diverging blade passages, providing the distance between the blades is not excessive. The only condition to be fulfilled is that the stream-filaments are straight.

12. EQUAL VELOCITY DISTRIBUTION IN THE BLADE PASSAGE

One may ask whether it is possible to obtain a constant velocity distribution with relative rotational motion similar to that found in stationary straight passages. Equating $dw/dn = 0$ and substituting this value in eqn. (30),

$$2\omega - \frac{w}{R} = 0; \quad \text{or } R = \frac{w}{2\omega} = \frac{r_1 w}{2u_1}.$$

This can actually be achieved if we apply this curvature to the passage, and form backward-curved blades. When w is constant, then from the above equation R is constant. This produces simple circular blades. Nevertheless, in comparison with eqn. (27) we find that a pressure difference perpendicular to the flow still exists and is

$$\frac{\partial p}{\partial n} = \frac{\gamma}{g} r \omega^2 \cos \beta.$$

Two terms have been eliminated in this particular case and a glance at Fig. 13 should give us the precise physical meaning. The centrifugal force $(w^2/R) dm$ on blade curvature is equal to the "Coriolis force" $2\omega w dm$ so that the only transverse pressure is caused by the centrifugal force $r \omega^2 dm$. This case has no practical significance since it would lead to blades that are far too short; moreover, because of the distinct backward curvature of these blades, only a very slight pressure would be produced.

13. EQUAL PRESSURE DISTRIBUTION IN THE BLADE PASSAGE

Is it possible to produce a blade passage which does not display a pressure difference perpendicular to the direction of flow? It might be considered that the "transfer of force" cannot occur in such a passage. But the contradiction which now arises has a simple explanation. Only the pressure difference at the leading and trailing edges of the blade governs the useful blade pressures which lie at the same radius, therefore points lying at the same radius must be examined with reference to their difference of pressure. One follows a line perpendicular to the flow, so that the length of the radius to the points on this line is in-

creased or diminished. One can also say that with reducing transverse pressure it is sufficient to have a pressure change in the direction of relative flow in order to permit the transfer of energy at the blade. The shape of this passage follows from the following calculation:

By substituting $\partial p / \partial n = 0$ in eqn. (27) we get

$$\frac{w^2}{R} + r \omega^2 \cos \beta - 2\omega w = 0.$$

From this R is calculated:

$$R = \frac{w^2}{\omega[2w - u \cos \beta]}.$$

It is possible to design the blade, point by point, from the radius of curvature R if, for example, one assumes the path of w . R can extend to infinity, which means the blades become straight if the denominator disappears, i.e. when $2w - u \cos \beta = 0$. From this point one establishes $w = \text{constant}$, so that the further blade path is straight, because for a straight line it is known that $u \cos \beta = \text{constant}$.

Grun⁽²⁾ was the first to refer to this form of blade, which has since gained a certain prominence in the field of turbocompressors.

14. CALCULATION OF VELOCITY AND PRESSURE DISTRIBUTIONS IN AN ARBITRARY BLADE PASSAGE

The starting point of these calculations is the differential equation of relative motion (30):

$$\frac{\partial w}{\partial n} = 2\omega - \frac{w}{R}.$$

The formal solution of this equation is relatively easy with the help of integrating factors. However, the evaluation of this equation presents considerable difficulty and hitherto has been successful in only a very few cases. With certain modifications, or rather simplification, an approximate solution is possible and might be adequate for practical purposes. Carrying out this calculation shows that the velocity distribution normal to the walls of the blade passage is nearly linear.⁽³⁾ In itself, particularly in the case of forward-curved blades, the difference between the true velocity distribution and a straight line is so small that it can be ignored. This simplification can be recommended as an adequate rule for frictionless flow. The maximum velocity difference Δw between the end points of the normal line only interests us from the practical aspect, and therefore on the assumption that a linear distribution prevails we get

$$\Delta w = 2\omega a \pm \frac{w_m}{R} a,$$

² Grun, Diss., Hanover, 1902.

³ Detailed explanations given in the first German edition are not given here in view of their limited meaning in practice.

where a is the width of the passage, R average radius of curvature, and w_m average velocity in the blade passages (negative for backward-curved blades and positive for forward-curved blades). With the help of this relationship the pressure distribution at the blades as well as a picture of the streamlines can be easily determined.

CHAPTER III

INFLUENCE OF A FINITE NUMBER OF BLADES

15. FUNDAMENTALS

In the previous section the flow was examined for a passage of finite width. The magnitude of the influence exerted by a finite number of blades on the transfer of energy will now be established in more detail. It is simple to visualise that such an influence must exist. In the case of an infinite number of blades the angle of discharge of the relative velocity is identical with the blade angle β_2 . If the blades are separated then "guidance" of the air becomes less effective, the average direction of discharge therefore varies from the blade angle β_2 as the number of blades decreases. The sense of direction of this change is easily determined: with less guidance, i.e. fewer blades, the air is less inclined to travel in the peripheral direction, *so that in every case the component c_u becomes less*. This causes a subsequent reduction in the theoretically obtainable pressure. According to eqn. (6) the theoretical pressure increase for an impeller having an infinite number of blades is $\Delta p_{th\infty} = \rho u_2 c_{2u}$, so that we can designate the theoretical pressure increase for a finite number of blades by Δp_{th} . It must be borne in mind at this stage that frictional effects are ignored. The ratio of these two theoretical changes of pressure introduce us to the following coefficient,

$$\varepsilon = \frac{\Delta p_{th}}{\Delta p_{th\infty}}. \quad (32)$$

The introduction of this coefficient, which has nothing to do with efficiency or with losses, may be justified on the basis that in the case of any design this factor must be known: it is sometimes known as the velocity coefficient.

Figure 19 gives a qualitative picture of the effects of a finite number of blades on the velocity triangles for the three most important cases in fan engineering (i.e. forward-curved, radial-tipped, and backward-curved blades). The full-line triangles are applicable to an infinite number of blades while the dashed-line triangles are valid for a finite number of blades. The practical effect of a finite number of blades can be readily interpreted from these diagrams:

- (1) The relative discharge angle β_3 is less than the blade angle β_2 in each case.
- (2) The average relative discharge velocity changes; in the case of backward-curved and radial-tipped blades it increases, and with forward-curved blades decreases.
- (3) In each case the average absolute discharge velocity c_3 is smaller than c_2 .
- (4) In each case the angle α_3 of the absolute velocity is more acute than α_2 (important for the construction of guide mechanisms, i.e. guide vanes, etc.).

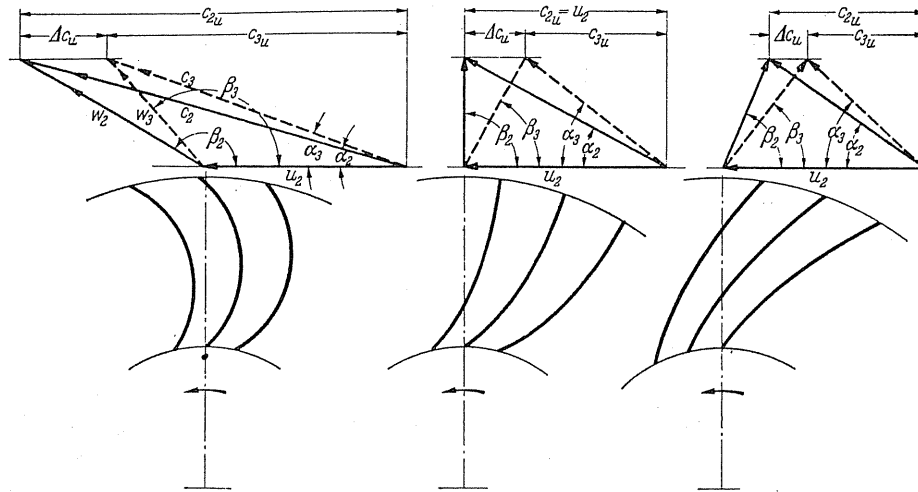


FIG. 19. Diagrams showing the effects of a finite number of blades upon the outlet velocity triangles for forward-curved, radial-tipped, and backward-curved blades.

(5) The velocity coefficient is proportional to Δc_u so that

$$\varepsilon = \frac{\Delta p_{th}}{\Delta p_{th\infty}} = \frac{\rho u_2 [c_{2u} - \Delta c_u]}{\rho u_2 c_{2u}} = \frac{c_{2u} - \Delta c_u}{c_{2u}} = \frac{c_{3u}}{c_{2u}}. \quad (33)$$

We notice that for practical purposes it suffices to calculate the reduction Δc_u from c_{2u} .

Reduction of output in consequence of a boundary layer. The formation of a boundary layer yields a small reduction of output. At the trailing edge of the blade, a boundary layer will gradually build up; this occurs even with separation-free flow until it reaches a maximum thickness at the blade tip. The effect of this build-up is more pronounced with forward-

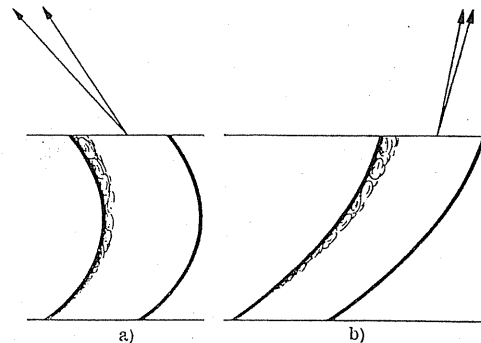


FIG. 20. (a) Deflection of the relative velocity due to formation of a boundary layer in the case of forward-curved blades. (b) Deflection of the relative velocity due to formation of a boundary layer in the case of backward-curved blades.

curved than with backward-curved blades. In Fig. 20 a, b these phenomena are illustrated in the blade cascades. By this means the active admission area of the blade passage is restricted. In consequence of this, there is a deflection of the relative velocity in the indicated sense and a reduction in output.

16. GRAPHICAL DETERMINATION OF THE REDUCTION IN OUTPUT

The determination of flow at the blade given in eqn. (14) presents us with a method of calculation of the reduction in output. This has the advantage of allowing one to calculate effectively the individual characteristics of the blading of an impeller.⁽¹⁾

Pressure forces are imparted to the air flowing through the passages by the blades. One should calculate the torque M exerted by all these pressure forces, so the output $M\omega$ is known, which can be equated to $\Delta p_{th\infty}$.

For the calculation of the pressure forces we shall employ eqn. (29):

$$\frac{w^2}{2g} + \frac{p}{\gamma_1} - \frac{u^2}{2g} = H'_t = \text{const.}$$

The pressure difference of the leading and trailing edges for a particular point of the blade is of interest to us (see also Fig. 26) when we apply Euler's equation to a point on the periphery of the impeller. It will be noted that $u_1 = u_2$ so that the term $u^2/2g$ is eliminated, hence

$$\Delta \bar{p} = \frac{\gamma}{2g} [w'^2 - w^2]. \quad (34)$$

The velocity for different sections and also for different points on the blade surface has already been calculated in a previous paragraph. Therefore, if we plot our calculated points over the developed side of the blade and join them up by means of a curve, we will obtain the values for all the intermediate points. Figures 21 and 22 illustrate the velocity distributions obtained in this manner for the radial impeller and the impeller with backward-curved blades. The velocity w for different points of equal radii on the leading and trailing edges can now be readily seen in the graphs. With this, $\Delta \bar{p}$ can be calculated according to eqn. (34). Pressure distributions obtained by this means were determined for six cases. Uncertainty, however, still arises at the blade tips. At this point the pressure difference must disappear, because an abrupt pressure drop in the flow is impossible; in other words the blade tips must be inactive, since a pressure difference at this point is non-existent. Thus we require only to complete a continuous curve to the origin as a result of this. If one draws various possible outlets, bearing in mind that discontinuous, i.e. irregular passages must be avoided, then possible error is only a small percentage of the total pressure.

¹ Kearton mentioned this in his noteworthy study. He did not approximate the velocity curve by a straight line. "The influence of the number of blades on the pressure generated in a centrifugal compressor and on its general performance", presented for discussion at the Institution of Mechanical Engineers, vol. 124, April 1933.

The torque one obtains by integration of

$$M = \int_{r_1}^{r_2} z \bar{\Delta p} br dr$$

(see Fig.26).

This is best accomplished graphically, because for the various points the value $\bar{\Delta p} br$ will be calculated. These values are plotted over the range of r and integrated:

$$M = z \int_{r_1}^{r_2} (\bar{\Delta p} br) dr.$$

The actual pressure-difference one obtains from the relationship

$$\Delta p = \frac{M\omega}{V}.$$

From the velocity triangles we obtain the values u_2 and c_{2u} , and with these, $\Delta p_{th\infty}$ can be calculated from the formula:

$$\Delta p_{th\infty} = \rho u_2 c_{2u}.$$

The results are given in Table 3.

TABLE 3

Blade shape	Shroud	Δp_{th} (mm WG)	$\Delta p_{th\infty}$ (mm WG)	$\varepsilon = \frac{\Delta p_{th}}{\Delta p_{th\infty}}$
Backward-curved	Tapered	279	324	0.862
Backward-curved	Parallel	338	396	0.855
Radial-tipped	Parallel	417.5	492	0.85
Radial-tipped	Tapered	426	492	0.866
Forward-curved	Parallel	463	588	0.79
Forward-curved	Tapered	514	662	0.778

The reduction in output varies here between 15% and 22%. In the case of radial blades and backward-curved blades it is almost equal, namely around 15%, while with forward-curved blades a considerably larger reduction (of about 22%) occurs.

A clear difference also exists with blades of the same shape, depending on whether the shrouds are tapered or parallel. With parallel blades c_{2m} is smaller. This indicates, as one can see from Fig.9, a larger c_{2u} in the case of backward-curved blades. In the same way the possible pressure must vary. A glance at Table 3 confirms this.

The method has the disadvantage of being lengthy, but, on the other hand, it gives a deeper insight into the frictionless flow of the impeller with the simplest of mathematical aids.

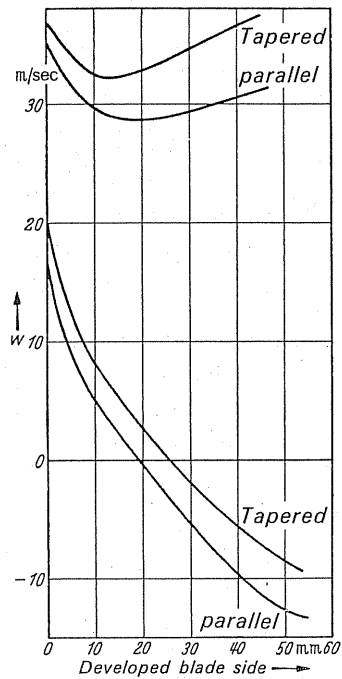


FIG.21. Distribution of velocity for leading and trailing edges of radial blades, with tapered and parallel shrouds. (Bottom curves represent the pressure side while the top curves represent the suction side.)

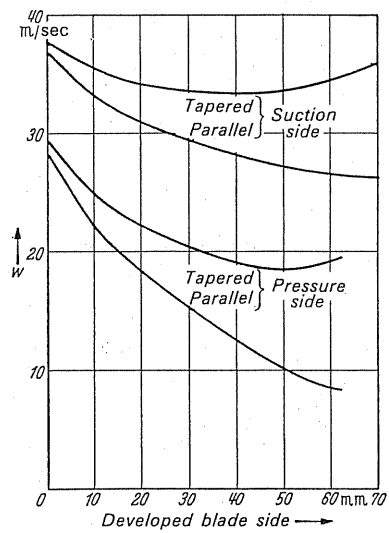


FIG.22. Velocity distribution for backward-curved blades.

17. APPROXIMATE CALCULATION ACCORDING TO STODOLA

Stodola⁽²⁾ developed the first useful method of approximation with which the influence of a finite number of blades can be easily calculated. The method is so simple and effective, that even today it still warrants mentioning.

Stodola claimed that the relative circulation is responsible for the reduction in output. Because of this, as previously established, velocity differences are produced in the blade passages, so that the velocity at the pressure side is less than that at the suction side. Stodola proceeds from the assumption that at the extremity of the blade passage the *back flow along the periphery* must be identical to the reduction of the c_u components. As a first approximation it is possible to calculate these relative back flows, if one assumes that at the blade tips fluid in the shape of sphere, of diameter a (passage width), moves relatively with an angular velocity ω (Fig. 23). Thus one obtains

$$\Delta c_u = \frac{a}{2} \omega.$$

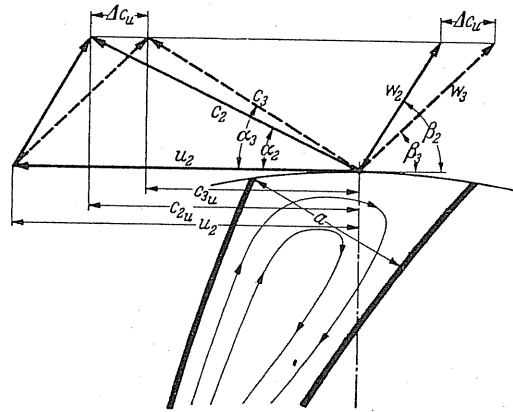


FIG. 23. Variation of circumferential components due to relative circulation in the passage.

From Fig. 23,

$$a \approx t \sin \beta_2; \quad t = \frac{\pi d_2}{z}; \quad a = \frac{\pi d_2 \sin \beta_2}{z},$$

$$\Delta c_u = \frac{\pi d_2 \sin \beta_2}{2z} \omega = u_2 \frac{\pi \sin \beta_2}{z}.$$

Therefore from the above we get the velocity coefficient

$$\varepsilon = \frac{c_{3u}}{c_{2u}} = \frac{c_{2u} - \Delta c_u}{c_{2u}} = 1 - \frac{\Delta c_u}{c_{2u}} = 1 - \frac{u_2}{c_{2u}} \frac{\pi \sin \beta_2}{z}. \quad (35)$$

² Stodola, *Dampf- und Gasturbinen*, 6th edn., Berlin, Springer, 1924.

According to Fig. 23,

$$c_{2u} = u_2 - \frac{c_{2m}}{\tan \beta_2} = u_2 - \frac{V}{\pi d_2 b_2 \tan \beta_2}.$$

Substituting this value in eqn. (35) gives

$$\varepsilon = 1 - \frac{u_2 \pi \sin \beta_2}{z \left(u_2 - \frac{V}{\pi d_2 b_2 \tan \beta_2} \right)}. \quad (36)$$

The method only takes into consideration the blade tip and precludes any consideration of the influence of the blade curvature.

In the case of backward-curved blades, a reduction of the velocity difference will be achieved—for example, according to eqn. (30) through a larger blade curvature. With forward-curved blades the influence is reversed, so that in the first case the method is too unfavourable and in the second case, works too favourably. Furthermore, the radial depth does not receive consideration. It follows that with relatively long blades and a larger number of blades, where the influence of the foregoing at the blade discharge is insignificant, the method is effective. *In point of fact, it is so effective in application that a better method could hardly be recommended.*

18. PRECISE ANALYTICAL DETERMINATION OF THE REDUCTION IN OUTPUT

From the investigations of the blade passage (page 29), the velocity distribution in a blade passage approximates closely to a linear path providing the blade distribution is not too great. Figure 24 illustrates the discharge cross-sections for the three fundamental blade

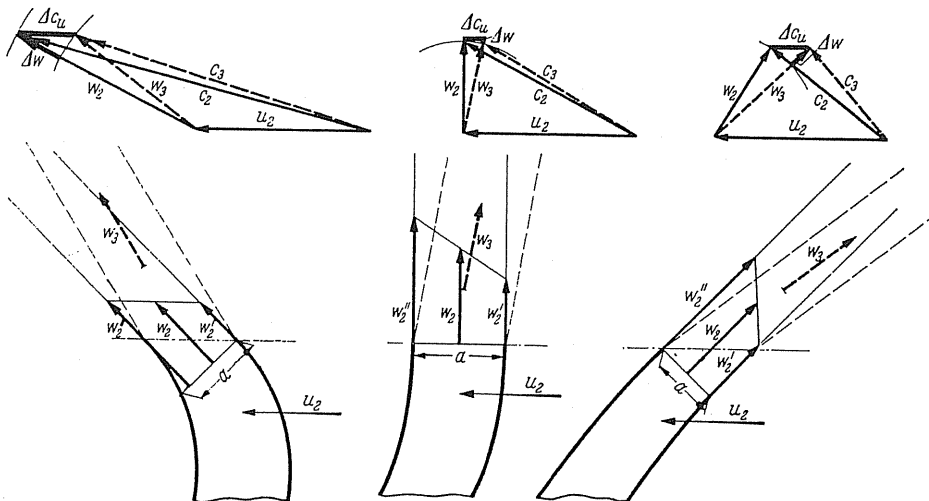


FIG. 24. Influence of a finite number of blades on the triangles of velocity and the direction of discharging streams for the three-blade forms.

forms. To emphasise the individual influence exercised by each of these forces, the blade ends are developed by straightline projections. The point where the stream is still guided on both sides shall be considered as the discharge section. Because a finite number of blades always causes a reduction in output, it results in a decrease of c_{2u} , which will be designated by Δc_u . From the velocity triangles one will recognise that *the relative flow at the blade, as established earlier, in each case will be deflected toward the direction of flow.*

The relative velocity w_2 indicated in the centre of each blade end section, on account of the linear distribution, must be identical with the relative velocity w_2 in the case of an infinite number of blades. The question now arises: can the known unequal velocity distribution be related in some way to the deviation of the relative velocity? This is, indeed, possible if one forms an analogy of Stodola's assumptions, *in which case the linear velocity gradient is equivalent to a rotation of the total flow across the passage.* To calculate the mean rotation, we shall consider a square body of a width a , a being the distance between the ends of the blades (Fig. 25). Owing to the greater velocity w_2 , the sides AB and CD

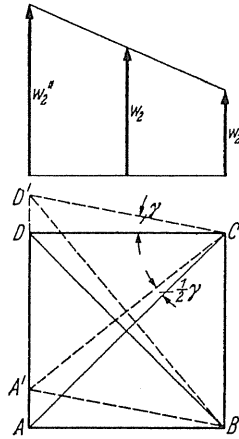


FIG. 25. Rotation of a square mass of fluid with a linear distribution of velocity.

will rotate with an angular velocity $\omega' = \Delta w/a$, while the sides AD and BC will not rotate. The average rotation is therefore half the total; a result which is also obtained if one considers the rotation in terms of a diagonal (Fig. 25).

This rotation $\omega'/2$ will produce a velocity $(a/2)(\omega'/2) = (\Delta w/4)$ at the centre, in the peripheral direction, which opposes c_{2u} . This approximates so closely to Δc_u that one can equate them, so that

$$\Delta c_u = \frac{\Delta w}{4}. \quad (37)$$

In practice $\omega'/2$, which is actually employed here, will differ from the angular velocity ω of the impeller because besides the "relative circulation", which Stodola alone took into consideration, there is an additional effect resulting from the curvature of the blades, which means the centrifugal force acting in the direction transverse to the relative flow becomes important.

The calculation of the reduction in output can therefore be related to the calculation of the velocity gradient at the blade discharge section.

The calculation can be considerably simplified if one assumes the average radial pressure at the blades to be constant. If the pressure gradient is $\bar{\Delta p}$, then it causes a torque to act on a blade element of radial depth dr . Thus

$$dM = \bar{\Delta p} b dr r.$$

Integrating for z numbers of blades we obtain

$$M = z \bar{\Delta p} \int_{r_1}^{r_2} (b dr) r = \bar{\Delta p} z S. \quad (38)$$

$$\int_{r_1}^{r_2} (b dr) r = S,$$

where S is derived from the known formulae of statics. Because the pressure gradient between the leading and trailing edges of the blades at the same radius must be substituted in eqn. (38), the corresponding velocity gradient can be calculated according to Bernoulli's equation:

$$\bar{\Delta p} = \frac{\rho}{2} (\bar{w}_2'^2 - w_2'^2).$$

Thus we have obtained the velocity gradient between C and B but not between A and B (Fig. 26). It may also be questioned as to whether a noticeable change of velocity can be expected between the points A and C on the suction side of the blade. As we have seen by the three cases calculated on page 35 (Figs. 21 and 22), the velocity change in the case of backward-curved blades, when expressed as a percentage of w , is relatively small. It is somewhat greater with a forward-curved blade impeller having tapered shrouds, while the change is practically zero in the case of radially tipped blades as the blade outlet cross-section lies on the outside circle. Therefore, no large errors will be incurred if we state that

$$\bar{w}_2'' \approx w_2''.$$

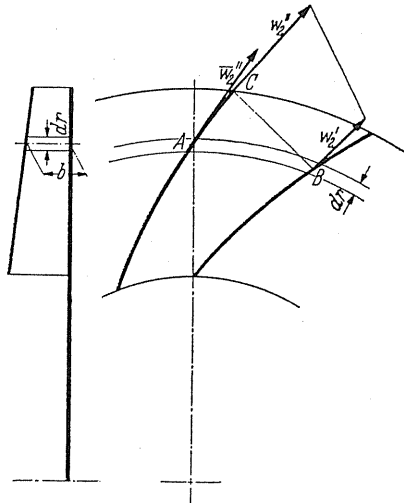


FIG. 26.

This approximation is then substituted in Bernoulli's equation to give

$$\bar{\Delta p} = \frac{\rho}{2} [w_2''^2 - w_2'^2] = \rho w_2 [w_2'' - w_2'] = \rho w_2 \Delta w, \quad (39)$$

where

$$w_2 = \frac{w_2'' + w_2'}{2}.$$

From the torque we obtain the output from the following relationship:

$$L = M\omega = V\gamma H_{th} = V\Delta p_{th},$$

where

$$V = c_{2m} \pi d_2 b_2; \quad \Delta p_{th} = \rho u_2 c_{3u}.$$

(The practical value of c_{3u} must naturally be inserted here.)

Substituting the values obtained from eqns. (38) and (39) for M and $\bar{\Delta p}$ respectively, we get

$$\omega S z \frac{\gamma}{g} w_2 \Delta w = c_{2m} \pi d_2 b_2 \frac{\gamma}{g} u_2 c_{3u},$$

from which we get

$$\Delta w = \sin \beta_2 \frac{\pi d_2^2 b_2 c_{3u}}{2 S z},$$

where

$$\sin \beta_2 = c_{2m}/w_2 \quad \text{and} \quad u_2 = \frac{d_2}{2} \omega.$$

By using eqn. (37), $\Delta c_u = \Delta w/4$, we have

$$\Delta c_u = \sin \beta_2 \frac{\pi d_2^2 b_2 c_{3u}}{8 S z} = c_{2u} - c_{3u}. \quad (40)$$

The velocity coefficient $\varepsilon = c_{3u}/c_{2u}$ is now readily changed to

$$\varepsilon = 1 / \left[1 + \frac{\sin \beta_2 \pi d_2^2 b_2}{8 S z} \right]. \quad (41)$$

With *parallel* shroud⁽³⁾ walls,

$$S = \frac{b_2}{8} d_2^2 \left[1 - \left(\frac{r_1}{r_2} \right)^2 \right].$$

Hence

$$\varepsilon = 1 / \left\{ 1 + \sin \beta_2 \frac{\pi}{z [1 - (r_1/r_2)^2]} \right\}. \quad (42)$$

³ With other types of shrouds we have the following values:

(a) Tapered shrouds:

$$S = \left[r_2 + \frac{r_2 - r_1}{3} \frac{2b_1 + b_2}{b_1 + b_2} \right] \frac{b_1 + b_2}{2} [r_2 - r_1].$$

(b) Shroud plates according to the formula $c_m = \text{const}$, i.e. $rb = \text{const}$:

$$S = r_2 b_2 [r_2 - r_1].$$

If with the help of this equation the numerous factors involved are considered for a finite number of blades, one can establish good agreement for β_2 between the range 30° and 50° , while the increment according to the sine rule in conformity with eqn. (40) is obviously too large for angles above this value. All the experimental values become comprehensible in the meantime, if we substitute $\sin \beta_2 \cdot \pi$ by $1.5 + 1.1 \beta_2/90^\circ$. In fan engineering, β_2 normally lies between the range 20° to 170° , so that, finally, we obtain

$$\varepsilon = 1 / \left\{ 1 + \frac{1.5 + 1.1 \beta_2/90}{z [1 - (r_1/r_2)^2]} \right\}. \quad (43)$$

VELOCITY COEFFICIENT WITH HIGH-EFFICIENCY FANS

The development of fans with efficiencies in the order of 83 to 90% showed that the above equation was not valid. In the meantime, the previous equation has been modified as follows:

$$\varepsilon = 1 / \left\{ 1 + \frac{a + b \beta_2/90}{z [1 - (r_1/r_2)^2]} \right\}. \quad (44)$$

Equation (44) is given in general terms, so that various ranges may be obtained by using different values of a and b . For new fans of high efficiency, one can use values of 0.9 for a and 3.7 for b , in the range $20^\circ < \beta_2 < 45^\circ$. With fans of low efficiency the exact relation of β_2 is not known, but the above relationship may help to obtain this when further data become available as a result of research.

Lewinsky-Kesslitz⁽⁴⁾ measured the following constructional features for the range $n_s = 66-160$:

$$z = 5-7,$$

$$d_1/d_2 = 0.4-0.52,$$

$$b_2/d_2 = 0.045-0.13,$$

$$\beta_1 = 29^\circ-37^\circ,$$

$$\beta_2 = 15^\circ-26^\circ.$$

In this range an accuracy of $\pm 3\%$ can be obtained with

$$\varepsilon = 1 - \frac{5}{z c_{2u}} [(0.5-0.56) u_2 - w_2 \cos \beta_2].$$

This deals with relatively narrow impellers, which are normally found in centrifugal pumps.

Traupel⁽⁵⁾ conducted an analysis of special designs of radial compressors, of which details are given in Fig. 27.

⁴ Lewinsky-Kesslitz, H.-P., Diss., Graz, 1959.

⁵ Traupel, W., *Thermische Turbomaschinen*, Vol. I, Berlin/Göttingen/Heidelberg, Springer, 1958, p.233.

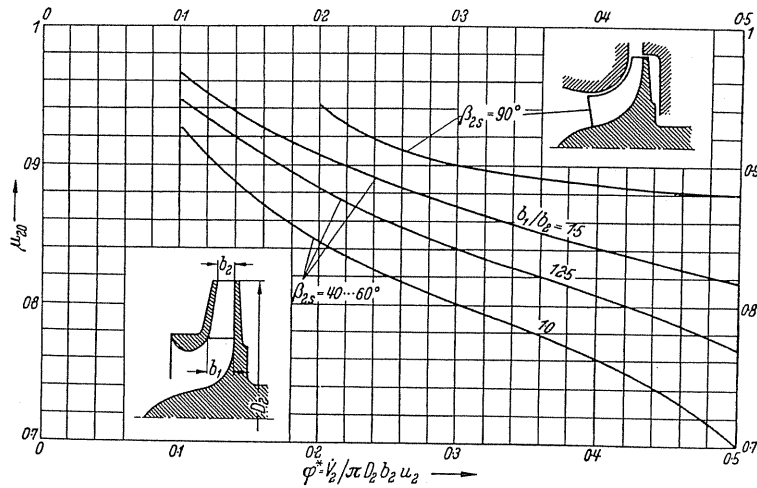


FIG. 27.

According to Traupel the simple formula

$$\varepsilon = 1 - (1 - \mu_{20}) \frac{20}{z}$$

can be applied, where μ_{20} is given in Fig. 27.

The values for enclosed impellers were obtained for $d_1/D_2 = 0.59$ and circular arc blades with a radius of curvature $r = 0.83 D_2$. For the open impeller with $\beta_2 = 90^\circ$ measurements were made on an impeller with $D_{N1}/D_2 = 0.3$; $D_{s1}/D_2 = 0.59$ and $b_2 = 0.067 D_2$.

For the remaining types, which on account of their cast-iron construction and risk of variation differ from the usual fan designs, precise information concerning the velocity coefficient has been given by Pfeiderer.⁽⁶⁾

19. INFLUENCE OF THE REACTION EFFECTS

When considering an impeller with a finite number of blades the question which now arises is whether the velocity coefficient originates at the expense of static pressure in the impeller or at the expense of kinetic energy. This question is answered by considering the coefficient of reaction r . According to eqn. (14)

$$r = 1 - \frac{c_{3u}}{u_2} \frac{1}{2},$$

Instead of c_{2u} the actual obtainable value c_{3u} has been substituted. Because $c_{3u} < c_{2u}$ the reaction is somewhat larger,

$$\frac{c_{3u}}{u_2} < \frac{c_{2u}}{u_2}.$$

⁶ Pfeiderer, C., *Die Kreiselpumpen für Flüssigkeiten und Gase*, 4th edn., Berlin/Göttingen/Heidelberg, Springer, 1955.

In consequence of a reduction of the discharge velocity, it will be seen from the velocity diagram that there has been a significant decrease in kinetic energy. *There is an increase in reaction effect due to the fact that there is a finite number of blades and in turn the efficiency of the fan is improved.*

Absolute angle of discharge. To make the construction of suitable guide arrangements possible, i.e. guide vanes, etc., the absolute angle of discharge of the air from the impeller must be known. From Fig. 23 one obtains the following relationships

$$\frac{c_{2m}}{c_{2u}} = \tan \alpha_2; \quad \frac{c_{2m}}{c_{3u}} = \tan \alpha_3.$$

from which α_3 is easy to calculate.

Summing up, it can be stated that in practice with the most important blade form (backward-curved) the approximate theory according to eqn. (43) gives satisfactory agreement with experimental values.

20. VISUALISATION OF THE ACTUAL FLOW AT THE BLADE

If a constructor is in a position to predetermine the reduction in output in accordance with calculations established in previous chapters and their satisfactory agreement with experimental values, he will be interested in the appearance of the actual flow in a blade passage. With adequate knowledge of the influence of friction in a rotating passage one can confidently state measures which could contribute to an improvement in efficiency.

One may ask in which direction will a *frictionless flow* be changed when *friction* is considered? First of all it is easy to understand that the relative passage circulation will be slowed down by friction. This causes an increase in output, which in the case of a larger number of blades can be amplified because of the increased frictional surface. Experience shows that with impellers which have large numbers of blades, experimental values are significantly higher than calculated values.

Only a guess could be hazarded as to further influences, because the difficulties encountered when investigating the flow in a rotating passage are very great. Only when it is possible to discern the details of flow at the blade can specific statements in respect of this be forthcoming. Because of the experimental difficulties, it is not surprising to find that this important problem has received little attention. To secure information, experiments were conducted by Oertli,⁽⁷⁾ Fischer,⁽⁸⁾ Escher-Wyss,⁽⁹⁾ Grünagel,⁽¹⁰⁾ Stiess,⁽¹¹⁾ Frietsch,⁽¹²⁾ Fette,⁽¹³⁾ and Prian and Michel⁽¹⁴⁾ in which air as well as water was used.

⁷ Oertli, Diss., Zürich, 1923.

⁸ Fischer, *Mitt. Hydr. Inst. TH München*, 4 (1931).

⁹ Escher-Wyss-Mitt., 1935, No. 6.

¹⁰ Grünagel, Diss., Danzig, 1934.

¹¹ Stiess, *Mitt. Inst. f. Strömungsmasch. TH Karlsruhe*, 3 (1933).

¹² Frietsch, E., *VDI ForschHft.*, 384 (1937).

¹³ Fette, H., *Z. techn. Phys.*, 1933, pp. 257-66.

¹⁴ Prian, V. D., and D. J. Michel, MACA TN 2584 (1951).

The prevailing methods of observation leave much to be desired. The surface appearances, mostly obtained with powdered aluminium in a flow tank, have far too small a Reynolds number and already lie partially in the laminar region. Various experiments with air have indicated the features that occur when solid bodies are introduced into the flow,

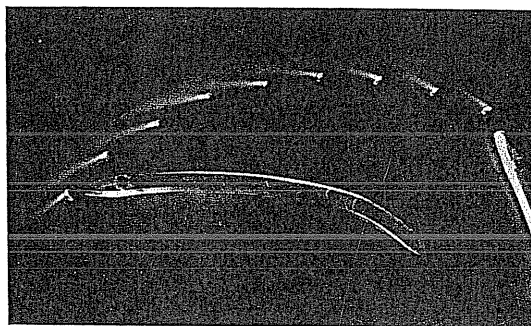


FIG.28. Visualisation of a normal volume flow.

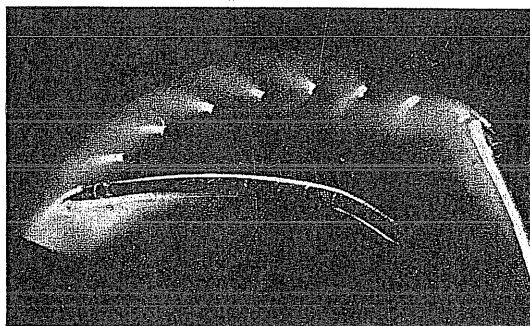


FIG.29. Visualisation of a small volume flow.

or ribbons of paper, wool, or similar materials are used somewhere in the passage. The use of these materials permits the visualisation of the direction of flow of the currents. Lewinsky-Kesslitz⁽¹⁵⁾ has shown that they are responsible for *considerable deviations*. The angle could vary by as much as 30° from the direction of flow, which means precise information with this method is not possible, particularly if certain effects as a result of it could also be made distinguishable. The author's method, in which thin laminar gas flames are used, was also used by Lewinsky-Kesslitz. We showed that the separate paths before the discharge can be made clearly distinguishable if one mixes fine soot with the gas. No discrepancy between the paths of the soot and air particles will be observed on account of the extremely small particle sizes of the glowing soot.

With this method Lewinsky-Kesslitz investigated centrifugal pump impellers while working on air. At various places on the impeller passages sooty flames were introduced and photographed. This yielded a good image of the actual internal flow in an impeller, with an accuracy hitherto unknown. Figures 28 and 29 show the photographs of this method, which were taken for an impeller working at a full volume and at a smaller volume. Various

¹⁵ Lewinsky-Kesslitz, Flow investigation in turbine rotor, Diss., Graz, 1959.

directions of flow can be very accurately distinguished. The back flow at the trailing edge of the blade before discharge is characteristic.

On completion of these tests the static pressures were subsequently measured by probes introduced in the flow. From the now known direction of flow in the blade passages it was then possible to measure the total pressure at different points with a Pitot tube.

The results of this work are noteworthy. First of all Fig. 30 shows the relative flow for a normal output. The dotted paths indicate places where the images of the sooty flames were measured. The disturbance of the blade outlet is characteristic.

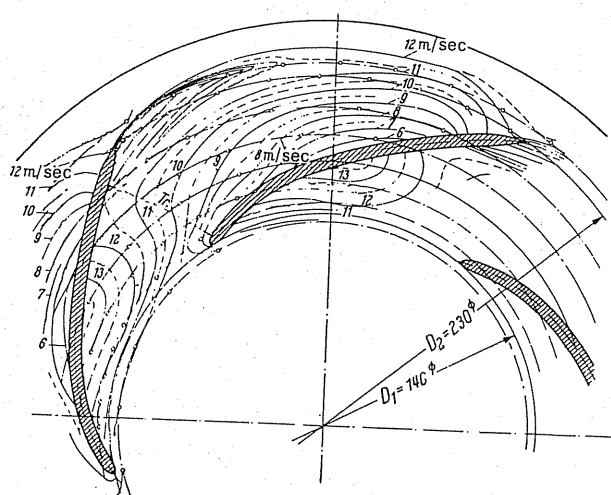


FIG. 30. Lines of equal speed ("isotachs") of the relative stream.

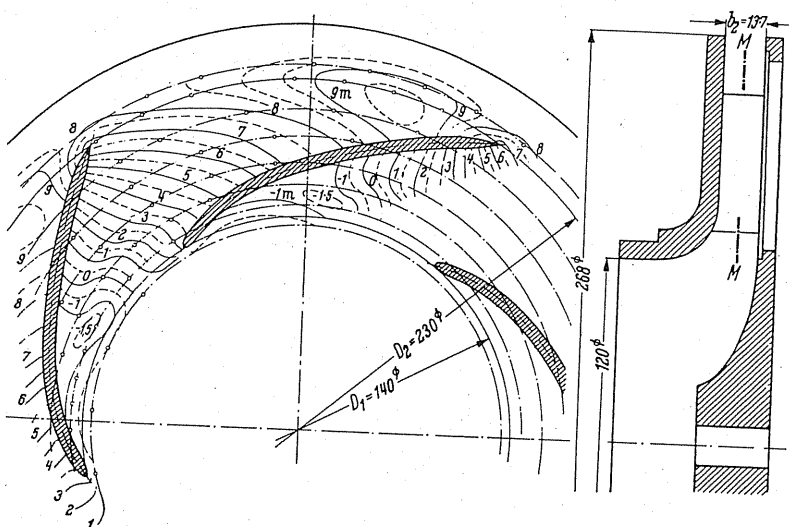


FIG. 31. Pressure distribution of the relative stream.

The pressure distribution in the blade passage (Fig.31) was surprising: the minimum and maximum pressures do not occur at the blade walls but in the centre of the flow. The minimum pressure is located almost in the middle of the entry section while the maximum pressure is found at the periphery, somewhat in front of the leading edge point of the blade. The equal pressures at the blade tips can be clearly seen. This position has changed according to the investigations into cavitation with increasing speed; meanwhile the zone of the lowest pressure moves almost to the side of the entrance.

The relative flow is also surprising inasmuch as its maximum value of the relative flow does not lie at the entrance, but almost at the centre of the trailing edge of the blade. Moreover, the average streamline displays an almost constant relative velocity throughout the blade passage.

Until now very little has been known about the fundamental relationship of a boundary layer in a rotating system. In recent times the work of Jungclaus⁽¹⁶⁾ gives one an insight into this problem. An analogy was found between the relative flow in a rotating passage and a flow in a stationary passage with equal shear, indicating that the boundary-layer equation was the same in both cases. For instance, this motion arises in a straight passage in which one wall moves in one direction and the other wall in an other direction. H. Reichardt⁽¹⁷⁾ studied this type of flow while investigating a space bounded by a rotating band immersed in a fluid (Fig.33). Comparison with relative eddies as they appear in the sector of a star impeller, as illustrated in Fig.32, shows a fundamental similarity between both types of flow.

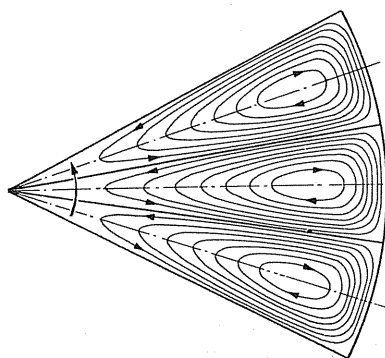


FIG.32. Relative circulation in a totally enclosed sector.

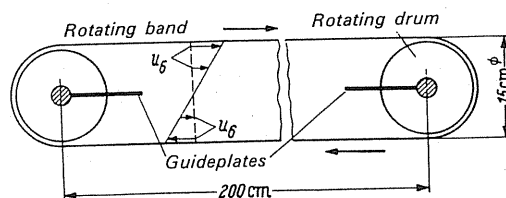


FIG.33. Diagram showing how shear flow is produced.

¹⁶ Jungclaus, G., *Boundary Layer Analysis of Shear flow in Rotating Channels*, Report No.11, 1955, Max-Planck Institute for Flow Research, Göttingen.

¹⁷ Reichardt, H., *Flow Field around Cylindrical Bodies in a Rectilinear Couette Flow*, Report No.9, Max-Planck Institute for Flow Research, Göttingen.

Visualisation of this type of flow brought several surprises. Parallel flow along a plate, illustrated in Fig. 34, shows a clearly defined separation beneath the leading edge and a stagnation point at the centre of the flow. This shows that much information is still needed before flow through a radial impeller can be sufficiently understood as in the long-standing case of axial-flow machines. Unfortunately, since the fan manufacturer cannot wait until such information is readily available, there remains little choice other than development on a purely experimental basis.

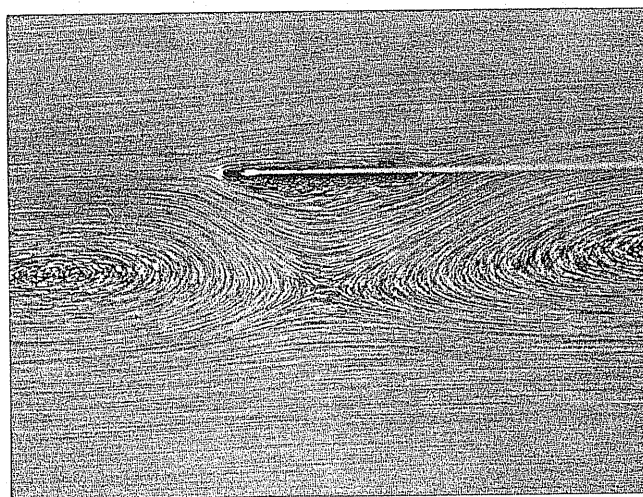


FIG. 34. Flow parallel to plate when there is a shear flow.

These investigations produced evidence, for example, that the flow must separate on the trailing edge of a blade. According to Kucharsky, Fig. 17, the separation of flow is only of a theoretical importance.

In spite of all this the following statement appears to be valid, i.e. that because the boundary layer is influenced by the action of centrifugal force, the extent of this influence being related to the shape of the blade, it will be projected outwards in a radial direction. This phenomenon causes a reduction in the degree of flow separation, so that it can be stated that *rotating diffusers are better than stationary ones*. This may also be the reason why radial-tipped blades are not as bad as they may often appear when considering greatly enlarged blade passages. For the same reasons, rotating curvatures are better than stationary ones. Use is made of this by making different blade forms.

Owing to the considerable uncertainty of the behaviour of the boundary layer in a rotating passage, the theoretical design of fans appears to be impossible without exhaustive test-bed measurements. Therefore, good testing is essential in all aspects of serious work with fans.

From the previously mentioned experiments, it is possible to obtain a rough outline of the flow separation. This knowledge may serve as a method to an approximate calculable estimate. We will assume that the area of the dead-space is more or less known. From Fig. 35, one can see that this dead space is the difference between the actual geometrical passage width a and the functional passage width a' . This change in the resultant velocity

triangles is illustrated in Fig.35. Because of this, there has been a considerable change in the angles relating to the relative and absolute velocities. In agreement with Stodola, Δc_u will be smaller for the passage width a' than for a . From our earlier calculations with reference to the velocity coefficient, we conclude that *in the case where blade angles are identical, narrower blades can be used. This means the number of blades will increase according to $z' = z (a/a')$* . Therefore, substituting the relationship $z' = z (a/a')$ for z in eqn. (43), we get

$$\varepsilon = 1 \left\{ 1 + \frac{1.5 + 1.1 \beta_2^2 / 90}{z (a/a') [1 - (r_1/r_2)^2]} \right\}. \quad (45)$$

Naturally this expression only serves as a guide for calculating the velocity coefficient in terms of known a' . On account of their much larger dead spaces on the suction side it is not often possible to assess the theoretical output of forward-curved and radial-tip blades with the same degree of accuracy obtainable in the case of backward-curved blades. The necessary correction factors are obtained experimentally.

Accurate velocity triangles at the discharge were established by the experiments of Kearton.⁽¹⁸⁾ The particular values were obtained from the measurement of rotation and of the amount of air. c_m designates average values only. Hence this case is not a true representation of the actual angle in the partially filled passage, according to Fig.35.

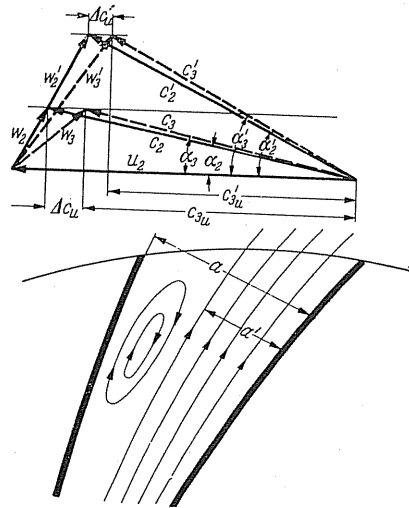


FIG.35. Partially filled blade passage. Velocity diagram for partially and completely filled blade passage.

Nevertheless, the interpretation of this diagram is justified, because its study leads to a clearer understanding of the problems associated with a finite number of blades (Fig.36). The direction of the discharge velocity in the case of an infinite number of blades and also the point of normal volume are plotted in all the diagrams. The case of an impeller possessing thirty-two blades is unusual. The effects of friction in the narrow blade passages

¹⁸ See footnote 1, Chapter III.

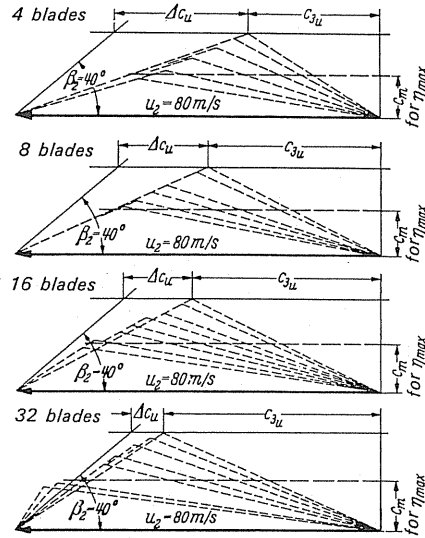


FIG. 36. Discharge velocity triangles derived from Kearton's experimental data.

appear to act in the reverse direction. There is no obvious reason for this. Impellers of this type have distinctly unsatisfactory efficiency curves owing to this phenomenon.

Only the over-critical volumes have been taken into account in the diagrams. The meaning of the following relationships now becomes apparent:

- (1) The direction of the actual relative exit velocities almost coincide.
- (2) The velocity coefficient increases with an increasing volume.

From (1), if one assumes that β_3 is constant, it is simple to determine a rule which says that as the volume increases, the output falls.

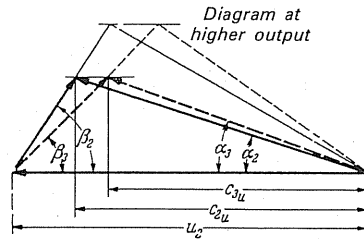


FIG. 37. Velocity triangles for various volumes, derived from Fig. 36.

From Fig. 37 it follows:

$$c_{3u} = u_2 - \frac{c_{2m}}{\tan \beta_3}; \quad c_{2u} = u_2 - \frac{c_{2m}}{\tan \beta_2}.$$

Hence

$$\varepsilon = \frac{c_{3u}}{c_{2u}} = \frac{u_2 - (c_{2m}/\tan \beta_3)}{u_2 - (c_{2m}/\tan \beta_2)} = \frac{\tan \beta_2}{\tan \beta_3} \frac{\tan \beta_3 - (c_{2m}/u_2)}{\tan \beta_2 - (c_{2m}/u_2)}. \quad (46)$$

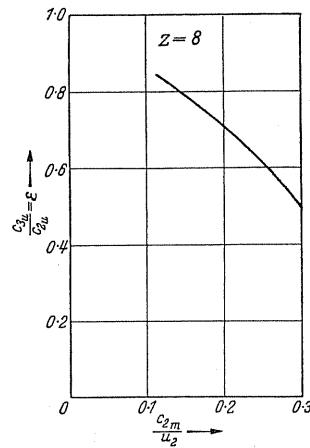


FIG.38. ϵ plotted against c_{2m}/u_2 , where ϵ is the ratio of theoretical pressure for a finite number of blades to the theoretical pressure for an infinite number of blades, and c_{2m}/u_2 is the axial velocity divided by the peripheral velocity.

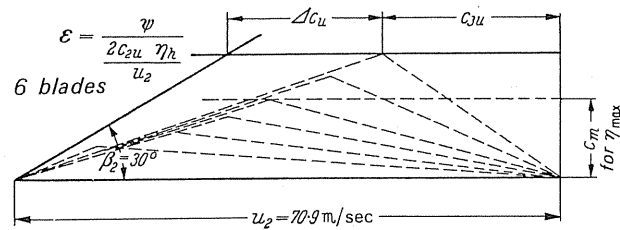


FIG.39.

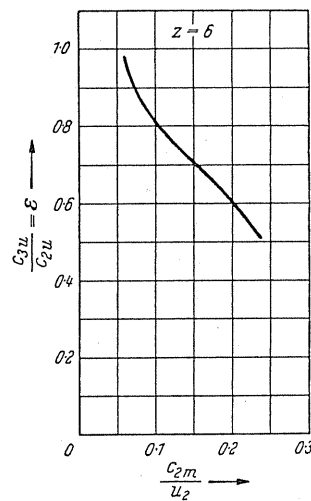


FIG.40.

Figure 38 shows the velocity coefficient ε for an impeller with eight blades plotted against c_{2m}/u_2 . The curve illustrates clearly how the value of this coefficient decreases as the volume increases. Assessment of these results appears to validate eqn. (18), so that, for a given impeller design, it is possible to assess the velocity coefficient for any arbitrary volume. For smaller volumes, the equation does not work because of discontinuity.

The observations of Kearton have been subsequently confirmed by the author. Experiments conducted with completely different types of impeller, as indicated by Figs. 39 and 40, showed a behaviour similar to the findings of Kearton.

It is most unfortunate that similar experimental data are not available for forward-curved and radial-tip blades.

21. NUMBER OF BLADES

Unfortunately, unlike the case with axial impeller there is no mathematical method to determine an optimum number of blades for a *radial* impeller. Care must be exercised in the design of the blade passages to ensure *reasonable flow* of the streamlines so that no separation occurs. We will stipulate a boundary condition for the ratio blade length/blade width, which will be in the order of 2. In fans, the angle of blade entry normally lies in the region of 30° , while the blade exit angles can be 90° and possibly higher. As an average we can assume the blade length l to be approximately 50% longer than the radial depth $r_2 - r_1$. At the discharge we will fix the passage depth because the blade elements determine the transfer of energy, and also the highest pressure occurs at this point. The passage depth is $a = t \sin \beta_2$; with $l = 1.5 (r_2 - r_1)$ and $l/a = 2$ we get

$$\frac{l}{a} = \frac{1.5 (r_2 - r_1)}{t \sin \beta_2} = \frac{1.5 (r_2 - r_1) z}{2 r_2 \pi \sin \beta_2} = 2, \quad (47)$$

$$z = \frac{4\pi}{1.5} \frac{\sin \beta_2}{(1 - r_1/r_2)} \approx 8.5 \frac{\sin \beta_2}{1 - r_1/r_2}.$$

Thus the number of blades depends only on the discharge angle β_2 and the radial ratio r_1/r_2 . The formula gives an approximate indication of the number of blades required for normal radial impellers, while multivane impellers require more specialised treatment. However, the optimum number of blades of a radial impeller can only be truly ascertained by experiment.

CHAPTER IV

SHAPE OF THE BLADE TIP

22. INACTIVE BLADE

In considering the shape of the blade tip we will consider the shape of a blade which has no capacity to do work and therefore no ability to transfer energy to the air. We shall call such blades *inactive*. Because eqn. (5) states that the consumption of energy is proportional to $(c_{2u} u_2 - c_{1u} u_1)$, care must be exercised to ensure that this expression is equal to zero, which means that $c_u u$ or $c_u r$ must remain constant in the impeller. An arbitrary element of the blade passage is considered in Fig. 41.

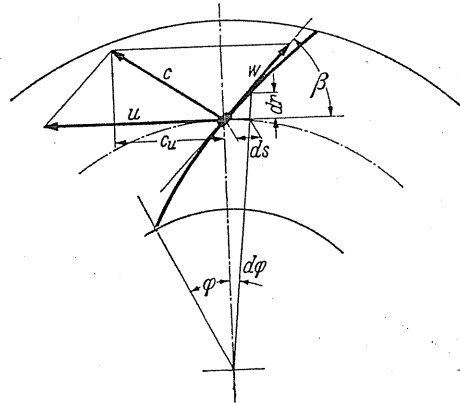


FIG. 41.

The relative velocity w possesses the same angle β as the blade. With the aid of the velocity triangle this angle can be expressed as $\tan \beta = c_m/(u - c_u)$ or, alternatively, by means of the blade element as

$$\tan \beta = \frac{dr}{r d\varphi}.$$

Equating both terms,

$$\frac{dr}{r d\varphi} = \frac{c_m}{u - c_u}. \quad (48)$$

c_u is dependent upon the inefficiency and in each case is derived from the formula

$$c_u = \frac{c_{0u} r_0}{r},$$

where the subscript 0 refers to a point immediately in front of the impeller. A variation in the value of c_m is dependent on variations of the axial length, i.e. breadth b and the radius r . The following cases will be dealt with:

(1) $c_m = c_{0m} = \text{constant}$.

The surface is hyperbolic in shape.

$$\frac{dr}{r d\varphi} = \frac{c_{0m}}{r\omega - (c_{0u} r_0/r)} \quad \text{or} \quad \frac{dr}{c_{0m}} \left[\omega - \frac{c_{0u} r_0}{r^2} \right] = d\varphi.$$

The solution is

$$\varphi = \frac{\omega}{c_{0m}} [r - r_0] + \frac{c_{0u}}{c_{0m}} r_0 \left[\frac{1}{r} - \frac{1}{r_0} \right]. \quad (49)$$

If the air is not prerotated at the entry, then $c_{0u} = 0$ and the above equation simplifies to

$$\varphi = \frac{\omega}{c_{0m}} [r - r_0] = \frac{1}{\tan \beta_0} \left[\frac{r}{r_0} - 1 \right], \quad (50)$$

where

$$\tan \beta_0 = \frac{c_{0m}}{u_0}.$$

Hence

$$r = r_0 [1 + \varphi \tan \beta_0]. \quad (51)$$

(2) $b = b_0 = \text{constant}$.

In this case, $c_{0m} r_0 = c_m r$, or $c_m = (c_{0m} r_0)/r$.

Equation (48) states:

$$\frac{dr}{r d\varphi} = \frac{(c_{0m} r_0)/r}{r\omega - (c_{0u} r_0/r)} \quad \text{or} \quad d\varphi = \frac{dr}{c_{0m} r_0} \left[r\omega - \frac{c_{0m} r_0}{r} \right]$$

The solution is

$$\varphi = \frac{1}{2} \frac{u_0}{c_{0m}} \left[\left(\frac{r}{r_0} \right)^2 - 1 \right] - \frac{c_{0u}}{c_{0m}} \ln \frac{r}{r_0}. \quad (52)$$

If the air is not pre-rotated at the entry, then only the first term is retained.

Therefore,

$$\varphi = \frac{1}{2} \frac{u_0}{c_{0m}} \left[\left(\frac{r}{r_0} \right)^2 - 1 \right] = \frac{1}{2} \frac{1}{\tan \beta_0} \left[\left(\frac{r}{r_0} \right)^2 - 1 \right]. \quad (53)$$

Figure 43 illustrates a blade obtained for the case applicable to eqn. (53). Angle β_0 selected was equal to 30° .

A very much elongated blade has been formed whose angle at the periphery reduces towards the outside, behaviour which, moreover, can be an immediate consequence of a velocity triangle where $c_u = 0$.

We consider the movement of air in the case of an inactive blade. Because $c_u = 0$, air can only move radially in the direction AB . The blade apparently glides past the air and causes no deflection.

If the blade, in direct contrast to this particular case, has an even more pronounced curve, so that c_u becomes negative, the resulting impeller acts as a turbine. Figure 42 illustrates the blade shapes applicable to turbines as well as pumps.

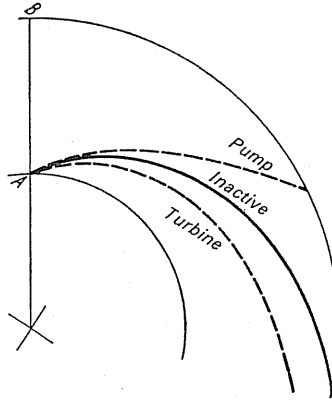


FIG.42. Inactive blade compared with pump and turbine blades.

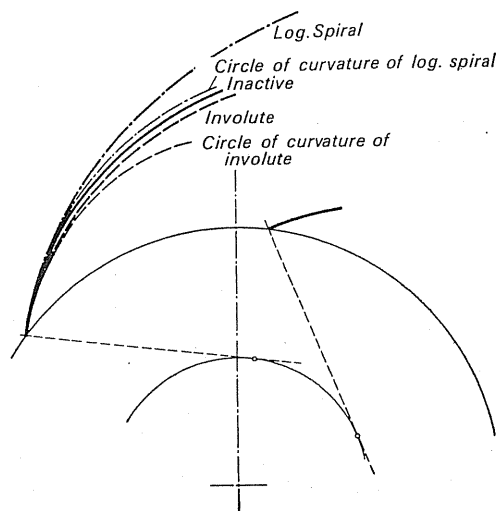


FIG.43. Inactive blade entry compared with spirals and their radii of curvature.

In particular, one should ensure with normal blades that the admission end of a blade is "inactive" to prevent a separation of flow. As this only entails dealing with relatively short sections, one may conceivably ask whether an "inactive" section can be eventually reproduced by the arc of a circle. Figure 43 illustrates a comparison between the exact curve, obtained with eqn. (53), and the curves of an involute, a circle of curvature of an involute, a logarithmic spiral, and a circle of curvature of a logarithmic spiral. All the curves have the identical angle β at the discharge point. One will notice that the circle of curvature of the logarithmic spiral and the involute curve coincide closely with the actual curve.

23. STUDY OF THE THICKNESS OF A BLADE

Owing to the finite thickness of a blade, the cross-sectional area available to the main flow is reduced in relation to the condition existing before the impeller blade. The resulting change in the velocity triangles is readily seen, if one considers the inner blade circle developed as a straight line, as shown in Fig. 44. First of all one will observe that because of the

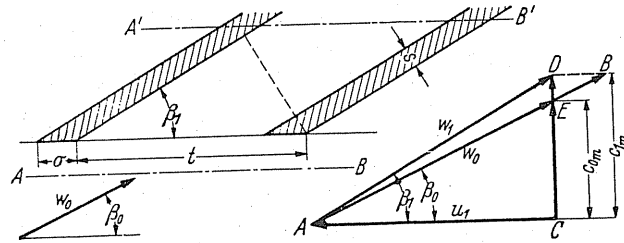


FIG. 44. Blade inlet straightened out to show narrowing due to blade.

finite thickness s of the blade, the meridional velocity c_{0m} is increased to c_{1m} , since the cross-sectional area $A' - B'$ is smaller in comparison with $A - B$ by the factor $(t - s)/t$. The value of c_m changes in the opposite way, hence

$$c_{1m} = c_{0m} \frac{t}{t - s}. \quad (54)$$

If the entry blade angle is the same as the relative angle of flow upon entry to the impeller β_0 , then w_0 must accelerate in the entrance of the blade passage to the value AB . This produces a negative value DB for c_u , which means that the blade entrance is not inactive as one normally assumes, but acts like a turbine. Of course, this effect must be avoided. The condition $c_u = 0$ can only occur if the blade entry β_0 is adjusted to β_1 so that an increase of w_0 to w_1 occurs, i.e. an acceleration is produced at the entry, so that the action described above is avoided. Accordingly, the blade angle may be obtained from the following formula:

$$\tan \beta_1 = \tan \beta_0 \frac{t}{t - s}; \quad \sigma = \frac{s}{\sin \beta_1}. \quad (55)$$

The variation from β_0 to β_1 , on the other hand, causes a shock, the effect of which can only be reduced by suitably small value of s . Of course, these effects cannot be entirely eliminated. With designs of centrifugal pumps it has been found advantageous to chamfer the blade at the inner end. In the case of designs of fans, there is less restriction and so less disturbance on account of the extensive use of sheet-metal blades in contrast to the castings used in the manufacture of pumps. Because of this, the above correction might be applicable to most fans.

It must be emphasised that *the geometrical requirement of shock-free entry is only valid in the event of an impeller having very narrow blade divisions*. If the distance between the

blades is large, as in an aerofoil, the shock-free entry extends over a fairly wide angular range. *In the case of the aerofoil, the angle at which the flow separates is very important.* From this it follows that shock losses are considerable with large number of blades, particularly when the delivered volume deviates from the normal shock-free volume. However, it must not be forgotten that an absolute shock-free entrance is impossible with impellers having blades of finite thickness.

CHAPTER V

DIMENSIONLESS CHARACTERISTICS

24. COEFFICIENTS

For the design, comparison, and critical assessment of all fans, one employs dimensionless coefficients. These coefficients must be dimensionless so that the numerical values which arise are independent of the actual increase in pressure, the mass flow, and other physical properties. Today we are in the fortunate position of being able to recommend a number of dimensionless coefficients which are the results of extensive study and which will most probably become standardised. These coefficients⁽¹⁾ will be of considerable assistance to manufacturers and users of fans who are not concerned with the theoretical aspects of designs.

From the point of view of the fan user, the pressure head $\Delta p/\gamma$ or pressure Δp as well as the volume flow per second V are the most important factors. We shall consider the relationship between these factors and the dimensions of the impeller.

Pressure coefficient ψ . The fan impeller shown in Fig. 45 has a typical outside diameter d_2 . Let us consider a typical peripheral velocity u_2 . As a possible basis of comparison for the pressure produced by the impeller, the dynamic pressure of the peripheral velocity

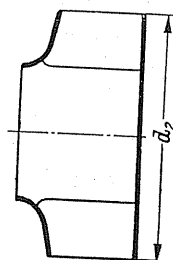


FIG. 45.

$(\rho/2) u_2^2$ may be considered. The pressure coefficient may be defined as the ratio of both these quantities

$$\psi = \frac{\Delta p}{(\rho/2) u_2^2}, \quad (56)$$

where Δp is the total pressure produced by a centrifugal machine.

¹ Eck, B., Turbine coefficients, *Konstruktion*, 12 (1960), No. 6, pp. 252-4.

We shall now consider the relationships

$$\Delta p_{th\infty} = \varrho u_2 c_{2u} = \psi_{th\infty} (\varrho/2) u_2^2,$$

$$\Delta p_{th} = \varrho u_2 c_{3u} = \psi_{th} (\varrho/2) u_2^2,$$

$$\Delta p = \varrho u_2 c_{3u} \eta_i = \psi (\varrho/2) u_2^2.$$

By rearrangement, we obtain the following:

$$\psi_{th\infty} = 2 \frac{c_{2u}}{u_2}, \quad (57)$$

$$\psi_{th} = 2 \frac{c_{3u}}{u_2} = 2\varepsilon \frac{c_{2u}}{u_2}, \quad (58)$$

$$\psi = 2\eta_i \frac{c_{3u}}{u_2} = 2\eta_i \varepsilon \frac{c_{2u}}{u_2}. \quad (59)$$

Volume coefficient φ . The volume flow per second V requires a similar basis of comparison. So one employs the circular area of the impeller $\pi d_2^2/4$ through which the flowing medium passes with a velocity u_2 . Thus the volume flow $V = u_2 \pi d_2^2/4$. Naturally, this volume differs from the actual volume, but we wish to know by how much this volume exceeds the actual volume, so that we obtain the volume coefficient

$$\varphi = \frac{V}{u_2 \pi d_2^2/4}. \quad (60)$$

The relationship with respect to the impeller breadth follows from

$$\varphi = \frac{V}{u_2 F_2} = \frac{c_{2m} \pi d_2 b_2}{u_2 (\pi/4) d_2^2} = 4 \frac{c_{2m} b_2}{u_2 d_2}.$$

In the case of axial-flow fans an earlier definition $\varphi' = c_m/u_2$ was also in use. The difference is easily ascertained if

$$\varphi' = \frac{c_m}{u_2} = \frac{V}{(\pi/4) (d_2^2 - d_1^2) u_2} = \frac{V}{(\pi/4) d_2^2 [1 - v^2] u_2},$$

then

$$\varphi = \frac{V}{u_2 (\pi/4) d_2^2}; \quad \left[\frac{d_1}{d_2} = v \right] \quad \text{and} \quad \varphi' = \frac{\varphi}{1 - v^2}. \quad (61)$$

Additional information on reactive fans is required before conclusions can be reached. Employing cross-sectional area as a parameter is not very reliable when applied to this type of fan, because by increasing the axial length of the impeller, the volume can be almost arbitrarily increased. The projected surfaces of the impeller, i.e. $(d_2 b)$ as shown in Fig. 46, should be used as a datum instead. Their connection with φ is simply obtained from the equation

$$V = \varphi_{rf} b d_2 u_2 = \varphi u_2 \frac{\pi d_2^2}{4}.$$

After transposition we get

$$\varphi_{\text{rf}} = \varphi \frac{\pi}{4} \frac{d_2}{b}. \quad (62)$$

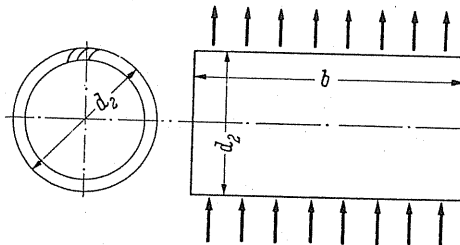


FIG. 46.

Volume coefficient in relation to the blade area at the entrance. Although the volume coefficients derived in relation to the outside diameter can be used for a general and very valuable comparison of all fans, it must be understood that, from the scientific point of view, the outside circular blade area is not sufficiently representative to be employed as a reference datum. In conclusion, it has been found that the volume flow of a cascade is defined at the entry area of this cascade while it is not so through the circular area of the outside diameter. In particular, narrow radial blades yield large differences by this means in contrast to axial flow fans. If one forms a relationship between a volume flow coefficient φ_1 at the actual entrance area and the peripheral velocity u_1 :

$$\varphi_1 = \frac{V}{(\pi/4) d_1^2 u_1^2} \quad (63)$$

then the mathematical relationship between the impeller and the volume flow is obtained for all impellers. Rüttschi⁽²⁾ compared values of φ with calculated from (a) the outside diameter and (b) the inlet area. This is illustrated in Fig. 47. The comparison, based on experiments conducted with centrifugal pumps, is characteristic. While curves obtained with outside diameter show an unorganised pattern, those obtained with the inlet area yield a systematic picture, which makes it possible to recognise the actual flow per unit area of the entrance approximately. Thus the volume flow in the case of narrow radial impellers is specifically greater than in the case of high-speed impellers.

This additional information gives a deeper understanding of the concept of volume flow without in anyway detracting from the purely practical value of the coefficients generally employed today.

Speed coefficient σ and diameter characteristic δ . In practice, both the coefficients φ and ψ have been found inadequate for numerical evaluation of the important characteristics of the centrifugal impeller. A given volume V and a given pressure increase Δp can be produced by various fans which are widely different in their dimensions. The price of a fan is

² Rüttschi, K., Reynolds' number and dimensionless coefficients for turbo machinery, *Schweiz. Bauztg.*, 1955, No. 46.

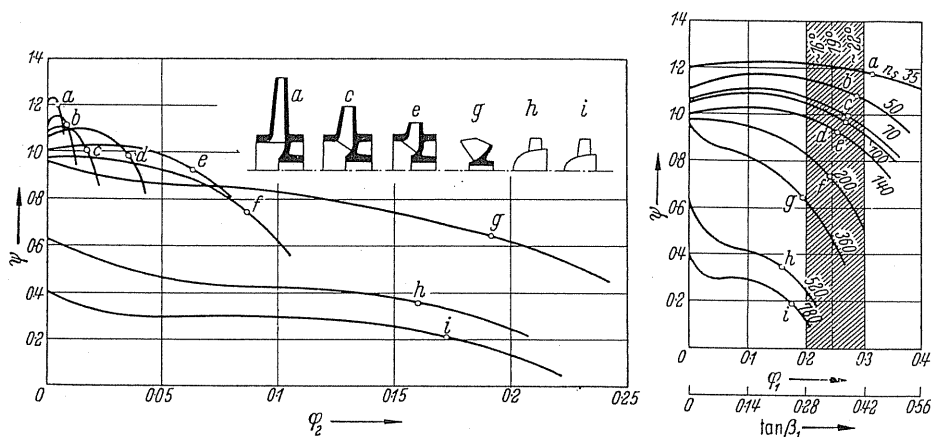


FIG.47. Characteristics of various impellers with ϕ_2 (left) and ϕ_1 (right) as abscissae according to Rutschi.

often dependent upon its size, and the importance of this from the point of view of the client cannot be over emphasised. Moreover, the client often requires a specified speed, so coefficients relating to the dimensions and speed of a fan are necessary.

The specific speed of water turbines has been found to be of considerable assistance in design. Success in this field has led to its use in the design of fans and pumps.

Specific speed is defined as that speed of a "unit turbine", i.e. a machine geometrically similar in all respects to the given turbine but of such a size that it would develop 1 hp. with a head of 1 m, and a flow of 1 m³/sec. To obtain this one uses the well-known formula

$$n_s = n \frac{\sqrt{N}}{H^{3/4}} = 3.65 n_q, \quad (64)$$

where H is the head in metres, N is the output power in horse-power, n is the speed in rev/min, and n_s is the specific speed.

This index is suitable for water turbines in general because in the case of larger machines the highest possible rotational speed is still desirable. The tendency in the development of water turbines is towards achieving the maximum possible speed.

The main reason for the adaptation of this index in industry, and later its application to centrifugal pumps and fans, was the university support for this field of applied science. There was little time spent on other types of centrifugal machines and almost none on fans.

The specific speed has since been superseded by the high speed coefficient σ , which was used in work connected with axial-flow fans.⁽³⁾ A conception such as this had already been presented by the author.⁽⁴⁾ In recent times, the diameter coefficient δ , has been proposed by Cordier,⁽⁵⁾ although it had in fact appeared in the study of Baashuus⁽⁶⁾ in 1905.

³ Keller, C., Axial flow fans from point of view of aerofoil theory, Diss., Zürich, 1934.

⁴ Eck, B., The effect of a specific speed of rotation, *Z VDI*, 1926, p.1015.

⁵ Cordier, Similarity conditions for turbo machinery, *BKW*, 1953, p.337.

⁶ Baashuus, Classifications of turbines, *Z VDI*, 1905, p.92.

Comparison with a model fan having $\varphi = 1$; $\psi = 1$. In the following a new derivation of these quantities will be given.

A centrifugal impeller is selected for a fixed volume V and pressure increase Δp and compared with another impeller with identical volume and pressure increase, but with a volume coefficient $\varphi = 1$ and pressure coefficient $\psi = 1$, in which $c_m = u$. The problem is to ascertain the size of this impeller and its speed.

An axial-flow fan (Fig. 48) has an outside diameter d_2 , number of revolutions n , volume V , and a total pressure increase $\Delta p = \psi (\rho/2) u_2^2$. Consider a smaller but geometrically similar machine of diameter d' and pressure rise Δp . Let c' be the outlet velocity, then $\Delta p = \rho/2 (c'^2) = \psi (\rho/2) u_2^2$, hence $c' = u_2 \sqrt{\psi}$.

The diameter d' is readily calculated from

$$V = \varphi u_2 F = c' F' \quad \text{or} \quad F' = F \varphi u_2 / c' = F \varphi / \sqrt{\psi}.$$

With $\varphi = 1$ and $\psi = 1$ we get an impeller with the peripheral velocity u_2' according to $\Delta p = 1 (\rho/2) u_2'^2$ and $V = 1 u_2' F' = c' F'$. Hence $u_2' = c'$.

From this it follows that the outside diameter d' of the comparative impeller is identical with the diameter of the outlet of the original fan.

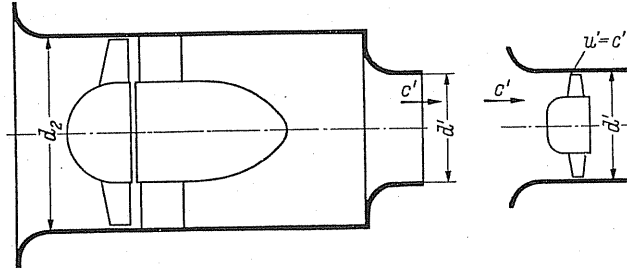


FIG. 48. Comparison of a fan (left) with standard fan (right).

From $F'/F = \varphi/\sqrt{\psi}$, we get

$$\left(\frac{d'}{d}\right)^2 = \frac{\varphi}{\sqrt{\psi}}, \quad \text{i.e.} \quad \frac{d}{d'} = \frac{\psi^{1/4}}{\varphi^{1/2}} = \delta. \quad (65)$$

It can be seen that d/d' is equivalent to the currently used coefficient of diameter δ : it expresses the number of times greater an impeller's diameter is in relation to that of a comparative impeller having $\varphi = 1$ and $\psi = 1$.

For the rotational speed n' (rev/min) of the comparative impeller, we get

$$u_2 = d_2 \pi n / 60, \quad u_2' = d_2' \pi n' / 60 = c', \quad c' = u_2 \sqrt{\psi}, \quad d_2' n' = d_2 n \sqrt{\psi},$$

then

$$\frac{n}{n'} = \frac{d_2'}{d_2} \frac{1}{\sqrt{\psi}} = \frac{\varphi^{1/2}}{\psi^{3/4}} = \sigma. \quad (66)$$

The ratio n/n' is usually known as the speed coefficient σ . For conversions it is necessary to know that

$$\psi = \frac{1}{\sigma^2 \delta^2}; \quad \varphi = \frac{1}{\sigma \delta^3}. \quad (66a)$$

By this means σ and δ are clearly defined. One compares the easily obtainable characteristics of a centrifugal impeller with the above described coefficients which are in the order of $\psi = 1$, $\varphi = 1$, $\sigma = 1$, and $\delta = 1$. Recent proposals, which suggested that a comparison could be made with a rotating jet, must be treated with reserve.⁽⁷⁾

The results may be summarised as follows.

The diameter coefficient δ indicates the number of times greater the diameter of an impeller is in relation to the diameter of a model impeller with $\varphi = 1$ and $\psi = 1$.

The speed coefficient σ indicates how many times greater the number of revolutions of an impeller is in relation to the number of revolutions of a model impeller having $\varphi = 1$ and $\psi = 1$.

Throughout, a model impeller has $\psi = 1$, $\varphi = 1$, and this is particularly true with multi-vane impellers or ducted axial-flow fan impellers.

The diameter coefficient δ can be less than 1 if $(\psi^{1/4})/(\varphi^{1/2}) < 1$, which means $\sqrt{\psi} < \varphi$. Such a case can arise, for example, with a normal high-speed axial-flow impeller with $\varphi = 0.2$ and $\psi = 0.04$.

If one substitutes the quantities V and H instead of the coefficients φ and ψ into the equation for σ and δ , we obtain

$$\begin{aligned} \sigma &= n_{\text{sec}} \sqrt[4]{\frac{V^2}{(2gH)^3}} \cdot 2\sqrt{\pi} = 0.379 n_{\text{sec}} \sqrt[4]{\frac{V^2}{H^3}} = \frac{1}{28.5} V^{1/2} \left(\frac{\Delta p}{\rho}\right)^{-3/4} n_{\text{min}} \\ &= nq \frac{1}{157.8} (nq \text{ in l/min}) = ns \frac{1}{578} (ns \text{ in l/min}): \end{aligned} \quad (67)$$

and

$$\delta = d \sqrt[4]{\frac{2gH}{V^2}} \sqrt{\frac{\pi}{4}} = 1.865 d \sqrt[4]{\frac{H}{V^2}}. \quad (68)$$

25. OPTIMUM CURVES

The coefficients σ and δ have gained considerable significance since Cordier demonstrated their use in choosing the most suitable impeller design. In this method, centrifugal machines are graphically represented in terms of δ and σ . The best impeller of each type is inserted in the appropriate position on the $\sigma - \delta$ graph so that all impellers are confined within a narrow band. To determine the most suitable impeller for a definite value of σ one is only required to read the corresponding value of δ plotted on the $\sigma - \delta$ curve. If one selects the

⁷ Mulsow, Operating characteristic of a fan and its significance, *Heizung-Lüftung-Haustechnik*, 1952, p.298.

design indicated at the point of intersection on the curve, an optimum efficiency is obtained providing the construction of the blades is also satisfactory. However, if the design is varied from that particular design indicated on the curve, then a relatively high efficiency is impossible, irrespective of how well the overall impeller has been constructed. (Assessment of the optimum operational point of an axial-flow fan by the σ - δ curves becomes unreliable when in the high σ range.)

With this an important connection becomes clear. The actual types of design were plotted in Fig. 49 according to scale so that the outside diameter would extend from the abscissa to the curve of Cordier. This form of representation⁽⁸⁾ permits the selection of the most favourable impeller design without the complications of numerous formulae. At the point on the graph, in Fig. 49, where $\sigma = 1$ and $\delta = 1$, the comparative or model impeller is shown in broken outline. It lies below the curve because it is not a high-efficiency impeller, but this is of small consequence when making a comparison.

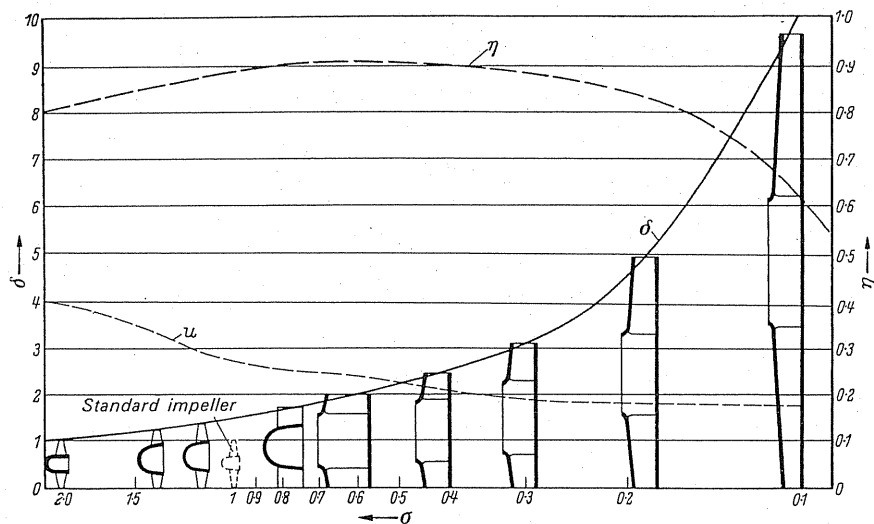


FIG. 49. Various impellers shown on a σ - δ diagram. Curves of maximum efficiencies and peripheral velocities.

Figure 49 is only intended to give an approximate review of the positions occupied by particular fans. Precise details will follow later under the treatment of individual fans.

For each design the model impeller, at $\sigma = 1$ and $\delta = 1$, was used as the standard of comparison. Therefore, all the impellers had the same volume flow and total pressure, and the outlines in Fig. 49 indicate the relative sizes of the individual impellers. To take one example, the size of a high-pressure fan at the extreme right of the graph is 9.7 times that of the model impeller, while its rotational speed is only one-tenth of the speed of the model impeller.

⁸ See footnote 1, Chapter V.

26. OTHER COEFFICIENTS

Throttling coefficient φ^2/ψ . There is an interaction between a fan and a duct to which it may be connected because of the retarding or throttling action of the resistance set up by the duct upon the air discharged by the fan. In general, the resistance is proportional to the pressure developed divided by the square of the output volume, i.e. $\Delta p = \bar{c} V^2$. To obtain a dimensionless constant, we substitute the appropriate values of $\varrho/2$ and F_2 into the above equation: hence

$$\Delta p = C V^2 = \frac{1}{\tau} (\varrho/2) \frac{1}{F_2^2} V^2.$$

We have introduced here dimensionless constant τ in the denominator. Further substitution with the coefficients φ and ψ gives

$$\Delta p = \psi (\varrho/2) u_2^2 = \frac{1}{\tau} (\varrho/2) \frac{1}{F_2^2} \varphi^2 F_2^2 u_2^2$$

from which we get

$$\tau = \frac{\varphi^2}{\psi}. \quad (69)$$

The ratio φ^2/ψ is called the *throttling coefficient*, and is employed with increasing frequency by various authors.

Coefficient of performance λ . For the driving power, which is associated with the previously mentioned coefficients, we shall define another coefficient called the output coefficient or coefficient of performance.:

$$\lambda = \frac{L_{\text{shaft}}}{(\pi d_2^2/4) u_2^3 \varrho/2},$$

where

$$L_{\text{shaft}} = \frac{\Delta p V}{\eta}.$$

By substitution we get

$$\lambda = \frac{\varphi\psi}{\eta}. \quad (70)$$

Equivalent orifice. In evaluation of the operational characteristics of a fan, a concept called the *equivalent orifice* has been employed for some time. When the pressure resistance is caused by a resistance to the flow of a fluid, the pressure is also proportional to the square of the velocity in the system and therefore is proportional to the square of the delivered volume. Therefore the equation $\Delta p = \bar{c} V^2$ is valid in this particular case and represents the characteristic of the connected system. One can consider the discharge point of a fan as an orifice which for the same volume flow has a pressure drop across it equivalent to the total pressure drop caused by the resistance of a delivery duct (Fig. 50). The size of the

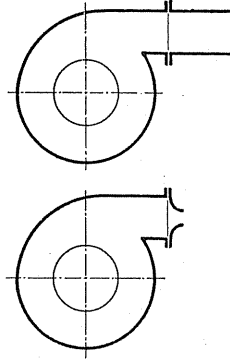


FIG. 50.

orifice is easy to determine. The discharge velocity is $c_0 = \sqrt{2g(\Delta p/\gamma)}$. To pass a volume V through an orifice it is necessary to know its area F_D , which can be easily calculated from $V = c_0 F_D$.

$$F_D = \frac{V}{\sqrt{2g(\Delta p/\gamma)}} \text{ [m}^2\text{]}. \quad (71)$$

F_D is called the equivalent orifice. It shows the effect of the total resistances acting upon a fan.

The area ratio is obtained by dividing F_D by F :

$$\vartheta = \frac{F_D}{F} = \frac{\text{Equivalent orifice area}^{(9)}}{\text{Fan discharge area}}. \quad (72)$$

Since

$$\frac{F_D}{F_{\text{impeller}}} = \frac{\varphi}{\sqrt{\psi}},$$

it follows that the square of the area ratio is identical to the throttling coefficient φ^2/ψ . The idea of the equivalent orifice was originally introduced for applications in mining.

In mining, an orifice plate is used which generally has a coefficient of contraction of 0.65. It is usual to use in calculations a constant density of 1.2 kg/m^3 for air. Thus the area of an equivalent orifice with a discharge volume V_{sa} is

$$F = \frac{0.38 V_{sa}}{\sqrt{\Delta p}} \text{ [m}^2\text{]} = F_{\text{impeller}} 1.537 \frac{\varphi}{\sqrt{\psi}}. \quad (73)$$

This is called the "equivalent area of a mine" and is designated by $A \text{ [m}^2\text{]}$.

Frequently the manufacturers of fans furnish the characteristics in terms of pressure as a function of ϑ . The advantage of this coefficient is that a few simple experiments will enable one to check the guaranteed output.

Another coefficient $\vartheta^2 = (F_D/F)^2$ is also used. The physical meaning of this coefficient can be shown by the following relation:

$$\vartheta^2 = \frac{F_D^2}{F^2} = \frac{V^2}{F^2 2g \Delta p/\gamma} = \frac{(\varrho/2) c_0^2}{\Delta p} = \frac{\text{Dynamic pressure in an equivalent orifice}}{\text{Total pressure}}.$$

⁹ Regeln für Abnahme und Leistungsveruche an Verdichtern, Berlin, VDI Verlag, 1934 (new rules in preparation).

Velocity coefficient $\bar{\varphi}$. Total pressure in the case of an equivalent orifice is expressed by the velocity pressure, which means that the dynamic pressure is the total pressure of the fan. Moreover, c_0 is the highest free-discharge velocity that the fan can generally achieve. This velocity is an easily demonstrable feature of a fan and can be employed to illustrate its aerodynamic characteristics. Comparing c_0 with the peripheral velocity, we obtain another nondimensional coefficient $\bar{\varphi}$, i.e. since $\Delta p = \psi (\rho/2) u_2^2 = (\rho/2) c_0^2$,

$$\bar{\varphi} = \frac{u_2}{c_0} = \frac{1}{\sqrt{\psi}}. \quad (74)$$

This coefficient is inversely proportional to the square root of the pressure coefficient and indicates the ratio of the peripheral velocity to the highest obtainable discharge velocity of a fan.

It is directly related to the effects of wear caused by dust-laden gases and to the noise generated by a fan, i.e. the effects are a function of the peripheral velocity. This is of considerable importance to the user of the fan. Table 4 illustrates values which are applicable to fans.

TABLE 4

$\bar{\psi}$	0.05	0.1	0.5	1.0	1.5	2.5	3	3.5
$\bar{\varphi}$	4.48	3.16	1.415	1.0	0.816	0.632	0.577	0.535

According to the type of design of a given fan, the limiting value, $4.48/0.535 = 8.32$, indicates that the number can change *eightfold* while the limiting pressure coefficient is in the order of 1:70, i.e. $3.5/0.05$.

In order to demonstrate clearly the important connection this has in practice, Fig. 51 shows in schematic form several fan designs with the peripheral velocity plotted to scale against a constant discharge velocity. The differences displayed by the fans in this form of representation appear quite striking.

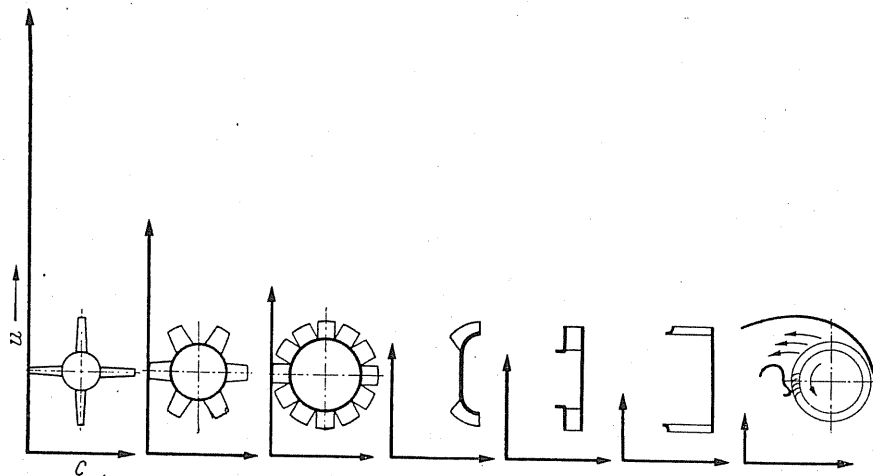


FIG. 51. The peripheral velocity required for each design in order to obtain the same discharge velocity.

27. BASIC FORMULAE

A number of important formulae can be obtained from the equations $\Delta p = \psi (\varrho/2) u_2^2$ and $V = \varphi u_2 F_2$ and the relationship $u_2 = (\pi d_2 n)/60$, and are as follows:

$$d_2 = \sqrt{\sqrt{\frac{\varrho}{2}} \frac{4}{\pi} \frac{(V/\varphi)^{0.5}}{(\Delta p/\psi)^{0.75}}} = 0.562 \frac{(V/\varphi)^{0.5}}{(\Delta p/\psi)^{0.75}} \quad \left(\text{where } \varrho = \frac{1}{8} \right). \quad (75)$$

$$n = \sqrt{\frac{900}{\pi (\varrho/2)^{3/2}} \frac{(\Delta p/\psi)^{0.75}}{(V/\varphi)^{0.5}}} = 135.4 \frac{(\Delta p/\psi)^{0.75}}{(V/\varphi)^{0.5}} \quad \left(\text{where } \varrho = \frac{1}{8} \right). \quad (76)$$

$$n = \sqrt[3]{\frac{1.73 \times 10^6}{\pi^4 \varrho}} \sqrt[3]{\frac{V \Delta p}{d_2^5 \varphi \psi}} = 52.2 \sqrt[3]{\frac{V \Delta p}{d_2^5 \varphi \psi}}. \quad (77)$$

From $\Delta p = \psi (\varrho/2) u_2^2$ and $V = \varphi u_2 F_2$ it follows:

$$d_2 = \sqrt[3]{\frac{240V}{\pi^2 \varphi n}}, \quad (78)$$

$$d_2 = \frac{60}{n\pi} \sqrt{\frac{2\Delta p}{\varrho\psi}} = \frac{240}{n\pi} \sqrt{\frac{\Delta p}{\psi}} \quad \left(\text{where } \varrho = \frac{1}{8} \right). \quad (79)$$

$$n = \frac{240V}{\pi^2 d_2^3 \varphi}, \quad (80)$$

$$n = \frac{60}{d_2 \pi} \sqrt{\frac{2\Delta p}{\varrho\psi}} = \frac{240}{d_2 \pi} \sqrt{\frac{\Delta p}{\psi}} \quad \left(\text{where } \varrho = \frac{1}{8} \right). \quad (81)$$

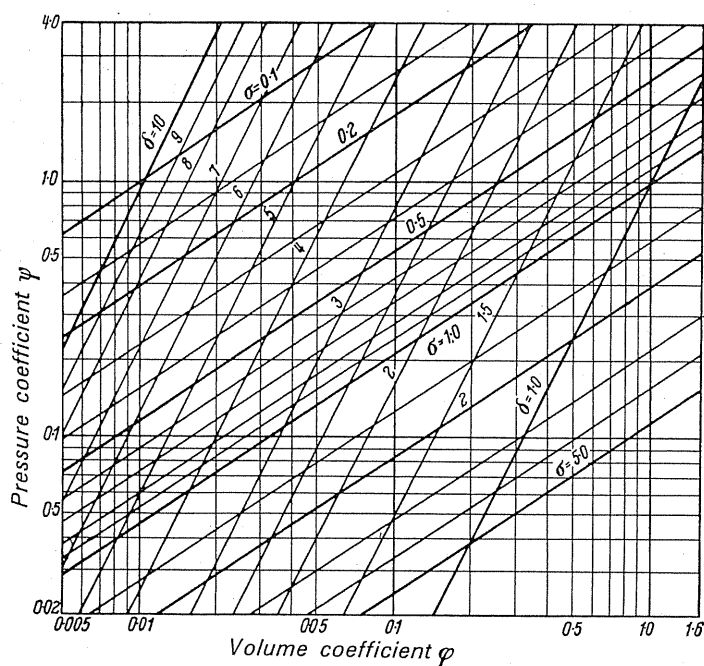


FIG. 52. Evaluation of dimensionless coefficients of a fan.

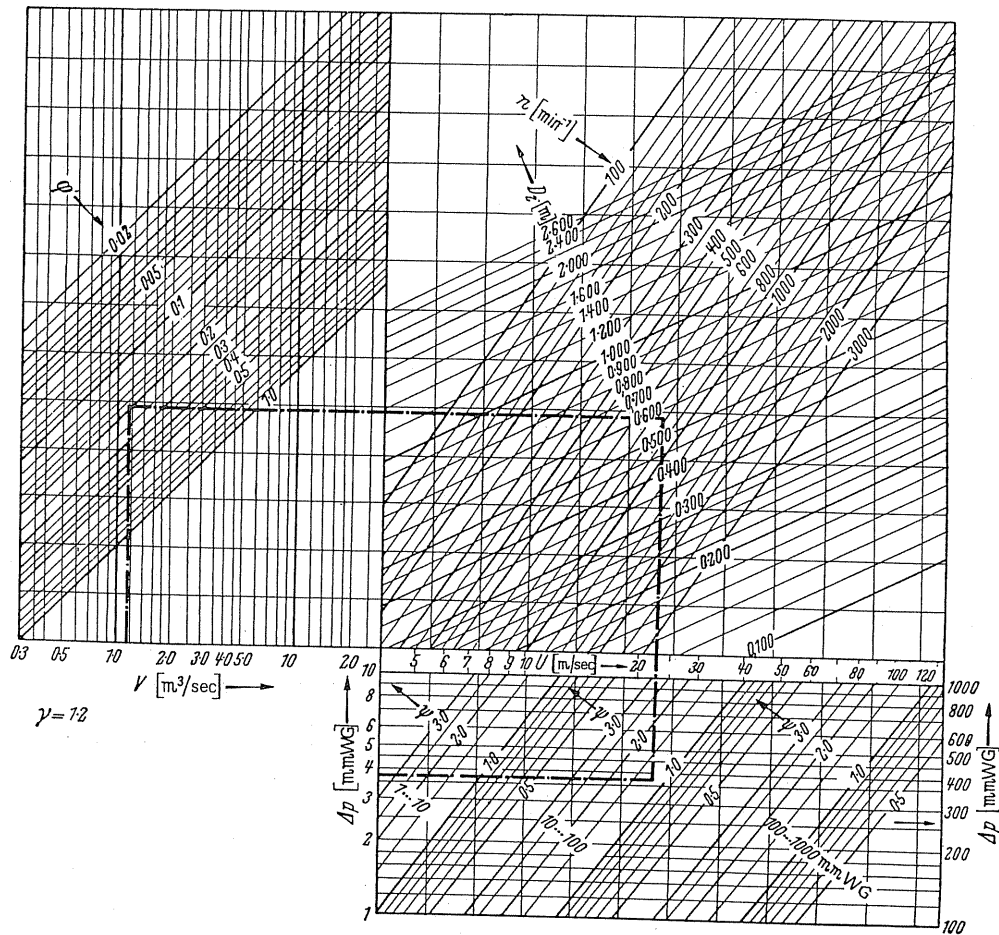


FIG. 53. Determination of the dimensions of an impeller by using coefficients.

These formulae can be used in a simple manner to obtain a graph from which the dimensions and rotational speed of an impeller are determined by means of the dimensionless coefficients if they are known, or vice versa (Fig. 52).

A further graph in Fig. 53 illustrates how the coefficients σ and δ are determined with the aid of the values of φ and ψ .

Example

Given:

$$V = 4150 \text{ m}^3/\text{h} \approx 1.15 \text{ m}^3/\text{sec} \quad \psi = 1.1$$

$$\Delta p_{\text{total}} = 37 \text{ mm WG} \quad \varphi = 0.19$$

find impeller diameter and speed.

From the graph (Fig. 53); we get impeller diameter $D_2 = 575 \text{ mm}$ and rotational speed $n = 770 \text{ rev/min}$.

28. REVIEW OF THE CHARACTERISTICS OF DIFFERENT TYPES OF FAN

The coefficient σ derived above is inadequate for a critical assessment of fans. It has little meaning because the design of each type of impeller implies a fixed range for this coefficient or for the specific speed. *Outside this range no design should be selected if the highest possible efficiency is desired.* This applies to centrifugal machines in general. With fans, however, overlapping of the different ranges of coefficients occurs, since different types of impeller can be selected in the same range of coefficients. This overlapping does not occur when other centrifugal machines are selected. There are certain practical applications where efficiency must inevitably be sacrificed. In practice the variables are so diverse that one does not make a satisfactory choice of design with the classical methods of constructing centrifugal machines. Often a representative of a firm may be in error when stressing the merits of a particular design of a centrifugal machine. It must be disconcerting that such designs as, for example, the multivane impeller, maintain their position with surprising stubbornness in spite of everything. The following list of desirable features may serve to throw some light on the matter in quantitative terms.

If we were to ask what are the factors which enable a definite choice of design to be made, the following should be considered:

- (1) **Maximum efficiency.** This requirement is satisfied by a design with a suitable value of the coefficient σ ,
- (2) **Minimal noise generation.** Maximum value of ψ and low peripheral velocity.
- (3) **Minimum wear in operation with dust-laden gases.** Maximum value of ψ .
- (4) **Large capacity.** Maximum value of φ ,
- (5) **Maximum capacity with minimum size, cheapest design.** The product of $\psi\varphi$ must be as large as possible.
- (6) **Characteristic requirements.** (a) steep, (b) flat, and (c) peakless characteristic.
- (7) **Power curve requirements.** (a) Minimum power requirement at zero volume flow, and (b) greater power requirement at normal volume flow.
- (8) **Regulation of capacity requirement.** For example, regulation at constant pressure or a definite change of pressure with the volume.
- (9) **Low weight.**
- (10) **Definite installation requirements.**
- (11) **Requirements of the inlet and discharge connections.**
- (12) **Impeller with the least moment of inertia [$G.D^2$].**
- (13) **Impeller possessing maximum strength.**

The selection of a fan becomes more difficult with the greater number of conditions that have to be simultaneously satisfied.

Figure 54 shows the main types of fan design tabulated with their ranges of the previously derived coefficients. Although no precise method for answering all the questions posed is available, this method greatly assists selection.

The values specified in Fig. 54 should be considered as approximations to assist the user

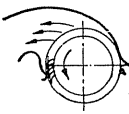
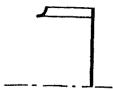
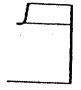
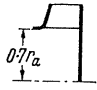
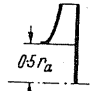

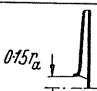
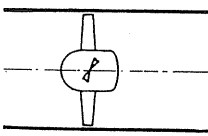
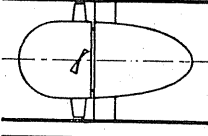
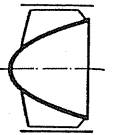
	φ	ψ	$\varphi \quad \psi = \lambda \quad \eta$	σ	δ	$n_q = 158 \cdot 1 \cdot \sigma$
	1.0	2-4	2-4	0.35-0.6	1.14-1.19	40-95
	1	2-3	2-3	0.438-0.592	1.19-1.32	69-93
	0.3	0.75	0.225	0.68	1.7	107.5
	0.2	0.6	0.12	0.657	1.965	104
	0.13	1.0	0.13	0.361	2.72	57.1
	0.03	1.1	0.033	0.162	5.92	26.6
	0.00185	1.1	0.00203	0.04	24.4	6.3
	0.1-0.2	0.05-0.01	0.005-0.02	1.6-3.8	1.0-1.78	250-600
	0.3	0.5	0.15	0.924	1.535	146
	0.3	0.7	0.21	0.715	1.62	113

FIG. 54. Tabulation of coefficients for different types of fan design.

in making an assessment: they can be changed by a skilful manufacturer to suit a particular requirement. Since numerical differences between individual designs are considerable, such a representation may nevertheless serve its purpose because it allows significant differences to be shown in order of magnitude.

Characteristic curves. Figure 55 illustrates the pressure-coefficient and power-consumption curves for six typical designs. These curves clearly show the characteristic of a fan in a striking manner.

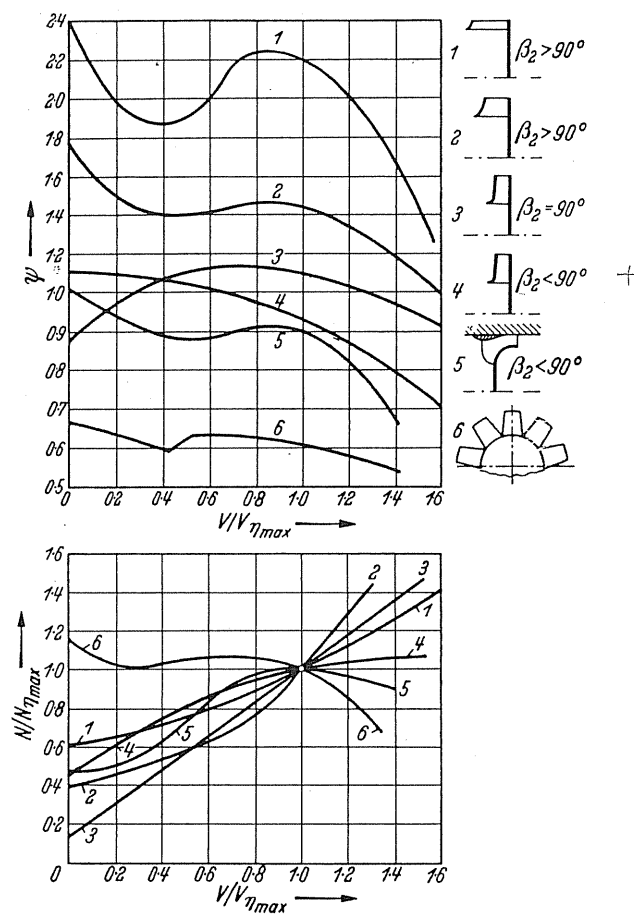


FIG. 55. Typical curves for characteristics and power consumption (dimensionless) of the main types of design.

CHAPTER VI

LOSSES

A PRECISE knowledge of losses is of interest for many reasons. At one time the power consumption depended to a large extent on the losses involved, particularly in the case of cheap designs where large losses had to be tolerated. Previously the designer was interested in a number of different forms of loss, because without knowledge of these, the precise determination of the dimensions of a fan is impossible. If one also desires to estimate performance with any reasonable degree of accuracy, it is advantageous to know the losses in order of magnitude. This is the least a designer should know when he needs to obtain a definite pressure from his design with any degree of certainty. Sources of losses will be investigated in the following sections in an attempt to offer guidance on numerical factors that assist in design.

29. IMPELLER FRICTION LOSSES

In this section we shall deal with the friction losses produced by the smooth disc of the impeller. This process can be described as follows; air adheres firmly to the surface of the rotating disc and is caused to move in an angular direction with the peripheral velocity of the disc. In the disc boundary layer, the velocity of the air which starts at a value equal to that of the peripheral velocity of the disc gradually becomes reduced to the velocity of the free stream. The air carried along by the disc is subject to a centrifugal force which tends to project the air from the centre towards the outer edge of the impeller, and in consequence of this a ring vortex is created within the impeller as shown in Fig. 56. This internal motion is at the expenditure of energy which therefore can be classified as a loss. This loss is usually called impeller friction or disc loss.

Numerous experiments have been conducted to investigate this loss; some have dealt with the influence of the space between the discs and the casing walls, and others the inlet diameter of the impeller. The first theoretical approach was made with the boundary layer theory by von Kármán.⁽¹⁾ Experiments conducted in Göttingen⁽²⁾ some years later put the physical side of the problem in a new light and, moreover, managed to validate the hypothesis illustrated by Fig. 56.

A thorough investigation of the "flow fields" produced the following surprising results. At the disc a thin boundary layer rotates with an angular velocity approximately equal to the angular velocity of the disc. This air, which is thrown outwards by the disc, moves in

¹ Kármán, V., *Abhandlungen des Aerodynamischen Instituts Aachen*, 1. Lieferung (Issue), Berlin, Springer, 1922.

² Schultz-Grunow, F., *V. angew. Math. Mech.*, **15** (1935) 191.

a thinner layer along the casing walls to return along the axis. This phenomenon is illustrated in Fig. 57. The centre portion (shaded in Fig. 57) does not take part in the above circular motion, *but rotates as a compact body and has an angular velocity equivalent to half that of the disc*. This flow pattern shows that the size of the casing does not play a great part. This has been confirmed by subsequent tests. Therefore we shall ignore the effects of the casing in our calculations because a completely valid explanation is not available.⁽³⁾

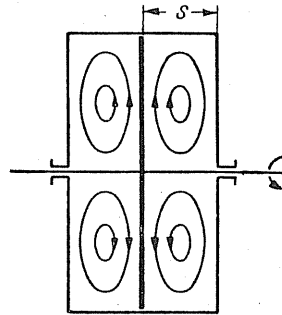


FIG. 56. Diagram of circulation caused by impeller friction.

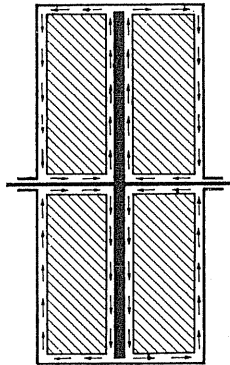


FIG. 57. Boundary-layer motion due to impeller friction.

A simple assessment of the factors upon which the "work done by friction" depends may be obtained if we consider the dimensions of an impeller. Because this is primarily a hydraulic loss, it must be represented by a relation such as the work done is equal to the product of pressure, area and velocity. Only the dynamic pressure $(\rho/2)u^2$ due to the peripheral velocity u_2 comes into the physical picture as far as pressure is concerned. Apart from the

³ A laminar parabolic velocity curve characterises the movement in the boundary layers, only in this case the medium rotates at half disc velocity. Below this range the Poiseuille-flow occurs, in which case the velocity curve becomes a straight line. Here the distance from the wall s/d is a very important factor, which falls away later, the loss being a minimum when $0.004 < s/d < 0.02$, but this lower range does not enter the picture in practical cases. If the condition of the flow at the disc is described by $Re_d = (d^2 u^2) \nu$, then at about $Re_d = 10^5$ the turbulence of the boundary layer is affected. The roughness of the wall becomes significant as in the case of flow through a pipe, but the effect of this roughness is not yet understood.

disc surface areas $(\pi/4) d_2^2$, no other elements play any significant part, while the only velocity to be considered is the peripheral velocity u_2 . Therefore with these values, the work done by impeller friction must take the form

$$N_r \sim \frac{\rho}{2} u_2^2 \frac{\pi}{4} d_2^2 u_2 \sim u_2^3 d_2^2 \sim \omega^3 d_2^5. \quad (82)$$

The usual way of writing this is

$$N_r = \frac{\beta}{10^6} u_2^3 d_2^2 \gamma \quad [\text{hp}] \quad (83)$$

where u_2 is in m/sec, d_2 is in m, γ in kg/m³, and N_r is the work done by friction.

According to Stodola, the value of β is between 1.1 and 1.2.

Therefore the impeller friction losses are dependent upon the cube of the peripheral velocity and the square of the diameter. In the case of a constant peripheral velocity—cf. impellers with identical pressure heads—the *impeller friction is proportional to the area of the impeller discs*. This implies that in order to reduce losses the impeller diameter should be as small as possible and the number of revolutions selected to be as large as possible.

The total amount of impeller friction is less important than its proportion of the total useful work. This is, $N_L = (\Delta p V)/75$, where N_L is the total useful work.

Substituting the pressure and volume coefficients in the above equation, we obtain

$$N_L = [\psi (\gamma/2g) u_2^2 \varphi u_2 \pi (d_2^2/4)]/75.$$

We also obtain the ratio

$$\frac{N_r}{N_L} = \frac{\beta u_2^3 d_2^2 \gamma \times 75}{10^6 \varphi u_2 (\pi/4) d_2^2 \psi (\gamma/2g) u_2^2} = \frac{\beta 8g \times 75}{10^6 \cdot \pi} \cdot \frac{1}{\psi \varphi}.$$

In the case of radial impellers, according to the relation $\varphi = 4 (b_2/d_2) (c_{2m}/u_2)$, for β we substitute the value 1.2 and obtain

$$\zeta = \frac{N_r}{N_L} = \frac{1}{1775} \frac{1}{[(b_2/d_2) (c_{2m}/u_2)] \psi}. \quad (84)$$

To obtain a formula in terms of the dimensions of the impeller, we introduce $\varphi = (d_1/d_2)^3 \times [(1/\sqrt{2}) \times 1.2]$. In consideration of the average value $\psi = 1$, we reduce the above coefficient to terms of the diameter ratio d_1/d_2 , so that

$$\zeta = \frac{1}{262 (d_1/d_2)^3}. \quad (85)$$

Calculations give the values shown in Table 5.

TABLE 5

d_1/d_2	0.15	0.3	0.5	0.7
ζ	1.135	0.142	0.0305	0.011

It can be seen that impeller friction plays a significant part only in the case of impellers having small diameter ratios. One should note that there is a marked effect on efficiency, e.g. where $d_1/d_2 = 0.15$, the impeller friction is greater than the useful output. This is the case with fans used in forges and organs, etc., and also at the last stage of turbo-compressor impellers where friction can be quite significant. This is the reason why one aims at designs⁽⁴⁾ with specially driven impellers so that better diameter ratios are obtainable.

The impeller friction of fans changes somewhat with variations in the volume. It is worth noting that in the case of higher velocities, i.e. larger volumes in the volute, impeller friction becomes less.

30. IMPELLER LOSSES

Entry losses. Losses may arise from a change of direction in the impeller, i.e. upon entry into the impeller intake, the air is diverted through an angle of approximately 90° before entry into the blade cascade. These losses, which are comparable to losses at bends, are

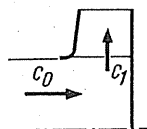


FIG. 58.

dependent upon the values of c_0 and c_1 (Fig. 58). If one relates this loss in the usual manner to the dynamic pressure of the maximum velocity, then

$$\Delta p_1 = \zeta_1 (\varrho/2) c_1^2.$$

Throughout, these losses are fairly small in relation to the total pressure

$$\zeta_1 \approx 0.15-0.25.$$

Friction losses in the impeller. The greatest losses arise from the passage of a fluid through an impeller. Determination of the degree of loss is difficult to calculate. This is because the losses arising from separation of flow are impossible to assess with accuracy. It must be remembered that the losses in consequence of discontinuity of flow at an aerofoil cannot be determined by calculation and that the aerofoil theory is no longer valid where the flow on the *suction side* breaks away, i.e. where $c_{a \max}$ occurs. The problem becomes more difficult when rotating aerofoils are taken into consideration as can be seen from the flow illustrated in Figs. 34 and 35. Therefore any calculation of the loss in question is subject to considerable uncertainty. This is true of experimentally derived coefficients obtained for a given condition. One should remember that applying a coefficient derived from an experiment with one impeller to another impeller of a different design will not be successful because the eddy zones are unstable. This means that the flow is no longer geometrically similar, and in consequence one experimental coefficient cannot be applied to different

⁴ Naumann, A., A new turbo compressor, *Technik*, 1948, p. 374.

designs of impeller. It should be explained that a purely theoretical approach has made no practical contributions in the recent improvements of radial flow fans. These resulted from experimental research.

Thus it should be clear there is no sense in undertaking a mathematical analysis of a flow through a passage subject to discontinuity. However, there are cases where no separation of flow exists. Such conditions are possible when the efficiency lies above 85%, where the only losses occurring are directly attributable to surface friction. These cases will be subsequently dealt with.

With theoretical formulae one has the choice of two approaches. One can consider the "blade throughout" as the "blade passage flow" and treat it in a manner applicable to losses arising from pipe friction. Alternatively, it can be dealt with, as a basis of comparison, in a manner applicable to pure surface friction as it arises in the case of circulation around a plate. The latter method is more profitable because the influence of the flow along the plate can be directly integrated in the known coefficients. If the problem is attacked along the lines of pipe friction, the effects of the flow along the plate are not so well known.

The resistance of a long plate immersed in a parallel flow of constant velocity is given by

$$W = c_f F (\rho/2) w^2.$$

Because the velocity in the blade passages changes from point to point, the friction given by $dW = c_f dF (\rho/2) w^2$ must be calculated for each element and then integrated. This system fails, however, because of our ignorance concerning velocity distribution. In the main, with fan impellers of high efficiency, the change of velocity is small so the subsequent error will not be great. The maximum velocity w_1 of the flow at the blade entry is reduced by the time the fluid reaches the exit to about $0.9 w_1$. Thus we can assume that the average velocity is given by $\bar{w} = (w_2 + w_1)/2$ for the blade passages. After this the losses caused by retardation can be correctly understood. Retardation loss may be reliably estimated from the following expression:

$$\Delta p'' = \zeta' \frac{\rho}{2} [w_1^2 - w_2^2] = (0.1-0.2) \frac{\rho}{2} w_1^2 \left[1 - \left(\frac{w_2}{w_1} \right)^2 \right]; \quad \frac{w_2}{w_1} = v^x$$

and because

$$w_1 = u_2 \frac{d_1}{d_2} \frac{1}{\cos \beta_1},$$

then

$$\Delta p'' = \zeta' \frac{\rho}{2} u_2^2 \left(\frac{d_1}{d_2} \right)^2 \frac{1 - v^{x2}}{\cos^2 \beta_1}.$$

Therefore the total resistance in the impeller is

$$W = c_f F_{\text{total}} \frac{\rho}{2} \bar{w}^2,$$

where F_{total} is the combined areas of both side walls and the total area of the blades. From W we get the total work done by the resistance

$$L = W \bar{w} = V \Delta p'.$$

Hence $\Delta p' = (W \bar{w})/V$ is the resultant pressure loss.

In a separate calculation we will determine the blade areas. The blade length with blade angles β_1 and β_2 gives a good approximation if we assume it to be a logarithmic spiral with the average angle of $\beta_m = (\beta_1 + \beta_2)/2$.

With this assumption the length of the curve is

$$l = \frac{r_2 - r_1}{\sin \beta_m}$$

and the total blade area

$$F_{\text{area}} = 2z l b_m, \quad \text{where} \quad b_m = \left(\frac{b_1 + b_2}{2} \right),$$

while the side areas $= 2\pi (r_2^2 - r_1^2)$, where

$$V = c_{1m} \pi d_1 b_1 = w_1 \sin \beta_1 \pi d_1 b_1,$$

then

$$\Delta p' = c_f F_{\text{total}} (\varrho/2) \bar{w}^2 \bar{w} / V = c_f \frac{[2z l b_m + \pi (r_2^2 - r_1^2) 2] (\varrho/2) \bar{w}^3}{w_1 \sin \beta_1 \pi d_1 b_1}.$$

We shall now consider

$$w_2/w_1 = v^x; \quad \bar{w} = w_1 \frac{1 + v^x}{2},$$

where

$$u_1 = u_2 (d_1/d_2)$$

and

$$w_1 = u_1 / \cos \beta_1.$$

(w_2 is the actual average relative velocity at the impeller discharge. This value is determined in relation to the influence of a finite number of blades.)

Hence

$$\Delta p' = c_f \frac{\varrho}{2} u_2^2 \left(\frac{d_1}{d_2} \right)^2 \left(\frac{1 + v^x}{2} \right)^2 2 \frac{z \frac{l b_m}{d_1 b_1} + \frac{\pi}{4} \frac{d_2^2}{d_1 b_1} \left[1 - \left(\frac{d_1}{d_2} \right)^2 \right]}{\pi \sin \beta_1 \cos^2 \beta_1}.$$

To this we add the loss caused by retardation $\Delta p''$. Hence

$$\Delta p_{\text{impeller}} = \Delta p' + \zeta' \frac{\varrho}{2} u_2^2 \left(\frac{d_1}{d_2} \right)^2 \frac{1 - v^{x2}}{\cos^2 \beta_1}.$$

Dividing this by the dynamic pressure of the peripheral velocity,

$$\begin{aligned} 1 - \eta_{\text{impeller}} &= \frac{\Delta p_{\text{imp.}}}{\psi (\varrho/2) u_2^2} = \frac{c_f}{\psi} \left(\frac{d_1}{d_2} \right)^2 \left(\frac{1 + v^x}{2} \right)^2 2 \frac{z \frac{l b_m}{d_1 b_1} + \frac{\pi}{4} \frac{d_2^2}{d_1 b_1} \left[1 - \left(\frac{d_1}{d_2} \right)^2 \right]}{\pi \sin \beta_1 \cos^2 \beta_1} \\ &\quad + \frac{\zeta'}{\psi} \left(\frac{d_1}{d_2} \right)^2 \frac{1 - v^{x2}}{\cos^2 \beta_1}. \end{aligned} \quad (86)$$

With smooth surfaces $c_f \approx 0.004-0.0045$. Rough surfaces, according to recent results, can be exactly evaluated.

For high efficiency fans the above calculation gives

$$1 - \eta_{\text{impeller}} \approx 0.07.$$

This value closely coincides with experimentally obtained values. Flügel⁽⁵⁾ dealt with impeller losses in a similar manner.

31. SHOCK LOSSES

(a) IMPELLER ENTRANCE LOSS

The direction of the relative flow will no longer coincide with the blade angle if the normal volume flow is varied. As a result of any variation from the normal volume flow, a loss called a "shock loss" arises. This can be readily understood from the entry velocity triangle illustrated by Fig. 59. An increase in the normal volume flow from V to V_x requires an increase in the meridional velocity from c_{1m} to c_{1mx} .

Hence

$$c_{1mx} = c_{1m} \frac{V_x}{V}.$$

As the air should enter radially in both cases, the blade angle must be increased to β'_1 in order to change the direction of flow before entry to a tangential flow into the impeller. The deflection towards β'_1 causes a so-called shock component c_s if c_{1m} is to remain constant. One can prove by the theorem of momentum⁽⁶⁾ that at impact the velocity head of the geometrical velocity gradient can be transformed to a pressure loss, i.e.

$$\Delta p_2 = \frac{\rho}{2} c_s^2. \quad (87)$$

In the case of a finite number of blades, the loss due to shock may be somewhat less. We shall consider this in terms of a coefficient μ which is in the order of $0.7-0.9$:⁽⁷⁾

$$\Delta p_2 = \mu \frac{\rho}{2} c_s^2.$$

According to Fig. 59 we calculate the value

$$c_s = u_1 \left[\frac{c_{1mx}}{c_{1m}} - 1 \right] = u_1 \left[\frac{V_x}{V} - 1 \right].$$

By substituting $u_1 = u_2 (d_1/d_2)$ we have

$$c_s = u_2 \frac{d_1}{d_2} \left[\frac{V_x}{V} - 1 \right].$$

⁵ Flügel, Optimum obtainable efficiency of turbo machinery, *VDI-Z*, 1954, pp. 722-55.

⁶ Eck, B., *Technische Strömungslehre*, 7th edn., Berlin/Göttingen/Heidelberg, Springer, 1966.

⁷ According to Hansen (Diss., Brunswick, 1936), valid for normal number of blades $\mu = 0.3 + 0.6 \beta/90$.

The loss is given by

$$\Delta p_2 = \mu \frac{\rho}{2} u_2^2 \left(\frac{d_1}{d_2} \right)^2 \left[\frac{V_x}{V} - 1 \right]^2. \quad (88)$$

For the introduction of our coefficient we take $(\rho/2) u_2^2 = (\Delta p/\psi)$. Again the absolute value of the loss is of little interest; the most important factor is its proportion of the actual pressure developed. The quotient $\Delta p_2/\Delta p$ gives this proportion.

$$\frac{\Delta p_2}{\Delta p} = \mu \frac{1}{\psi} \left(\frac{d_1}{d_2} \right)^2 \left[\frac{V_x}{V} - 1 \right]^2. \quad (89)$$

One may notice that d_1/d_2 has a decided influence on the loss. In order to minimise shock loss the ratio d_1/d_2 should be as small as possible. The influence of the coefficient ψ is easy to see. High ψ values, which are obtained especially with multivane impellers, reduce shock losses.

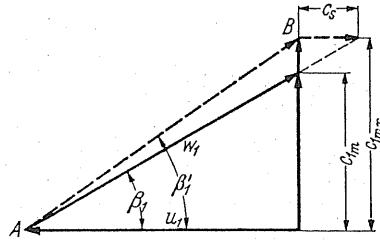


FIG. 59.

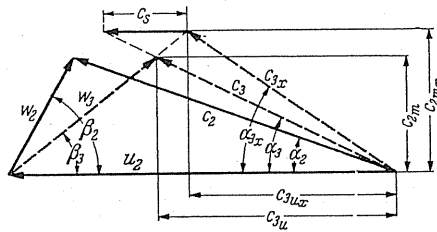


FIG. 60.

(b) GUIDE VANES LOSS

A second form of shock loss arises from the use of guide vanes at the entry. The velocity triangle (Fig. 60) also furnishes the explanation for this particular case. One may recall that, in the case where there is a finite number of blades, the absolute discharge velocity c_3 undergoes a noticeable increase towards α_3 and the angle of the guide vanes will agree with α_3 . When the volume flow is increased from V to V_x , c_{2m} increases to c_{2mx} . However, with changes in volume, c_{3u} changes to c_{3ux} . From previous considerations we will assume a shift of the apex of the velocity triangle on the arm of β_3 as a result of a change in the volume. Figure 60 shows two apices, the normal point, whose angle α_3 determines the guide blade, and a point for a higher volume designated by c_{2mx} . A shock component c_s arises here.

From the data given in Fig. 60,

$$c_s = u_2 \left[\frac{c_{2mx}}{c_{2m}} - 1 \right] = u_2 \left[\frac{V_x}{V} - 1 \right].$$

Since the shock loss is

$$\Delta p_3 = \mu \frac{\rho}{2} c_s^2,$$

then on substituting for c_s ,

$$\Delta p_3 = \mu \frac{\rho}{2} u_2^2 \left[\frac{V_x}{V} - 1 \right]^2,$$

and substituting

$$\frac{\rho}{2} u_2^2 \quad \text{by} \quad \frac{\Delta p}{\psi},$$

$$\Delta p_3 = \mu \frac{\Delta p}{\psi} \left[\frac{V_x}{V} - 1 \right]^2.$$

Dividing the above expression by Δp , we get

$$\frac{\Delta p_3}{\Delta p} = \mu \frac{1}{\psi} \left[\frac{V_x}{V} - 1 \right]^2. \quad (90)$$

Apart from the term in brackets in eqn. (90), which will be discussed later, the shock loss is inversely proportional to ψ , which means that as the peripheral velocity increases for a given Δp , ψ decreases; the result is an increased shock loss.

32. CLEARANCE LOSSES

An impeller is sealed in a casing with the smallest possible clearance between impeller and sealing lip of the casing. In consequence of this clearance, a small quantity of the total volume passed through the impeller will not emerge in the volume discharged, so that work done on this quantity to raise its pressure to that at discharge will be lost.

Only in rare cases are fans fitted with complex sealing arrangements, e.g. a labyrinth gland. With blower impellers operating at high pressures this form of seal is indispensable.

Generally, fans are installed in sheet metal housings (Fig. 61), suitably strutted to give them rigidity, so that a clearance width δ has to be reckoned with. Between the shaft and

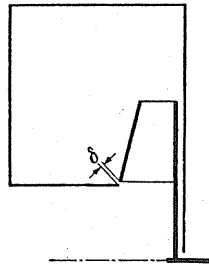


FIG. 61.

impeller there is also a small clearance through which leakage can occur, but this is neglected because of the relatively small shaft diameter.

To calculate the volume flow through this clearance the pressure gradient existing across the gap must be known. The total pressure at the fan discharge is $\Delta p = \psi (\rho/2) u^2$, while at the periphery of the impeller it is less on account of the "static regain" in the volute. In the case of backward-curved blades the static pressure at the outlet of the impeller is approximately equal to $\frac{2}{3} \Delta p$. The pressure is slightly less at the sealing clearance because, owing to the rotation of the air, the pressure reduces towards the centre. The shape of the casing greatly affects this influence, so if we ignore this fact and calculate the loss on the assumption of the pressure being equal to $\frac{2}{3} \Delta p$, then the resulting theoretical loss will be possibly larger than the actual loss. The coefficient ψ increases from 2 to 3 with forward-curved blades, whereby the reaction is probably only half as large as in the first case. Generally most of the conditions will be reasonably well covered if we assume $\psi \approx 1$ but, however, one should calculate with $\Delta p'_{\text{stat}} = \frac{2}{3} (\rho/2) u_2^2$.

The velocity c of the air passing through the clearance is given by

$$\Delta p'_{\text{stat}} = \frac{\rho}{2} c^2 = \frac{2}{3} \frac{\rho}{2} u_2^2,$$

i.e.

$$c = u_2 \sqrt{\frac{2}{3}}.$$

Because we are dealing with sharp-edged openings we shall assume that a coefficient of contraction $\mu = 0.7$ is applicable to the gap.

Thus the volume leakage through the gap is

$$V' = F\mu c = d_1 \pi \delta_i \mu u_2 \sqrt{\frac{2}{3}}.$$

If we relate this loss to the total volume flow $V = \varphi (\pi d^2/4) u_2$ and introduce the internal width of the clearance δ_i into our equation we get:

$$\frac{V'}{V} = \frac{d_1 \pi \delta_i \mu u_2 \sqrt{\frac{2}{3}} 4}{\varphi \pi d_2^2 u_2} = \frac{d_1}{d_2^2} \delta_i \frac{\mu}{\varphi} \sqrt{\frac{3}{2}} 4.$$

From past experience it has been found that the required clearance of a machine increases with the size of the machine, other ratios remaining the same, so that we can equate the clearance gap width δ_i to the ratio d_2/u , i.e. $\delta_i = d_2/u$, in order to make it a function of the diameter. The size of a fan is best indicated by means of its diameter so that reference to d_2 may be justified.

$$\frac{V'}{V} = \frac{d_1}{d_2} \frac{\mu}{u \varphi} 4 \sqrt{\frac{2}{3}}. \quad (91)$$

From eqn. (112) we substitute $\varphi = (1/1.7) (d_1/d_2)^3$ to give

$$\frac{V'}{V} = 1.7 \times 4 \sqrt{\frac{2}{3}} \frac{\mu}{u} \frac{1}{(d_1/d_2)^2} = \frac{3.89}{u (d_1/d_2)^2}. \quad (92)$$

This reduces the clearance loss to a function of the diameter ratio d_1/d_2 . Results for the values $u = 100$ and $u = 200$ substituted in eqn. (92) are plotted in Fig. 62. The standard of workmanship for $u = 100$ is *not* required to be very high, therefore a rotor having a diameter of 500 mm will have a clearance of 5 mm when $u_2 = 100$.

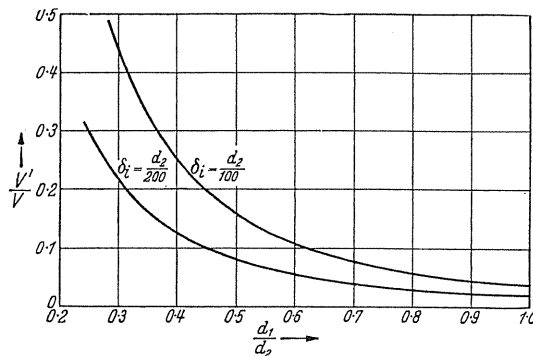


FIG. 62. Losses for different clearances as a function of the diameter ratio.

In Fig. 62 one will see the loss is already 8% of the total output when $d_1/d_2 = 0.68$ and $u = 100$. When $u = 200$ (again a value which does not put too great a demand on workmanship), a ratio of $d_1/d_2 = 0.5$ is achieved before the same loss becomes apparent. Above this value the clearance loss is very small. This calculation shows the reason for dispensing with the use of special sealing arrangements on fans. Should the diameter ratio d_1/d_2 be less than approximately 0.6, then higher values can only be obtained with narrower clearances. To obtain higher efficiencies one will find labyrinth seals⁽⁸⁾ worth while for the value $d_1/d_2 \approx 0.6$.

The situation basically changes if the type of seal employed is not of the crude type as shown in Fig. 61 but of the type designed for high-performance fans. Recently a lower pressure across the clearance gap has resulted from the introduction of a stagnation point on the inner side of the passage, which in turn has reduced the volume leakage. The remaining portion of this leaking volume can be used to advantage by disturbing the boundary layer, thus it only represents a partial and not an absolute loss. By this means success has been achieved in fans with large diameter ratios where the reduction of output is of little importance. The initial designs of high-performance fans required a clearance of 0.1 mm, but today with efficiencies of over 90%, a clearance of 2.0 mm is common in small models having a diameter of 400 mm. In conclusion, it can be said that with special designs disregard of output decrease due to leakage give satisfactory results, while by contrast, clearance losses in axial flow fans produce an undesirable loss of efficiency.

⁸ Detailed explanations for the calculation of labyrinth seals can be found in W. Traupel, *Thermische Turbomaschinen*, vol. I (1958) and vol. II (1960), Berlin/Göttingen/Heidelberg, Springer; also in W. I. Kear-ton and T. H. Keh, Leakage of air through labyrinth glands, *Proc. (A) Instn. Mech. Engrs. London*, 166 (1952), 180-95. New formulae are contained in B. Eck, *Technische Strömungslehre*, 6th edn.

33. DIFFUSER LOSSES

The kinetic energy of air discharged by the impeller, i.e. $(c_3^2/2g)\gamma$, must be converted into pressure in a diffuser. This conversion is called "static regain", and with fans it is effected in the volute in the majority of cases. It is a process which generally causes comparatively large losses. Because of this, the ratio of the kinetic to the total energy is kept at a minimum level in good designs. This requirement results in a maximum reaction. The design of a diffuser or volute will be treated more fully in Chapter XI, so at this point we shall only concern ourselves with the losses involved. Providing the enlargement of the guide channel is small, so that separation of flow does not occur, the pressure losses can be given by

$$\Delta p = \frac{\rho}{2} [c_3^2 - c_4^2] (0.2-0.3) \quad (93)$$

(c_4 is the discharge from the fan and generally similar to the entry velocity).

In simpler terms we relate the losses to $(\rho/2) c_3^2$ so that a smaller constant can be selected so that

$$\Delta p_4 = \frac{\rho}{2} c_3^2 (0.15-0.25). \quad (94)$$

By substituting c_3 by c_{3u} we will not incur excessive losses because the angle with which c_3 emerges is generally small, i.e. ($\alpha_3 < 20^\circ$). At the same time, in agreement with the remaining calculations, we shall express this loss in terms of the total pressure $\Delta p = \psi(\rho/2)u_2^2$:

$$\frac{\Delta p_4}{\Delta p} = \frac{1}{\psi} \left(\frac{c_{3u}}{u_2} \right)^2 (0.15-0.25).$$

Substituting

$$\frac{c_{3u}}{u_2} = \frac{\psi}{2\eta_{\text{hydr}}}$$

we get

$$\frac{\Delta p_4}{\Delta p} = (0.15-0.25) \frac{\psi}{4\eta_{\text{hydr}}^2}. \quad (95)$$

This loss is directly proportional to ψ . With the large values of ψ generally met with in fan engineering it is exceedingly important to ensure the correct shape of the diffuser.

34. BEARING LOSSES

In the majority of cases, losses arising from bearing friction are exceedingly small. Let G = weight of the rotor and u' = the peripheral velocity of the shaft journal; then the work done in overcoming friction of a plain bearing is

$$N_{\text{mech}} = \mu \frac{Gu'}{75} \quad [\text{hp}]. \quad (96)$$

The following values may be taken for μ , the coefficient of friction:

Ball-bearings	0.0015μ
Sleeve or plain bearings	0.005μ
Michell self-aligning bearings	0.003μ .

35. EFFICIENCY

For the analysis of fan performance there are distinct advantages in subdividing efficiency into appropriate sections according to the type of loss involved. This subdivision is convenient, for example, if individual losses are examined at a later date or if only certain losses can be measured.

(a) HYDRAULIC EFFICIENCY

If we were to trace a particle of air from its entry point into the fan to its discharge from the fan, we would find it subject to the pressure losses $\Delta p_1 + \Delta p_{\text{imp}}$ in the impeller and Δp_4 in the diffuser so that with an actual pressure head of Δp the theoretical pressure head would be

$$\Delta p + \Delta p_1 + \Delta p_{\text{imp}} + \Delta p_4.$$

The hydraulic efficiency is therefore

$$\eta_{\text{hyd}} = \frac{\Delta p}{\Delta p + \Delta p_1 + \Delta p_{\text{imp}} + \Delta p_4} = 1 / \left(\frac{1 + \Delta p_1 + \Delta p_{\text{imp}}}{\Delta p} + \frac{\Delta p_4}{\Delta p} \right). \quad (97)$$

If the fan being considered does not have a shock-free entrance, the losses Δp_2 and Δp_3 must also be included. Undoubtedly hydraulic efficiency is an important factor in the design of an impeller.

(b) VOLUMETRIC EFFICIENCY

With respect to the clearance loss already discussed, we introduce the so-called volumetric efficiency η_{vol} ,

$$\eta_{\text{vol}} = \frac{V}{V + V'} = \frac{1}{1 + (V'/V)}. \quad (98)$$

Volumetric efficiency gives the ratio of the outlet to the inlet quantities of air. The ratio V'/V has already been calculated in Section 32.

(c) MECHANICAL EFFICIENCY

One can assume that the purely mechanical losses are made up of bearing and transmission losses, i.e. gear, belt and V-belt losses. This overall loss is designated by N_m . Two methods of obtaining the mechanical efficiency can be adopted: one is to subtract N_m from the total input power, i.e. brake horse power, the other is to add this loss to the impeller shaft output, i.e.

$$\eta_{\text{mech}} = \frac{N - N_m}{N} = \frac{N_w}{N_w + N_m}. \quad (99)$$

(d) TOTAL EFFICIENCY

The ratio of the actual work done on the air N_L to the work done at the coupling $N_w + N_m$ is called the total efficiency, η_{total} , i.e.

$$\eta_{\text{total}} = \frac{N_L}{N_w N_m} = \frac{V \Delta p}{75 (N_w + N_m)}.$$

This is most effectively determined by experiment. The denominator includes terms representing useful work, and numerous losses involved which include disc friction N_r , hence,

$$\eta_{\text{total}} = \frac{V \Delta p}{V + V' [\Delta p + \Delta p_1 + \Delta p_{\text{imp}} + \Delta p_2 + \Delta p_3 + \Delta p_4] + N_m \times 75 + N_r \times 75}.$$

$$\eta_{\text{total}} = \frac{1}{\left(\frac{V'}{V} + 1\right) \left[1 + \frac{\Delta p_1 + \Delta p_{\text{imp}}}{\Delta p} + \frac{\Delta p_2}{\Delta p} + \frac{\Delta p_3}{\Delta p} + \frac{\Delta p_4}{\Delta p}\right] + \frac{N_m \times 75}{V \Delta p} + \frac{N_r \times 75}{V \Delta p}}. \quad (100)$$

In the case of shock-free entry, the terms Δp_2 and Δp_3 are eliminated.

Substituting the following: η_{vol} , η_{hyd} , η_{mech} , and ζ , then

$$\eta_{\text{total}} = 1 / \left[\frac{1}{\eta_{\text{vol}}} + \frac{1}{\eta_{\text{mech}}} + \frac{1}{\eta_{\text{total}}} - \frac{1}{\eta_{\text{total}}} \eta_{\text{mech}} + \zeta \right] \quad (101)$$

from which we derive the hydraulic efficiency:

$$\eta_{\text{hyd}} = \frac{\eta_{\text{total}}}{\eta_{\text{mech}} - \zeta \eta_{\text{total}} \eta_{\text{vol}}} \cdot \frac{1}{\eta_{\text{vol}}}. \quad (102)$$

For a predetermined total efficiency $\eta_{\text{tot}} = 0.65$ we determine the hydraulic efficiency η_{hyd} as follows. From eqn. (85) $\zeta = 0.04$ and from Fig. 62 we get the value $\eta_{\text{vol}} = 0.97$. If it is assumed $\eta_{\text{mech}} = 0.99$, then we get $\eta_{\text{hyd}} = 0.694$. This efficiency is higher than the value obtainable if all the efficiencies were multiplied.

(e) CHANGE OF TOTAL EFFICIENCY OWING
TO A VARIATION IN MECHANICAL LOSSES PRODUCED
BY VARIATION IN SPEED

Purely frictional bearing losses vary with the rotational speed; while the air output and hydraulic losses vary as the cube of the rotational speed. Therefore, under certain circumstances, a reduction in speed will result in a sharp fall in total efficiency. Denoting a fixed number of revolutions with the subscript 0, then for an arbitrary number of revolutions n per minute we get

$$L = L_0 \left(\frac{n}{n_0} \right)^3,$$

where L is the total work of the combined hydraulic work where the speed ratio is raised to the third power, and

$$L_M = L_{M0} \left(\frac{n}{n_0} \right)^3,$$

where L_M is the mechanical work for the mechanical losses. From this we get

$$\eta_{\text{mech}} = \frac{L}{L + L_M} = \frac{L_0 (n/n_0)^3}{L_0 (n/n_0)^3 + L_{M0} (n/n_0)} = \frac{1}{1 + (L_{M0}/L_0) (n_0/n)^2}.$$

Since

$$\frac{\eta_{\text{total } n}}{\eta_{\text{total } n_0}} = \frac{\eta_{\text{mech}}}{\eta_{\text{mech}_0}} \quad \text{and} \quad \frac{L_{M0}}{L_0} = \frac{1}{\eta_{\text{mech}}} - 1,$$

$$\frac{\eta_{\text{total } n}}{\eta_{\text{total } n_0}} = \frac{1}{\eta_{\text{mech}_0} + (1 - \eta_{\text{mech}_0}) (n_0/n)^2}.$$

The ratio $\eta_{\text{total } n}/\eta_{\text{total } n_0}$ is plotted in Fig. 63 for the values $\eta_{\text{mech}} = 0.95, 0.9, 0.85$.

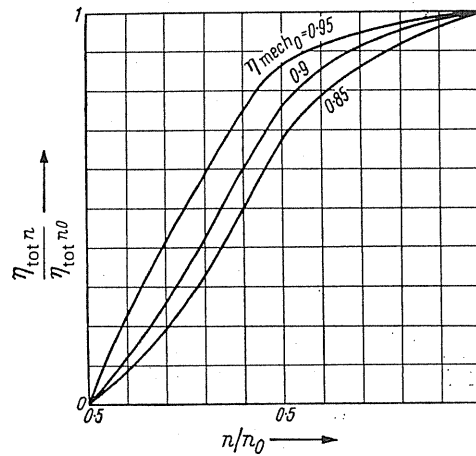


FIG. 63.

The graph indicates a sharp fall in efficiency under certain conditions when there is a reduction to half the normal rotational speed. This is because the proportion of the mechanical losses involved is very large.

These effects are noticeable and often most undesirable with V-belt and belt drives.

36. HYDRAULIC EFFICIENCY BY THERMAL ASSESSMENT

Sometimes the hydraulic efficiency of an uncooled fan can be simply ascertained thermodynamically. The pressure increase in a fan produces a slight compression. The necessary expenditure of work is simple to calculate by employing the principles of thermodynamics

in conjunction with temperature. Without losses the change in condition is isentropic and the work done for 1 kg of air (expressed in kcal) is $q_s = c_p (t_2 - t_1)$, where t_1 is the entry temperature and t_2 is the discharge temperature.

Internal losses produce an actual temperature t'_2 which is higher than t_2 . This process is called polytropic and the work done in kcal is

$$q_{\text{poly}} = c_p (t'_2 - t_1) \text{ kcal.}$$

For the efficiency,

$$\eta_s = \frac{q_s}{q_{\text{poly}}} = \frac{t_2 - t_1}{t'_2 - t_1}.$$

Temperatures t_1 and t'_2 can be measured while t_2 is easy to calculate. For an isentropic process the ratio of the absolute temperatures gives

$$\frac{T_2}{T_1} = \frac{273 + t_2}{273 + t_1} = \left(\frac{p_2}{p_1} \right)^{(\kappa-1)/\kappa},$$

where the temperatures are measured in the Celsius scale. On account of the small pressure gradients generally encountered in fans, the last equation can be expressed in terms of $\Delta p/p_1$, i.e.

$$\begin{aligned} \frac{T_1 + \Delta T}{T_1} &= \left(\frac{p_1 + \Delta p}{p_1} \right)^{(\kappa-1)/\kappa}, \\ 1 + \frac{\Delta T}{T_1} &= \left(1 + \frac{\Delta p}{p_1} \right)^{(\kappa-1)/\kappa} \approx 1 + \frac{\kappa-1}{\kappa} \frac{\Delta p}{p_1}, \\ \Delta T &= T_1 \frac{\kappa-1}{\kappa} \frac{\Delta p}{p_1}. \end{aligned}$$

Substituting $T_1 = 273 + 15$ and $p_1 = 10,000 \text{ kg/m}^2$, we get

$$\Delta T = \frac{\Delta p (\text{mm WG})}{121.5}. \quad (103)$$

For each change in pressure of 121.5 mm WG there is a resulting isentropic change of temperature of 1°C. The temperature differences throughout an experiment can be reliably measured with a thermometer graduated in tenths of a degree.

At higher pressures these measurements might be affected by the radiation of heat from the fan; however, this is relatively small and may be neglected. By means of this method the hydraulic efficiency is determined and the efficiency curve can be easily obtained as well. This curve lies somewhat above the values determined with a dynamometer.

This appears to be the simplest practical method of deriving the efficiency. This method is little known and rarely used in industry.

Example

The following results were obtained in the author's laboratory:

$$\Delta p = 280 \text{ mm WG},$$

$$\text{Inlet temperature } t_1 = 13^\circ\text{C},$$

$$\text{Outlet temperature } t'_2 = 16.5^\circ\text{C},$$

so that $\Delta t = 16.5 - 13 = 3.5^\circ\text{C}$.

From eqn. (103)

$$\Delta T = \frac{280}{121.5} = 2.3^\circ\text{C}$$

and

$$\eta_{\text{hyd}} \approx \eta_s = \frac{2.3}{3.5} = 0.658.$$

CHAPTER VII

THE DESIGN OF IMPELLERS

37. INTRODUCTION

The following questions are often asked when the design of an impeller is considered. What will the shape of an impeller be for optimum efficiency? This is an important question when one considers the overall design of a fan, but other questions are equally important.

Should a fan exhibit definite operating characteristics? Is it possible to give a satisfactory practical answer to this question?

Answers to these questions become clear when one examines the parameters that affect the losses in a fan. These are as follows:

- (1) Ratio of entry and exit diameters: d_1/d_2 .
- (2) Rotational speed: n .
- (3) Entry and exit axial breadths: b_1 and b_2 .
- (4) Blade angles: β_1 and β_2 .
- (5) Number of blades: z .
- (6) Shape of blade.
- (7) Design of diffuser.

We can combine these factors more easily for centrifugal than for axial-flow fans. On the other hand, losses can be calculated for axial-flow fans but not for centrifugal fans because of lack of data. This is a formidable problem and one should attempt to find a partial if not a complete solution.

38. OPTIMUM ENTRY BREADTH b_1

The factors involved in determining the size of the axial breadth b_1 of a blade entry can be readily obtained. Before the introduction of air into the impeller, the air must be turned through an angle of 90° (approximately) from the axis of the suction of intake duct. This is analogous to a change of direction occurring at a bend. The inside radius of curvature, however, is not always adequate in fans because of the insufficient room. In order to save expense in manufacture it will often be found that the rounding-off of the shoulder is omitted. Generally, such an abrupt change of direction as this is not detrimental to the fan because even with a small radius a separation of flow will occur (Fig. 64). This phenomenon in itself is detrimental not because of loss occurring at the bend, which can represent a small fraction of the total pressure, but because of the indirect influence it exercises upon the impel-

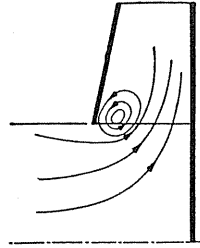


FIG. 64. Back flow at inlet of impeller due to large inlet breadth.

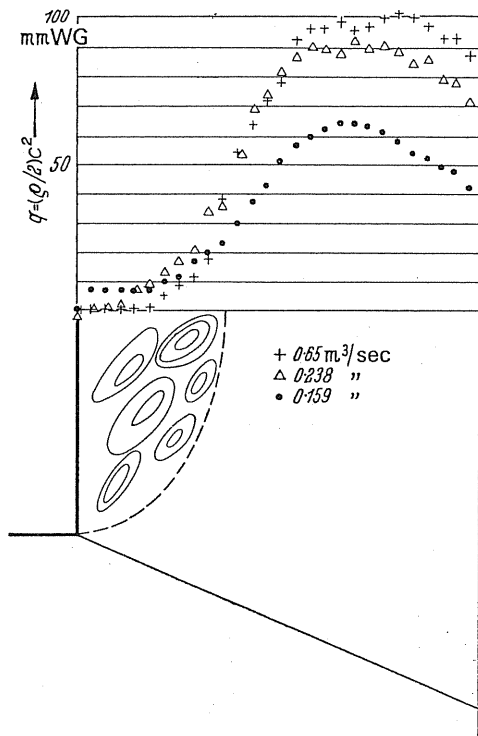


FIG. 65. Distribution of total energy immediately behind impeller, for various outputs.

ler. Owing to the separation of flow at this point, the entry breadth is only partially filled by the active stream which contributes towards a significant increase in the meridional velocity at this point. On account of this, a highly undesirable shock occurs here with normal volume flow. A secondary effect is a "back flow" which could arise in the remaining portion of the impeller entrance. The air flowing back into the suction or intake is often responsible for large losses of energy.

Figure 65 shows the results obtained by the author during experiments conducted with an impeller that was too wide. The impeller was open, i.e. running without a casing, and a pitot tube was positioned in the direction of flow to obtain the measurements. The experimental results indicate the flow-separation zone quite clearly and show that it does not vary to any great degree with different volumes.

To avoid this detrimental influence upon the impeller, separation of "flow at the bend" must be prevented. *The most effective measure to combat separation at this point is to accelerate the main stream.* Therefore the impeller entry area $\pi d_1 b_1$ must be smaller than the intake opening $(\pi/4) d_1^2$. This change in area will be designated by ξ .

Thus

$$\frac{\pi}{4} d_1^2 = \xi \pi d_1 b_1,$$

from which

$$b = \frac{d_1}{\xi \times 4}. \quad (104)$$

Generally,

$$\xi = F_1/F'_1,$$

where F_1 is the axial intake area and F'_1 is the impeller ring entrance area.

On account of a reduction in area caused by a hub of diameter d_0 , we get

$$b_1 = \frac{d_1}{\xi \times 4} \left[1 - \left(\frac{d_0}{d_1} \right)^2 \right] = \frac{d_1}{\xi \times 4} [1 - \bar{v}^2], \quad (105)$$

where

$$\bar{v} = d_0/d_1.$$

With an acceleration of 20%, i.e. $\xi = 1.2$, then

$$(\pi/4) d_1^2 = 1.2 \pi d_1 b_1, \quad (106)$$

therefore, $b_1 = (d_1/4 \cdot 8)$.

The impeller shapes which yield such an acceleration are schematically illustrated in Fig. 66.

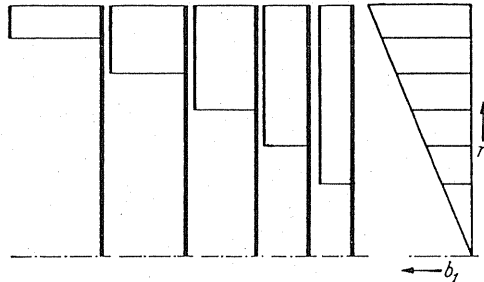


FIG. 66. Possible shapes of impellers at 20% inlet acceleration.

Recent investigations have shown, as opposed to earlier opinion, that an acceleration is not necessary. In fact, under certain circumstances, a considerable deceleration can be possible and even desirable. The 90° change of direction of flow cannot be adequately supported by the simple analogy of "flow at a bend" because the energy is being transferred from the blades to the fluid (Fig. 113b) and in certain cases a phenomenon occurs similar to boundary-layer suction. In the following discussion the change in area will still be designated by the coefficient which will also be employed for values less than unity.

39. OPTIMUM INLET DIAMETER AND BLADE ANGLE AT ENTRY⁽¹⁾

In considering the shape of an impeller there are still questions to be answered, e.g. what are the deciding factors to be considered when selecting the diameter ratio d_1/d_2 ? It is to be expected that the impeller losses are dependent upon the ratio d_1/d_2 as previous calculations have already shown.

Because the maximum velocity—which generally appears in the impeller—is the entry velocity w_1 , we must pay due attention to its magnitude.

The simplest assumption to be made is that the smallest possible entry velocity w_1 is required. The losses in the impeller may be expressed as $\Delta p_{\text{imp}} = c (\varrho/2) w_1^2$. The problem is to find a minimum value for w_1 .

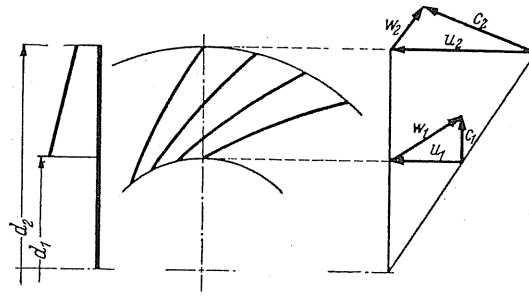


FIG. 67. Impeller with velocity triangles.

From Fig. 67 we get $w_1^2 = u_1^2 + c_{1m}^2$. c_{1m} is obtained from the output V per second, taking into consideration the narrowing of the blades, where

$$c_{1m} = \frac{V}{\pi d_1 b_1 [(t - \sigma)/t]} = \frac{c_{0m}}{(t - \sigma)/t}$$

(c_{0m} is immediately before the blading); b_1 is derived from the previous condition of acceleration at the entrance and possible reduction in the area because of the impeller hub,

$$b_1 = \frac{1}{4} \frac{d_1}{\xi} [1 - \bar{v}^2].$$

Substituting for $u_1 = \omega (d_1/2)$,

$$w_1^2 = c_{1m}^2 + u_1^2 = \frac{16\xi^2 V^2}{\pi^2 d_1^4 [(t - \sigma)/t]^2 [1 - \bar{v}^2]^2} + \omega^2 \frac{d_1^2}{4}.$$

For a given volume V and angular velocity ω , i.e. the rotational speed n , with a fixed value for d_1 , a minimum velocity w_1^2 will be obtained. Figure 68 shows how the velocity w_1 varies as d_1 changes from its optimum value.

¹ The following calculation, which first appeared in the first edition, 1937, was completed later in B. Eck, New calculation method for axial and centrifugal fans, *Schweiz. Bauztg.*, 1939, No. 4.

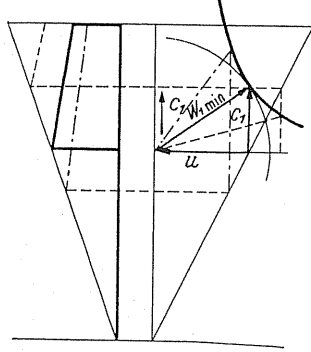


FIG. 68. Variation of relative entry velocity with the inlet diameter, where $V = \text{constant}$, $n = \text{constant}$. The diagram shows the minimum relative velocity.

From the inlet velocity triangle,

$$w_1 = \frac{u_1}{\cos \beta_1} \quad \text{and} \quad w_1^2 = \frac{u_1^2}{\cos^2 \beta_1}.$$

Substituting for

$$u_1 = \frac{\pi d_1 n}{60},$$

we get

$$w_1^2 = \frac{\pi^2 d_1^2 n^2}{60^2 \cos^2 \beta_1}.$$

To establish d_1 we shall calculate the volume of flow according to

$$V = c_{0m} \pi d_1 b_1 = c_{1m} \frac{t - \sigma}{t} \frac{\pi}{4} d_1^2 [1 - \bar{v}^2] \frac{1}{\xi},$$

from which

$$d_1^2 = \frac{4V\xi [t/(t - \sigma)]}{[1 - \bar{v}^2] c_{1m} \pi}.$$

Inserting this into the equation for w_1^2 ,

$$w_1^2 = \frac{\pi^2 n^2}{60^2 \cos^2 \beta_1} \frac{4V\xi [t/(t - \sigma)]}{[1 - \bar{v}^2] c_{1m} \pi},$$

and multiplying both sides by w_1 ,

$$w_1^3 = \frac{4\pi n^2 V\xi [t/(t - \sigma)]}{60^2 [1 - \bar{v}^2] \cos^2 \beta_1 (c_{1m}/w_1)} = \frac{4\pi n^2 V\xi [t/(t - \sigma)]}{60^2 [1 - \bar{v}^2] \cos^2 \beta_1 \sin \beta_1}.$$

The minimum value of w_1 is a function of the angle β_1 and is obtained by equating $(dw_1^3/d\beta_1) = 0$. Calculation yields the simple result

$$\tan \beta_1 = \frac{1}{\sqrt{2}}. \quad (107)$$

To obtain the corresponding diameter of the entry d_1 we take the above equation for d_1^2 into consideration and substitute it into

$$c_{1m} = u_1 \tan \beta_1 = \frac{\pi d_1 n}{60} \tan \beta_1,$$

from which

$$d_1 = \sqrt[3]{\frac{240\xi V [t/(t - \sigma)]}{[1 - \bar{v}^2] \pi^2 n \tan \beta_1}}. \quad (108)$$

For the case where

$$\xi \approx 1; \quad \frac{t}{t - \sigma} \approx 1; \quad \bar{v}^2 \approx 0,$$

$$d_1 = \sqrt[3]{\frac{240V}{\pi^2 n \tan \beta_1}}$$

or

$$V = \frac{d_1^3 \pi^2 n \tan \beta_1}{240}. \quad (109)$$

To obtain a dimensionless form we shall consider

$$V = \varphi u_2 \frac{\pi d_2^2}{4} \quad \text{and} \quad u_2 = d_2 \frac{\pi n}{60}.$$

Thus we derive the important ratio d_1/d_2 :

$$\frac{d_1}{d_2} = \sqrt[3]{\frac{\xi \varphi [t/(t - \sigma)]}{[1 - \bar{v}^2] \tan \beta_1}}, \quad (110)$$

from which the simple formula for the volume coefficient φ is obtained, i.e.

$$\varphi = \tan \beta_1 \left(\frac{d_1}{d_2} \right)^3 \frac{1 - \bar{v}^2}{\xi} \frac{t - \sigma}{t}.$$

This can be simplified because in most cases

$$\bar{v}^2 \approx 0, \quad \xi \approx 1 \quad \text{and} \quad \frac{t - \sigma}{t} \approx 1,$$

so that

$$\varphi = \tan \beta_1 \left(\frac{d_1}{d_2} \right)^3. \quad (111)$$

Figure 69 graphically illustrates this equation.

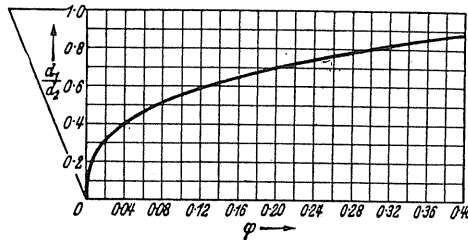


FIG. 69. Optimum value of d_1/d_2 as a function of φ .

An examination of the impeller losses has already shown that besides w_1 they are also a function of the diameter ratio d_1/d_2 . With a decreasing ratio d_1/d_2 the blade passage becomes narrower and longer. Neglecting this affects the result in the sense that the equation with $\xi = 1.2$ gives a low value for d_1/d_2 :

$$\left(\frac{d_1}{d_2}\right)^3 = \varphi \sqrt{2} \times 1.2$$

or

$$\frac{d_1}{d_2} = 1.194 \sqrt[3]{\varphi}, \quad (112)$$

while at the same time the angle β_1 from eqn. (107) is somewhat large. In each case the calculation results in a minimum value for d_1/d_2 and a maximum value for β_1 . With the following conditions fulfilled, eqns. (107) and (112) become practical propositions.

$$\beta_1 \leq 35.26^\circ, \quad (113)$$

$$\frac{d_1}{d_2} \geq 1.194 \sqrt[3]{\varphi}. \quad (114)$$

40. INFLUENCE OF THE CURVATURE OF THE ENTRANCE UPON THE OPTIMUM BLADE ANGLE

The right-angled inlet passage in the impeller necessarily demands—under certain conditions—a considerable increase in the meridional velocity c_{1m} at the curvature. Because of this the maximum relative velocity w_1 will be even larger than that derived from

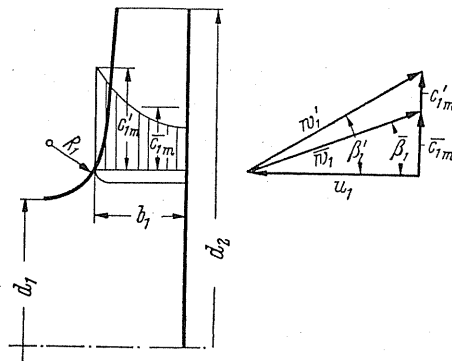


FIG. 70. Influence of the inlet curvature on the blade angle β_1 .

previous calculations when the average value was calculated and which we will designate by \bar{w}_1 . Without doubt this maximum velocity, generally found within the impeller, is a decisive factor where losses are concerned. The problem is to maintain w'_1 at a minimum level.

Denoting the ratio $(c_{1m'}/c_{1m}) = n$, for $w_1'^2$ we get

$$w_1'^2 = \frac{u_1^2}{\cos^2 \beta_1'} = u_1^2 (1 + \tan^2 \beta_1') = u_1^2 (1 + n^2 \tan^2 \bar{\beta}_1).$$

Let

$$u_1^2 = \frac{\pi^2 d_1^2 n^2}{60^2} \quad \text{and} \quad d_1^2 = \frac{4\xi V}{\pi \bar{c}_{1m}}.$$

Transformation of these values gives

$$w_1'^3 = \frac{4\pi\xi V n^2}{60^2} \frac{(1 + n^2 \tan^2 \bar{\beta}_1)^{3/2}}{\tan \bar{\beta}_1}.$$

From

$$\frac{dw_1'^3}{d \tan \bar{\beta}_1} = 0,$$

we get

$$\tan \bar{\beta}_1 = \frac{1}{\sqrt{2}} \frac{1}{n}. \quad (115)$$

That means, in contrast to an earlier result, $\tan \beta_1$ is small on account of the factor $1/n$. Consideration of the influence exercised by the curvature leads to a smaller average blade angle. In the light of earlier work⁽²⁾, an approximation was first produced to cover this factor.

$$\frac{1}{n} = \frac{1}{3} (1 + 2e^{-b_1/2R_1})$$

(where R_1 is the radius of curvature at the impeller entrance). The result is also a function of b_1/R_1 .

b_1/R_1	0.2	0.4	1.0	2.0	3.0	4.0
$1/n$	0.952	0.88	0.74	0.58	0.472	0.424
β_1	34°	31.9°	27.7°	22.3°	18.5°	16.7°

The table shows that all the angles are smaller than the angle of 35.2°, obtained previously.

In addition, one can ascertain the diameter of the entrance from the formula

$$d_1 = \sqrt[3]{\frac{240 V \xi}{\pi^2 n \tan \beta_1}}$$

according to eqn. (109).

² See footnote 1, Chapter VII.

41. CALCULATION OF THE OPTIMUM BLADE ANGLE IN THE CASE OF PRE-ROTATION

It may happen that, perhaps through an adjustable distributor, air is pre-rotated before entry—either in the same direction as the impeller or otherwise. This case is of considerable significance. One should consider whether there is an “optimum blade angle”.

From the velocity triangle (Fig. 1) we take

$$w_1 = \frac{u_1 - c_{1u}}{\cos \beta_1} = \frac{u_1}{\cos \beta_1} \left(1 - \frac{c_{1u}}{u_1} \right).$$

By substituting $c_{1u} = c_{1m}/\tan \alpha_1$ in the above equation we obtain

$$w_1 = \frac{u_1 - (c_{1m}/\tan \alpha_1)}{\cos \beta_1} = \frac{u_1 - (c_{1m}/w_1)(w_1/\tan \alpha_1)}{\cos \beta_1} = \frac{u_1 - \sin \beta_1 (w_1/\tan \alpha_1)}{\cos \beta_1},$$

from which

$$w_1 = \frac{u_1}{\cos \beta_1 + (\sin \beta_1/\tan \alpha_1)}; \quad w_1^2 = \frac{u_1^2}{[\cos \beta_1 + (\sin \beta_1/\tan \alpha_1)]^2}.$$

In order to substitute u_1^2 we consider

$$V = \frac{\pi d_1^2}{4} \frac{1}{\xi} c_{1m}, \quad c_{1m} = \frac{4V\xi}{\pi d_1^2}$$

as well as

$$u_1 = \frac{\pi d_1 n}{60}; \quad u_1^2 = \frac{\pi^2 d_1^2 n^2}{60^2}; \quad u_1^2 = \frac{4V\xi\pi n^2}{60^2 c_{1m}}.$$

Thus substituting for u_1^2 we get

$$w_1^2 = \frac{4\pi n^2}{60^2} \frac{V\xi/c_{1m}}{[\cos \beta_1 + (\sin \beta_1/\tan \alpha_1)]^2}.$$

Where $c_{1m} = w_1 \cdot \sin \beta_1$ we get, by substitution,

$$w_1^3 = \frac{4\pi n^2 V\xi}{60^2} \left/ \left[\sin \beta_1 \left(\cos \beta_1 + \frac{\sin \beta_1}{\tan \alpha_1} \right)^2 \right] \right. \quad (116)$$

We have now derived the velocity w_1 as a function of β_1 . To verify the existence or nonexistence of a minimum value of w_1 for a definite angle β_1 the denominator term $\sin \beta_1 [\cos \beta_1 + (\sin \beta_1/\tan \alpha_1)]^2$ should be differentiated with respect to β_1 . This gives

$$\tan \beta_1 = \frac{3}{4} \frac{1}{\tan \alpha_1} + \sqrt{\frac{9}{16} \frac{1}{\tan^2 \alpha_1} + \frac{1}{2}}. \quad (117)$$

If, according to this equation, we plot the angle β_1 against α_1 , we see that β_1 increases when rotation is in the direction of the impeller and decreases with counter rotation. Where $\alpha_1 = 90^\circ$, i.e. without rotation, it gives the previously determined value (Fig. 71).

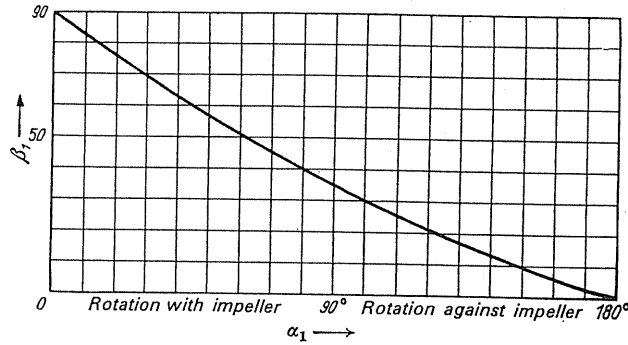


FIG. 71. Angle β_1 as a function of α_1 , when the rotation is with and against the impeller.

To obtain the diameter d_1 from the equation $d_1^2 = (4V/\pi c_{1m}) \xi$ we take the following equation into consideration:

$$\tan \beta_1 = \frac{c_{1m}}{u_1 - (c_{1m}/\tan \alpha_1)}$$

from which we get

$$c_{1m} = \frac{(\pi d_1 n/60) \tan \beta_1}{1 + (\tan \beta_1/\tan \alpha_1)}.$$

We substitute this value in d_1^2 and get

$$d_1 = \sqrt[3]{\frac{240V\xi}{\pi^2 n \tan \beta_1}} \sqrt[3]{1 + \frac{\tan \beta_1}{\tan \alpha_1}}. \quad (118)$$

42. TAPERED OR PARALLEL IMPELLER SHROUDS

No information is yet available to enable the discharge width b_2 to be determined from one definite aspect. In practice, one finds both parallel as well as tapered shrouds enclosing the blades of an impeller.

The shape of the shroud will depend on the shape of the blade. The decisive factor is the blade passage, not the meridional area. The mean velocity reduces from w_1 to w_2 in the blade passage. This deceleration is a very important factor in the design of an impeller. In the absence of reliable experimental data about the separation of flow in a rotating passage, one makes use of an analogy with stationary diffusers.

Accordingly care must be exercised to ensure that the tapering angle does not exceed 9° to 12°. ⁽³⁾ One plots the cross-sectional area of the shroud or the diameter of an equivalent circle against the *mean velocity of the streamlines* so that the enlargement of the blade passage area can be easily examined. The shorter the blade passages, i.e. a larger value for d_1/d_2 , the less the area. In general, one can relate the permissible enlargement of the blade

³ Because of the throwing off of particles on the boundary layer, due to centrifugal forces, the diffuser angle should be larger than for stationary diffusers.

passages, which is dependent on w_2/w_1 , to the diameter ratio. Therefore as an approximation

$$\frac{w_2}{w_1} \cong \frac{d_1}{d_2}. \quad (119)$$

In the case of two fans with identical d_1/d_2 values, the ratio w_1/w_2 can vary according to the coefficient ψ . One must assess each case on its merits in order to determine whether a tapered construction will be effective or not. This type of construction will keep deceleration within known limits. This general statement does not give any indication of when a tapered or parallel shroud should be used.

43. DETERMINATION OF THE BLADE SHAPE

So far we have been considering optimum design of the impeller casing as well as the blade entry and discharge angles. What is the form of a blade conforming to the inlet and outlet angles of the blades? With given angles β_1 and β_2 there is a wide choice of possibilities.

(a) STRAIGHT BLADE

The straight blade is the simplest form of design. Therefore the relationship between the entry and discharge angles, according to Fig. 72, is as follows:

$$\cos \beta_2 = \frac{r_1}{r_2} \cos \beta_1.$$

For $\beta_1 = 30^\circ$ the values of β_2 calculated from the above expression for different radii are shown in Table 6.

TABLE 6

r_1/r_2	0.3	0.5	0.7
β_2°	74.5	64.3	52.7

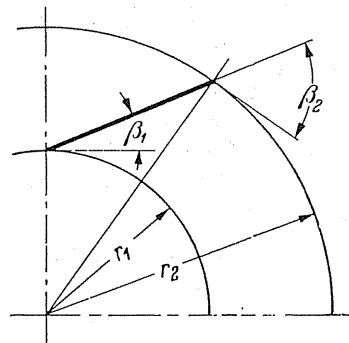


FIG. 72. Geometrical relations for straight blades.

(b) CIRCULAR ARC BLADE

Amongst other advantages, the circular arc blade⁽⁴⁾ permits the use of arbitrary entry and discharge angles. Its construction is illustrated in Fig. 73. The radius of curvature R is calculated from the following formula:

$$R = \frac{r_2^2 - r_1^2}{2(r_2 \cos \beta_2 - r_1 \cos \beta_1)}. \quad (120)$$

The construction of its outline is as follows. At the centre point O an angle equal to $\beta_1 + \beta_2$ is constructed. A straight line connects the inner and outer circle intersection points B and C ; the line is then produced to point A . AB is the chord of the required circular

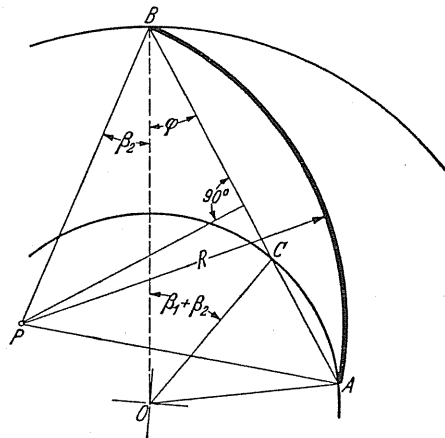


FIG. 73. Construction of blade from a circular arc; entry and discharge angles being given.

arc. At the point B an angle β_2 is constructed which cuts the perpendicular drawn from the mid-point of the chord AB . At the point of intersection of these two lines lies the required point P .

(c) DETERMINATION OF THE BLADE PASSAGE

With straight blades and blades curved in the form of a circular arc the entry is not shaped correctly. This produces, in certain circumstances, too high a blade pressure which leads to separation of flow. At the point of entry a smaller radius of curvature is required. This could be achieved by means of two radii of curvature or alternatively by a gradually changing curve. Simple circular constructions are not worth considering. The entry is most suitable when designed to produce no acceleration or deceleration of the flow. It has been shown that this region may approximately be delineated by an arc of a circle with its centre

⁴ Quantz, *Kreiselpumpen*, 3rd edn., Berlin, Springer, 1930.

at point A which leads to a logarithmic spiral; we shall select this form of curve up to cross-section BC (Fig. 74). From this region we construct a parabola which has a constant radius of curvature up to point C . This is best done with the aid of French curves. The blade passage thus obtained will need further investigation. The construction of a number of circles assists one in finding the width of the area of flow as well as the path of the streamlines. One can easily obtain the areas by means of the diameters of the constructed circles as well as the average width. The average width is obtained by taking the widths corresponding to the centre points of the various circles as shown on the side of the figure. The figure also shows the area of the various circles plotted against the points on the line joining the centres of the circles (Fig. 74). It is of importance that this area should increase

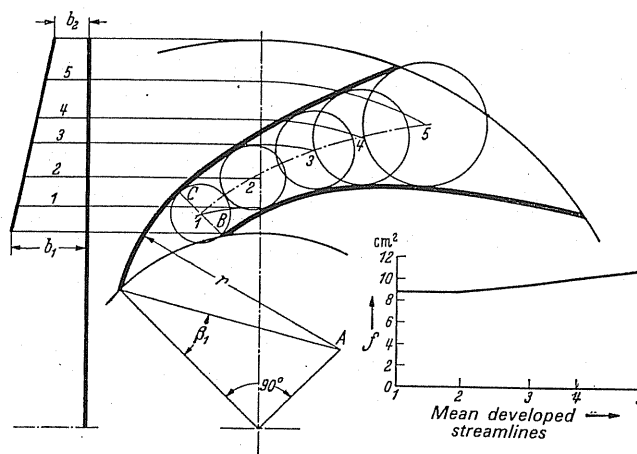


FIG. 74. Construction and investigation of blade passage.

steadily. If this is not the case then the passage must be modified. A sharp fall followed by a rise of the curve is undesirable because the resulting deceleration may be greater than required at a given point for a given length of passage. The best way of ascertaining the degree of deceleration is to plot the diameters of the equivalent circles instead of the areas, and the slope of the resulting curve should not exceed $8-10^\circ$.

The requirement that there should be a gradual increase of the area in relation to the maximum permissible increase in size of a diffuser is the *most important factor, governing the dimensions of a blade passage*. The design of the blade passage becomes more critical when the blade passage becomes narrower in relation to the blade length.

In the case of an impeller with few blades, circular arc blades may be acceptable because the flow conditions at the entrance resemble aerofoil flow.

Blade passage with constant deceleration. It is generally assumed that the reduction of w is linear and, in this case, Pantell⁽⁵⁾ first pointed out that the deceleration in the passage reduces sharply from a peak value in the beginning. It was suggested that a blade passage

⁵ Pantell, K., Impeller-profile of turbomachinery, *Konstruktion*, 1949, p. 77.

should be chosen in which *deceleration remains constant*. The following relationship, i.e.

$$\frac{dw}{dt} = \frac{dw}{ds} \frac{ds}{dt} = \frac{dw}{ds} w = \text{const.}$$

shows that if deceleration is to remain constant when w decreases, dw/ds must increase.

(d) GRAPHICAL DETERMINATION OF THE BLADE FORM

The shape of a blade can be determined simply providing definite assumptions are made. In Fig. 75 we shall consider a blade element Δs and resolve it into its vector components Δr and Δu . From $\tan \beta = \Delta r / \Delta u$ one obtains

$$\Delta u = \frac{\Delta r}{\tan \beta}.$$

If we draw Δr in a radial direction, it is possible to determine the corresponding value Δu , providing the curve of β is given. Because $\tan \beta = c_m/u$, c_m can be employed instead of β or the cross-sectional area of the blade passage may be substituted. The method, which is extremely quick to use, will be applied in the following case.

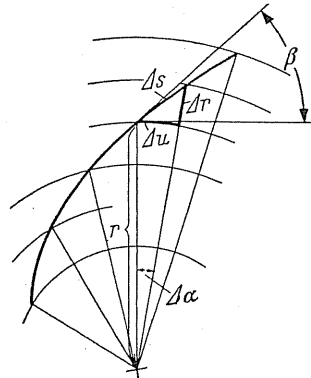


FIG. 75. Resolution of a blade element into its components Δr and Δu .

Blade passage of constant deceleration. From

$$w \frac{dw}{ds} = -C \quad \text{we get} \quad w dw = -C ds,$$

which after integration gives $w^2 = w_1^2 - 2sC$. This equation may be represented by a parabola. Assuming constant deceleration, $w = f(s)$, it follows that the curve of relative velocity w versus the developed passage length s is parabolic in each case. A number of different cases based on this assumption will be treated in the following paragraphs.

Constant meridional velocity (Fig. 76). In general there will be little variation of c_m in the impeller so that the case where $c_m = \text{const}$ is of special interest. By substituting

$ds = dr/\sin \beta$ in the equation $w dw = -C ds$, we obtain $w \sin \beta (dw/dr) = -C$. Because $w \sin \beta = c_m$ we get

$$c_m \frac{dw}{dr} = -C_1 \quad \text{or} \quad dw = \frac{-C}{c_m} dr,$$

and

$$w = w_1 - \frac{C}{c_m} (r - r_1); \quad (121)$$

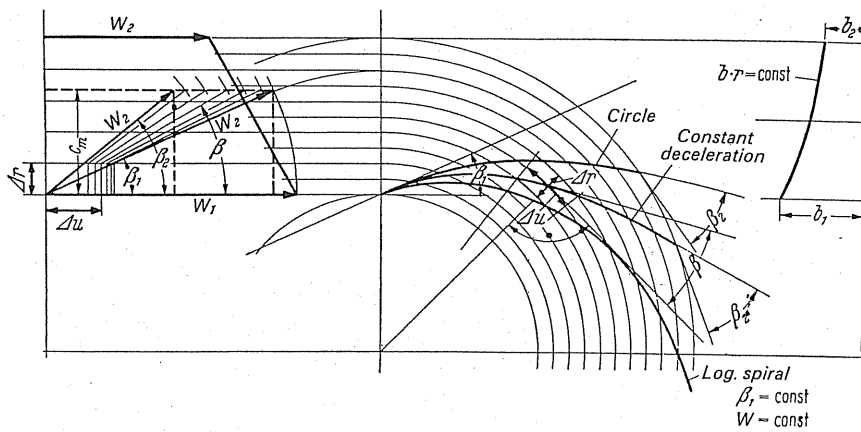


FIG. 76. Blade shape for constant deceleration in the case of constant meridional velocity c_m .

w , in this case, is also *linear* along the radius, and β is constant, since the blades are in the shape of a logarithmic spiral (Fig. 76). The equation

$$w \frac{dw}{ds} = -C = w \sin \beta \frac{dw}{dr}$$

can be easily integrated with β constant.

For the boundary conditions $w = w_1$ for $r = r_1$ and $w = w_2$ for $r = r_2$, we get

$$\frac{w^2}{2} = \frac{w_1^2}{2} - \frac{w_1^2 - w_2^2}{2(r_2 - r_1)} (r - r_1). \quad (122)$$

In this case the relation between w and the radius is parabolic. An exception arises if we maintain w constant, i.e. construct the passage so that deceleration does not occur. In the case of a logarithmic spiral shape β is constant and it follows that c_m is also constant, because $c_m = w \sin \beta$. This means that where the product of b and r is constant, the shroud is shaped like a hyperbola (Fig. 76). One can therefore conclude that blades with *logarithmic spiral shapes associated with hyperbolic shrouds result in blade passages having similar areas, i.e. $w = \text{constant}$.*

For this case it is easy to determine the pressure coefficient. Because $c_{2u} = u_2 - u_1$, one gets

$$\Delta p = \rho u_2 c_{2u} \varepsilon \eta = \rho u_2 (u_2 - u_1) \varepsilon \eta$$

$$\Delta p = \rho u_2^2 \left(1 - \frac{d_1}{d_2}\right) \varepsilon \eta \quad (123)$$

$$\psi = 2 \left(1 - \frac{d_1}{d_2}\right) \varepsilon \eta. \quad (124)$$

Graphical constructions. In general cases a graphical method can be employed which takes into consideration all possibilities.

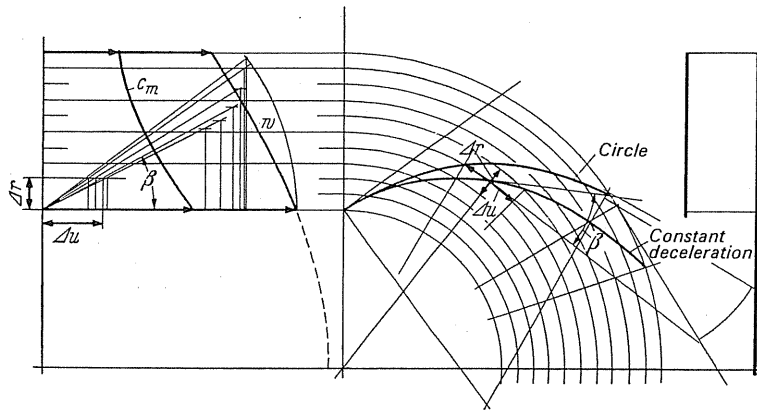


FIG. 77. Impeller having constant axial breadth.

Impeller of constant breadth (Fig. 77). On the basis of continuity of flow this type of impeller has a volume flow

$$V = c_m 2\pi r b = \text{const.}$$

i.e.

$$\frac{1}{c_m} = \frac{2\pi}{V} r b.$$

The basic equation of acceleration leads to

$$w \frac{dw}{ds} = w \sin \beta \frac{dw}{dr} = c_m \frac{dw}{dr} = -C,$$

or

$$dw = -C \frac{dr}{c_m},$$

and

$$w_2 - w_1 = -C \int_1^2 \frac{dr}{c_m} = -C \sum \frac{\Delta r}{c_m}. \quad (125)$$

The constant C may be obtained from the following equation:

$$C = (w_1 - w_2) \left/ \left(\int_1^2 \frac{dr}{c_m} \right) \right. = (w_1 - w_2) \left/ \left(\sum \frac{\Delta r}{c_m} \right) \right.$$

Where integration is not possible or, if a graphical solution is required, the summation formula can be used.

With constant breadth the integral can be solved. We get

$$C = V \frac{w_1 - w_2}{\pi b (r_2^2 - r_1^2)}. \quad (126)$$

By substituting this value in the basic equation,

$$w = w_1 - \frac{w_1 - w_2}{r_2^2 - r_1^2} (r^2 - r_1^2). \quad (127)$$

Plotting w against r gives a parabola, c_m being constant (Fig. 77). Previously (see Fig. 76) the velocity w varies linearly with the radius r , so that in both curves c_m and w can be considered as functions of the radius r . The radius is divided into equal divisions. In the centre of these divisions angle β is constructed, according to Fig. 76, from w and c_m . By this means exact values of β are obtained for all sections. The extended parallels in the Δr interval bisect the section Δu , which according to the equation $\Delta u = \Delta r / \tan \beta$, represents the extension of each of the Δr sections in the peripheral direction. From the origin of the inside radius, the curve of the blade can be easily determined. On the right-hand side of the figure the curve of the axial breadth is also plotted, and the curve in this particular case is a hyperbola. For the purpose of comparison, the circular blade has also been plotted, with the same angles of entry and exit as the logarithmic spiral with $\beta = \beta_1 = \text{constant}$. The variations of this blade from the shape required for constant deceleration are quite considerable.

$b = \text{constant}$. In this case, the curve of c_m is a hyperbola while that of w is a parabola. Both of these curves are plotted on the left side in Fig. 77. The blade shapes are then determined in Fig. 77 by the same method. Again for the purposes of comparison the circular blade with identical end angles has been included in the graph.

General case. First of all we shall select a *straight sloping* shroud. Values of w_1 and w_2 depend on the energy transfer from the blade. *We are looking for a blade shape which will produce constant deceleration.*

From the continuity equation $C' = c_m br$, we get $c_m = C'/br$. This is substituted into the basic equation,

$$dw = - \frac{dr}{c_m} C \quad \text{or} \quad \Delta w = - \frac{\Delta r}{c_m} C$$

to give

$$\Delta w = - \frac{\Delta r}{c_m} \frac{(w_1 - w_2)}{\sum \Delta r / c_m} = \frac{\Delta r br (w_1 - w_2)}{\sum (br) \Delta r} = - \frac{br}{\sum (br)} (w_1 - w_2). \quad (128)$$

For $w_1 - w_2 = 79 - 52.8 = 26.2$

$$\Delta w = -26.2 \frac{br}{\sum (br)}.$$

Calculations are given in Table 7.

TABLE 7

r	b	br	$\frac{br}{\sum(br)}$	Δw	c_m
5.5	2.45	13.5	0.223	5.84	33
6.5	2.06	13.4	0.221	5.79	33.2
7.5	1.7	12.75	0.212	5.55	34.9
8.5	1.33	11.30	0.1868	4.88	39.3
9.5	0.98	9.6	0.1585	4.15	46.3

$$\sum(br) = 60.55$$

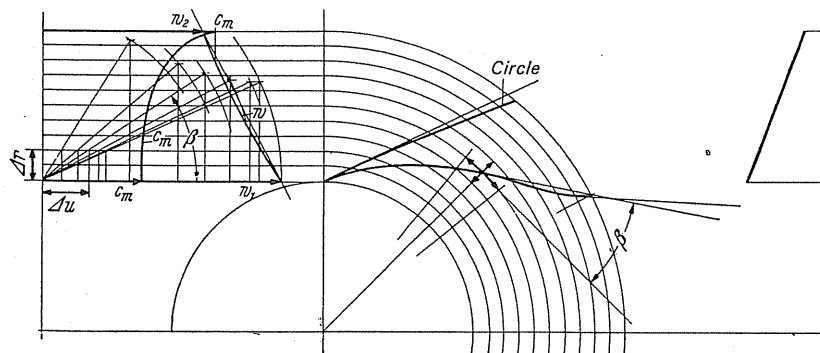


FIG. 78. Rectilinear but arbitrarily sloping shroud. Blade form for constant deceleration.

The shape of the blade is constructed graphically as in the previous example Fig. 78. In this particular case, the outline of the blade has a double curvature. The circular blade with identical end angles is almost straight.

In this example, although an extreme form of shroud was chosen, the curve w is almost straight. If we make a comparison with the other cases previously dealt with, which represent a reasonable cross-section of the actual feasible designs—the following statement is approximately true. *The relative velocity w varies in linear fashion with the radius.*

Designing of radial-flow fans with some characteristics of axial-flow fans. In considering fans with high peripheral velocities, it is interesting to note that purely radial blades have an axial-flow appearance at the entry of the impeller. The design of this type of entry has been discussed by Hasselgruber,⁽⁶⁾ Oberländer and Homola.⁽⁷⁾

⁶ Hasselgruber, H., Streamlining the shape of the rotor of axial compressors, *Konstruktion*, 1958, p. 22.

⁷ DAS 1065 559.

CHAPTER VIII

OPERATING CHARACTERISTICS OF CENTRIFUGAL FANS

A DECISIVE factor affecting the operational characteristics of a fan is the relation between pressure and volume. Fans are usually driven by electric motors rotating at constant or only slightly varying speed. If one considers a fan to be operating at a fixed speed, it is important to know how the pressure varies in relation to the volume.

44. THEORETICAL CHARACTERISTICS AS A REFERENCE

It is useful to consider in the first place a purely theoretical characteristic of a fan with an infinite number of blades and no losses.

Consider the following equation:

$$\psi_{th\infty} = 2 - \frac{\varphi}{2 \tan \beta_2 (b_2/d_2)}.$$

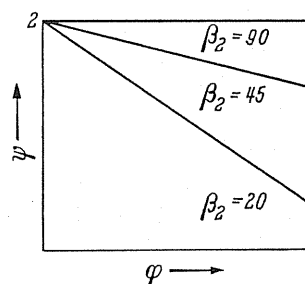


FIG. 79.

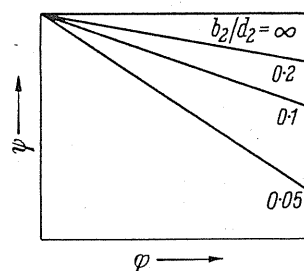


FIG. 80.

The characteristics $\psi_{th\infty} = f(\varphi)$ are straight lines and their slope is a function of the blade angle β_2 and the ratio b_2/d_2 . Figures 79 and 80 show this relationship. The figures show that as the blade angle β_2 and the ratio b_2/d_2 decrease, the slope of the characteristic becomes *steeper*. According to the above equation, if the ratio $(\tan \beta_2) b_2/d_2$ remains constant, there is only one characteristic curve.

45. INFLUENCE OF A FINITE NUMBER OF BLADES UPON THE CHARACTERISTIC

The pressure-volume curve of a fan is usually termed the characteristic. Although the effects of friction are considerable, it is nevertheless profitable to study the characteristic of frictionless motion in an endeavour to obtain a reference for comparison.

For an infinite number of blades the function $\Delta p = f(V)$ has already been explained. It gives a straight line which begins at $V = 0$ in the case of $\Delta p = \rho u_2^2$. With backward-curved blades the pressure Δp decreases as the volume increases; it remains constant with radial-tipped blades and increases with forward-curved blades.

Assuming absence of friction, we now consider the effect of a finite number of blades on the characteristic. The characteristic also remains linear⁽¹⁾ in this particular case. For special forms of backward-curved blades, Schultz⁽²⁾ found the position was exactly the same. He also found that the characteristic for a finite and an infinite number of blades intersected at a point *A* below the V axis. Figure 81 shows the resultant characteristic of backward-curved blades.

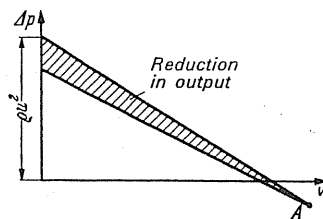


FIG. 81. Influence of finite number of blades on the characteristic.

46. EFFECTS OF FRICTION ON THE CHARACTERISTIC

(a) FRICTION IN THE BLADE PASSAGE

Frictional losses within the impeller and shock losses have a considerable effect on the characteristic of a fan, and these losses are, as a first approximation, proportional to w_1^2 . Here the value w_1 represents the average relative entry velocity which is proportional to the volume V . The *purely frictional* loss can be represented by $\Delta p' = C V^2$. Because the volume,

¹ Eck, B., *Beitrag zur Turbinentheorie*, Werft, Reederei, Hafen, 1925.

² Schultz, Delivery head of centrifugal pumps, *Z. angew. Math. Mech.*, 1927.

when there are shock losses, differs from that when there are no shock losses, and the effects of friction are influenced by flow-separation and back-flow, this formula is unsuitable for accurate numerical calculation. Therefore we can only expect an approximate assessment of frictional loss from this formula. Figure 82 shows a parabola derived from the previous equation. One subtracts the value $\Delta p'$ from the theoretical pressure Δp and plots the curve, which turns out to be parabolic and intercepts the volume V axis at some considerable distance from the theoretical linear characteristic. This point gives the greatest volume produced by a given fan.

(b) SHOCK LOSSES

Shock losses can be determined more accurately because they can be calculated directly from the deviating volume V_x in eqn. (88). Therefore,

$$\Delta p'' = \mu \frac{\rho}{2} u_2^2 \left(\frac{d_1}{d_2} \right)^2 \left[\frac{V_x}{V} - 1 \right]^2.$$

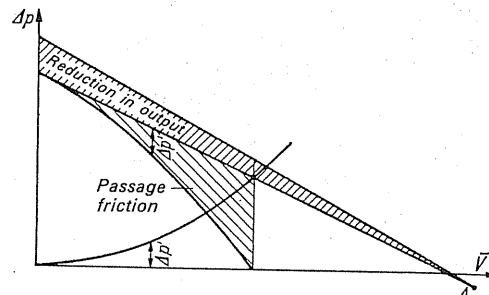


FIG. 82. Change of theoretical characteristic due to frictional losses $\Delta p'$.

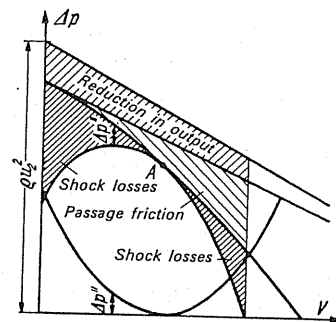


FIG. 83. Influence of shock losses $\Delta p''$ on characteristic.

From this we obtain a parabola: at its minimum value the volume is shock-free. This curve is illustrated in Fig. 83; it is similar to a test curve. Friction and shock losses in the entry guide vanes act in a manner similar to that of the corresponding impeller losses so that the general picture is not altered to any significant degree.

Because of the impossibility of determining the passage friction at outputs which deviate from shock-free condition with any degree of accuracy, a reliable calculation of the estimated

performance is out of the question. However, it is possible to make a qualitative statement about the influence of different methods of construction on the characteristic. The following conclusions may be found useful in practice.

(1) The point of maximum efficiency does not coincide with the point indicating shock-free entry. Because the friction losses to the left of point *A* are less than those to the right of this point (Fig. 83), the minimum total loss is located somewhat to the left of *A*. From this it follows that it will be to the designer's advantage to take a value for the volume somewhat greater than that corresponding to point *A* in his calculations.

(2) With equal blade angles and equal numbers of blades, the characteristic becomes steeper as the shock losses increase. With casings of the volute type these are almost the only shock losses in the impeller. These losses may be calculated using eqn. (88). This formula shows that the losses depend to a large extent upon the diameter ratio d_1/d_2 . As this ratio increases the losses become considerably larger. From this it follows that *impellers with very short radial blades have the steepest characteristic. A flatter characteristic occurs when the fan has long radial blades, i.e. the value of d_1/d_2 is small.*

Using eqn. (89), the characteristics given in Fig. 84 have been derived for diameter ratios d_1/d_2 of 0.3, 0.5, and 0.8. The importance of this ratio is readily recognised. When the characteristic is steep it cuts the abscissa sooner, which means that with a reducing radial depth the volume flow through the fan falls, i.e. the maximum obtainable volume from any particular fan is indicated at the point of intersection of the characteristic and the abscissa.

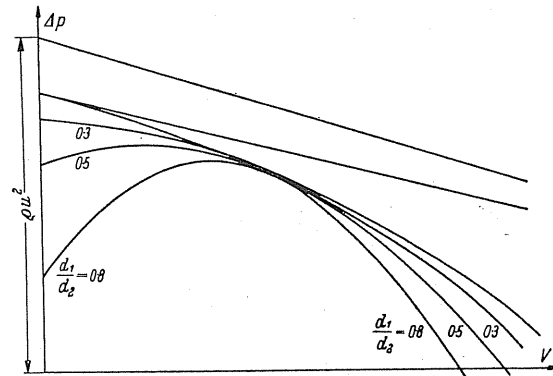


FIG. 84. Influence of the diameter ratio on the characteristic.

(3) If diffusers are employed the shock losses are determined by means of eqn. (90).

$$\Delta p_3 = \mu \frac{1}{\psi} \Delta p \left[\frac{V_x}{V} - 1 \right]^2.$$

Because ψ changes according to the value of V_x a purely parabolic curve is not obtained in this particular case.

In consequence, all fans equipped with guide vanes have steeper characteristics than fans without guide vanes. A flatter characteristic can be obtained if volute casings are used instead of guide vanes.

By reducing the entry velocity c_4 the effects of the guide vanes losses can be considerably reduced. This is possible if one allows a large free space between the impeller and guide vanes, i.e. a so-called smooth guide ring. This expedient, particularly important in the case of turbines because of the generation of noise, produces a flatter characteristic.

(4) The peripheral velocities of radial-tipped and forward-curved blades are less than these of backward-curved blades for exactly the same rise in pressure. The shock losses are, according to eqn. (88), proportional to u_2^2 , and therefore are substantially less than for backward-curved blades. Under certain circumstances, e.g. with Sirocco-rotors, the shock losses can be halved if, at the same time u_2^2 is halved. The theoretical characteristic of a fan will be modified due to shock losses.

47. VARIATION OF THE BREADTH/DIAMETER RATIO

A study of the theoretical characteristic has already shown that the gradient of a characteristic can be altered by a variation in the ratio b_2/d_2 . It is extremely important to possess information concerning the behaviour or the actual characteristic when there is a variation in the ratio b_2/d_2 , and one takes into consideration losses and a finite number of blades. The development of high-performance fans has resulted in worthwhile information on this problem being obtained.

In an endeavour to obtain an optimum arrangement, the breadth/diameter ratio was systematically changed. The characteristics obtained by this means showed that a change occurred which was similar to the variation obtained when the blade angle of an axial-flow fan is altered. Previously, advantage was taken of this principle to bring about volume regulation by installing a disc within the impeller, which was adjustable along the axial length, so that the width could be changed at will (Fig. 328).

The difference between the theoretical and experimental characteristic ε is obtained for a finite number of blades and efficiency η_i from

$$\psi = \psi_{\text{th}\infty} \varepsilon \eta_i = \left[2 - \frac{\varphi}{2} \frac{1}{(b_2/d_2) \tan \beta_2} \right] \varepsilon \eta_i.$$

Hoffmann⁽³⁾ first discovered the fact that, given one characteristic obtained experimentally, the characteristic of any other b_2/d_2 ratio can easily be determined. Hoffmann decided that there existed definite corresponding points on the characteristics obtained by using two different b_2/d_2 ratios whose product $\varepsilon \eta_i$ is constant. This supposition is almost correct and is true if an identical condition of thrust exists in each fan. Although it is true that at or near the point of maximum efficiency only minor shock losses occur, it is not without significance that it is also the middle of the shock-loss curve. In the case of similar velocity triangles the same probable shock condition may be achieved, which means $\varepsilon \eta_i$ is constant. In this case the ratio c_{2u}/u_2 , i.e. ψ , is constant, but with this the term in brackets must remain constant:

$$\left[2 - \frac{\varphi}{2} \frac{1}{(b_2/d_2) \tan \beta} \right],$$

³ VDI-Z, 1960, pp. 269-70.

which means that the coefficient φ varies with the ratio b_2/d_2 in the following way:

$$\varphi'/\varphi'' = \frac{b'_2/d'_2}{b''_2/d''_2}. \quad (129)$$

Figures 85 and 86 are based on Hoffmann's data for the diameter ratios 0.72 and 0.5. The agreement with the measured experimental points is remarkable. In Fig. 86 the broken lines indicate those curves derived by means of another method of calculation.⁽⁴⁾

However, there is no available information to suggest whether an alteration in the b_2/d_2 ratio will have any effect on efficiency. This will have to be decided by experiment.

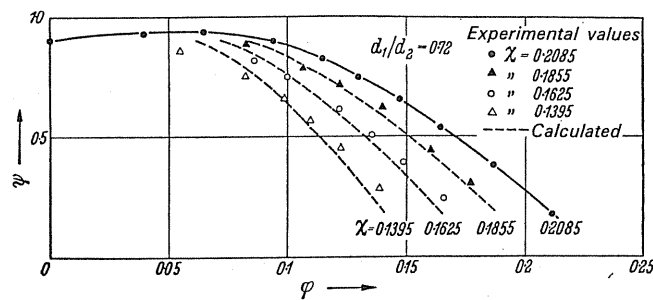


FIG. 85. Calculation of characteristics according to Hoffmann for various values of $\kappa = b_2/d_2$.

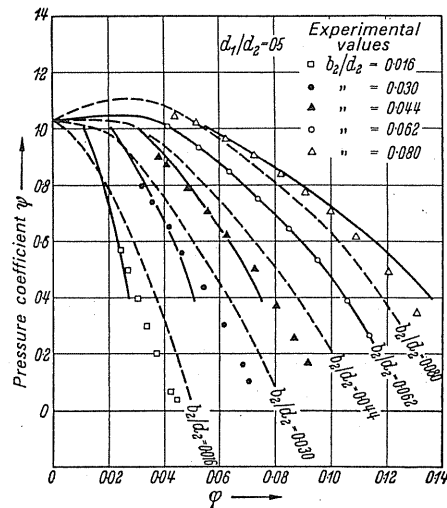


FIG. 86. Plotted curves: calculation according to Hoffmann shown as a dotted line: calculation with reference to throttling.

⁴ According to Bommers, if one assumes that the value of $\epsilon\eta$ is constant for points of equal throttling on the resistance curve φ^2/ψ const, further calculation is possible, (VDI-Z, 1959, p.445). The procedure is complicated and does not give good agreement with experimental results, and so Bommers applied certain corrections. Hoffmann plotted these results as dotted lines in Fig. 86.

GAP PRESSURE CHARACTERISTIC

The static pressure characteristic at the impeller discharge is of further interest to us. This, along with the "gap pressure characteristic", has previously been determined for an infinite number of blades in conditions of loss-free flow. The reduction in output due to a finite number of blades may be measured with the help of the results of Kearton. In this case a smaller angle β_3 is taken instead of β_2 . In the case where the angle is 90° , a parabolic curve is obtained instead of a straight line. With $\beta_2 = 90^\circ$ a characteristic peak occurs in every case, while backward- and forward-curved blades produce among other things a peakless characteristic (Fig. 87).

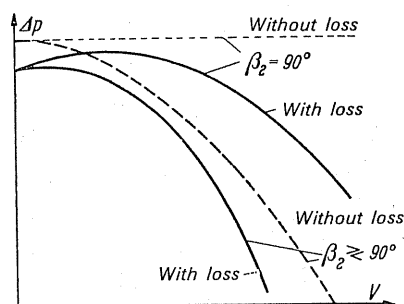


FIG. 87. Gap characteristic with different blade angles.

48. THE EFFECTS OF REDUCED VOLUME-FLOW ON THE FAN CHARACTERISTIC

The previous study has not given the complete picture. In fan engineering it is established that with radial-tipped and forward-curved blades agreement is usually obtained: a characteristic similar to that illustrated in Fig. 83. The characteristic of a Sirocco-rotor (see Fig. 88) clearly shows that when the volume flow is very low the value of the pressure

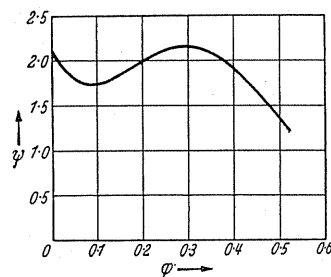


FIG. 88. Characteristics of a multivane impeller.

coefficient falls with increasing volume flows, and that when a critical volume flow is reached the coefficient increases with increasing volume flow.

The author believes that this phenomenon may be explained as follows. With a greatly reduced volume flow the blade passage is only partially filled by the active stream of fluid.

The flow settles itself on the pressure side of the blade, as the experiments of Thoma and Escher-Wyss have shown. This condition is illustrated in Fig. 89 for forward- and backward-curved blades. Instead of the passage breadth a only the breadth a' is effective for flow, so that the relative velocity is increased. This increases the value of the ratio $w'_2 = (a/a') w_2$. Accordingly, there is a significant change in the velocity triangles. As shown in Fig. 89,

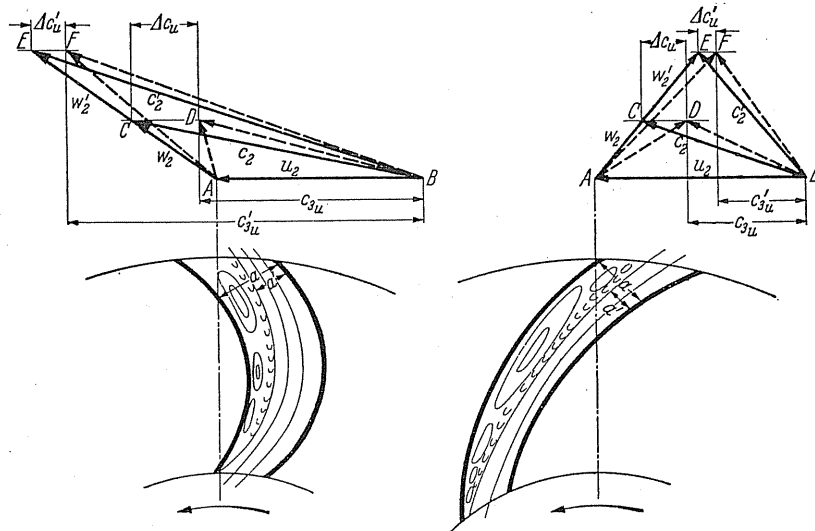


FIG. 89. Influence of a partially filled passage on the velocity triangles of forward- and backward-curved blades.

velocity triangle ABC indicates the condition where the blade passage is fully utilised; triangle ABD represents the situation where the impeller has a finite number of blades. The velocity triangle ABE is constructed with a relative velocity w'_2 or ABF where there is a finite number of blades. The line CD represents the situation when the blade passage is completely utilised for flow; line EF indicates that the blade passage is only partly utilised by the flow, hence EF is smaller than CD , and this is Stodola's interpretation.

One will note that with backward-curved blades the reduction in c_{3u} is less than is suggested in Fig. 83, so that the pressure curve must fall again here. Circumstances are different in the case of forward-curved blades. A significant increase occurs here, so that c_{3u} exceeds c'_{3u} and in consequence with smaller volumes the value of $qu_2 (c'_{3u} - c_{3u})$ becomes positive. This change in the characteristic is illustrated in Fig. 90 and coincides very closely with the true picture shown by Fig. 88.

Changing from a partially filled passage to, at least in the centre, a completely filled passage results in instability. Kearton's experiments showed this quite distinctly. The characteristics as well as the schematic drawings of the impellers from which they were derived are illustrated in Fig. 91. There are discontinuities in the power and pressure curves. With smaller volume flows, the angle between the peripheral velocity and the absolute stream velocity, i.e. α_3 , is large, but with larger volume flows unexpectedly small values result which are very similar in value to those which might be expected with an infinite number of blades.

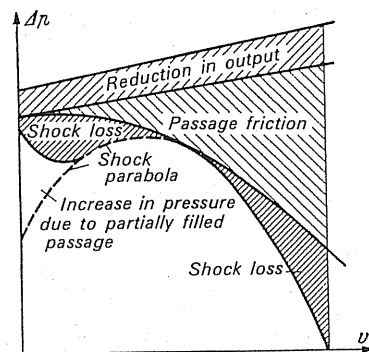


FIG. 90. Variation in the characteristic owing to a partially filled passage.

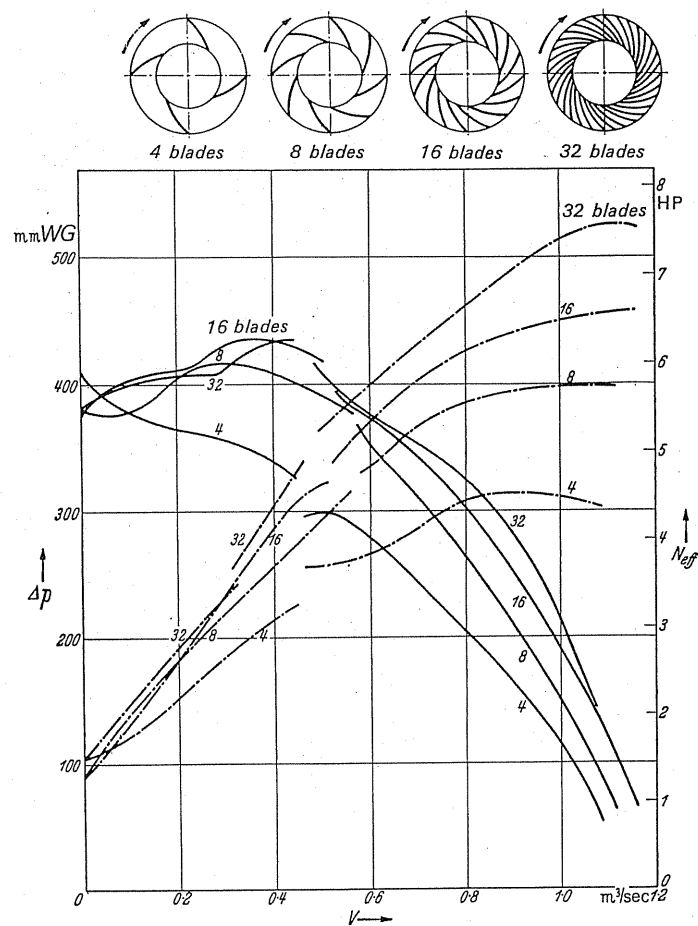


FIG. 91. Characteristics and power curves for impellers with different numbers of blades according to the experiments of Kearton.

49. PRESSURE COEFFICIENTS IN THE CASE OF RADIAL IMPELLERS

The pressure coefficients obtained with radial impellers can be easily understood if we consider

$$\psi = 2\eta \frac{c_{3u}}{u_2} = 2\eta \varepsilon \frac{c_{2u}}{u_2} \quad \text{and} \quad c_{2u} = u_2 - \frac{c_{2m}}{\tan \beta_2}.$$

By substitution we get

$$\psi = 2\eta \varepsilon \left[1 - \frac{c_{2m}}{u_2} \frac{1}{\tan \beta_2} \right].$$

Average ratios are satisfied by $c_{2m} = c_{1m}$. By substituting $c_{1m} = c_1 = u_1 \tan \beta_1$,

$$\psi = 2\eta \varepsilon \left[1 - \frac{d_1}{d_2} \frac{\tan \beta_1}{\tan \beta_2} \right]. \quad (130)$$

Figure 92 shows the graph obtained for the diameter ratios $d_1/d_2 = 0.5$ and 0.7 and $\beta_1 = 30^\circ$ (when $\eta = 0.7$; $\varepsilon = 0.8$). From this curve it appears that with backward-curved blades ψ -values may exceed unity and with higher efficiencies, ψ increases in proportion.

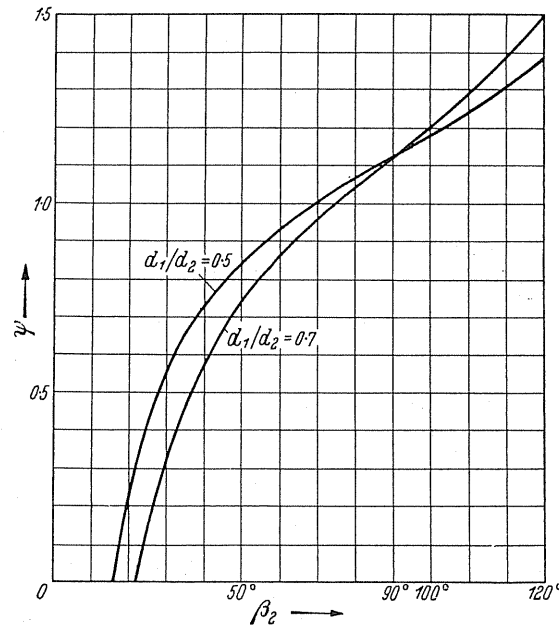


FIG. 92. ψ values for the diameter ratios 0.5 and 0.7 with $\eta = 0.7$ and $\varepsilon = 0.8$.

CHAPTER IX

THE MAIN TYPES OF CENTRIFUGAL FAN

50. HIGH-PERFORMANCE FANS

The characteristic feature of fan engineering up to the Second World War was the development of the axial-flow fan. Efficiencies of over 80% could be obtained with this type of fan. In one important application, e.g. for the induced draught, the centrifugal fan was completely replaced by the axial-flow fan. Andritzky⁽¹⁾ in 1943 reviewed the types of fan employed as induced-draught fans. This report was confined almost entirely to axial-flow fans with efficiencies of around 80%. For the ventilation of mines the radial-flow fan had long been in use. From the experience obtained with centrifugal pumps, particularly with the earlier developments of Rateau, a newer type of impeller with a small diameter ratio appeared and with this an efficiency of about 80% was achieved. The dimensions, and therefore the price of centrifugal fans, was prohibitive in comparison with the new axial-flow fans, and in consequence of this the former were unacceptable. Figure 93

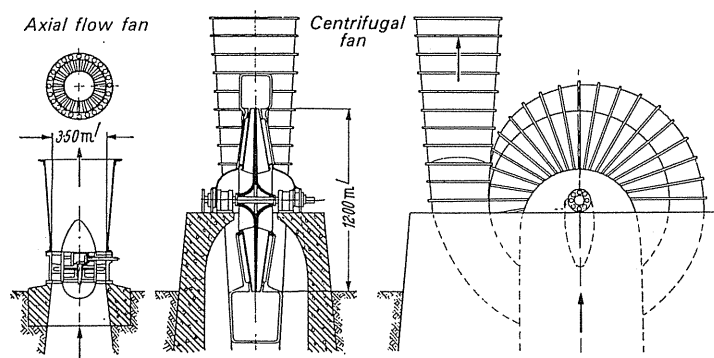


FIG. 93. An axial mine fan and a radial mine fan of an old type compared in size for identical duties.

shows an axial-flow fan⁽²⁾ and a centrifugal fan of the older type being employed as mine ventilators. The unimaginative engineer might well conclude that centrifugal fans were obsolete.

Why were axial-flow fans developed and why were they better than centrifugal fans? It is not possible to give a definite answer to this, but it is related to the success of the aerofoil

¹ Andritzky, M., Axial-flow fans for induced draught plant, *Braunkohle*, 1943, p.497.

² Linsel (Mine ventilation, *VDI-Z*, 1953, p.429) assessed the best efficiency of German mine axial-flow fans at 83%.

theory immediately after the First World War. This success was due in part to the assumption of a frictionless fluid, and aerofoil theory achieved a remarkable correlation with actual results. In 1922 Bauersfeld⁽³⁾ already showed a way in which aerofoil theory could be applied to turbines. In this case also the theory was applied with great success. The same method was applied to centrifugal fans. Kucharski⁽⁴⁾ had already opened this line of inquiry. Subsequently considerable progress was made in solving purely mathematical problems. The theory of frictionless flow is, unlike the theories of aerofoil and axial-flow machines, divorced from reality. Although the user did not benefit directly from the theoretical analysis, it was instructive. At that time research was confined almost entirely to the types of impeller commonly used in centrifugal pumps and compressors, i.e. impellers with narrow rims and small diameter ratios. The construction of fans received little attention. The centrifugal fan, therefore, was neglected. But a few individual engineers and companies were working on the problems of centrifugal fans, and thus slowly brought about a change.

From the point of view of purely scientific research, fundamental problems arose owing to the difficulties of the mathematical analysis of the boundary layer. This necessitated an additional term to the existing differential equation describing the boundary layer.

About 1951 and 1952 a significant event occurred in the development of centrifugal fans, i.e. the appearance of new high-performance fans (Fig. 96). The way in which the improvements were achieved will be understood when we consider the impellers. At one time investigations were carried out to find out how the design of centrifugal pumps could be applied to the design of centrifugal fans. Figure 94 illustrates a typical impeller which

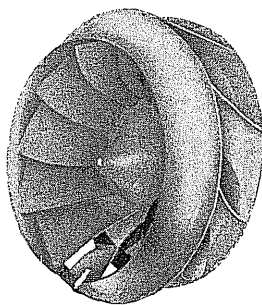


FIG. 94. Impeller with blades brought deep into the suction chamber.

resulted from this type of investigation. It is interesting to note that the blades go deep into the intake chamber, a procedure usually adopted in pumps to offset the effects of cavitation. The efficiency of this design is in the order of 80%, the speed coefficient σ is in the region of 0.4. On the other hand, the designer has the opportunity of taking the advantage of aerofoil blades. The Babcock-Stork blower, for example, was designed with aerofoil blades (Fig. 95). An improvement in the efficiency curve was obtained with a speed coefficient σ of approximately 0.43. A completely new method was then used in the design of high performance fans (Fig. 96). In contrast to previous designs, *the discharge width was increased*

³ Bauersfeld, The basis for calculation of high speed impellers, *Z VDI*, 1922, p. 41.

⁴ Kucharski, W., *Strömungen einer reibungsfreien Flüssigkeit bei Rotation fester Körper*, Munich, Oldenbourg, 1918.

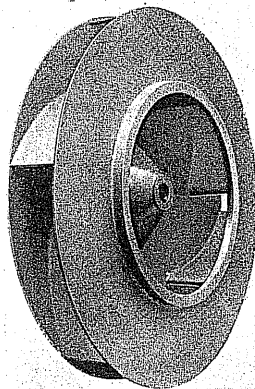


FIG. 95. Impeller with aerofoil blades. Babcock Stork.

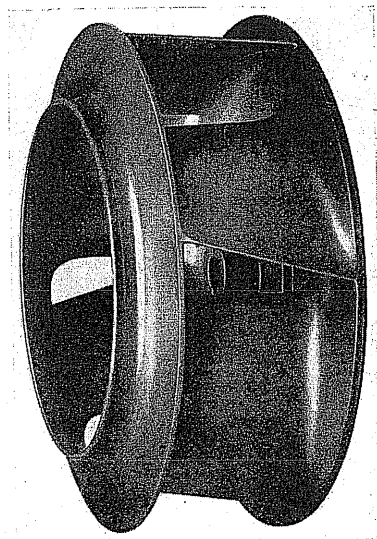


FIG. 96. High-performance impeller.

considerably; it was, in fact, almost doubled. The blades had a pronounced backward curvature and the entry was well rounded off. There was no aerofoil profiling or projection protruding into the suction chamber. With this type of impeller a speed coefficient σ of 0.66 was obtained, and it opened up new prospects for the centrifugal fan. For the very first time the efficiency could be raised to nearly 90%. Figure 97 shows the first design of a large mine fan, which at the acceptance trial gave an efficiency of 90%. This impressive result raised the centrifugal fan from the position of being the worst machine to that of the best. A speed coefficient $\sigma = 0.66$ gave the designer, *for the first time, the opportunity of obtaining smaller dimensions.* Impellers with the highest efficiencies and smallest dimensions were obtained in the new fields of application. Both features are of vital importance to fans in all applications.

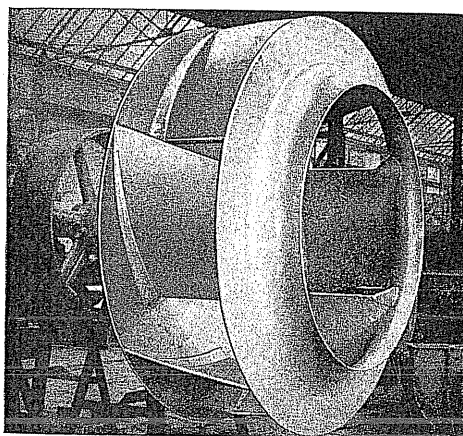


FIG. 97. High-performance impeller. "Our Fritz."

The new representative method of fan selection in Fig. 49 gives a clear review of the whole range of fans. By means of the curve in which σ is plotted against δ a comparison of the characteristic of different types of fan can be made and the model fan with $\varphi = 1$ and $\psi = 1$ is shown as a broken line in the diagram.

The different types of impeller are shown diagrammatically together with their corresponding mean widths and diameter ratios. Since all the impellers shown have the same values for the volume V and the pressure rise Δp , their power outputs are identical. However, the rotational speed, which is proportional to σ , differs. If one compares, for example, the axial-flow fan with $\sigma = 1$ with the centrifugal fan with $\sigma = 0.1$, then the speed of the axial-flow fan is ten times that of the centrifugal fan for the same air output. The broken line curve u denotes the peripheral velocity.

The efficiency curve shown in Fig. 49 is derived from values obtained with reliable designs. Axial-flow fans must be considered in the light of a later explanation which describes the necessity for adequate clearance at the blade tip and how this is achieved in a foolproof manner, but unfortunately at the expense of efficiency. The diagram shows the highest efficiency of nearly 91% occurs in the newly discovered range. To the right and left of this point the curve declines. In the case of high-performance fans, designers gained more experience and thus succeeded in raising the efficiency at $\sigma = 0.32$ to 89% (Fig. 49). *These impellers are considerably larger in size and therefore more expensive.* However, in the case of certain applications they should not be dismissed altogether, because relatively wide rotors are unsatisfactory for high pressures because of constructional weakness.

It is important that the impellers shown in Fig. 96 should have a definite curvature at the shroud, and, furthermore, that the ratio b_2/d_2 , the blade angle, the number of blades, the diameter ratio, and the blade curvature should be suitably chosen. The higher velocity at the shroud must be matched with the different velocity triangles for the impeller and the shroud. The author suggests that blades should be designed so that they are twisted as shown in (Fig. 98). In this way one avoids the double curvature of the Francis turbine blade.

In addition to the design of the curve of the shroud at the inlet, it proved important to design the passage between the impeller shroud and the casing lip as a cone whose optimum

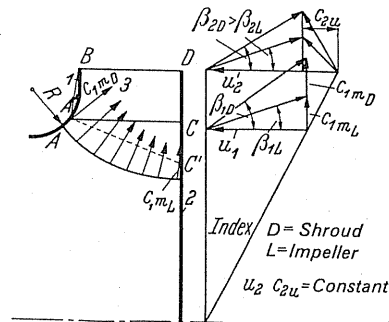


FIG. 98

contour will change according to requirements. Figure 99 shows the originals of four of the author's sketches of the "jet-like entry" which he drew for his colleagues in December 1952. Detailed tests conducted with models in the author's laboratory threw considerable light on the problems.

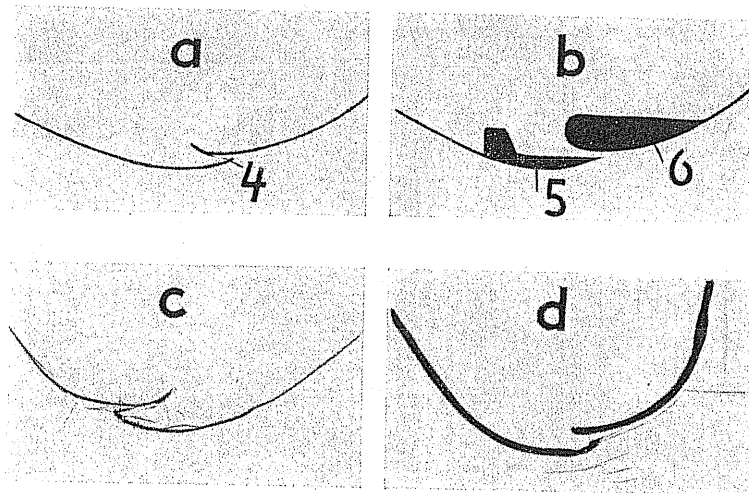


FIG. 99. Copies of original photographs of inlet jets 1952/3. (a) and (b) taken from PAE 6523 I a 27c (1952), (c) sketch (1952), (d) sketch (1953).

The test showed that the simple rectangular casing is best providing that it is well designed. The best-designed impeller and casing resulted in a large spiral casing with very flat "flow-in" and very low absolute velocities. By this means the casing losses were reduced to a very low level.

The preparatory work and completion of the main designs took place in the author's laboratory at Cologne. As soon as the investigations looked promising, the author in 1951 approached Messrs. P. Pollrich of Mönchen-Gladbach, who expressed their willingness to undertake a more detailed investigation. In these tests all the important parameters were systematically varied until the best design was achieved. The ratio b_2/d_2 , the diameter ratio,

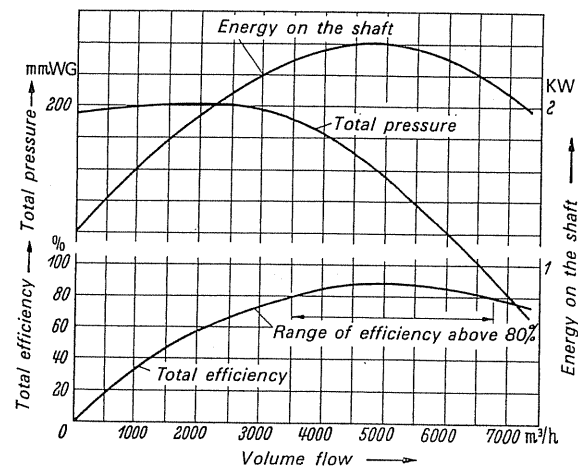


FIG.100.

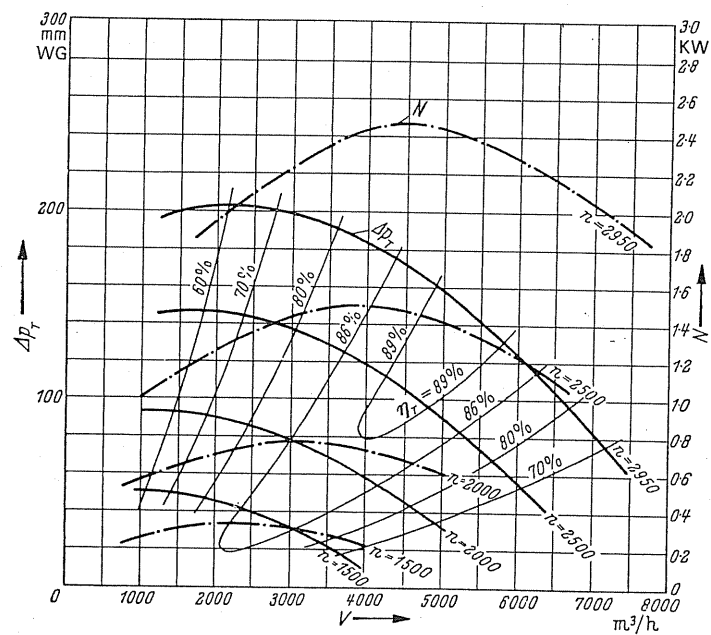


FIG.101.

the number of blades, the deceleration in the impeller, the entry curvature, and blade twisting, etc., were changed in many different tests.

The first publication was made after Mulsow⁽⁵⁾ had confirmed the results. Further confirmation of these measurements was later received from the ventilating station in Bochum. A similar but somewhat improved model was employed by Flügel⁽⁶⁾ in very detailed investigations in which all the present techniques of measurement were used. During these experiments with an impeller of 533 mm diameter (Fig. 96) a maximum efficiency of somewhat above 90% was obtained. Later Flügel⁽⁷⁾ gave an account of the optimum obtainable efficiency curve.

The characteristic of the fan is illustrated by Fig. 100. It is typical that the power curve reached its maximum approximately at the point of maximum efficiency. Owing to this, the practice of oversizing the driving motor is completely unnecessary. One should note the extended working range above 80%. Figure 101 illustrates the variations of characteristics obtained by varying the rotational speed. In the meantime a considerable improvement of the high-performance fan has been achieved. Figure 102 illustrates the difference between the original and more recent designs⁽⁸⁾. This particular comparison has a bearing on designs lacking in finish and rounding off corner sections. By means of this the efficiency increases from 89% to 91% while the power consumption is increased considerably with impellers having at the same time reduced dimensions. Because of this, losses due to leakage are reduced. While in the case of the first fan there was a tolerance of 0.1 mm, a clearance of around 2 mm could now be accepted between the impeller and casing on a runner or

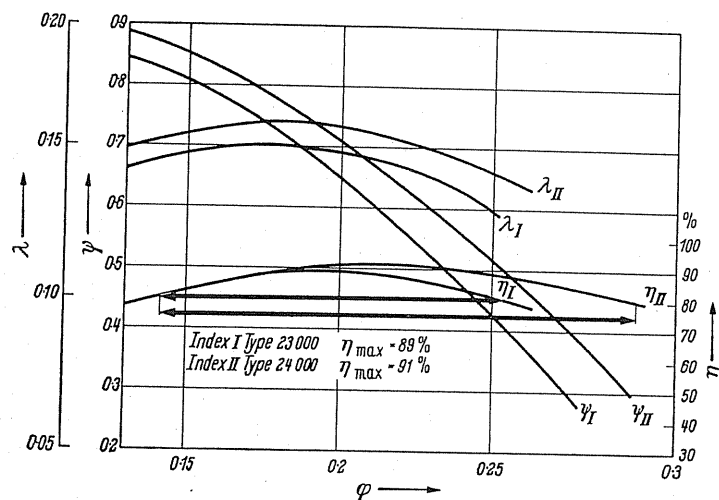


FIG. 102. I, old design, 1951; II, new design, 1960.

⁵ Mulsow, R., Centrifugal fan with 89% efficiency, *Melliand Textilberichte*, 33 (1952), 665. Mulsow investigated all fans on the market at that time for a particular purpose. *High-performance fans gave easily the best results.*

⁶ Flügel, *Gebläse hohen Wirkungsgrades*, Glückauf, 1954, p. 919.

⁷ Flügel, The optimum obtainable efficiency of turbomachinery, *VDI-Z*, 1954, p. 752.

⁸ Herr Ing. Kister carried out investigations on a model.

impeller having a diameter of 500 mm. The range of operation above 80% is again greatly increased. Presumably this may be the limit obtainable.

Similar efficiency has been achieved with experience gained with small pressure ratios. Figure 103a illustrates the results for a diameter ratio of 0.4.

BLADE PROFILES

The profiling of blading of centrifugal fans is for various reasons problematic as is stated below.

(1) For the first time the fundamental researches of Schmitz^(9, 10) show that at Reynolds numbers below 80,000 to 100,000 bent sheet-metal is—without any doubt—considerably superior to aerofoil blades. Furthermore, it has been found that many types of thin profile which approach sheet-metal profiles are equal to the latter in practice. Other experiments were conducted by Schmitz and Muesmann.⁽¹¹⁾ As a result of this work it appears that there are two distinct groups of profile. The first group comprises those profiles which fail completely below certain critical conditions, i.e. $Re < 80,000$. In most instances these are profiles of over 9–10% thickness. The second group includes those thin profiles which have the same critical properties as bent sheet-metal, i.e. $Re > 80,000$.

It is apparently a hopeless task to design even thicker profiles (i.e. those over 9–10% thickness) in such a way as to save them from failure, at the lower Reynolds numbers. This is shown, for example, by the work of Charwat.⁽¹²⁾ In these, however some quite odd shapes have been designed which cannot have any practical application.

(2) Following the work of Schmitz,⁽⁹⁾ Muesmann⁽¹¹⁾ investigated the effects of these phenomena on axial-flow fans. It was shown that aerofoil blading is advantageous up to Reynolds numbers of 10,000–20,000. This can be explained by the fact that the fluid at the boundary layer is ejected perpendicular to the direction of the main flow and laminar separation is made ineffective. Himmelskamp⁽¹³⁾ previously demonstrated this phenomenon with flow visualisation.

With backward-curved blades of a well-designed centrifugal fan such a phenomenon is impossible.

(3) Quite independent of the foregoing, the effect of shear flow should be considered in centrifugal fans. It will superimpose itself on the crossflow and produces a completely different position.

The aerofoil wing is the best shape for plane circumferential flow with a cross force, whereby a maximum buoyancy can be achieved with a minimum resistance. According to Fig. 103b(i) flow without separation will be achieved up to a stalling angle of about 15°.

⁹ Schmitz, F.W., *Aerodynamics of Flight Models*, Volckmann, Berlin, 1942.

¹⁰ Schmitz, F.W., *Measurements in Wind Tunnels and Two Aerofoil Wing Profiles for Small Reynolds Numbers*, Report 57/A/07, Aerodynamic Testing Station, Göttingen, 1957.

¹¹ Muesmann, G., Connections between the flow qualities of the impeller of an axial flow fan and a single wing, *Z. Flugwiss.*, 1958, p. 149.

¹² Charwat, A.F., Experiment on the variation of aerofoil properties with Reynolds number, *J. of Aeronaut. Sci.*, 1957, p. 386.

¹³ Himmelskamp, H., *Researches into Profiles on a Rotating Impeller*, Report 2 of the German Institute of Aviation, Göttingen, 1950.

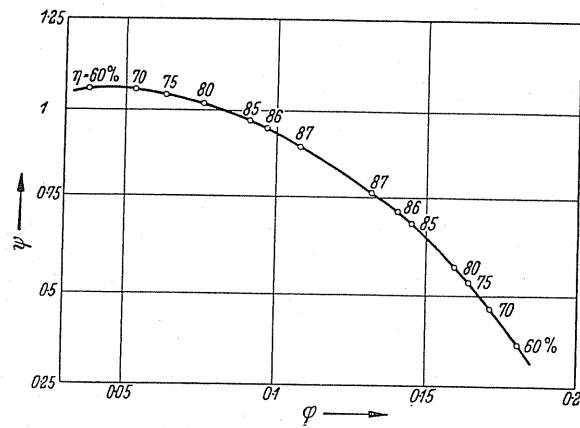


FIG.103a. Characteristic and efficiency of a high-performance fan with a small-diameter ratio.

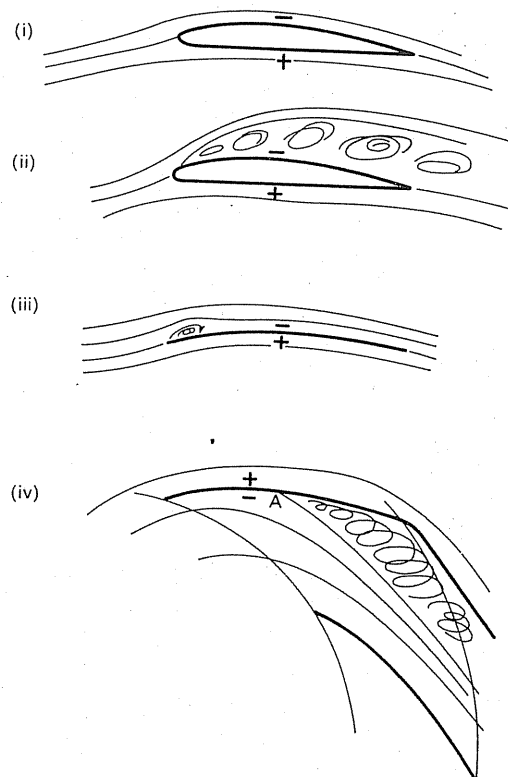


FIG.103b. (i) Fully developed boundary layer flow, on aerofoil wing. (ii) Flow separation on aerofoil wing. (iii) Circulation around a bent plate with vortex. (iv) Circulation around a radial blade with flow separation.

The identical buoyancy will be accomplished with an appropriately bent plate. Here the so-called "curl vortex" according to Fig. 103b(iii) will be formed at the front which will consequently force the flowing fluid to close in, thereby automatically producing some resistance. It seems appropriate to point out this view point because the literature of fan manufacturers frequently describes and shows wrongly the principal difference between aerofoil blades and bent plates. Furthermore, it should be specially mentioned that for the aerofoil blade (Fig. 103b(ii)) as well as for the bent plate practically the same $c_{a\max}$ will be produced, that the total flow will break at nearly the same stalling angle and be followed by a very similar flow pattern.

If one now observes for the centrifugal fan the flow pattern through blades on which the shearing flow is superimposed, one will get completely new conditions. Pressure and suction sides are interchanged. The decisive separation is not as with aerofoil wings on the upper but on the under surface and approximately at point A, Fig. 103b(iv). A further fundamental difference is caused by the effect of the Coriolis forces. These forces of pressure which are acting perpendicular to the relative flow will cease suddenly at the end of the blade, thus causing unsteady conditions. By this a discontinuity of the radii of the curvature of the flow at the exit rim of the blade is caused so that a nearly sudden change of reversion takes place towards the suction side of the blades. The Kutta discharge flow conditions as observed with standard aerofoil wings must be complemented for centrifugal fans in this direction.

Only recently has it been possible to investigate thoroughly the shear flow.^(14, 15, 16) It was found that the well-known boundary-layer equations will fail for shear flow, but that the rotation of the whole system has no influence on the boundary-layer equations. This purely theoretically assessed knowledge will permit investigation of such flows in ducts with contra-rotating partitions. These first investigations showing such flows were surprising as they had been completely unknown up to that date. Still lacking, however is the continuation of these tests by which one would consider the superposition of a moderately retarded flow to get the exact boundary-layer conditions as they occur with centrifugal fans. It is most desirable that such basic research is undertaken.

CONCLUSIONS

The above explanations should make one realise that the flow around blades of a centrifugal fan has primarily no connection with the plane flow around the aerofoil wings, and that even no similarity exists between both flows. One should not assume that it is advantageous to make the blades of a centrifugal fan of aerofoil shape. As a matter of fact, some 12 years ago it was found that efficiencies of 90% and 91% were obtained with simple sheet-metal blades.

¹⁴ Reichardt, H., *Circumferential Flow over Cylindrical Bodies in a Straight Line Couette Flow*, Report No. 9, Max-Planck Institute of Flow Research, Göttingen, 1954.

¹⁵ Jungclaus, G., *Investigations into Boundary Layers in Rotating Ducts and for Shearing Flows*, Report No. 11, Max-Planck Institute of Flow Research, Göttingen, 1955.

¹⁶ Reichardt, H., *Regularities of Straight Line Turbulent Couette Flows*, Report No. 22, Max-Planck Institute of Flow Research, Göttingen, 1959.

However, the problem is not yet solved. It could be that, owing to thickening of the walls and profiling of the sheet-metal blade, small advantages might be achieved. In this case it is assumed, as Schmitz, does that thin, profiled, steel blades are equivalent to thin sheet-metal blades. As 91 % efficiency has been achieved with thin sheet-metal blades, i.e. values which are nearly equal to the maximum⁽¹⁷⁾ possible, and with characteristic numbers which approximate to those of axial-flow fans, the question will arise regarding the reasons for these findings.

Already it has been found that under certain circumstances sheet-metal plates could be made considerably thicker without any disadvantage if, somehow, both ends were tapered. This observation was utilised to design dual panel, i.e. two parallel, blades of special shape because with higher circumferential speeds, single blade would not be strong enough. This is a rational design procedure in order to achieve greater strength at higher velocities. If certain sections of these dual-panel blades are tapered, the above-mentioned profiles will be obtained in plate form which, however, are not so strong. It seems obvious that the aerofoil blades will give an ideal aerodynamic shape for plane circumferential flow, but such a shape is not the best form for strength, and, moreover, an aerofoil blade is more expensive to make than a dual-panel.

In the meantime one of the technical universities has undertaken theoretical research to find the optimum shape for centrifugal fans.⁽¹⁸⁾ It was found that a decisive separation of flow can be avoided without any kind of profiling. The blade shape is very similar to that of a high-efficiency booster. As, however, other characteristics are missing, an efficiency of only 87 % is reached instead of 91 % for high-efficiency boosters. In this case the practical solution of the problem was confirmed by subsequent theoretical analysis.

51. CENTRIFUGAL FANS WITH VALUES OF STATIC REGAIN ABOVE UNITY

A surprising development in high-performance fans was the discovery that the optimum static regain was obtained with a simple rectangular spiral casing. The casing particularly must be considered in all its aspects and especially the width-to-depth ratio in order to obtain the best design. It transpired that an unusually large discharge outlet was required. This area in high-performance fans is substantially larger (almost double) that of the suction area. Despite this, it has been shown that the velocity distribution at this point is very nearly uniform. This result bringing the old rectangular spiral casing into prominence once more is fortunate because the casing is simple to produce. Up to this time the highest efficiencies have been obtained with axial-flow fans, but now *higher efficiencies* are attainable with high-performance centrifugal fans. This means that there are designs available which have *neither guide vanes no diffusers behind or in front of the impeller*. This is particularly important from the point of view of noise. A high-performance fan achieved a total reaction effect, according to an earlier definition, of 0.96, which is indeed a remarkable value. This

¹⁷ Flügel, The optimum efficiency of turbo engines which can be achieved, *Z VDI*, 1954, pp.752-5.

¹⁸ Albring, W. and Schlender, F., The development of a centrifugal fan with high efficiency, *Maschinenbautechnik*, 1959, p.560.

means that with free suction, i.e. no connected system on the suction side of the fan, only 3.6% of the total energy exists in the discharge area of the fan as dynamic pressure. With this total reaction effect some fans do not require any form of diffuser in many applications. This is often a very important point because, firstly, the restrictions of an installation might not permit the use of a diffuser on account of the shortage of space available, and, secondly, the shock losses have normally to be considered, and these can spoil an otherwise good fan.

High-performance fans now give characteristics that previously were unobtainable. If a fan is installed in an enclosed system of ductwork and the air pressure is obtained from the *difference in static pressure between the suction and discharge areas of a fan*, and a comparison is made with the work done at the shaft, then we get the ratio

$$\frac{\Delta p_{\text{stat}} V}{N_{\text{shaft}}}$$

This ratio, together with the static pressure, total pressure, and efficiency, are plotted against volume flow in Fig. 104. The ratio-curve is above the curve for the total efficiency. At high volumes the value of the ratio exceeds unity, and the total efficiency curve is lower than the static regain efficiency curve. Until now this ratio has been called "static efficiency" in practice, and has given rise to so much lively discussion and writing that it is necessary to comment on it.

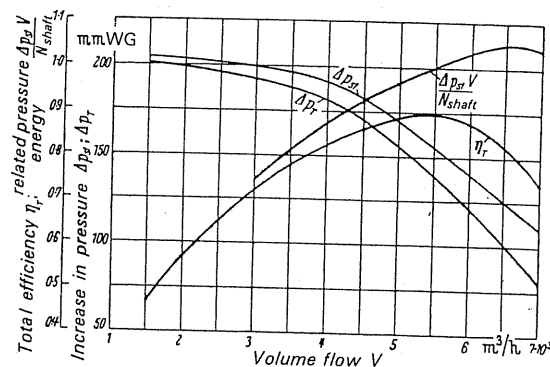


FIG. 104. Fan with a static regain > 1 .

In fan engineering it is usual to relate the efficiency to the difference in static pressure between the suction and discharge points of a fan. Overseas instructions are often still issued to the effect that this static efficiency must be the accepted basis in all tests. The emergence of new fan designs with values above unity must change the standards usually accepted.

First of all it must be stated that the previous numerical values have nothing at all to do with the total efficiency, therefore it is proposed that we designate "static regain" by ϵ_{stat} . The total pressure defining the efficiency is, as previously, $[p_2 + (\rho/2) c_2^2] - [p_1 + (\rho/2) c_1^2] = \Delta p_{\text{total}}$, while the static regain is a calculable quantity which gives the power consumption by the gas whilst being transferred from one point to another when a definite difference of static pressure exists between these two points. This is a question often posed in industry.

On account of the difference in areas existing in any one piece of apparatus there must be a resulting difference in static pressures. For various reasons, it is probably more meaningful for the fan user to compare the air output referred to the static conversion pressure with the driving energy of the fan. The fan-user is not concerned with the type of apparatus which is used to solve this problem; he probably has little interest in fan coefficients. His prime interest is the role of a fan in a given system. This is how the concept of static regain originated. Should this idea be abandoned? It is difficult to answer this question, but it must be borne in mind that static regain has little or nothing to do with efficiency and it is only employed as a basis for calculations. To the user it is indispensable because it is important for him to know, for instance, which volume gives him the highest possible value. According to Fig. 104, the highest value of static efficiency does not occur at the volume flow of maximum efficiency, but at a delivery volume which is considerably larger (about 27% larger than the optimum volume). It is clear that it is essential to know the static regain curve.

One should now realise that the use of static efficiency as an index of total fan efficiency was a *mistake*. The following argument should remove any remaining doubts. If one considers a wind tunnel (see Fig. 105), then only the *kinetic energy* is of interest to the student of aerodynamics in the test section. By comparing this with the *fan output*, he firmly establishes that the *fan has only to apply a fraction of this output*, i.e. the value of the ratio of the kinetic energy and fan energy exceeds unity. Values of $N_{kin}/N_{fan} = 6 \cdots 8$ are achieved in modern wind tunnels.

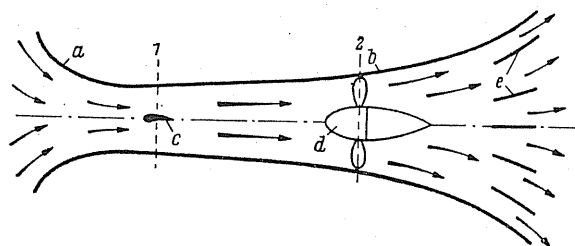


FIG. 105. Diagram of a wind tunnel of open design. 1, measurement section. 2, fan. *a*, entry cone; *b*, diffuser, *c*, model under test.

It is instructive to examine the streamlines in Fig. 106. Despite the resistance acting in the direction of flow, the streamlines are drawn in because behind them a strong excessive static pressure produces a resultant force *against* the direction of flow.

Now it has often been argued in the case of fans that a similar effect could be achieved if the discharge area of the fan was enlarged or the intake area reduced. It is true that the intake area can be extensively altered. An increase in the intake area can occur without loss in efficiency, but a reduction in efficiency readily occurs when the area is decreased. This deterioration in performance can be somewhat offset if the intake is shaped like a venturi tube, but also the losses arising in the diffuser will be detrimental to the fan. It is disastrous with the discharge vent. An arbitrary enlargement will test the workmanship of the spiral casing and it will result in additional losses. In these circumstances one obtains clear indications that *the static pressure across the fan is higher than the total pressure* (Fig. 107). However, one obtains this at the expense of the total efficiency which is now smaller than before,

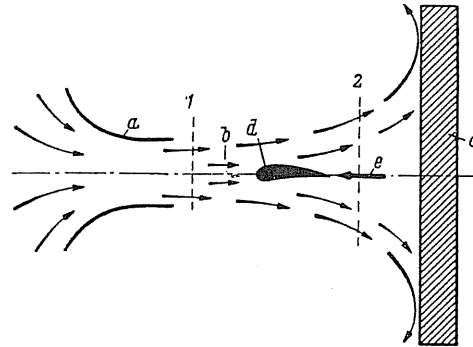


FIG. 106. Diagram showing a profile in an airstream impinging on a plate. *a*, jet or cone; *b*, velocity before profile; *c*, baffle; *d*, profile; *e*, back pressure on profile.

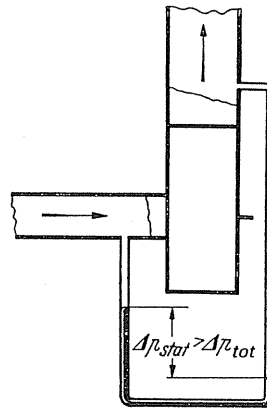


FIG. 107. Radial fan with the discharge area greater than the inlet area.

so that such measures are useless. In fact because of this, and despite the previously held view which had almost become a law in practice, *the total efficiency always exceeds the so-called static efficiency*. It is still in use today because there is, so to speak, a certain amount of safety in using static efficiency as a criterion. Actually the author cannot cite a case where the total efficiency is less than the static efficiency. If one considers all the possibilities involved in the preceding theory it appears that with all the fans to date *it is impossible for the numerical value to exceed unity*. It is hoped that the following analysis will make matters clear.

If the discharge area F_3 is larger than the intake area F_1 , from Fig. 107 the static pressure across the fan is greater than the total pressure, and the excess is given by

$$(\rho/2) [c_1^2 - c_3^2] = \Delta p_{\text{stat}} - \Delta p_{\text{tot}}.$$

We indicate the impeller area by $F_2 = (\pi/4) d^2$, so that it is possible to obtain an expression for the volume V :

$$V = \varphi u_2 F_2 = c_1 F_1 = c_3 F_3.$$

Therefore

$$c_1 = u_2 \varphi \frac{F_2}{F_1} \quad \text{and} \quad \frac{c_3}{c_1} = \frac{F_1}{F_3},$$

from which we get

$$\Delta p_{\text{stat}} - \Delta p_{\text{tot}} = (\varrho/2) c_1^2 \left[1 - \left(\frac{F_1}{F_3} \right)^2 \right].$$

At the same time if we consider $\Delta p_{\text{tot}} = \psi(\varrho/2) u_2^2$, the above static pressure difference can be covered by the following formula:

$$\begin{aligned} \Delta p_{\text{stat}} - \Delta p_{\text{tot}} &= (\varrho/2) u_2^2 \varphi^2 \left(\frac{F_2}{F_1} \right)^2 \left[1 - \left(\frac{F_1}{F_3} \right)^2 \right] \\ \Delta p_{\text{stat}} &= \Delta p_{\text{tot}} + (\varrho/2) u_2^2 \varphi^2 \left(\frac{F_2}{F_1} \right)^2 \left[1 - \left(\frac{F_1}{F_3} \right)^2 \right]. \end{aligned} \quad (131)$$

The pure static regain is

$$\varepsilon_{\text{stat}} = \eta_{\text{tot}} \frac{\Delta p_{\text{stat}}}{\Delta p_{\text{tot}}} = \eta_{\text{tot}} \left\{ 1 + \frac{\varphi^2}{\psi} \left(\frac{F_2}{F_1} \right)^2 \left[1 - \left(\frac{F_1}{F_3} \right)^2 \right] \right\}. \quad (132)$$

When $\varepsilon_{\text{stat}} > 1$ we will investigate the boundary condition of $\varepsilon_{\text{stat}} = 1$.

Therefore, with $\varepsilon_{\text{stat}} = 1$,

$$1 = \eta_{\text{tot}} \left\{ 1 + \frac{\varphi^2}{\psi} \left(\frac{F_2}{F_1} \right)^2 \left[1 - \left(\frac{F_1}{F_3} \right)^2 \right] \right\}.$$

For simplicity we assume $F_1 \approx F_2$ —an assumption often necessary to permit impeller to be removed from the front of its casing. Further, it will be assumed that $F_1/F_3 = \frac{1}{2}$. With the aid of these values we obtain the following formula:

$$\psi = \frac{3}{4} \varphi^2 \frac{\eta_{\text{tot}}}{1 - \eta_{\text{tot}}}. \quad (133)$$

Figure 108 shows the curves of the $\psi - \varphi$ graph for various values of η_{tot} . The condition $\varepsilon_{\text{stat}} > 1$ could occur beneath the curves. In the same figure the dotted curve indicates the minimum value of ψ/φ , i.e. below the range of the above curves, could be achieved with known types of radial impeller.

The figure also shows that for values of $\psi \approx 0.45$ and $\varphi \approx 0.25$ the dotted curve is first intersected by the *total efficiency curve* of 90%. This phenomenon was seen for the first time with high-performance fans, and it also occurs with larger φ values. The other types of constructions cannot ever come within the region of the dotted curve. One can see that with efficiencies below 80% it is hardly possible for a centrifugal fan to reach this region.

Two conditions are necessary if static regain is to exceed unity. Firstly, the discharge area must be considerably larger than the intake area (nearly twice as large), and, secondly, the efficiency must lie between 85 and 90%.

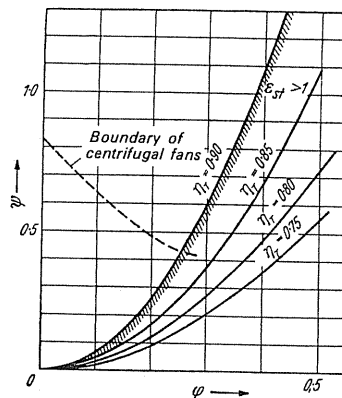


FIG. 108.

Value of static regain above unity for axial flow fans. With axial-flow fans also there are cases where static regain above unity can be achieved. This occurs at high efficiencies, i.e. above 85%, with very high rate of flow. These cases come within the range of possibility. The exact calculation is to be found elsewhere (Eck, 3rd German edition of this book).

52. THE DESIGN OF FANS FOR THE TRANSPORT OF DUST-LADEN GASES

The transport of dust-laden gases by fans poses serious problems for the designers. It is important to prevent adhesion of dust to the impeller, while, at the same time, wear to the impeller must be reduced to a minimum. Special axial and radial impellers have been designed to meet these requirements.

About 30 or 40 years ago, radial impellers with very steep blades, frequently with an exit blade angle of 90° , were used in most cases. With an exit blade angle of 90° it was possible to prevent the adhesion of dust, but one had to accept a low efficiency of 60–70%. At this time axial-flow fans with aerofoil blades were designed with efficiencies as high as 80%. Attempts were made to use such fans for transport of dust-laden gas, but unfortunately there was so much wear that so far as suction fans were concerned their use was not practicable. The wear occurred just in those parts of the aerofoil blade which are decisively important for the aerodynamic characteristic of the aerofoil, i.e. on the front part of the suction side. This means that the efficiency of such fans drops very considerably. Often the efficiency of such fans is reduced within a few days of use.

Improvements followed the design of a completely new type of axial-flow fan, that is the so-called meridian-accelerated axial-flow fan. In this type of fan the meridian section gradually decreases in the direction of flow. Such fans can be built with blade channels unprofiled, i.e. from sheet steel on account of their accelerated through-flow. Despite this, efficiencies of 80% and more have been obtained. It is essential that inevitable wear will not be associated with decreased efficiency. Two types of axial-flow fan emerged from subsequent designs, viz. the constant-pressure type as developed by Schicht and the reaction-pressure

type.⁽¹⁹⁾ These types became predominant, and for further details the reader is referred to an interesting report by Andritzky.⁽²⁰⁾

However, about 40 years ago fans with efficiencies of 90 % were designed and it was hoped to use these new fans for exhaust purposes,⁽²¹⁾ but when tests began it was not long before important operational disturbances were reported. The fans began to vibrate so much that it became necessary to switch them off. When the fans were examined it was found that quite thick layers of dust had been deposited on the back of the blades which considerably reduced the spaces between the blades. When the fans were running, some of the dust fragments came away from the blades suddenly. The effect of this was to set up vibration and instability which made it necessary to stop the fan. The first attempt to overcome this problem consisted in allowing a small Laval jet, operated by compressed air, to move slowly to and fro over the whole width of the blade at fixed intervals of time. The apparatus is shown in Fig. 109a. The layers of dust deposited on the blades were removed as if they had been cut by a steel tool. Depending on the nature of dust it would be necessary to do this at intervals of days or once a week. Some of these installations are still operating satisfactorily today.

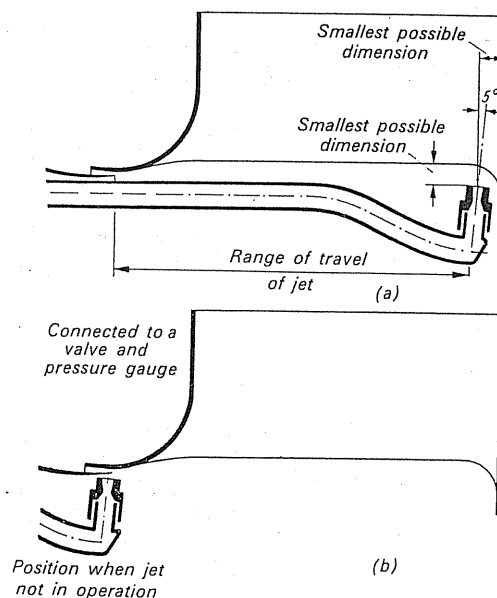


FIG. 109

However, a radical solution of the problem would involve the design of a radial-flow fan so that no dust would adhere to the blades. The highest possible efficiency would be achieved and wear reduced to a minimum.

The size of the particles of dust is an important factor in design. Tests have shown that only very fine dust adheres to the blades.

¹⁹ Eck, B., *Ventilatoren*, 4th edn., 1962.

²⁰ Andritzky, M., *Axial-flow fans for suction installations*, Braunkohle, 1943, p. 497.

²¹ Linsel, E., *Mine ventilating*, VDI-Z, 1953, p. 429.

At the entry to the impeller and also in the passage through the blade channels, dust becomes separated into two streams. On account of the 90° turn at the entry into the impeller the larger particles impinge on the impeller side plate and thereafter travel along it. Smaller particles, however, are rotated earlier and become separated from the larger particles relative to the impeller side plate. This is illustrated in Fig. 110a. It may be noted that

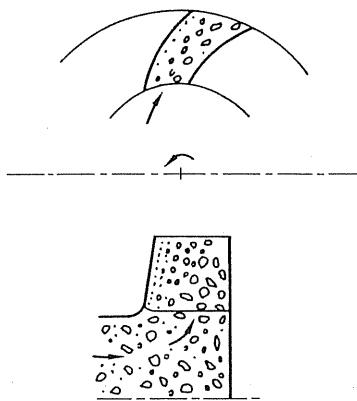


FIG. 110a.

after entry into the impeller ducts no more suction effect can be exerted on the solid particles. The particles will bounce to a greater or less extent on to the pressure side of the blade and they will rebound or continue to glide or roll along. The separation which occurs is shown in Fig. 110a. The larger particles move directly on to the pressure side, whilst the very fine dust will glide along the suction side. The explanation of the adhesion of the very fine dust is given by the results of research on turbulence and friction. One of the most important results of this research is that the roughness of a plate which is totally immersed in a fluid will only become significant if the particles suspended in the fluid exceed a certain size. The explanation is that even for turbulent-flow conditions, a very thin laminar surface layer, i.e. a laminar boundary layer, will be produced, inside of which any kind of roughness is just smoothed out and no increase of the laminar thrust forces takes place. The magnitude of these forces may be assessed fairly accurately. It is given by the equation

$$\frac{Wk_{zul}}{v} \approx 100,$$

where W is the velocity in the free stream and k_{zul} is the particle size which does not produce hydraulic roughness, so that the particle size in the boundary layer is known in relation to the velocity in the free stream. Apart from this, the average roughness of the various materials is related to the process by which they are manufactured. For rolled steel, as it is used in manufacturing, the average dimensions of the "projections and depression" are about 0.05–0.12 mm, i.e. 50–120 μ .

The following calculation is based on a relative velocity of 25 m/sec. This gives a circumferential velocity twice as large, i.e. about 50 m/sec. Therefore, according to the above

formula,

$$k = \frac{100v}{W} \frac{100 \times 15 \times 10^{-6}}{25} \times 10^6 \mu = 60 \mu,$$

which means that a boundary roughness of 60μ will have no significant effect. As a matter of fact, dust particles which adhere to the suction side are in most cases less than 60μ in diameter. These small particles therefore can be deposited in the depressions of the sheet-steel blades. Under these circumstances these particles will be situated in the boundary layer without being exposed to air currents, and thus these particles will be subject to analysis. Figure 110b shows a small particle in this situation. The centrifugal force acting on the particle is composed of a perpendicular force N and a tangential force Z . According to the

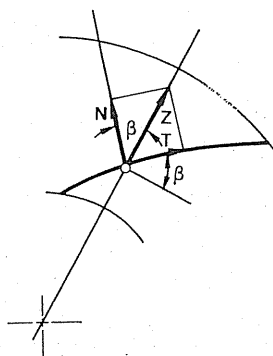


FIG. 110b.

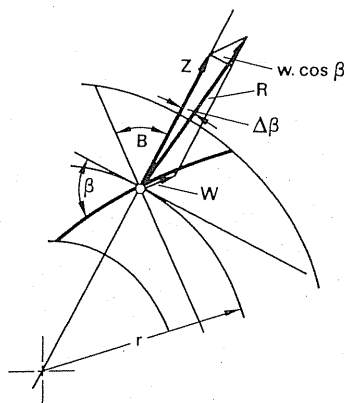


FIG. 110c.

well-known laws of friction, slip will occur, if the angle β is greater than the angle of friction, which is valid for particle and wall. This means that the blade angle will have to be slightly greater than the friction angle. The behaviour of the larger particles is schematically shown in Fig. 110c. It is clear that the particle is affected by the velocity W , which will depend on the thickness of the boundary layer. The forces acting on the particles are the centrifugal force Z and the resistance W . The resultant R is, however, inclined towards the

circumferential velocity by a small angle $\Delta\beta$. This means that the angle of friction will have to be increased by $\Delta\beta$, or, if β is the friction angle, these particles would have started to slip already. Figure 110c shows the following relationship:

$$\Delta\beta = \frac{W \cos \beta}{Z}.$$

Assuming as before that the local relative velocity is 25 m/sec and that the particle diameter is about 2 mm, one can also assume a quadratic law of resistance. Other assumptions are that the coefficient of resistance $\xi = 0.5$, and the local radius $r = 1$ m. With these data, the following empirical results can be obtained, if d_0 is the diameter of the particles:

$$\Delta\beta = \frac{W \cos \beta}{Z} = \frac{\pi d_0^2}{4} \frac{(\rho/2) \xi W 0.5 \mu \cos \beta}{(\pi d_0^3/6) \rho k \mu^2}$$

$$\Delta\beta = \frac{3}{4} \frac{\mu}{d_0} \frac{w_2^2 \gamma_2 \cos \beta}{u^2 \gamma_{\text{coll}}}$$

$$\Delta\beta^\circ = \frac{3}{16} \times 500 \times \frac{1.2}{1400} \times 0.707 \times 57.3 = 3.26^\circ.$$

Dependent on the particle size and the position of the boundary layer which—one can assume—will increase considerably towards the end of the blade, one will get for a given size of particle different angles of friction which are not only a function of the particle size but also of their position on the suction side of the blade.

Observations with a stroboscope have shown dust, e.g. lignite dust, settling on the suction side. Initially small spots appear; these become bigger until the whole suction side of the blade is covered with dust. When this side is covered, layers of dust are built up. Once the initial layers have been deposited, dust which settles subsequently will produce a pattern of its own.

It seems very likely that the outer end of the back of the blade plays a special role (see Fig. 110d). For backward-curved blades⁽²²⁾—and we are only concerned with such blades—separation of the stream occurs at A with only a small vortex formation. The position of A depends on the type of blade. Yet, even with the best of fans, small vortices can be expected. In all probability fine dust moves in a reverse direction at this point and then will

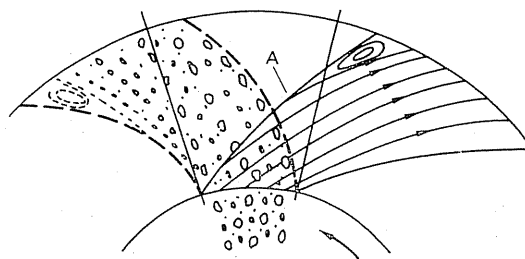


FIG. 110d.

²² The new development of radial flow fans, *Tech. Rundschau*, Bern, 1962, No. 20.

settle on the back of the blade. The circumferential velocity carries the smaller particles of dust, whereas the larger particles move towards one side of the back of the blade.

The total picture is complex according to the size of the particle. The effective angle of friction varies, and in fact as the particle is entrained by the stream of the boundary layer in one direction or another, the static friction angle will vary. It appears that the relative velocity will affect all but quite small particles. Accordingly one can state as an approximate rule that at the back of the blades the blade angle should exceed the angle of friction of the given dust. These blade angles vary between about 40° and 60° .

Complete solution of the problem could be achieved if the fan had a high efficiency. Analysis of the high-efficiency blower shows that high efficiency is associated with fairly small blade-angles.⁽²²⁾ The efficiencies increase if the blade angle is reduced to about 25° . It has already been noted that these angles must exceed the angle of friction if one wants to avoid deposition of dust, and the blading must therefore be designed in such a manner that the angles at the back of the blade just exceed the angles of friction. In practice this means that the blade angles on the suction side are approximately equal and lie within the range of 40 – 60° .

For high-efficiency fans optimum performance can be obtained only for certain ratios of blade width to the space between the blades, when, at the same time there are small blade angles. These criteria are also valid for fans moving dust-laden air, but there is another factor to consider. The passage of dust through the fan causes a certain amount of wear. For very narrow impellers considerable wear occurs on the impeller disc. In the case of very wide impellers wear is not uniform. It is essential to design a fan so that wear is uniform in order to achieve the longest possible working life. It is now possible to specify dimensions of the impeller.

The characteristics of three very good types are given in Fig. 111.

	φ	ψ	$\eta\%$	Type
I	0.13	1.1	86.5	27,500
II	0.2	0.95	87.5	28,50
III	0.3	0.75	81.0	28,65

The efficiencies of these fans are practically the same as those of high-performance fans, whilst the maximum volume flows are as high as those for the best axial-flow fans.

53. DOUBLE-ENTRY FAN

If one places two identical fans with their intakes facing outwards, then one has an arrangement similar to a double-entry fan. In ventilation work this type of fan is readily chosen because the volume can be easily increased. It is particularly advantageous when the location permits a *free* intake, i.e. there is no ductwork connected from, say, the atmosphere to the fan intake. Should the gas handled require that there be some form of ductwork, then

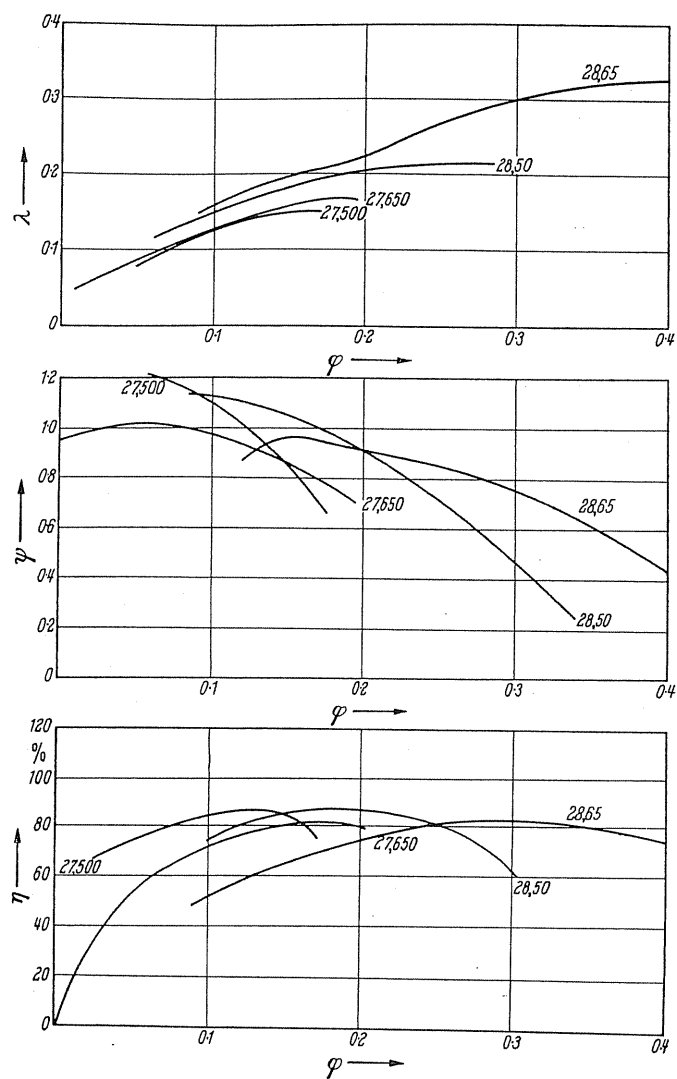
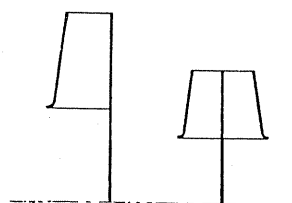


FIG.111. Radial fans with steep-angled blades of old and new design. Old type 27,650, new types 27,500, 28,50 and 28,65.



Single inlet	Double inlet
d_1	$d'_1 = d_1/\sqrt{2}$
F_1	$F'_1 = F_1/\sqrt{2}$
d_2	$d'_2 = d_2/\sqrt{2}$
n	$n' = n \sqrt{2}$
b_1	$b'_1 = b_1/\sqrt{2}$
b_2	$b'_2 = b_2/\sqrt{2}$

FIG.112. Single- and double-intake fans with equal output.

a complicated arrangement is required and the installation becomes altogether much more expensive than for a single-intake fan. As the bearing construction lies more or less in the suction opening, additional losses occur, so that the efficiency is always smaller than with single-entry fans.

The comparison given in Fig. 112 illustrates typical differences between a double- and single-inlet impeller. The volume, pressure, and peripheral velocities are identical. The impellers are geometrically similar.

The question now is which design is the most favourable if the outputs are identical. If a fan has a free intake then the following differences exist. While a single-intake fan can be supported from one side, the double-intake fan must have a shaft passing through the impeller which must be mounted on bearing supports on both sides. This leads to an obstruction in the entry. If the intake must be enclosed by ductwork, then two entry envelopes must be constructed and joined together for the double-entry fan. For the majority of cases the bearing must be installed within the suction envelopes so that considerable operational disadvantages arise in contrast to the single-intake fan. Therefore in both cases the double-entry fan is at a distinct disadvantage to the single-entry fan. However, an acoustical advantage does exist because of the staggered blade distribution in many of the sizes. By means of this we get double the rotational acoustic speed.

When the outputs are compared it is found that the main advantage of the double-entry fan is the small moment of inertia. With extremely large fans this is important because on starting up the plant a larger electric motor is required. Apart from this, only small mechanical advantages are obtained. The axial thrust is absent because both bearings are equally loaded, while a single-entry fan requires a thrust bearing (mainly segmental) and a heavy-duty bearing at the approach of the impeller. This presents no difficulty today.

54. DESIGN OF THE MULTIVANE IMPELLER (SIROCCO RUNNER)

In many applications a choice of fan is governed by the space available for its installation and the permissible noise level. One requires a design giving a minimal value for the coefficient δ . This problem was solved by the design of the multivane impeller. It is some 60 years old and is widely known. Its main features are its large diameter ratio, large relative width, and number of blades which are of the forward-curve design, thus forming a "drum". The original design of the Sirocco fan had the following dimensions:

$$d_1/d_2 = 0.875; \quad b = \frac{3}{5} d_2; \quad \beta_1 = 64^\circ; \quad \beta_2 = 22^\circ; \quad z = 54.$$

The blades were formed precisely as circular arcs.

This design received no attention in the field of research. Although the circular arc was blamed for the poor efficiency ($\eta = 50\%$), it has enjoyed a success unrivalled by any other design and has been manufactured in greater numbers than any other form of flow machine. Apart from its compactness it is remarkably silent in operation. There is no other fan which operates as silently at comparable pressures. One will find quiet operation a

criterion in many applications even if it is at the expense of efficiency. In this aspect the multivane impeller fulfils uncontested an important operational problem that is no less important today than it was in previous years.

This impeller differs quite considerably from others, and there is a lack of fundamental knowledge of the design and calculations.

(a) IMPELLER WIDTH

Air entering the radial impeller must be turned through an angle of 90° from the axis of the shaft. To avoid separation of flow it is reasonable to accelerate the flow, since the expected separations will behave in accordance with Fig. 65.

However, we find in multivane impellers that instead of an acceleration there is a considerable deceleration (around 2:1) which is created by the width of the blades. There are, however, ratios that would be impossible to obtain with certain bends. Bends with such

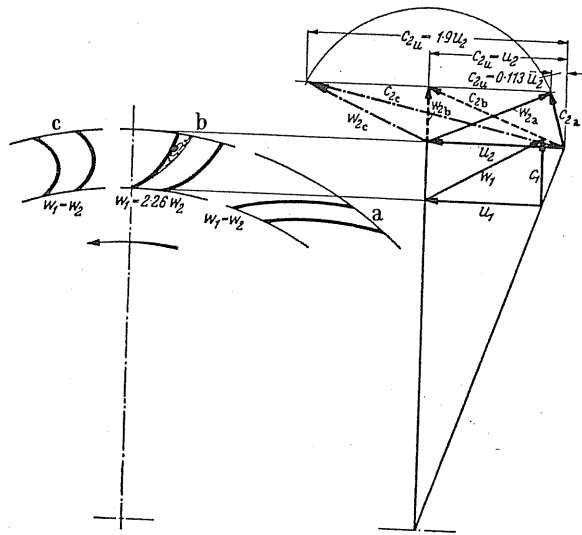


FIG. 113a. Investigation of various forms of blades in a multiblade impeller.

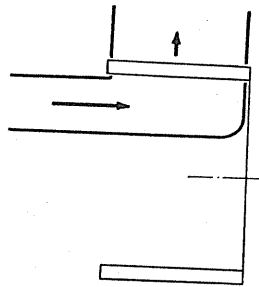


FIG. 113b. Stream of air entering a rotating impeller.

decelerations are unavoidable here, and they are responsible for pronounced separation of flow. In the case of multivane and high-performance impellers this separation of flow is not always seen. This means that other phenomena are concerned. The author considers another unknown factor to come into effect here, which is described as follows. According to Fig. 113a we consider a 90° bend with a large deceleration occurring with a pronounced separation of flow. Now at the surface of deflection, the blade cascade passes through an otherwise totally enclosed bend, in the manner indicated, perpendicular to the direction of flow. What will happen at this point then? At the point on the bend where the flow normally breaks away, the blade cascade imparts additional energy to the stream. The effect is probably so great that the air loses its tendency to flow separation and almost passes around the bend in a sharp right-angled sweep. Such flow is quite different from the normal flow at a bend.

(b) BLADE SHAPE

Because in attempting to achieve the highest possible value of d_1/d_2 the inlet diameter of the impeller is approximately established, the arguments for obtaining the most favourable blade angle lose their significance.

First of all, according to Fig. 113a for a ratio $d_1/d_2 = 0.85$ and an assumed blade angle of β_1 we will examine all the possible blade designs. Assuming $b_1 = b_2$, the corresponding c_u values are drawn on the diagram. Because we are dealing with blades which are particularly short in length it is hardly possible to permit *a deceleration of the relative velocity w in the blade passages which is worth mentioning*. The question concerning the form of blade design which is most suitable for maintaining a constant relative velocity w is closely related to this statement. In Fig. 113a all the possible cases are examined:

1. **Backward-curved blades (a).** When $w_1 = w_2$, a very small value of $c_{2u} = 0.113u_2$ is obtained. As deceleration does not occur here, the accompanying blade passage is acceptable. Special constructions make use of this fact.

2. **Radial-tipped blades (b).** This blade produces a marked deceleration. We get $w_2/w_1 = 0.443$, i.e. a value which with impellers of the *smallest* inside diameter is still possible. It is clear that this design is completely unsuitable. Figure 113a illustrates the large separation of flow which clearly causes further heavy losses.

3. **Forward-curved blades (c).** In this case the requirement $w_1 = w_2$ is easily fulfilled. It produces a blade design as illustrated by Fig. 113a. One obtains a value for $c_{2u} \approx 2u_2$ which means that a large pressure conversion is possible in this case. Therefore this blade design fulfils both requirements.

Therefore in practice the forward-curved blade has been almost exclusively employed in multivane impellers.

The problem now is how to obtain a large change of direction in a relatively short distance. A glance at Fig. 114 shows that c_{2u} increases as w_2 exceeds w_1 .

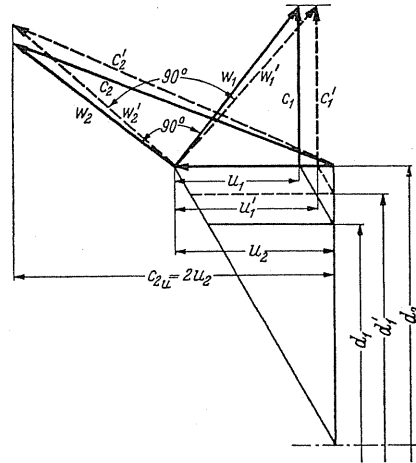


FIG.114. Velocity triangles for two diameter ratios at 90° deflection.

By studying the flow in the bend one can see that a change of direction of 90° is still possible if the average velocity is not reduced and the radius of curvature is selected as large as possible. This requirement $180^\circ - (\beta_1 + \beta_2) \leq 90^\circ$ with $w_1 = w_2$ and considering the continuity equation

$$\pi d_1 b_1 w_1 \sin \beta_1 = \pi d_2 b_2 w_2 \sin \beta_2 \quad \text{gives} \quad \sin \beta_2 = \sin \beta_1 \frac{d_1}{d_2}.$$

Therefore with $\beta_2 < \beta_1$ the following relationships result:

$$\begin{aligned} \tan \beta_1 &= \frac{d_2}{d_1}; \quad \tan \beta_2 = \frac{d_1}{d_2}; \quad \frac{c_{2u}}{u_2} = 1 + \frac{c_{1m}}{u_1} \frac{d_1}{d_2} = 1 + \tan \beta_1 \frac{d_1}{d_2} \\ &= 1 + \frac{d_2}{d_1} \frac{d_1}{d_2} = 2. \end{aligned}$$

Independent of d_1/d_2 , c_{2u} is twice as large as u_2 . This is valid for an infinite number of blades and no losses. Figure 114 illustrates the velocity triangles for two diameter ratios.

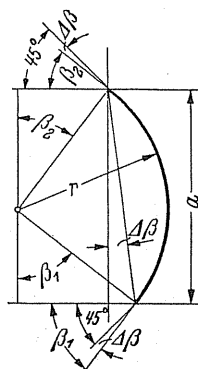
(c) NUMBER OF BLADES

The geometry of this blade is illustrated by Fig.115. It gives

$$a = r_2 - r_1 = r(\cos \beta_1 + \cos \beta_2); \quad \Delta\beta = \frac{1}{2} \frac{1 - (d_1/d_2)^2}{d_1/d_2}.$$

TABLE 8

d_1/d_2	0.8	0.85	0.9
$\Delta\beta^\circ$	12.9	9.35	6.05

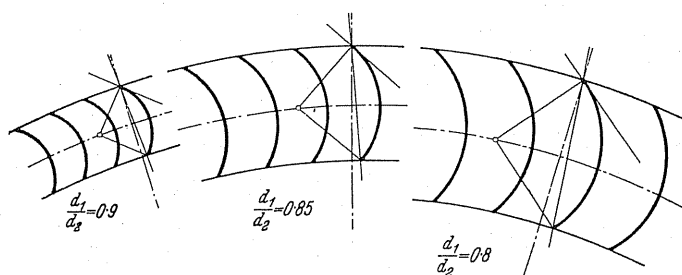
FIG.115. Geometrical relation of a circular arc blade rotated by $\Delta\beta^\circ$ with respect to the radius.

In relation to the pitch of the blade it can be said: that with $180^\circ - (\beta_1 + \beta_2) = 90^\circ$ a pitch t of $0.7-1.0 r$ should suffice. For the number of blades see Table 9.

TABLE 9

d_1/d_2	0.8	0.85	0.9	0.95
$t = 0.7 r$	64	85	127	254
$t = r$	44	60	89	178

With $t = 0.7 r$ blades result which are in accordance with Fig.116.

FIG.116. Blades of multivane impeller at $t = 0.7 r$.

(d) REACTION EFFECT

According to eqn. (10)

$$\Delta p = \frac{\rho}{2} (c_2^2 - c_1^2) + \frac{\rho}{2} (u_2^2 - u_1^2) + \frac{\rho}{2} (w_1^2 - w_2^2).$$

The static and kinetic components of the energy transfer are easily traced. Because in this case $w_1 = w_2$, the last term disappears so that the static pressure produced is given by

$$\Delta p_{\text{stat}} = \frac{\rho}{2} (u_2^2 - u_1^2) = \frac{\rho}{2} u_2^2 \left[1 - \left(\frac{d_1}{d_2} \right)^2 \right].$$

Substituting $\Delta p_{\text{total}} = \psi (\rho/2) u_2^2$ for the reaction effect we get

$$r = \frac{\Delta p_{\text{stat}}}{\Delta p_{\text{tot}}} = \frac{1}{\psi} \left[1 - \left(\frac{d_1}{d_2} \right)^2 \right]. \quad (134)$$

Because the coefficient ψ is approximately equal to 2, it becomes

$$r = \frac{1}{2} \left[1 - \left(\frac{d_1}{d_2} \right)^2 \right].$$

Table 10 gives the values for the reaction coefficient r for the usual diameter ratios d_1/d_2 ; from this one can see that the *reaction effect* for values of d_1/d_2 between 0.85 and 0.8, i.e. values at which it mostly occurs, is *only of the order of 15%*.

TABLE 10

d_1/d_2	0.8	0.85	0.9	0.95
r	0.18	0.139	0.095	0.049

(e) DETAILED STUDY

The previous considerations served as a preliminary examination of the situation; they do not give a comprehensive understanding of the newer development of multivane impellers.

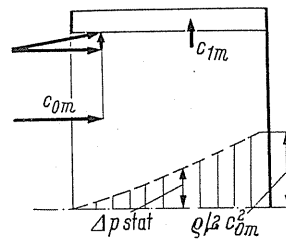


FIG. 117.

According to Fig. 114 the meridional velocity $c_{1m} \approx u_2$. If one is guided by the designs of today and selects $b \approx d_1/2$, then

$$V_2 = \pi d_1 b c_{1m} \approx \pi \frac{d_1}{2} d_1 u_2 = \frac{\pi d_2^2}{4} u_2 \varphi;$$

from which $\varphi = 2 (d_1/d_2)^2$.

TABLE 11

d_1/d_2	0.8	0.85	0.9
φ	1.28	1.45	1.62

Theoretically this would mean that abnormally high values for the coefficient φ are attainable. Actually, values in the order of $\varphi = 1\text{--}1.2$ are obtained today, so that the theoretical considerations are approximately established. Above all, these high φ values are only obtainable with the new blade shapes. In comparison, the earlier blades had values about 0.5–0.7.

If we consider the diameter ratio $d_1/d_2 = 0.9$ in conjunction with the coefficient $\varphi \approx 1$, which today is readily achieved, then the following ratios are obtained:

$$V = \varphi u_2 \frac{\pi}{4} d_2^2 = c_{0m} \frac{\pi d_1^2}{4} = c_{1m} \pi 0.5 d_1 d_1,$$

i.e.

$$c_{0m} = \varphi \left(\frac{d_2}{d_1} \right)^2 u_2 = \varphi \left(\frac{1}{0.9} \right)^2 u_2 = \varphi 1.235 u_2.$$

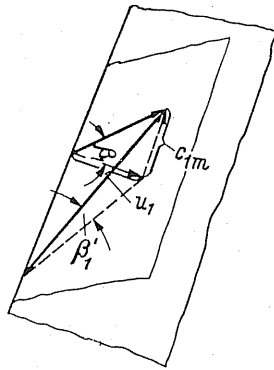


FIG. 118.

In the case where $\varphi = 1$,

$$c_{0m} = 1.235 u_2 = 1.37 u_1$$

which gives

$$c_{1m} = \frac{c_{0m}}{2} = 0.6175 u_2,$$

$$c_{2m} = 0.9 c_{1m} = 0.555 u_2.$$

It follows that the entry velocity c_{0m} is larger than u_2 , which means a drop in pressure at the entry of about $(\varrho/2) c_{0m}^2 = 1.52 (\varrho/2) u_2^2$, i.e. a drop in pressure related to the magnitude of the total pressure. Because c_{0m} decreases steadily to zero on account of the lateral downward stream, the blades yield a necessary static pressure gradient at the entry width in the order of $1.52 (\varrho/2) u_2^2$.

Now we will consider the flow entering an impeller at an angle. If we first of all assume a uniform distribution of $c_{1m} = 0.6175u_2$ for $b = d_1/2$, we get the air entering at a considerable angle. At the inner diameter of the shroud the angle to the axis is α_0 , which gives $\tan \alpha_0 = 0.6175$, so that the value of $\alpha_0 = 31.7^\circ$. This angle increases until the impeller disc is reached when $\alpha_0 = 90^\circ$. The blade will be set at a considerable angle at the inlet. There is no other fan which has a similar angle of incidence. First of all the effective blade angle at entry changes on account of the occupying in-flowing stream from

$$\tan \beta_1 = \frac{c_{1m}}{u_1} \quad \text{to} \quad \tan \beta'_1 = \frac{c_{1m}}{\sqrt{u_1^2 + c_{0m}^2}} \quad (\text{see Fig. 118})$$

$$\tan \beta'_1 = \tan \beta_1 \frac{1}{\sqrt{1 + (c_{0m}/u_1)^2}} = \frac{\tan \beta_1}{1.7} \quad \text{for} \quad d_1/d_2 = 0.9 \quad \text{and} \quad b = d_1/2.$$

Now if β_1 does not agree with the calculated figure and a much higher value is selected, it gives rise to shock, not one in the accepted sense, but an inclined shock illustrated in Fig. 119 where the eddies roll along the blade in the approximate direction of the axis. The assumption is that this inclined shock with an inclined separation of flow displays small losses in comparison with the frontal thrust because the boundary layer can perhaps deflect laterally. The first insight into the flow separation problem originates from Roy.⁽²³⁾ Roy gives an explanation for selecting a larger entry angle without incurring too much of a disadvantage. The "increased angle" has the advantage that the blade passage can be reduced. The meridian asymmetry can be effectively influenced by twisting the blades, twisting of the spiral tongue, or installing the tongue at an incline.

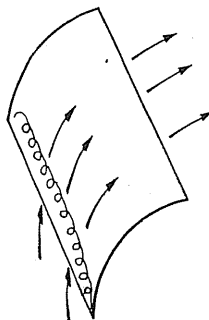


FIG. 119.

(f) BLADES WITH ACCELERATING BLADE PASSAGES

It has been recently shown that with high φ values the disturbance on entry could be damped down by a strong acceleration in the blade passages. Actually the present progress of the multivane impeller is due to this acceleration.

²³ Roy, M., The origin of eddy zones in flows with low viscosity, *WGL Vortrag Hannover*, 21 May 1959.

If blade design is accomplished in the simplest manner by profiling, it does not help to solve the problem for the reason amongst other factors that the weights of the blades would be excessive. In the case of wide blades, the resulting bending stresses would permit only very low peripheral velocities. For this reason pure sheet-metal blades or the newer discontinuous profiled blades have come into use. The existing blade forms arise from circular arcs. According to Fig. 120 we shall now consider such a blade with a pronounced acceleration. The acceleration will be obtained when β_2 is considerably smaller than β_1 . The ratios at the blade discharge are significantly different from those of all other fans.

The blade discharge is of a jet-like character. The blade stream is finally held in the cross-section a of the two walls and thus enclosed the stream can move freely. Naturally the circular arc still lies to the left of the angle γ . This gives rise to the question whether the stream can eventually be one-sided on this section.

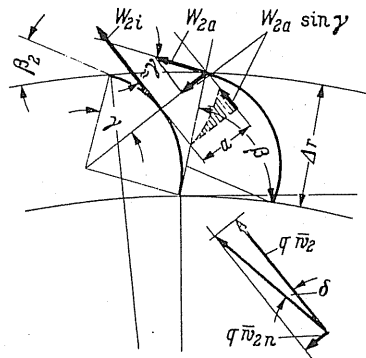


FIG. 120. Diagram of the main relationships in a strong accelerating flow of air between the blades.

Thus if we consider the discharge area a , the following picture will emerge. As a result of the curvature and the Coriolis force, the velocity on the inside is significantly greater than that on the outside, which means $w_{2i} > w_{2a}$. The second point is that the directions of these streamlines are somewhat different. The effects will now be considered.

The difference in velocity can be calculated approximately. For this we assume that the moment of rotation produces an average blade pressure $\bar{\Delta p}$. This is resolved in the following calculation:

$$\bar{\Delta p} \Delta r b u_m z = \Delta p_{\text{total}} V = \psi (\varrho/2) u_2^2 \varphi u_2 F_2$$

from which

$$\bar{\Delta p} = \psi (\varrho/2) u_2^2 \frac{2\pi\varphi}{z [1 - (d_1/d_2)^2]} \frac{r_2}{b},$$

so that we could insert reliable numerical values in this expression. We shall take as a basis the experimental results of a constructional type which was obtained with $\beta_2 = 0^\circ$, an angle of wrap $180^\circ - (\beta_1 + \beta_2) = 108^\circ$ and a new discontinuous profiling as in Fig. 121. $\psi = 3$; $\varphi = 1$; $\eta = 0.7$.

Upon substitution of these values

$$\bar{\Delta p} = (\varrho/2) u_2^2 1.42.$$

The mean value of w_2 is derived from $azbw_2 = V$, where V is the volume. One obtains the value here of $w_2 \approx u_2$.

The pressure discontinuity $\overline{\Delta p}$ at the front and rear sides of the blades can also be expressed in terms of Bernoulli's equation if we define the average excess velocity Δw as above or below the average value \bar{w}_2 , so that

$$\overline{\Delta p} = (\rho/2) [(\bar{w}_2 + \Delta w)^2 - (\bar{w}_2 - \Delta w)^2],$$

$$\overline{\Delta p} = (\rho/2) 4 \Delta w \bar{w}_2 = 1.42 (\rho/2) u_2^2,$$

$$\Delta w = 0.355 u_2.$$

The requisite values of a and γ for the purpose of further calculation are obtained from the drawing of the blade. The calculation is extremely complicated, but for our purpose an approximation will suffice.

$$a = t \left[\frac{t}{2R} + \sin \beta_2 \right]; \quad \tan \gamma = \frac{\cos \beta_2}{\sin \beta_2 + R/t}.$$

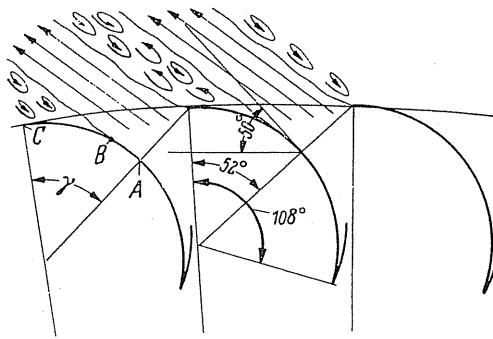


FIG. 121.

Together with a large change in velocity the discharge stream displays a *difference of direction*, which is approximately equivalent to γ . With this the discharging stream possesses a momentum perpendicular to $(w_2 + \Delta w) = w_{2i}$. This momentum deflects the free discharging stream so that it lies in the direction of the total momentum vector. This means a deflection to the periphery. The largest perpendicular component of momentum lies on the outside and acts with a velocity $(\bar{w}_2 - \Delta w) \sin \gamma$. This component steadily reduces to zero in the depth of the stream. If we assume a parabolic distribution for the reduction of the perpendicular component as in Fig. 120 in this manner we shall obtain an approximately correct ratio.

Thus with this an average value is realised:

$$\bar{w}_{2n} = \frac{1}{3} (\bar{w}_2 - \Delta w) \sin \gamma,$$

$$\bar{w}_{2n} = \frac{1}{3} (u_2 - 0.355 u_2) \sin \gamma$$

$$= \frac{1}{3} 0.645 u_2 \sin \gamma.$$

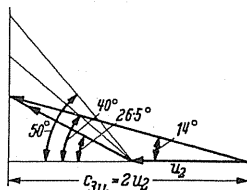


FIG. 122.

The total stream momentum can be resolved into two perpendicular components:

$$q \bar{w}_{2n} \quad \text{and} \quad q \bar{w}_2$$

(Fig. 120). With this the stream deflection is

$$\tan \delta = \frac{q \bar{w}_{2n}}{q \bar{w}_2} = \frac{\frac{1}{3} 0.645 u_2 \sin \gamma}{1.355 u_2}.$$

With $\gamma = 50^\circ$ it gives

$$\delta \approx 0.1645 \cong \approx 10^\circ.$$

This stream is also deflected *inwards* by approximately 10° . In strong contrast to all other problems, finite numbers of blades here give a decrease in the angle. With this the flow separation is found at point *B* instead of point *A* (Fig. 121). Between points *B* and *C* there is a zone where flow separation occurs. The streams discharging from the blade passages are separated by these eddy zones.

The turbulent mixing results in losses and has a tendency to stabilise the flow as well. The final direction can be obtained from the continuity of the stabilised flow providing that the relationship of the twist remains constant. Moreover, it will be found that a further decrease in the angle occurs. For our purpose we shall return to the previously mentioned test. With $\varphi = 1$ we get

$$V = c_{2m} \pi d_2 b = \varphi u_2 \frac{\pi d_2^2}{4}, \quad \frac{c_{2m}}{u_2} = \frac{1}{4} \frac{d_2}{b} = \frac{1}{2}.$$

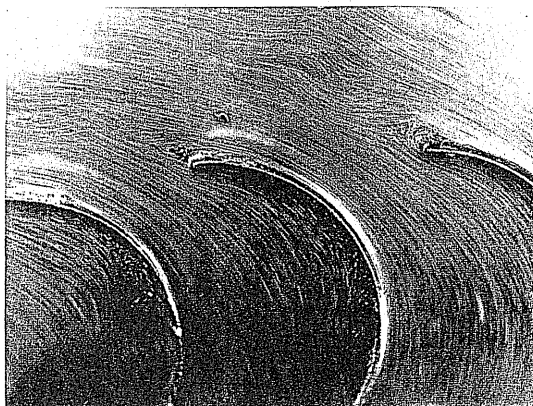


FIG. 123.

With this we can draw the actual diagram at the discharge point. This gives an actual relative angle of 26.5° and an absolute angle of 14° . The air is finally discharged with this angle at the periphery. The problem is characterised by a *double reduction* of the angle from 50° to 40° and from 40° to 26.5° (Fig. 122).

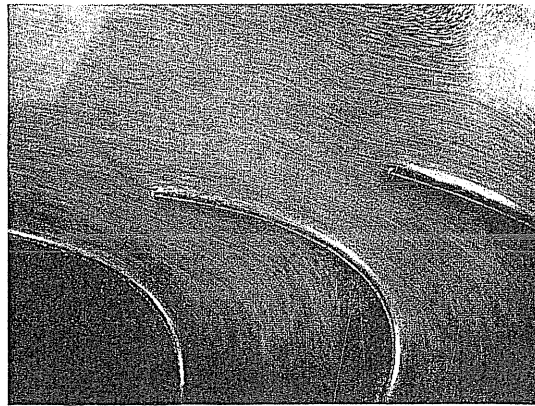


FIG. 124a.

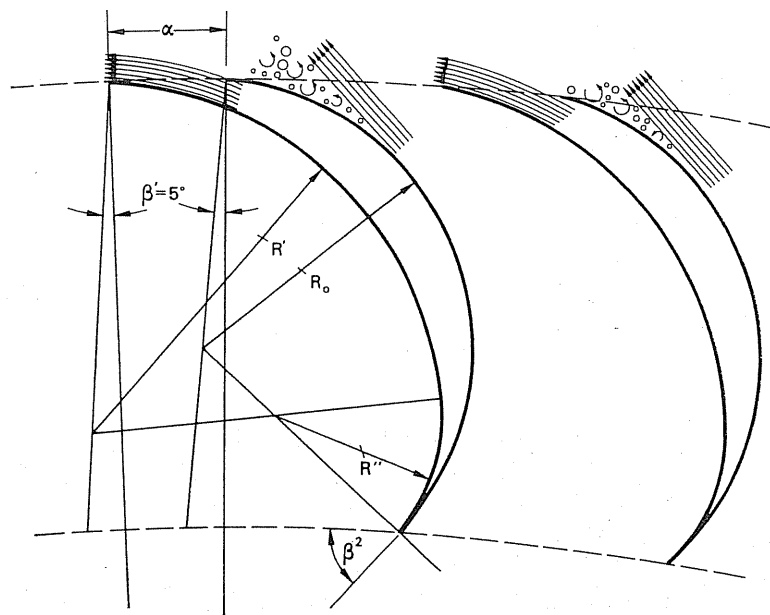


FIG. 124b.

During the course of experiments with multivane impellers the author found a typical eddy at the blade tip as illustrated in Fig. 123. It was also discovered that this eddy could be eliminated through suitable blade design (Figs. 124a and 124b).

(g) EXPERIMENTAL VALUES OBTAINED WITH MULTIVANE IMPELLERS

Economic production costs were the prime consideration with the previous form of multivane impeller. Such impellers are very simple and cheap if they are produced from sheet-metal stampings. By this method of production the circumference of the impeller is the sum of the unwrapped blades. The disadvantage with this type of construction is the blade spacing. This is often excessive. As the diameter ratios decrease, the resulting efficiency is reduced. The characteristics for the diameters 400, 130, and 78 mm were tested by the author under identical conditions and the results obtained are shown in Fig. 125. In the first case the efficiency is around 50%, then it reduces to 30%, and subsequently to 21%. By employing new blade forms the author secured a significant improvement for quite small impellers. Figure 126 shows an example where the efficiency could be raised from 22% to 37%. Subsequently small fans were developed which operated almost noiselessly.

As a result of recent research into multivane impellers, new blade shapes were obtained which gave definite optimum values.⁽²⁴⁾ Figure 127 shows a typical example of a model test (400 mm dia.) which gives an indication of what can be achieved today. In the layout, care must be exercised to avoid noise and any effects detrimental to the capacity. φ values of ≈ 1.2 and ψ values of ≈ 3.0 are obtainable. The efficiency related to the narrowest discharge cross-sectional area lies at 0.7 and rises somewhat higher with larger models.

There must be distinct differences between a datum referred to the smallest discharge cross-section and that referred to the design with an enlarged discharge area. The latter is

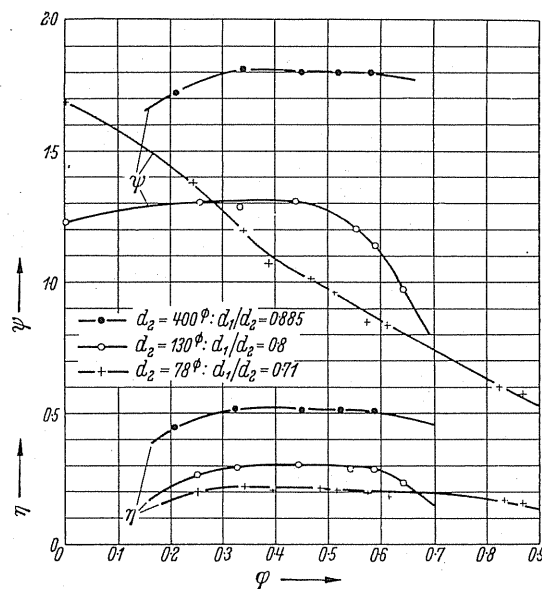


FIG. 125.

²⁴ According to DAS 1,047,980 wrapping angles between 115° and 145° were recommended for circular-arc blades.

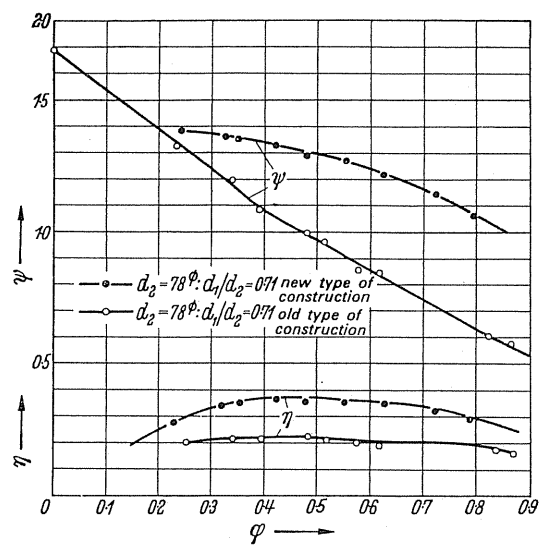


FIG. 126.

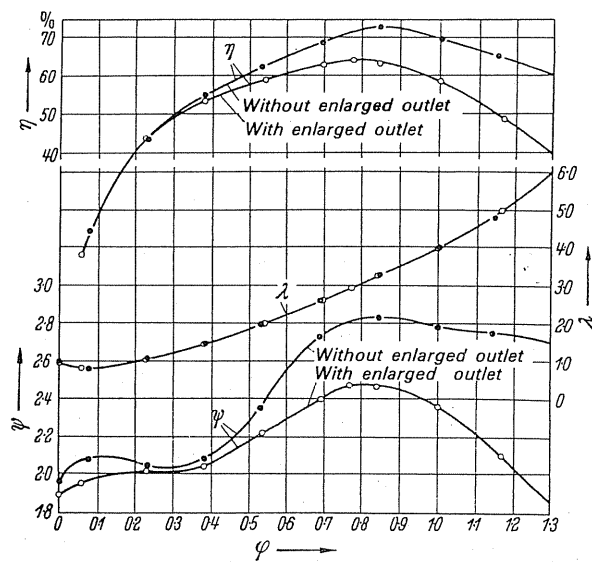


FIG. 127.

mostly employed in practice, because multivane impellers are almost always furnished with suddenly enlarged diffusers. The modern multivane impeller was developed by Messrs. P. Pollrich of Mönchen-Gladbach.

55. RADIAL IMPELLER WITH AN AXIAL PRE-RUNNER

In order to obtain better efficiencies with impellers of larger capacities (φ) and larger pressure coefficients (ψ) new methods have been evolved. To increase the blade area the axial intake was equipped with blades while at the same time the connected axial section possessed a jet-like restriction. These designs are illustrated in Fig. 128. For the purposes of manufacture the division of the blade along AB is necessary (Fig. 128a). A further variation of the same idea is that, according to Fig. 128b, a jet-like restricting pre-impeller, i.e. axial flow jet fan,

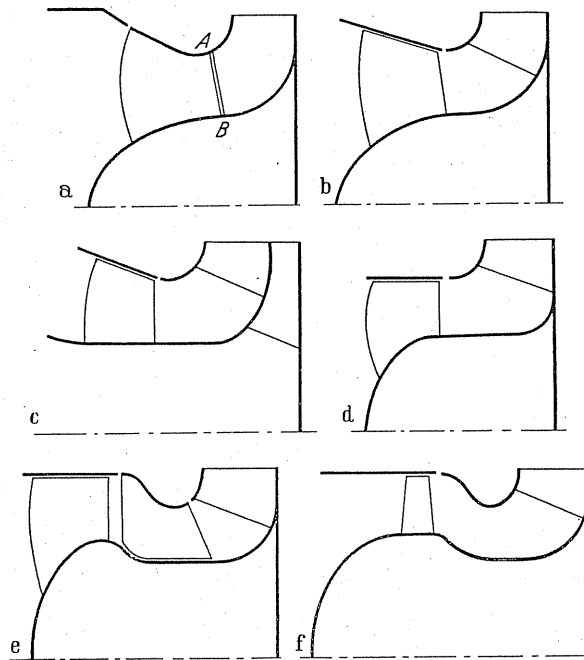


FIG. 128. (a) Impeller with a jet-like restriction in the intake. (b) Radial impeller with jet-like pre-runner. (c) Impeller as (b) but with an additional impeller with its intake through the hub. (d) Radial impeller with a meridionally accelerated axial flow impeller as a pre-runner. (e) Radial impeller with axial pre-runner whose outside diameter is larger than the intake diameter of the radial impeller and fitted with intermediate guide vanes. (f) A normal axial flow impeller whose outer diameter is in excess of the inlet diameter of the impeller inlet.

is connected in series with the radial impeller. To obtain a reduction of the meridional cross-section one could possibly use a hub with a rapidly increasing diameter, i.e. a spherical cone. Because the diameter of the hub must be proportionally large, it creates a relatively thicker core which introduces an unused "dead-space". If a problem should arise whereby it is required to produce the highest air output with the smallest space, according to Fig. 128c

one can guide the air through the hollow hub to a narrow terminal radial impeller which, because of its large radial depth, easily achieves the same pressure gradient as the main stream.

On account of the pre-runner the air receives a pre-rotation in the same direction as the movement of the impeller. As is already known from the experience derived with entry guide vanes, this produces an improvement in the performance of the main impeller. The larger blade entry angles into the radial impeller, which are now possible, yield favourable cross-sections which bring about an improvement of the impeller.

One might ask how the pre-runner should be arranged in order to yield a noticeable increase in the total pressure. It is evident that adequate peripheral velocities are required for the pre-runner. This condition is fulfilled only when the diameter ratio of the impellers is large, therefore the multivane impellers are most suitable, while impellers with small diameter ratios could hardly influence the total pressure even if they were fitted with a pre-runner. Moreover, the pressure coefficient of the selected pre-runner plays a decisive role. Because of this the meridian acceleration axial-flow impeller comes first into mind. Figure 128d schematically illustrates an arrangement with a meridian acceleration axial-flow impeller with a cylindrical outer cover connected in front. It is possible to achieve higher pressures by increasing the outside diameter of this pre-runner, so that it is larger than the entry diameter of the radial impeller. These designs provide new openings for even normal axial-flow impellers as illustrated by Fig. 128f. A further improvement of pressure is possible if one installs a permanent *guide-vane arrangement* between the pre-runner and the radial

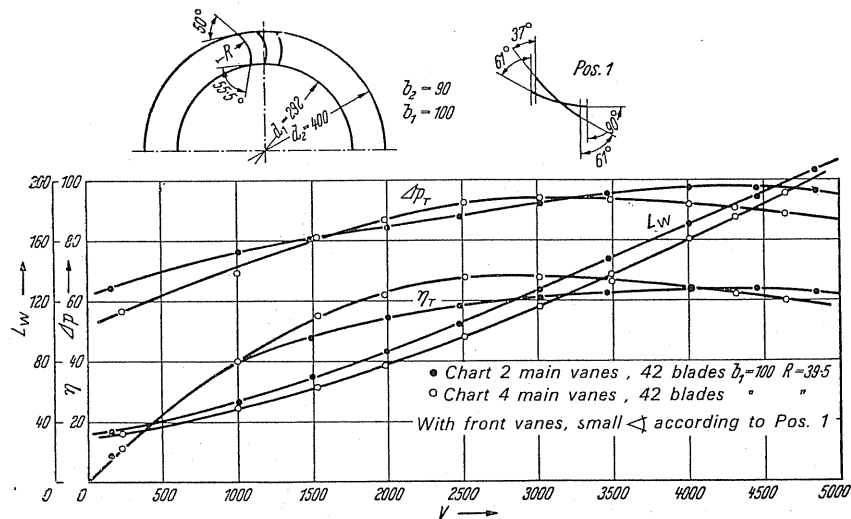


FIG. 129. Improvement of a multivane impeller with forward-curved blades.

impeller, as shown in Fig. 128e. With such designs constructed simply out of sheet metal it is possible to obtain a total pressure of around 800 mm WG whilst still maintaining moderate, noiseless, peripheral velocities.

All the arrangements illustrated by Fig. 128 are no more expensive than the simple fan with a volute casing, because the pre-runner only occupies the same intake space which is

already an integral part of the fan anyhow. This means that existing fans as well could be simply modified without having to resort to a new casing or additional ductwork.

Figure 129 illustrates an example where a multivane impeller with forward-curved blades was improved. From the characteristics obtained the improvement can be seen quite clearly. By this means it is quite typical to obtain an increase in efficiency while the capacity decreases.

CHAPTER X

CROSS-FLOW FANS. DOUBLE PASSAGE THROUGH CASCADE FANS

56. HISTORY OF THE DEVELOPMENT OF THE CROSS-FLOW FAN

As early as 1892 Mortier⁽¹⁾ sketched the detail of the cross-flow fan as illustrated by Fig. 130. By the turn of the century its application to mine ventilation⁽²⁾ had become widely known. However, it was soon displaced by the then superior Capell-and-Rateau fan. Subsequently many American inventors busily engaged themselves with the cross-flow fan

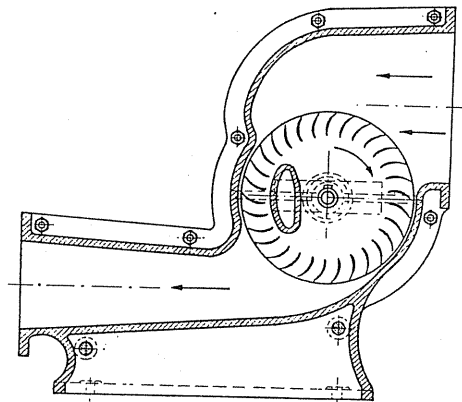


FIG. 130. Original fan of Mortier.

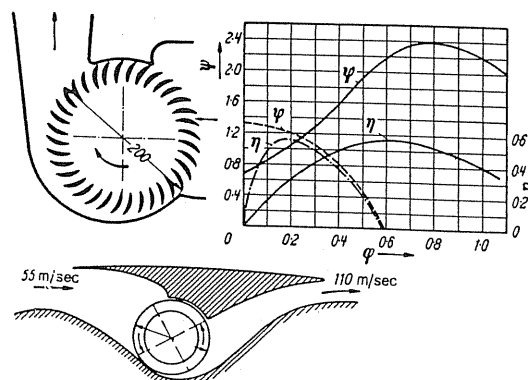


FIG. 131. Experiments of Sprenger (1938). (Broken line curves normal radial fan.)

¹ DRP 146,464.

² Thering, A.V., *Die Gebläse*, Berlin, Springer, 1903.

without any application being known or even apparent, whilst in Europe the fan remained almost completely forgotten; even the literature hardly mentioned it. So it is understandable that this type of fan had to be practically rediscovered in recent times. In 1938 an article by Ackeret⁽³⁾ appeared which made reference to the control of the boundary layer of aerofoil wings as being a possible application. In a footnote to this article mention was also made of the work of Sprenger in this field. Figure 131 illustrates the new feature, which is the profile blading, in contrast to the earlier design of Mortier and Schmarje.⁽⁴⁾ After the reference in the article by Ackeret, which aroused little interest, the subject appeared 21 years later in a publication of the Zürich circle.⁽⁵⁾

In constructing a small wind tunnel De Fries tried to keep the dimensions and noise level of the multivane impeller to a minimum. In doing so it was found that the impeller produced a sharply defined stream without a casing providing a firm guide arrangement was fitted internally. This property can be clearly demonstrated by Fig. 132, which shows a ball

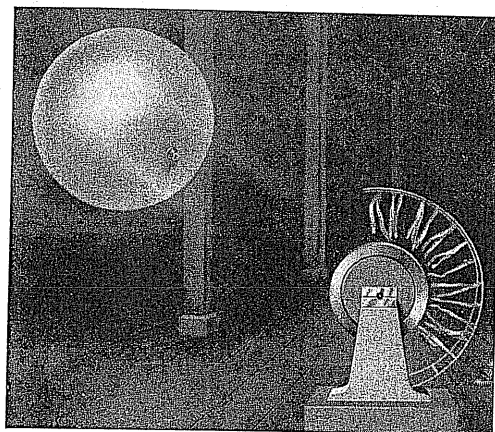


FIG. 132. Rubber ball held in suspension by multivane impeller with free suction and discharge.

held in suspension in the oblique stream. The author further found that this sharp stream can be enlarged by special walls and a method of diffusion so that a fan could be produced. Thus the installation of internal guide arrangements gave rise to a different method from that adopted with Mortier fans (Fig. 133). By this means one obtains the highest possible pressure coefficients, namely 2.5, ..., 3.5. The efficiencies lay around 55–58%. The first fan of this type was built in the author's laboratory at Cologne in 1948 to 1950.⁽⁶⁾ With this model the author went to Messrs. P. Pollrich in Mönchen-Gladbach and suggested that this concept be utilised. This suggestion was readily accepted by Messrs.

³ Ackeret, J., Present and future problems of aircraft propulsion, *Schweiz. Bauztg.*, 1938, No. 1.

⁴ DRP 242,076 (1910).

⁵ De Fries, J.R., 66 years of cross-flow fans, *VDI-Berichte*, 38 (1959). From this review one learns details of the work in Zürich from 1938. It is strange that neither numerous U.S.A. patents nor Schmarje patent DRP 242,076 were known to such a well-informed institute. Due to the outbreak of war, work in Zürich had obviously to be abandoned. De Fries states: "Sprenger did not later work intensively with cross-flow fans."

⁶ DP 807,978 of 8 February 1950.

Pollrich. The first short article was published in 1952.⁽⁷⁾ This publication might have value in stimulating interest in the study of cross-flow fans. Very probably the result has been that more work is being done on this problem. If one looks back through pre-war literature not leading to any practical applications, it is possible that no other publication or patents may be found preceding this publication of 1952. The term "cross-flow fan" was first proposed by the author.

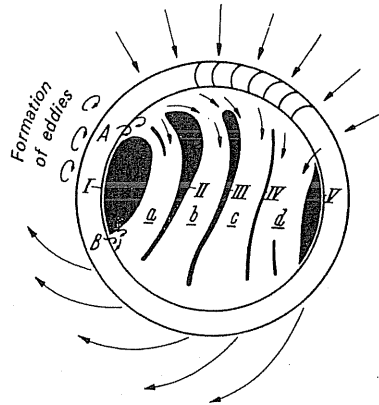


FIG. 133. Internal guide arrangement for a cross-flow fan.

During the co-operation in this work with Messrs. Pollrich a number of industrial applications soon followed: cross-flow fans for air curtains and induction fans for small waste gas flues have originated since that time. Most likely these were the first practical applications since Mortier, and this is most certainly true of Germany and Europe.

57. GENERAL PRINCIPLES OF DOUBLE PASSAGE THROUGH RADIAL BLADING

If we follow the path of a streamline in the case of a double traverse through the cascade impeller (Fig. 134), i.e. cross-flow fan, we find in fact there are *four* entries and exits, whereby the air flows radially inward and finally is discharged radially outwards. The first question which comes to mind is whether a blade arrangement exists where at all the four points the action involved is free from shock. Further one may ask: how efficient will be the transfer of energy with different blade angles? Because we get ratios which differ fundamentally from those of other types of fan, unknown elementary relationships must still be derived.

Velocity diagram. Figure 135 shows two pieces of the blade cascade and to ensure clarity the blade cascade has been unrolled into a straight line and the exit and entry of the air are drawn next to one another. For the case of the radial entry, i.e. free from pre-rotation, the applicable velocity triangles are illustrated above and below the cascade sections. The outlet angle at the periphery is β while the inlet angle assumes a radial discharge, i.e.

⁷ Eck, B., *Ventilatoren*, 2nd edn., Berlin/Göttingen/Heidelberg, Springer, 1952.

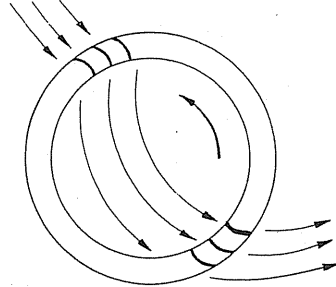


FIG. 134. Diagram of the flow through a cross-flow fan.

an angle of 90° . One can see immediately that the possibility exists in this case of achieving shock-free operation for both passages through the cascade. The total pressure is also proportional to Δc_u which is drawn as a thick line in all following diagrams for the sake of clearness. The general case where $c_{2m} > c_{1m}$ was considered.

Figure 135 illustrates the only case where shock-free operation is possible. Shock-free operation is possible only where the inlet angle is 90° (relatively radial in direction). The ratios which are given by other inlet angles are represented in Fig. 135. With these a shock

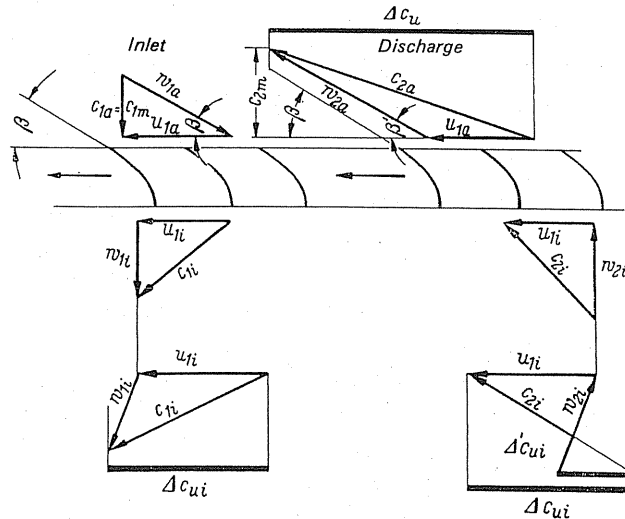


FIG. 135.

component originates on entry into the second cascade. Here one must exercise care to ensure that the flow relative to the cascade enters and leaves radially. Where the effects of a finite number of blades have to be considered, one can permit an angular increase of 15° .

According to the equation of momentum, only the entry and discharge are the decisive factors of the total blading for the overall transfer of energy. What happens between these points is really unimportant. This means that for the assessment of the theoretical pressure head, $\Delta c_{2u} - \Delta c_{1u}$ is the decisive quantity. Therefore if we define the factors on which the pressure head depends it will be sufficient to permit a study of the entry and discharge velocity

triangle for the whole impeller. On account of the double passage through the cascade yielding an identical angle β , both the discharge velocity triangles could be superimposed to simplify the following study.

We could go a step further and completely depart from the double passage impeller for a while. For the present it is sufficient to consider a simple cascade according to Fig. 136.

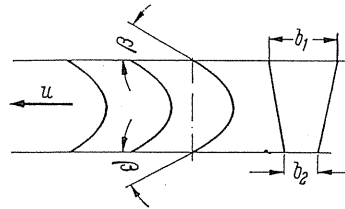


FIG. 136.

with straight blades and identical entry and exit angles. So that different meridional velocities can be obtained, there is a reduction in the blade spacing width from b_1 to b_2 . The simple hypothetical model permits the following analysis. The possible cases will be treated and, in particular, the influence of the blade angle β will be examined.

1. Radial entry (without pre-rotation); $c_{1m} = c_{2m}$ which means identical inlet and outlet curves. For all values of β there are velocity triangles whose apices lie on a perpendicular (two angles β and β' are examined at a given time). This means it does not matter which blade angle one selects. In each case $\Delta c_u = 2u$. With other values of β' the capacity changes considerably (Fig. 137, top).

2. Radial entry (without pre-rotation); $c_{1m} > c_{2m}$. The inlet curve is larger than the outlet curve in this case, which means the meridional velocity at the discharge is higher than it is at entry. The blade angle will be changed so that the corresponding values of the entry and discharge arcs remain constant, i.e.

$$\frac{c_{1m}}{c_{2m}} = \frac{c'_{1m}}{c'_{2m}}.$$

In this case there is also no resultant change of Δc_u , i.e. of the pressure, with a change in the angle β . In contrast to 1 the pressure is considerably increased. $\Delta c_u = 2.87u$ (Fig. 137, centre) (inverted where the inlet curve is less than the outlet curve).

3. Entry where pre-rotation is in the same direction as the impeller; $c_{1m} = c_{2m}$. The blade angle will be so changed that the direction α of the pre-rotation in the direction of the impeller remains the same (Fig. 137, lower). One sees that with angle β increasing, the value of Δc_u decreases and it is, of course, from $1.52u$ to $1.0u$. The resulting pressure reduction is strikingly large in consequence of the pre-rotation in the direction of the impeller. The deductible entry pre-rotation components are specially stressed in the representation so that a study without calculation is possible. This is valid for all the following diagrams.

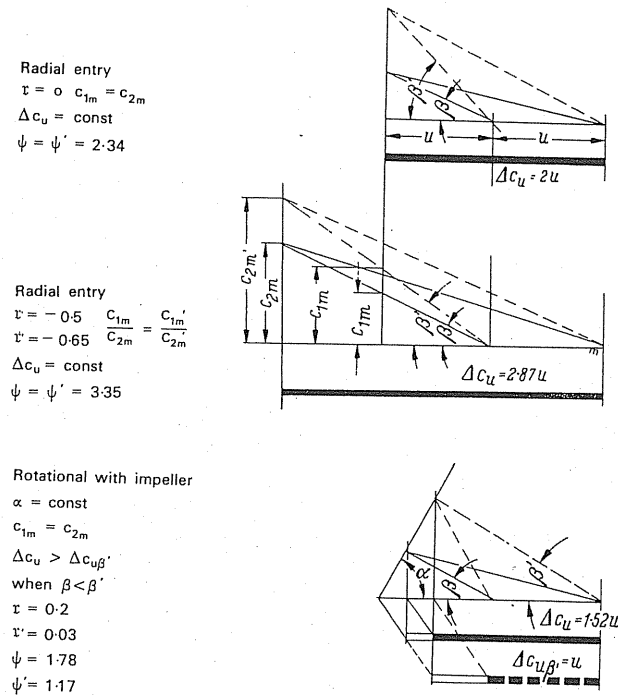


FIG. 137.

4. **Pre-rotation counter to impeller;** $c_{1m} = c_{2m}$. Also here the blade angle β will be so altered as to maintain a constant direction α for the counter pre-rotation. With an increase in the blade angle, Δc_u can only be increased from $2.654u$ to $2.97u$ (Fig. 138).

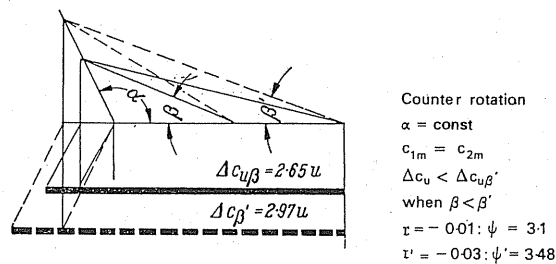


FIG. 138.

5. **Pre-rotation counter to impeller;** $c_{2m} > c_{1m}$; $\alpha = \text{constant}$. As in the previous case, the blade angle will be so altered to ensure a constant entry and discharge ratio, i.e.

$$\frac{c_{1m}}{c_{2m}} = \frac{c'_{1m}}{c'_{2m}}.$$

One will see with an alteration of the blade angle β , the pressure Δc_u only increases from $3.25u$ to $3.92u$. Extremely high pressure coefficients are characteristic here (Fig. 139).

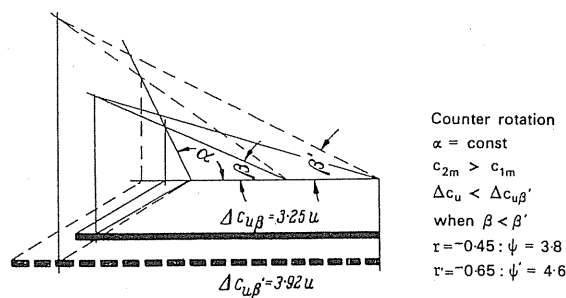


FIG. 139.

The results of this analysis can be summarised as follows. With irrotational entry no variation of the pressure results from a change in the blade angle. With positive and negative pre-rotation the apparent change is that with pre-rotation counter to the impeller, the pressure *increases* with larger blade angles and *decreases* in the case of pre-rotation with the impeller. Figure 140 illustrates this point.

We also firmly establish that *in the case of double passage impellers the blade design is reasonably independent of the pressure*. In all other cases the converse is true and there is a strong dependency of the pressure on the blade angle β .

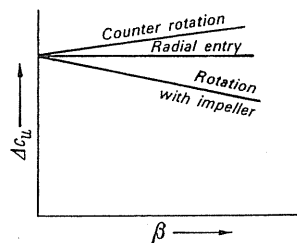


FIG. 140.

It is significant to note the influence exercised over the pressure by positive and negative pre-rotations. Pressure is similarly affected by the ratio c_{1m}/c_{2m} , i.e. the ratio of the inlet and outlet blade curves. The moment one makes the outlet curve considerably smaller than the inlet curve it is possible to obtain a significantly increased pressure. The pressure coefficients obtained with cross-flow fans can be examined with relative ease if we resort to the equation previously derived,

$$\psi = 2\eta \varepsilon \frac{\Delta c_u}{u}.$$

Assuming an average value of $\eta = 0.65$ and for the influence exerted by a finite number of blade $\varepsilon = 0.8$ (mean value) we get from the above diagrams the limiting boundary $\psi = 1.04$ ($\Delta c_u/u$). According to the diagrams the values of $\Delta c_u/u$ are within the boundaries

$$1 < \frac{\Delta c_u}{u} < 4.$$

Therefore we obtain $1.04 < \psi < 4.16$. This value is in reasonable agreement with values obtained in practice.

(a) REACTION EFFECT ω

For the purpose of calculating the reaction effect we consider

$$r_{th} = \frac{\Delta p_{stat th}}{\Delta p_{total th}} = \frac{\rho u \Delta c_u - (\rho/2)(c_2^2 - c_1^2)}{\rho u \Delta c_u} = 1 - \frac{c_2^2 - c_1^2}{2u \Delta c_u}. \quad (135)$$

In this form the equation may be used for the evaluation of the reaction effect from the diagrams (Figs. 137-9).

In case 1 we get a zero value; case 2 produces a large negative value -0.5 and -0.65 ; case 3 yields positive values of 0.2 and 0.03 ; while case 4 yields low values around the zero -0.01 to 0.03 ; and in case 5 a large negative value arises, -0.45 to -0.65 .

In general, the reaction oscillates around zero, which means that throughout it deals with *similar pressure fans*, with higher pressures it yields a negative value. This theoretical value is increased somewhat by consideration of the efficiency and a finite number of blades. However, despite this the rule still stands whereby the reaction is around zero and this is borne out by actual measurement.

These fans are more or less *producers of velocity pressures of air*.

(b) SELECTION OF THE DIAMETER RATIO
AND OF THE BLADE ANGLE

With an alteration of the diameter ratios there are a number of advantages and disadvantages which must be carefully assessed in each case. For the first flow in cross-flow fans it is a necessary condition to have a *decrease* of the relative velocity and for the second flow an *increase* is essential. The deceleration is what one might term as a necessary evil, while the acceleration at the second passage through the cascade is absolutely essential in order to achieve a high blade loading. If one reduces the diameter ratio of the impeller, the resultant deceleration as well as acceleration becomes smaller. The small advantage obtained by this means at the first passage through the impeller is negated somewhat by the disadvantage incurred with a reduced acceleration at the second passage. Naturally the degree of change involved in this process is dependent upon the blade angle. In the case of small blade angles the resultant accelerations and decelerations are larger than with larger blade angles, so that in the first case to achieve a balance a smaller internal inside diameter is necessary than with larger blade angles. Because the magnitude of the blade angles primarily governs the capacity afterwards, one must choose a suitable diameter ratio. Throughout one can assume $0.85 > d_1/d_2 > 0.7$. One cannot give precise numerical values because the shape of the housing also exerts an influence. There remains little to be done except to establish the optimum arrangement by experiment. For small designs the flow can be rendered visible in experiments by some means or other in order that the blade angle can be so adjusted that the main streamlines do not display signs of separation.

58. VORTEX MOTIONS WITHIN THE IMPELLER

For some considerable time the author has studied the flow in a cross-flow fan. The flow was rendered visible to facilitate the study. The author found that a vortex existed acting to one side of the periphery on the inside of the impeller, which dominates the whole stream. Figure 141 shows this phenomenon quite clearly. It is almost a precise potential vortex.

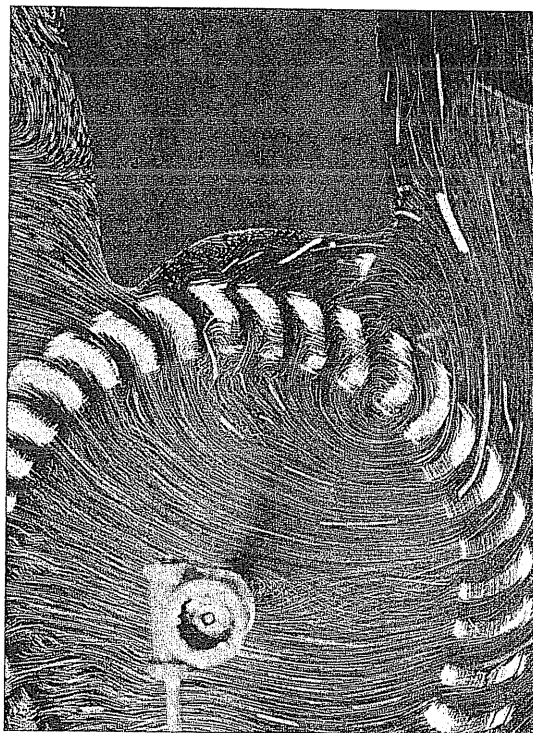


FIG. 141.

The vortex centre lies somewhere on the inner edge of the blade. Depending upon the throttling circumstances, the vortex centre moves towards the periphery.

The discovery of this vortex structure within the impeller was a decisive turning point in the development of this type of fan.

Fortunately it is already possible to calculate the vortex motion in a comparatively simple manner. For this purpose, according to Fig. 142, we will assume that the vortex centre is located at point O on the edge of a circle of diameter d . According to our previous analysis it will be assumed that a constant velocity c_u exists at the periphery of the circle. It is possible to prove that this eddy motion is a simple potential vortex. For this it must be proved that the ρc is constant. From the triangle AOC we get $\rho = 2r \cos \alpha/2$; further, it gives $c_u/(\cos \alpha/2)$. With this

$$\rho c = 2r \cos \alpha/2 \frac{c_u}{\cos \alpha/2} = 2r c_u = d c_u = \text{const.}$$

motion a turning eddy of equal strength asymmetrically opposed, left and right of the vortex O , at O_1 and O_2 (Fig. 143). These vortices have the characteristic of inducing velocities only perpendicular to the periphery of the circle which passes through them, i.e. c_u constant is unaltered. The flow pattern which now occurs is illustrated by Fig. 143; and it comes close to the actual pattern. A characteristic of this flow is that on the inside it is strongly accelerated. The magnitudes of the entry and outlet curves are indicated by heavy lines in Fig. 143, which permits easy recognition of the situation that exists in the majority

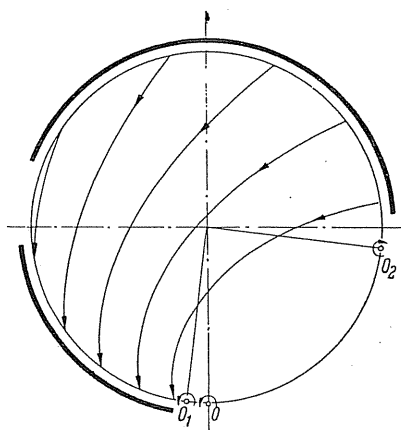


FIG. 143.

of cases with reactive fans. Such cases were also examined theoretically by Coester. It is significant that almost all the flows could be obtained by superposition purely according to the rules of drawing.⁽⁹⁾ A small disturbance arises by the fact that at O_1 and O_2 additional singularities appear. This defect could be easily overcome if one sets into operation a "line-like" eddy distribution instead of a single eddy. The deceleration on the inside could be achieved in an analogous manner.

The user may ask how it is possible to bring the flow to an orderly arrangement on the inside of the impeller. This is possible by resorting to suitable external measures, i.e. the casing.

Also it is possible to state that the eddy or vortex motion at the inside of the impeller arises from a vortex with a freely moving vortex core, which can wander around according to circumstances. The streamlines on the inside could be determined with relatively simple means. In a simple symmetrical case the distribution of c_m is proportional to $\tan \alpha/2$.

59. VORTEX CONTROL

Firstly, after finding the free internal vortex during the course of his work the author finally came to the decision that this vortex can be controlled by appropriate measures applied internally and externally to the impeller. By these means the characteristic can be altered. According to the means selected, the eddy can be controlled to produce a fan with

⁹ Eck, B., *Technische Strömungslehre*, 6th edn., Berlin/Göttingen/Heidelberg, Springer, 1961.

smaller capacities and larger pressure coefficients or vice versa. Moreover, further regulation can be effected through the positioning of a suitable arrangement.

A back flow of the air already transmitted to the inside of the impeller is caused by the unavoidable internal vortex. This back flow is responsible for a loss of energy which can be quite considerable. The efficiency of a fan will depend on the proportion of the total volume this circulating back flow represents. Depending upon the means chosen for controlling the vortex this volume can be relatively *small* or very *large* according to the circumstances. Figure 144 illustrates two cases: (a) with a small back flow, and (b) with a larger back flow. In favourable cases one-third of the total flow is effected by this circulation. This proportion can be increased to half and possibly more of the volume flow. If one were to assess a fan approximately in terms of these proportions, then an efficiency of approximately 65% would result.

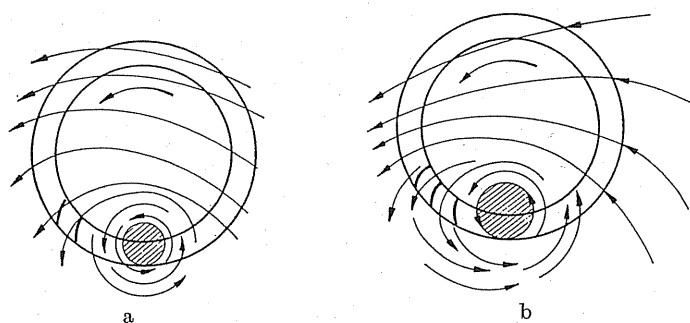


FIG. 144.

It is extremely interesting to compare this discussion and the earlier views of Mortier. Mortier employed a means which, for the sake of clarity, is shown in Fig. 145a, together with more recent methods. He used an "internal displacer" which served the following purpose: "to prevent the air drawn through the impeller vane from rotating with the impeller, so that the air is forced to emerge again from the lower blade and as a result has a continuous wake from above."

Firstly, tests were made in order to achieve control on the inside, and special guide blades were employed for this purpose. Figure 133 has already shown this arrangement. It shows that even with one blade, effects were produced. Through a relatively small rotary displacement of the internal guides or an independent internal blade, a significant amount of regulation could be achieved. However, measures adopted for the casing are more important.

For 60 years it has been the accepted custom to separate the suction and pressure zones by a partition which according to Fig. 145a has a narrow, concentric clearance between it and the impeller so that a straight "pick up" is avoided. Mortier gave an account of this arrangement which was left exactly as he described it by all the later inventors (e.g. see Figs. 130 and 131).

The overall development of reactive fans received a considerable stimulus with the appearance of a new design in 1953 (DP 963,809). For the very first time the space between casing and impeller was widely extended, so that at this point instead of having the usual fine clearance there was a large gap. Because of this gap a balancing of the suction and pressure

zones could take place. It was then found that the concentric gap according to Fig. 145*b* could even be improved by profiling so that the gap reduced radially in the direction of rotation. Variations of this form of gap are illustrated by the examples in Fig. 145, *c-h*.

By these means a smoother confluence of the suction and pressure zones can be obtained and this is a significant improvement on the design of Mortier. Figure 146 shows two characteristics of the experiments of that time which along with an improvement of the efficiency show a larger capacity.

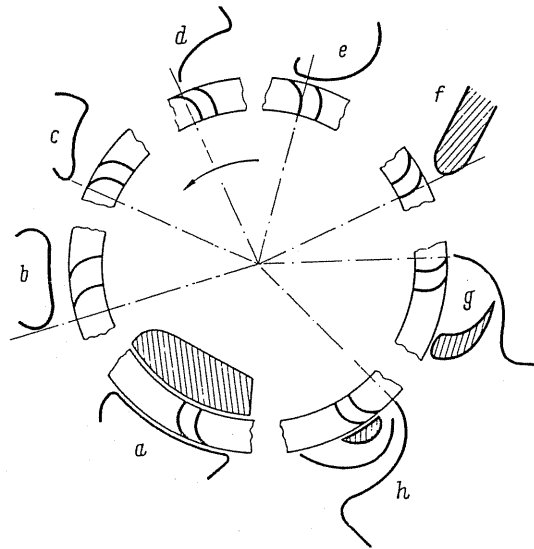


FIG. 145.

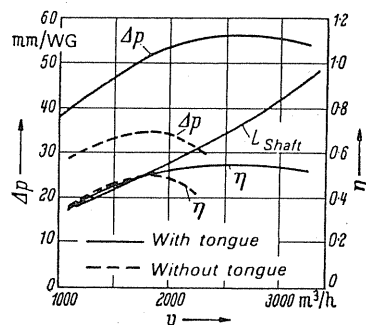


FIG. 146.

Of particular interest in application are the fans of large capacities and small dimensions. To this end it was important to maintain the circulating volume according to Fig. 144 at lowest possible level. Figure 145*f* already shows an arrangement to meet this requirement to within a reasonable margin. In an extreme case one would presume the tongue would fulfil this requirement with a simple sharp plate design (Fig. 147*a*). This design is not of practical use mainly because of the loud whistling noise the fan produces. The author, therefore,

developed a new fan. The tongue was developed to form a narrow blade cascade, as shown in Fig. 147*b*, in order to guide the recirculation around it along a very narrow space. In addition it gave a boundary-layer suction for the diffuser as well as the possibility of greater deceleration. There is a significant possibility of obtaining almost arbitrary characteristics (also stable) by suitably designing the cascade.

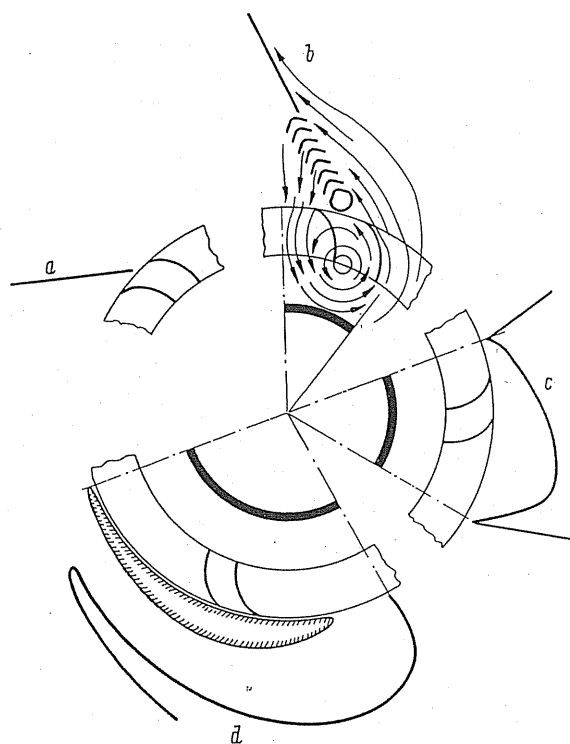


FIG. 147.

A further group for vortex control is composed of the "pocket type". The outside back-flow can be completely isolated by such pockets from the rest of the fan. This idea has already been indicated earlier by Palin⁽¹⁰⁾ and the more recent designs are modifications of the basic idea. Figure 147*c* illustrates the earlier suggestion of Palin, while Fig. 147*d* represents a new design by Coester. The pocket arrangement is well suited to designs requiring a small volume at high pressures; however, there are large circulating volumes which are costly. The thickly drawn lines in Fig. 147 indicate the circumferential ranges necessary for the different designs. These peripheral angles are a rough scale for judging the magnitude of the circulating volumes. One will note the differences are considerable.

¹⁰ DRP 471,551.

THE FLOW IN THE IMPELLER AT ZERO DELIVERY

It is very characteristic that in the case of zero delivery, i.e. completely throttled condition, the asymmetry of the impeller stream remains unchanged. After observations of the flow, the streamlines obtained are shown by Fig.148. It depicts two circular streams such

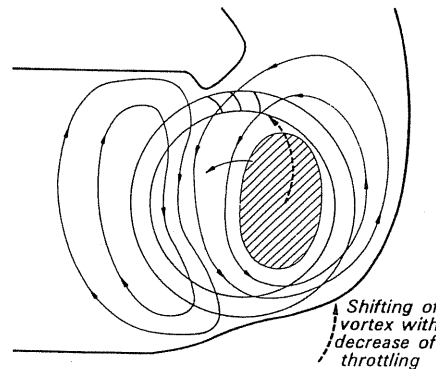


FIG.148.

that the pressure and suction zones each display an enclosed circulation. The vortex core is displaced towards the inside and simultaneously against the direction of rotation. The enclosed circulation of the suction zone shows no perceptible vortex centre point. It is significant to find the condition in this case where the streamlines within the impeller have the same curvature as exists with other larger circulations in the pressure zone. The overall picture of Fig.142 remains somewhat the same in that the vortex core lies at approximately half the radius. Figure 147*b* modifies this pattern.

60. ARRANGEMENT OF THE DIFFUSERS OF CROSS-FLOW FANS

The mostly negative reaction effect of the cross-flow fan shows that this type of fan gives primarily *velocity pressure*. To obtain a static pressure above atmospheric pressure, the velocity head at discharge must be converted into pressure. The efficiency of this type of fan stands or falls by the effectiveness of the diffuser. Now the construction of the diffuser is particularly difficult, because the velocity and also the energy profile exhibit a strong concentration at the discharge from the impeller on the tongue side. Figure 149 shows an energy profile as it appears without suitable vortex control. To add to that, the low energy side or its boundary layer has a considerable distance to travel before reaching the enclosed diffuser section. Because the velocity gradients are very small as well, the separation of flow criterion is quickly reached. In the case of normal diffusers, owing to the turbulent mixture, the boundary layer is again always supplied with energy so that a separation of flow can be avoided. For the low energy side this is much more difficult with reactive dif-

fusers. There an effect which was first detected with the volute casing as being extremely useful assists us in our problem. Namely it was found that a curved volute with a diffuser effect superimposes a secondary circulation upon the main stream (see Fig. 202). These secondary circulations produce the same effect in a curved diffuser as the known turbulent flow. Recent experiments of Sprenger⁽¹¹⁾ with comparatively flat sections, and having a curved path,

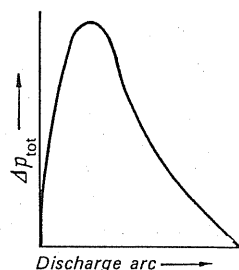


FIG. 149.

have shown that they can generate such secondary flow. In the case of sections having a small width in relation to their height this effect mainly disappears. This means for good reactive diffusers the ratio of the impeller width to the height at the diffuser entry should lie between 2:1 and 1:1. Depending upon the circumstances, the step diffuser has also the same effect but with low Reynolds number produces a particularly strong rolling up vortex.

A recent proposal of the author is, according to Fig. 147b, to use vortex control for boundary-layer control in order to achieve a very pronounced enlargement and good diffuser efficiency. Further, one can often artificially assist the formation of the secondary flow if, according to Sprenger, one employs special guiding or control surfaces in the diffuser.

The author also found that a break-up of the unequal energy distribution is possible if one fits guide vanes or a similar arrangement on the intake side so that at the beginning rotation with the impeller, then irrotational entry and finally counter rotation is produced (Fig. 150).

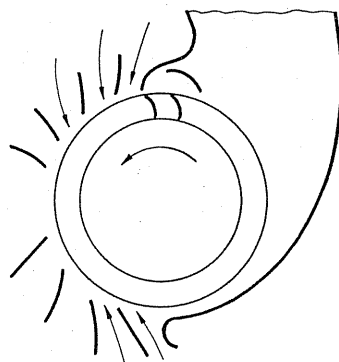


FIG. 150.

¹¹ Sprenger, H., *Experimental Investigations of Straight and Curved Diffusers*, Report of the Institute of Aerodynamics, Zürich, 1958.

61. THEORETICAL AND ACTUAL CHARACTERISTICS

The theoretical total pressure increase varies with the volume flow. The behaviour is the same in all the previously described cases so that it will suffice to examine the first case. Figure 151 illustrates this investigation. With a change in the volume flow the operating point wanders along the arm of the blade angle β . For a smaller volume it gives, for example, the point B with a smaller $\Delta c_u'$, while in the case of larger volumes the point C arises with a larger value for $\Delta c_u''$ as in the case of the previously described forward-curved blades. The total pressure reduces linearly with smaller volume till reaching $\psi = 2$ at the point of zero volume flow.

In order to obtain the actual characteristics, we plot first of all the friction losses which, according to our earlier study, are given by a parabola of $\varphi = 0$; finally, the parabola of the shock-losses is plotted on the graph from the turning point. By this means we obtain a characteristic (Fig. 152) which is close to the actual curve.

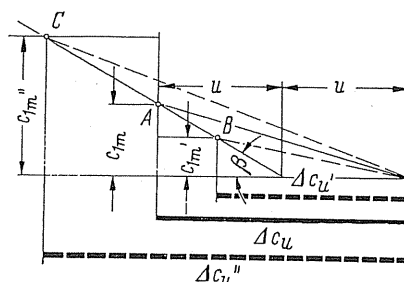


FIG. 151.

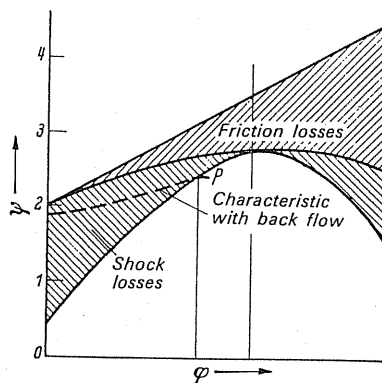


FIG. 152.

The decaying branch of the characteristic to $\varphi = 0$ is a usual feature. Correspondingly it gives an extremely small value when operating at low and zero volumes as was similarly observed in multivane impellers. For different applications the decaying branch indicates an unstable characteristic which can produce complications with fans operating in parallel.

Operationally the steep gradient of the decaying branch can be effectively reduced by bleeding some of the discharged air back into the fan at a definite point around P . By this

means it is possible to obtain a point below which the branch will no longer fall. Figure 152 illustrates the correction as a dotted line extending from point P to $\varphi = 0$.

By the new arrangement shown in Fig. 147b it is possible to influence the characteristic externally, making it stable or even extremely stable, i.e. with steeply falling lines.

62. CHARACTERISTICS, EFFICIENCY, EVALUATION, APPLICATIONS

With cross-flow fans the "through-put" stream of the impeller is unsteady. Because of this the main equation of motion⁽¹²⁾ changes with respect to its characteristic term

$$e \int_1^2 \frac{\partial c}{\partial t} ds.$$

Another effect in consequence of this form of motion is that the blade-tip discharge is not necessarily identical with the tangent to the blade. Most probably the influence is small as long as the radial depth of the blade is very small. In his investigations Coester came to the conclusion that this factor was not overcome by the magnitude of the blade friction. Perhaps undoubted advantage may ensue from the character of unsteady flow.

It is very important that the volume flow at the blades near the core has a greater velocity, i.e. considerably larger Reynolds number than with other types of flow machine. This higher Reynolds number, together with the possible reduction of friction because of non-steady admission, may be the reason for designing a cross-flow fan to give efficiencies worthy of consideration whereas *axial flow* and *radial* machines already possess poor efficiencies. N. Laing, Stuttgart, is particularly responsible for the work done in this field. Other types of centrifugal machine have a considerable fall in efficiency with smaller dimensions and exhibit efficiencies of around 10–15% in many applications.

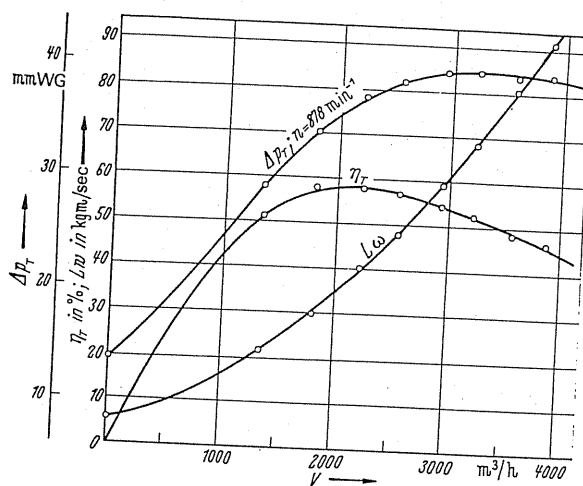


FIG. 153. Characteristics of a cross-flow impeller according to Fig. 145b.

¹² See, for example, Eck, *Technische Strömungslehre*, 7th edn., Berlin/Göttingen/Heidelberg, Springer, 1966.

61. THEORETICAL AND ACTUAL CHARACTERISTICS

The theoretical total pressure increase varies with the volume flow. The behaviour is the same in all the previously described cases so that it will suffice to examine the first case. Figure 151 illustrates this investigation. With a change in the volume flow the operating point wanders along the arm of the blade angle β . For a smaller volume it gives, for example, the point B with a smaller $\Delta c_u'$, while in the case of larger volumes the point C arises with a larger value for $\Delta c_u''$ as in the case of the previously described forward-curved blades. The total pressure reduces linearly with smaller volume till reaching $\psi = 2$ at the point of zero volume flow.

In order to obtain the actual characteristics, we plot first of all the friction losses which, according to our earlier study, are given by a parabola of $\varphi = 0$; finally, the parabola of the shock-losses is plotted on the graph from the turning point. By this means we obtain a characteristic (Fig. 152) which is close to the actual curve.

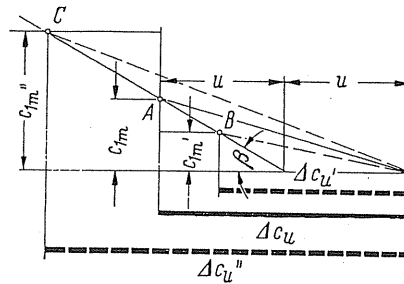


FIG. 151.

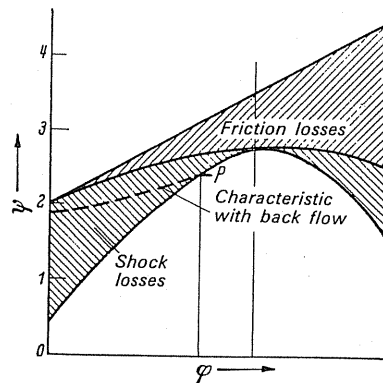


FIG. 152.

The decaying branch of the characteristic to $\varphi = 0$ is a usual feature. Correspondingly it gives an extremely small value when operating at low and zero volumes as was similarly observed in multivane impellers. For different applications the decaying branch indicates an unstable characteristic which can produce complications with fans operating in parallel.

Operationally the steep gradient of the decaying branch can be effectively reduced by bleeding some of the discharged air back into the fan at a definite point around P . By this

means it is possible to obtain a point below which the branch will no longer fall. Figure 152 illustrates the correction as a dotted line extending from point P to $\varphi = 0$.

By the new arrangement shown in Fig. 147b it is possible to influence the characteristic externally, making it stable or even extremely stable, i.e. with steeply falling lines.

62. CHARACTERISTICS, EFFICIENCY, EVALUATION, APPLICATIONS

With cross-flow fans the "through-put" stream of the impeller is unsteady. Because of this the main equation of motion⁽¹²⁾ changes with respect to its characteristic term

$$e \int_1^2 \frac{\partial c}{\partial t} ds.$$

Another effect in consequence of this form of motion is that the blade-tip discharge is not necessarily identical with the tangent to the blade. Most probably the influence is small as long as the radial depth of the blade is very small. In his investigations Coester came to the conclusion that this factor was not overcome by the magnitude of the blade friction. Perhaps undoubted advantage may ensue from the character of unsteady flow.

It is very important that the volume flow at the blades near the core has a greater velocity, i.e. considerably larger Reynolds number than with other types of flow machine. This higher Reynolds number, together with the possible reduction of friction because of non-steady admission, may be the reason for designing a cross-flow fan to give efficiencies worthy of consideration whereas *axial flow* and *radial* machines already possess poor efficiencies. N. Laing, Stuttgart, is particularly responsible for the work done in this field. Other types of centrifugal machine have a considerable fall in efficiency with smaller dimensions and exhibit efficiencies of around 10–15% in many applications.

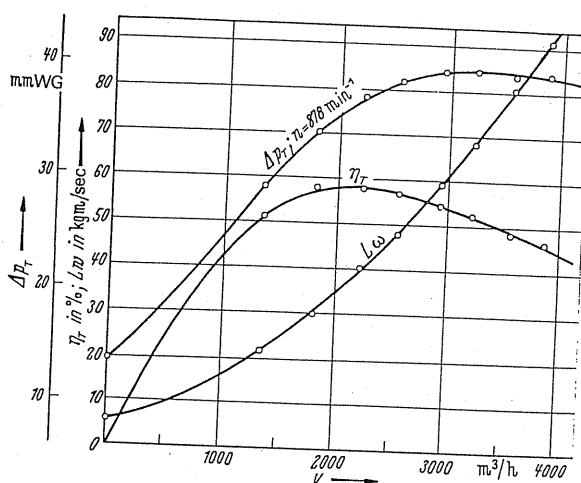


FIG. 153. Characteristics of a cross-flow impeller according to Fig. 145b.

¹² See, for example, Eck, *Technische Strömungslehre*, 7th edn., Berlin/Göttingen/Heidelberg, Springer, 1966.

Even today nothing can be stated about the evaluation of the cross-flow fan by calculation. This uncertainty does not arise only through the change of the Reynolds number and the frequency of pulsations but also through a phenomenon which does not exist in any other type of centrifugal machine, viz. the fact that the position of the internal vortex can change. Because of this, all the characteristics of a fan change immediately. With the enlargement of the cross-flow fan, cases were found where a noticeably different value appeared with larger designs; it was also found, though, that there were designs with which the opposite occurred. Finally, it must be remembered here that the accepted assumed principles of the reassessment—the exclusive dependence on the Reynolds number—is losing considerable ground because of the recent work of Rüttschi.

To facilitate an understanding of what has been achieved to date, the following diagrams will be found useful. Figure 146 illustrates the original diagram obtained with the conical tongue. The resulting improvement was considerable. Figure 153 shows the overall diagrams of a then existing design with which an efficiency of 58% was already reached. Figure 154 shows:

- (a) the value, according to Mortier, when the same small model as with other fans is used;
- (b) the first established large pressure increase through the use of internal guide vanes according to Fig. 133;
- (c) design with a gap;
- (d) an arrangement for an extremely large capacity with a tongue design in accordance with Fig. 145 *b*;
- (e) the best design for small capacity and large pressure coefficients according to the work of Coester.

The differences in noise levels are considerable. Consistent information which permits recognition of a definite principle is not yet available. Unfortunately the requirements for quiet operation and high efficiency are not always possible to fulfil.

According to the size and the Reynolds number and to any special construction used, some noticeable deviations arise, so, for special cases, pressure coefficients above 5 can be obtained. Also in special cases efficiencies of 70% are attainable.

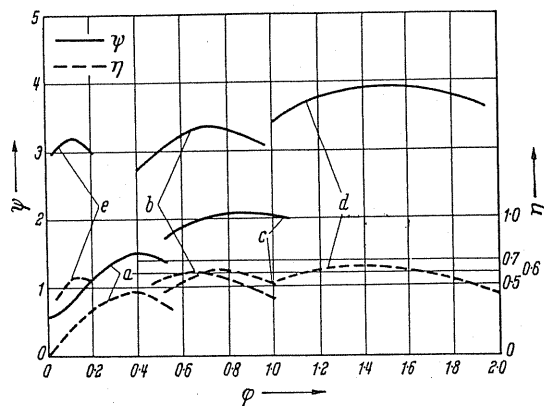


FIG. 154. *a*, design by Mortier; *b*, internal guide blades; *c*, gap with radially decreasing width; *d*, design according to Fig. 145 *b*; *e*, design with pocket according to Coester.

(a) APPLICATIONS

Numerous new applications have been forthcoming with the new trend of development in cross-flow fans. A typical example will be given.

Figure 155 shows a fan by Messrs. P. Pollrich for use in air curtains. This design belongs to the first of the new applications. The space limitations imposed by this type of installation cannot be readily satisfied by any other type of fan.

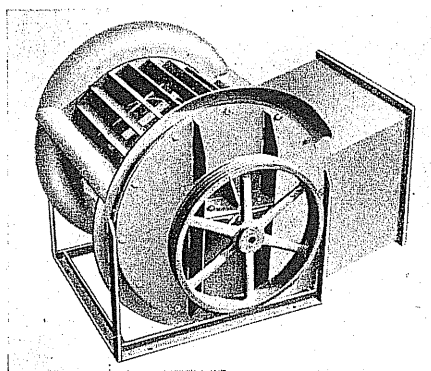


FIG. 155.

Applications arising from the field of household equipment are basically new and constitute a landmark in this field. N. Laing, Stuttgart, was particularly responsible for this undertaking. Figure 156 shows a 2 kW air heater manufactured by Messrs. Max Braun, Frankfurt, which was produced in conjunction with Laing. A comparison is made in Fig. 156 between this form of heater and a standard telephone to give some idea of its compactness.

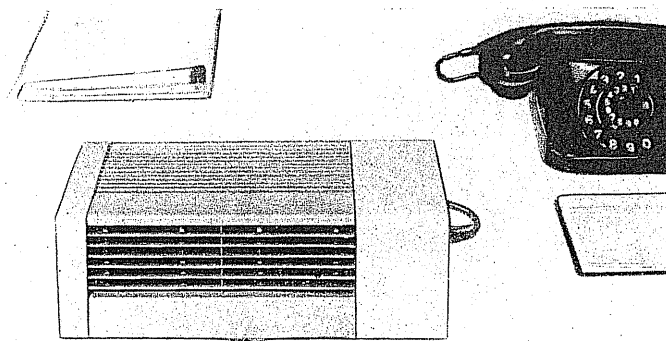


FIG. 156.

The apparatus can be easily carried in a briefcase. A section, Fig. 157, shows the internal construction. This type of heater has the advantage over the previous heating appliances equipped with axial or propeller fans of producing a stream deep into the space or room that is neither turbulent nor in possession of a vortex core.

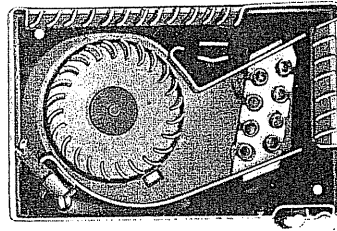


FIG. 157.

Figure 158 shows a schematic arrangement of a spin dryer by Messrs. Meyer (developed by Laing). This arrangement clearly shows the advantage of the drum-type of construction. There are many small applications where this characteristic plays a decisive part. If one

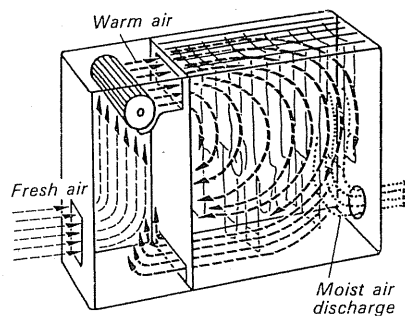


FIG. 158.

builds a small cross-flow free-flowing impeller coupled to a small electric motor, a neat compact arrangement results suitable for any number of applications. Figure 159 shows such an arrangement of Laing (manufactured by Standard Lorenz Electric).

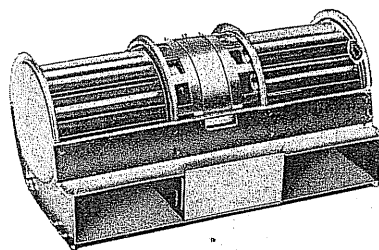


FIG. 159.

From Laing there comes a design which could change the fundamental conception of electric motor cooling. In this design the rotor of the machine acts as a cross-flow impeller and the cold air is carried through to produce air cooling of the machine. By this means the cooling is superior to that given by the previous conventional designs. Figure 160 illustrates a cross-section of this type of arrangement where the cold air flows twice through the machine.

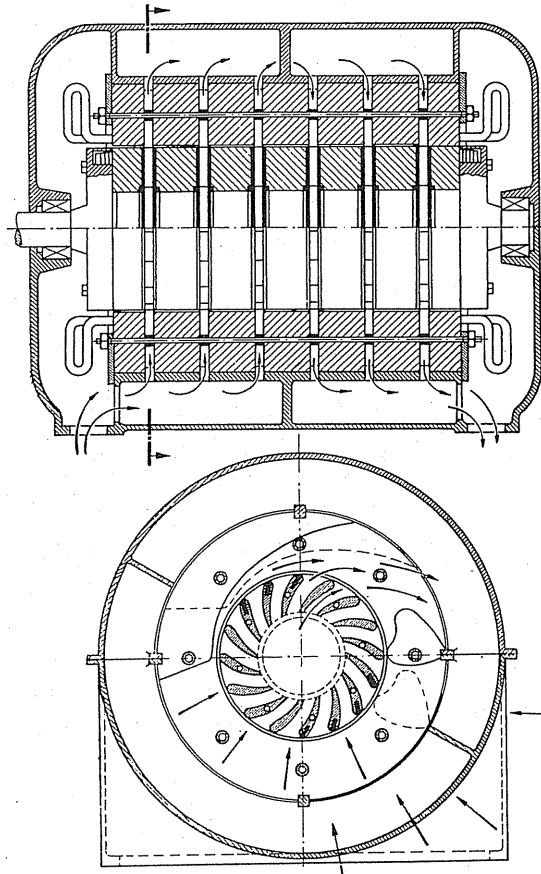


FIG. 160.

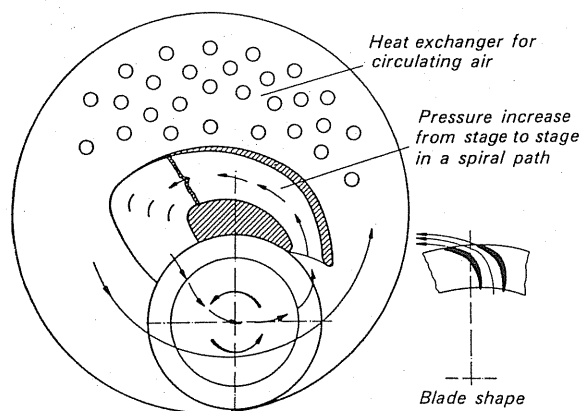


FIG. 161.

It is worthy of note that the Zürich circle around Ackeret has succeeded in developing a small reactive compressor. In this design one takes part of the air stream at the zone of high velocity and conveys it from stage to stage through a spiral passage. The remaining portion of the air is allowed to circulate and to cool at the same time. Figure 161 schematically represents this process while Fig. 162 shows the overall arrangement.

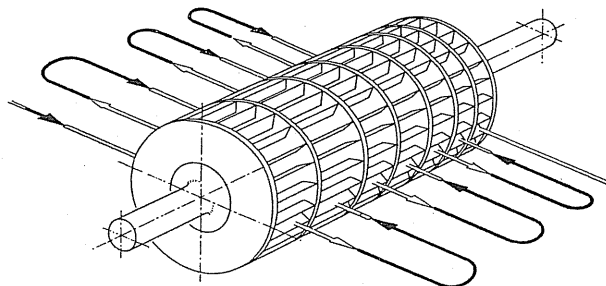


FIG. 162.

(b) CROSS-FLOW MULTIVANE IMPELLER

The volume flow of a cross-flow impeller has already shown that this flow is highly concentrated in the proximity of the vortex and on the opposite side it is considerably reduced. This relatively poor utilisation of the impeller area can be improved according to a proposal of the author if one only uses the section in the immediate vicinity of the vortex as the reactive fan. This section is isolated by a wall *W*, Fig. 163, mounted internally. The remaining section, somewhat around two-thirds to three-quarters of the circumference, will then work as a normal multivane impeller, so that two types are realised in a single impeller.

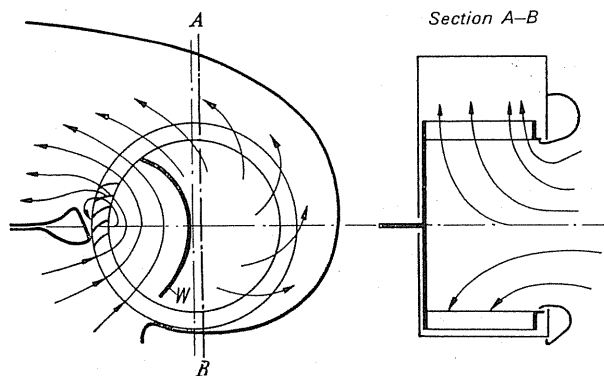


FIG. 163.

63. CROSS-FLOW IN IMPELLERS WITHOUT CASING

For a long time the author searched for a simple device to agitate a fluid and to circulate air. This question was again taken in connection with the work on cross-flow fans. It has now been found that this problem is soluble with a simple multivane impeller without casing

and without an inlet guide vane. The flow from such a free multivane impeller takes the form of a sharply defined free stream. Photographs of the flow are shown by Figs. 164 and 165 for such a case when an impeller is immersed in a small and a large tank. The internal flow is almost identical with the theoretical conception of Fig. 142. Figure 165 is most distinctive because the influence of the tank walls is no longer perceptible. A sharp stream arises in the proximity of the vortex. The range of the entry and discharge streams can be readily identified. The external in-flow shows clearly the stagnation point. Suction occurs at one side of this stagnation while circulation around the impeller occurs on the other side

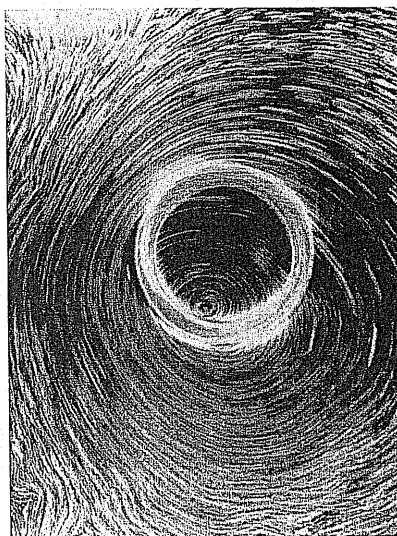


FIG. 164.

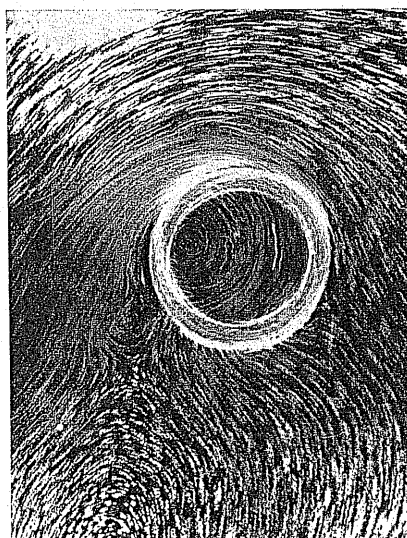


FIG. 165.

without penetration into the impeller. The flow-in develops a counter pre-rotation; between the discharging stream and inlet flow there is a vortex zone. In the case of immersion in a small tank the flow pattern changes somewhat. The discharging currents flow almost directly back and into the impeller again with pre-rotation in the same direction as the impeller. A vortex zone between the inlet and discharge currents is not discernible. It was also found that the discharging stream itself turns very slowly in the direction of rotation of the impeller.⁽¹³⁾

A study of the start up of the process, Fig. 166, is highly informative. As well as in the interior, the external edge itself constitutes a kind of vortex street. This form of turbulence

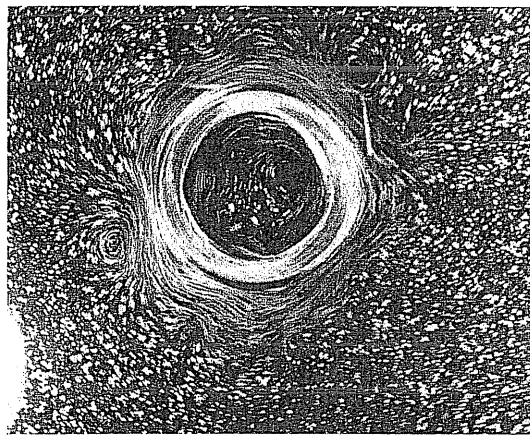


FIG. 166.

always brings portions of the stationary fluid—whose extent can be identified from the picture—into motion. Already on the inside a strong vortex is displaced to one side. This can be clearly recognised from Fig. 166, which also shows how already at the start the circular symmetry of the flow pattern is disturbed.

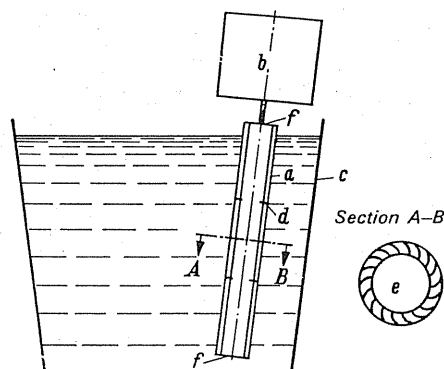


FIG. 167a. *a*, cylinder; *b*, motor; *c*, container; *d*, blade width; *e*, cross-section of the cylinder; *f*, end plate of the cylinder.

¹³ Depending on the blade design the stream may become practically stationary or, under vortex diffusion no isolated stream is formed.

Accordingly the desired agitator⁽¹⁴⁾ (also blower) could be built along these lines (Fig. 167a). One such agitator, therefore, can arise from a rotating cylinder only and produce a uniform circulation at all planes with a pronounced velocity gradient at individual places around the periphery of the cylinder. This characteristic is very important with agitators because particles and droplets of secondary components must be sheared away from the bulk of the stationary fluid (loosening, reaction). By an external rotary impulse the vortex slowly rotates in the direction of rotation of the impeller and controls the slow rotation of the stream in this manner. In the case of the model, the rotational velocity of the stream was one-twentieth of the number of revolutions of the cylinder. New investigations have shown some further possibilities in combining the cross-flow blower with the centrifugal impeller. With certain guide vanes it has been found that a nearly open impeller operates partly as a cross-flow and partly as a centrifugal impeller. This is illustrated in Fig. 167b which shows

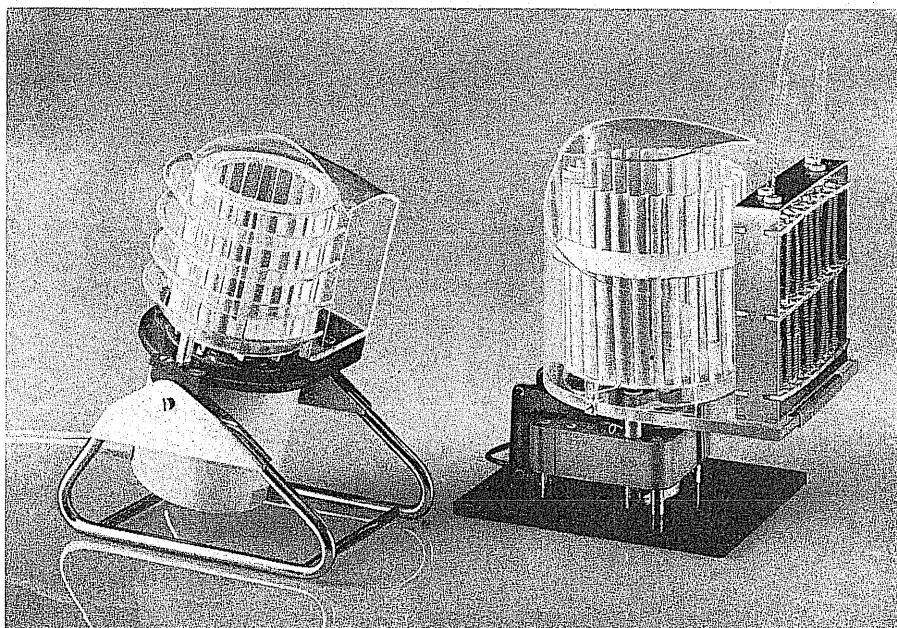


FIG. 167b.

that a part of the upper suction surface is covered by the casing, whereas the casing at the side, as can be easily seen on the right-hand side of the figure, will cover only part of the impeller. This ensures that the upper part of the impeller operates as a cross-flow blower, whereas the lower section will act as a centrifugal impeller. Looking more closely into this arrangement one will find that such impellers blow out over the whole width of the impeller projection, that is to say they operate virtually without a casing. By applying special techniques it is possible to arrange the guide vanes in such a manner that the highest efficiency can be attained. This arrangement permits a fan to be used in places, e.g. in a corner of some apparatus where an ordinary fan would be useless. Fans of this type can be used in air heaters as shown in Fig. 167b.

¹⁴ Eck, B., New equipment for milling fluids, *Chemiz-Ingenieur-Technik*, 1959, p. 260.

64. OSCILLATING BLADE IMPELLER

One of the great disadvantages of the cross-flow fan is that some of the blade ranges can only operate in a turbulent manner and that there is back flow which involves approximately one-third of the total volume. This means that the efficiencies are defined within certain limits.

It was found that the disadvantage could be avoided if a relative rotation of the blades could be realised during the rotation of the impeller. By this means the point of first entry is different from that of the second passage through the cascade, while the side length can be practically controlled to yield a cylindrical wall covering in the circumferential direction. During rotation the blades must oscillate and this is achieved by the new oscillating blade impeller⁽¹⁵⁾ whose blades oscillate during a revolution around a centre line which lies in the peripheral direction.

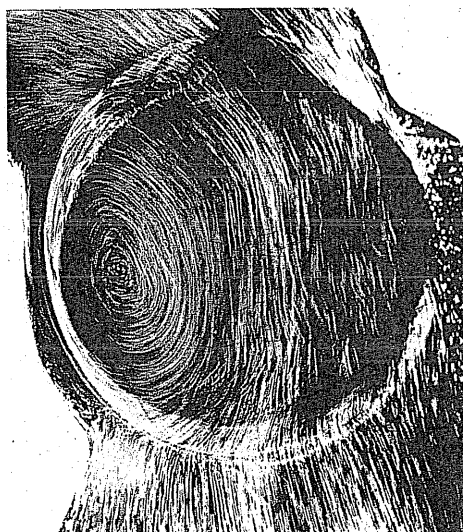


FIG. 168.

Figures 168 and 169 show flow patterns obtained with the new impeller. Typically here is also a vortex on the inside of the impeller. It is found at a place where the blades are swung round, which means that they almost constitute a wall. The vortex ensures by this means that the flow pursues its course on the other side free from any disturbance. The difference between the cross-flow and free impeller is that the main flow fills the interior of the impeller to the right of the vortex while with the cross-flow impeller a pronounced circulation round the vortex appears and the remaining portion of the impeller is occupied by a flow with a very low velocity—almost a dead zone. This difference is schematically represented by Fig. 170. The vortex centre point is displaced towards the centre if the blade amplitude is smaller (Fig. 169). With an enclosed blade cascade only a symmetrical rotary

¹⁵ Eck, B., The oscillating blade impeller, a new impeller for fans and pumps, *Chemie-Ingenieur-Technik*, 1960, p. 94.

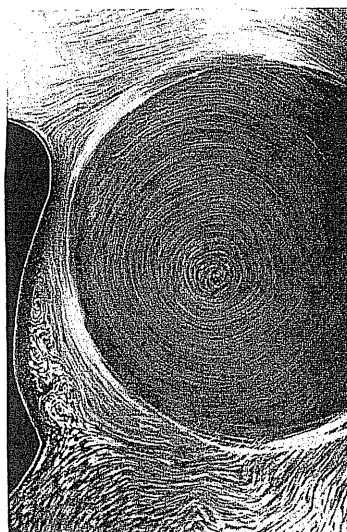


FIG. 169.

flow on the inside is seen. With smaller blade amplitudes, a sharply defined stream appears in the peripheral direction, while in the case of larger admission the diffuser will be reasonably well filled. Between the impeller and separating wall one observes a back flow in the suction zone which can be reduced by a small clearance. Here the inner vortex does not intersect the blading at any point: it rotates more or less within an enclosed space and by doing so may only cause minor losses. It prevents the active flow from deflecting into the dead region within the impeller.

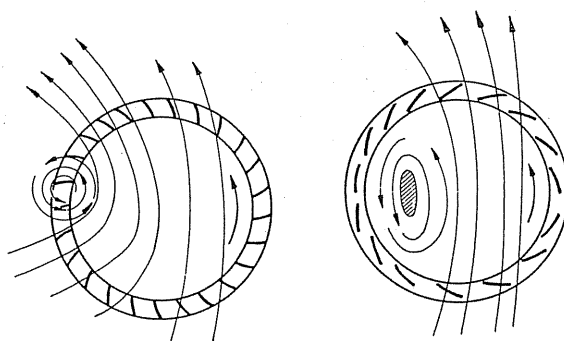


FIG. 170.

Experiment indicates one possibility. It now appears that one can move the blades with twice the frequency and thus allow the blades to be in the position of forward-curved blades for the second passage through the impeller such as exists in the case of cross-flow fans. For many applications it is interesting to note that a complete reversal of the direction of flow can be achieved. In the zero position the blades almost constitute a cylinder, which in

effect means a shaping with rapidly disappearing resistance, a feature one also cannot find in other flow machines. The regulation capacity of the impeller is almost unlimited. The extremely large volume-handling capacity of the impeller, supplemented by the almost complete absence of a casing, makes it possible to attain a small compact unit which until now has been impossible.

The cross-flow blower is unsuitable for use with water on account of cavitation, but, in this case the difficulty does not arise. There is now a possibility of being able to build pumps which can be driven by a shaft projecting perpendicularly from the piping. This could be achieved if a reliable kinematic solution could be found.

CHAPTER XI

GUIDE ARRANGEMENTS

IN THE guide arrangement or, as it is more commonly called, the diffuser of a fan, the air is decelerated from its higher velocity at the impeller discharge, a process which is essential for the connected ductwork. By this means a static pressure is produced in the diffuser which is superimposed on the static pressure obtained in the impeller. Technically it is a process of pressure recovery—"static regain"—by deceleration of the flow and depending upon the circumstances it can be responsible for fairly heavy losses. We have also seen that in the impeller, decelerations occur, yet, as experience has shown, a rotating diffuser is not so prone to losses as an expanding stationary passage. This is because the boundary layer is ejected by centrifugal force in a rotating diffuser, a process completely absent with stationary diffusers. This knowledge has been gradually acquired by research work and other observations have justified the guide arrangement. But in order to reach high efficiencies, appropriately high reactions must be aimed at. In view of this, special attention must be paid to the diffuser of a fan.

65. GUIDE BLADES

Although guide blades in the single-stage fan are almost an exception, at least the main aspects of its design can be grouped together here. The problem of a diffuser is to convert the high absolute discharge velocity c_3 into static pressure whilst incurring the smallest possible losses. If one puts the problem thus, that this must be carried out on the smallest possible outside diameter, then guide blades are unavoidable. There are applications, e.g. aeroplane superchargers, with which there is no disadvantage in having an annular discharge section.

After leaving the impeller the air has an absolute velocity c_3 at an angle to the periphery of α_3 . The resolving of $c_3^2 = c_{3u}^2 + c_{3m}^2$ is therefore essential because from the principle of pre-rotation and from the stability equation a simple change of these components can be given with r :

$$c_u = \frac{c_{3u} r_2}{r}; \quad c_m = \frac{c_{3m} r_2}{r}.$$

One obtains

$$\tan \alpha = \frac{c_m}{c_u} = \frac{c_{3m}}{c_{3u}} = \text{const.}$$

Since the angle is constant, the air moves with a logarithmic spiral. The equation of this spiral states

$$\varphi \tan \alpha = \ln \frac{r}{r_3} \quad (137)$$

(designated according to Fig. 171).

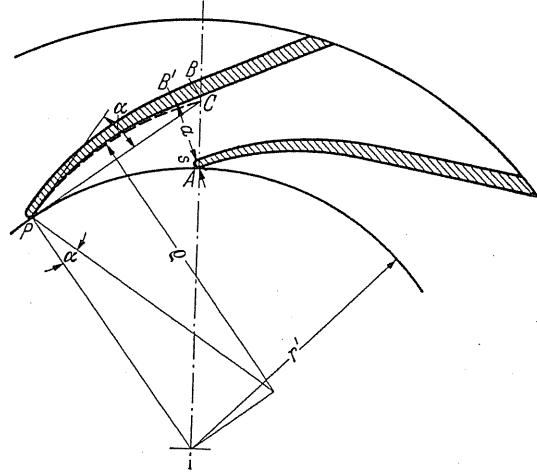


FIG. 171. Logarithmic spiral and its radius of curvature as a guide blade inlet.

The guide blades must, therefore, begin with a logarithmic spiral at least to section AB' so that the entry shall be inactive. Instead of which one selects the corresponding curvature mostly in the case of large numbers of blades whose construction is easily recognisable from Fig. 171. It has the value

$$\varrho = \frac{r'}{\cos \alpha}.$$

In the case of only a few blades, i.e. when known designs out of the centrifugal pump field are assumed, a particular radius of curvature gives a guide blade section which is too small. Figure 171 shows the relationship for ten guide blades and an angle $\alpha_4 = 20^\circ$. The circle of curvature, which begins at P , is indicated by a dashed line, while the point B was precisely calculated according to the equation $\varphi \tan \alpha = \ln (r/r')$.

From this equation the passage width $(a + s)$ can be easily calculated. With $AB = r - r'$, $a + s = (r - r') \cos \alpha$. For an approximation:

$$\ln \frac{r}{r'} \sim \frac{r - r'}{r'}.$$

Because φ corresponds to the blade pitch, it gives $\varphi = 2\pi/z$. One then substitutes this into eqn. (137) to get

$$\frac{2\pi}{z} \tan \alpha = \frac{a + s}{r'} \frac{1}{\cos \alpha},$$

from which we get

$$a + s = r' \frac{2\pi}{z} \sin \alpha = t \sin \alpha,$$

where t is the blade pitch.

Because we have introduced the blade pitch, the equation acquires a simple significance.

In consideration of the contraction caused by a finite blade thickness, an increase in the angle will occur according to the equation

$$\tan \alpha_4 = \tan \alpha_3 \frac{t_3}{t_3 - \sigma_3} \quad \left[\sigma_3 = \frac{s}{\sin \alpha_3} \right]. \quad (138)$$

From the section AB' onwards, the air is confined within an enclosed passage. Beyond this point the maximum permissible deceleration can be undertaken, which is applied in the case of a diffuser. It then gives a form, as may be seen from Fig. 171, which is known from the field of centrifugal pumps.

This blade form is rarely selected in fan engineering. The materials generally employed in this field are different. Whilst castings are commonly employed for centrifugal pumps, sheet-metal constructions are predominant in fans and this leads to other blade forms. From this and other factors the guide blades in use on fans are usually straight. The number of blades in this case is simply arrived at, providing one does not allow an undue enlargement. Allowing for an enlargement angle of 14° ,⁽¹⁾ then as the least number of blades required, we get $z = \frac{360}{14} \approx 25$. A familiar design can be seen in Fig. 172.

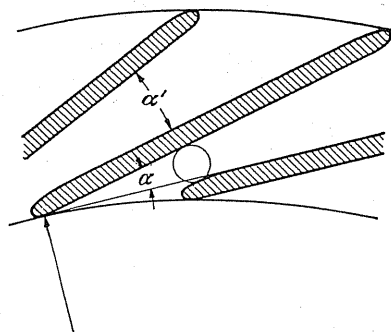


FIG. 172. Straight guide blades.

In the calculation of these guide blades, whose basic form also occurs in rotating guide vanes, *the narrowest section plays a larger part than the blade angle*. The narrowest section must be such that only slight or no acceleration occurs. The complete treatment of this aspect is more comprehensively dealt with in the field of turbo-compressors.

In the case of curved guide vanes the width a must be increased by 20–30% in contrast to the calculated value, whereas with straight guide blades a significant increase is unnecessary.

66. INTERCHANGE ACTION

Between the guide vanes and impeller one finds a more or less large interchange of motion taking place. This is understood more readily as the back flow from the guide vanes into the impeller. The air is again caught into the impeller and flows into the guide vane with

¹ These larger values could be left here because the strong turbulence which air displays behind the impeller suppresses separation.

greater energy. On account of this it is true that the resultant pressure increase is in excess of the calculated value, although the reduction of efficiency in consequence of this is undesirable. This interchange action increases if the guide vanes lie closer to the impeller and the volume reduction is greater than the designed normal condition. With volume flows in excess of the normal condition this effect diminishes quite considerably. Even with a smooth guide ring a similar backflow would be observed. According to Schrader,⁽²⁾ the main pressure increase did not—as until now one assumed—take place in the guide passages but in the first part of the oblique section instead. Figure 173 schematically illustrates this process quite clearly. The back-flow width of the boundary layer increases as the volume decreases, up to the point of zero flow where it completely fills the passage.

With fans, a suitable clearance between the impeller and guide vanes must be provided to counteract the generation of undue noise. Unfortunately this necessary step introduces a reduction in the efficiency.

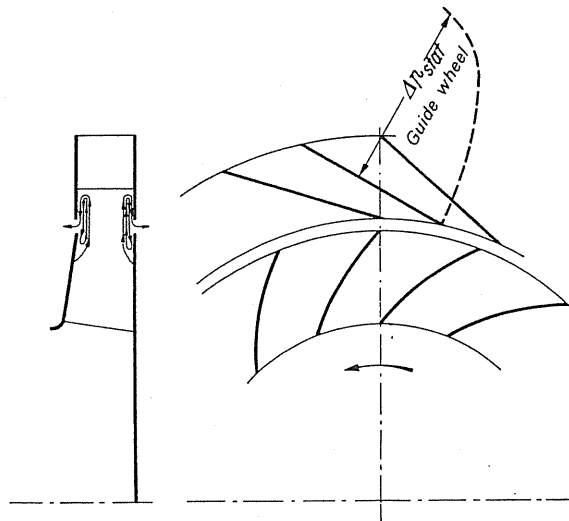


FIG. 173. Interchange moment and actual distribution of pressure in the oblique section.

Only in the case of special designs (turbo-compressors, aircraft superchargers) are various rotary guide vanes employed. In the case of small dimensions one will also resort more frequently to guide vanes.

In general, results obtained with smooth guide rings and spiral housings or volutes are better than those obtained through the use of guide vanes. In particular, without guide vanes one gets a flatter characteristic and flatter efficiency curves.

² Schrader, H., Measurements on guide vanes of axial-flow pumps, Diss., Brunswick, 1939.

67. SPIRAL HOUSING

In the case of single-stage blowers, particularly with ventilation fans, the volutes casing is almost exclusively employed as the guiding device. *This form of guide arrangement is so simple in its construction and efficient in operation that it would be difficult to recommend an alternative.* In view of its importance it is necessary to describe its design.

(a) FUNDAMENTALS

To be able to grasp the flow relationships within a simple volute, one starts from a simple flow that is symmetrical about an axis. For this condition one very important case is if an isolated vortex is thought of as a source. For the case of parallel side walls one gets streamlines which take the path of a logarithmic spiral (Fig. 174). A centrifugal impeller of diameter d_0 can be replaced for its total effect by such a system. For a point lying outside the impeller with a radius r one obtains the peripheral velocity c_u from the condition that the rotation must remain constant ($rc_u = \text{const}$). (In practice this rule is valid with the restriction that one must be so far displaced from the impeller that deflections conditioned by the consideration of a finite number of blades can be ignored.) This rule constitutes the basis for the dimensioning of a volute for the case where friction has been ignored.

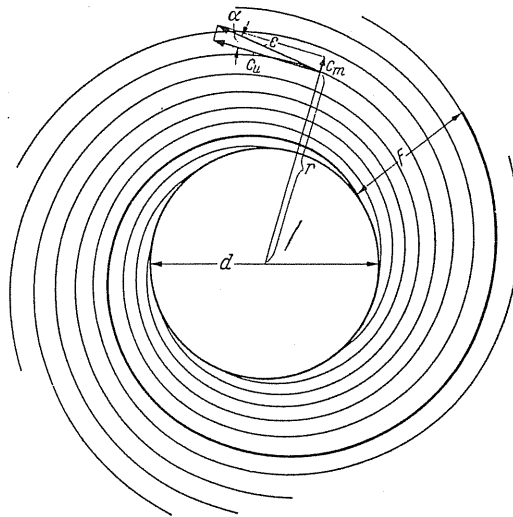


FIG. 174. Formation of a volute casing from the streamline of a vortex source.

Figure 174 illustrates simply how one produces a volute. One substitutes a streamline (the heavy drawn line indicates the streamline in question, Fig. 174) by a firm wall which after a full revolution will confine the flow within the end section F , so that at that point the transition into a pipe can be simply accomplished. Now because the discharge must be straight and does not follow a volute, there are deviations from the above-mentioned flow. Often these will be insignificant if one attempts to obtain the steadiest possible transition.

A necessary hypothesis to the above rule is again mentioned; i.e. that the side walls of the casing must be symmetrical with respect to rotation. If one does not observe this condition with the shape of housing as, for example, in the case of a circular section, then the flow will no longer be exactly symmetrical about the axis. In particular the law $r c_u = \text{const}$ is no longer valid because the peripheral velocities at the periphery of a circle are no longer constant. In spite of this, in the hydrodynamical sense the flow is still free from vortices. Small deviations from the rotational body naturally could not evoke any large changes. Only in this sense is it permitted to look on the previous rule as valid in the following calculations.

(b) CONSTRUCTION OF VOLUTES WITHOUT CONSIDERING FRICTION

For most of the basic forms encountered it is possible to calculate the boundary curves of a volute mathematically. Where this is not possible, the graphical method is of great assistance.

(α) **Parallel side walls.** The velocity c at an arbitrary place can be calculated from its components c_u and c_m . From previous work⁽³⁾

$$c_u = \frac{c_{0u} r_0}{r}.$$

From the condition that the same volume flow must flow (continuity equation) through all the circles it gives the relationship

$$c_m 2r \pi b = c_{0m} 2r_0 \pi b;$$

from which follows (Fig. 175)

$$c_m = \frac{c_{0m} r_0}{r}.$$

One gets the directions of a streamline from

$$\tan \alpha = \frac{c_m}{c_u} = \frac{c_{0m}}{c_{0u}} = \tan \alpha_0,$$

which means the angle of inclination to the periphery is constant because

$$\tan \alpha = \tan \alpha_0 = \frac{dr}{r d\varphi} = \frac{c_{0m}}{c_{0u}}. \quad (139)$$

³ In the following the basic circle of the spiral will always be indicated with the subscript 0. In many cases however one can substitute the subscript 0 by the subscript 2 which refers to the outside diameter of the impeller and then, for example, for eqn. (140) one gets:

$$\ln \frac{r}{r_2} = \varphi \frac{c_{2m}}{c_{2u}} \frac{b_2}{b} = 2.302 \lg \frac{r}{r_2}.$$

See the example on p. 192.

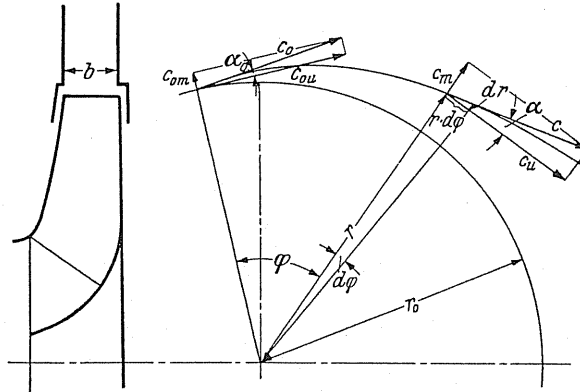


FIG. 175. Spiral space with parallel sidewalls.

Thus it gives the equation

$$\ln \frac{r}{r_0} = \varphi \frac{c_{0m}}{c_{0u}} = \varphi \tan \alpha_0. \quad (140)$$

This is the equation of a logarithmic spiral, which can be assumed to be the outside boundary curve for the volute.

For the outline one requires the radius of curvature:

$$R = \frac{r}{\cos \alpha}.$$

(β) **Parallel side walls which are wider than the impeller.** This type is illustrated in Fig. 176. With most ventilation fans this is the normal form of design. Its calculation is very simple. If we designate the constant width of the casing by b , then for the cylindrical section r the continuity equation states:

$$2r\pi b c_m = 2r_0\pi b_0 c_{0m},$$

from which

$$c_m = c_{0m} \frac{r_0 b_0}{rb}.$$

For c_u the same rule as previously is valid:

$$c_u = \frac{c_{0u} r_0}{r}.$$

With this we obtain the following inclination α of the streamlines:

$$\tan \alpha = \frac{c_m}{c_u} = \frac{c_{0m}}{c_{0u}} \frac{b_0}{b} = (\tan \alpha_0) \frac{b_0}{b}.$$

Because we can obtain the boundary of a volute from a streamline, again it yields

$$\tan \alpha \frac{dr}{r d\varphi}; \quad \frac{dr}{r} = d\varphi \tan \alpha = d\varphi (\tan \alpha_0) \frac{b_0}{b}.$$

The solution states

$$\ln \frac{r}{r_0} = \varphi (\tan \alpha_0) \frac{b_0}{b} = \varphi \frac{c_{0m}}{c_{0u}} \frac{b_0}{b} = 2.302 \lg \frac{r}{r_0}. \quad (141)$$

The only difference between this and the first case is the factor b_0/b .

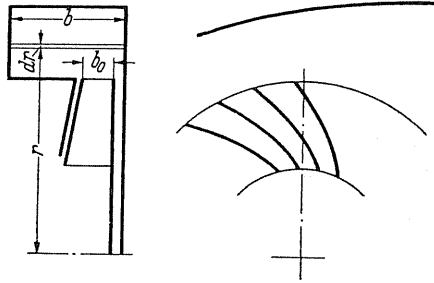


FIG. 176. Rectangle of same width as the basic form of the spiral.

Example

Calculate the volute for a blower impeller of $b_0 = 60$ mm outside width; $r_0 = 200$ mm, $c_{0u} = 15$ m/sec and $c_{0m} = 5$ m/sec. Selecting 150 mm for b and employing eqn. (141):

$$\varphi = 2.302 \frac{b}{b_0} \frac{c_{0u}}{c_{0m}} \left(\lg \frac{r}{r_0} \right) = 2.302 \frac{150}{60} \frac{15}{5} \lg \frac{r}{r_0} = 17.3 \lg \frac{r}{r_0},$$

$$\varphi^\circ = 57.3 \varphi = 990 \lg \frac{r}{r_0}.$$

Table 12 shows the calculated values from which the volute can be easily plotted.

TABLE 12

φ°	0	45	90	135	180	225	270	315	360
$\lg \frac{r}{r_0} = \frac{\varphi^\circ}{990}$	0	0.0455	0.091	0.137	0.182	0.227	0.273	0.318	0.364
r/r_0	1	1.113	1.233	1.395	1.52	1.685	1.88	2.08	2.31
r	200	222	246	279	305	337	376	416	462

In many cases we will require that the discharge area is square. By integration in the discharge section the necessary width of the volute casing can be calculated. If we assume the velocity in the discharge area to be $c \approx c_u = (c_{0u} r_0)/r$, then for the total discharge volume we get

$$V = \int_{r_0}^{r_0+b} b \frac{c_{0u} r_0}{r} dr = b c_{0u} r_0 \ln \frac{r_0 + b}{r_0}.$$

Because this formula is inconvenient for the calculation of b , as an approximation we will assume that the velocity c at the point of concentration of the discharge area is equal

to the mean velocity:

$$c = \frac{c_{0u} r_0}{r_0 + (b/2)}.$$

So that for the discharge cross-section of the volute it gives

$$V = \frac{b^2 c_{0u} r_0}{r_0 + (b/2)}.$$

Substituting for $V = 2r_0 \pi b_0 c_{0m}$ and after rearranging the terms we obtain a quadratic equation for b :

$$b = \frac{\pi}{2} b_0 \frac{c_{0m}}{c_{0u}} + \sqrt{\left(\frac{\pi}{2} b_0 \frac{c_{0m}}{c_{0u}}\right)^2 + 2r_0 \pi b_0 \frac{c_{0m}}{c_{0u}}}. \quad (142)$$

For the last example with this formula we get $b = 200$ mm.

(γ) **Tapering side walls.** The previous statement for c_u is applicable in this case. However, c_m on account of the changing width (Fig. 177) is

$$c_m = \frac{c_{0m} r_0 b_0}{rb}.$$

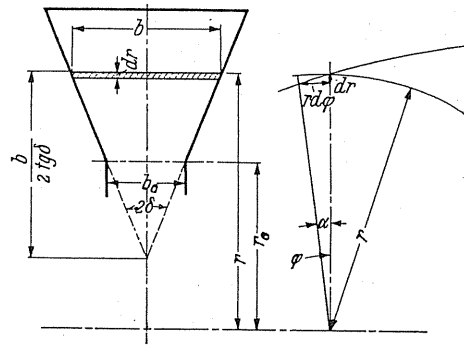


FIG. 177. Spiral with tapering walls. Trapezoidal form as a basis for the cross-section.

With the designations of Fig. 177 for b ,

$$b = b_0 + 2(r - r_0) \tan \delta.$$

Substituting for this value we get

$$c_m = \frac{c_{0m} r_0 b_0}{[b_0 + 2(r - r_0) \tan \delta] r}; \quad c_u = \frac{c_{0u} r_0}{r};$$

$$\tan \alpha = \frac{c_m}{c_u} = \frac{dr}{r d\varphi} = \frac{c_{0m} b_0}{c_{0u} [b_0 + 2(r - r_0) \tan \delta]}.$$

The solution to this differential equation is given by

$$\varphi = \frac{1}{\tan \alpha_0} \left[\left(1 - 2 \frac{r_0}{b_0} \tan \delta \right) \ln \frac{r}{r_0} + 2 \frac{r_0}{b_0} \left(\frac{r}{r_0} - 1 \right) \tan \delta \right]. \quad (143)$$

By the substitution of arbitrary values of r one obtains

$$\varphi = f(r).$$

The equation consists of a logarithmic and a linear term; the former disappearing for

$$1 - 2 \frac{r_0}{b_0} \tan \delta = 0,$$

which means

$$\tan \delta = \frac{b_0}{2r_0}.$$

As one recognises from Fig. 177, i.e. the case if the side walls meet at $r = 0$, the preceding equation is modified to

$$\varphi = \frac{1}{\tan \alpha_0} \left(\frac{r}{r_0} - 1 \right) = \frac{1}{\tan \alpha_0} \frac{\Delta r}{r_0}, \quad (144)$$

where $\Delta r = r - r_0$.

This equation states that the outside envelope increases proportionally to the curvature of admission. This relationship shows that with certain constructions which permit such a kind of angle, a significant simplification for the first design is possible.

The selection of δ is dependent upon the separation of flow. One must investigate the magnitude of the actual angle of enlargement in the direction of the absolute stream. This may not exceed the approved value of 8–12°. However, in the meantime it is assumed that if this requirement is not observed it does not necessarily cause large losses, *because the factor mainly involved is the conversion of the meridional velocity which is proportionally small.*

(δ) Rectangular cross-section. The individual section whose basic shape is rectangular should be altered radially and axially so that it results in similar areas. These constructions naturally yield no body of rotation with reference to the side walls, so that deviations from the law $r c_u = \text{const}$ are to be expected.

If the radial extension is not large in relation to the radius, then the following calculation may represent a good approximation. With the designations of Fig. 178 we put $h/b = C$ (const). At the position x

$$c_u = \frac{c_{0u} r_0}{r_0 + x};$$

with the angle φ the volume $(\varphi^\circ/360) V$ flows through the section $b_\varphi h_\varphi$. Consequently

$$\frac{\varphi^\circ}{360} V = \int_0^h \frac{c_{0u} r_0}{r_0 + x} \frac{h}{C} dx,$$

which gives the equation

$$\varphi^\circ = \frac{360 c_{0u} r_0 h}{VC} \ln \left(1 + \frac{h}{r_0} \right). \quad (145)$$

(ε) **Circular cross-section.** A precise calculation is possible in this case also and it gives

$$\frac{d}{2} = \sqrt{\varphi \frac{[r_0 + (d/2)] V}{360\pi c_{0u} r_0}} - \varphi^2 \left(\frac{V}{720\pi c_{0u} r_0} \right)^2. \quad (146)$$

As it is so complicated, the formula rarely comes into practical calculations and can for this purpose be replaced by a simple approximate formula. The change of c_u in the radial direction is hyperbolic on account that $c_u = (c_{0u} r_0)/r$ (plotted in Fig. 179). If the diameter d

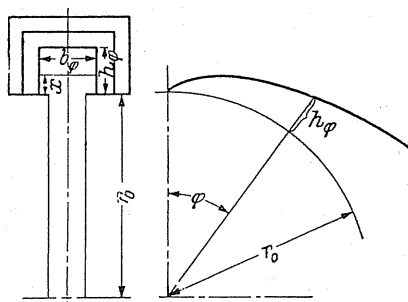


FIG. 178. Volute with a rectangular section. (Section geometrically similar.)

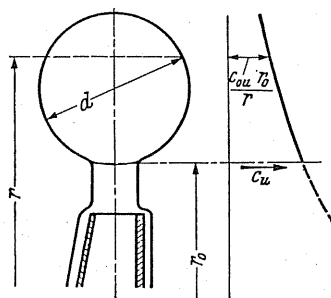


FIG. 179. Volute with a circular cross-section. (To the right is the curve of the peripheral component of the absolute velocity.)

of the volute section is not too great in relation to the total casing diameter, then the hyperbolic path over the circular section is very flat. If the path were straight, then the average velocity would be equal to the velocity at the point of concentration of the area, which means

$$c_{av} = \frac{c_{0u} r_0}{r_0 + (d/2)}.$$

This assumption may suffice in most cases; with this one gets

$$\frac{\varphi^\circ}{360} V = \frac{\pi}{4} d^2 c_{av} = \frac{\pi d^2}{4} \frac{c_{0u} r_0}{r_0 + (d/2)}$$

from which

$$d = \sqrt{\frac{\varphi^\circ [r_0 + (d/2)]}{c_{0u} r_0} \frac{V}{90\pi}} \quad (147)$$

so that

$$\varphi^\circ = \frac{\pi d^2}{4} \frac{c_{0u} r_0}{r_0 + (d/2)} \frac{360}{V}. \quad (148)$$

The outer envelope d also increases proportionally as

$$\sqrt{\varphi^\circ [r_0 + (d/2)]}.$$

Because d^2 is proportional to the section, this does not increase proportionally to the curvature of admission, which was the case with constant velocity in the volute, but is considerably greater, namely in the order of

$$\text{prop } \varphi^\circ [r_0 + (d/2)].$$

The application of this formula presupposes the knowledge of d . At best, one first of all selects d approximately, meanwhile one calculates the cross-section which gives a constant velocity c in the complete volute. In this case, the section increases proportionally to the admission arc. A successive calculation with the value of d corrected by the use of the preceding calculation is often unnecessary, because the result converges very sharply.

(ζ) **Inner volute.** One can establish the volute from the inside. By the means the air flows around the impeller and will be divided on one or both sides of the impeller. According to the law of rotation the peripheral component will be subsequently larger. This gives rise to a *significantly smaller volute*. The impeller friction falls off because the air flows along the

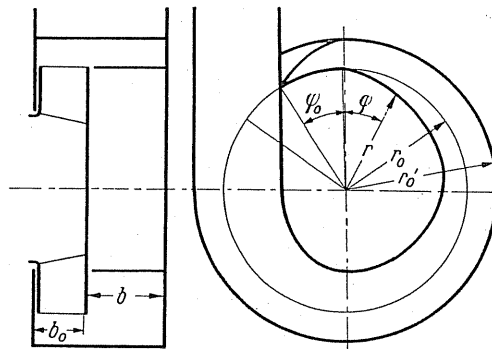


FIG. 180. Internal volute.

discs with a still larger velocity. The friction path in the volute is *significantly shorter* than in the case of normal construction. How far this advantage is balanced out by the increased friction in consequence of the greater velocity it is not yet possible to say. In the case of impellers with small delivery coefficients φ this is the form of volute often indicated.

Along with the opportunity of obtaining a dimensionally small unit they present the advantage that the outside boundary can be cylindrical.⁽⁴⁾

The calculations for Fig. 180 are available. First of all such a form of tongue section is necessary for an angle φ_0 . Firstly, the air will enter the outer rectangular section $(r'_0 - r_0) \times (b_0 + b)$ at this angle. For this

$$\varphi_0 = \frac{c_{0u}}{c_{0m}} \frac{b_0 + b}{b} \ln \frac{r'_0}{r_0}.$$

The volume flow to φ_0 is easily calculated by $V_{\varphi_0} = (V \varphi_0^\circ)/360$. From this angle on, the discharging air must be transferred to the inside rectangle and for this we again use eqn. (141).

$$\ln \frac{r}{r_0} = \varphi \frac{c_{0m}}{c_{0u}} \frac{b_0}{b}.$$

From this the internal spiral can be readily calculated.

In the case of this construction depending upon circumstances the discharge velocities are rather high so that possibly a diffuser must even be fitted to the outlet connection.

(η) **Axial volute.** An interesting form is derived if the "volute" is developed between two co-axial cylinders in the axial direction. Purely from the point of view of construction this type has the great advantage of arising from cylindrical surfaces. Because the overall c_u distribution is equal the lateral boundaries must increase in simple proportion to the angle of admission. We use the average value of c_u in our calculations and designate the lateral width by b , the curvature of admission φ , and the height h . Thus,

$$b = \frac{V}{c_u h} \frac{\varphi^\circ}{360}. \quad (149)$$

In order to achieve the outside diameter of the entry to the volute the air already divides before the tongue so that according to Fig. 181 the volume which flows in at φ° goes through the complete casing. On account of the narrow rectangular sections of these volutes essential losses arise through secondary flows. If one subdivides the lateral passage by means of walls, as suggested by the author, these losses can be avoided. Figure 181 clearly illustrates the cylindrical section AB . Through two walls, which one can consider to be forms of guide vanes, the air will be taken off immediately after the impeller in a lateral direction, and can be carried away in the side passage uninfluenced by the impeller flow on a favourable passage. Figure 181 illustrates one such form of subdivision which produces square sections.

(θ) **Helix volute.** If one poses the problem of how to collect the air so that the velocity existing behind the impeller is neither changed in magnitude nor in direction, then there is the hope that the air can be collected loss free. The conversion of the high velocity of the discharge into static pressure must then be carried out in a connected straight diffuser. Just

⁴ In place of a cylindrical boundary this can also be developed simultaneously from outside or as an axial lying volute.

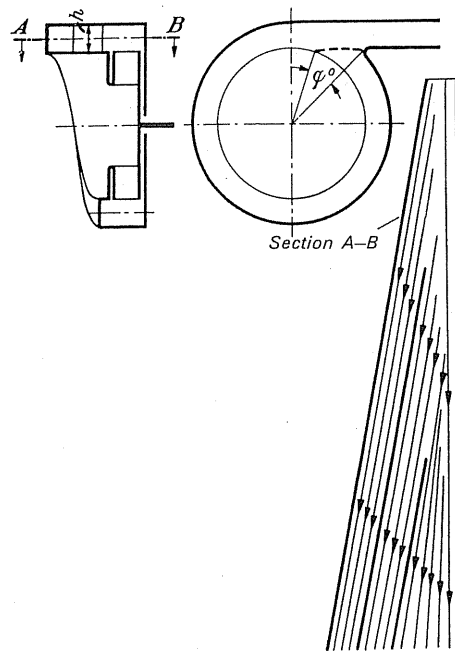


FIG.181. Axial spiral with a discharge subdivided by means of guide blades at the side.

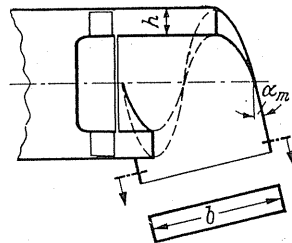


FIG.182. Axial spiral with oblique discharge. (Helical spiral.)

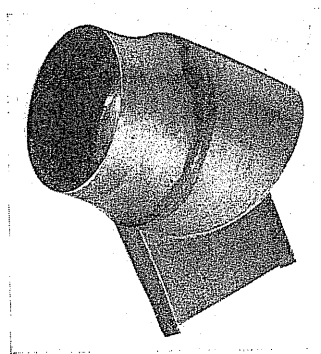


FIG.183. Helical volute. Experimental model.

here the deceleration process is often easier to govern than in the case of special guide arrangements. This means that one only has to provide a collecting arrangement behind the impeller for the air. From this consideration the author developed the helix diffuser (Fig. 182). The air enters the annulus without a change in direction and will slip out laterally into an oblique pocket lying along the spiral angle of the streamline, on which a diffuser may be connected if necessary. The spiral angle with which the streamlines move is in accordance with the law of rotation: smaller on the outside than is the case on the inside. For the discharge a suitable average angle will be selected. If α_m is the mean angle with a section perpendicular to the axis, then for the discharge width

$$b = \sin \alpha_m \pi d_m.$$

This design is especially suitable for axial-flow fans. Figure 183 illustrates the experimental model of the author.

(*l*) **Volute casing for axial-flow fans.** In some cases the arrangement of a volute casing behind the axial-flow fan is desirable. The advantage of this construction lies in the fact that by dispensing with guide vanes the characteristic and efficiency curves become smoother. However, it has the disadvantage of creating a dimensionally larger unit. Depending upon the circumstances the discharge velocities can be considerable, so that care must be taken to avoid any rapid changes of direction or deflections. The construction shown in Figs. 184 and 185 proved successful. The calculation followed the principles previously developed so repetition can be spared.

(*n*) **Helix-formed construction of volute casings.** The volute casing is the best and simplest guide or diffusion arrangement for radial-flow fans which is known in fan engineering. This is not so for axial-flow fans. This is all the more regrettable as the use of volute casing with axial-flow fans, as shown for example in Figs. 184 and 185, produces a large unit, and in addition to this numerous experiments have shown it can cause undue losses.

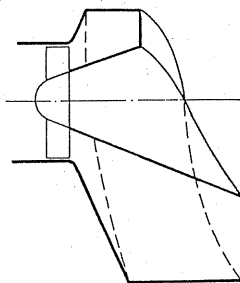


FIG. 184.

It is possible to develop a kind of volute casing in an axial direction in certain cases. A half helix can be formed so that the discharge lies on the circular segment. This construction yields small losses in comparison to the volute casing built around the axial-flow fan. It also permits clear access to the drive motor. Figure 186 shows a small example of this design.

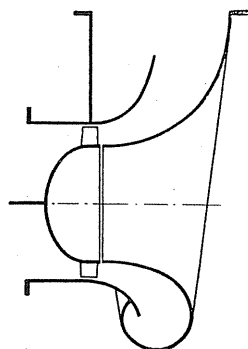


FIG. 185. Volute casing for axial-flow impellers.

(λ) **Subdivided volute casing.** With large radial extent of the volute casing undue disturbances arise through secondary streams. Depending upon the circumstances, this influence can be modified if, according to Fig. 187, one resolves an average tongue into two or more spirals.

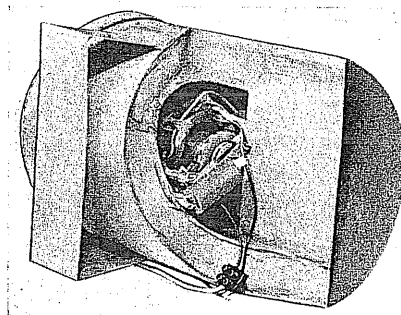


FIG. 186. Axial half-helix as a volute casing.

If one requires to decrease the discharge velocity at the same time in the shortest possible space, then to get this one can subdivide the discharge section with a number of guide blades. Such a solution is shown in Fig. 188 in which three guide blades are installed in a staggered arrangement in the volute casing. With cheap designs these guide blades are omitted.

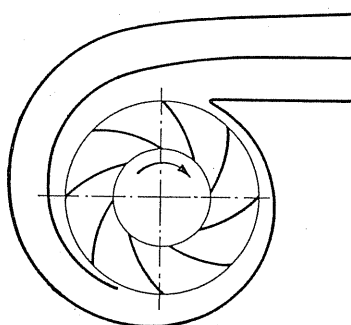


FIG. 187. Volute with single subdivision.

When in the interest of economics one requires cheap construction for large volumes by avoiding a perhaps enormous normal volute casing, then one can go a step further. By subdivision and partial profiling of the guide blades according to Fig. 189, air is discharged at a width which is more than double the diameter of the impeller. Particularly with impellers

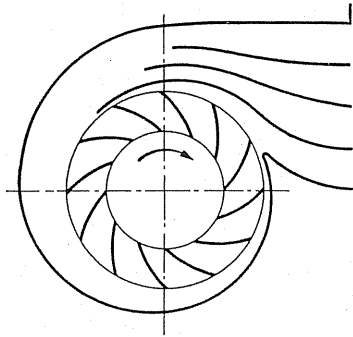


FIG. 188. Volute with a number of subdivisions of the discharge section.

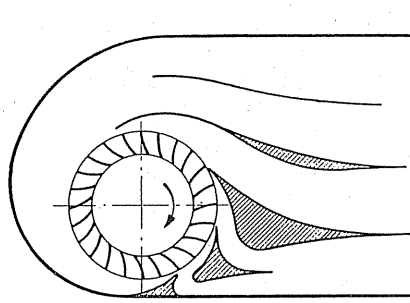


FIG. 189. Half-volute with profiled discharge blades.

having high volume coefficients, i.e. multivane impellers, this construction produces surprisingly small units, which could be easily built into a piece of equipment as an integral unit.

Figure 190 shows how diverging casing walls are arrived at with profiled blades. Often for different applications a double discharge, each discharge in different directions, is essential, as Fig. 191.

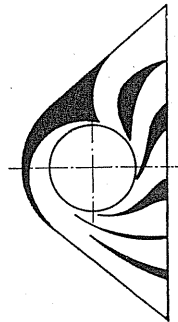


FIG. 190. Diverging casing walls with profiled blades.

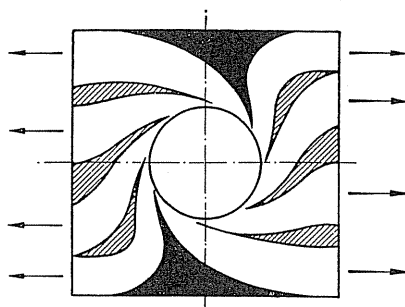


FIG.191. Discharge in two directions. Diverging casing walls.

(μ) **Volute casing with an adjustable tongue.** The requirements often demand that a volute casing must satisfy different volumes in order to avoid too large a loss when the duty falls below normal design conditions. Particularly in mine ventilation, for example, the conditions are continuously changing so that this aspect is extremely important. Attempts to solve this problem were made by investigating the effects of adjusting the volute tongue. For example, Fig. 192 shows how one can employ a swivelling arrangement of the tongue. Therefore adjustable tongue ends are available for different positions. The effect of such measures is limited.

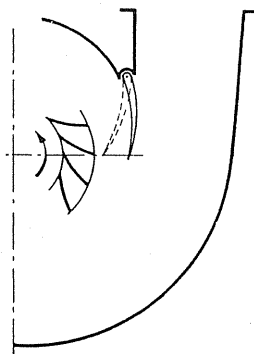


FIG.192. Volute with an adjustable tongue.

(ν) **Volute casing with a number of discharge points.** If the air is required to be drawn off from a number of pick-up points, depending upon the circumstances it can be suitably arranged to design the existing volute casing to accommodate these branches. Designs of this type are familiar in aircraft engine superchargers (Fig. 193). The figure shows a supercharger blower for a Hispano-Suiza engine whose volute is comprised of two component volutes. The necessity of even further take-offs exists with radial engines where the air pressure must be branched off to each cylinder. The symmetry of this design is that a particular discharge is provided for a particular cylinder. Figure 194 shows a design with nine discharge points. A guide wheel behind the impeller is provided in most cases with this supercharger.

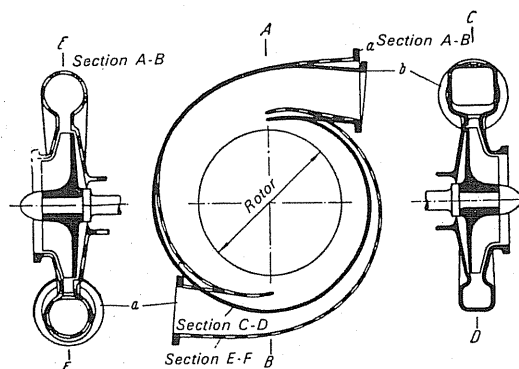


FIG.193. Volute casing with two dischargers for circular or rectangular cross-sections. *a*, dashed line: circular cross-section; *b*, full line: rectangular cross-section.

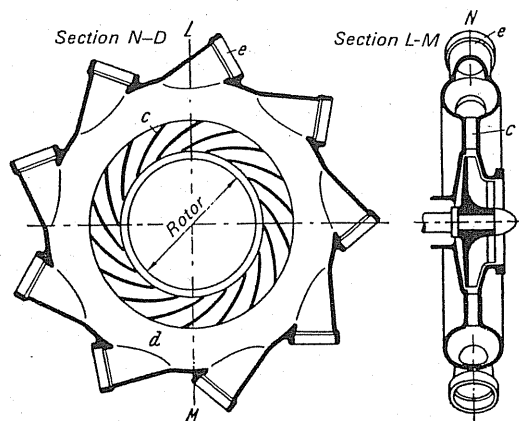


FIG.194. Volute casing with nine discharge points. *c*, guide arrangement; *d*, diffusers without blades.

It is to the credit of W. Karrer⁽⁵⁾ to have found that with the correct design of the multiple discharges the losses arising with a number of branches can be considerably reduced in contrast to the usual volute casing. From the detailed experiments of Karrer this improvement is so large that it justifies the use of a number of discharge points and the joining of them together again in a common manifold. This could constitute a completely new form of diffuser arrangement. Figure 195 shows a design of this type. The four component volutes are laid around each other from the inside out and lie in a common plane. The design takes into consideration earlier experience so that the decelerated flows shall be conducted rectilinearly. Curvatures to the passage are only accomplished when the deceleration of the straight section terminates free from separation. Figure 196 shows the compressor of a gas-turbine plant of Messrs. Oerlikon in Zürich which is equipped with such volutes. Because peak efficiencies are necessary in this plant, a proportionally high constructional cost is unavoidable.

⁵ Karrer, W., The Oerlikon experimental gas turbine establishment, *Technik*, 1947, 16 July, supplement to the *Neue Zürcher Zeitung*.

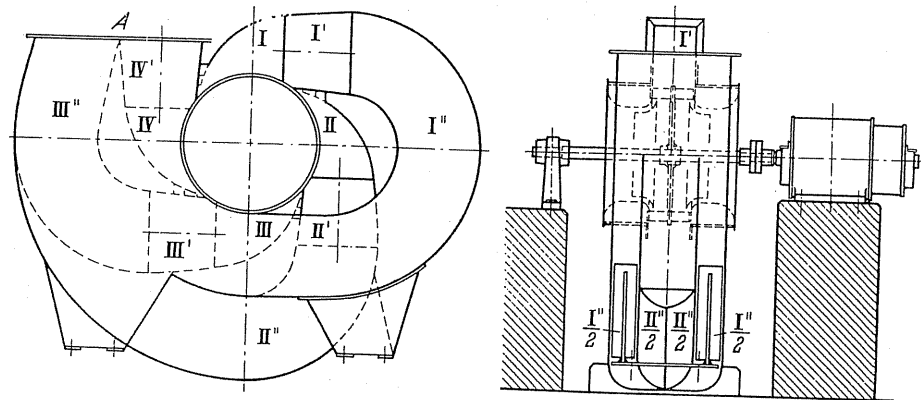


FIG. 195. Volute casing with four adjacent partial volutes combined according to Karrer.
 $n = 1430 \text{ rev/min}$. $V = 625 \text{ m}^3/\text{min}$. $\Delta p = 175 \text{ mm WG}$. $N = 30.5 \text{ h.p.}$ $\eta \approx 80\%$.

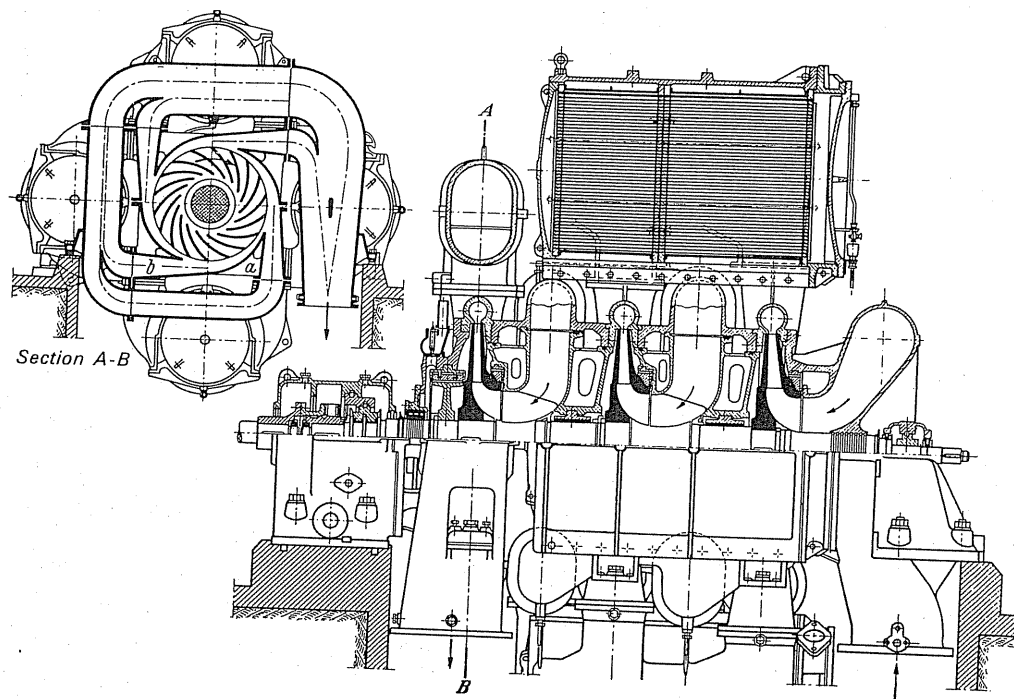


FIG. 196. Volute casing with four discharges combined in a common duct, according to Karrer.
 Radial compressor of a gas turbine of Messrs. Oerlikon, Zürich.

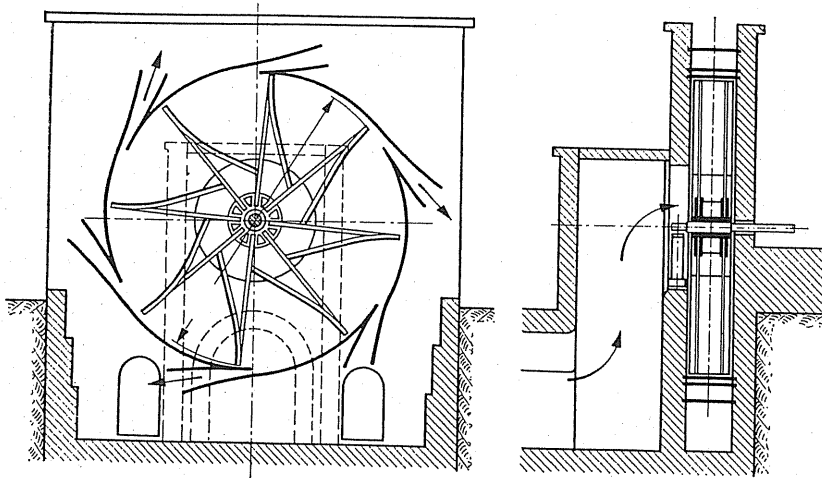


FIG. 197. Mine fan of Harzé with free-discharging partial diffusers.

According to the information from the inventor, Mr. Karrer, efficiencies of 85% were achieved with the highest outputs, while at 30 h.p., 80% was established. The proportionally expensive type of Karrer becomes economical with outputs above 100 h.p.⁽⁶⁾

(ξ) **Graphical methods.** For the numerous forms of cross-sections employed with volutes the calculations will be very complicated. Both the following methods are suitable in practice because of their simplicity.

(c) PRECISE METHOD

It is taken for granted that the principles for development of a section are known. The section will be developed from a trapezium and a rectangle both having the same height (Fig. 198). Thus one is in the position to find any cross-section with the prescribed total height h . However, the position occupied by any particular section on the periphery remains unknown. If the position is fixed by the curvature of admission φ , then a volume $V(\varphi/360)$ flows through the section under consideration; this is equal to

$$\int_0^h c \, dF = \int_0^h cb \, dr.$$

The velocity c is given by $c \approx c_u = (c_{0u} r_0)/r$. Defining the mean velocity as c_{av} , then

$$\frac{V\varphi^\circ}{360} = c_{av} F = \int cb \, dr \quad \text{or} \quad c_{av} = \frac{1}{F} b_{\max} \int_0^h c \frac{b}{b_{\max}} \, dr.$$

⁶ It is noteworthy that in the early days of fan engineering a similar concept was evident. Figure 197 shows an illustration of a design by Harzé which was used in Belgium as a mine ventilator.

First of all c_{av} will be evaluated. To achieve this one plots c against the radial range of the section, which in effect is a parabola. Then c is multiplied by the ratio b/b_{max} and determines the discharge area A bounded by the new curve. After calculation of the area $F (=A)$ of the section one obtains the value of c_{av} from the last formula. The corresponding angle is derived from the equation

$$\varphi^\circ = \frac{360^\circ}{V} c_{av} F.$$

One repeats this operation a number of times in order to obtain sufficient points to permit the plotting of a number of curves for the volute to be conveniently drawn.

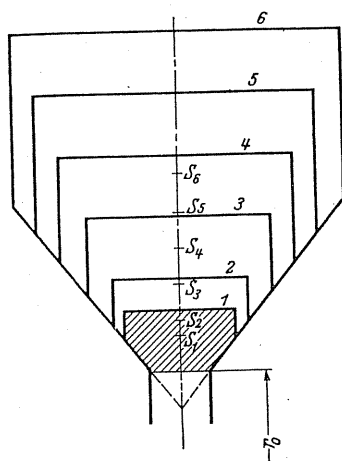


FIG. 198. Volute cross-section comprising a trapezium and a rectangle of equal height.

Example

The method described above is employed for the following assumptions (Fig. 199).

Diameter at the beginning of the volute $2r_0 = 535$ mm.

Peripheral component at the beginning of the volute $c_{0u} = 136$ m/sec. Volume delivered referred to the intake $= 4000$ m³/h. Reduction of volume in volute on account of the static pressure in the impeller $= 1.22$. Actual volume delivered in volute $V = 4000/(1.22 \times 3600) = 0.91$ m/sec. Pressure increase in the complete fan, 0.4 atmospheres.

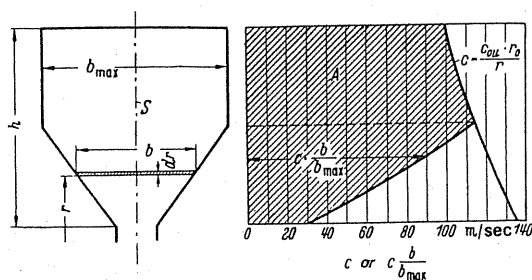


FIG. 199. Graphical procedure for defining a volute for any cross-section.

Now

$$\int c_u \frac{b}{b_{\max}} dr = 90.65.$$

$$c_{av} = \frac{b_{\max}}{F} \int c_u \frac{b}{b_{\max}} dr = 113 \text{ m/sec.}$$

$$\varphi = \frac{360}{V} c_{av} F = \frac{360}{0.91} \times 113 \times 74.7 \times 10^{-4} = 334^\circ.$$

Often with a new design one will have no indication when calculating the cross-section as to which starting point one should assume for this method. It is, therefore, recommended that the end section ($\varphi = 360^\circ$) is approximately determined by this means and it is to be presumed that the section is circular and a constant velocity $c_u = c_{0u}$ prevails.

From this one gets the first approximation

$$F_{360} \approx \frac{V}{c_{0u}}.$$

(d) APPROXIMATE METHOD

If instead of graphical integration one assumes that the average velocity c_{av} at the area centre point is available, this substitution will give a simple method. This has already been recommended for the calculation of the circular section. This assumption is correct if the velocity changes linearly. However, in the case of large volute sections this assumption yields deviations which are useful to consider.

One now continues to determine the point of concentration or centre of the area and the magnitude of the area, then suitably (see Figs. 198 and 199 and also Table 13) plots the velocity which in Fig. 199 is the velocity curve on the right. The corresponding angle φ° one gets from the equation

$$\varphi^\circ = \frac{360}{V} \frac{c_{0u} r_0}{r_0 + s} F.$$

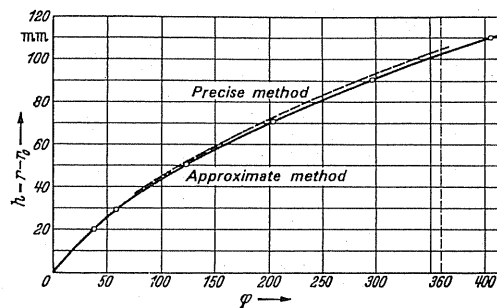


FIG. 200. Path of a volute evaluated according to two different graphical methods.

If one has determined about four to eight sections from the end section it gives an outer boundary through which it is easy to draw a curve. The division of the section is shown in Fig. 198.

For the previous example the method was carried out in Figs. 198 and 199 and then plotted in Fig. 200. As a comparison the velocity in the point of concentration was deter-

mined and compared with the section arrived at by the previous method with an actual velocity of 113 m/sec. It gave 112 m/sec, a negligible error.

According to precise calculation the outer boundary is somewhat larger. Because the correction factor is still to be applied, a precise evaluation of a frictionless section is not necessary so that the last method given is completely sufficient in practice.

TABLE 13. GRAPHICAL EVALUATION OF A VOLUTE WITHOUT CONSIDERATION OF FRICTION (Cross-section of volute according to Fig. 198). S indicates the distance of the point of concentration from the base circle $2r_0$ of the volute

No.	F	S	$r_0 + S$	φ°	h
6	93	6.4	33.15	405	110
5	65.25	5.2	31.95	294	90
4	43.4	4.0	30.75	204	70
3	25	2.88	29.65	121.5	50
2	11.3	1.6	28.35	57.5	30
1	7.4	1.2	27.95	28.1	20

68. THE INFLUENCE OF FRICTION IN VOLUTES ON THE TOTAL ENERGY CONVERSION

The influence of friction on the effectiveness of volutes. In every volute, friction between the fluid and the walls of the casing will result in losses. These losses will manifest themselves as a fall in pressure in the direction of flow. This means that a fall in pressure will occur at the origin of the volute, i.e. just after the impeller. The volute, however, is designed precisely so that the static pressure can remain constant over the whole periphery of the impeller. Apart from genuine friction losses a pressure fluctuation will occur at the impeller. These fluctuations will occur periodically and thus will cause unsteady flow through the impeller. It can, therefore, be assumed that impeller losses will increase. Friction in the volute will have two effects, (a) friction loss in the volute, and (b) reduction of flow through the impeller as an effect of unsteady static pressure at the periphery of the impeller.

It can be demonstrated that the reduction of flow through the impeller can be overcome by a slight increase in sectional area of the volute. This will be proved on a conical diffuser. Using the symbols of Fig. 201,

$$c_1 d_1^2 = c_2 d_2^2 = c d^2; \quad c = c_1 \left(\frac{d_1}{d} \right)^2;$$

and

$$d = d_1 + 2x \tan(\alpha/2).$$

The pressure drop along dx is

$$dH_r = \lambda \frac{c^2}{2g} \frac{dx}{d}.$$

Introducing

$$c = c_1 \left(\frac{d_1}{d} \right)^2$$

one gets

$$H_r = \int_1^0 \frac{\lambda c_1^2 d_1^4}{2g d^5} dx = \frac{\lambda c_1^2 d_1^4}{2g} \int_1^0 \frac{dx}{[d_1 + 2x \tan(\alpha/2)]^5}.$$

The solution is

$$H_r = \frac{\lambda c_1^2 d_1^4}{2g} \frac{1}{8 \tan(\alpha/2)} \left(\frac{1}{d_1^4} - \frac{1}{d_2^4} \right). \quad (150)$$

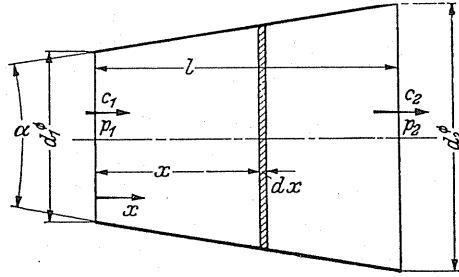


FIG. 201. Conically enlarged diffuser.

This fall in pressure—caused by friction—will now be compensated by a rise in pressure produced by increasing the cross-sectional area of the diffuser. This will be explained by reference to the Bernoulli equation

$$\begin{aligned} \frac{p_2}{\gamma} - \frac{p_1}{\gamma} &= \frac{c_1^2 - c_2^2}{2g} = \Delta H; \\ \Delta H &= \frac{c_1^2 - c_2^2}{2g} = \frac{c_1^2}{2g} \left[1 - \left(\frac{d_1}{d_2} \right)^4 \right]. \end{aligned} \quad (151)$$

Equalising H_r and ΔH one will obtain $\tan \alpha/2 = \lambda/8$. For small angles $\tan \alpha \approx \alpha$, so that $\alpha = \lambda/4$. For example, $\lambda = 0.04$ the diffuser angle becomes $\alpha^\circ = (0.04/4) (180/\pi) = 0.573^\circ$, or approximately $\frac{1}{2}^\circ$. This calculation is valid only for small diffuser angles (up to about 8°) as the coefficient of friction λ rises considerably for larger angles on account of separation of the flow.

Similarly, one can compensate for the fall in pressure caused by friction in the volute, when the cross-sectional area increases so that pressure along the periphery of the impeller remains constant. The calculation, however, becomes much more involved, as constantly new quantities of fluid enter the volute cross-sectional area, and the velocity distribution through this area follows other laws.

Before one can proceed to apply the above calculation to the volute, it is necessary to consider other factors. Within the volute the flow is not only retarded but also follows a curved path. We shall, therefore, have to alter the shape of the diffuser illustrated in Fig. 201 by curving it. The curvature will produce a further disturbance. It is well known that where streamlines are curved and also when they are retarded in a duct, secondary flow occurs. This can be understood easily. The centrifugal force in the centre of the section is bound to be greater than at the sides because air particles in the centre have a greater velocity than those which are retarded at the walls of the duct by friction. These particles in the centre are

pushed more vigorously towards the outside. At the discharge section a so-called double vortex will occur which becomes super-imposed on to the main flow. The streamlines at the centre of the section are steeper than those at the boundaries. On account of this secondary air movement, the path of each particle becomes longer; in addition each particle will have a greater velocity on the average than without the secondary movement. *In consequence the influence of friction is even greater than if calculations are based only on mean velocities.*

According to tests⁽⁷⁾ the double vortex will cause considerable separation of the intermediate layer (Fig.202) especially the air stream entering the discharge section. Therefore Oesterlen⁽⁸⁾ suggests the conversion of the double vortex into a simple straight vortex by arranging the volute asymmetrically towards the outer side (Fig.203). This suggestion was verified experimentally⁽⁹⁾ with a spiral flow with a straight vortex; losses were considerably lower. The undesirable separation at the lip was avoided. The effect of a straight vortex can be explained similarly to those which are observed in double bends.

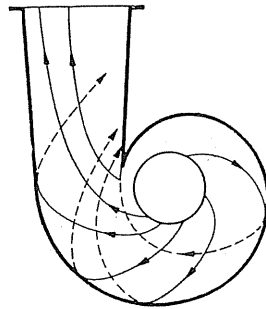


FIG.202. Diagram of streamlines in a spiral case according to Kranz.

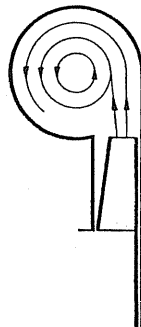


FIG.203. Asymmetrical spiral according to Oesterlen.

According to tests by Kranz and Broer it seems unnecessary to take friction into account. Dimensions which are based on the assumption that friction can be neglected, turn out to be satisfactory in most cases. It may, however, be objected that in the tests of Kranz and Broer, measurements were made *without an impeller*, so that any interchange of energy

⁷ Kranz, *Flow through Volute*, Forschungsheft 370.

⁸ Oesterlen, *Deutsche Wasserwirtschaft*, 1935, p. 41.

⁹ Broer, F., *Volute of pumps with twisted flow*, *Z VDI*, 37, 391.

between the impeller and the fluid was completely absent and there were considerable variations in the straight-line discharge. Because of this one cannot come to any final conclusions.

Fans usually have larger volutes; thus the influence of friction is insignificant and can be ignored in most instances. However, the conditions for narrow volutes which are used with high-pressure compressors are different; friction cannot be ignored in any calculations.

For the case of a circular volute the computation will proceed as follows:

$$\frac{\Delta F}{F} \approx \frac{\lambda \pi^2}{2} \frac{C_{0u} r_0}{V} d \quad (152)$$

(d is the diameter of the circular volute). The effect in the first instance depends on the expression $c_{0u} r_0 (d/V)$. It is only important where d is small compared with r_0 .

69. REDUCTION OF ROTATIONAL FLOW OWING TO FRICTION IN ANNULAR SPACES AND STATIONARY GUIDE VANES

The rotational flow between smooth surfaces is greatly influenced by surface friction. Rotation can be reduced and absorbed completely by friction. This is shown by the example in Fig.204 in which a free annular space is located behind the axial impeller. The pressure

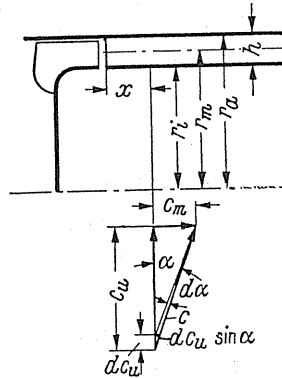


FIG.204. Effect of friction in a ring channel with axially rotating flow.

drop for a very small section of the fluid ds will be $d[\Delta p] = \lambda (\varrho/2) c_m^2 (ds/2a)$, where a is the hydraulic radius of the fluid which will be calculated here as h . The pressure drop has two effects. The c_u -component will become reduced considerably, whereas the c_m -component owing to continuity remains constant. In addition to the reduction of the actual *kinetic energy* $d[(\varrho/2) c_u^2]$, a purely *static* pressure drop will also take place. One can assess it by calculating the effect of friction of the constant component c_m along the sectional length ds $\lambda (\varrho/2) c_m^2 (ds/2h)$, thus we get

$$d \Delta p_{\text{loss}} = \lambda \frac{\varrho}{2} c^2 \frac{ds}{2h} = d \left(\frac{\varrho c_u^2}{2} \right) + \lambda \frac{\varrho}{2} c_m^2 \frac{ds}{2h}; \quad (153)$$

on account of $c^2 = c_u^2 + c_m^2$ we get

$$\lambda \frac{ds}{4h} = \frac{dc_u}{c_u}; \quad (154)$$

this equation can be integrated easily

$$\lambda \frac{s}{4h} = \ln \frac{c_u}{c_{0u}}; \quad c_u = c_{0u} e^{(\lambda/4h)s}.$$

Thus we see how c_u will vary with s . Owing to the fact that we have a curved streamline and an unknown function for s , the equation does not appear to be very helpful in the first instance. If, however, we take into consideration that $ds = dx/\sin \alpha$ and according to Fig. 204

$$c \, d\alpha = dc_u \sin \alpha \quad \text{and} \quad c = \frac{c_u}{\cos \alpha}, \quad \frac{dc_u}{c_u} = \frac{d\alpha}{\sin \alpha \cos \alpha}$$

and we introduce these expressions into eqn. (154), we get

$$\frac{\lambda}{4h} dx = \frac{d\alpha}{\cos \alpha}. \quad (155)$$

This basic equation appears to be the most suitable for solving the problem, and can be integrated easily provided that the angle α is small and if one can assume that $\cos \alpha \approx 1$. In this case we get $(\lambda/4h) dx = d\alpha$, and it follows $(\lambda/4h) x = \alpha - \alpha_0$. As the angle has to be small, one can apply—if more suitable—the following form: $(\lambda/4h) x = \sin \alpha - \sin \alpha_0$. One can also find an exact solution for the basic equation (155). The result of the integration is

$$\frac{\lambda}{4h} x = \ln \frac{\tan [(\pi/4) + (\alpha/2)]}{\tan [(\pi/4) + (\alpha_0/2)]}. \quad (156)$$

If one introduces into the basic equation (155) $dx = ds \sin \alpha$, it is possible to calculate the exact relation between α and s . The solution is

$$\frac{\lambda}{4h} s = \ln \frac{\tan \alpha}{\tan \alpha_0}; \quad \tan \alpha = \tan \alpha_0 e^{\frac{\lambda}{4h}s}.$$

In order to estimate the loss of energy in relation to x we enter the values $c = (c_u/\sin \alpha)$ and $ds = (dx/\sin \alpha)$ into the main equation (153) $d\Delta p_{\text{loss}} = \lambda (q/2) c^2 (ds/2h)$.

The following approximation, $(\lambda/4h) x = \sin \alpha - \sin \alpha_0$, may be used and this leads to the following equation:

$$\Delta p_{\text{loss}} = \frac{q}{2} \left[c_m^2 \frac{1}{\sin^2 \alpha_0} - \frac{1}{[x (\lambda/4h) + \sin \alpha_0]^2} \right]. \quad (157)$$

To obtain quantitative values we start with the basic equation $(\lambda/4h) dx = (d\alpha/\cos \alpha)$ and convert it to an equation of finite differences:

$$\frac{\Delta x}{h} = \frac{4 \Delta \alpha}{\lambda \cos \alpha} = \frac{4 \Delta \alpha^\circ}{57.3 \lambda \cos \alpha}. \quad (158)$$

A graphical evaluation of this equation is easy. To do this we choose a constant angle difference of $\Delta\alpha^\circ = 5^\circ$ and enter into a table the corresponding values $\Delta x/h$. The cylindrical development of the streamline can be plotted easily. In Fig. 205 the curve is shown where $\lambda = 0.03$ and the initial value of α_0 is 20° . We get a curve which shows gradually increasing values of α . As α and x are now known and in addition c_m remains constant, the velocity c_u can be determined for every angle α . This is done in Fig. 205. In the beginning c_u decreases considerably.

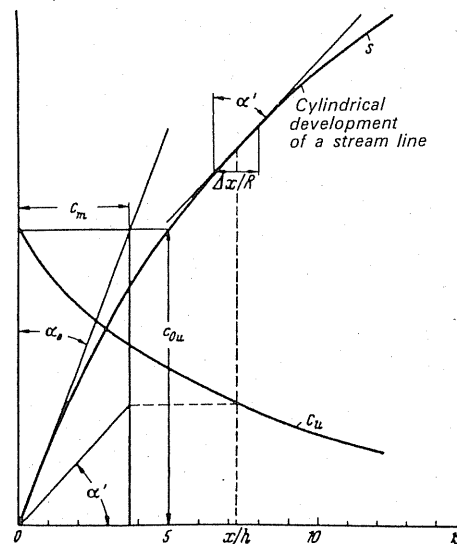


FIG. 205. Cylindrical development of a streamline, path of c_u .

Similar calculations can be made for smooth stationary guide blades. In this case Pfeleiderer⁽¹⁰⁾ obtained the approximate equation

$$\frac{1}{c_u r} = \frac{1}{c_{0u} r_0} + \frac{\lambda \pi}{2V} (r - r_0). \quad (159)$$

The width of a smooth stationary guide blade is practically equal to the width of the impeller. The best running conditions will be achieved with comparatively small angles between the entrance velocity and the periphery. If $r/r_1 < 1.5$, the effect of the diffuser is annulled by friction and the losses due to separation. Conical stationary guide blades are worse.

Secondary flow due to friction. Previously it was assumed that friction is distributed uniformly over the area concerned similar to the distribution in straight tubes. In the present case the flow may vary. At the boundary zones the velocities will be considerably reduced, whereas the flow in the centre will remain unaffected at the start. In Fig. 206 this condition is schematically indicated. This means that, owing to friction, the angle α will become larger

¹⁰ Pfeleiderer, C., Research relating to turbine wheel machinery, *Forschungsarbeiten*, No. 295.

in the boundary zones than in the centre. Unrolling of the fluid and secondary flow can take place as one noted with volute casings. These possibilities have not yet been investigated thoroughly. Therefore it is not practicable to pursue theoretical calculations beyond those which have already been given.

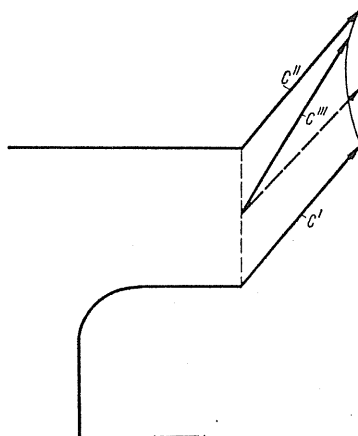


FIG. 206. The effects of friction on velocity vector.

70. EFFECT OF SMALL CHANGES ON THE BEHAVIOUR OF VOLUTES

A fairly constant pressure on the periphery of the impeller for a given flow can be achieved if the volute is correctly designed. A certain disturbance is, however, caused by the lip, and the nearer the lip to the impeller the greater the effect. To obtain a clearer picture one will have to investigate the flow in the vicinity of the lip. The lip splits the flow coming from the impeller; one part flows directly into the fan outlet whereas the other will be returned to the volute: it will have to retrace a path corresponding to the whole circumference of the volute before being re-discharged into the outlet. The flow circulating around the lip will vary according to the relations between the flow quantity with respect to the standard flow. For the standard flow quantity the turning point of the branch flow line is fairly close to the edge of the lip; if the flow quantity increases, this turning point moves to the inside of the volute casing and if it decreases, it will move into the discharge piece. Figure 207 shows the branch flow lines as they would occur in accordance with the theoretical calculations of

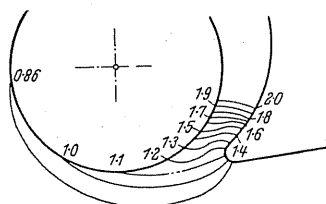


FIG. 207. Branching of streamlines according to Straszacker.

Straszacker⁽¹¹⁾ which agree well with tests. This diagram shows that for non-standard flow quantities considerable disturbances of the pressure symmetry may be expected. The distribution of the static pressure along the periphery of the impeller for given flow quantities can be seen in Fig. 208, as the result of tests made by the author.⁽¹²⁾ The figure shows that

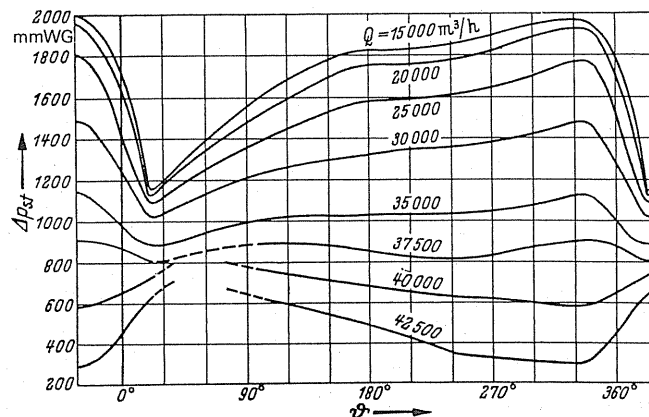


Fig. 208. Distribution of static pressure on the circumference of the impeller for various volume flows.

the pressure distribution for a mass flow of $37,500 \text{ m}^3/\text{h}$ will produce a fairly constant pressure distribution. Such deviations from a constant pressure which are shown in the curve may be removed by widening the volute in the vicinity of the lip, preferably by increasing the angle on the inner side of the lip. The success of this procedure will be dependent on the design of the volute and the specific speed. On account of noise it is often necessary to increase the distances between the lip and the impeller, so that further correction will become unnecessary.

For a mass flow which is less than standard, the pressure beyond the lip in the direction of flow will increase, whereas for a larger mass flow the opposite will occur. This phenomenon may be explained as follows. For a small flow the volute casing is too large; the velocity head of the flow will be converted to pressure so that the volute acts like a diffuser. For large flows the volute is too small. In this case the pressure loss due to the mass flow causes a considerable reduction of pressure in the region from the lip to the discharge of the volute. The asymmetric distribution of static pressure corresponds to an asymmetric entry of the impeller. The mass flow through any section of the impeller depends on the static pressure at the periphery of the impeller. The pressure characteristic of the gap is a decisive factor in the mass flow. The relation between the impeller and the pressure in the gap is indicated in Fig. 87 which shows that the greater the flow the smaller the gap pressure. If one relates this to the pressure distribution shown in Fig. 208, the following interpretation can be given: for smaller flows the dimensions of the entry must decrease with

¹¹ Straszacker, K., Computation of flow conditions in volute cases, *Ing. Arch.*, 2 (1931) 92; Broer, F., Flow in volute casing of pump, Diss., Hanover, 1939.

¹² Tests of this kind are of value only if measurements are taken with the impeller operating. The impeller cannot be replaced by internal stationary guide vanes which have the same shape because the flow through these vanes does not follow the equation of Bernoulli. The pressure distribution along the periphery of a rotating impeller will be governed by laws which indicate that pressure in the gap is a significant factor.

the volute angle. This means that the greater part of the flow occurs in the vicinity of the lip, and the remaining part of the impeller does not play an important part in the transfer of energy. For larger flows the opposite will take place. The impeller sections nearest to the inlet duct will have the largest flow. This means that the individual blade passages are intermittently supplied and that during their rotation the flow is temporarily either accelerated or retarded. With smaller flows the velocity decreases during rotation, but a temporary retardation will occur, whereas for larger flows acceleration will take place. This can cause a reduction of the impeller losses for large flows. These phenomena have not been investigated yet. Generally speaking, it appears that no great disadvantages have been observed with an asymmetric flow. This is possible because the efficiency of the volute casing is higher than that of multistage axial-flow fans.

71. THE DIMENSIONS OF THE LIP

Figure 209 shows the structure of flow in the region of the lip. At the top of the lip a turning point S is formed by which the flow is divided into two parts; one part will move to the left into the volute, whereas the other will flow directly into the discharge outlet. If one changes the position of the lip on the streamline representing the division of flow, the flow conditions will not be altered. The top of the lip will have to be thickened to avoid interference of the flow when the lip is enlarged. Two designs are shown as I and II in Fig. 209. Experience has shown that a fairly large lip should be aimed at, especially as one will thereby reduce noise. If the lip is put too near the impeller, the fan will "howl".

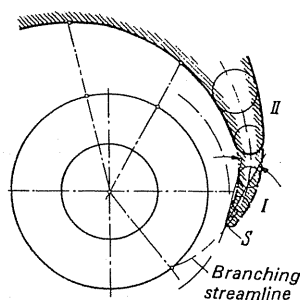


FIG. 209.

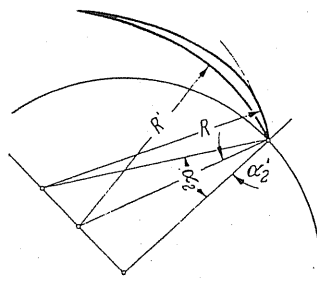


FIG. 210.

Near the impeller the angle of discharge exceeds the angle of the volute and the difference between the angles is increased as the ratio B/b_2 becomes larger. Obviously if one increases the angle near the lip, one must enlarge the neighbouring volute casing at the same time. Figure 210 shows the geometric construction of the lip where α_2 is the angle of discharge at the impeller and α'_2 the angle of the volute. The lip begins with a logarithmic spiral with the angle α_2 , i.e. with the radius of curvature R , whilst a smooth transition to the main spiral takes place. This well-tried practical method⁽¹³⁾ has recently been verified experimentally.⁽¹⁴⁾

The designer must not retract the lip without considering the lip angle, otherwise there will be a frequent wasteful circulation in the volute casing: if the lip is moved it should always be on the dividing streamline. According to Fig. 192 it is possible to control the flow by displacements of the lip in a radial direction.

72. THE DISTRIBUTION OF PRESSURE AND FORCE IN THE VOLUTE CASING

Given the pressure distribution in the volute casing one can ascertain the effects of changing the flow on conditions in the volute casing. Figure 211 shows the total force P which acts on the casing and the distribution of the pressure difference along the casing. It is characteristic that at about 43 m³/h the direction of the total force suddenly increases by nearly 180°. The greatest pressure difference occurs with the greatest flow.

73. LOSSES IN THE VOLUTE CASING

The development of high-efficiency blowers showed that the losses can be kept astonishingly low even for a simple, rectangularly shaped volute casing if they are designed exactly in accordance with the law of areas.

As the problem of loss is a problem of retardation, one must obviously take diffuser losses into account. Where the entry velocity into the volute casing is c_3 and the discharge velocity c_4 , the diffuser loss is

$$\Delta p''_{\text{loss}} = (0.1-0.2) (\varrho/2) [c_3^2 - c_4^2].$$

For the majority of blowers the width of the casing B is often considerably greater than the width of the impeller b . The meridian velocity c_{2m} will change to $c_{3m} = (b/B) c_{2m}$. This will cause a shock loss which will increase considerably as the width increases reaching a maximum value:

$$\Delta p''_{\text{loss}} = (\varrho/2) (c_{2m}^2 - c_{3m}^2)^2 = (\varrho/2) c_{2m}^2 \left[1 - \left(\frac{b}{B} \right)^2 \right].$$

¹³ Strassacher, R., *Ing.-Arch.*, 1935, No. 3.

¹⁴ Moser, Research paper on volute casing of radial fans, *Heizung-Lüftung-Haustechnik*, 1957, p. 319.

In addition there is a loss due to friction. Broecker⁽¹⁵⁾ has shown that these losses can easily be expressed by the equation $\Delta p_{\text{loss total}} = (\varrho/2) c_{2m}^2$. This means that the loss is to be considered throughout as the dynamic pressure of the meridian entry velocity c_{2m} in the

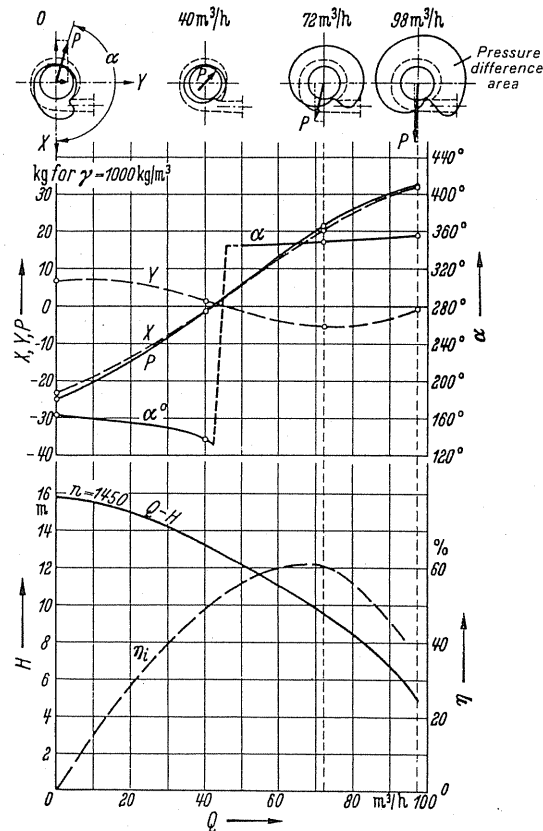


FIG. 211. The effect of various loads on the resultant force and its direction in a spiral housing. according to Lewinsky-Kerslitz.

diffuser. If one relates the total loss coefficient to the dynamic pressure of the entry velocity into the volute of the casing c_2 , one will get

$$\Delta p_{\text{loss total}} = \zeta \frac{\varrho}{2} c_2^2, \quad \zeta = \frac{\Delta p_{\text{loss total}}}{(\varrho/2) c_2^2} = \frac{(\varrho/2) c_{2m}^2}{(\varrho/2) c_2^2} = \left(\frac{c_{2m}}{c_2} \right)^2 = \sin^2 \alpha_2.$$

It is also advantageous to keep the slope of the streamlines entering the volute casing as small as possible. The question now arises as to how far one may increase. According to Broecker,

$$B/b_2 = \alpha_2^\circ/6,$$

¹⁵ Broecker, E., Optima problems for radial fans, *Heizung-Lüftung-Haustechnik*, 1959, p.155.

where B is the width of the casing, b_2 is the width of the impeller at the discharge, and α_2° is the slope of the flow when entering the casing. This formula is valid up to 45° .

Rotating diffuser. Independent of the volute casing and other types of guide vanes, one can achieve a retardation of flow at the discharge of the impeller casing by a direct method, viz. providing diffuser type enlargement of the discharge openings of both impeller side plates, as can be seen in Fig.212. For narrow impellers such a measure is very effective. As particles are thrown off the boundary layer, such diffusers are very suitable. Specially flat characteristics and greater power can thus be achieved.

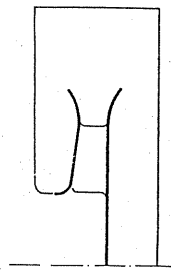


FIG.212.

74. DIFFUSERS FOR IMPROVING THE PERFORMANCE OF VOLUTE CASINGS

One should not increase the volute merely because, for example, the duct is too large to be connected. Whatever the circumstances the volute should be designed according to the rules already given in order to avoid disturbance of the impeller and other unfavourable influences. In such cases, however, a special diffuser as illustrated in Fig.213 can be fitted.

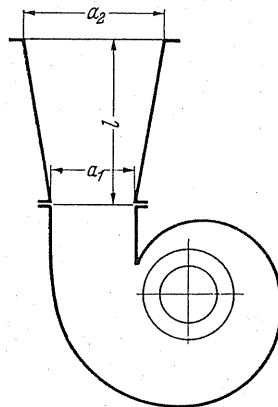


FIG.213. Improvement of a spiral housing by adding a diffuser.

This will gradually reduce the air velocity as the sectional area of the diffuser gradually increases. Similar diffusers which are very large are often used in the ventilation of mines.

Research work on venturi meters has been limited to smaller Reynolds numbers. This showed that, under certain circumstances, it is useful to *increase the cross-sectional area abruptly after a short initial conical enlargement*. It is best to limit the diffuser to the point where flow separation begins. For diffuser angles between 15° and 20° and a sectional area ratio of 1:4, efficiencies of 0.8–0.85 can still be achieved. Diffusers with abrupt expansions occur, e.g. with drum-type impellers.

Even for small radial-flow fans, the fundamental laws of fluid mechanics still apply. The larger the Reynolds number, the smaller the optimum angle of enlargement will become. Whereas $8-9^\circ$ is often given as a good average value, one will have to reduce the angle to 6° , even to 5.5° , for very high Reynolds numbers.

The design of large diffusers and their connection with duct work under different conditions of joining will have to be investigated in every individual case. Under difficult circumstances the only way to obtain feasible solution will be to investigate the problem by means of a model test. Design criteria for the shaping of diffusers are much better now than they were in the past. Further discussion of this topic from the point of view of the practical engineer is outside the scope of the present book. The author discusses this topic elsewhere.⁽¹⁶⁾

To minimise the losses in a diffuser it is, under certain circumstances, worth while to use annular baffles or guide vanes. This procedure was first used in the design of large wind tunnels⁽¹⁷⁾ (Fig. 214).

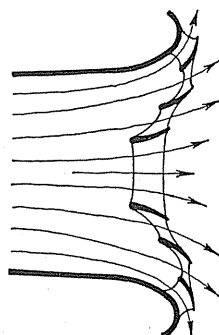


FIG. 214. Outlet diffuser subdivided by ring guide blades.

75. DISCHARGE FILTERS

In many installations, draughts from a free-discharging fan can be very disagreeable. Even with the best diffusers this cannot be entirely avoided. At the cost of a small drop in pressure, a filter (Fig. 215) will be an ideal remedy. Such a filter is well known in vacuum cleaners. The loss of pressure in such cases is indicated in Fig. 215. If the filter is sufficiently

¹⁶ Eck, B., *Technische Strömungslehre*, 7th edn., Berlin/Göttingen/Heidelberg, Springer, 1966.

¹⁷ Darrieus, G., *Account of the Erection of Wind Tunnels*, BBC Report No. 143, p. 168.

large the loss can be kept extraordinarily small. It is wrong in principle to leave out the diffuser between the fan outlet and filter. The diffuser will regain a greater pressure in most instances than the filter will lose.

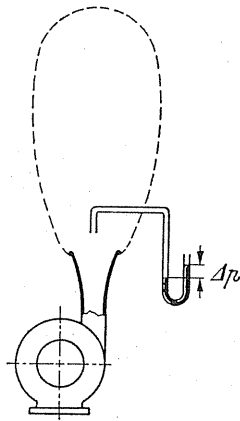


FIG.215. Discharge filter for straightening the outlet flow of air.

PART B

THEORY AND CALCULATION
OF AXIAL-FLOW FANS

CHAPTER XII

CALCULATION OF THE NORMAL AXIAL-FLOW FAN

76. GENERAL REMARKS

The designation "axial-flow fan" like the designation "radial-flow fan" originates from the main flow path through the rotor. The rotor is in the path of the axis of rotation. Accordingly, the rotor consists of a hub which is fitted with aerofoils in a radial direction. The aim in the design is to profile these aerofoils in such a way that all air particles are given the increase in energy and the unavoidable losses are kept as low as possible.

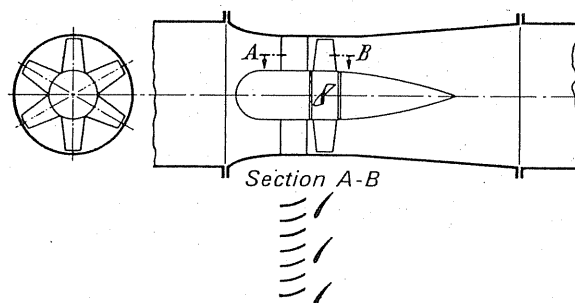


FIG. 216. Diagram of an axial-flow fan.

In general application, the fan, according to Fig. 216, becomes the "armature of a duct". By its introduction into a duct the axial-flow fan simplifies the design. This is because owing to the basically axial-flow path, the fan forms the part of the duct externally.

The following components are mainly present in axial-flow fans:

- (1) A piece of duct constricted into a nozzle and a duct expanded into a diffuser. In many cases, in the interests of efficiency and convenience, it is necessary for the diameter of the rotor to be less than that of the duct.
- (2) Rotor consists of a hub and aerofoil blades, the number of which generally varies from 4 to 8. The limits lie between 2 and 50 blades.
- (3) Upstream and downstream guide vanes.

As the flow through the fan is symmetrical to the axis, uniform flow conditions will be encountered on any random section of the cylinder. Therefore it is advisable to develop this cylinder on a plane. This is shown in Fig. 216 (at the bottom). Guide vanes and rotor appear here as a cascade of blades of infinite length. Each section of the cylinder therefore will have a different appearance. If we look at the section AB close to the hub, cascades of blades are

seen, the pitch of which is less than at the periphery, and their blade cross-section—according to length, form, and angle—must look different from there since, of course, the peripheral speed varies from radius to radius. It will be presumed that the flow through the cascade of blades will be the governing factor for the design of fans of this kind. In actual fact the knowledge of the so-called cascade flow is the basis for the whole calculation.

77. SIMPLE RELATIONSHIPS OF CASCADE FLOW

(a) STATIONARY CASCADE

Let the air entering at an angle α_1 be deflected at an angle α_2 by means of a static cascade of infinite length. The curve blades drawn in Fig. 217 are, for example, intended to indicate by what means it is possible to effect a deflection of this kind structurally. Let angles α_1 and α_2 be measured at a distance before or after the cascade so that there is not the slightest inkling of a blade effect. Since as a rule the blades are set far apart from each

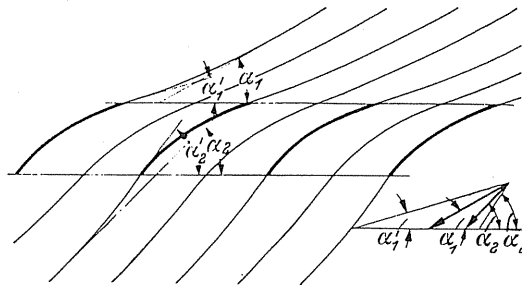


FIG. 217. Streamlines in a cascade.

other, the angle differences close to the cascade will have to be greater. The flow line running at a direct tangent to the blades will enter at the angle α'_1 , which is smaller than α_1 and will discharge at the angle α'_2 , which is greater than α_2 . The flow path obtaining between two blades will be deflected considerably less since the lateral "travel" is very slight. It is clear that the total deflection from α_1 to α_2 can only be achieved if $\alpha'_1 < \alpha_1$ and $\alpha'_2 > \alpha_2$, and this can be applied for the blade angle. The angles will only coincide as $\alpha'_1 = \alpha_1$; $\alpha'_2 = \alpha_2$, at a very narrow pitch. The designation "excess angle" is invariably used to imply the necessary variations of angles due to the finite number of blades. Figure 217 shows this cascade flow with this excess angle.

Figure 218 shows an investigation into the flow through a full division, and the designation laid down there will be used for the succeeding calculations. The expression $c_{1m} tb = c_{2m} tb$, i.e. $c_{1m} = c_{2m} = c_m$ (b is the width perpendicular to the plane of the drawing), and is taken from the continuity equation. From this it follows that the velocity triangles all have the same level c_m .

This gives

$$c_1 \sin \alpha_1 = c_2 \sin \alpha_2.$$

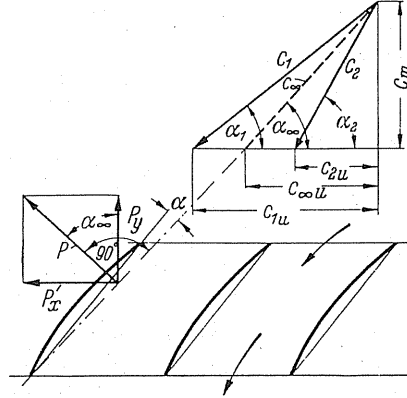


FIG.218. Diagram of forces in a cascade.

Frictional losses will be neglected at present so that the pressure difference before and after the cascade can be ascertained by the Bernoulli formula.

$$\Delta p_{\text{stat}} = \frac{\gamma}{2g} [c_1^2 - c_2^2]. \quad (160)$$

This pressure entails a force perpendicular to the axis of the cascade

$$P_y = \Delta p_{\text{stat}} tb = \frac{\gamma}{2g} [c_1^2 - c_2^2] tb = \frac{\gamma}{2g} [c_{1u}^2 - c_{2u}^2] bt.$$

The force in the direction of the cascade can be calculated readily according to the momentum principle. The mass $q = tb c_m (\gamma/g)$, flows through division t in 1 second. In the direction of the cascade this mass varies its speed.

$$c_2 \cos \alpha_2 - c_1 \cos \alpha_1 = c_{2u} - c_{1u}.$$

To do this the cascade must exert a force P'_x on the air:

$$P'_x = q (c_{2u} - c_{1u}) = tb c_m \frac{\gamma}{g} (c_{2u} - c_{1u}), \quad (161)$$

whereas the opposing force P_x is exerted by the air on the cascade

$$P'_x = tb c_m \frac{\gamma}{g} (c_{1u} - c_{2u}).$$

Applying the formula $P = \sqrt{P_x^2 + P_y^2}$ we obtain from P_x and P_y the resultant

$$P = \frac{\gamma}{g} (c_{1u} - c_{2u}) c_{\infty} tb.$$

(The reaction forces are described in Fig.218, i.e. the forces which the air exerts on the blades.)

Our interest is in this resultant and for this purpose we calculate as follows:

$$\frac{P_y}{P_x} = \frac{\frac{1}{2} (\gamma/g) [c_1^2 - c_2^2] t b}{\frac{\gamma}{g} [c_{1u} - c_{2u}] c_m t b} = \frac{(c_{1u} + c_{2u})/2}{c_m} = \cot \alpha_\infty$$

or, in general,

$$P_y : P_x : P = \frac{c_{1u} + c_{2u}}{2} : c_m : c_\infty.$$

The mean value $(c_{1u} + c_{2u})/2$ has been inscribed in Fig. 218. Designating the appropriate angle as α_∞ it follows from this equation that the path of the resultant lies perpendicular to this direction. However, no conditions were laid down beforehand regarding the form and number of blades. It can be generalised that: *If by any means it has been possible to deflect a flow of finite widths from angles α_1 to angle α_2 or to alter it from c_{1u} to c_{2u} , then forces to do this are required which lie perpendicular to a mean path which is formed from the meridional velocity and the mean components in the direction of the cascades.* (This still applies for variable axial speeds.)⁽¹⁾

(b) ADJUSTABLE CASCADE

As soon as the cascade is moved in the cascade axis the force P'_x carries out work in the path of the cascade. If the cascade moves to the opposite direction of P'_x , the work is transferred to the cascade (turbine), whereas the reverse direction of movement transfers work to the flowing medium (pump). There is no alteration to the validity of the cascade formulae derived previously on account of the movement. If a specified deflection of the absolute velocity is achieved, the conditions of the momentum principle remain in force independent of how this is achieved or with which cascade, i.e. stationary or running.

If the cascade velocity is u , then a power $P'_x u$ is transmitted to the air volume corresponding to the cascade pitch. In the same way as with radial-flow fans we imagine this work being converted to lift. The weight of air qg flowing through the cascade division t per second is lifted to a height H . By comparing both work equations we get

$$P'_x u = qgH; \quad q(c_{2u} - c_{1u}) u = qgH$$

$$H = \frac{1}{g} u [c_{2u} - c_{1u}]. \quad (162)$$

In fans it is generally more practical to work with a pressure Δp instead of the pressure head. As stated before, for this we arrive at

$$\Delta p = \rho u [c_{2u} - c_{1u}]. \quad (163)$$

Here again, therefore, the Euler turbine formula is obtained.

¹ Pollmann, *Konstruktion*, 1950, p. 373.

In order to observe the details relevant to the cascade we form the velocity triangle in accordance with Fig. 219. The cascade moving at u (m/sec) is swept at an intake velocity c_1 . The absolute discharge velocity is c_2 . The relative velocities w_1 and w_2 are obtained from $c_1 = u \hat{+} w_1$ and $c_2 = u \hat{+} w_2$.

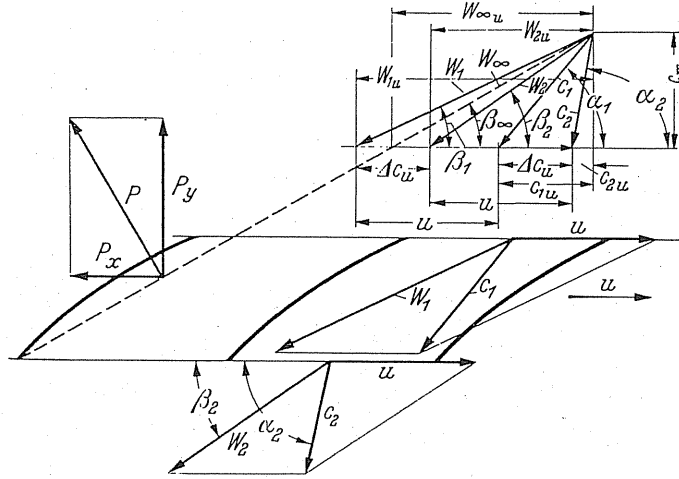


FIG. 219. Effect of forces on a moving cascade.

If we move along with the cascade we only see a stationary cascade with the intake and discharge velocities of w_1 and w_2 . The relationship derived above must be applicable also to the relative cascade flow since the Bernoulli equation as well as the impulse equation are still applicable to this flow free of vortices. It is found in particular, therefore, that the force acting on a blade is perpendicular to w_∞ . w_∞ is derived readily by halving the extreme points of w_1 and w_2 . Let the path of w_∞ towards the axis of the cascade be designated as β_∞ . Analogous to the calculation carried out under (a) we obtain

$$\Delta p_{\text{stat}} = \frac{\gamma}{2g} (w_1^2 - w_2^2)$$

$$P_y = \Delta p_{\text{stat}} t b = \frac{\gamma}{2g} (w_1^2 - w_2^2) t b = \frac{\gamma}{2g} (w_{1u}^2 - w_{2u}^2) t b$$

$$P_x = q (w_{1u} - w_{2u}) = q (c_{1u} - c_{2u}) = t b c_m \rho (w_{1u} - w_{2u}) \\ = t b c_m \rho (c_{1u} - c_{2u})$$

$$P = \sqrt{P_x^2 + P_y^2} = \rho t b (w_{1u} - w_{2u}) w_\infty.$$

The direction of the resultant P again is obtained from

$$\frac{P_y}{P_x} = \frac{(w_{1u} + w_{2u})/2}{c_m} = \cot \beta_\infty;$$

the more general relationship also is present:

$$P_y : P_x : P = \frac{w_{1u} + w_{2u}}{2} : c_m : w_\infty. \quad (164)$$

The following general relationship occurs between the angles:

$$\cot \beta_\infty = \frac{1}{2} [\cot \beta_1 + \cot \beta_2] = \frac{1}{2} \frac{\sin(\beta_1 + \beta_2)}{\sin \beta_1 \sin \beta_2}. \quad (165)$$

(c) THE FOUR MAIN CASES OF AXIAL-FLOW FAN

In axial-flow fans the inlet and discharge flow can be either axial or oblique, since an axial alignment takes effect by means of upstream or downstream guide vanes. Such arrangements, however, only occur in fans where a duct is connected before and after the fan. Since in these ducts rotational flow cannot be accommodated, we will have to limit ourselves mainly to arrangements where the intake and discharge flow is free of rotation, i.e. a curve in the axial direction. The following four main cases emerge, and for each case the following relationship applies:

$$\Delta p = \rho u \Delta c_u = \rho u [c_{2u} - c_{1u}].$$

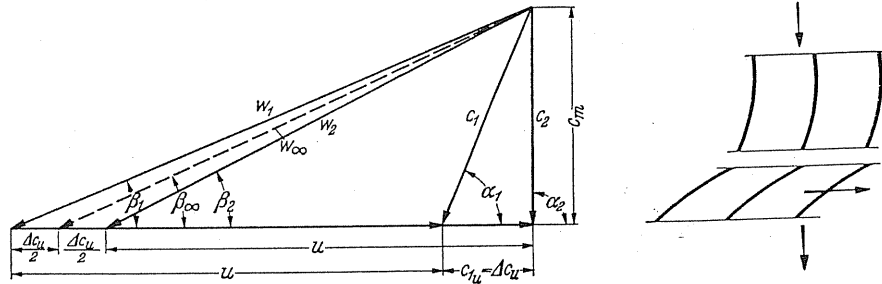


FIG. 220. Velocity diagram with pre-rotation; axial outlet.

(α) A rotation against the movement of rotor is generated by means of guide vanes in front of the impeller as shown in Fig. 220. This is then cancelled in the rotor, so that we obtain the velocity diagram as shown in Fig. 220 with axial discharge flow. We obtain

$$\Delta P = \rho u c_{1u}.$$

Reaction effect,

$$\tau = \frac{w_{\infty u}}{u} = \frac{u + \Delta c_u/2}{u} = 1 + \frac{1}{2} \frac{\Delta c_u}{u} > 1.$$

This arrangement at first glance would appear attractive because the flow through the guide vanes is accelerated. Nevertheless, the results are not so marked because the speed in the rotor is relatively so much higher and therefore the rotor losses rise.

(β) The air is delivered to the rotor in an axial direction, i.e. without guide vanes. The axial direction is deflected by means of guide vanes following the rotor (Fig.221). This is the most common case. As shown in Fig.221, the formula $\Delta p = \rho u c_{2u}$; $r = w_{\infty u}/u < 1$ apply.

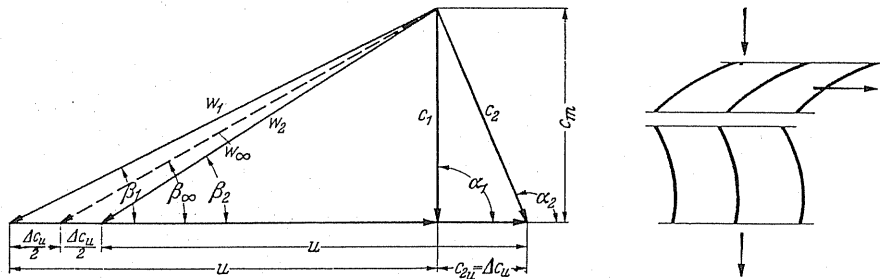


FIG.221. Downstream guide wheel $r < 1$.

(γ) Before and after the rotor guide vanes are fitted in accordance with Fig.222. It will be observed from the velocity triangles that the intake and discharge flows are arranged in mirror image. *Therefore the absolute inlet velocity is exactly identical with the absolute outlet velocity.* This means that the rotor only generates static pressure:

$$\Delta p = \rho u 2c_{1u} = \rho u 2c_{2u};$$

since $w_{\infty u} = u$, then $r = 1$.

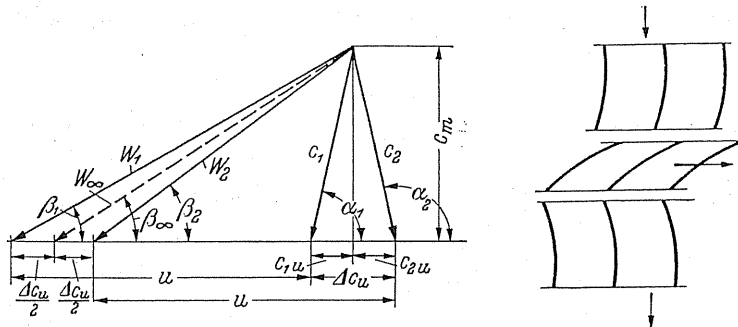


FIG.222. Upstream and downstream guide wheel. Symmetrical intake and discharge flow at impeller $r = 1$.

(δ) At the same total pressure, i.e. at the same value of $u \Delta c_u$, the peak of the diagram is displaced to show that the relative speeds and absolute speeds are of equal size and can be arranged in mirror image (Fig.223). This means that the flow through the rotor and guide vanes can be at a slope. In this case the velocities occurring are smaller than in the three other cases. Since the actual losses in the rotor and guide vanes are proportional to the square of the flow passing through, minimum losses may be expected if at otherwise equivalent conditions (i.e. the same c_m , u , and c_u) the expression $(w_\infty^2 + c_\infty^2)$ reaches its minimum. This is the case when $w_\infty = c_\infty$, i.e. the full symmetry is achieved in accordance with Fig.223. In multistage compressors this is the best case. In single-stage arrangements

the advantages are less since in this case *two* guide vane arrangements are required. The blading of the rotor and the guide wheel are identically the same. The time lag in the rotor is just as large as in the guide vanes. The reaction effect is 0.5. The arrangement corresponds exactly to the case of the reaction turbine. In multistage axial-flow fans, especially axial compressors for gas turbines, the same blade arrangement is applied as it produces the lowest Mach numbers.

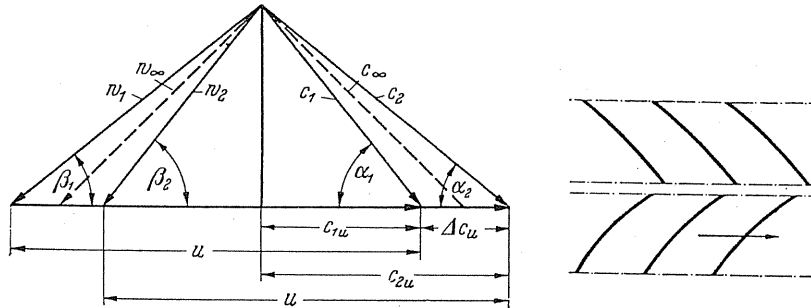


FIG. 223. Fully symmetrical inlet and outlet flow (gas turbine arrangement). $r = 0.5$.

The cases (α) and (γ) have advantages for the guide wheels especially where in the case (α) the flow through the guide wheel is *accelerated*. There is, however, a disadvantage in that at (α) as well as at (γ) the relative velocities in the rotor are greater than at (β) under otherwise equivalent conditions, i.e. equal u , c_m , Δp .

(ϵ) Alongside these main instances which apply solely for the single-stage axial rotor many other forms of layout can be mentioned which, however, have only a purely theoretical

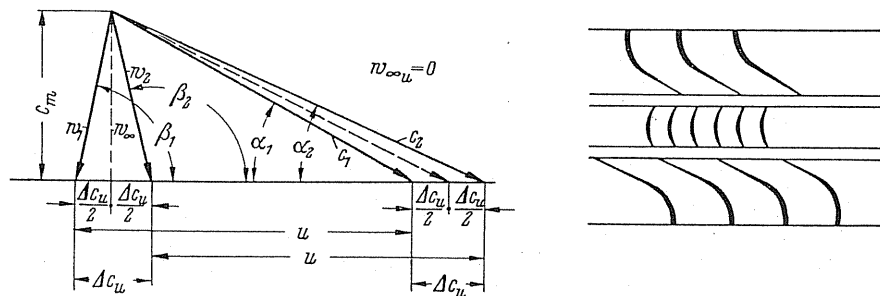


FIG. 224. Symmetrical inlet and outlet flow. Reaction rate $w = 0$.

significance. For example, as shown in Fig. 224, only constant pressure can also be realised. In this case a symmetrical curved blade such as used in steam turbines is evolved. These blades have a very bad performance owing to the large deflection. Since the deflection increases at the hub, a particularly adverse form of blade is evolved. In addition the downstream guide vanes have to convert the velocity into total pressure. The layout becomes still worse if static pressure below atmospheric pressure is produced with $w_2 > w_1$ in the rotor, i.e. a negative reaction effect.

The disadvantages of the constant pressure rotor are reduced if one moves meridionally accelerated layers.

78. REACTION EFFECT OF MOVING CASCADE

A knowledge of the static pressure increase in proportion to the total pressure increase, i.e. the reaction effect r introduced previously is essential for assessing a turbo rotor. As the conversion of the kinetic energy present behind the impeller into static pressure is always associated with fairly high losses, the aim will be to realise as high a reaction effect as possible.

By applying the Bernoulli equation to the relative flow we obtain the static pressure increase

$$p_2 - p_1 = \frac{\rho}{2} (w_1^2 - w_2^2) = \frac{\rho}{2} [(u + \Delta c_u)^2 + c_m^2 - (c_m^2 + u^2)]$$

$$p_2 - p_1 = \rho \left[u \Delta c_u + \frac{\Delta c_u^2}{2} \right] = \rho w_{\infty u} \Delta c_u.$$

The total pressure is obtained from

$$\Delta p = \rho u \Delta c_u.$$

This produces the reaction effect

$$r = \frac{p_2 - p_1}{\Delta p} = 1 + \frac{\Delta c_u}{2u} = \frac{w_{\infty u}}{u} \quad (166)$$

(upstream guide vanes). For downstream guide vanes, we have

$$r = 1 - \frac{\Delta c_u}{2u} = \frac{w_{\infty u}}{u}. \quad (167)$$

The last formula agrees accurately with eqn. (14). It is significant that a reaction effect is obtained in the first case *which is above 1*, i.e. the static pressure generated in the rotor is greater than the total pressure. This is, indeed, the case, for the upstream guide vanes the pressure for generating the peripheral component c_{1u} drops and therefore a pressure below atmosphere $(\rho/2) c_{1u}^2$ is present in front of the rotor. The rotor therefore has to generate a pressure increase which is greater by the pressure drop stated. The rotor only generates positive static pressure.

The case of the downstream guide vanes appears in a rather worse light. The peripheral component has to be converted to pressure again in the guide wheel. The movement is retarded in the widened guide wheel ducts, a procedure which is always associated with losses.

Since the Δc_u values are always very small, r values are obtained here which lie close to 1. *These persistent high reaction effects explain the high efficiencies which can be achieved with axial-flow fans.*

79. CALCULATION BY THE AEROFOIL THEORY

The actual change of direction of the relative flow is very slight in many axial-flow fans, i.e. the corresponding cascades. The velocity diagrams from Figs. 220 to 223 represent real conditions. In cases such as these it is useful to apply the aerofoil theory for calculating the deflection because it is just at this point that the deflection achieved with the aerofoil profile is slight, and the calculation and tests are in satisfactory agreement. Although for the blade cascades used, the pitch is of such a size that there is no longer a question of air "control" in the sense of the old turbine theory, *aerofoil theory in this case enables a solution almost as accurate as the streamline theory to be found with infinitely closely pitched blades.*

If an aerofoil is set against the direction of flow having an air velocity w at an angle of incidence α , in other words the aerofoil moves, which is the same thing with this velocity w in the still air, a considerable force perpendicular to the flowpath will be found, given appropriate profiling. This is called lift A , but, on the other hand, the force in the direction

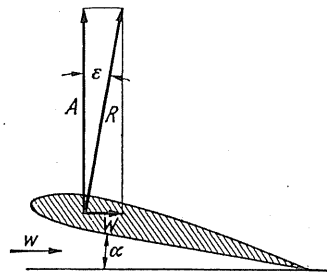


FIG. 225. Different forces acting on an aerofoil.

of the flow, the so-called drag W is small compared to A (Fig. 225). The main characteristics of a given aerofoil profile, as far as they concern our fans, are represented by the lift and drag. To enable dimensionless characteristics to be used instead of the actual forces dependent on measurements and velocities, coefficients c_a and c_w have been introduced according to the following equations:

$$A = c_a qF \quad (F, \text{aerofoil area in m}^2), \quad (168)$$

$$W = c_w qF \quad (q, \text{velocity pressure in kg/m}^2 \cong \text{mm WG}). \quad (169)$$

Usually $c_a = f(c_w)$ is expressed and the angle of incidence is indicated at the actual measuring points. This method of illustration, called polar diagram, has the advantage that the joining of any point with the zero point indicates the magnitude and directions of the resultant R or

$$c_r = \sqrt{c_a^2 + c_w^2}.$$

Geometrically it is similar to the analogous force indication (Fig. 226). The angle ϵ gives the glide angle. It is at its lowest for the tangent at the polar $\tan \epsilon \approx \epsilon = c_w/c_a$. The polar diagrams are given in well-known profile literature,⁽²⁾ mainly for the aspect ratio 1:5. Since

² Results of the Aerodynamic Testing Station, Göttingen, Supply 1-LV, Munich, Oldenbourg, or NACA Report No. 460 (1936) as well as NACA Tech. Note 3916 (1957).

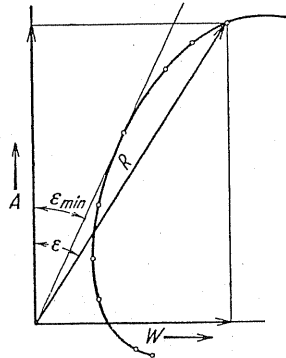


FIG.226. Polar diagram of an aerofoil.

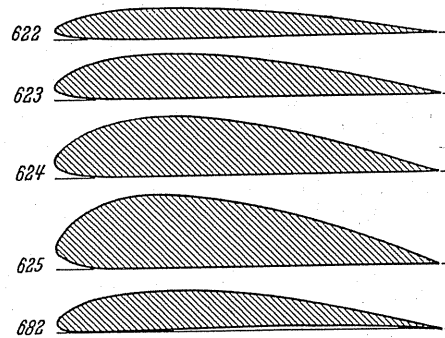


FIG.227. Aerofoils drawn to scale ($l = 50$ mm).

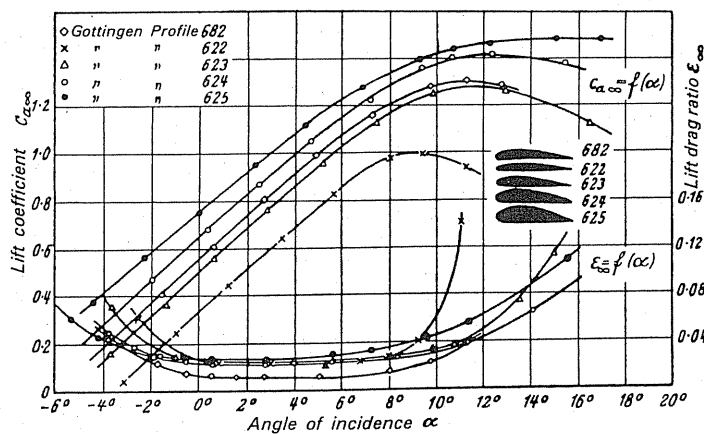


FIG.228. Lift coefficient and angle of glide for infinite aspect ratio according to Eckert.

in our fans the aerofoils end at the hub and at the external wall, there is hardly any influence of the finite aerofoil (circulation round the ends of the aerofoils) present; actually the aspect ratio $1:\infty$ is available. The polar diagrams for $1:5$ therefore must be converted according to the well-known formulae for aerofoil theory. The following alterations emerge.

(1) The incidence angle is to be reduced by the angle $\Delta\alpha$:

$$\Delta\alpha^\circ = \frac{c_a l}{\pi b} 57.3, \quad (170)$$

(l = span of aerofoil; b chord of aerofoil); for 1:5 the correction then is

$$\Delta\alpha^\circ = \frac{c_a}{\pi} \frac{57.3}{5} = c_a 3.65. \quad (171)$$

(2) The drag coefficient c_w is to be reduced by the following value:

$$\Delta c_w = \frac{c_a^2}{\pi} \frac{l}{b}. \quad (172)$$

For $l/b = 1/5$ we have

$$\Delta c_w = \frac{c_a^2}{15.7}. \quad (173)$$

In calculating for axial flow fans the dependencies $c_a = f(\alpha)$ are mainly used. Within the scope of the common incidence angle this is a linear function; there is no alteration to this in the conversion to infinite aspect ratio. Figure 227 shows a range of profiles suitable for propeller fans. These are the Göttingen profiles 682, 622, 623, 624, and 625 which have been converted according to eqn. (172) to infinite aspect ratio. Figure 228 shows the curve $c_{a\infty} = f(\alpha)$ as well as the gliding angles ε_∞ . The dimensions of the profile are shown in Fig. 227 and in Table 14. The dimensions can also be taken directly from Fig. 227. The profile span, of course, is 50 mm, and therefore any desired size can be obtained in $\frac{1}{2}\%$ of the profile span.

For the profiles 622, 623, and 624 the formula can be stated as

$$c_a = 4y_{\max}/l + 0.092\alpha^\circ$$

(y_{\max} camber, i.e. maximum distance between the chord and mean chord).

TABLE 14

	x	0	1.25	2.5	5.0	7.5	10	15	20	30	40	50	60	70	80	90	95	100
622	y_0	2.40	3.75	4.50	5.45	6.15	6.60	7.30	7.70	8.00	7.80	7.10	6.15	5.00	3.55	1.95	1.15	0.20
	y_u	2.40	1.45	1.05	0.60	0.35	0.25	0.15	0.05	0.00	0.00	0.00	0.00	0.00	0.00	0.00	0.00	0.00
623	y_0	3.25	5.45	6.45	7.90	9.05	9.90	10.95	11.55	12.00	11.70	10.65	9.15	7.35	5.15	2.80	1.60	0.30
	y_u	3.25	1.95	1.50	0.90	0.35	0.20	0.10	0.05	0.00	0.00	0.00	0.00	0.00	0.00	0.00	0.00	0.00
624	y_0	4.00	7.15	8.50	10.40	11.75	12.85	14.35	15.30	16.00	15.40	14.05	12.00	9.50	6.60	3.55	2.00	0.50
	y_u	4.00	2.25	1.65	0.95	0.60	0.40	0.15	0.05	0.00	0.00	0.00	0.00	0.00	0.00	0.00	0.00	0.00
625	y_0	5.50	9.00	10.80	13.30	14.95	16.35	18.25	19.30	20.00	19.05	17.35	15.05	12.10	8.60	4.75	2.25	0.65
	y_u	5.50	3.30	2.35	1.25	0.75	0.40	0.15	0.10	0.00	0.00	0.00	0.00	0.00	0.00	0.00	0.00	0.00
682	y_0	2.50	4.55	5.55	7.00	8.05	8.90	10.00	10.65	11.20	10.90	10.05	8.65	6.90	4.85	2.55	1.35	00.0
	y_u	2.50	1.05	0.60	0.25	0.10	0.06	0.05	0.20	0.55	0.75	0.80	0.85	0.75	0.60	0.35	0.15	00.0

The equation shows how by means of steady variation from y_{\max} any random thickening or thinning of a profile can be achieved and in certain circumstances the same basic profile with steady thickening towards the hub can be applied with any aerofoil. It is desirable that y_{\max}/l should not exceed the value 0.18.

80. INFLUENCE OF REYNOLDS NUMBERS. ADVANTAGE OF PROFILING

Whilst for isolated aerofoils below $Re = 80,000$ – $100,000$ the boundary layer becomes laminar and there is a gradual drop in the c_d values and a strong rise in the c_w values, the latest tests by Muesmann⁽³⁾ have shown that this transfer only takes place in rotating aerofoils below the value 20,000–40,000. At the same time, however, the centrifugal forces and the Coriolis forces act on the roots of the blade in a particular direction. For instance, they accelerate the boundary layers in the direction of flow, and the boundary layers therefore to a large extent act like an accelerated layer. Hence, even if with a laminar boundary layer, contact is still possible in certain circumstances. This means, however, that these effects can prevent separation, and it is worth noting that there is no sudden deterioration as in the single aerofoil but a slow and notable deterioration is observed. This apparently satisfactory phenomenon, however, is nullified as soon as there is any appearance of *hub dead space* which results in immediate separation.

Former ideas will have to be modified to suit these new findings. Accordingly it pays to have profiles up to these critical Re -values of 20,000–40,000. It should be pointed out, however, that at a turbulent boundary layer, i.e. greater Re -values, there are no differences between calculation and measurement.

B. Eckert (see *Z. VDI*, 1944) carried out accurate tests with aerofoils of variable smoothness. An unmachined grey iron aerofoil was compared with an accurately polished design. It was found that the grey iron aerofoil brought about a 10% deterioration in the efficiency.

Another restriction for profiling is produced by narrow pitching of blade s for high-pressure impellers. The cross-section becomes fairly restricted due to profiling, and the high speeds thus generated with correspondingly greater friction often offset the advantages of profiling. In any case it will have to be weighed carefully whether profiling pays.

Another aspect favouring profiling is noise generation. In this case profiling is a distinct advantage as opposed to steel blades.

Circular arc profiles. For many fans the simple circular arc is the most practical form of aerofoil. The characteristics of these profiles applicable for steel fabrication therefore must be known exactly. The Göttingen measurements of arc profiles and straight plates⁽⁴⁾ are shown in Fig. 229 in a representative form with all interesting characteristics which might be particularly suitable for the requirements of fan engineering. l/R and f/l were selected as

³ Muesmann, E., Association of flow properties of an axial fan with those of a single aerofoil, *Z. f. Flugwiss.*, 1958, p. 345.

⁴ Results of the Aerodynamic Testing Station, Göttingen, IV, p. 96.

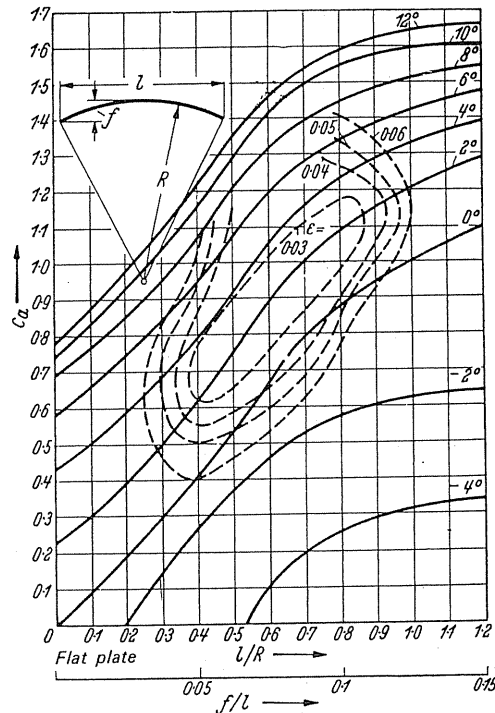


FIG. 229. Aerodynamic characteristics of arc profiles.

abscissa. Curve $\alpha^\circ = \text{const}$ and $\varepsilon = \text{const}$ were plotted. The chart shows clearly that the best gliding values lie in the range $0.05 < f/l < 0.1$.

Construction of arbitrary profiles. Each profile and its curvature properties are best investigated through the *mean camber line*. This is understood to be a line which is obtained by halving all profile thicknesses. Whereas in aircraft this line has to be curved most towards the nose, in cascades used in fans the circular arc is mostly a better proposition than mean camber line. In order to be able to design profiles at will the following criteria apply:

- (1) The greatest thickness d shall be less than $0.184l$ and should lie between 0.3 and $0.5l$.
In narrow cascades it is advisable to move the greatest thickness to the centre.
- (2) Rounding of the nose, which must diminish with lesser thicknesses, should not exceed $0.03l$.

Figure 230 shows one of these constructive profiles. For this the equation

$$c_a = (7.5 - 9.4)f/l + \alpha^\circ 0.094$$

applies almost exactly: 7.5 if the greatest thickness is at $0.31l$; 9.4 if the greatest thickness is at $0.5l$.

A basis for the application of aerofoil theory to cascade flow. In individual aerofoils the total deflection of the flow is equal to zero at some distance from the aerofoil. Greater

deflections of individual flow lines are only present in the immediate proximity. *In cascades, on the other hand, at a greater distance from the aerofoil, there is a rather small but still finite deflection present.* The question arises as to how and whether the aerofoil theory can be applied in this case. In the cascade the velocity w_1 is turned from the direction β_1

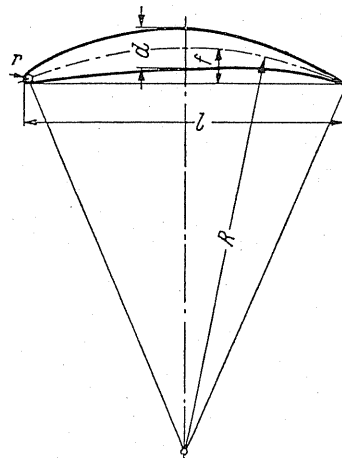


FIG.230. Construction of profiles from arcs.

into direction β_2 . In between a rather marked direction β_∞ was obtained from a former calculation, which direction is the one on which, of course, the resultant of the air force acts vertically. If an individual aerofoil were to be driven in the direction β_∞ , a resultant of air force perpendicular to this direction would be obtained. Even if it were not anticipated that both cases coincide, the question arises whether by this comparison it is possible to find a new way for direct application of the results of the single wing to a cascade of aerofoils.⁽⁵⁾

Obviously this would mean a considerable simplification if the aerofoil of the cascade could be replaced by a single aerofoil which would be set below β_∞ . The decision on this question would depend on whether in both cases the c_a values agree (c_w has primarily a small role). The following causes lead to an assumption of a deviation compared to the single aerofoil.

- (1) The aerofoils lie in curved flow in contrast to the average straight-line flow for a single wing.
- (2) The finite thickness of aerofoils constricts the pitch and thus accelerates the mean velocity which is discarded in an individual aerofoil.
- (3) The cascade flow is retarded on the average (reduction from w_1 to w_2).
- (4) The friction in boundary layers for cascades operates like the constriction of the effective pitch and therefore similar to the finite thickness.

Owing to the high importance of axial turbines as well as of axial-flow fans, a great deal of ingenuity has been applied to the study of these problems and particularly from the

⁵ Stated for the first time by Bauersfeld, Basic principles for calculating high speed turbo wheels, Z VDI, 1922, p.41.

mathematical aspects. In certain cases an accurate solution⁽⁶⁾ has been found for flow without friction. It appears that, according to conditions, the values of the cascade aerofoil can lie well above and also below the values of the individual aerofoils.

For turbine flow (i.e. acceleration of cascade flow) the proof was provided by Amstutz⁽⁷⁾ *that in treating the cascade aerofoil as an individual aerofoil, i.e. without so-called cascade correction, good agreement with test values from Kaplan turbines is available* (see footnote 7).

In a work by Keller,⁽⁸⁾ which cited far-reaching influence on the development of the axial-flow fan, the proof was provided that the theory of first approximation generally is of ample importance in pump flow.

According to this theory it suffices in the *first approximation* for calculation of axial-flow fans to treat the cascade aerofoil as an individual aerofoil subject to the application of the known c_a and α_∞ values of the individual aerofoils. *It would appear that the influences which govern the variation of the ϵ_{\min} values in the cascade flow without friction are offset in the first approximation by the friction.*

81. BEHAVIOUR OF BOUNDARY LAYER IN AXIAL-FLOW FANS

Whilst it may not be possible at the moment to give any more accurate information on the behaviour of the boundary layers in rotating channel, some basic observations can be defined which are of practical importance.

As the boundary layers adhere more or less firmly to the rotating blade areas, they are subject also to the effect of centrifugal forces. Thus result radial movements which are superimposed on the main flow. Ruden⁽⁹⁾ was able to prove such movements clearly in his tests. Separated particles were thrown outside and so, by their accumulation, the flow is disturbed. This gave rise to a kind of boundary-layer suction which prevents a separation. Gutsche⁽¹⁰⁾ made this movement visible by means of a propellor driven in water, the propellor being provided with oil paint stripes which ran in the direction of the boundary-layer discharge flow. Figure 231 shows the suction end of a propellor at which a separation at the hub is inhibited through these influences. Further investigations were made by Himmelskamp.⁽¹¹⁾ In this work for the first time accurate profile measurements were carried out with the propellor running. The results have provided great surprises. In the aerofoil sections close to the hub c_a values above 3 were found. This means an almost threefold rise of the maximum lift values compared to the same profile in plane flow. A large increase of resistance was observed at the same time. Figure 232 depicts these flows by small streamers.

⁶ Konig, E., Potential flow through cascades, *Z. angew. Math. Mech.*, 1922, p.422. Schilhansl, Calculation by approximation of elevation and pressure distribution in aerofoil cascades, *J. b. wiss. Ges. Luftf.*, 1927. Numachi, *Aerofoil Theory of Propellor, Turbines and Pumps*, Technol. Report Tōhoku Univ., 1929, Vol. 8. Weinig, *Die Strömung um die Schaufeln von Turbomaschinen*, Leipzig, 1935. Ackeret, *Schweiz. Bauztg.*, 1942, p.103. Betz, *Ing.-Arch.*, 1931.

⁷ Amstutz Memorial Lecture, Stodola, Zürich, Orell Füssli, 1929.

⁸ Keller, Axial fans, Diss., Zürich, 1934; English translation, *The Theory and Performance of Axial Flow Fans*, McGraw-Hill, Aldwych House, London, 1937.

⁹ Ruden, Diss., Hanover, 1937.

¹⁰ Gutsche, *Jb. Schiffbautechn. Ges.*, 41 (1940).

¹¹ Himmelskamp, Diss., Göttingen, 1945.

In the meantime some information has been gathered regarding the processes involved in the separation. The separation in a blade starts close to the hub. Owing to the dead-space forming with the separation, the cross-section between two blades becomes narrow. The flow is deflected in such a way that the angle of incidence for the adjacent blades on the pressure side becomes smaller (diminished separation risk), whilst for the blades adjacent to the suction side the angle of incidence increases and the separation continues in this

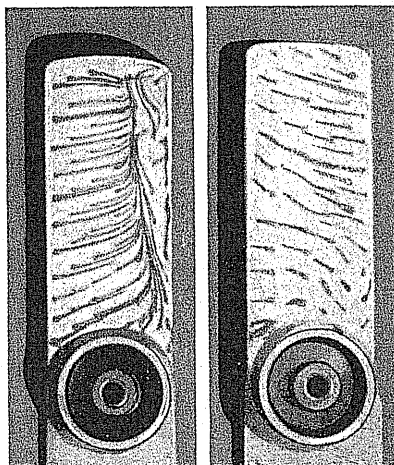


FIG.231. Boundary-layer movement in axial impellers according to Gutsche.



FIG.232. Visualisation of boundary-layer movements in axial-flow fans by small streamers according to Himmelskamp.

direction. Viewed as a whole the separation in this way migrates at a speed of rotation which is smaller than the peripheral speed of the impeller. Thus we have here the phenomenon of a progressive separation⁽¹²⁾ which is primarily found at the blade tip in impellers and at the hub in guide wheels.

From these observations alone it follows that special care is needed if measured values obtained from smooth flow have to be applied to axial-flow fans. At the same time they open up the great problem of cascade calculations.

82. CALCULATION WITHOUT CONSIDERING THE AEROFOIL FRICTION

Let us assume a cascade arrangement with aerofoil as shown in Fig. 233. Let there be a guide wheel in front of the impeller which generates a rotation opposite to the velocity u . The impeller will be composed of aerofoils arranged to follow each other at a distance t . The velocity diagram of Fig. 220 applies. If by virtue of former considerations the cascade aerofoil is looked upon as an individual aerofoil where w_∞ is at an angle β_∞ to the axis of the cascade, the actual angle of incidence of the aerofoil is the angle shown in Fig. 233.

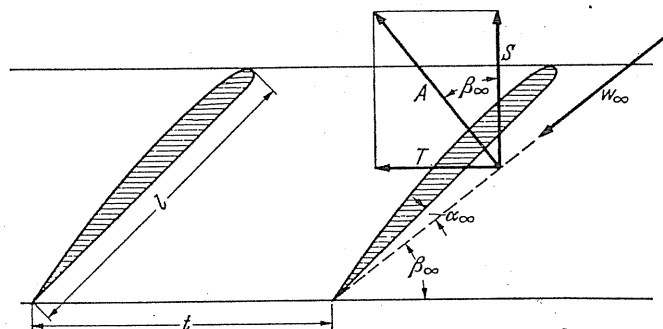


FIG. 233. Effect of forces on cascade aerofoils in flow without friction.

Since for the present it is intended to ignore the resistance, we only have to consider the lift A which is to be calculated by the following formula:

$$A = c_a \frac{\gamma}{2g} w_\infty^2 l b.$$

The components in peripheral direction and in axial direction $T = A \sin \beta_\infty$ and $S = A \cos \beta_\infty$ are of particular interest.

According to the momentum principle the force in the direction of the cascade is equal to the air mass q times the variation of velocity Δc_u in this direction, appropriate to the pitch:

$$T = q \Delta c_u.$$

¹² Jura Rannie, Experimental investigations of propagating stall in axial flow compressors, *Trans. of the ASME*, April 1954, pp. 436-71.

For T we express the value just found. Moreover, we take into account

$$q = t b c_m \frac{\gamma}{g}$$

$$T = A \sin \beta_\infty = c_a \frac{\gamma}{2g} w_\infty^2 l b \sin \beta_\infty = t b c_m \frac{\gamma}{g} \Delta c_u.$$

With $c_m / \sin \beta_\infty = w_\infty$ we have $q \Delta c_u = (l/t) c_a w_\infty q/2$. By putting this in eqn. (163) $\Delta p = q u \Delta c_u$, we obtain

$$\Delta p = c_a \frac{l}{t} w_\infty u \frac{q}{2}, \quad (174)$$

which gives us

$$\frac{c_a l}{t} = \frac{\Delta p \cdot 2}{u q w_\infty}.$$

Taking $\psi = 2 (\Delta c_u / u)$ into account we obtain further

$$\frac{c_a l}{t} = \psi \frac{u}{w_\infty} = 2 \frac{\Delta c_u}{w_\infty} = 2 \frac{\Delta c_u}{c_m} \sin \beta_\infty.$$

We then express

$$u = \frac{d}{2} \omega \quad \text{and} \quad t = \frac{\pi d}{z} \quad (z = \text{number of blades}):$$

$$c_a l = \frac{\Delta p \cdot 4\pi}{w_\infty q \omega z}. \quad (175)$$

The right-hand side of eqn. (175) is constant for the whole aerofoil up to w_∞ . This gives us the following rule: *For each aerofoil cross section $c_a l$ is always inversely proportional to w_∞ .*

These equations form the basis for designing the axial-flow fans.

By simple rearrangement the following practical equations are obtained:

$$\frac{c_a l}{t} = \frac{2 \Delta c_u}{w_\infty} = \frac{2 \Delta c_u \sin \beta_\infty}{c_m}. \quad (176)$$

By substituting, $\Delta c_u = w_1 \cos \beta_1 - w \cos \beta_2$ (see, for instance, Fig. 220) we obtain

$$\frac{c_a l}{t} = 2 \sin \beta_\infty [\cot \beta_1 - \cot \beta_2] = 2 \sin \beta_\infty \frac{\sin (\beta_2 - \beta_1)}{\sin \beta_1 \sin \beta_2}. \quad (177)$$

83. GENERALLY APPLICABLE RELATIONSHIPS

It is easy to derive a few general applicable relationships from the velocity diagrams, and these are to be summarised for the most frequent case of the downstream guide vanes.

(a) *Volume coefficient $\varphi' = c_m / u$.*

(b) *Pressure coefficient ψ .*

From

$$\Delta p_{\text{tot}} = \rho u \Delta c_u \eta = \psi \frac{\rho}{2} u^2 \quad \text{we get} \quad \psi = 2\eta \frac{\Delta c_u}{u}. \quad (178)$$

Figure 234 shows ψ as a function of $\Delta c_u/u$ for various values of η .

(c) *Reaction effect* r .

$$r = \frac{\text{static pressure}}{\text{total pressure}} = \frac{\Delta p_{\text{tot}} - \Delta p_{\text{dyn}}}{\Delta p_{\text{tot}}} = 1 - \frac{\Delta p_{\text{dyn}}}{\Delta p_{\text{tot}}} = 1 - \frac{(\rho/2) \Delta c_u^2}{\rho u \Delta c_u \eta}. \quad (179)$$

The r values are summarised for different efficiencies as a function of $\Delta c_u/u$ in Fig. 234.

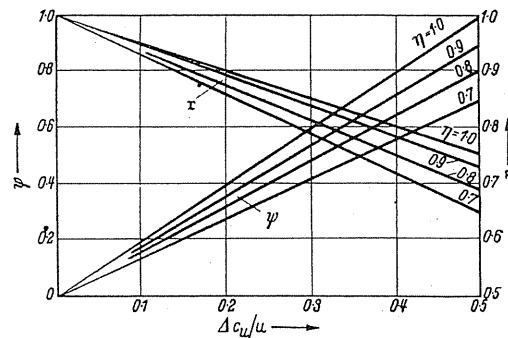


FIG. 234. Reaction effect and pressure factor for different efficiencies as a function of $\Delta c_u/u$.

(d) *Retardation* in the impeller illustrated by w_2/w_1 . The risk of separation⁽¹³⁾ at the suction side of the impeller increases correspondingly with the retardation in the relative speed. This retardation is expressed numerically most simply by the ratio w_2/w_1 . The dependency of this quantity on the main quantities c_u/u and $c_m/u = \varphi'$ was the subject of

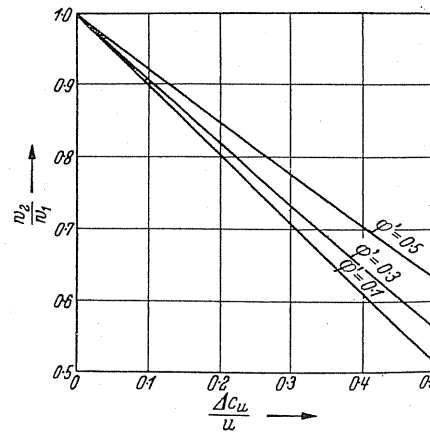


FIG. 235. Retardation in the impeller w_2/w_1 , for different φ' values as a function of $\Delta c_u/u$.

¹³ The pressure gradient on the suction side of the blade alone is the governing factor for separation. Since this pressure gradient is approximately constant in cascades, the risk of separation here can be expressed by w_2/w_1 .

calculation. A simple calculation gives us

$$\frac{w_2}{w_1} = \sqrt{\frac{(\varphi')^2 + (1 - \Delta c_u/u)^2}{1 + (\varphi')^2}} \approx 1 - \frac{\Delta c_u}{u}$$

for small values of φ' . In Fig. 235 w_2/w_1 as a function of $\Delta c_u/u$ was plotted for different values of φ' .

The maximal retardation w_2/w_1 occurs near the hub. According to Keller, De Haller, and Marcinowsky,⁽¹⁾ for single-stage axial-flow fans it is advisable for the values of w_2/w_1 to be below 0.7–0.65, and (2) for multistage axial-flows fans values of w_2/w_1 should lie between 0.6 and 0.55.

84. CALCULATION TAKING FRICTION INTO ACCOUNT

The next problem is to consider in eqn. (175) the losses arising in the aerofoil and in a diffuser which may be related later by means of a correspondingly higher Δp . If η is the total efficiency the fan aerofoil blades must generate a higher Δp , namely $\Delta p/\eta$, to give us the following equation:

$$c_a l = \frac{\Delta p \, 4\pi}{\eta \, w_\infty \, \rho \, \omega z}. \quad (180)$$

If we also consider, according to eqn. (178), that the efficiencies increase to $\Delta p/\eta$ the pressure to be generated at the blade

$$\frac{\Delta p}{\eta} = \rho u \Delta c_u,$$

and this gives us

$$\Delta c_u = \frac{\Delta p}{\eta \rho u}. \quad (181)$$

This is the actual Δc_u which is essential for generating the pressure Δp .

If we take into account the losses in the previous equations according to eqn. (176), the following final practical formulae are obtained:

$$c_a l = \frac{\Delta p \, t \, 2}{\eta u \rho \, w_\infty} = \frac{\psi u t}{w_\infty \eta} = \frac{2t \Delta c_u}{w_\infty} = \frac{2t \Delta c_u \sin \beta_\infty}{c_m}. \quad (182)$$

Substituting $\Delta c_u = w_1 \cos \beta_1 - w_2 \cos \beta_2$ (see, for instance, Fig. 221) we obtain

$$c_a l = \frac{2t}{\eta} \sin \beta_\infty [\cot \beta_1 - \cot \beta_2] = \frac{2t}{\eta} \sin \beta_\infty \frac{\sin(\beta_2 - \beta_1)}{\sin \beta_1 \sin \beta_2}. \quad (183)$$

However, it is quite important to divide up the efficiencies according to individual losses so that during the design an outline of the influence of various restrictions can be obtained.

A simple outline is obtained by the following calculations.

By taking $T = R \sin(\beta_\infty + \varepsilon)$ from Fig. 236, and since $V = c_m t b$, we obtain

$$\Delta p c_m t b = R u \sin(\beta_\infty + \varepsilon).$$

If we still take into account

$$\Delta p = \varrho u \Delta c_u \quad \text{and} \quad R = \frac{A}{\cos \varepsilon} = \frac{c_a (\varrho/2) l b w_\infty^2}{\cos \varepsilon}$$

this gives us

$$\begin{aligned} \varrho u \Delta c_u c_m t b &= \frac{c_a (\varrho/2) w_\infty^2 l b}{\cos \varepsilon} u \sin(\beta_\infty + \varepsilon) \\ c_a l/t &= 2 \frac{\Delta c_u}{w_\infty} \frac{c_m}{w_\infty} \frac{1}{\sin(\beta_\infty + \varepsilon)} = 2 \frac{\Delta c_u}{w_\infty} \frac{\sin \beta_\infty}{\sin(\beta_\infty + \varepsilon)} \\ c_a l/t &= \frac{2 \Delta c_u}{c_m} \frac{\sin^2 \beta_\infty}{\sin(\beta_\infty + \varepsilon)}. \end{aligned} \quad (185)$$

By retaining Δp we obtain

$$\frac{c_a l}{t} = \frac{2 \Delta p}{\varrho w_\infty^2} \frac{c_m}{u} \frac{\cos \varepsilon}{\sin(\beta_\infty + \varepsilon)}.$$

For $\varepsilon \approx 0$ we have

$$\frac{c_a l}{t} = \frac{2 \Delta p c_m}{\varrho w_\infty^2 u \sin \beta_\infty} = \frac{2 \Delta p}{\varrho u w_\infty}.$$

The following refined analysis gives us deeper insight. In Fig. 236 the resultant force of air R is resolved first in the direction of the lift A and the drag W and then in the direction of the cascade, namely the tangential force $T = R \sin(\beta_\infty + \varepsilon)$ as well as perpendicular to the cascade, namely the so-called thrust force $S = R \cos(\beta_\infty + \varepsilon)$.

The ratio of both forces is

$$\frac{S}{T} = \frac{1}{\tan(\beta_\infty + \varepsilon)}.$$

We now look for the magnitude of this ratio where there is no friction. Obviously then the following relationship will result:

$$\frac{S_{th}}{T_{th}} = \frac{1}{\tan \beta_\infty}.$$

If for obtaining simple basis for comparison in both cases we assume an equal tangential force owing to similarity, we obtain

$$\frac{S'}{T} = \frac{1}{\tan \beta_\infty}.$$

In this way the ratio of *actual* thrust force to the ideal *thrust force*, which would be available if the friction were not there, can easily be calculated. Since these thrust forces are responsible for the static pressure differences so it is necessary to express this ratio as static

efficiency. This gives us

$$\eta_{\text{stat}} = \frac{S}{S'} = \frac{\tan \beta_{\infty}}{\tan (\beta_{\infty} + \varepsilon)} \approx \frac{1 - \varepsilon \tan \beta_{\infty}}{1 + (\varepsilon / \tan \beta_{\infty})}. \quad (186)$$

This is the equation originating from the air-screw theory. As in air screws the thrust force is only of interest, and rotational components, etc., are unimportant, this efficiency gives the only useful basis for comparison of air screws. The maximum $\eta = \tan^2 \beta_{\infty}$.

The static efficiency η_{stat} is obtained also by comparison of the pressure rise $p_2 - p_1$ (such as can be measured, for instance) with the possible theoretical pressure rise. This is known as $(\rho/2)(w_1^2 - w_2^2)$, i.e. a value which has arisen due to the retardation of the relative velocity.

$$\eta_{\text{stat}} = \frac{p_2 - p_1}{(\rho/2)(w_1^2 - w_2^2)}. \quad (187)$$

The gliding angle can be calculated from eqn. (186), as

$$\varepsilon = \frac{\tan \beta_{\infty} (1 - \eta_{\text{stat}})}{\eta_{\text{stat}} + \tan^2 \beta_{\infty}}. \quad (188)$$

This formula may serve the purpose of verifying the gliding angle ε of profiles according to tests.

85. THE EFFICIENCY AS A FUNCTION OF DIMENSIONLESS QUANTITIES

To facilitate the calculations, it is useful to rearrange the former formula based on the parameter φ' and $\Delta c_u/u$.

The peripheral force T for a blade pitch, according to the momentum principle, works out to

$$T = \rho c_m b t \Delta c_u,$$

whilst the force S perpendicular to the wheel is obtained from the static pressure difference, as

$$S = (p_2 - p_1) t b.$$

This gives us

$$\tan (\beta_{\infty} + \varepsilon) = \frac{T}{S} = \frac{\rho c_m \Delta c_u}{p_2 - p_1}$$

and

$$p_2 - p_1 = \frac{\rho c_m \Delta c_u}{\tan (\beta_{\infty} + \varepsilon)}.$$

From the velocity diagram we obtain

$$\tan \beta_{\infty} = \frac{c_m}{u - c_u/2} = \frac{c_m/u}{1 - c_u/2u}.$$

If the same considerations are applied for the downstream guide wheel, we obtain

$$\tan(\alpha_{\infty L} + \varepsilon_L) = \frac{\rho c_m \Delta c_u}{p_3 - p_2}$$

(index L for values in wheel), and this gives

$$p_3 - p_2 = \frac{\rho c_m \Delta c_u}{\tan(\alpha_{\infty L} + \varepsilon_L)}$$

and

$$\tan \alpha_L = \frac{c_m}{\Delta c_u/2} = \frac{c_m/u}{\Delta c_u/2u}.$$

The static pressure increase $p_2 - p_1$ of the rotor corresponds to an effective power

$$(p_2 - p_1) V_{tb} = (p_2 - p_1) c_m b t,$$

whereas the power generated by the impeller, according to the momentum principle, has the following value:

$$uT = u \rho c_m b t \Delta c_u.$$

This gives us the rotor efficiency

$$\eta_{\text{rot}} = \frac{(p_2 - p_1) c_m b t}{u \rho c_m b t \Delta c_u} = \frac{\rho c_m \Delta c_u c_m b t}{\tan(\beta_{\infty} + \varepsilon) u \rho c_m b t \Delta c_u}.$$

$$\eta_{\text{rot}} = \frac{c_m/u}{\tan(\beta_{\infty} + \varepsilon)} \quad (189)$$

Since $c_m/u \approx \tan \beta_{\infty}$ in high-speed impellers, this gives us

$$\eta_{\text{rot}} = \frac{\tan \beta_{\infty}}{\tan(\beta_{\infty} + \varepsilon)}, \quad (190)$$

i.e. the value already found above.

Using the addition formulae the impeller losses alone amount to

$$1 - \eta = \frac{\tan \beta_{\infty} + \varepsilon - c_m/u + \varepsilon (c_m/u) \tan \beta_{\infty}}{\tan(\beta_{\infty} + \varepsilon)}.$$

By ignoring the small quantities and putting $\tan \beta_{\infty} \approx c_m/u$ we obtain for high-speed rotors

$$1 - \eta = \frac{\varepsilon}{\varphi' + \varepsilon}. \quad (191)$$

If, furthermore, ε is small compared with φ' , we obtain the most simple formula

$$1 - \eta = \varepsilon/\varphi'.$$

The analogous considerations for the guide wheel leads to a guide-wheel efficiency

$$\eta_L = \frac{c_m/u}{\tan(\alpha_{\infty} + \varepsilon_L)}.$$

The efficiency of impeller plus guide wheel, for practical purposes called the stage efficiency, works out to be

$$\eta_{\text{stage}} = \frac{c_m}{u} \left[\frac{1}{\tan(\beta_{\infty} + \varepsilon)} + \frac{1}{\tan(\alpha_{\infty L} + \varepsilon_L)} \right]. \quad (192)$$

By applying the addition formulae and

$$\tan \alpha_\infty = \frac{c_m}{\Delta c_u/2}; \quad \tan \beta_\infty = \frac{c_m}{u - \Delta c_u/2}; \quad \text{and} \quad c_m/u = \varphi',$$

we obtain

$$\eta_{\text{stage}} = \varphi' \left[\frac{1 - \Delta c_u/2u - \varepsilon\varphi'}{\varphi' + \varepsilon - \Delta c_u\varepsilon/2u} + \frac{\Delta c_u/2u - \varepsilon_L\varphi'}{\varphi' + \varepsilon_L\Delta c_u/2u} \right]. \quad (193)$$

It is very remarkable and this was pointed out first by Keller that specific optimum values result from this and these vary according to the choice of ε and ε_L . Some of these curves according to Buhning⁽¹⁴⁾ are shown in Fig. 237 for cases where $\varepsilon = 0.03$ was selected for the rotor and $\varepsilon_L = 0.06$ for the guide wheel. Thus the condition is taken into account that in the rotor the effect of profile due to removal of the boundary layer by the centrifugal forces is *considerably better*. Figure 237 is a typical illustration that definite optimum values are obtained. They move to greater φ' values at lower ψ values, whilst the efficiency is reduced somewhat.

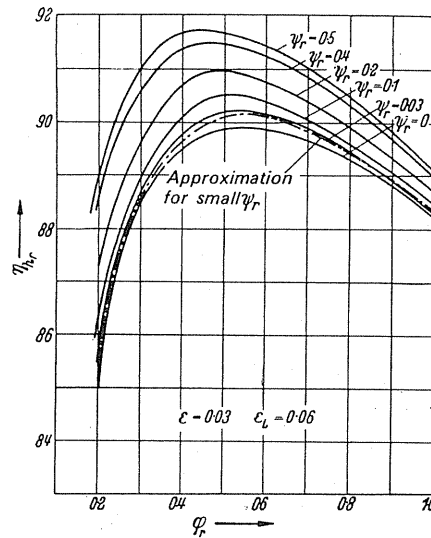


FIG. 237. Optimum characteristics for axial-flow fan according to Buhning.

The improvements which have been brought about since Keller⁽¹⁵⁾ are to be credited to the work by Buhning⁽¹⁴⁾ and Marcinowski.⁽¹⁶⁾

These fundamental considerations should demonstrate that the axial-flow fan satisfactorily opens up fruitful theoretical analysis. The results of these calculations simplify the design.

Primarily the calculations only apply for one-blade element. To obtain the total efficiency various assumptions can be made. First of all the blade section can be designed in such a

¹⁴ Buhning, Concerning the behaviour of extreme high speed axial machines, Diss., Karlsruhe, 1957.

¹⁵ Keller, C., Axial-flow fans from the point of view of the aerofoil theory, Diss., Zürich, 1934.

¹⁶ Marcinowski, H., Optimum problems in axial-flow fans, Diss., Karlsruhe, 1956.

way as to have the same efficiency available at all points. This is only possible if the lift-drag ratio varies in a specific manner. In the second method, which is the most used, a mean constant value is assumed for the lift-drag ratio ε and the integral mean value of the efficiency is then obtained. In addition to this there are other lift-drag ratios which are described below.

The lift-drag ratios for rotor and guide wheel. The lift-drag ratios mainly are known from aerofoil and cascade measurements. For each aerofoil there is a minimum value in the vicinity of which the angle of incidence can be modified somewhat without any notable influence on the best value.

The value of ε varies according to the roughness and Re . Another factor is whether the aerofoil is at rest or rotating. Special phenomena are associated with rotation which are brought about by *the removal of the boundary layer to the outside and a movement to the inside due to the impeller gap*. Fortunately the lift-drag ratios of the rotating aerofoil are better than those of the aerofoil at rest. Moreover, differences are created according to whether the flow accelerates or retards through the profile cascade. If a mean lift-drag ratio is stated for the rotating aerofoil, then the gap and edge losses have to be taken into account some way or other as they are a function of the hub ratio.

A formula can be stated temporarily for the impeller which embraces all losses:

$$\varepsilon_{LA} = 0.02 + \frac{0.008}{1 - \nu}. \quad (194)$$

Here $\nu = r_i/r_a$.

For the maximum retarded flow through the guide wheel, higher values of $\varepsilon \approx 0.05-0.06$ have to be taken. In the case of the upstream guide wheel when the accelerated flow moves through it, smaller values $\varepsilon \approx 0.035-0.045$ can be used.

The results of calculations subject to these assumptions are summarised below. Generally they concern refinements of the former fundamental calculations by Keller. Here it should be noted that the results of Keller have been confirmed in the main. The main deviations according to Bühning and Marcinowski appear in the range of very high-speed axial-flow fans and recently, according to Laux (Diss., Berlin), for freely discharging fans.

86. EFFICIENCY OF FREELY DISCHARGING AXIAL-FLOW FANS

The efficiency has to be specially defined for some particular problem in ventilation. In wall fans, according to Fig. 238, at the right the following situation arises. The fan has to blow a quantity of air $V \text{ m}^3/\text{sec}$ into a space which has a higher pressure Δp_{stat} . The power required for this task is $V \Delta p_{\text{stat}}$. Let L_a be the power required by the fan, thus we have an efficiency

$$\eta = \frac{V \Delta p_{\text{stat}}}{L_a}.$$

Clearly the purchaser is only interested in this efficiency. When designing a fan, moreover, it should be taken into account that the outlet energy $(\varrho/2) c_2^2$ also has to be considered. The

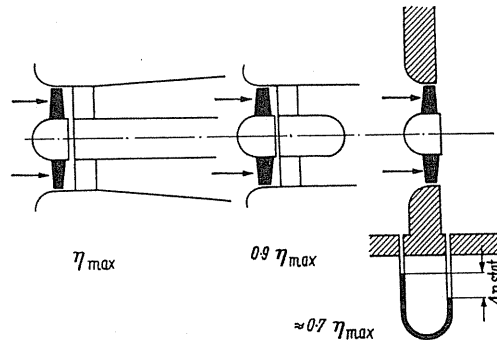


FIG. 238. Three different methods of fixing axial fans.

actual fan efficiency which governs the design hence is

$$\eta_{\text{tot}} = \frac{V [\Delta p_{\text{stat}} + (\rho/2) c_2^2]}{L_a}$$

It is a matter of keeping c_2 as low as possible, i.e. d_2 as high as possible.

The situation is considerably improved by recovering energy from rotation

$$\eta_{\text{rec}} = \frac{\int_r p_{\text{stat}} c_m r \, dr}{\int_t \frac{1}{2} \rho c_u^2 r \, dr},$$

which may amount up to 65% at free discharge (Diss., Laux).

If the efficiency is related to the technically most calculable static pressure difference, characteristic differences emerge according to whether the impeller and diffuser are absent. The differences in quantities thus arising in the efficiencies is shown in Fig. 238, and it depends on a certain often-used type of construction. The values alter a little according to the design of the rotors.

Diagrams for optimum rating for all axial-flow fans. It is remarkable that the theoretically optimum considerations are in good agreement with numerous tests for axial-flow fans of all types. From these the actual $\sigma - \delta$ value can be obtained by means of a few curves.

The main result of the latest investigations by Bühning and Marcinowski is that at higher σ -values no uniform curve is available in the $\sigma - \delta$ diagram, but branching arises according to the installations which increase in size as the σ -value rises. In Figs. 239–242 a fundamental survey of all coefficient ranges is shown. The differences in installations to be taken into account have the following features,

- (1) Curve a_1 . Rotor + downstream guide wheel, i.e. use in one duct. What is meant is one stage without diffuser and without free discharge. The energy of the air is utilised directly at the junction to the guide wheel.
- (2) Curve a_2 . Rotor + guide wheel + diffuser. The air is utilised directly after the diffuser. This is the most popular case.

(3) Curve a_3 . After the stage, i.e. after the guide wheel, there is a direct discharge so that all energy after the guide wheel may be considered as loss. The lower curve $0.6 < \sigma < 3$ differs a little from the thick-line curve. This is due to the fact that for the lower curves Marcinowski has based his conclusions on discharge without rotor.

Figure 239 shows the upper coefficient range where the differences in mounting are the greatest. These concern arrangements without rotors.

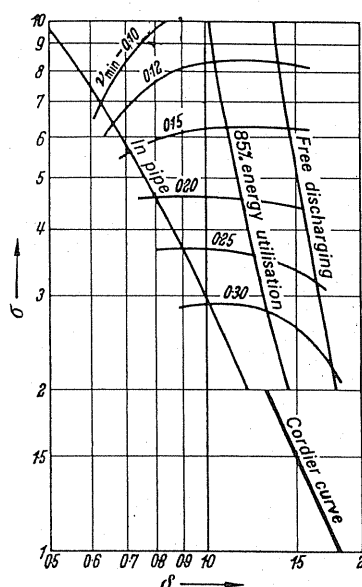


FIG. 239. Minimum values of hub ratios for optimum performance of impellers—without guide vanes for various methods of mounting.

Figure 240 is a survey of the smaller coefficient ranges; in this illustration the smallest hub ratios are also entered. It is clear from this graph that the divergence of the curves decreases as the value σ becomes less.

At the boundary the curves by Bühning and Marcinowski do not agree exactly as shown in Fig. 241, which is due to the fact that correct rules cannot be made here. This has to be equalised somewhat in the transition zone.

The results alter somewhat with the lift-drag ratio. For the lift-drag ratio in ranges $0.02 < \varepsilon < 0.04$, displacements of curves according to Fig. 242 occur.

In addition to the former results by Keller we have the knowledge today that the method of mounting plays a role which becomes all the greater the higher the speed of the fan. In considering the values for three typical installations at the same high-speed, considerable alterations are likely to occur. For the most used stage arrangement: rotor + guide wheel, the former findings by Keller agree almost exactly with the latest ones. According to the latest findings by Laux, the whole field of the free discharging fans has to be excluded from integration into the $\sigma - \delta$ scheme. It has been found that in these fans the conditions for hub diameter are absolute governing factors according to formula in Fig. 251.

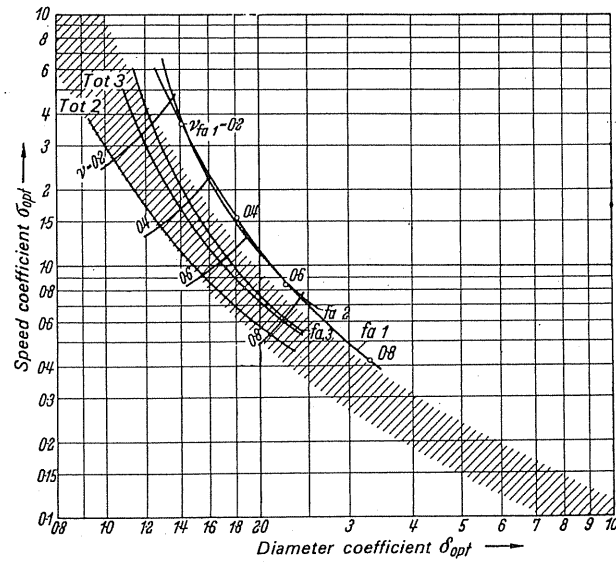


FIG.240. Optimum curves with minimal hub ratios for different methods of installation for impellers with low characteristics.

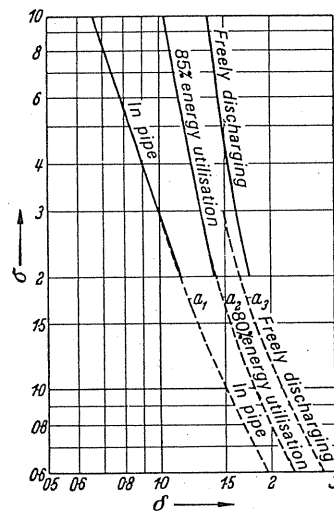


FIG.241. Comparison of optimum curves from the data of Bühning (thick line) and Marcinowski (dotted line).

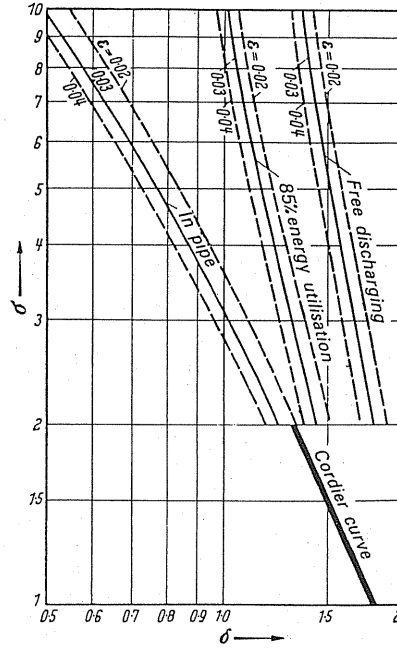


FIG. 242. Optimum curves at various lift-drag ratios for different installations.

The use of the diagrams will now be explained. As is known, the delivery volume V and the total pressure increase Δp can be discussed first of all. Generally an approximate assumption on the desired speed n is possible to make either that the speeds of the electrical motors are available or other requirements in this respect. This means that the three values V , Δp , and n are present. This allows the speed coefficient to be calculated

$$\sigma = \eta_{\text{sec}} \left[\frac{V^{1/2}}{(2gH)^{3/4}} 2\pi^{1/2} \right]. \quad (195)$$

The appropriate value of δ can be read from the diagrams to suit the arrangement envisaged. The diameter is obtained from the formula

$$d = \delta \frac{2V^{1/2}}{(2gH)^{1/4} \pi^{1/2}}. \quad (196)$$

At the same time the minimum permissible value of the hub ratio is obtained from the diagrams. This leads to further coefficients:

$$\psi = \frac{1}{\sigma^2 \delta^2} \quad \text{and} \quad \varphi = \frac{1}{\sigma \delta^3}.$$

In this way the *first* part of the problem has been solved. The *second part of the problem* is concerned with arrangement of the blading which will be dealt with subsequently.

87. REDUCED OUTPUT OWING TO BOUNDARY-LAYER EFFECTS

In passing through the rotor and owing to retardations of varying degree, boundary layers arise at the cylindrical walls, i.e. of the hub and of the external casing wall. The flow velocity c_m decreases in these boundary layers. For reasons of continuity this is only possible if the central portions are correspondingly accelerated. At the entry into the rotor this kind of effect will not usually be present because owing to the well-rounded hub a more or less strong acceleration practically precludes any boundary-layer decelerations. Thus we obtain the velocity diagram shown at the top in Fig. 243. In front of the impeller a fairly

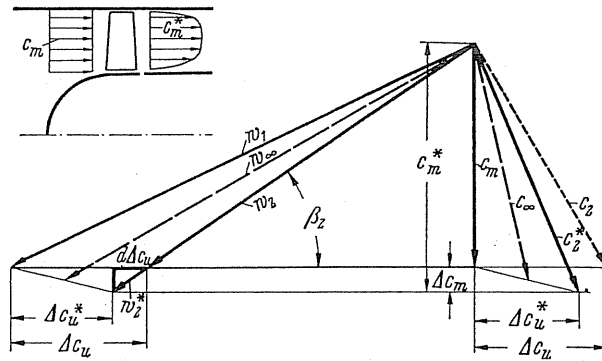


FIG. 243. Velocity diagram for flow in the impeller taking into consideration the boundary layer.

constant distribution of the meridional velocity can be expected, whilst at the outlet in the centre in certain circumstances a considerably greater meridional velocity, c_m^* can be observed. This gives a *reduced output*. From the velocity diagram it is easy to see the ratios. While w_1 remains unchanged the outlet velocity w_2 , retaining its direction, is increased to w_2^* , corresponding to the increase of c_m to c_m^* . Thus similar ratios are obtained as in meridionally accelerated axial-flow fans. It will be appreciated that the peripheral deflection from Δc_u to Δc_u^* is diminished. Taking away from the small triangle, which contains the reduction $d \Delta c_u$, the relationship

$$d \Delta c_u = \Delta c_m / \tan \beta_2,$$

it is easy to calculate the decrease of pressure if the ratio $(c_m/c_m^*) = \eta$ is introduced.

$$\varepsilon^* = \frac{\Delta c_u^*}{\Delta c_u} = 1 - \frac{u}{\Delta c_u} \frac{1 - \eta}{\eta}.$$

Obviously the effect will be greater the higher the hub ratio ν . According to tests the first approximation gives a dependency on ν according to

$$\varepsilon^* = 1 - \nu^2 \times 0.28. \quad (197)$$

88. GEOMETRY OF THE CIRCULAR ARC BLADE

In reference to the applications of simple, circular, arc-shaped blades which have to be dealt with, the typical geometrical characteristics are summarised below.

From Fig. 244 first of all the relation between the angles, the radius of curvature, and the depth of cascade can be derived.

$$\left. \begin{aligned} a &= R (\cos \beta'_1 - \cos \beta'_2); \\ R &= \frac{a}{\cos \beta'_1 - \cos \beta'_2}; \\ l &= R (\beta'_2 - \beta'_1) = R 2\beta'; \\ R &= \frac{l}{\beta'_2 - \beta'_1} = \frac{l}{2\beta'}; \\ \beta' &= \frac{1}{2} \frac{l}{R}; \quad \frac{f}{l} = \frac{1}{8} \frac{l}{R}; \\ \beta' &= \frac{\beta'_2 - \beta'_1}{2}. \end{aligned} \right\} \quad (198)$$

These formulae still apply if the centre of the radius of curvature lies within the cascade strip (Fig. 244, bottom). In the guide wheel this is the case, for example.

The lift coefficient $c_{a\infty}$ will be determined accurately for circular arc blades.

$$c_{a\infty} = 2\pi \left(\alpha + \frac{\beta'}{2} \right) = 2\pi \left(\alpha + 2 \frac{f}{l} \right) = 2\pi \left(\alpha + \frac{l}{4R} \right) = 2\pi \left[\alpha + \frac{1}{4} (\beta'_2 - \beta'_1) \right]. \quad (199)$$

$\alpha, \beta', \beta'_1, \beta'_2$ are in radians (f camber height). Due to the friction we have

$$\frac{dc_{a\infty}}{d\alpha} < 2\pi.$$

This value decreases throughout to 5.5. By introducing a profile efficiency η_{pr} this can be taken into account.

$$\frac{dc_{a\infty}}{d\alpha} = \eta_{pr} 2\pi. \quad \eta_{pr} \approx 0.85-0.9.$$

Thus the following final formulae are obtained

$$\begin{aligned} c_{a\infty} &= 2\pi\eta_{pr} \left(\alpha + \frac{\beta'}{2} \right) = 2\pi\eta_{pr} \left(\alpha + 2 \frac{f}{l} \right) \\ &= 2\pi\eta_{pr} \left(\alpha + \frac{l}{4R} \right) = 2\pi\eta_{pr} \left[\alpha + \frac{1}{4} (\beta'_2 - \beta'_1) \right]. \end{aligned} \quad (200)$$

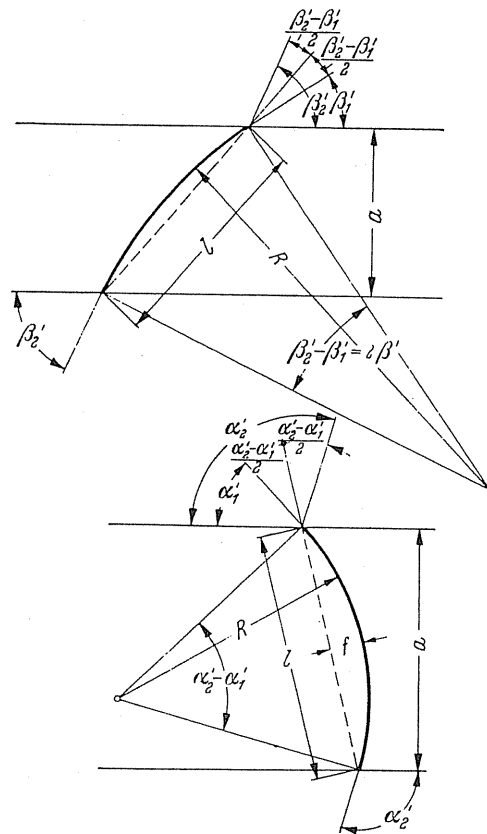


FIG. 244. Geometrical relationships for arc profile blades. *Top*: centre point of curvature outside the cascade. *Bottom*: centre point of curvature within the cascade.

The measured values of circular arc profile blades (Fig. 229) can be readily obtained by the following formula:

$$c_{a\infty} = 1.12 \frac{l}{R} + 0.095 \alpha^\circ. \quad (201)$$

By relating this formula to the general equations, simple formulae can be derived for the radius of curvature:

$$\begin{aligned} \frac{l}{R} &= \frac{1.79t/l}{\eta} \sin \beta_\infty \frac{\sin(\beta_2 - \beta_1)}{\sin \beta_1 \sin \beta_2} - 0.85 \alpha^\circ, \\ \frac{l}{R} &= \frac{1.79t/l}{\eta} \sin \beta_\infty \frac{\sin(\beta_2 - \beta_1)}{\sin \beta_1 \sin \beta_2} \quad \text{for } \alpha^\circ = 0. \end{aligned} \quad (202)$$

These equations offer the possibility of calculating a cascade from purely geometrical data. All hydraulic details, velocities, etc., have been left out.

It may be interesting to know within what limits in a given case a circular arc profile can be designed. For this purpose let us assume that $c_a = 1$ and the span of the profile l is constant. To keep within the range of minimum lift-drag ratios the angle of incidence, according to Fig. 229, must be kept within the limits $0-6^\circ$. Four possibilities ($0^\circ, 2^\circ, 4^\circ, 6^\circ$) are shown in Fig. 245. It will be observed that there is an extensive scope for variation with rather variable curvatures.

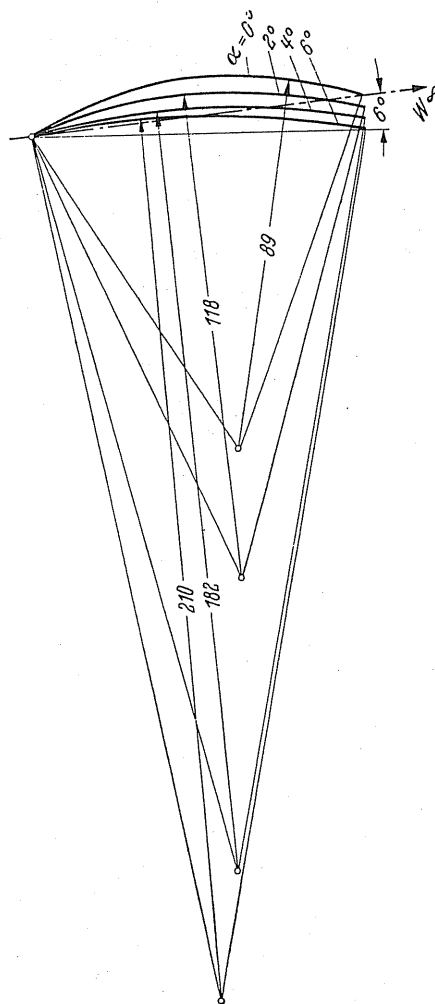


FIG. 245. Four different arrangements of an arc profile blade for equivalent ψ and ϕ .

Increase of the outlet angle β_2 only. In respect of the opinion invariably expressed, one should open up the angle of incidence in the interests of adequate intake cross-section. The case is interesting where the intake angle β_1 is equal to angle β'_1 , whilst the outlet angle $\beta'_2 > \beta_2$. Since $(\beta_1 + \beta_2)/2$ in the first approximation equals the angle β_∞ , we obtain, according to Fig. 246, the angle of incidence α from the difference in path of the two chords. The rule will be readily appreciated.

Angle opening,

$$\Delta\beta'_2 = \beta'_2 - \beta_2 = 2\alpha.$$

The following result is obtained:

$$\Delta\beta'_2 = \frac{4}{3} \frac{t}{\eta \eta_{pr} l \pi} \sin \beta_\infty \frac{\sin(\beta_2 - \beta_1)}{\sin \beta_1 \sin \beta_2} - \frac{1}{3} (\beta_2 - \beta_1). \quad (203)$$

For the radius of curvature we obtain

$$\frac{l}{R'} = \frac{4}{3} \frac{t}{\eta \eta_{pr} l \pi} \sin \beta_\infty \frac{\sin(\beta_2 - \beta_1)}{\sin \beta_2 \sin \beta_1} + \frac{2}{3} (\beta_2 - \beta_1). \quad (204)$$

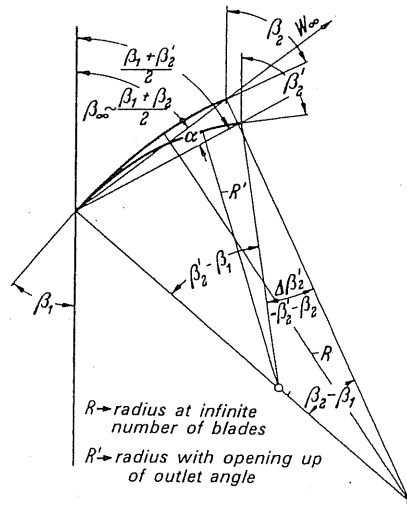


FIG. 246. Single opening-up of outlet blade angle at unvaried intake angle.

89. THE MOST FAVOURABLE BLADE PITCH ACCORDING TO ZWEIFEL

Blade number and blade pitch according to former opinion were derived from the assumption that conditions similar to the single aerofoil could be presumed. This means that by and large the c_a -value of the best gliding angle ought to be chosen. This was understood to be subject to the fact that the individual blade encountered by the flow at the ideal direction w_∞ was fairly identical with the blade in the cascade relationship. We justified this by the assumption that here it was only a matter of approximation but we took it into account because the accurate layout according to the cascade theory does not affect the efficiency very much. When going over to narrower blade pitches, i.e. to larger a/t values, the former conditions become very unstable. This becomes all the more impressive when considering the blading of a drum impeller and also the steam-turbine blading. Here the deflection through the blades is so great that the normal aerofoil calculations lose their

meaning. Long before there was an aerofoil theory in existence, engineers found the correct path by instinct. The blade channels were designed according to the aspects which had become known for bends. The Briling rule⁽¹⁷⁾ should be mentioned, according to which the thickness of the jet is equal to the half median radius of curvature of the duct. If, as a trial, the cascade aerofoil theory first stated by Bauersfeld⁽¹⁸⁾ be applied to cascades of this kind, c_a values of 20 and more are obtained. These values show clearly the problem of the aerofoil theory. It may be asked what should be done in the intermediate zone, which is very important to us. The question to be answered can be outlined in the following way. Where the blade pitch is too narrow the *surface friction* will lower the efficiency. Where the pitch is too large *separations* occur with high losses. In between there will be an approximate best value, the safe choice of which will be the governing factor for the efficiency to be achieved.

Zweifel⁽¹⁹⁾ has the credit of having found a satisfactory answer to this question from the engineering point of view. His idea will be elaborated in an example of fan-blading as shown in Fig. 247.

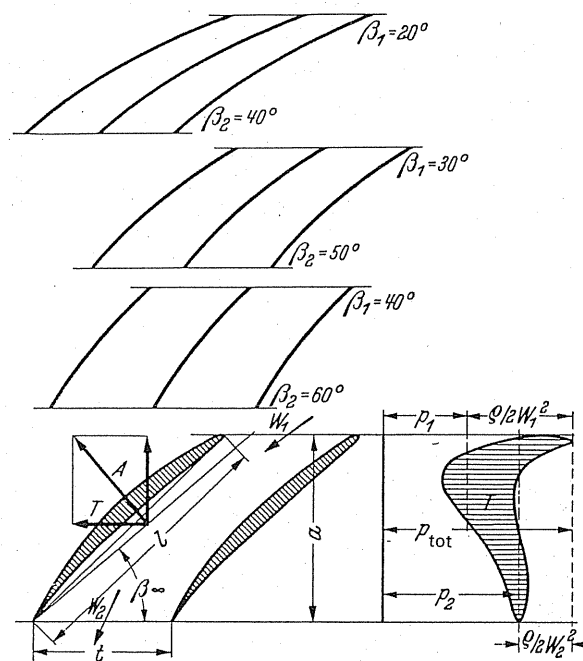


FIG. 247. Top: Three-blade cascades with optimum pitch according to Zweifel. Bottom: The effect of force and pressure distribution on cascade blade.

In the blade channel the mean velocity is retarded from w_1 to w_2 . This corresponds to a static pressure increase

$$p_2 - p_1 = (q/2) (w_1^2 - w_2^2).$$

¹⁷ Briling, Forschungsheft 68.

¹⁸ Bauersfeld, Z VDI, 1922, p. 461.

¹⁹ Zweifel, BBG-Mitteilungen, 1945, p. 463.

The pressure distribution around a blade is shown on the right. At the front there is the *velocity head* at which the velocity w_1 is retarded to zero. This corresponds to the pressure increase by $(\rho/2) w_1^2$ so that the total pressure $p_{\text{tot}} = p_1 + (\rho/2) w_1^2$. This is the highest pressure which can actually occur in the flow. On the hollow side of the blade the pressure due to stagnation is greater than on the back side. The difference provides the blade pressure which has to be developed by the driving machine. At the rear-blade pitch both pressure lines converge again. At both sides the pressure p_2 and the outlet velocity w_2 prevail. The pressure distribution, as will be observed, differs somewhat in this cascade profile from the distribution at the individual profile. The area formed by the two pressure curves corresponds to the overall tangential force T which acts on the blade. It will now be asked what pressures are *characteristic* and *physically important* to the problem. Two points are outstanding, namely the front stagnation point with p_{tot} and the back edge with p_2 . What is remarkable is that in contrast the pressure p plays no significant role. A difference $p_{\text{tot}} - p_2$, is obtained from the two absolute pressures, and this is exactly equal to $(\rho/2) w_2^2$, i.e. equivalent to the stagnation pressure of the mean outlet velocity. It is therefore advisable to compare the tangential force acting on the blade with an ideal force which occurs due to the fact that the stagnation pressure of w_2 is allowed to act on the full blade width. Thus we have the force $(\rho/2) w_2^2$ which obviously is closely bound up with the problem. We shall, therefore, be curious as to the magnitude of the ratio $T/[(\rho/2) w_2^2 a] = \psi_T$, since a coefficient ψ_T has been introduced for this at the same time. It is appropriate at the same time to consider the lift force A which by definition must be located perpendicular to w_∞ . Let us take the analogous case where the velocity head $(\rho/2) w^2$ acts on the aerofoil chord l and we have a force which may possibly have some relationship with the lift A . Let us look at the ratio

$$\frac{A}{(\rho/2) w_2^2 l} = \psi_A,$$

which is designated by a coefficient ψ_A . Zweifel found this value in all cascade tests which are known, and wherein also acceleration cascades (turbine cascades) were integrated. Here, surprisingly, Zweifel has found that the best values of all known cascades are situated between the values 0.9 and 1.0, whereas for conventional examination, i.e. when recording above the c_a values, a very wide spread is observed, which shows that these former investigations did not go to the root of the problem.

By this means, however, a rule of practical use for finding the most favourable blade pitch is realised immediately. All that is necessary is to see that the ψ_T or ψ_A values are situated between 0.9 and 1. Thus by easy calculation, if we still want to be rather cautious in our deceleration cascades, and based on a value $\psi_T \approx 0.8$, we arrive at the following formula for the most favourable pitch:

$$\frac{a}{t} = 2.5 \sin^2 \beta_2 [\cot \beta_1 - \cot \beta_2]. \quad (205)$$

For typical angles occurring in fan blades this formula is plotted in Fig. 248. For further illustration three cascades are shown in Fig. 247 in which the same change of deflection of 20° is available.

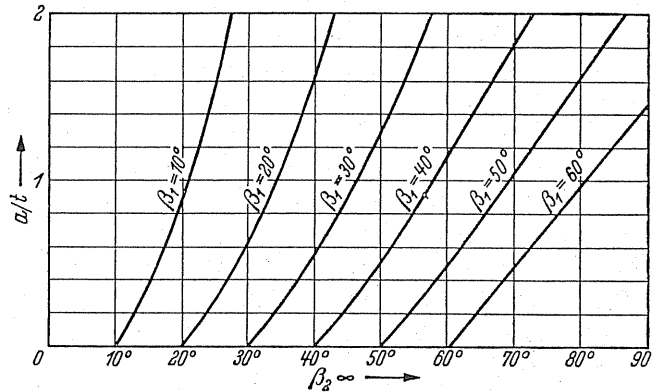


FIG. 248. Evaluation of eqn. (205).

Simple approximation calculations. In the cases dealt with beforehand regarding narrow blading it is possible to carry out simple approximate calculations on the lines of remarks made on p. 38. In this way, for increasing the angle at the blade tip according to a calculation by the author (see Eck, *Ventilatoren*, 3rd German edition), we obtain the simple formula

$$\Delta\beta = 0.25 \frac{t}{l} (\beta_2 - \beta_1).$$

Howell⁽²⁰⁾ arrives at a similar equation:

$$\Delta\beta = 0.25 \sqrt{t/l} (\beta_2 - \beta_1).$$

The comparison by means of tests shows that the suitable value is 0.4.

90. CASCADE CALCULATIONS ACCORDING TO WEINIG

For cascades running at low loads Weinig instituted accurate potential-theoretical calculations which are easy to evaluate in practice. Let us start from the circular arc section profile which shows intake and discharge flow angles at infinite blade numbers and which agree exactly with the flow angles. If, for example, the flow is deflected from the angle β_1 to the angle β_2 , then circular arcs with these inlet and outlet angles would have to be realised at infinite number of blades. The overall deflection of the flow in this case is $\beta_2 - \beta_1 = \vartheta_\infty$. According to Weinig an excessive bending is selected in such a way that circular blades with a deflection $\vartheta > \vartheta_\infty$ are obtained. For the ratio $\mu = \vartheta_\infty/\vartheta$ Weinig has found the formula

$$\mu = \frac{t/l}{\pi/2} \sin \beta_m \ln \frac{R^2 + 1}{R^2 - 1}, \quad (206)$$

in which the quantity R is a characteristic value of the conformal transformation $\beta_m = (\beta_1 + \beta_2)/2$. The solution actually only applies for shallow-arched cascades. It would appear, however, that they are also useful for deep arches and fairly narrow pitches. In

²⁰ Howell, A. R., and Bonham, R. P., Overall and stage characteristics of axial-flow compressors, *Proc. Instn. Mech. Engrs. London*, **163** (1950).

Fig. 249 the formula is illustrated in simple form. The total excess angle is now to be divided up uniformly over a correction of the inlet and the outlet angle, so that the local excess takes the value $\nu = (\vartheta - \vartheta_\infty)/2$. The following relationships are also found easily:

$$\nu = \frac{\vartheta - \vartheta_\infty}{2} = \frac{\vartheta_\infty}{2} \frac{1 - \mu}{\mu} = \frac{\vartheta}{2} (1 - \mu); \quad \vartheta = \frac{\vartheta_\infty}{\mu}. \quad (207)$$

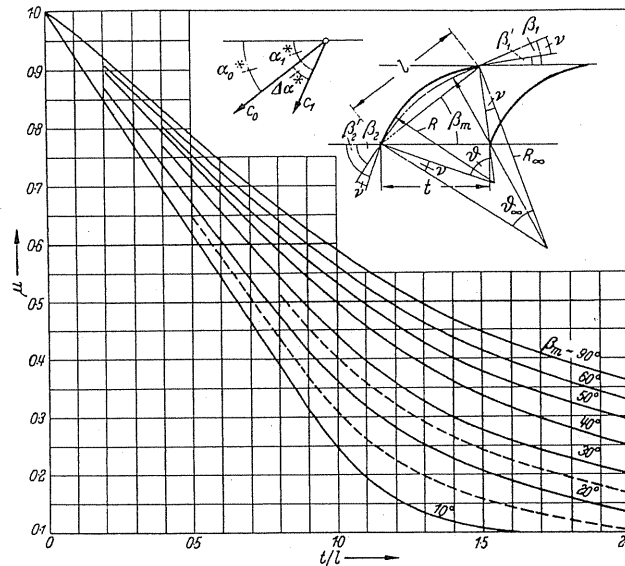


FIG. 249. Cascade calculation according to Weinig.

This gives us the following blade angles,

$$\beta'_1 = \beta_1 - \nu; \quad \beta'_2 = \beta_2 + \nu. \quad (208)$$

As the angles β_1 and β_2 for any problem are known, all that is missing for calculation of the excess is the value t/l . For this, however, according to eqn. (176), the value $t/l = (c_a w_\infty)/(2 \Delta c_u)$ can be inserted and the value of $c_a \approx 1$ not exceeded, but a mean value $c_a \approx 0.5-0.6$ can be chosen as average. The best values lie at $0.5 < t/l < 1.5$, and therefore simply this value can be chosen. The procedure, however, may take the form that according to the assumptions by Zweifel the value of t/a according to eqn. (205) is found. Thus the reckoning is reverted to a minimum size. It should be emphasised here that it is recommended by different authorities only to carry out the excess curvature at the blade outlet and to leave the inlet unaltered.

Very accurate cascade investigations were carried out by Schlichting⁽²¹⁾ and Scholz.⁽²²⁾ These exact calculations were then verified by means of many examples using the calculat-

²¹ Schlichting, H., Calculation of the frictionless incompressible flow for an upstream flat blade cascade, *VDI ForschHft.*, **447** (1955).

²² Scholz, N., Investigations on blade cascades, *VDI ForschHft.*, **442** (1954).

ing method of Weinig and the correction due to thickness effect. It was found that these simple calculations agreed very accurately with the results obtained by Schlichting and Scholz. This procedure is to be highly recommended in practice.

91. INCREASE OF OUTLET ANGLES IN PROFILING

The calculation according to Weinig only applies to simple steel blading. Shemoyama⁽²³⁾ has found, however, that when transferring to a profile, additional velocities are induced to the intake flow and lead to the direction of β_∞ , having to be increased a little. Viewed superficially it is an increase of outlet angle which has already been used in the streamline theory for taking into account the finite blade thickness. It is a fortunate fact that for cascades this effect can be calculated accurately with the aid of the conformal transformation. A correction dependent on thickness and pitch is obtained which obeys the formula

$$\Delta\beta = \Delta\beta_1 \left(\frac{l}{t} \right)^2. \quad (209)$$

Here $\Delta\beta_1$ is an intermediate calculation quantity which is equivalent to $\Delta\beta$ for $l = t$. The value of $\Delta\beta_1$ can be taken from Fig. 250 for different profile thicknesses.

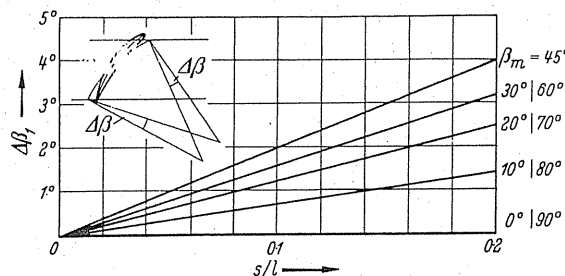


FIG. 250. Chart for determining the increase of angle by profiling. s , profile thickness; l , chord length.

Working out of profiling. We start from the circular arc section form mentioned before, which is turned by the angle $\Delta\beta$ for taking into account the profile thickness. Then the profiling is plotted simultaneously on both sides. Here care should be taken that in cascades as opposed to individual profiles the greatest thickness should lie at about 40% of the depth. For the profiling itself it is best to use approved profiles in accordance with Fig. 227.

92. MINIMUM HUB DIAMETER

Particularly difficult conditions exist at the hub of the axial-flow fan. At this point the peripheral speed is at its lowest. This can only be compensated by deeper blades and by a larger angle of incidence. The limit is set by the possible separation of the flow. The value $c_a \approx 1$ therefore cannot be exceeded very much if the conditions for individual aerofoils are considered on their own. This was pointed out first by Keller. On the other hand, in

²³ Shemoyama, Y., Experiments with rows of air foils for retarded flow, *Mem. Fac. Engrg. Kyushu. Imp. Univ. Fukuoka*, 1938.

the interest of high efficiency it should be as large as possible. Therefore the cascade value becomes $c_a l/t = 0.5-1.5$. Recent research has shown that the upper limit of $c_a l/t$ lies between 1.5 and 2.

De Haller⁽²⁴⁾ in experiments with flat cascades found that when a specified retardation $w_2/w_1 = 0.75$ was achieved, the boundary layers at the side walls increase so greatly that the outlet velocity cannot be decreased any further. This causes a cascade to be choked.

Moreover, for constructional reasons Keller recommended a limitation to pitch ratio at the hub $l/t < 1.1$.

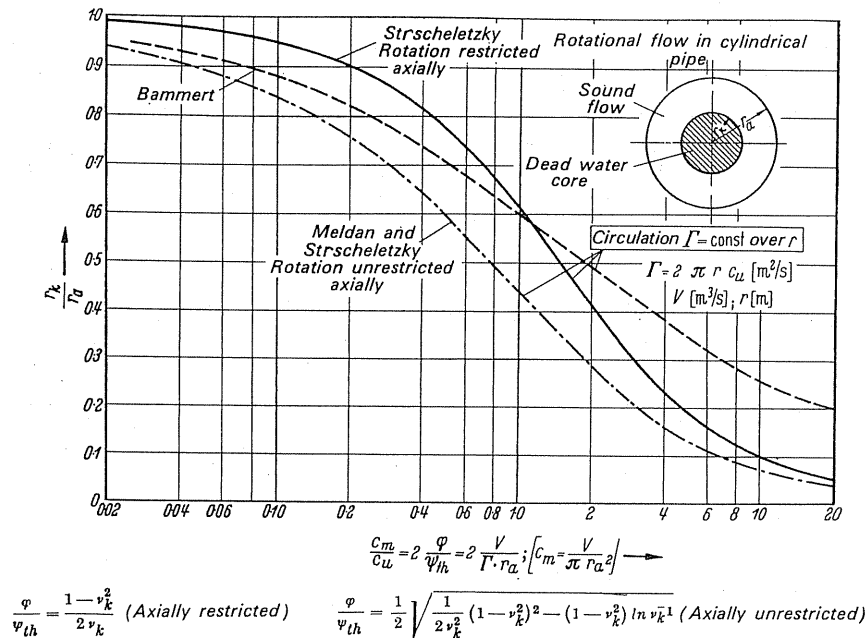


FIG.251.

Two distinct physical phenomena, however, are more decisive factors for many fans. First we have the *Strscheletzky boundary layer conditions of the hub dead space* (Fig.251) and the later knowledge that at least in *free discharging rotational flow there is a considerable recovery of rotation*. These findings enable the application of fans without guide wheels to be extended into the field of application dominated by fans having guide wheels.

93. VORTEX CORE FORMATION

The vortex core formation is highly important for the selection of the smallest hub diameter of axial-flow fans as well as for profiling of guide appliances for generating rotation. Since the researches of Meldau⁽²⁵⁾ and Bammert⁽²⁶⁾ into this problem and the new rules

²⁴ De Haller, P., The behaviour of aerofoil cascades in axial-flow fans and in the wind tunnel, *BWK*, 5 (1953) 332-7.

²⁵ Meldau, E., Rotating flows in hollow rotating spaces, Diss., Hanover, 1933.

²⁶ Bammert, K., and Klünkes, H., Hub dead-space following guide wheels of axial-flow machines, *Ing.-Arch.*, 1949, p.367.

due to Strscheletzky⁽²⁷⁾ and Schlünkes,⁽²⁸⁾ much information is now available. Accordingly it is possible to state the core dimensions as a function of rotation. The following results merit attention.

(1) There is a difference between a rotational flow in an axially unrestricted flow and a shorter axial path, following which there is an appliance in action for straightening the rotation. Figure 251 shows the two curves and their formulae which clearly portray this difference.

(2) According to Fig. 251 the core diameter can be increased by straightening the flow. At a distance of $0.3d$ in front of the arrangement the theoretical core diameter of the axially restricted rotational flow is achieved. At a distance of $3d$ this core starts to increase.

(3) If the rotation is generated by a radial rotating appliance, the core diameter at first is lower than the theoretical value due to the momentum components directed radially inwards. The theoretical value is only achieved after $2d$ (important for guide appliances).

(4) The theoretical core diameter is achieved immediately when using an axial rotational generator and remains constant for a long distance.

Hausenblas has shown that the following simple relation, $0.8 < c_m/c_{au} < 1.0$, is valid near the hub; this means that the direction of the relative velocity w_2 should not be less than 45° .

Rotational effect of free jets. Whilst the rotational effects of flow within closed ducting can be recognised to some extent by means of Fig. 251, there are other manifestations in free jets. Later, important knowledge has been gained in appropriate research on nozzle jets.⁽²⁹⁾

If, for instance, we follow a jet leaving a nozzle with a variable swirl imparted by an internal guide appliance, we find the following phenomena.

At lower rotation the round jet structure is fairly well maintained. The pressure below atmosphere in the core holds the whole jet together. At higher swirl the jet falls apart suddenly. This occurs in the case where the total pressure in the interior of the jet drops below the surrounding static pressure. Thus outside air penetrates into the jet; the jet then becomes a free jet. The transition occurs fairly abruptly.

The jet issuing at a slope to the outside can easily be deflected backwards by guide blades. Recently a complete reversal by 180° has been achieved by sucking the boundary layer at the nozzle curvature. In this way the reaction forces of the jet alter their direction which is important for jet aeroplanes for shortening their landing path. Figure 252 is a diagram of these processes.

A straightening of rotation takes place. At a 50° rotational angle and free exhaust, for instance, the pressure below atmosphere drops in the centre of the jet in one diameter only to 60% of the maximum value behind the outlet. A recovery also takes place even in rotational flow restricted by walls.

²⁷ Strscheletzky, M., Equilibrium forms of rotation symmetrical, rotational flow with constant rotation in straight cylindrical hollow rotational spaces, *Voith-Forschung u. Konstruktion*, 1959, No. 5.

²⁸ Schlünkes, F., Measurements on air flows with constant rotation in a straight circular duct, *Voith-Forschung u. Konstruktion*, 1959, No. 5.

²⁹ Iserland, K., Experiments comparing deflection of a free jet with the aid of twist, *Mitt. Inst. f. Aerodynamik*, No. 25, Zürich.

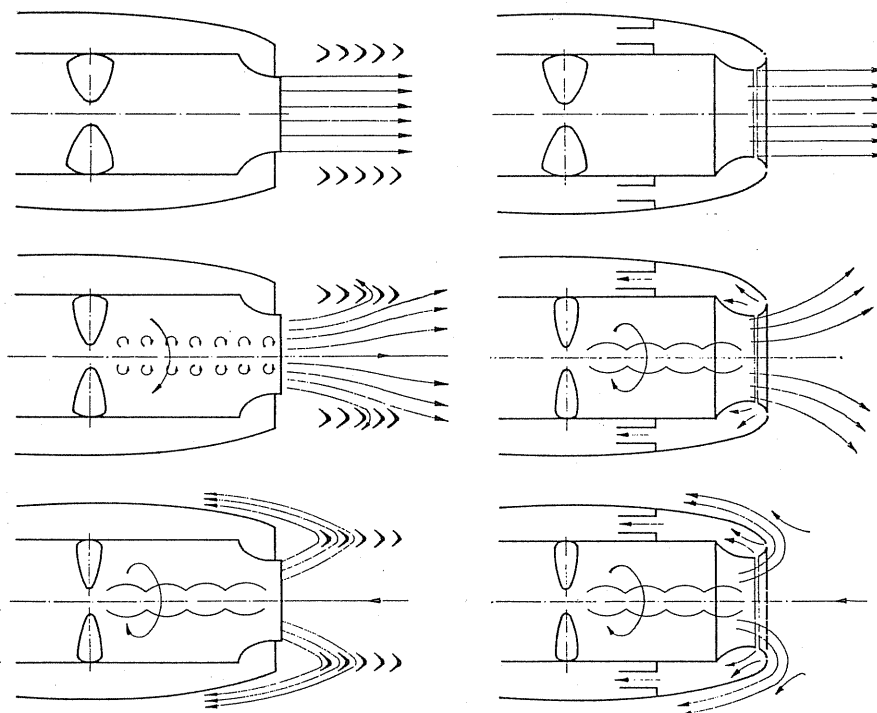


FIG. 252. Behaviour of an irrotational flow.

94. EFFECT OF TIP CLEARANCE

Between the outside wall of the housing and the external diameter of an axial rotor it is essential to have a gap. The size of the gap, i.e. the ratio s/d , has a great effect on the efficiency, delivery volume, and delivery pressure. Efficiency falls catastrophically as the gap increases in size. In the case of small gaps the fall is particularly great in high-class profile blading. According to the latest measurements⁽³⁰⁾ a fall $\Delta\eta \approx 2\%$ can be stated to be the rule for a gap increase of 1% .

This means that given the width of the gap the maximum efficiency of an axial-flow fan can be estimated approximately. The gapless axial-flow fan has an optimum upper limit of 90% so that the following optimum values result for various s/d ratios.

$s/d \text{ ‰}$	1	2	3	4	5
η_{\max}	0.88	0.86	0.84	0.82	0.80

Figure 253 shows the measurement on profiled and twisted blades (top curves) and untwisted steel blades (B 3, 4, and 6). The steep drop in profile blades is worthy of note. The results agree with similar ones obtained on Kaplan turbines by Canaan.⁽³¹⁾

³⁰ Marcinowski, H., The influence of the impeller gap in free discharging axial-flow fans without guide wheel, *Voith-Forschung u. Konstruktion*, 1958, No.3.

³¹ Canaan, 30 years of Caplan turbines, *Wasserkraft u. Wasserwirtschaft*, 1944, No.2, pp.29 and 39.

In the range of relatively large gaps starting from 10% there is hardly any difference between profiled and steel blades.

The correction of the delivery volume and of the pressure can be carried out by enlarging the blade angle or by raising the velocity.

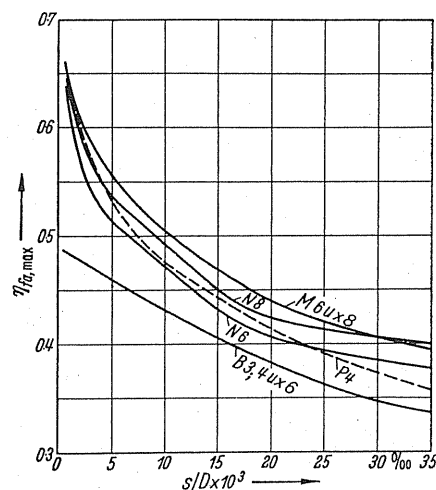


FIG. 253. Influence of gap on axial impellers without guide wheels according to Marcinowski.

More recent investigations⁽³²⁾ demonstrate further that by increasing the gap a cross-flow appears at this place. The separation conditions are altered thereby. For reasons of manufacture the gap is never evenly distributed around the circumference, and this gives rise to another inconvenient source of noise.

Influence of the Reynolds number on the efficiency. At smaller sizes, i.e. lower Reynolds numbers, the efficiency of axial-flow fans falls drastically. The fall, moreover, depends on the volume coefficient φ . According to Eckert the governing parameter therefore is taken as the value φRe . Approximately starting from $\varphi Re = 80,000$ the efficiency falls almost linearly to 10%. Above it the efficiency rises slowly up to 90%.

95. CALCULATION AND CONSTRUCTION OF GUIDE WHEELS

In general a guide wheel is essential before or after the rotor. The problem is either to deflect any intake air towards the periphery or conversely. The designs of the guide wheels necessary for this purpose are dealt with below.

With the guide wheel arranged *in front* there is an accelerated flow. According to observations on turbines the influence of the finite number of blades in these accelerated cascades can be ignored as a first approximation. We would like to recommend this layout here. In the cylindrical or untwisted design which is often encountered, the layout will be considered

³² Stanley P. Hutton, Tip clearance and other three-dimensional effects in axial-flow fans, *Festschrift Ackeret*, 1958, p. 359.

for a medium diameter. The question is how the excess angle shall be determined with the downstream guide wheel, where the excess only relates to the outlet angle, whilst the inlet angle for practical purposes is selected equal to the angle resulting from velocity triangle at the impeller outlet. For calculating the outlet angle excess the ideas formerly mentioned shall be applied.

From the velocity diagram we obtain the absolute direction of the velocity before or after the impeller, the problem is how a finite number of blades should be arranged in order to obtain the desired deflection. Generally the guide wheel is in a worse position than the rotor. The centrifugal effect, i.e. whirling effect on the boundary layer, is absent. For this reason an effort must be made to keep the load of the guide wheel as low as possible. The reaction effect $r = \Delta p_{\text{stat}} / \Delta p_{\text{tot}}$ indicates numerically what pressure conversions take place in the impeller and guide wheel. In normal single stage axial-flow fans it is advisable not to select the reaction effect below 0.7. One exception is the guide wheel in an axial compressor. In this case nowadays a reaction effect of approximately 0.5 is chosen. The function in the compressor, however, cannot be compared with the one in a single-stage fan. Therefore, for single-stage fans the above recommendations are appropriate. If a guide blade cascade is intended to deflect air from angle α_1 to angle α_2 , then the outlet angle must be increased and $\alpha_3 > \alpha_2$. The deviation on the curve, c_u thereby is increased by Δc_u . According to a previous calculation we obtain

$$\Delta c_u = 0.33 \frac{c_m}{c_2} \frac{t}{a} (c_{1u} - c_{2u}).$$

For the two most important cases of the upstream and downstream guide wheel the formulae are:

Upstream:

$$\Delta \hat{\alpha} = \left(\frac{1}{4} \dots \frac{1}{3} \right) \frac{t}{a} \sin^2 \alpha_2 \cos \alpha_2, \quad (210)$$

Downstream:

$$\Delta \hat{\alpha} = \left(\frac{1}{4} \dots \frac{1}{3} \right) \frac{t}{a} \frac{1}{\tan \alpha_1}. \quad (211)$$

Let us consider in accordance with eqn. (205) the most favourable blade pitch according to the formula $a/t = 2.5 \sin^2 \alpha_2 (\cot \alpha_1 - \cot \alpha_2)$. Thus we obtain:

Upstream:

$$\frac{a}{t} = -2.5 \sin^2 \alpha_2 \cot \alpha_2 = -2.5 \sin \alpha_2 \cos \alpha_2 = -1.25 \sin 2\alpha, \quad (212)$$

Downstream:

$$\frac{a}{t} = 2.5 \cot \alpha_1. \quad (213)$$

By integrating the above equations, we obtain

Upstream:

$$\Delta \hat{\alpha} = \left(\frac{1}{10} \dots \frac{1}{7.5} \right) \sin \alpha_2, \quad (214)$$

Downstream:

$$\Delta\hat{\alpha} = \left(\frac{1}{10} \cdots \frac{1}{7.5} \right) \cong 5.73^\circ - 7.65^\circ, \quad (215)$$

but this implies that a constant excess angle of approximately $6^\circ - 7^\circ$ occurs if the most favourable pitch is realised.

For the angle $\alpha'_1 = 75^\circ, 60^\circ, 45^\circ$, the guide blades for the case of the downstream guide wheel are drawn in Fig. 254 to suit the results of eqn. (215). In the case of blades which are far apart, the aerofoil calculation ought presumably also lead to the same result $\alpha'_1 = 75^\circ$. Checking back gives $\Delta\alpha \approx 5^\circ$, i.e. a fairly uniform correction.

Independent of this simple layout the process by Weinig can also be applied.

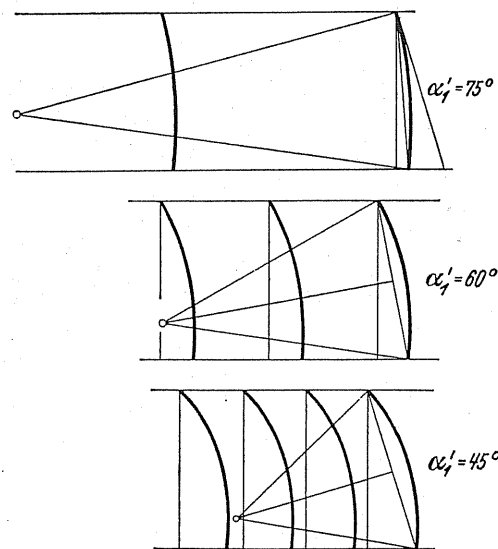


FIG. 254. Three different guide wheels with excess angle and optimum blade pitch.

Guide blades gap. It was proved by tests by Fickert⁽³³⁾ that with *fixed decelerating* cascades improvement can be achieved by means of gaps. Accordingly, gaps of a width of approximately 6–8% of the depth of upstream aerofoils are advantageous if the depth of upstream aerofoil is designed with 1–2% of overlap. In this case, of course, high loads with c_a values of 1.2 must be realised, whereas gapless guide wheels achieved $c_{a \max}$ values of 0.7. Arrangements where the blades are staggered by a half pitch, such as are found in many designs, have proved to be ineffective.

96. COMPARISON BETWEEN CONSTRUCTIONS WITH UPSTREAM GUIDE WHEEL AND DOWNSTREAM GUIDE WHEEL

The question is often raised whether an upstream guide wheel or a downstream guide wheel should be chosen. In many cases the decision is governed by the type of installation and the overall arrangements. Over and above this, however, there is the question whether,

³³ Fickert, K., Tests on blading on retarding cascades with a high deflection, *Forschung*, 1949/1950, p. 141.

in principle, one of these arrangements promises a better efficiency. Primarily the upstream guide wheel appears to have advantages since the flow is accelerated with these whilst the downstream guide wheel is situated in the zone of retarded flow. This advantage, however, is offset by a disadvantage, because the static pressure drop which has arisen in the upstream guide wheel has to be generated additionally in the downstream guide wheel by way of static pressure with retarded relative flow. For this reason greater losses occur than in the case of the downstream guide wheel, since the static pressure rises in the impeller as well as in the guide wheel. The question now is whether the advantage of the upstream guide wheel is greater or lesser than the disadvantage just mentioned. Marcinowski⁽³⁴⁾ investigated this problem very thoroughly by way of various examples and reached the conclusion that the upstream guide wheel is only of benefit at very low hub ratios and particularly bad lift-drag ratios. This statement only applies to the case where no rotation is present behind the rotor, i.e. only for the design level. Moreover, it was assumed that the layout will be carried out with constant rotation. The tendency in practice to design axial impellers with downstream guide wheels is therefore justified in a general way.

97. UPSTREAM GUIDE BLADES WITH CONSTANT OUTLET ANGLE (CYLINDRICAL BLADE)

For simplifying manufacture alone, the problem whether upstream guide blades with constant outlet angles should be used, is interesting. Then a simple cylindrical curved blade would arise which would have no twist.

In any case a rotational flow would be generated which is given by a constant rotational angle α . This flow can be easily determined. Let us start with the Bernoulli equation $P = p + (\varrho/2) c^2$, the validity of which we accept. This means that constant energy for all streamlines is assumed. The alteration of the total energy in the direction dr therefore must be equal to zero.

$$\frac{dP}{dr} = \frac{dp}{dr} + \varrho c \frac{dc}{dr} = 0.$$

Due to the c_u component, centrifugal forces occur which can only be absorbed by a static variation of pressure in the radial direction in accordance with the relationship

$$\frac{dp}{dr} = \varrho \frac{c_u^2}{r}.$$

By substituting this in the above equation we have

$$c \, dc + \frac{c_u^2}{r} \, dr = 0. \quad (216)$$

This differential equation must always apply if we assume the validity of the Bernoulli equation and the conditions of equilibrium normal to the flow.

³⁴ Marcinowski, H., Optimum problems in axial-flow fans, *Voith-Forschung u. Konstruktion*, 1958, No. 3.

The assumption $\alpha = \text{const}$ implies that for all radii, c moves on the side of the angle α . By substituting $c = c_u / \cos \alpha$ we obtain

$$\frac{dc_u}{c_u} + \cos^2 \alpha \frac{dr}{r} = 0.$$

By integrating and simplifying,

$$c_u r^{\cos^2 \alpha} = c_{au} r_a^{\cos^2 \alpha} = \text{const.} \quad (217)$$

The rule $c_u r = \text{const}$ therefore is no longer complied with. Since $c_m / c_u = \tan \alpha = \text{const}$, we can express the formula also by c_m .

$$c_m r^{\cos^2 \alpha} = c_{ma} r_a^{\cos^2 \alpha} = \text{const.} \quad (218)$$

c_m , however, is no longer constant. It increases from the outside to the inside. For the case $\alpha = 30^\circ$ the c_m distribution is shown in Fig. 255.

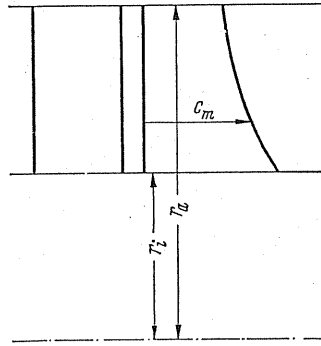


FIG. 255.

Distribution of rotation with $c_u = \text{const}$. Where the rotational component c_u is constant it is possible also to integrate. We express $c^2 = c_u^2 + c_m^2$; $d(c^2) = d(c_m^2)$ and obtain

$$\frac{1}{2} d(c_m^2) + \frac{c_u^2}{r} dr = 0,$$

$$\frac{c_m^2}{2} + c_u^2 \ln r = C,$$

$$c_m^2 = c_{im}^2 - 2c_u^2 \ln \frac{r}{r_i}. \quad (219)$$

It follows from this equation that here also c_m increases as we approach the hub.

It is also easy to get an expression for the angle α . For this purpose we divide the last equation by c_u^2 and obtain

$$\left(\frac{c_m}{c_u} \right)^2 = \left(\frac{c_{im}}{c_u} \right)^2 - 2 \ln \frac{r}{r_i}.$$

Since $c_m/c_u = \tan \alpha$, we have

$$\tan^2 \alpha = \tan^2 \alpha_i - 2 \ln \frac{r}{r_i}. \quad (220)$$

This means that the angle α decreases towards the outside. Hence a *reverse* rotation to that of the standard case is obtained.

Distribution of rotation by the general exponential law. Let us now take the general power law $c_u = C'/r^n$. The integration is then possible. We put $c_u = C'/r^n$ in the general eqn. (216) and obtain $c \, dc + (C'^2/(r^{2n+1})) \, dr = 0$, from which

$$\frac{c^2}{2} - \frac{C'^2}{2^n} \frac{1}{r^{2n}} = C''.$$

If we express

$$c^2 = c_u^2 + c_m^2 = \frac{C'^2}{r^{2n}} + c_m^2,$$

we obtain

$$c_m^2 = c_{im}^2 + \frac{n-1}{n} C'^2 \left[\frac{1}{r_i^{2n}} - \frac{1}{r^{2n}} \right]. \quad (221)$$

Three different cases now arise according to whether n is equal to or greater or less than 1.

$$n = 1 \quad c_m = c_{im} \text{ (normal case),}$$

$$n > 1 \quad c_m > c_{im},$$

$$n < 1 \quad c_m < c_{im}.$$

It is worth noting in this solution that the case $c_m > c_{im}$ can also be realised.

The results are significant owing to the adjustability of single-stage axial-flow fans by means of adjustable upstream guide blades. At air intake without rotation it would be desirable for reasons of the lower flow resistance if upstream guide blades were without twist and without curves. If, for example, in the mechanical design only the rear edges are twisted, an upstream guide blade having a cylindrical form is obtained in which, therefore, the rotation angle generated is constant. In this case mainly only rotational angles in the direction of motion come into question, because only here at least do they give good regulating effects. However, the simple axial wheel without pre-rotation already demonstrates a c_m distribution, with c_m values decreasing outwards at delivery volumes which are lower than normal. It will be appreciated that the cylindrical upstream blade is eminently suitable in such cases and the question arises whether any benefit at all can be obtained by twist.

Other small c_m distributions which have been achieved, as stated above, by suitable form of the upstream guide wheel are very useful in cases where the upstream guide wheel is situated in the nozzle-shaped, i.e. externally curved, intake zone.

98. RADIAL PRESSURE DISTRIBUTION IN AXIAL-FLOW FANS

The custom of relating coefficients to the external diameter or the peripheral speed should not lead one to believe that these values vary from radius to radius. For instance, the pressure coefficient ψ which is used throughout the calculation actually is only present at the outside periphery. For smaller radii ψ varies as follows:

$$\Delta p = \psi_a \frac{\rho}{2} u_a^2 = \psi \frac{\rho}{2} u^2 \quad \text{which gives} \quad \psi = \psi_a \left(\frac{r_a}{r} \right)^2.$$

The ψ values are thus inversely proportional to r^2 . The more important question is how the static pressures vary. Consider the case where the air supplied to the fan free of rotation is led to straight flow by means of a guide wheel following the rotor. In this case the overall pressure consists of a static and a dynamic portion.

$$\Delta p_{\text{tot}} = \Delta p_{\text{stat}} + \frac{\rho}{2} c_u^2.$$

The dynamic pressure expressed as a proportion of the total pressure is

$$\frac{\Delta p_{\text{dyn}}}{\Delta p_{\text{tot}}} = \frac{(\rho/2) c_u^2}{\eta/\rho u_a c_{au}}.$$

For reasons of equivalent energy transferred for all streamlines we must have

$$u c_u = u_a c_{au},$$

$$c_u = \frac{u_a c_{au}}{u}.$$

By inserting this and with simultaneous consideration of $\psi_a = 2(c_{au}/u_a)\eta$, we obtain $\Delta p_{\text{stat}}/\Delta p_{\text{tot}} = r$. The static portion which interests us, i.e. the reaction effect, which here varies from radius to radius, is then easy to calculate.

For ψ values between 0.05 and 0.8 the pressure distributions are plotted in Fig. 256. It will be observed that the decrease of the pure static pressure takes place with increase of ψ . The restriction of hub dimension, according to relationship $\nu = \sqrt{0.8\psi}$ in this case, is a vertical straight line and plotted in Fig. 256. Hence $r = 0.25$. For illustrating the importance of the different curves the pressure distribution adjacent to an impeller is shown at the side of the graph for the case $\psi_a = 0.4$.

The point of intersection of the curves with the coordinate axis represents the case that $\Delta p_{\text{stat}} = 0$. This, however, signifies uniform pressure. Rough calculation gives the radius at which this uniform pressure is achieved:

$$\frac{r_a}{\sqrt{2}} \frac{\sqrt{\psi}}{\eta}.$$

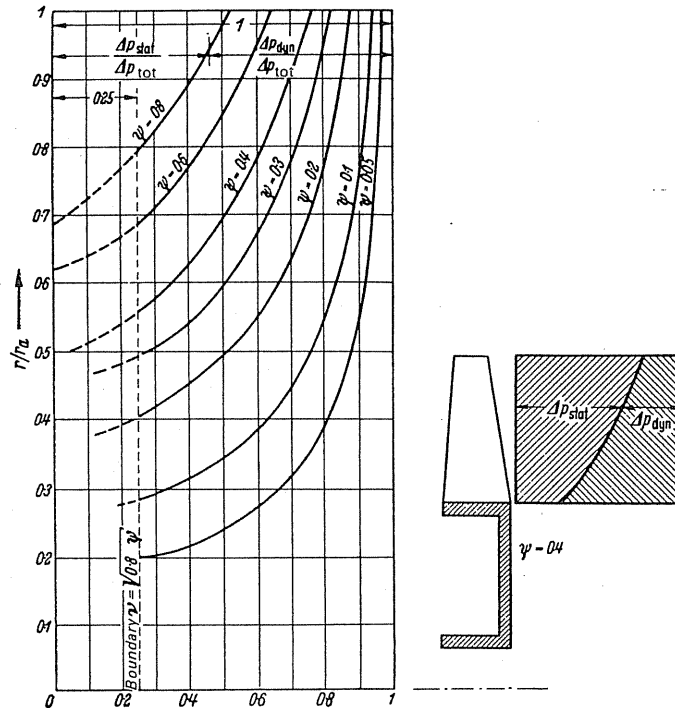


FIG. 256. Pressure distribution in axial impellers.

It will be observed from Fig. 256 that for an axial impeller, uniform pressure at the hub is only achieved if the hub ratio is lower than the one previously recommended. At $\eta = 0.914$ we obtain $\nu = 0.858 \sqrt{0.8\psi}$, i.e. uniform pressure occurs at the hub at a 15% lower ratio.

99. DIFFUSER LOSSES

After leaving the impeller as a rule the flow passage cross-section of the fan expands. Even taking the simplest case of the blower to be a part of duct (Fig. 257b), we obtain with a hub of greater or smaller diameter an expansion of the cross-section after the aerofoil. This enlargement can be unsteady in the simple cases (Fig. 257a), probably due to hub discharge or sudden enlargement of the housing. Even if obvious causes of separation such as these, which in many cases cannot be prevented in practice, are not present, diffusers which are useful to a greater or lesser degree can be obtained by means of *hub discharge*

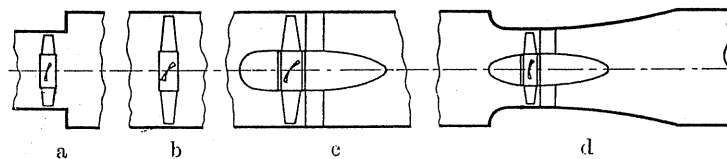


FIG. 257. (a-d) Various forms of diffusers and hubs of normal axial flow fans.

or by *steady enlargement of the external casing* or by both measures. If high efficiencies are essential the form of such diffusers is of great importance. The constructional form is difficult because this problem cannot be overcome by purely theoretical methods and often comprehensive tests are indispensable. Only the main points can be elaborated and an outline of the various possibilities given here.

(a) GENERAL RELATIONSHIPS

Let the velocity at the narrowest cross-section be c_{1m} and at the end of the diffuser c_{2m} , then with an output free of losses a pressure rise $(\rho/2)(c_{1m}^2 - c_{2m}^2) = \Delta p''$ would be achieved according to the Bernoulli equation. In actual fact, however, only $\Delta p''' = \eta \Delta p''$ would be gained, and therefore $(1 - \eta) \Delta p''$ is lost. With well-designed diffusers, $\eta \approx 0.8$ can be used for calculation. Larger dimensions and higher speeds reduce the losses.

On the other hand, the question arises: how big can the losses become in the most unfavourable case? This case obviously occurs if the cross-section alters steadily according to Fig. 257 without any transfer component. Shock losses arise which can be easily calculated according to the momentum principle. We obtain

$$\text{pressure loss} = \frac{\rho}{2} [c_{1m} - c_{2m}]^2.$$

If the ratio of the initial to the final cross-section of the diffuser is $F_1/F_2 = m'$ we obtain for the sudden enlargement alone a conversion rate⁽³⁵⁾ $\eta = 2 [m'/(1 + m')]$. If we relate the loss not to $(\rho/2)(c_{1m}^2 - c_{2m}^2)$ but to $(\rho/2)c_{1m}^2$ in order to remain in immediate proximity to the fan, we obtain

$$\left. \begin{aligned} 1 - \eta' &= \frac{(\rho/2)[c_{1m} - c_{2m}]^2}{(\rho/2)c_{1m}^2} = \left[1 - \frac{c_{2m}}{c_{1m}}\right]^2 = (1 - m')^2, \\ \eta' &= 2m' - m'^2. \end{aligned} \right\} \quad (222)$$

(b) DIFFUSER LOSSES AS PROPORTION OF TOTAL LOSS

We use this method of recording progressively and thus obtain for the total diffuser losses $\Delta p_{\text{loss}} = (1 - \eta')(\rho/2)c_{1m}^2$. If the overall pressure rise actually achieved in the fan, as already determined, is $\Delta p = \psi(\rho/2)u_a^2$, then through the definition $\Delta p_{\text{loss}}/\Delta p$ we obtain the proportion of these losses in relation to the total pressure. We obtain

$$\frac{\Delta p_{\text{loss}}}{\Delta p} = \frac{(1 - \eta')c_{1m}^2(\rho/2)}{\psi(\rho/2)u_a^2} = (1 - \eta')\frac{\varphi'^2}{\psi}. \quad (223)$$

In this way these losses are likewise converted to dimensionless co-efficients.

³⁵ Eck, B., *Technische Strömungslehre*, 7th edn., Berlin/Göttingen/Heidelberg, Springer, 1966.

(c) INFLUENCE OF HUB DISCHARGE AT EQUAL PASSAGE WIDTHS

Even in the absence of the diffuser type of enlargement, there is still an increase in cross-section because in the screw circular area the hub of the propeller reduces the effective cross-section. The ratio of the effective cross-section then is

$$\frac{f_1}{f_2} = \frac{(\pi/4) (d_a^2 - d_i^2)}{(\pi/4) d_a^2} = \left[1 - \left(\frac{d_i}{d_a} \right)^2 \right] = 1 - v^2 = \frac{c_{2m}}{c_{1m}}.$$

Here the value v has been substituted for d_i/d_a .

First the magnitude of the losses under the best conditions will be calculated. This is done in cases where there is no hub discharge available at all. According to the momentum principle the quantity

$$\frac{\rho}{2} [c_{1m} - c_{2m}]^2 = \frac{\rho}{2} c_{1m}^2 \left[1 - \frac{c_{2m}}{c_{1m}} \right]^2 = \frac{\rho}{2} c_{1m}^2 [1 - (1 - v^2)]^2 = \frac{\rho}{2} c_{1m}^2 v^4$$

is then lost again. If we relate the loss again to the total pressure

$$\Delta p = \psi (\rho/2) u_a^2,$$

we obtain

$$\frac{\Delta p_{\text{loss}}}{\Delta p} = \frac{(\rho/2) c_{1m}^2 v^4}{\psi (\rho/2) u_a^2} = \frac{\varphi'^2}{\psi} v^4. \quad (224)$$

The smallest possible hub diameter for the actual design is closely associated with the pressure coefficient ψ . This can be assessed approximately through the relationship $\psi = v^2/0.8$.

If we substitute this ψ we obtain

$$\text{loss} = 0.8 \varphi'^2 v^2. \quad (225)$$

For different φ' values (0.2–0.5) the losses are listed in Table 15. The smallest v values which can be used in practice will be $v = 0.2$. The table only contains values where the losses are above 1%.

TABLE 15. VALUES OF LOSSES FOR HUBS

v	$\varphi' = 0.2$	$\varphi' = 0.3$	$\varphi' = 0.4$	$\varphi' = 0.5$
0.3			0.0115	0.018
0.4			0.0205	0.032
0.5		0.018	0.032	0.05
0.6	0.0115	0.026	0.046	0.072
0.7	0.0157	0.035	0.0627	0.098
0.8	0.0205	0.046	0.082	0.128

The hub ratio according to the φ' values lie between 0.3 and 0.5 for cases where the losses are lower than 1% when the hub discharge is ignored. Eddy losses through vortex core formation are of greater importance than these relatively small losses in cases where there is no hub discharge.

100. THE SHAPE OF DIFFUSERS

In normal diffusers there are basically three geometrical possibilities for the shape.

As already stated in the discussion of the diffusers for radial-flow fans, it is impossible to state exact rules for diffusion angles. The angles may vary between 5° and 20° according to Re -values and stream turbulence, even if in most cases the narrower range $7-9^\circ$, is envisaged. Since the basic tests are mostly carried out on the round tapering diffusers, an interesting problem is how a transfer to the present cases can be effected where the internal space becomes an annular cross-section due to the hub discharge. A comparison is possible by plotting the diameter of circular areas of equivalent content above the streamlines and taking care that the diffusion angle thus obtained does not exceed the permissible values of taper nozzles. This rule is not a scientifically strict one, but it gives the engineer some guidance. According to the latest studies it appears, moreover, that the assumption of a *straight* cone, taken as a matter of course, is no longer supported.

Possibly better diffusers are obtained if the diffuser is steadily curved outwards.

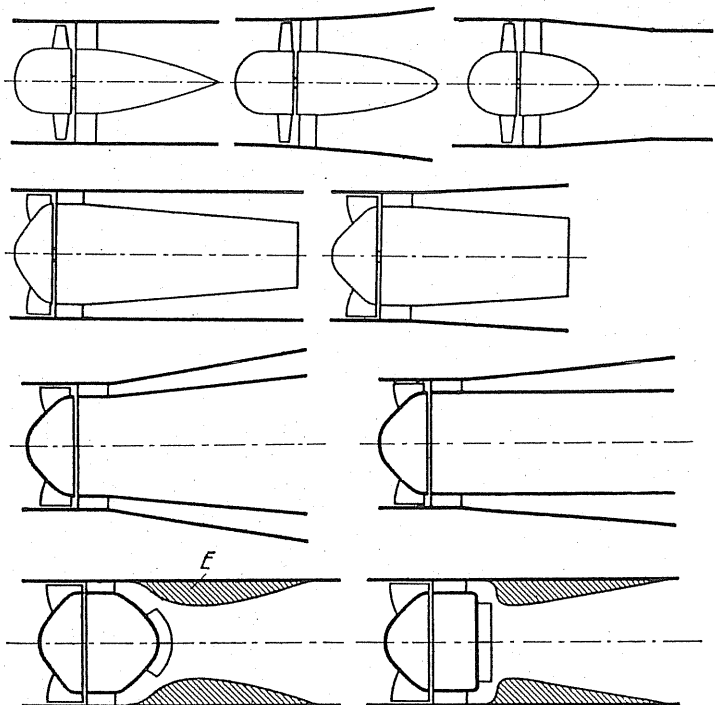


FIG.258a. Diffusers for normal axial-flow fans: External casings cylindrical: hub discharge. External casings enlarged outwards, hub discharge. External casings constricted, short hub discharge. Diffusers for meridionally accelerated axial-flow fans: External casing cylindrical, hub discharge as a blunted cone. External casing enlarged outwards, hub discharge as a blunted cone. External casing enlarged outwards, hub discharge as a blunted cone enlarged outwards. External casing enlarged outwards, hub discharge as a cylinder. External casing cylindrical with internal bulge E constricted hub discharge with cross plate. External casing cylindrical with internal bulge, no hub discharge. Residual rotation destroyed by cross-plate or guide vanes.

Greater difficulties are met with diffusers of meridionally accelerated axial-flow impellers. The percentage pressure conversion in the diffuser is so high in this case that these designs vary in a well-working diffuser. Externally the problem arises of enlarging a very narrow, annular cross-section on a full, round cross-section. The danger of vortex core formation is particularly great in this case, and here the hub discharge is dispensed with entirely. Therefore the following *four* possibilities emerge (Fig. 258a, second and third rows).

All four solutions have the same feature. After achieving a specified cross-section the hub is suddenly broken off. This implies that at this point Carnot losses will have to be envisaged which by means of correct sizing must be reduced to very low percentage.

Unfortunately diffusers of this type have an inconvenient length which often is difficult to accommodate. Another disadvantage is that such diffusers with narrow annular ring cross-sections tend to instability, since separation comes about at any one section.

To obviate both disadvantages a new solution is proposed. By inserting an annular bulge in accordance with Fig. 258a at the bottom, the annular cross-section is changed into the concentric annular cross-section where the hub is shortened. From then onwards a standard taper diffuser connects up, the flow of which is easier to overcome, in case of emergency by inserting cross-plates. Any prevailing residuary swirl is then best removed by means of guide blades.

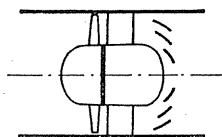


FIG. 258b. Hub diffuser with subdivided guide blades.

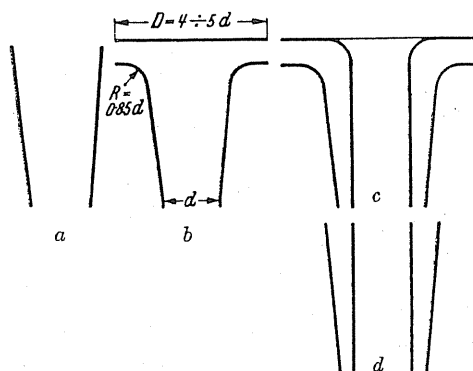


FIG. 259. (a-d) Different shapes of exhaust diffusers.

Still shorter designs can be obtained if, according to Fig. 258a the hub discharge is dispensed with altogether and a wall limiting the hub is fitted directly behind the guide wheel, and which is well rounded externally.

In larger designs the annular bulge can be formed readily in concrete.

According to Fluegel, in certain circumstances shorter diffusers are obtained by means of subdivided guide blades if it is possible to eliminate separation at the outside casing (Fig. 258b).

Freely discharging diffusers. In the same way as in radial-flow fans the problem often arises in axial-flow fans of having to discharge from a diffuser to atmosphere. In the first place all the solutions previously given for radial-flow fans are applicable. Besides these, there are special solutions which are conditional upon the nature of the axial type. There are numerous possibilities and a few typical ones are shown in Fig.259. According to Fig.259 the core must be continued up to the plate in ring diffusers with thrust plates.

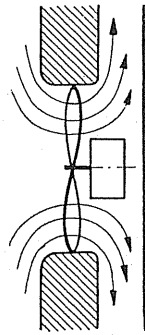


FIG.260. Stream deflection of a wall cooling fan by an impact plate. Simple diffuser.

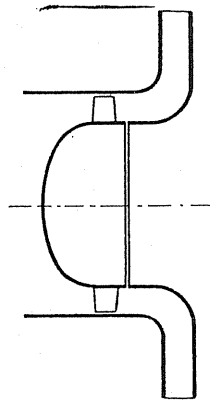


FIG.261. Radial guide ring to replace guide blades of an axial-flow fan.

Without a plate the last solution, according to Fig.259c, applies. A plate as shown in Fig.260 fitted directly behind a wall fan will immediately show high gains. A design according to Fig.261 certainly offers the possibility of utilising the rotation also when a guide wheel is partly dispensed with, because it is known that the c_u components decrease as the radii increase.

101. WHEN DOES IT PAY TO USE A GUIDE ARRANGEMENT?

Where there is no guide wheel the air must be supplied to the impeller in axial direction so that the same conditions are present for the guide wheel as with the guide wheel following on. We shall calculate the losses which arise when there is no guide wheel. Let a peri-

pheral component c_u be present on radius r . We will assume first of all that the velocity head of c_u is lost by shock. Thus the mean value of the pressure $(\rho/2) c_u^2$ must be formed.

$$\Delta p' = \frac{1}{F} \int_{r_i}^{r_a} \frac{\rho}{2} c_u^2 2r \pi dr.$$

If Δp is the actual stage pressure attained and η the efficiency, then we have

$$\rho c_u u = \frac{\Delta p}{\eta}$$

from which we obtain

$$c_u = \frac{\Delta p}{\rho u \eta} = \frac{1}{r} \frac{\Delta p}{\rho \omega \eta}.$$

By substituting this in $\Delta p'$ we get

$$\Delta p' = \frac{\pi \rho \Delta p^2}{F \rho^2 \omega^2 \eta^2} \int_{r_i}^{r_a} \frac{dr}{r} = \frac{\pi \Delta p^2}{F \rho \omega^2 \eta^2} \ln \frac{r_a}{r_i}.$$

We relate the loss again to the stage pressure Δp and also consider the ratio

$$\frac{\Delta p'}{\Delta p} = \frac{\pi \Delta p}{F \rho \omega^2 \eta^2} \ln \frac{r_a}{r_i}.$$

Here we substitute again:

$$\Delta p = \psi (\rho/2) u_a^2; \quad \frac{r_i}{r_a} = \nu \quad \text{and} \quad F = \pi [r_a^2 - r_i^2] = \pi r_a^2 [1 - \nu^2].$$

$$\frac{\Delta p'}{\Delta p} = \frac{\pi \psi \rho u_a^2}{2 \rho \omega^2 \pi r_a^2 [1 - \nu^2] \eta^2} \ln \frac{1}{\nu} = \frac{\psi}{[1 - \nu^2] 2 \eta^2} \ln \frac{1}{\nu}. \quad (226)$$

For different ψ and ν values associated with the practical range the percentage losses have been calculated according to this formula and listed in Table 16. It will be seen that a guide unit can only be dispensed with at lower ψ values. At $\psi > 0.1$ a guide wheel would always be a practical proposition.

TABLE 16

ψ	$\frac{\Delta p'}{\Delta p (\nu = 0.3)}$	$\frac{\Delta p'}{\Delta p (\nu = 0.5)}$	$\frac{\Delta p'}{\Delta p (\nu = 0.7)}$
0.05	0.052	0.036	0.027
0.1	0.1033	0.0724	0.0547
0.3	0.31	0.217	0.164
0.6	0.62	0.434	0.328

Another aspect is the problem of when the guide-wheel resistance is equal to zero. This condition can be readily obtained from eqn. (193).

$$\frac{1}{2} \frac{\Delta c_u}{u} \varepsilon_L \varphi' = 0; \quad \varphi' = \frac{1}{2} \frac{\Delta c_u}{u} \frac{1}{\varepsilon_L}.$$

The results of both considerations are equal. The limits of the usefulness of guide wheels are shown in the diagrams of Figs. 240 and 241.

New investigations by Laux show that this problem cannot be correctly answered without taking into account the marked recovery of rotational energy. According to his views the fan without guide wheels has the advantage throughout the whole range $1.1 < \delta < 1.5$. This means that the fan and no guide wheel might be used in cases hitherto reserved for guide wheel fans. Independent of the coefficient φ and ψ , Laux found the following boundary conditions for the critical hub ratio, which if it comes to a lower figure causes the guide wheel losses to be higher than the swirl losses, quite independent of the method of installation.

$$\frac{\varepsilon_1 (1 - \nu) (4 + \nu)}{2\nu (1 - \eta_{re})} = \ln \nu^{-1} \quad (\eta_{re} \text{ rotational regain factor}).$$

102. LAYOUT OF MULTISTAGE AXIAL-FLOW FANS

It would appear first of all that the layout of multistage axial-flow fans and axial-flow compressors can be designed in such a way that the principles of layout advocated here for single-stage fans are arranged systematically in sequence. Accordingly, for each stage *constant rotation*, *constant meridional velocity distribution* over the radius and *constant energy* distribution over the radius, would be assumed. Actually, initially we proceed in this way and look upon the multistage compressor as the "algebraic sum" of individual axial-flow fans.

Very soon, however, it was noticed that the symmetrical development of impeller and guide blades having a reaction effect of 0.5 in accordance with Fig. 223 offered advantages. The maximum velocities c_{\max} and w_{\max} arising in the machine are equal and have the absolute minimum value. It is clear that this is an advantage in view of the closely associated sound velocity limits in compressors. (In present-day terms the minimum Mach number $M = c/a$ is achieved with this blading.) Subsequently it was found that not only is the reaction effect 0.5 advantageous, but that above this it is practical *to maintain this reaction effect constant over the whole length of the blade*. It should be remembered that in standard blade design the reaction effect decreases from the outside to the inside (Fig. 256). It is, however, only possible to maintain a constant reaction effect under the condition of the same energy content for all radii if the c_u distribution differs from the assumed constancy. Thus we find that c_u is *greater at the hub* than at the *outside*. Traupel⁽³⁶⁾ and Eckert⁽³⁷⁾ were able to show proof that in this case *vibrational movements* of the meridional streamlines occur through the whole compressor.

The trend in Anglo-Saxon countries is in the direction of an inlet flow to the rotors which is identical with the rotary movement of a solid body where the peripheral components increase proportionately to the radius (forced vortex). This rotational movement must be enforced by means of a rotating preliminary guide wheel whilst in the last stage the

³⁶ Traupel, W., New general theory of multistage axial-flow turbomachines, Diss., Zürich, 1942.

³⁷ Eckert, B., and Schnell, H., *Axial- und Radialkompressoren*, 2nd edn., Berlin/Göttingen/Heidelberg, Springer, 1961.

unevenness of the energy content arising from the inlet stage must be eliminated again. With an inlet flow such as this, the condition that all streamlines have the same energy can no longer be maintained. At present it is not clear how it is possible to have stable behaviour in the compressor when these fundamental conditions do not obtain. It may be that even for this blading the flow in some way adjusts itself to the conditions on its own, so that all streamlines obtain the same energy increase. It is significant that compressors which had been fitted with this type of blading should have better efficiencies than former designs.

To explain the above differences between former interpretations it should be stated that the effects of boundary layers already produce variable velocity distribution. The case of constant energy transfer probably takes effect asymptotically quite automatically in multi-stage machines. It is presumed by some authorities that a vortex form between potential vortex and cross-flow is probably the most stable and the best. Departing from the second stage of the multistage arrangement, the through-flow probably has an extremely complicated periodically unstable character. Perhaps in this case it is a matter of a "rough" turbulence, the average movement of which was only noticed hitherto. The fact is that rather unclarified physical flow phenomena, which have not yet been taken into account in our cascade calculations, overshadow the whole problem. This is the reason for *dealing with the single-stage axial-flow fan separately*.

In axial-flow compressors the first rotor must be treated separately and does not follow the design rules mentioned above. Moreover, it must be designed according to the basic principles which have already been given for single-stage axial-flow fans. It is outside the scope of this book to elaborate the special designing methods for axial-flow fans.

103. PRACTICAL DESIGN CALCULATION. REVIEW OF THE CALCULATION PROCEDURE

In most cases primarily the delivery volume V and the stage pressure Δp are known. The speed is mainly adapted to the choice of the driving machine and, therefore, especially for electrical drives, the speeds 3000, 1500, and 750 are the most popular. Therefore for the present purpose the quantities V , Δp , and n can be assumed as known.

With the aid of eqn. (67),

$$\sigma = \frac{1}{28.5} V^{1/2} \left(\frac{\Delta p}{\rho} \right)^{-3/4} \quad n = 0.379 n_{\text{sec}} \frac{V^{1/2}}{H^{3/4}},$$

it is possible to calculate σ immediately.

Thereupon the appropriate best values of the diameter characteristic δ as well as the minimum value of the possible hub diameter ratio ν are taken from Figs. 239–242. Then coefficients φ and ψ can be calculated.

$$\varphi = \frac{1}{\sigma \delta^3}; \quad \psi = \frac{1}{\sigma^2 \delta^2}.$$

The peripheral speed is taken from

$$u = \pi d n / 60.$$

The external fan diameter is obtained from

$$d_2 = \frac{60}{\pi n} \sqrt{\frac{2\Delta p}{\psi \rho}}.$$

The meridional speed is obtained from

$$c_m = \frac{V}{(\pi/4)(d_2^2 - d_1^2)}.$$

The coefficient φ' is obtained from $\varphi' = c_m/u_2$.

Finally, the equation

$$c_a l = \frac{\Delta p \ 4\pi}{\eta \ w_\infty \ \rho \omega z} = \frac{\Delta p \ t \ 2}{\eta u \rho \ \omega_\infty}$$

could be solved.

A decision as to the choice of the number of blades can be made when the value t/l is known approximately. It should be remembered that $0.5 < t/l < 1.5$ is a practical formula. Now $(\Delta p \ 4\pi)/(\eta \rho \omega z) = C$ can be calculated, which gives $c_a l = (C/w_\infty)$.

Continuing, it is possible to calculate c_u . Now the equation $c_u = (\Delta p)/(\rho u \eta)$ is used for this purpose.

The velocity triangles can now be drawn. This gives us the angles.

Further calculation is best carried out by tables after the velocity diagrams have been drawn beforehand. For the c_a curve the increase of c_a should be as large as possible towards the hub.

104. EXAMPLES OF CALCULATION

Example

Calculation of an axial-flow fan without guide wheel for the following condition:

$\Delta p = 30$ mm WG;

$V = 45,000$ m³/h = 12.5 m³/sec;

$n = 1500$ rev/min;

$\gamma = 1.225$ kg/m³.

According to eqn. (67) we obtain

$$\sigma = 0.379 \ n_{\text{sec}} \sqrt[4]{\frac{V^2}{H^3}} = 3.05.$$

From Fig. 240 for $\sigma = 3.05$ we obtain $\delta = 1.2$.

By applying eqn. (66a) we obtain

$\psi = 0.0748$ and $\varphi = 0.1895$.

The diameter works out at

$$d_2 = \frac{60}{\pi n} \sqrt{\frac{16 \Delta p}{\psi}} = 1.02 \text{ m}.$$

We select $d_2 = 1$ m and will assume the hub diameter $d_1 = 300$ mm, considering the size of electric motor.

By rounding off in this way we obtain the ultimate values

$$u_2 = 78.5 \text{ m/sec}; \quad c_m = \frac{V}{\frac{\pi}{4} [d_2^2 - d_1^2]} = 17.55 \text{ m/sec}.$$

The final φ' is obtained from

$$\varphi' = \frac{c_m}{u_2} = \frac{17.55}{78.5} = 0.2237.$$

For the overall efficiency taking into account the design without guide wheels let us take $\eta = 0.75$.

$$N = \frac{V \Delta p}{75\eta} = \frac{12.5 \times 30}{75 \times 0.75} = 6.67 \text{ hp}$$

For equation (180) we now calculate for all radii constant the value

$$\frac{\Delta p \cdot 4\pi}{\eta \rho \omega z} = \frac{30 \times 4\pi}{0.75 \times \frac{1}{8} \times 157 \times 4} = 6.4,$$

thus we obtain $c_a l = 6.4/w_\infty$.

For the number of blades we select $z = 4$.

For determining the velocity diagrams we require the c_u -value; this is calculated from the eqn. (181).

$$c_u = \frac{\Delta p}{\rho u \eta} = \frac{30 \times 8}{u \cdot 0.75} = \frac{320}{u},$$

Further calculation is by means of the simplest tabular method with simultaneous application of the velocity diagrams plotted previously. For the course of c_a an increase towards the hub is advisable.

Table 17 shows the calculations for six different radii. The aerofoil cross-section as well as the diagrams are given in Fig. 262 underneath each other. The Göttingen profile (564) was selected.

TABLE 17

r (mm)	u (m/sec)	c_u (m/sec)	W_∞ (m/sec)	$c_a l$ (cm)	c_a	l (cm)	β_∞	α_∞	$\beta = \beta_\infty + \alpha_\infty$	Profile 564
500	78.5	4.075	82	7.8	0.60	13.0	12° 13'	2.1	14.6	564
430	67	4.78	71.5	8.95	0.68	13.15	14°	3.1	17.1	564
360	56	5.71	61.5	10.4	0.75	13.85	16° 40'	3.8	20.47	564
290	45.5	7.02	52	12.3	0.82	15.00	20° 20'	4.6	24.93	564
220	34.4	9.3	43	14.86	0.90	16.5	24° 15'	5.5	29.75	564
150	23.5	13.6	35	18.27	0.90	20.3	30° 33'	5.5	36.05	564

It may eventually be necessary to change to thick profiles at the hub. The centrifugal loading present there as well as the possibility of achieving higher c_a -values at thicker profiles may be decisive factors. At peripheral speeds below 100 m/sec, however, the loads do not give rise to any complications, as yet.

Example 2

The procedure is according to that laid down by Weinig.

$$\Delta p = 100 \text{ mm WG}; \quad V = 10,800 \text{ m}^3/\text{h} = 3 \text{ m}^3/\text{sec}.$$

$$n = 3000 \text{ rev/min}; \quad \gamma = 1.225; \quad H = 81.5 \text{ m}.$$

The factor σ is again used in the calculation.

$$\sigma = 0.379 n_{\text{sec}} \sqrt[4]{V^2/H^3} = 1.21.$$

From Fig. 240 we read the values of δ and ν for the arrangement with guide wheel and diffuser:

$$\delta = 1.65; \quad \nu = 0.55.$$

Then we obtain

$$\psi = \frac{1}{\sigma^2 \delta^2} = \frac{1}{(1.21 \times 1.65)^2} = 0.252; \quad \varphi = \frac{1}{\sigma \delta^3} = \frac{1}{1.21 \times 1.65^3} = 0.1845.$$

This allows the diameter to be determined.

$$d_2 = \frac{60}{\pi n} \sqrt{\frac{2 \Delta p}{\psi \rho}} = \frac{60}{\pi 3000} \sqrt{\frac{16 \times 100}{0.252}} = 0.506.$$

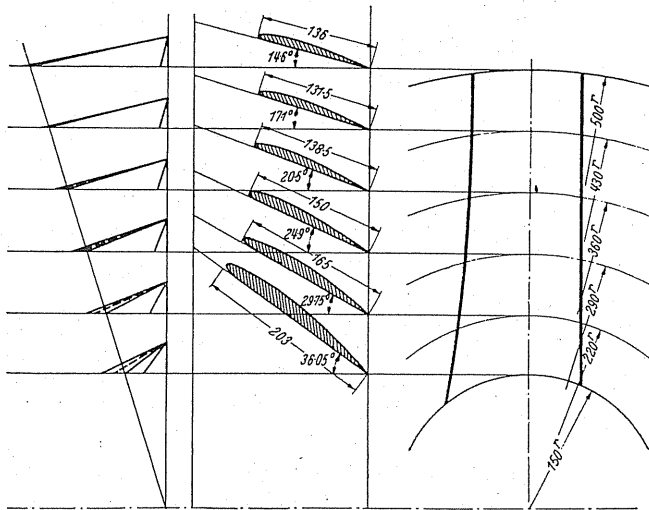


FIG.262. Design of an axial-flow fan with profiled blades.

We take formula

$$d_2 = 500 \text{ mm}; \quad d_1 = 500 \times 0.55 = 275 \text{ mm}; \quad \eta = 0.83;$$

$$c_m = \frac{V}{(\pi/4)(d_2^2 - d_1^2)} = \frac{3}{0.137} = 21.85 \text{ m/sec};$$

$$u_2 = \frac{d_2 \pi n}{60} = 78.5 \text{ m/sec}; \quad \varphi' = \frac{c_m}{u_2} = \frac{21.85}{78.5} = 0.279;$$

$$c_u = \frac{\Delta p}{\rho u \eta} = \frac{100 \times 8}{0.83 u} = \frac{964}{u}.$$

For t/l , the best values of which range between 0.5 and 1.5, it is advisable to choose values between 1.25 and 0.75, the first value being at the tip of the blade. Thus we have the number of blades $z = 12$.

Further calculation is done in tabular form. After calculating u and c_u , the velocity triangle can be plotted. From this we obtain β_1 and β_2 . In this way we know the value of the angle $\vartheta_\infty/2 = (\beta_2 - \beta_1)/2$ and $(\beta_1 + \beta_2)/2$. From Fig.249 we then take the value μ . From this we obtain for the increase of outlet angle

$$\nu = \frac{\vartheta_\infty}{2} \frac{1 - \mu}{\mu}$$

To determine the further increase of the outlet angle due to profiling the greatest profile thickness d/l is selected at 0.06 externally and at 0.065 internally. Accordingly, $\Delta\beta_1$ can be read from Fig.250. The ultimate angle opening comes to $\Delta\beta = \Delta\beta_1(l/t)^2$.

From this we obtain small angle corrections which are marked in the table. Fig.263 shows the profiles to scale.

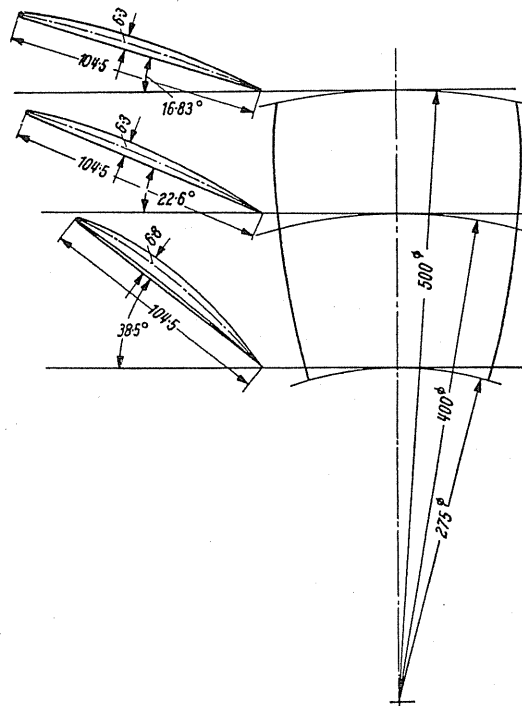


FIG. 263. Design of an axial-flow fan with profiled blades.

TABLE 18

d (mm)	u (m/sec)	c_u (m/sec)	s/l	β_1^0	β_2^0	$\frac{\vartheta_\infty}{2} = \frac{\beta_2 - \beta_1}{2}$	$\beta_m = \frac{\beta_1 + \beta_2}{2}$	t/l	u
500	78.5	12.25	0.06	15	18	1.5	16.5	1.25	0.235
400	62.8	15.36	0.06	19	24.8	2.9	21.9	1.0	0.375
275	43.1	22.3	0.065	27	46	9.5	36.5	0.742	0.600

$\frac{1-\mu}{\mu}$	$\nu = \frac{\vartheta_\infty}{2} \frac{1-\mu}{\mu}$	$\beta'_1 = \beta_1 - \nu$	$\beta'_2 = \beta_2 + \nu$	$\Delta\beta$	$\beta_m + \Delta\beta$	l	$\beta''_1 = \beta'_1 + \Delta\beta$	$\beta''_2 = \beta'_2 + \Delta\beta$
3.25	4.87	10.13	22.87	0.33	16.83	104.5	10.46	23.2
1.67	4.85	15.15	29.65	0.70	22.6	104.5	15.85	30.35
0.667	6.32	20.68	52.32	2	38.5	97	22.68	54.32

105. BEHAVIOUR OF AN AXIAL-FLOW FAN AWAY FROM THE BEST OPERATING POINT

Calculation and design of axial-flow fans should be carried out for the level of highest efficiency. In practice it is rare that fans can be rated to give the best level in operation. Often considerable under and over deliveries have to be set. The question then arises how

does the axial-flow fan behave on other levels of the characteristic. The disturbances which may be expected are often very considerable in axial flow fans. For small delivery volumes most axial-flow fans show an unstable characteristic, which means that the characteristic drops and rises ultimately at delivery quantities reducing to zero. Figure 264 is a diagrammatic overall outline. At $V_{\eta_{\max}}$, according to Fig. 264d, a uniform throughflow is present.

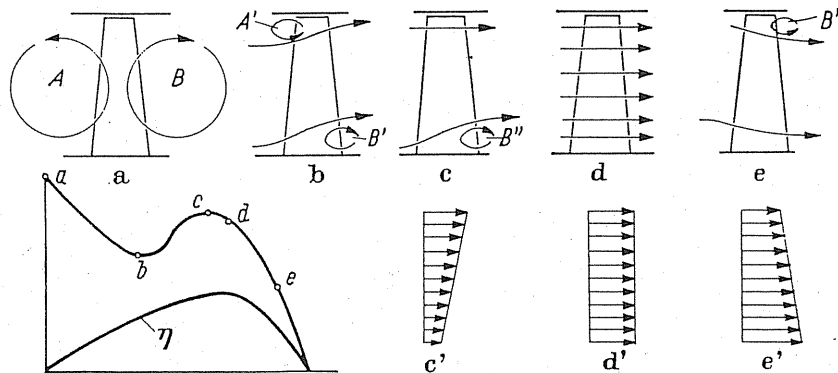


FIG. 264. (a-e) Diagrams of different flow conditions of an axial-flow fan at different throttling positions.

At overload (e) the throughflow moves a little to the inside. Ultimately a small back flow B''' forms. In this zone only very slight deviations are available throughout and even a favourable noise behaviour is observed. Very great disturbances start up at $V < V_{\eta_{\max}}$ which are typical of axial-flow fans. Close to the state c the characteristic has an apex. At this operating point a vortex B'' is observed in the wake of the hub, and this is caused by a separation on the back of the blade. The particles separated here are collected on the front side of the succeeding blade, so that a vortex structure helical in shape is obtained. At the deepest point of the characteristic the vortex B' has become still greater at b whilst simultaneously at the entry a new vortex A' appears. The flow passes the rotor no longer axially but at a slope. At delivery zero (a) the two vortices A and B have increased so much that the suction and pressure spaces are filled up. In general the noise increases with the growth of A and B . If, in spite of lack of main flow often the highest pressure occurs at a, this can be readily observed from the diagram of main flow. The flow passes the rotor more or less radially and therefore the pressure rises as in the radial blades. Typical variations of the meridional loadings are shown in Fig. 264c', d', e'. This means that away from the point d the c_m distribution is no longer uniform and, moreover, radial components arise.

Measures for stabilising the characteristics of axial-flow fans. The unstable zone of the characteristic of axial-flow fans situated to the left of c gives rise to complications in many applications. Over and above this, the considerable power consumption under low load conditions is a disadvantage and because of this oversizing of the driving machine may be necessary. It is also a very disturbing fact that the highest efficiency is so close to the point of the separation. Because of this an accurate rating is almost impossible.

The following measures can be used for modifications and sometimes for remedying the characteristics:

- (1) Almost in every case axial-flow fans without guide wheels have stable characteristics but unfortunately at mostly worse efficiencies.
- (2) The smaller the inlet angle of the blades the less the instability. This behaviour is clearly apparent by changing the rotor blades. The characteristic field at this adjustment shows clearly that with a smaller inlet angle the characteristics become steadily steeper and more stable.
- (3) Large numbers of blades and large hub ratios reduce the output peak with partial throttling particularly at zero delivery.
- (4) A radial guide area in front of the impeller has a great stabilising effect, because by this means the vortex A is sheared.⁽³⁸⁾
- (5) A concentric ring before the impeller in the vicinity of the external casing has a stabilising effect.⁽³⁹⁾ Unfortunately this is offset by a reduction of velocity in the external c_m distribution.

106. CHARACTERISTIC AND PART CHARACTERISTIC OF AXIAL-FLOW FANS

A preliminary theoretical calculation of the characteristics of good axial-flow fans which do not show the same problems as in radial-flow fans is closely connected with the nature of flow without separation, even if accurate determination is rather inconvenient. It will suffice to calculate the trends of the characteristics at the point of the highest efficiency.

Let us start from the basic eqn. (176) $c_a = (2\Delta c_u t)/lw$ and insert in the denominator the value $w_\infty = (u - \Delta c_u/2)/\cos \beta_\infty$. Furthermore, we express the aerodynamic incidence angle α in accordance with the equation $c_a = A\alpha$, and we obtain

$$c_a = A\alpha = \frac{2\Delta c_u t \cos \beta_\infty}{l(u - \Delta c_u/2)}.$$

(α is then calculated from the zero direction of the lift.)

We obtain from Fig. 221

$$\tan \beta_\infty = \frac{c_m}{u - \Delta c_u/2}.$$

By means of the known relationship of angles $\alpha = \gamma - \beta_\infty$ we obtain

$$\sin \alpha = \sin (\gamma - \beta_\infty) = \cos \beta_\infty [\sin \gamma - \cos \gamma \tan \beta_\infty].$$

³⁸ Scheer, W., Investigations and observations on the working method of axial-flow pumps with particular reference to the part-load range, *Brennstoff-Wärme-Kraft*, 1959, p. 503.

³⁹ Marcinowski, H., Experimental investigations in the aircraft division, *Voith-Forschung u. Konstruktion*, 1958, No. 4.

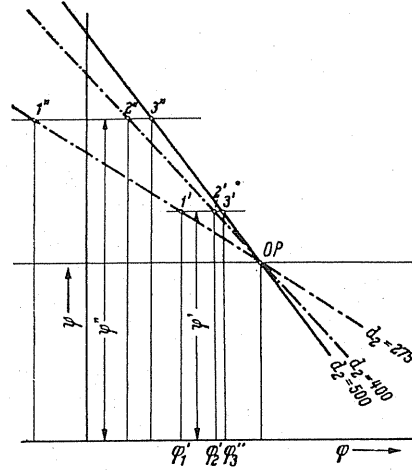


FIG. 265. Calculation of three-part characteristics.

By substituting the value for

$$\tan \beta_{\infty} = \frac{c_m}{u - \Delta c_u/2}$$

$$\sin \alpha = \cos \beta_{\infty} \left[\sin \gamma - \cos \gamma \frac{c_m}{u - \Delta c_u/2} \right]$$

and comparing with

$$\sin \alpha = \frac{c_a}{A} = \frac{1}{A} \frac{2 \Delta c_u t \cos \beta_{\infty}}{l(u - \Delta c_u/2)},$$

we obtain

$$\cos \beta_{\infty} \left[\sin \gamma - \cos \gamma \frac{c_m}{u - \Delta c_u/2} \right] = \frac{1}{A} \frac{2 \Delta c_u t \cos \beta_{\infty}}{l(u - \Delta c_u/2)}.$$

This gives us the value of Δc_u

$$\Delta c_u = \frac{2(u \sin \gamma - c_m \cos \gamma)}{(4t/Al) + \sin \gamma}.$$

By substituting it in eqn. (181) we obtain

$$\Delta p_{\text{tot}} = \rho u \Delta c_u \eta = 2 \rho u_a \frac{r}{r_a} \eta \frac{u \sin \gamma - c_m \cos \gamma}{(4t/Al) + \sin \gamma}.$$

In order to obtain the slope of the part characteristic, we differentiate the above expression:

$$\frac{d[\Delta p_{\text{tot}}]}{dc_m} = -2 \rho u_a \eta \frac{\cos \gamma}{(4t/Al) + \sin \gamma} \frac{r}{r_a}.$$

By applying equation

$$\varphi' = c_m/u_a \quad \text{and} \quad \Delta p = \psi(\varphi/2) u_a^2,$$

for practical purposes we introduce again the dimensionless coefficients φ' and ψ , formerly introduced.

$$\frac{d\psi}{d\varphi'} = -4\eta \frac{\cos \gamma}{(4t/Al) + \sin \gamma} \frac{r}{r_a}. \quad (227)$$

The three part characteristics were calculated for one example and represented in Fig. 265.

In order to obtain the resultant characteristics from the part characteristics we have to simplify very much in order at least to obtain the first approximation. Primarily it is advisable to apply the condition $\Delta p = \text{const}$. The advantage of this is that a line $\Delta p = \text{const}$ would represent the operating points of the part characteristics in the diagram of the part characteristics.

If, for example, we consider the points of intersection 1', 2', 3' for the pressure factor ψ' it will be appreciated that the lower φ' is at smaller radii and vice versa. The loading, therefore, would not be uniform any more, but such that the greater velocities could be encountered in the outside radii. In considering φ' values which are greater than the normal value at OP a greater c_m is obtained towards the hub. This produces the representation in Fig. 264 for the main flow at different operating points.

The assumption formerly made that at delivery volumes deviating from OP the same overall pressure is available for all part characteristics is invalid. The losses alter from radius to radius, the axial direction of the meridional flow is no longer maintained, and the partly curved flow occurs in which additional centrifugal forces are in action and so on. This is the reason why the above assumption $\Delta p = \text{const}$ is only a very rough approximation which only enables certain basic phenomena to be recognised, as, for instance, the varied c_m distribution. Other ways will have to be found for obtaining an overall characteristic agreeing to some extent with reality. The simplest assumption which can be made is that such part characteristics should be considered as overall characteristics which are located in the centre of the annular area, i.e. at $d_m = (d_i + d_a)/2$, or better still in the point of gravity of an area which is created due to r^2 being expressed in the annular space of the blade. An accurate method was developed by Ruden⁽⁴⁰⁾ but it is so complicated that it is used very little for practical calculations.

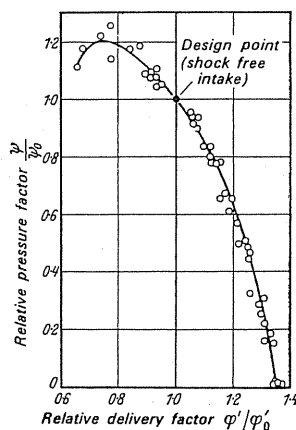


FIG. 266.

⁴⁰ Ruden, Tests on axial-flow fans, *Luftfahrtforschung*, Vol. 14.

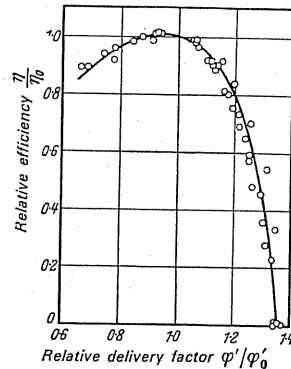


FIG. 267.

Eckert, however, has made an interesting discovery. By expressing for axial impellers the relative characteristics, i.e. $\psi/\psi_0 = f(\varphi'/\varphi_0)$ and $\eta/\eta_0 = f(\varphi'/\varphi_0)$, it is rather astonishing to find that these characteristics coincide very accurately for a range $0.552 < \nu < 0.8$ (without upstream guide blades). These curves are shown in Figs. 266 and 267. They were obtained on the basis of a very large number of axial impellers which were all rated for optimum values. Thus there is a certain *uniformity* of characteristic available which in many cases dispenses with the necessity of a theoretical calculation.

107. PRELIMINARY CALCULATION OF THE OPERATING CHARACTERISTICS IN BLADE SETTING

The control of an axial-flow fan by adjusting the blades is so important that the question arises whether the alteration occurring in the operational behaviour cannot be stated in advance. This is so if the blade setting hereafter expressed as $\Delta\beta$ is not too great. With the setting restricted to $\Delta\beta \leq 10^\circ$, it will be observed that the alterations follow simple functions. For easy grasp of these characteristics we will compare for each blade position the values at *optimum efficiency* and develop the ratio to the corresponding values at blade position 0° .

Efficiency curve. The optimum efficiency falls approximately as a parabola with positive and negative blade setting. The following function can be assumed up to approximately $\pm 10^\circ$ blade setting:

$$\frac{\eta_{\max \Delta\beta}}{\eta_{\max \Delta\beta=0}} = 1 - \frac{0.04}{100} \Delta\beta^2. \quad (228)$$

Delivery factor. At negative setting, i.e. in the direction of a lower suction capacity, the best delivery factor drops whereas it rises at positive angles again; a formula can be stated

up to approximately $\pm 10^\circ$ blade setting.

$$\frac{\varphi'_{\text{opt}}}{\varphi'_{\text{opt}}}_{\Delta\beta=0} = 1 + 0.022\Delta\beta^\circ - \frac{0.04}{100}\Delta\beta^{\circ 2}. \quad (229)$$

Pressure factor. The curve in principle is similar to the delivery factor. For $\Delta\beta \leq \pm 10^\circ$ we apply

$$\frac{\psi_{\text{opt}}}{\psi_{\text{opt}}}_{\Delta\beta=0} = 1 + 0.14\Delta\beta^\circ - \frac{0.06}{100}\Delta\beta^{\circ 2}. \quad (230)$$

The formulae have been derived in comparing many designs.

108. TEST RESULTS OF AXIAL-FLOW FANS

A survey of characteristics of axial-flow fans is shown in Figs. 268–274 which have been taken from the well-known studies by Keller. The outstanding significance of the rotor blade setting is very impressive.

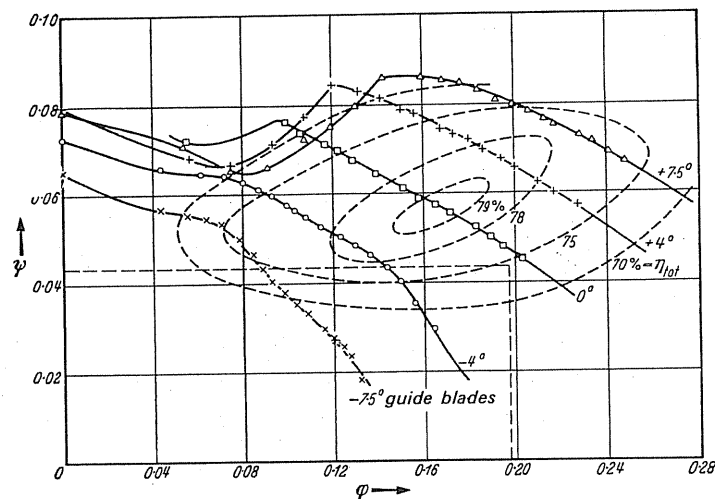
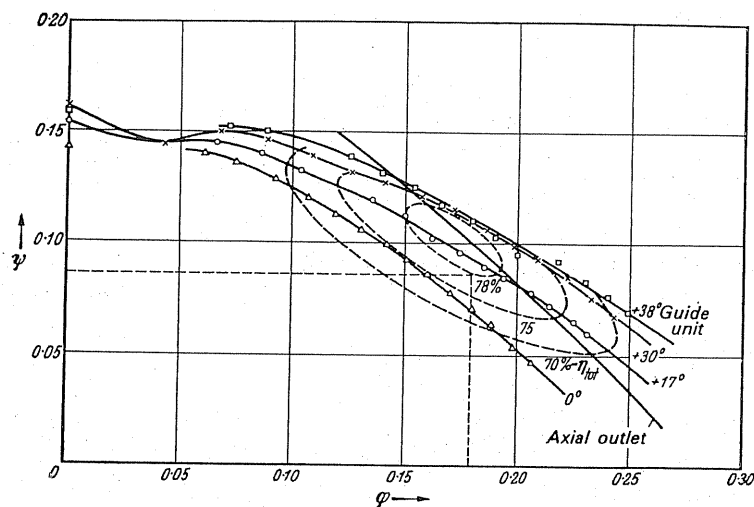
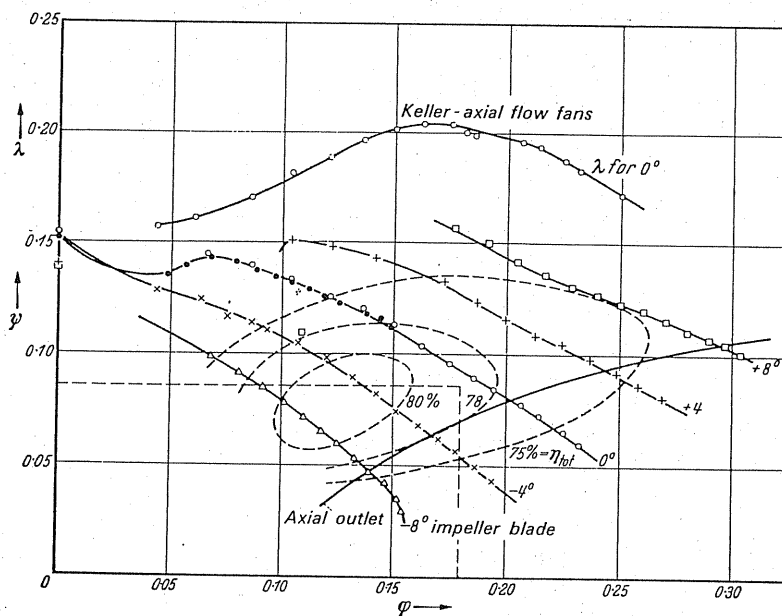


FIG. 268. Rotor 1 fixed guide unit $+17^\circ$, rotor blades -7.5° ; -4° ; 0° ; $+7.5^\circ$.

It might be assumed from Fig. 269 that adjustable guide blades are absolutely ineffective in front of axial-flow fans. This is not so. In the test by Keller there was a radial inlet guide unit at some distance from the rotor. On account of this, as we now know, vortex cores can form, which make the effect of the inlet rotation illusory. Therefore we must endeavour to arrange the guide unit directly in front of the impeller. In this case effective regulation is provided even with adjustable guide units. On the other hand, increased noise must be taken into account.


 FIG. 269. Rotor 2 guide unit variable 0° ; $+17^\circ$; $+30^\circ$; $+38^\circ$.

 FIG. 270. Rotor 2 guide unit fixed $+17^\circ$; rotor blades -8° ; -4° ; 0° ; $+4^\circ$; $+8^\circ$.

Apart from blade-setting remedies there are also possibilities of regulation by altering the number of blades and by introducing other blades.

Our thanks are due to the work of Ruden^(40a) for the first insight into the effect of radial velocities at working conditions which differ from the standard delivery volume. Only by assuming radial velocities is it possible to explain the actual operational behaviour of the axial-flow fans, as was outlined briefly previously. By interesting theoretical and experi-

^{40a} Ruden, Investigations on axial fans, *Luftfahrtforschung*, Vol. 14.

mental investigations, Ruden was able to obtain a distribution which can be seen in Fig. 275. Tip-clearance loss, rotor loss, pressure factor, guide wheel, and diffuser loss are noted here as a function of the volume factor. The guide wheel and diffuser losses increasing with φ' demonstrate the upper limit of the characteristic very well, whilst at smaller values due to the separation of the flow the characteristic is gradually terminated. The causes of the fairly pointed characteristics are easy to detect from this. Figure 275 also shows the limits of the finding. The obvious difference between η_{th} and η_m shows up to what degree it is possible to carry out a preliminary calculation at the time. Figure 276 also shows $\bar{\psi}/\eta$; an entry indicates to what degree a linear dependency of the pressure factor without losses is justified.

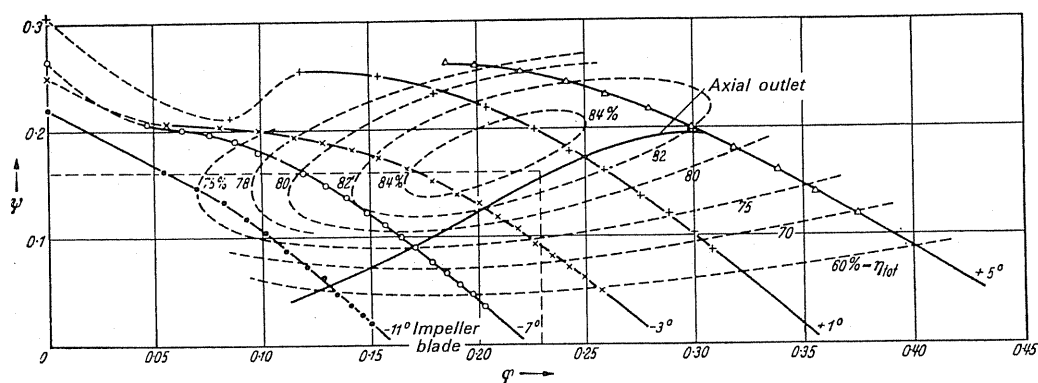


FIG. 271. Rotor 3 guide unit fixed at 31° ; rotor blades $-11^\circ, -7^\circ, -3^\circ, +1^\circ, +5^\circ$.

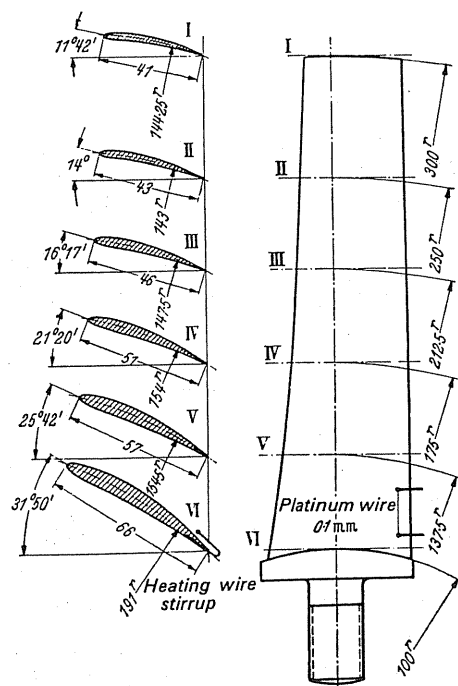


FIG. 272. Rotor 1, 4 blades.

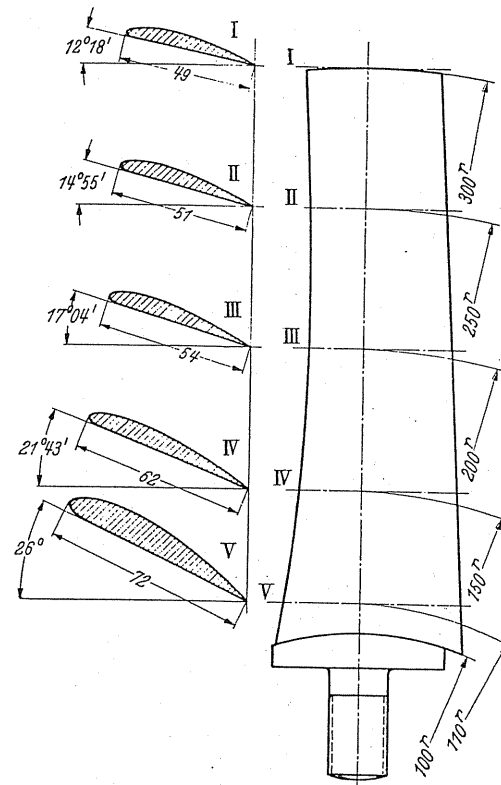


FIG. 273. Rotor 2, 6 blades.

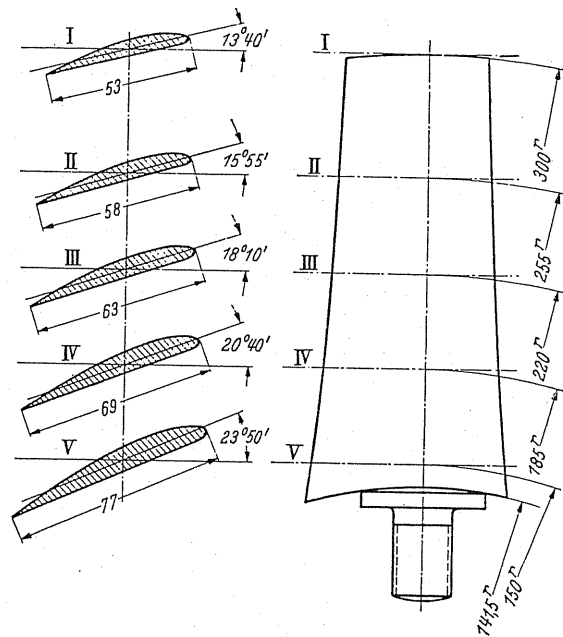


FIG. 274. Rotor 3, 10 blades.

The *nose fairing* of an axial impeller is of some importance. In ducted type fans this view has been accepted for a very long time. In these cases a semi-spherical nose fairing was indicated as a rule. Investigations by Eckert⁽⁴¹⁾ confirm this old practical rule almost exactly. In this reference Eckert also reports on part loading by means of segment-type blade caps. This type of measure according to Eckert is practical if the operating point with the rotor fully loaded moves into the unstable portion of the characteristic. This, for instance, is often the case in high-pressure rotors.

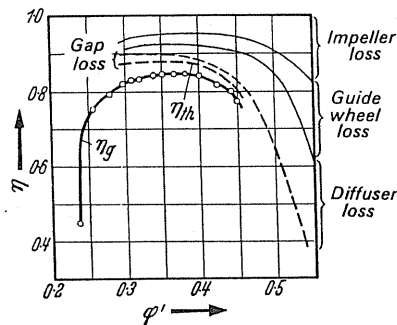


FIG. 275. Losses and efficiencies as a function of ϕ' .

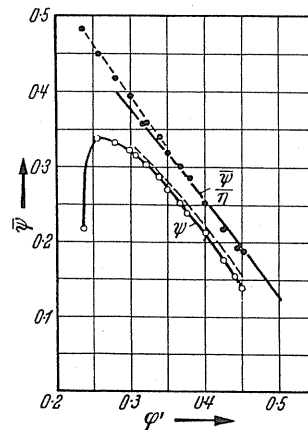


FIG. 276. Pressure factor measured ψ and calculated $\bar{\psi}$. Pressure factor without losses as a function of ϕ' .

Axial-flow fans can also be designed for higher pressure factors. As an example we refer to tests by Eckert⁽⁴²⁾ from which the example shown in Fig. 277 has been taken. It refers to a rotor with twelve blades and $\nu = 0.365$. In the zero setting the angles of the profile chord are set at 30.7° inside to the peripheral part and 12.4° external. The profile depth increases outwards (outside 45 mm, inside 40 mm). With this rotor pressure factors of approximately 0.5 were achieved. Only a relatively small part of the characteristic is useful. The flow soon separates at smaller delivery volumes. Accordingly, as shown in Fig. 277, pointed efficiency curves are obtained. Pressure factors even up to about 1 can be obtained. Rotors like these

⁴¹ Eckert, B., Experiences with high-pressure axial-flow fans, *Z VDI*, 1944, p.156.

⁴² Eckert, B., Cooling fans for air-cooled motor vehicle engines, *Dtsch. Kraftfahrtforsch.*, 1942, No. 67.

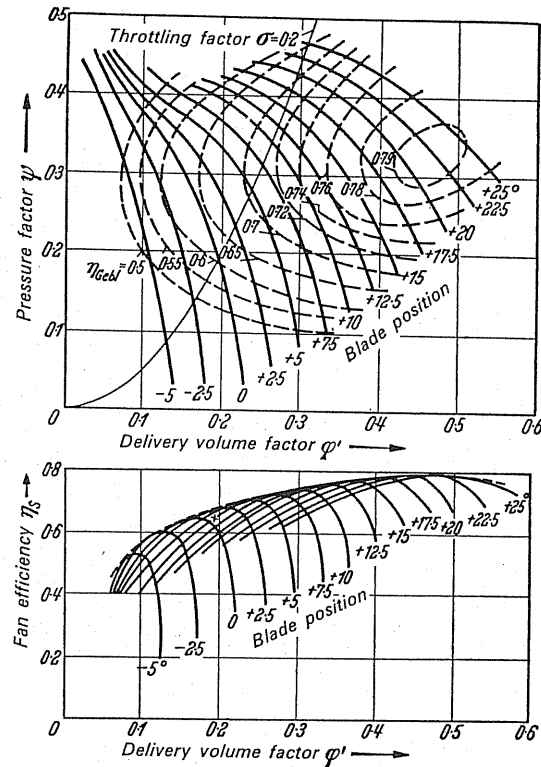


FIG.277. Characteristics and efficiency curves of a high-pressure axial impeller at different blade positions according to Eckert.

can only work without separation on a very narrow delivery range. This disadvantage can be compensated to a great extent by means of blade adjustment. If blade adjustment is not possible or cannot be carried out economically, axial impellers of this type can only be used if the operating point, i.e. the pressure and delivery volume, are known very accurately. In gas turbines and jet blowers this is the case, and hence axial-flow fans with very high-pressure factors give complete satisfaction in these applications.

One example of this type according to Eckert is shown in Fig.278; this refers to the characteristic of an axial stage which covers nine different blade positions. The very narrow range of useful characteristics and the short distance of the point of separation from the point of optimum efficiency are typical.

109. IRREGULAR INLET-FLOW CONDITIONS

Hitherto it has always been assumed that a uniform inlet-flow velocity is available over the whole radius in front of the fan, i.e. in ideal conditions. In every case a check should be made in order to ascertain whether considerable deviations from this case occur. It is intended to demonstrate on a few typical examples what are the practical effects.

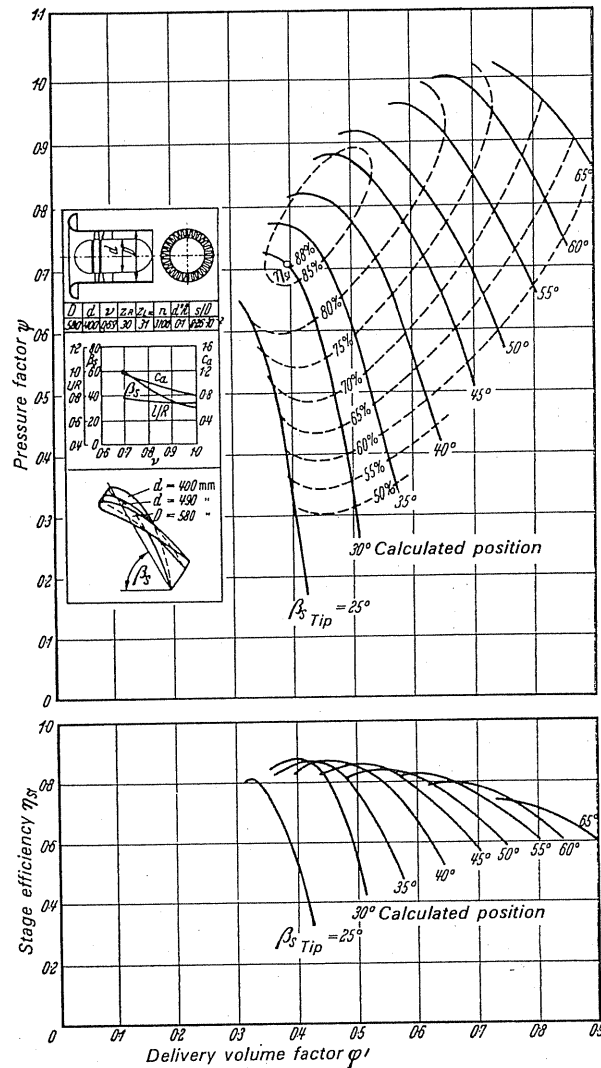


FIG.278. Characteristic of an axial compressor stage according to Eckert.

Figure 279 shows the case which often arises in which there is a considerable increase of velocity in the vicinity of the blade roots. It is due to the form of the nose fairing. The effects may be taken from the velocity diagrams in particular. The differences in blade angles β_{1i} and β_{1a} become greater than in the normal case. In the aerofoil design the c_m distribution must be accurately known.

Increase of velocities also occurs often at the external diameter. Figure 279 (centre) shows the example which often occurs in coolers of internal combustion engines. The change from the square shape of coolers into the round one of the fan brings about increase of velocities. The velocity diagrams portray the peculiarity that the inlet blade angles may perhaps be *similar*. Under certain circumstances, therefore, *untwisted* blades can be used.

Much more defined is the situation in Fig.279 at the bottom where the air is sucked from atmosphere radially. In this particular case an untwisted blade can be useful.

At this opportunity it might be worth while to mention an installation fault which is often observed in simple fans. Figure 280 shows typical cases.

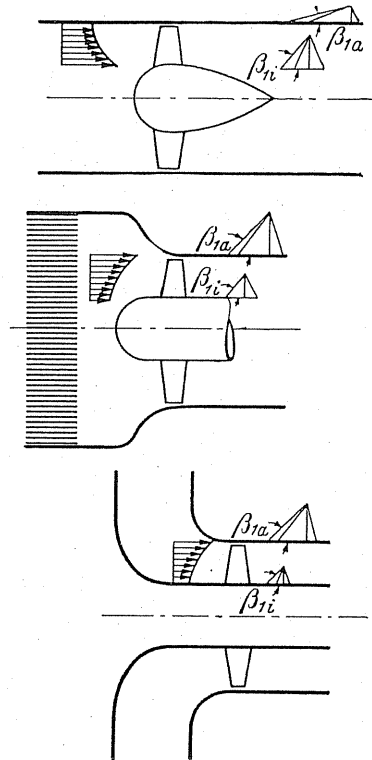


FIG.279. Examples of irregular inlet flow towards axial-flow fans. *Top*: excess velocity at hub; *centre and bottom*: excess velocity outside.

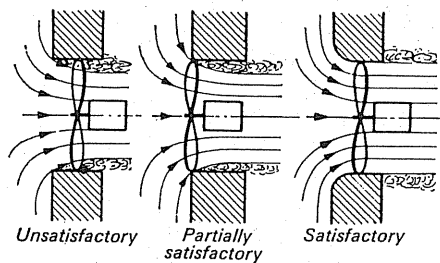


FIG.280. Satisfactory and unsatisfactory installation of axial-flow fans.

110. AXIAL-FLOW FANS WITH VARIABLE PRESSURE DROP

In one case the author had to reduce simultaneously various considerably different pressures for a single-stage axial-flow fan. It has been found that this problem can be solved if the characteristic is very steep and stable up to delivery zero. Characteristics such as these (Fig. 281) can be obtained by a higher specific speed coefficient with axial-flow fans without

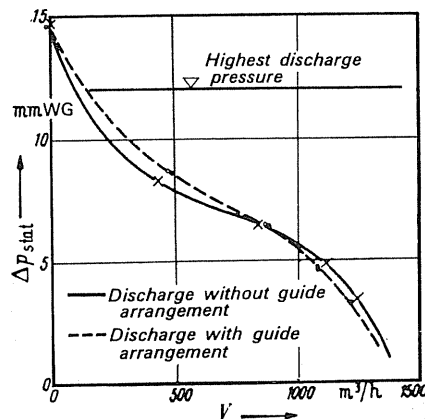


FIG. 281. Steep characteristic of axial-flow fans without guide wheels.

guide vanes. At the outside periphery a part sector of the guide wheel was cut out from the main flow (Fig. 282). In this way a maximum pressure of 10 mm WG was attainable whilst at the same time the main flow had a pressure of 5 mm WG. In place of guide wheels a part spiral housing can be fitted for this sector, which discharges on to a guide blade. The alteration of the main characteristic due to this cross-leak is very small as will be seen from Fig. 281.

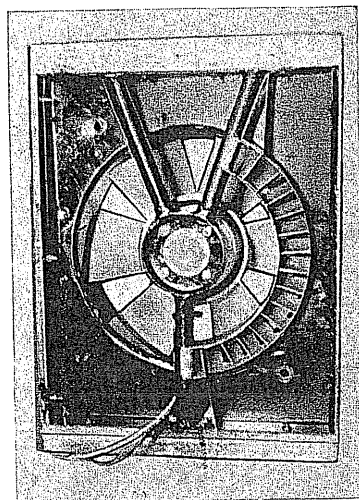


FIG. 282.

111. OPEN-RUNNING AXIAL-FLOW FANS

An air circulation can readily be achieved inside rooms by means of free-open-running axial-flow fans. These forms of ventilation appearing as table fans, ceiling fans, etc., are very useful and simple in their application.

In order to design this type of fan some attention must be paid to its very peculiar flow. According to Fig. 283 this type of fan sucks uniformly from all sides (theoretically also from the rear) and blows backward a concentrated stream with *rotation and internal vortex core*.

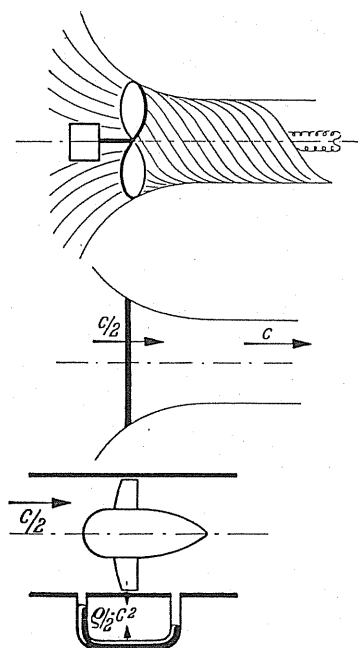


FIG. 283. Comparison of open flow of the free-running axial impeller with axial-flow fan of equivalent effect.

The suction in front of the fan—seen from a distance—can be compared to a space sink. The exceptional feature of this inlet flow is that in front of the fan there is hardly a trace of air movement. In order to arrive at a simple method of calculation let us imagine an ideal fan which is finitely thin and accelerates the air purely in axial direction on to velocity c without rotation and vortex core (Fig. 283 centre). According to the momentum equation it can be proved that the meridional transit velocity in the plane of the stream is exactly half of the ultimate velocity, i.e. $c/2$. It is practical therefore to compare the fan with a propellor fan which in accordance with Fig. 283 produces an overall pressure $\Delta p = (Q/2) c^2$. In order to gain the first guiding factor for the peripheral speed we introduce also here the pressure factor

$$\Delta p = \psi (Q/2) u^2 = (Q/2) c^2; \quad u = \frac{c}{\sqrt{\psi}}.$$

The construction of these types of fan without guide wheel gives small ψ values, on the one hand, whereas the call for low noise leads to larger ψ values. To compromise between these two demands it is recommended to use mean ψ values approximately $0.08 < \psi < 0.18$. Using in this case, however, the volume factor φ' is

$$\varphi' = \frac{c_m}{u} = \frac{c/2}{u} = \frac{1}{2} \sqrt{\psi}. \quad (231)$$

Since flat velocity triangles are obtained throughout, we can make use of the following simplifications:

$$w_\infty \approx \frac{c/2}{\sin \beta_\infty}; \quad \frac{c/2}{u} \approx \tan \beta_\infty.$$

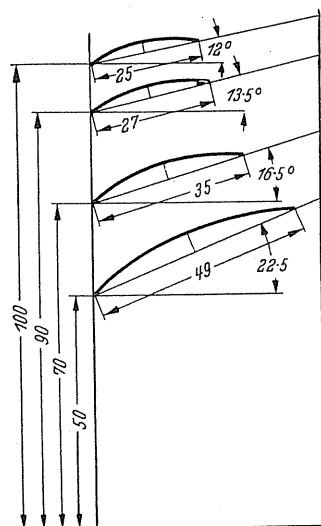


FIG. 284. Example of design of fan blades.

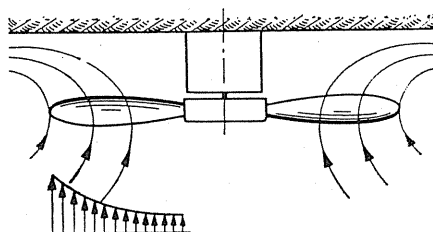


FIG. 285. Irregular inlet flow in ceiling fans.

Thus the equation formerly derived $c_a l = (\Delta p t 2/\eta u_0 w_\infty)$ can easily be used. We obtain

$$c_a l \approx 4 \frac{t}{\eta} \tan^2 \beta_\infty. \quad (232)$$

It is easy to carry out the calculation with this basic equation.

Example

It is required to design a fan of $z = 4$ and $n = 1450$ rev/min, which gives the discharge velocity of 6 m/sec. We take $\psi = 0.16$ and from this we find $u = c/\sqrt{\psi} = 15$ m/sec; $d = 200$ mm. The value β_∞ is obtained from $\tan \beta_\infty = c/2u = c/2r\omega$ therefore β_∞ can be

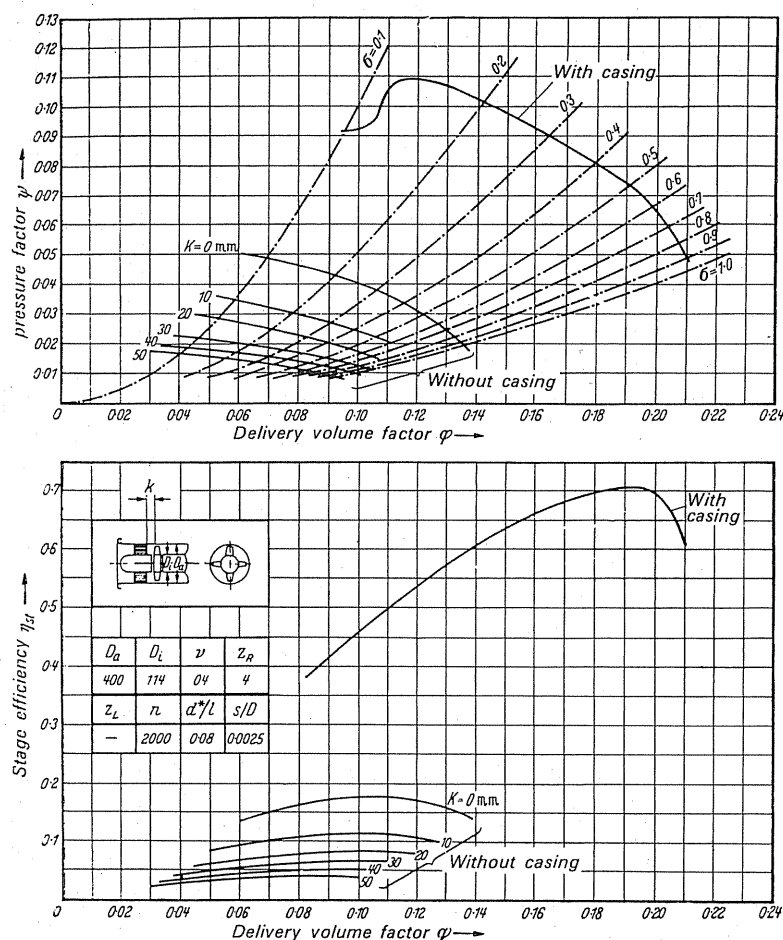


FIG. 286. Axial-flow fan with and without a casing according to Eckert.

readily calculated for different values of r . We want a circular arc profile with $f/l = 0.1$ at $c_a = 1$. For this we take from Fig. 229 an incidence angle of 1° which should be added to the angle β_∞ . For different radii, therefore, the layout shown in Fig. 284 is easily obtained. On the outside the finished aerofoil must be rounded off in order to avoid disturbing and noise-generating pressure increases at this point. The calculations of Re gives us on the outside $Re \approx 25,700$, i.e. values at which the aerofoil starts to fail. Steel blades are the best proposition here.

Axial-flow fans freely exhausting without guide wheels such as are used particularly for cooling internal combustion engines were investigated very thoroughly by Marcinowski.⁽⁴³⁾ The efficiencies which can be achieved at maximum are shown in Fig. 253. In view of the circumstance that with the larger impeller gaps necessary for practical reasons, efficiencies below 50% can only be achieved, the problem arises whether it is not high time to replace these fans with other types. Furthermore, the practicability of standardising by design with $\eta = 31\%$ must be doubted because thereby it is possible that the application of such bad fans will be promoted still more.

In ceiling fans which are generally of large size, the further circumstance should be taken into account that in accordance with Fig. 285 a greatly increasing inlet flow velocity for the periphery may be present.

In a recent work by E.J. Lyons⁽⁴⁴⁾ there are noteworthy and practical hints concerning agitators for gas and liquids.

Open running axial-flow fans without casing are best avoided if the air flow is to be sucked from a prearranged resistance, for instance, a condenser. Figure 286 shows tests by Eckert⁽⁴⁵⁾ which clearly demonstrate the deleterious effects of the lack of casing. In every case, therefore, casing is practical.

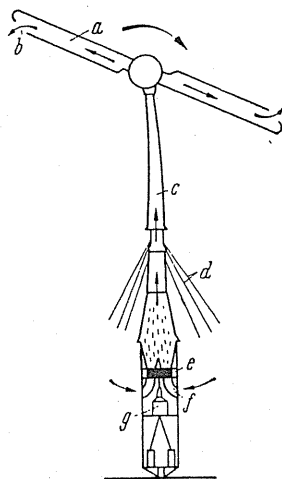


FIG. 287. Wind power plant. *a*, hollow axial impeller; *b*, outlet nozzle for exhausted pressure air; *c*, inlet for exhaust pressure air; *e*, air turbine; *f*, air inlet to air turbine; *g*, generator.

A fan in the form of a *rotating tube* has been known formerly.⁽⁴⁶⁾ A most original application is shown in a new type of wind power plant in St. Albans, England. The wind rotates a propeller of 25 m diameter mounted on a mast 30.5 m high. Air is discharged outwards through the hollow propeller aerofoil and is emitted to atmosphere from ports around the

⁴³ Marcinowski, H., The influence of the tip clearance in freely exhausting axial-flow fans without guide wheels, *Voith-Forschung u. Konstruktion*, 1958, No. 3.

⁴⁴ Lyons, E.J., *Chem. Eng. Progr.*, 44 (5) (1948) 341-6.

⁴⁵ Eckert, B., *Axialkompressoren*, Berlin/Göttingen/Heidelberg, Springer, 1953, p. 147.

⁴⁶ Eck, B., and Kearton, *Turbo-Gebläse und Kompressoren*, Berlin, Springer, 1929, p. 179.

periphery. The considerable air power thus generated is used, as shown in the diagrammatic representation in Fig.287, to drive an air turbine arranged at the foot of the mast, which is used for driving a generator.

The result in this way is to become to a far extent independent of the choice of the speed of the unit and there is no need to arrange any sensitive machine component on the wind vane itself. At a wind speed of 50 km/h, power of 100 kW is generated.

CHAPTER XIII

MERIDIONALLY ACCELERATED AXIAL-FLOW FANS

112. GENERAL OUTLINE

It is rather striking that a very good type of axial-flow fan has been left unnoticed for a long time. In this type the meridional cross-sections diminish greatly in the direction of flow in contrast to the type previously discussed. The various possibilities are sketched in Fig. 288.

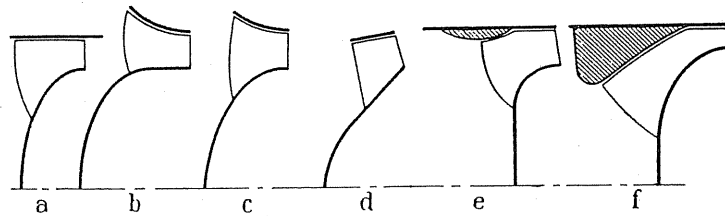


FIG. 288. (a-f), possible designs of meridionally accelerated axial impellers. (a) Increasing hub, cylindrical outside casing. (b) Outside casings, diminishing in diameter i.e. nozzle shape constriction, cylindrical internal casing. (c) Nozzle-shaped outside casing with greatly expanding hub. (d) Greatly expanding hub, slight expansion outside casing (inclined blade blower) (e) Greatly expanding hub from cylindrical outside casing at outlet and bulge-shaped constriction at inlet. (f) Design as (e) but inlet bulge drawn further inwards (high-pressure impeller).

The basic difference from the standard axial impeller is obvious immediately if we look at the velocity diagrams. The thick-line diagram (Fig. 289) applies to standard axial impeller with a pressure factor $\psi = 0.7$ corresponding to an internal deceleration $w_2/w_1 = 0.65$. If the same impeller is now provided with meridional acceleration at the same peripheral deflection, i.e. same c_u components, we obtain the dashed-line diagram. Now the value becomes $w_2/w_1 = 0.755$; therefore there is a considerably smaller deceleration in the rotor and; there-

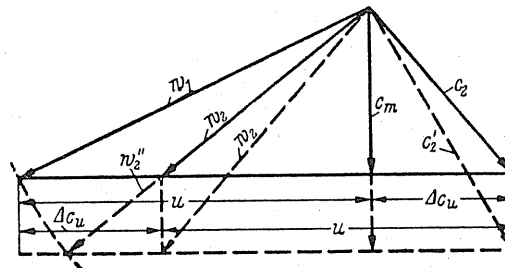


FIG. 289. Velocity diagram of a meridionally accelerated axial flow fan.

fore, a correspondingly less risk of separation. If, conversely, we now compare wheels of the same deceleration and same blade inlet angle β_1 (Fig. 290), a considerably greater peripheral deflection and a correspondingly greater pressure is created. Whilst the inlet diagrams are identical, considerable differences are obtained in the c_u components. The

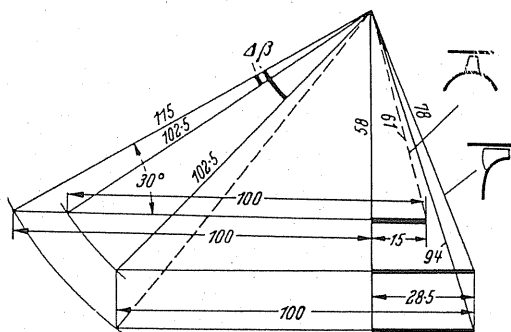


Fig. 290. Comparison of velocities between meridionally accelerated and standard axial-flow fans.

meridionally accelerated rotor shows almost double the value of c_u . This means a pressure twice as great or a pressure factor ψ twice as great. The directions of the absolute outlet velocities, however, hardly vary. The deflection angle $\beta_2 - \beta_1$, however, varies and is considerably greater than in the normal axial impeller. One of the main differences is in the magnitude of the absolute outlet velocities. It will be appreciated that the greater pressure conversion is a result of a greater outlet energy. In these fans, accordingly, the succeeding diffuser plays a greater part than in the standard axial-flow fan. The success of this design is governed by the shape of the diffuser. Primarily one advantage is a considerably higher pressure, the disadvantage being that the need of developing a more sensitive diffuser.

In Fig. 291 a comparison with standard axial-flow fans is shown in more detail. The ratio of the overall pressure achieved in both cases as a function of the meridional acceleration is expressed by c_{2m}/c_{1m} required in the meridionally accelerated impeller. Various curves for constant deceleration of relative velocity, expressed by means of the ratio w_2/w_1 have been indicated. It will be observed that even at moderate meridional accelerations a considerable rise in the overall pressure is obtained.

At otherwise equal meridional accelerations, the differences increase as the w_2/w_1 increases. If, in the middle, the pressure achieved is calculated as twice as high as in the normal axial impeller, this describes the situation which has also been confirmed in practice.

The reaction effect at meridionally accelerated axial impellers. In the design with cylindrical casing there is no alteration of the peripheral speed for the outside streamline. Consequently, there is a static excess pressure $(\rho/2)(w_1^2 - w_2^2)$ generated in the impeller due to deceleration of the relative velocity. Hence for the reaction effect we obtain

$$r = \frac{(\rho/2)(w_1^2 - w_2^2)}{\rho u_2 \Delta c_u}.$$

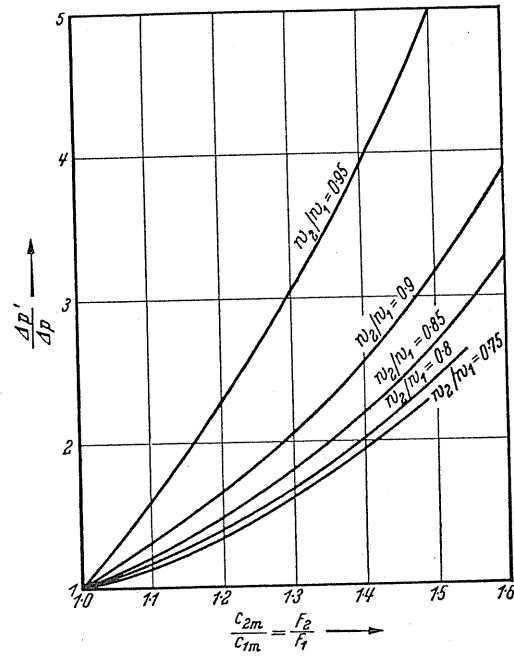


FIG. 291. Comparison between meridionally accelerated and standard axial-flow fans. Overall pressure ratios.

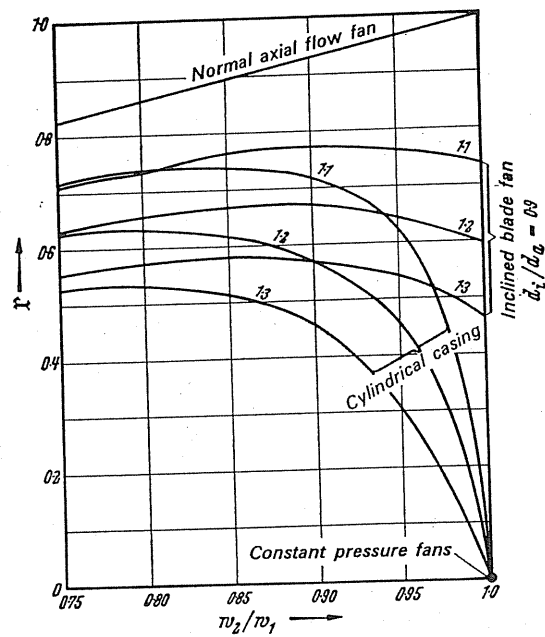


FIG. 292. The reaction effect as function of w_2/w_1 .

For the meridional acceleration $F_1/F_2 = 1.1, 1.2$, and 1.3 the reaction effects r are plotted in Fig. 292. At decelerations of $w_2/w_1 < 0.9$ reaction effects are obtained throughout which lie above 0.5. The values naturally come below the values of the standard axial-flow fan which is also represented in Fig. 292 for the purpose of comparison. The overall representation applies for an inlet blade angle of 30° .

The case of uniform pressure impeller has been defined as a dot for the purpose of comparison.

In meridionally accelerated inclined blade fans according to Fig. 293, apart from the amount mentioned before, there is still the pressure increase due to rise of the peripheral speed. This brings us to the amount $(\rho/2)(u_2^2 - u_1^2)$. Therefore the total static pressure rise

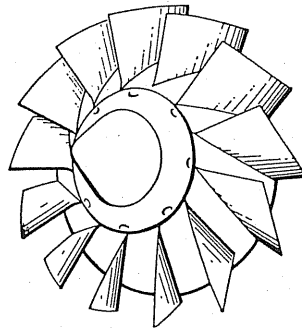


FIG. 293. Meridionally accelerated inclined blade fan (Büttner-Eck).

is $[(\rho/2)(w_1^2 - w_2^2) + (\rho/2)(u_2^2 - u_1^2)]$. For equal meridional accelerations the reaction effects have also been plotted in Fig. 292. The reaction effects are even considerable at moderate decelerations of the relative velocities. Values above 0.8 are possible to achieve in this case. In comparison to the cylindrical external casing, the case of $w_1 = w_2$ still gives a high reaction effect.

Table 19 shows the characteristic numerical values.

TABLE 19

	w_2	w_1	c_u	c_u/u	ψ	c_2
Axial-flow fans—normal	102.5	115	15	0.15	0.24	61
Meridional accel. cyl. casing	102.5	115	28.5	0.285	0.456	78
Constant pressure fan	115	115	28.5	0.285	0.456	95
Inclined blade fan	93.6	104	33	0.33	0.528	73
Inclined blade fan (unretarded)	104	104	33	0.33	0.528	87.5

The advantage of meridionally accelerated axial-flow fans becomes noticeable in the zone of higher pressures. Whilst for lower pressures up to approximately 0.25–0.3 standard axial-flow fans have no superiors and have many advantages, their characteristics deteriorate steadily when the zone of higher pressure values is entered. High diameter ratios with very many blades are required. The adjustment possibilities of the blades which is one of the best characteristics of the axial-flow fan become more difficult. Above all, however,

characteristics are obtained which are unsuitable for engineering practice. The useful range of characteristics becomes very small. The point of separation comes very close to the point of the best efficiency. This "incompatibility" is not so serious for typical application in aircraft design, i.e. nozzle compressors, but in mechanical engineering it is extremely disturbing as there is almost always a wide area of the characteristic which has to be covered and which cannot be met with the necessary good designing, required in these types. Despite all these reasons meridionally accelerated axial-flow fans in which the so-called phenomena are considerably milder have gained a footing. They have also the advantage that profiling can be dispensed with and simple steel blading will do.

The achieved pressure factors (about 0.7–0.8) are similar to those which are in high-performance fans. Table 19 gives comparison with axial-flow fans.

113. CONSTANT-PRESSURE FANS

In meridionally accelerated impellers there is a possibility of obtaining an *unaccelerated* relative velocity in the impeller, i.e. where $w_1 = w_2$ which is impossible to achieve in standard axial impellers. *To a degree better ratios are obtained for the flow through the impeller.* Thus a decisive advantage is obtained that *no profiling* is necessary and simple steel blades will do. In the case $w_1 = w_2$ the *constant pressure* is obtained for the external streamline with cylindrical casing, i.e. the impeller only generates kinetic energy. Schicht considers this

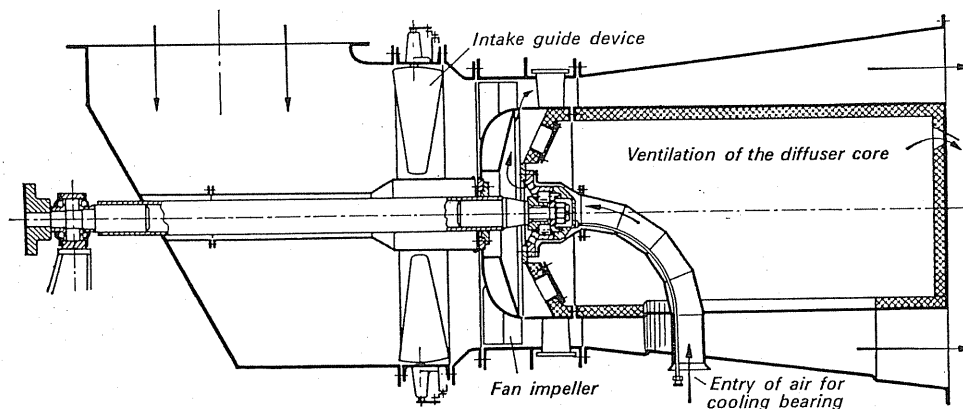


FIG.294. Induced-draught fan designed by Schicht with adjustable intake blades.

constant pressure important for effectiveness and efficiency and, as stated by Sørensen⁽¹⁾ lays greater value on constant pressure for the total behaviour of the outside streamline. This means that the streamlines closer to the hub are accelerated and very much accelerated at the hub itself. The total static pressure is generated in the diffuser and therefore the design of the highly loaded diffuser is a governing factor. The fans developed on the principle for which Schicht is noted are therefore called *constant-pressure fans* (DRP 633 155).

¹ Sørensen, E., *Z VDI*, 1939, p.925.

Schicht paid a great deal of attention to the principle of constant pressure in meridionally accelerated types and created a type which is very popular for use as induced draught fans. Figure 294 shows an induced-draught fan with adjustable-inlet guide blades. By adjustment of guide blades a high degree of adjustment is possible as shown in Fig. 295. Figure 292 shows the constant pressure fan as a dot.

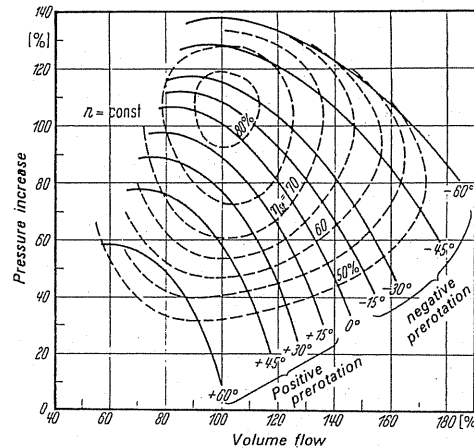


FIG. 295. Adjustment of a Schicht fan by guide blade adjustment according to Eckert.

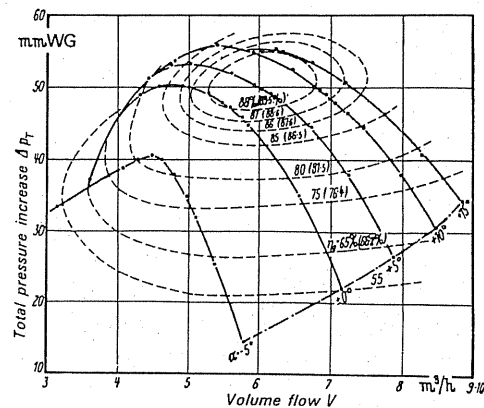


FIG. 296. Characteristic field for different blade positions meridionally accelerated axial-flow fan by Eck. P. Pollich, Mönchen-Gladbach; Büttner A. G., Krefeld-Ürdingen.

114. MERIDIONALLY ACCELERATED HIGH-PRESSURE FAN

Whilst in the constant-pressure fan a fairly large static pressure after the rotor was intentionally dispensed with, the author worked in the opposite direction. The aim was to achieve *the highest possible static pressure* in the rotor, i.e. a reaction effect as large as possible, in order to relieve the succeeding diffuser. A further factor was that a *rotating diffuser is better than a stationary diffuser*. The first design (Fig. 293) has the distinguishing feature that the external inlet ridge was drawn in somewhat and thus an external casing line was obtained

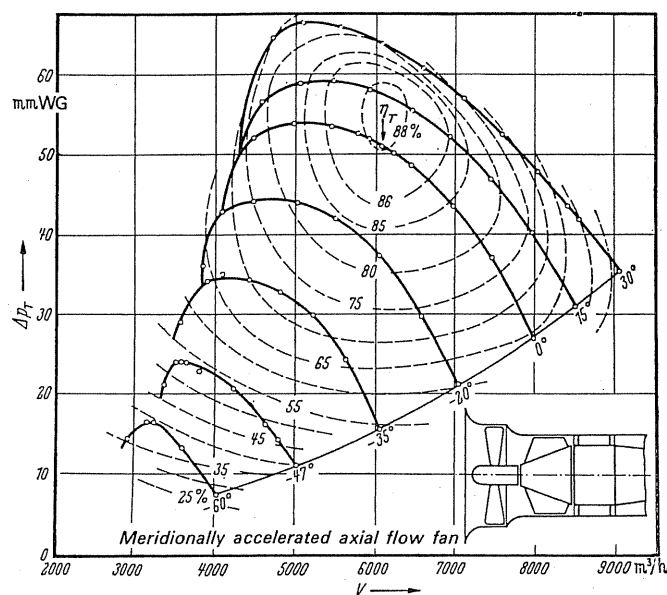


FIG.297. Family of characteristics when adjusting the preliminary guide unit according to Eck (Pollrich and Büttner).

arising at a slope. First of all, in this way the relative intake velocity was lower at the external intake which is a factor having a favourable effect on the shock losses at this point, also on the characteristic. Of greater importance is the fact that the outside streamlines no longer have an axial path but run outwards somewhat. Therefore *the static pressure is increased by the centrifugal forces*, and it may be anticipated that the reaction effect which is so important will increase. Thus we obtain designs, the meridional representation of which have some similarity with inclined blade centrifugal pumps. The difference apart from the obvious meridional acceleration, however, lies in a different design of blades.

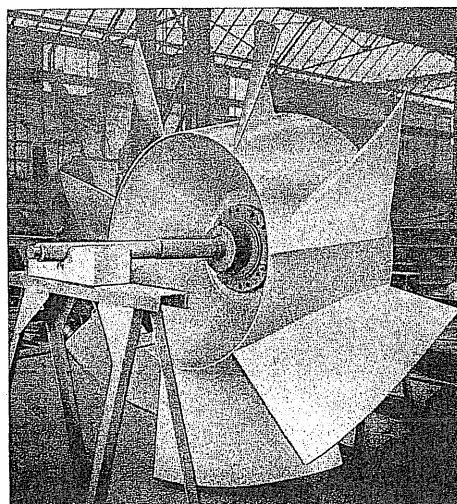


FIG.298. Meridionally accelerated impeller (Büttner-Werke A.G.).

In the meantime, a new type of high-pressure rotor with cylindrical external casing has been developed which brought about considerable advances. It has been found that with definite shape and optimum meridional acceleration and the number of blades, efficiencies of 88–89% were possible to achieve. Figure 296 shows the family of characteristics of this design for different blade angles which has been confirmed by tests carried out by Professor Fritzsche and the Mining Ventilation Establishment.⁽²⁾ By adjusting the upstream guide blades, a further range of adjustment is obtained (Fig. 297).

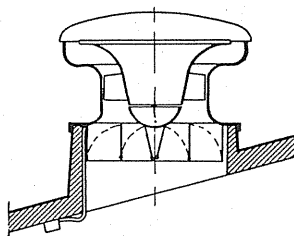


FIG. 299. Ceiling fan by the firm P. Pollrich. Roof ventilator.

Meridionally accelerated axial-flow fans, as well as other axial-flow fans with high-pressure factors, can be regulated by means of guide units arranged immediately in front. In contrast to most radial-flow fans these fans also react to counter rotation. Unfortunately, this characteristic was considerably impaired by the severe wear which was observed with certain dusts in fans which were not of the regular design.

At pressure coefficients of 0.65–0.7 the same values were obtained as in the high-duty fans. The reaction effect was 0.73. The total reaction effect with diffuser was 0.965 and, therefore, where free suction is concerned only 3.5% is left over for dynamic pressure energy. Figure 298 shows a large size type manufactured by Büttner-Werke.

A special application of this type is the one shown in Fig. 299 which is a roof ventilator by the firm Pollrich. The ventilator provided with external rotor motor is distinguished for its astonishing noiseless running capacity.

A standard design by the firm Pollrich is shown in Fig. 300.

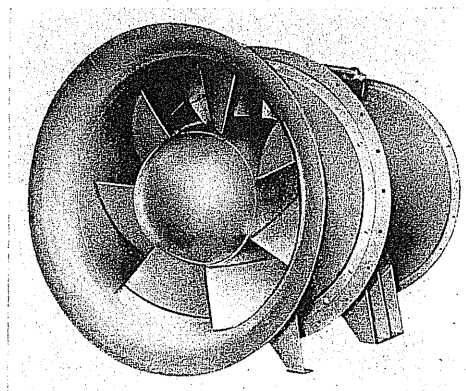


FIG. 300. Meridionally accelerated axial-flow fan designed by the firm P. Pollrich.

² Fritzsche, C.E., A new propeller fan meridionally accelerated type, *Glückauf*, 1956, pp. 161–4.

CHAPTER XIV

CONTRA-ROTATING AXIAL-FLOW FANS

115. DESIGN AND TEST VALUES

The arrangement of two fans, axial-flow type, arranged one after the other and running counter to each other is one of the most attractive fan designs. The guide wheel becomes superfluous, the pressure achieved corresponds to a two-stage fan, and a considerably shorter construction is obtained. The only disadvantage is the drive. Two separate driving machines running in opposite direction are required (lately also oil engines) or the rotor is driven by means of a belt from an external motor. A reversing gear is provided at or in the hub; usually it is costly for assembly owing to the difficulties of the drive, and it is seldom justified.

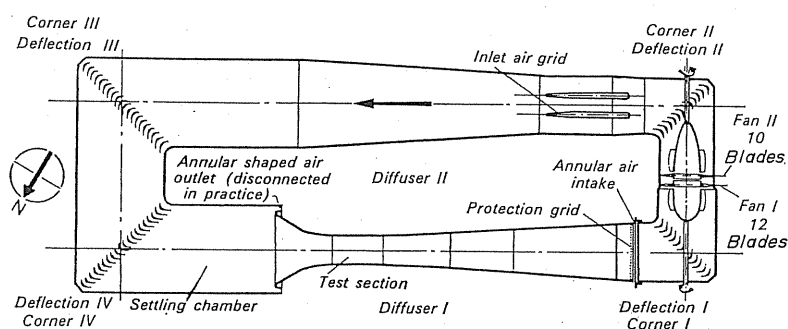


FIG. 301. Plan view of the wind tunnel in Modane.

A typical case where the contrarotating type has provided a good solution is the large wind tunnel of ONERA⁽¹⁾ in Modane. The drive possibilities by means of two Pelton turbines each of 55,000 hp and the prospect of being able to have the two drive shafts passing through the two corners of the wind tunnel created the ideal solution in the arrangement of contrarotating axial-flow fans.

Figure 301 shows a plan view of the wind tunnel with the turning vanes in the corners as well as two diffusers. The diffuser 1 covers the test section 14 m long and 8 m diameter in which the speed of sound can be obtained without any testing components. The fan blowing upstream has twelve blades and the one blowing downstream has ten blades. There is no mechanical connection between these two fans. Figure 302 is a fan viewed transversely through the opening made in the side wall. The picture of the workman gives an idea of

¹ ONERA (Office National d'Études et de Recherches Aéronautiques). M. Director Maurice Roy kindly supplied Figs. 301-303.

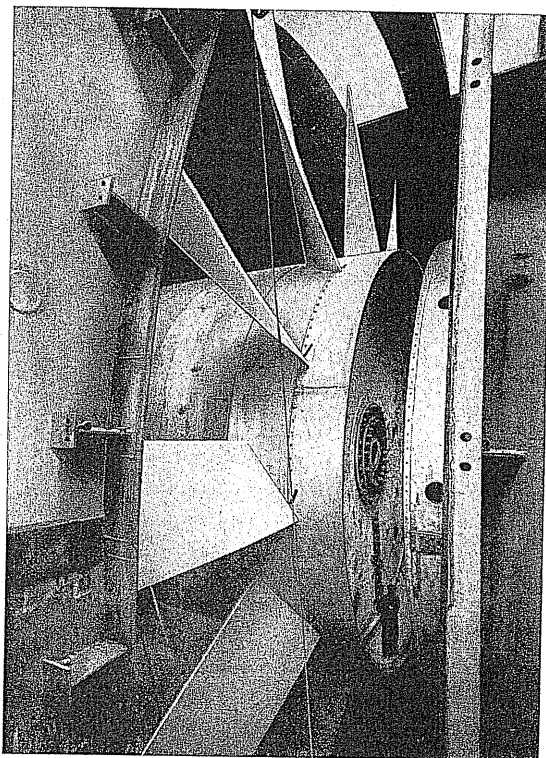


FIG.302. Photograph of the fan of the wind tunnel at Modane.

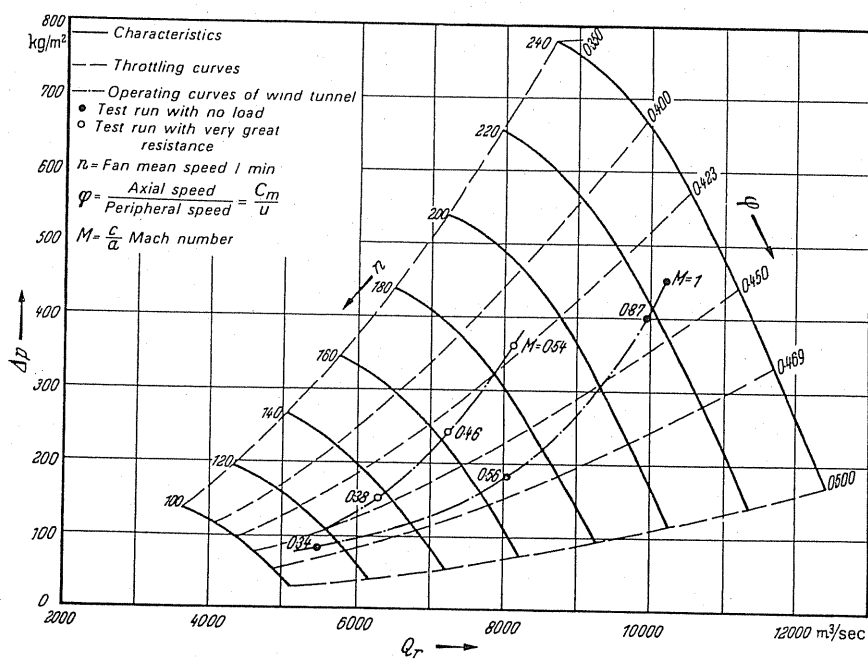


FIG.303. Characteristics of the wind-tunnel fan.

the immense size. The blade angles can be adjusted at the hub. Figure 303 shows the characteristics of the fan at speeds $n = 100\text{--}240$ rev/min. The resistance curves for the test run with and without trial inserts are supplied by the actual operating points (curves are dotted).

A more recent design by the LTG⁽²⁾ is worth looking at. Here the speed of the front impeller is adjusted whilst the speed of the back impeller is unaltered. Figure 304 shows the

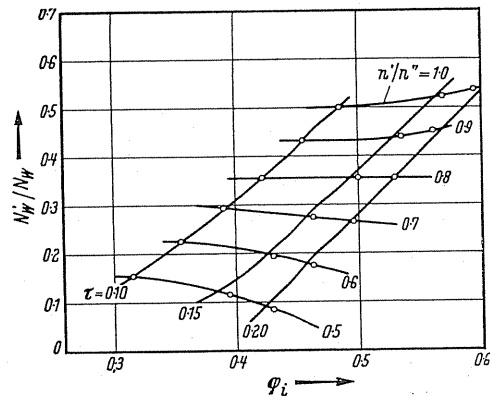


FIG. 304. Power absorption of the first stage related to the overall power absorption. (N' and n' relate to the first stage.)

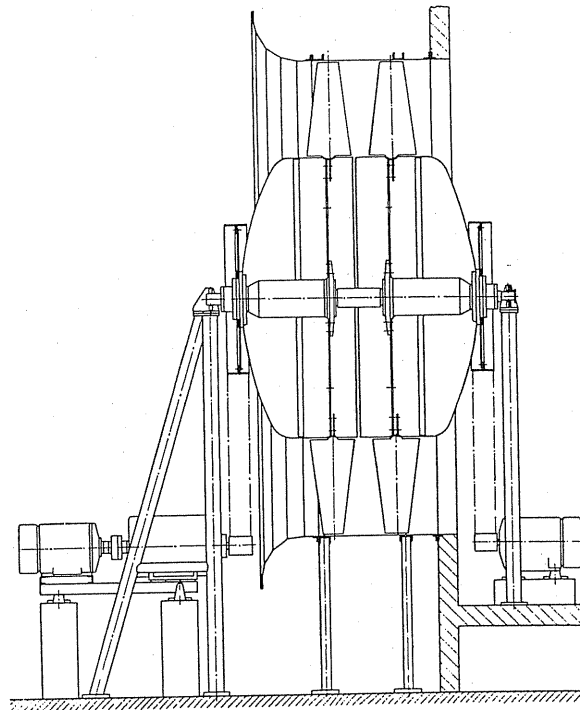


FIG. 305.

² Traupel, W., Tests on contrarotating axial-flow fan, *Heizung-Lüftung-Haustechnik*, 1959.

total relative power absorption in which values are achieved which are situated close to the cubic parabola, i.e. the pure speed regulation. Figure 305 is a section of the design which is distinguished by its short construction and its lack of diffuser. This construction achieved an overall efficiency of 90% but, of course, with the very small clearance of $1.31 \text{ }^{\circ}/_{00}$ (4.6 mm at 3522 outside diameter). As already emphasised previously, these efficiencies can only be obtained with such low clearances. With $\psi = 0.81$ and $\varphi_{\sigma} = 0.215$ values are obtained which signify a lower high-speed factor than in high-duty radial-flow fans, whilst the specific diameter δ is greater.

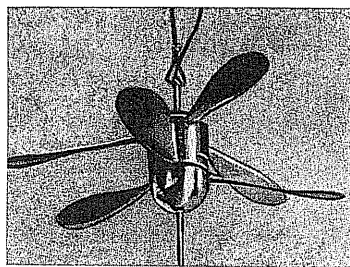


FIG.306. Fan with counter-rotating aerofoils. Stator and rotor are in opposed rotation.
Fa. W.Salonska, Schwertzing.

An interesting miniature design which is a ceiling fan is shown in Fig.306. Here a fan is formed out of two contra-rotating motor parts, i.e. starter and rotor. The whole set-up can be suspended firmly on a wire.

It is interesting to know that about 35 years ago contra-rotating axial-flow fans were known in small demonstration wind tunnels.⁽³⁾

³ Berlage, F., A wind tunnel with two contra-rotating air propellers, *Luftfahrt und Schule*, 1936, p.178.

PART C

GENERAL PROBLEMS RELATING
TO BLOWERS

CHAPTER XV

REGULATION OF BLOWERS

116. GENERAL PRINCIPLES

The necessity for the correct design of fans was stressed in previous chapters and various means of achieving this aim were described.

However, even if it has been possible to design the blower correctly and if the operating point coincides with maximum efficiency, the problem has been only partly solved. A completely satisfactory design can only be achieved if the delivery volume and the pressure remain constant, and this seldom, if ever, occurs. Alterations in the delivery volume which the fan has to accept are almost always the rule. For example, the induced-draught and forced-draught fans of a boiler must always adjust themselves to the fluctuating load of the boiler. The resistance to be overcome are lower in boilers producing smaller flue gas volumes and they increase with the size of the boiler. The fan designer has to deal with this contingency. If the duct and other devices, etc., connected up to the inlet and the outlet of the fan are considered as single resistances, the question arises as to how the pressure varies with the volume when air is blown through this resistance. This is known as the system characteristic.

It has been found from former investigations that, in the majority of cases, the operating characteristic takes the form of a parabola. This will be assumed throughout the following discussion.

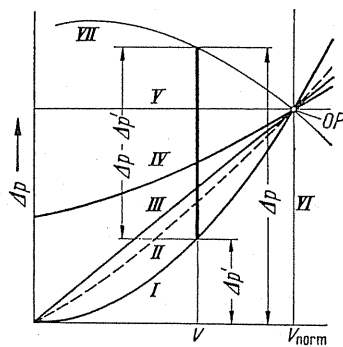


FIG. 307. Operating characteristics at various system resistances.

The fan running at constant speed develops different pressures for different volumes as shown in the curve VII of Fig. 307. The deviation from the required value is considerable. Therefore all that is left is to reduce the difference $\Delta p - \Delta p'$. This undesirable behaviour is true for almost every fan and blower, and the range of throttling is not further considered.

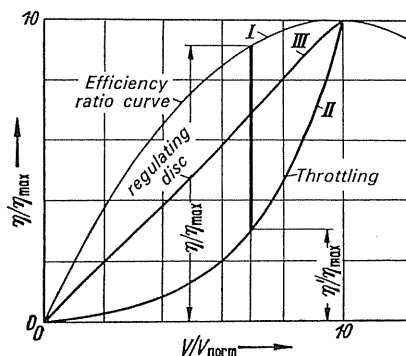


FIG.308. Relative efficiency curves with and without adjustment.

If the fan has been correctly designed initially, this behaviour refers to one point on the efficiency curve, which is the point of maximum efficiency. For all other delivery volumes the original efficiency curve is of no importance. The efficiency of real interest is considerably smaller than the value obtained from the blower characteristics, viz.

$$\eta = \eta' \frac{N_{\text{velocity}}}{N_{\text{throttle}}}$$

(η value according to characteristic Fig. 308.) Calculating point for point we obtain curve II (Fig. 308). It will be realised that with greatly fluctuating delivery volumes no useful efficiency can be achieved particularly away from the peak efficiency. One has to be satisfied if about half the peak efficiency is achieved. With greater variations of delivery volume not even one-third is achieved. Therefore it is imperative to take measures which will obviate these serious disadvantages.

There are two ways by which regulation can be obtained; firstly, hydraulic modifications are made within the blower at a velocity which is more or less constant, and secondly, the drive may be modified so that the speed is adjusted in some way. Subsequently, only those means which have given satisfaction in practice will be mentioned.

The possible hydraulic modifications include variations on the impeller itself, in front of or behind the impeller, alterations to the housing, or even alterations outside the blower.

Blade adjustment is the major factor affecting the impeller. In axial blowers which do not have too large pressure coefficients, i.e. for rotors with small diameter ratios and small numbers of blades, blade adjustment is one of the best methods of regulation. It has proved very satisfactory and at times gave the axial blower a fair lead over the radial blower, since in the latter the blade adjustment, though feasible in principle, could hardly be used in practice owing to constructional difficulties. The blade adjustment in axial blowers is so important that Kaplan turbines, for instance, could hardly be imagined without this control. In addition to blade adjustment, other measures are available; for instance, extending the blades, division of the impeller in such a way that one part could be driven on its own whilst the other part could continue to rotate at no load. Exterior to the impeller it is possible to take the following measures. Guide vanes which can be adjusted before or after the impeller. The latter are only used in turbo-compressors. Gap slides before and after the

impeller might be used: they are very simple to design but unfortunately they only regulate in the region of zero delivery. Displacement of the whole impeller was also tried out for control purposes,⁽¹⁾ and also lateral constriction of the whole guide ducts by means of sliding walls.⁽²⁾ Alterations in the housing is in general only a matter of varying the width of the spiral housing.

One of the simplest but most wasteful measures is the throttling damper arranged before or after the blower: in this case the excess pressure which is not utilised periodically is simply wasted. For working safety and simplicity, however, this method is the best. The serious engineer should regard every throttling damper as warning that he may by making use of this "control", create a situation which he cannot control.

A new control component namely, a flap, inducing rotation, has proved to be satisfactory recently in centrifugal machines.

As well as actual control devices, measures should be mentioned where continuous variation of the impeller is necessary. In radial impellers the outside diameter, for instance, can be machined off if the pressure is too high. The volume can be affected since the impeller is compressed in width (as is known from turbo-compressor impellers). By making some quite new modification to the blades it has been possible recently to increase the pressure by up to 50% (see p. 416, Fig. 412).

117. ADJUSTABLE INLET GUIDE VANES

It is known that the operation of a blower for smaller delivery quantities can be improved by means of adjustable downstream guide vanes. The guide vanes are set in the direction of the actual absolute outlet velocity so that the impact losses occurring otherwise are eliminated. These rotating guide vanes introduced by BBC have been adopted practically only in turbo-compressor engineering because, *inter alia*, the so-called pump limit can be reduced considerably by means of rotating guide vanes. Since this phenomenon is not observed in fan engineering there has been little call for this type of construction.

Inlet guide vanes, however, have been known for some time in fan engineering. It can be demonstrated that in specific circumstances these appliances bring certain advantages and enable the working range of a fan to be extended considerably. It is possible in many cases to adapt larger fans whose delivery volumes for various reasons have to be enlarged in due course, to be adapted to the new operating conditions by fitting inlet guide wheels.

If the delivery volume is greater than that of the shock free intake, shock losses occur which combined with the greater duct friction reduce the blower pressure considerably and ultimately cut short the suction capacity of the blower very quickly. Obviously the shock loss can be avoided by means of an inlet guide wheel. The velocity vector diagram shown in Fig. 309 gives a graphic representation of how circumstances alter in larger delivery volumes. The meridional component c_{1m} , for instance, has to be varied by Δc_{1m} . A shock would then be avoided if the air in the direction α'_1 were to enter with the negative c_u component c_{1u} .

¹ Widmar, H. U., *Techn. Rundschau, Bern*, 1953, No. 39.

² Weber, P. U., A new method for generating annular flow (1953), Supplement of the *Neue Zürcher Zeitung*, No. 1470.

This condition can be achieved by means of an inlet guide wheel. Apart from eliminating shock components there is an additional important factor; that due to the c_u components, according to the main formula $\Delta p = \rho [u_2 c_{2u} - u_1 c_{1u}]$ which alters the pressure. The value of c_{1u} is negative and therefore a lower pressure increase does not occur. An inlet guide wheel handling larger than normal delivery volumes for two reasons, produces a pressure rise compared with the normal characteristic due to counter rotation.

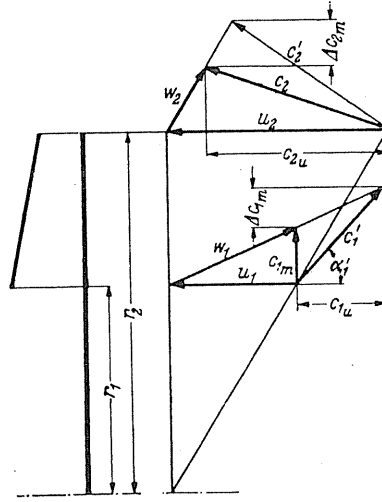


FIG. 309. Velocity vector diagrams for normal and excess delivery volumes.

The shock loss is $\mu (\rho/2) c_{1u}^2$, whereas according to the main formula $\rho u_1 c_{1u}$ is still gained. The gain over the normal characteristic therefore is

$$\Delta p' = \mu \frac{\rho}{2} c_{1u}^2 + \rho u_1 c_{1u} \varepsilon.$$

The reduction of the second expression due to the effect of a finite number of blades must be accounted for here by means of a coefficient ε in the same way as at the outlet.

Figure 309 readily gives us $c_{1u} = (\Delta c_{1m}/c_{1m}) u_1$. By considering $u_1 = u_2 d_1/d_2$ we obtain

$$\Delta p' = \mu \frac{\rho}{2} \left(\frac{\Delta c_{1m}}{c_{1m}} \right)^2 u_2^2 \left(\frac{d_1}{d_2} \right)^2 + \rho u_2^2 \frac{\Delta c_{1m}}{c_{1m}} \left(\frac{d_1}{d_2} \right)^2 \varepsilon.$$

Expressing the delivery volume of the shock free intake as V_0 and the variation compared to this quantity as ΔV , we then have $\Delta c_{1m}/c_{1m} = \Delta V/V_0$.

Thus we obtain

$$\Delta p' = \frac{\rho}{2} u_2^2 \left(\frac{d_1}{d_2} \right)^2 \left[\mu \left(\frac{\Delta V}{V_0} \right)^2 + 2\varepsilon \frac{\Delta V}{V_0} \right].$$

Expressing the pressure at normal delivery volume as

$$\Delta p = \psi (\rho/2) u_2^2$$

the gain can be easily stated:

$$\frac{\Delta p'}{\Delta p} = \frac{1}{\psi} \left(\frac{d_1}{d_2} \right)^2 \left[\mu \left(\frac{\Delta V}{V_0} \right)^2 + 2\epsilon \frac{\Delta V}{V_0} \right]. \quad (233)$$

From this equation it is obvious that a guide vane adjustment, other conditions being equal, is all the more effective the greater the expression $(1/\psi) (d_1/d_2)^2$ becomes.

These expressions has been calculated for main types, as Table 20 shows.

TABLE 20

Type	ψ	$\frac{d_1}{d_2}$	$\frac{1}{\psi} \left(\frac{d_1}{d_2} \right)^2$
High-duty blower	0.6	≈ 0.7	≈ 0.818
Radial blower, normal	1.2	0.5	0.208
Sirocco blower	2.2	0.85	0.325

This statement shows that the high-duty blowers are by far the best machines for the application of adjustable guide vanes. In actual practice, adjustments of this kind have given every satisfaction for this type of blower.

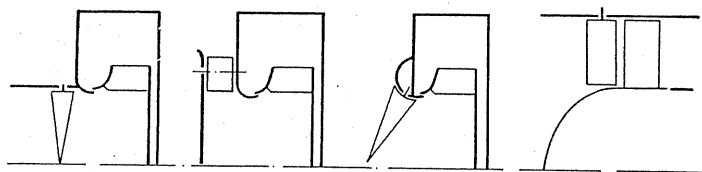


FIG.310. Different arrangements of adjustable guide vanes.

Adjustable guide vanes can be used in radial, axial, and semi-axial machines as well as for radial and for axial blowers. Figure 310 is a diagrammatic representation of these possibilities. A disadvantage in the radial arrangement is that the resistance has to be as low as possible in the zero position in order not to reduce the peak efficiency unnecessarily. However, this is only possible if the blades are not twisted. For this reason and also in order to be able to use these blades to induce counter rotation, there is no other choice available for the conventional type. The author has suggested that the disadvantage can be eliminated

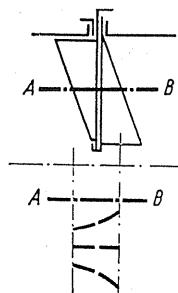


FIG.311. Guide vanes in two parts producing curved blades when adjusted.

if, as shown in Fig.311, the guide vane is made in two parts and these parts are adjusted coaxially. A straight vane can then be set in the zero position and when setting to either side of this a curved blade is always presented.

Even for unilateral arrangement of suction pockets, guide vanes can be used, as shown in Fig.312, so long as they are variably shaped due to the uneven inlet flow.

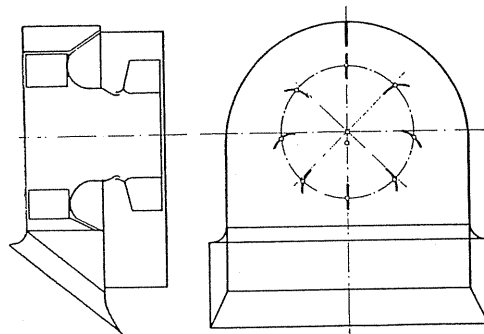


FIG.312.

One disadvantage of the adjustable upstream guide vanes is that they are fairly costly and therefore not often used. For this reason there is an interest in designs in which the applied adjustment is simple, even if not in exact form. The kinematics of adjustment becomes considerably simpler if, as suggested by the author, the adjustment is not made in a cross-section but in a longitudinal section of the pipe. The principle is represented diagrammatically in Fig.313. Rows of blades are arranged in a plane passing through the centre of the

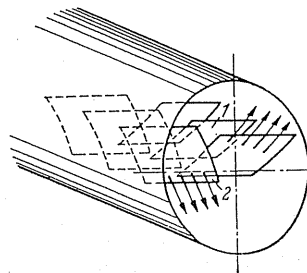


FIG.313. Imparting rotation along the duct. 1, right-hand rotation baffles directed upwards. 2, left-hand rotation baffles directed downwards.

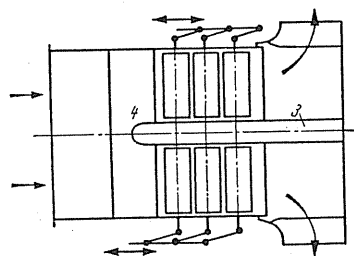


FIG.314. Baffle control mechanism according to Fig.313. 3, hub; 4, guide vane retainer.

pipe and are adjustable in series. The principle is applicable if an ample length of pipe is available. In this way mechanisms, as shown in Fig. 314, are obtained which are identical and adjustable by means of a lever. Since, according to Fig. 315 the centres of rotation are variably arranged, a staggered arrangement can be provided. The principle can also be used in more than two planes: for instance, three planes are shown in Fig. 316. According to Fig. 317 rotation can also be achieved by means of a row of blades.

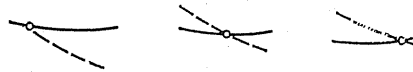


FIG. 315. Different arrangements of baffle centres of rotation.

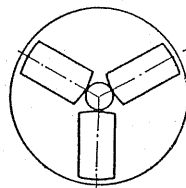


FIG. 316. Arrangements of baffles in three planes.

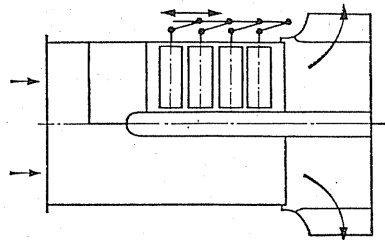


FIG. 317.

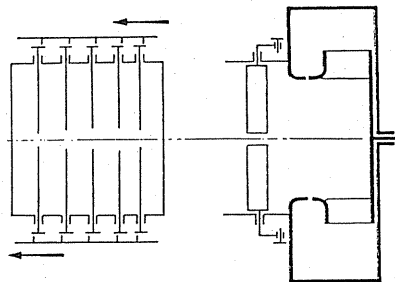


FIG. 318. Rotation produced by adjustable guide vanes in a square cross-section.

The same basic kinematic principle can also be applied in a cross-section perpendicular to the ducting if, as shown in Fig. 318, the cross-section is square or polygonal in shape.

When imparting rotation entailing a deterioration of efficiency it does not matter whether the rotation embraces all the parts of the cross-section uniformly.

There are many cases in the fields of application of fan engineering where a bend directly before the fan cannot be avoided, and it is not possible to accommodate the guide vanes

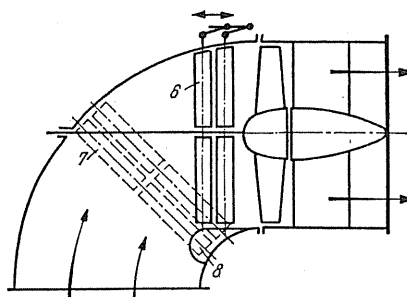


FIG.319. Arrangement of baffles in a curved duct. 6, baffles at the beginning of the curve. 7 and 8, baffles in the middle of the curve.

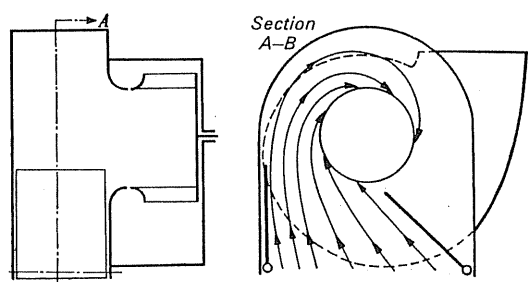


FIG.320. Imparting rotation by means of shrouded guide vanes.

previously shown. It is, of course, an attractive proposition to use the available flow in a bend for creating rotation. If the bend for instance is utilised as an inlet pocket, a rotation can be created at the periphery by means of baffles as shown in Fig. 320 since, for example, a baffle will now act as guide tongue of an improvised spiral housing. By simple means, e.g. using only two baffles, left-hand or right-hand rotation can be created.

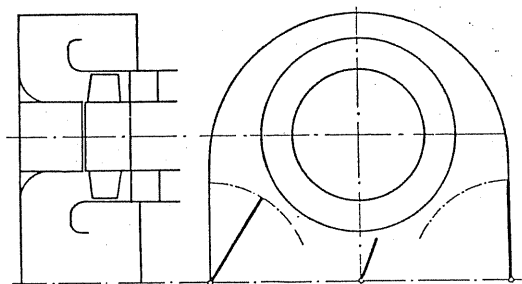


FIG.321.

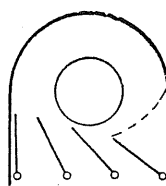


FIG.322. Imparting rotation by means of a number of baffles.

As shown in Fig. 322, by arranging several baffles which can be variably adjusted, an improvement is possible. The arrangement can be readily adapted to axial blowers as shown in Fig. 321. The principle of an adjustable guide blade, described beforehand, can also be used. This is shown in Fig. 319. There the guide vanes can be arranged directly in front of the impeller or also in the centre of the bend. A surprising effect can be achieved if, as suggested by the author, the curved guide vanes, often used for reversing with low loss, are used for imparting rotation in a right-angle bend, e.g. in Fig. 323. For this purpose the guide vanes are divided in the centre and set to enable one half to be adjusted in oppo-

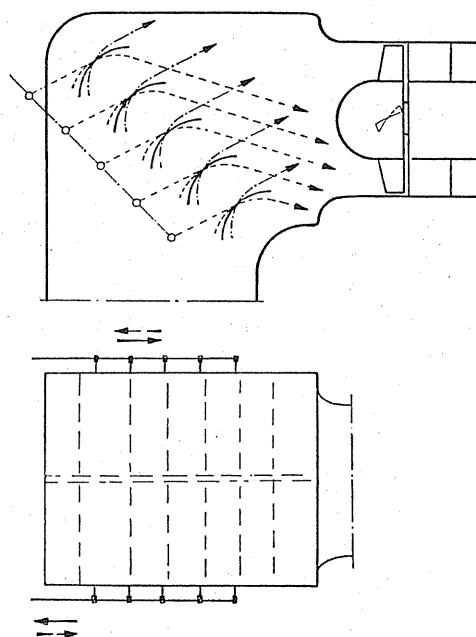


FIG. 323.

sition to the other half. This arrangement has the additional advantage that in the "zero" position there is almost no additional resistance present. Also it is often possible in existing installations to arrange this type of rotation adjustment subsequently.

What can be achieved with rotation in practice is shown in Fig. 324.

Hydraulic adjustment of rotation. Even without guide vanes adjustment can be made in a simple way if, as shown in Fig. 325, compressed air is injected into the spiral casing in the direction of the periphery through two adjustable slots.

A particular condition occurs with blades extended into the suction chamber axially. The control of rotation is particularly effective in this case. This might be due to the fact that between the guide wheel blade and the impeller blades the gap is very small. Hence formation of *vortex cores* can be prevented. This improvement, however, is only relative because these wheels have no particular suction capacity and are discarded for most purposes.

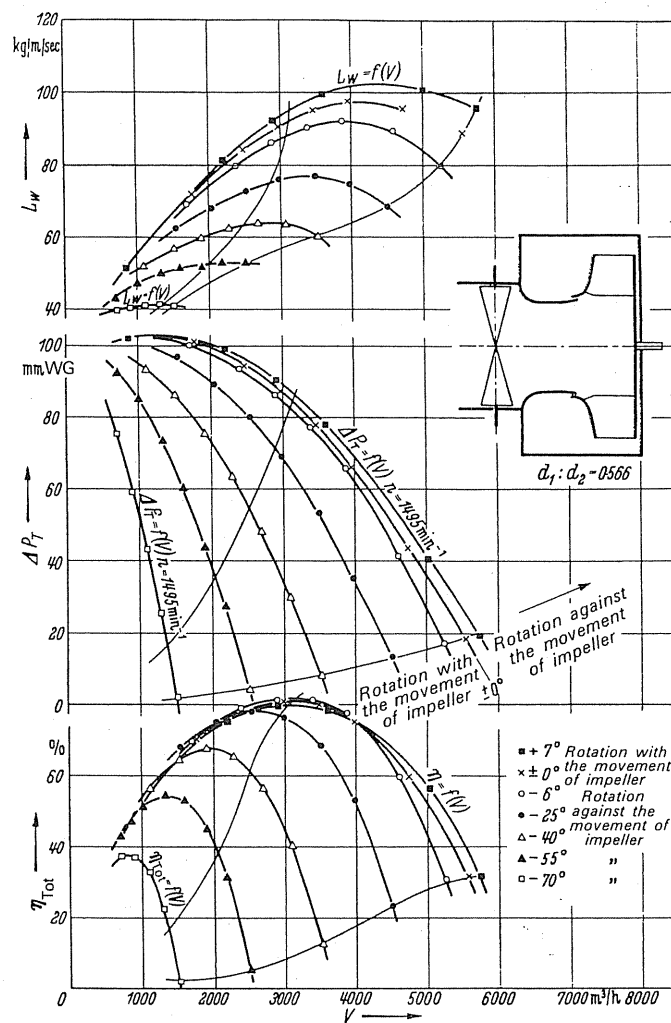


FIG. 324.

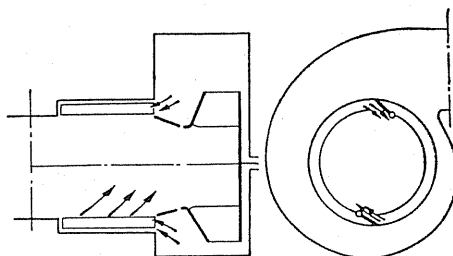


FIG. 325. Imparting peripheral rotation by means of adjustable slots.

Usefulness of inlet guide wheel adjustment in different types of fan. The effect of guide-wheel regulation for the various types of impeller differs widely. The following approximate rules can be stated. In axial-flow fans the effect depends on the pressure coefficient, at lower pressure coefficient the effect is less than with higher coefficients. The excellent effect of counter rotation at high-pressure values as shown in Figs. 295 and 297 is also remarkable.

In radial-flow fans the effect according to eqn. (233) depends very much on the diameter ratio. At very large diameter ratios of 0.9 which are, however, rarely used in practice, an astounding effective range is obtained for rotation as well as for counter-rotation with respect to the movement of the impeller. This is shown very clearly from the tests by E. Pollmann.⁽³⁾ In these tests, however, the guide vanes were arranged radially directly in front of the impeller blade. As the diameter ratio decreases, the useful range of the counter-rotation disappears steadily until ultimately *only the rotation* in the direction of the movement of the impeller is effective.

118. ADJUSTABLE BLADE TIPS

The firm of Babcock adjusts the blade tips for radial-flow fans according to Fig. 326. This measure is most effective but for reasons of strength remains limited to small impellers where the peripheral speed is not too great.

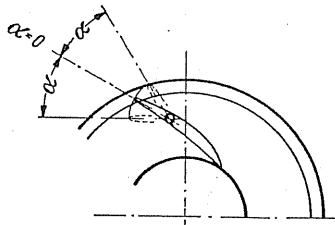


FIG. 326.

119. THE ADJUSTABLE DISC

A profound alteration of the characteristics of a radial impeller is possible if a disc passing through the blade and rotating along with the impeller is displaced in an axial direction. A portion of the impeller is cut out thereby, and no longer participates in active flow. The active portion flows past at almost constant velocity without shock. Thus it was to be expected that the impeller would require a smaller driving power for smaller delivery quantities. This is desirable, taking into consideration the relationship described above. The suggestion was first tested on a high-duty blower as has been described elsewhere.⁽⁴⁾ Figure 327 shows the result. The top curve I shows the power consumption of the fan at constant speed, *without regulation*. The effect of using the adjustable plate is shown, curve II. At about 50%

³ Pollmann, E., Calculation of fans for air-cooled motors, *MTZ*, 1951, pp. 142 and 143.

⁴ Eck, B., The adjusting base, a new control member for radial centrifugal machines, *Konstruktion*, 1955, pp. 68-72.

of the normal delivery volume *the driving power is down to half*. For comparison curve III shows the power with pure speed regulation only. For the same fan the power was also determined when only pre-rotation was controlled. So as not to make the known pre-rotation controller appear too unfavourable, a special set of correctly shaped guide vanes

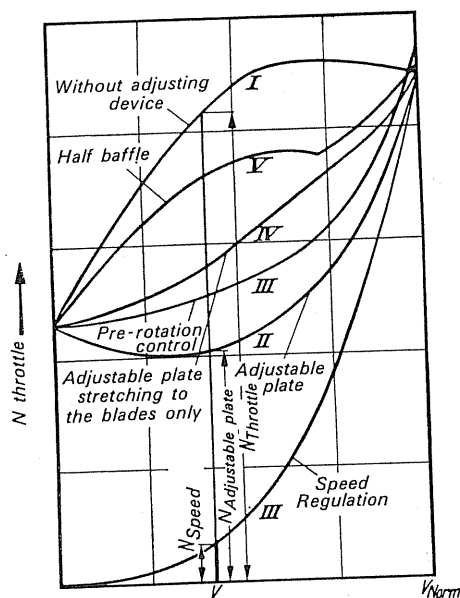


FIG.327. Power consumption with and without adjustable plate, pre-rotation, and speed control.

was used for each pre-rotation setting. Furthermore, the position and arrangement were decided upon in such a way that no vortex core could arise under any conditions. The result is plotted in curve III and Fig.329. It will be observed that the power absorption is considerably higher than in the case of the adjusting plate. It is also striking that for normal volume the power lies above the normal points. The cause of this is that the pre-rotation controller has an unavoidable residual resistance in the zero position and this reduces the peak efficiency of the fan. This disadvantage occurs in almost every other type of speed regulation. Hydraulic coupling, for instance, has a wasteful slip, whereas the adjustable electric motors have to some extent a considerably worse efficiency than squirrel-cage motors.

The effects of the adjustable disc stretching only to the blade, a design where entrainment of the disc is unnecessary (Fig.327), is shown in curve IV. The result is worse than that with the pre-rotation controller. Nevertheless, this arrangement is still worth consideration because of the low cost. Even if, as in Fig. 328, a simple semi-elliptical disc is used directly in front of the impeller for regulation purposes, there is still a certain amount of regulating effect available as shown in curve V. This arrangement is still considerably better than an ordinary throttling damper.

If the actual efficiency according to curve II is calculated when using an adjustable plate, we obtain curve III (Fig.308). It shows that the use of this device prevents the efficiency drop which occurs with other throttling devices.

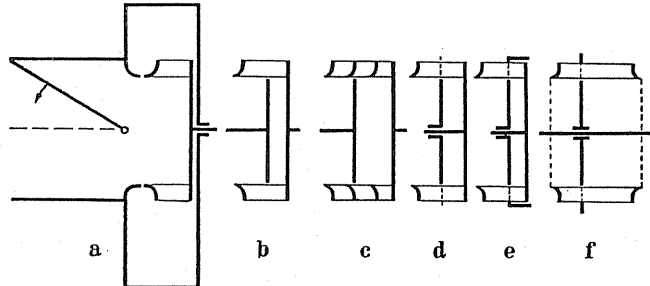


FIG.328. Various regulating devices. (a) Elliptical half-plate. (b)-(f) Various arrangements of adjustable plates.

The problem as to whether by combining the adjustable plate with pre-rotation regulation would bring about some change was answered by a test using a dust blower. At different points of the adjustable plate the pre-rotation control was fully opened. The actual power gain is shown in the shaded portion of Fig.329. With the adjustable plate fully opened, the additional control of pre-rotation has little effect. It is, however, noteworthy that by using the adjustable plate alone (bottom curve) practically all the advantages of the pre-rotation controller are realised. In comparison with the pre-rotation controller this means that the same results are achieved if the adjustable plate is moved a little more. The pre-rotation controller in this case, therefore, is of no benefit and can be omitted.

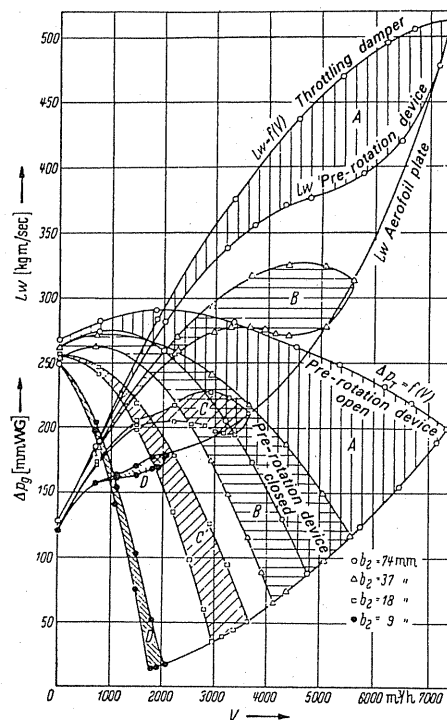


FIG.329. Power gain by means of pre-rotational control at various positions of adjustable plate.

Figure 328 presents various ways of using adjustable plates. Figure 330 represents a design from the firm Messrs. P. Pollrich where the adjustment is made automatically by means of a servo-motor. The adjustment can be made by hydraulic or pneumatic means quite easily.

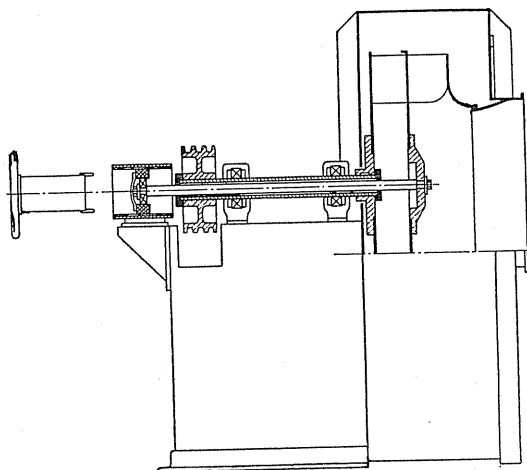


FIG. 330. Power transmission to an adjustable plate by means of a hollow shaft.

120. ADJUSTABLE GUIDE DEVICES

In view of the high cost, i.e. a 50% extra outlay, of the adjustable guide equipment, other methods have been developed. Regenscheit,⁽⁵⁾ for instance, suggests a movable guide appliance which can be used in freely discharging fans. Figure 331 shows that the guide appliance can be moved around the component *s*. In the zero position the guide appliance is firmly seated and provides full inlet rotation. If the device is moved back, it will provide a gap

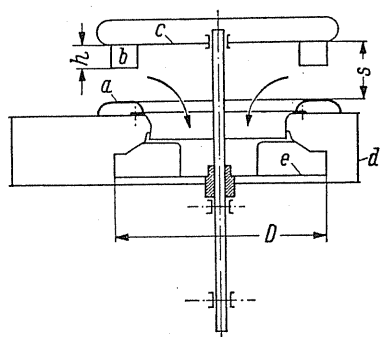


FIG. 331. Adjustable inlet guide devices (Regenscheit). *a*, housing; *b*, fixed guide vane; *c*, guide plate; *h*, guide vane depth; *e*, impeller; *s*, free intake width.

⁵ Regenscheit, B., Possibility of regulating the power saving volume flow regulation in radial-flow fans, *Heizung-Lüftung-Haustechnik*, 1957, p.317.

through which the air can enter without any rotation, whilst another part flows through the rotation appliance which is open at one end. The greater the displacement, the smaller the quantity of air which is flowing through the rotation appliance, thus producing a similar effect as in the adjustable rotation appliance.

121. CONTROL OF ROTATION

As suggested by the author, it is possible to take a step further and aim at achieving a rotational effect by simply opening one throttling damper. This problem has been solved as will be seen in a few typical examples.

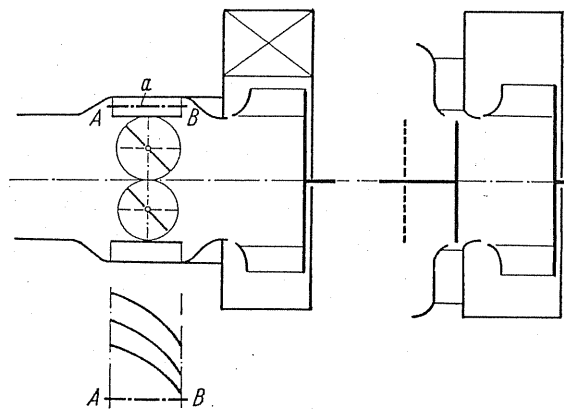


FIG. 332. *a*, fixed guide vanes.

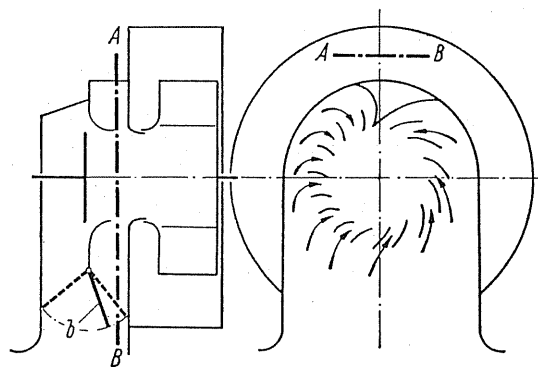


FIG. 333.

Figure 332 shows the suction duct provided with a short axial annular duct in which fixed blades are mounted for inducing rotation. In the internal cross-section there are simple throttling dampers which, to suit the space available, consist of one damper or of a flap. When the dampers are open, the air flows through the central cross-section to the fan

without any rotational effect. When the dampers are closed, air is forced through the annular ducting fitted with blades inducing rotation. The air will then enter the impeller with rotation. If the dampers are partly open, a portion can enter directly free of rotation, whilst one portion is passing through the blades inducing rotation. This causes the pressure drop through the throttling zone to become just as great as the negative pressure produced in the branch ducting through the blades inducing rotation.

Figure 332 (right) shows how the method can be used for a freely discharging fan. The fixed radial guide appliance can be used partly or wholly by means of a movable plate. When the plate is pushed out, any amount of swirl free air can be admitted.

Figure 333 shows the application to an inlet zone. By moving a single damper it is possible to regulate the flow by simultaneous movement of a plate.

122. SELF-ADJUSTMENT BY CHARACTERISTIC

Steepness of characteristic. For many practical operations the steepness of the characteristic is an important feature. For comparison, Fig. 334 shows a flat curve and a steep curve which both intersect at the same operating point. Let us consider the results of forcing a

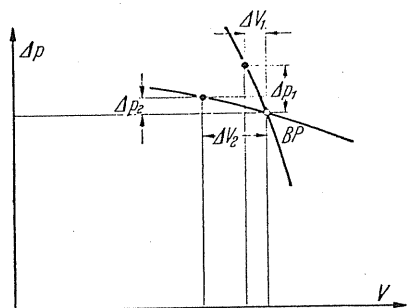


FIG. 334.

quantity of air through a liquid bath when the pressure remains fairly constant and the case when a constant quantity of gas is forced through a filter which is becoming slowly blocked up. In the first case a flat curve and in the second case a steep curve is desired because a kind of *self-adjustment* takes place under *constant pressure* and under *constant volume*. At considerable variations of volume in the first case and at wide range of pressure variations in the second case it would be possible to use a suitable fan having a constant speed without any further regulation.

It is not apparent which types of blower will give steep and which types will give flat characteristics. It is often stated that axial-flow fans present steep characteristics and radial-flow fans flat characteristics. At a first glance this statement appears to be supported by plausible evidence. It could be pointed out, of course, that in radial flow fans the purely static pressure portion remains constant, whilst this is not so in axial flow fans.

Indeed, for radial-flow fans as well as for axial-flow fans flat and steep characteristics can

be found. On looking closer into the matter it is necessary to understand the basis of a characteristic. It is a fact that, primarily, deductions must be made for finite number of blades and then other losses have to be deducted from the theoretical characteristic. According to the magnitude of these deductions and according to the position of the initial theoretical line, it is possible to obtain in practice a flat and steep characteristic.

In axial-flow fans really steep characteristics are obtained at very high pressure factors as shown, for instance, in Fig.278. The characteristics in the range shown in Fig.271 are rather less steep, namely at medium pressure factors, whereas at smaller pressure factors even flat characteristics can arise. Profiling causes flatter and plate construction leads to steeper characteristics.

In radial-flow fans still greater differences are obtained. Here there are differences due to the diameter ratio since steep characteristics are obtained with large diameter ratios, and flat characteristics arise at small diameter ratios. The variation of the width ratio also alters the slope. With improved design, i.e. higher efficiency, the characteristics become steeper. Spiral housings without guide wheels produce flatter characteristics than designs with guide wheels. The numerous characteristics illustrated in the book testify to the fact that at the present time it is very difficult to state exact rules. In individual cases, therefore, it is essential to undertake practical tests.

123. MECHANICAL AND HYDRAULIC SPEED ADJUSTMENT

There are several appliances which enable infinitely variable adjustment of power transmission to be effected. Most of them are only useful for low powers and have not the fool-proof safety which is absolutely necessary for driving fans. Hitherto devices of this kind were

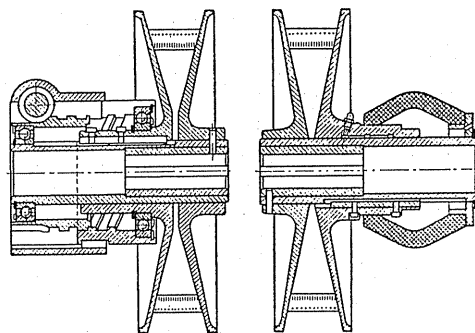


FIG.335. Speed regulation by movable V-belt drive.

rare. In one method the distance between the V-belt pulley halves can be varied. In this way the belt moves into other radii and thus alters the gearing, and in the meantime a high degree of operational safety has been achieved.

Figures 335 and 336 show a design due to the firm of Mulco in Hanover, in which a pulley is displaced by means of a worm drive whilst the other follows on and is pressed by

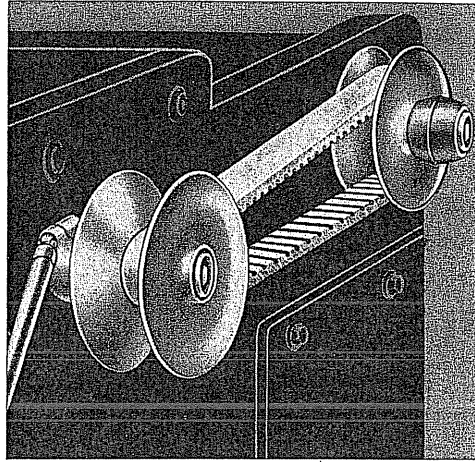


FIG. 336. Adjustable belt drive.

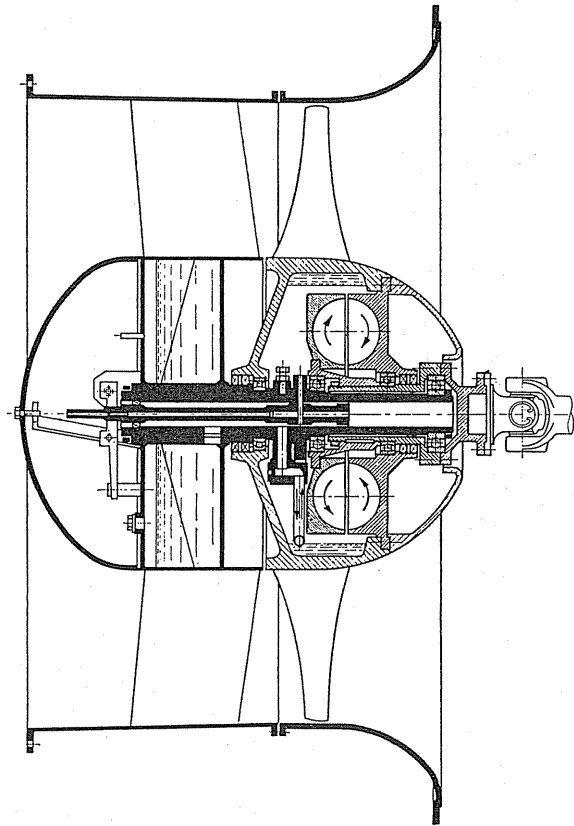


FIG. 337. Hydraulic coupling for axial-flow fans.

a rubber spring. Infinitely variable regulation 1:9 and power transmissions up to 10 hp are possible.

Voith hydraulic coupling for continuous speed regulation. The Voith hydraulic coupling is a flow coupling based on the Föttinger principle. It transfers the torque to the driven shaft by means of a liquid. Oil is used for transfer of momentum and it circulates between a centrifugal pump impeller mounted on the primary shaft and the turbine wheel mounted on the secondary shaft.

The speed is varied continuously by varying the volume of liquid circulating in the coupling by means of an electrically driven pump. The control range is about 4:1 (Fig. 337).

The oil is ejected from the working circuit constantly through nozzles into the outer coupling casing. A ring of oil is formed in that casing due to centrifugal forces and a fixed scoop pipe is dipped in the ring. The velocity head drives the oil, a thin mineral oil, through a distributor. The oil flows outwards and returns into the working circuit.

For removal of heat caused by slip if there is insufficient self-cooling, the oil is pumped through a cooler.

Primary and secondary parts of the hydraulic coupling are supported in opposition axially and radially by roller bearings, so that the hydraulic axial thrust does not act outwards. The motor coupling flange connects the primary portions with the motor and a rather flexible Voith-Maurer coupling, which is adjustable longitudinally, connects the secondary

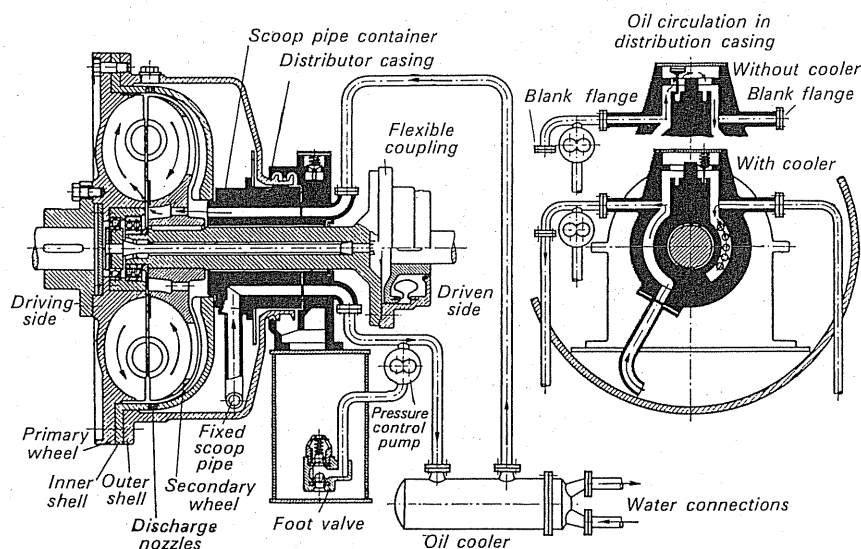


FIG. 338. Voith hydraulic coupling.

portion with the shaft of the driven machine (Fig. 338). These Voith controllers are an essential complement for axial rotors which have also been designed by this firm in many different well-known forms. The modern design is shown in Fig. 339.

The efficiency of the hydraulic coupling is taken as the ratio of output to input power. Further, this efficiency for the same torque on the input and output sides in the whole speed range, is equal to the ratio of the driven speed to the driving speed, $\eta = n_2/n_1$.

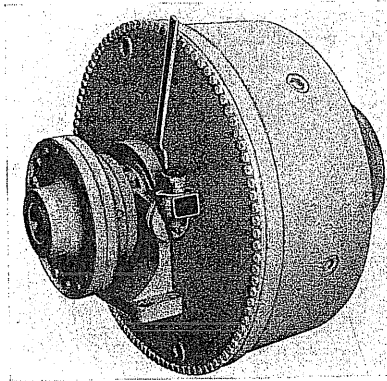


FIG. 339. Voith hydraulic coupling.

124. GEARS

Gear units are increasing in importance in fan engineering. Since these gears can be built for safe operation and with low losses for high outputs, gears can be used for long-term control of high-duty blowers if, for instance, the sets of gears are made interchangeable. In mine fans with long-term variation due to new openings, gears of this type have worked well. Reversible gears also, which are adjusted during stoppages, are very interesting propositions. Figure 340 shows one of the designs by Voith.

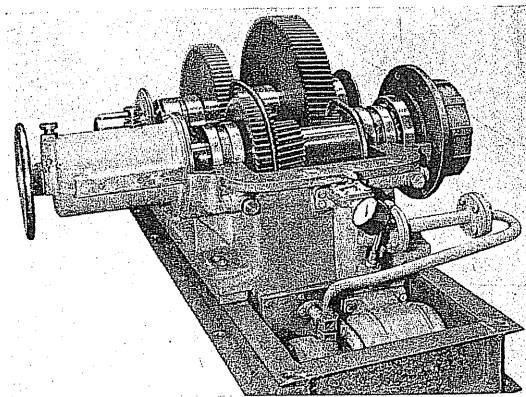


FIG. 340. Voith gearbox.

Recently, planet gears have also been coming to the fore, especially in combination with the Stöckicht gear. This is a gear with hydrostatic superimposed control. The internal pinion of a planet gear drives the fan shaft through the planet wheel. The external sun wheel is stationary at normal speed. The sun wheel is able to turn in both directions through the intermediary of a gear annulus. It is driven by an oil engine. This engine is powered by an oil-pump driven by an electric motor. In this way it is possible to reduce or increase the

speed constantly, allowing the main motor to retain its speed and its basic power throughout and thus always to work at optimum efficiency.

A remarkably large unit of a ventilator propeller of immense size was recently fitted with this gear.⁽⁶⁾

125. RELATIONSHIP DUE TO THE SPEED VARIATION

How do the pressure, delivery volume, and power alter when the speed is varied? This is an interesting problem in speed control. In tests one is often obliged to compensate for small speed variations.

Operating conditions similar to these will now be examined. In this problem it is understood that similar velocity triangles occur at variable speeds. The percentage effect of impact losses, etc., will then be the same. All points with an intake free of shock losses in particular should present similar velocity diagram.

Since the peripheral velocity is proportional to the speed and the other velocities alter in the same ratio, it can then be said that all velocities vary in proportion to the speed.

$$\frac{c_{2u}^I}{c_{2u}^{II}} = \frac{n_I}{n_{II}} = \frac{c_{2m}^I}{c_{2m}^{II}} = \dots \quad (234)$$

The volume of air delivered is proportional to c_{2m} which leads to the following linear dependency on the speed for the delivery volume.

If, for instance, the speed varies by 2%, the delivery volume also varies by 2%

$$\frac{V_I}{V_{II}} = \frac{n_I}{n_{II}}. \quad (235)$$

The pressure according to the formula $\Delta p = \psi (\varrho/2) u_2^2$ is proportional to the square of the peripheral velocity and therefore also of the speed.

$$\frac{\Delta p_I}{\Delta p_{II}} = \left(\frac{n_I}{n_{II}} \right)^2. \quad (236)$$

Hence if the speed varies by 2%, the pressure will actually vary by 4%.

As the variation of pressure and volume is known, each point of a characteristic can be transferred to the corresponding point of a different speed. If a characteristic is known, the characteristic for every other speed can be calculated. (The only limitation to this rule is that a number of sources of loss do not increase exactly with the square of the velocity.)

Substituting from eqn. (235) n_I/n_{II} in eqn. (236) we obtain

$$\frac{\Delta p_I}{\Delta p_{II}} = \left(\frac{V_I}{V_{II}} \right)^2; \quad \Delta p_I = \Delta p_{II} \left(\frac{V_I}{V_{II}} \right)^2. \quad (236a)$$

By means of this equation all points of the same shock state are connected together, i.e. with similar velocity triangles. A parabola is obtained. Starting from a different point of

⁶ Schmiederer, B., Fan propellers for large cooling towers, *VDI-Nachr.*, 1960, No.35.

the characteristic a different parabola is obtained and so the converted characteristics and this family of parabolas represent a comprehensive picture of the operating conditions at all speeds. Figure 341 is a diagram of this kind. The points of equal efficiency are joined by curves. They show up as ellipsoidal curves which indicate the contour lines of the "efficiency" peaks. The "highest" point (in Fig. 341) is representative of the optimum efficiency

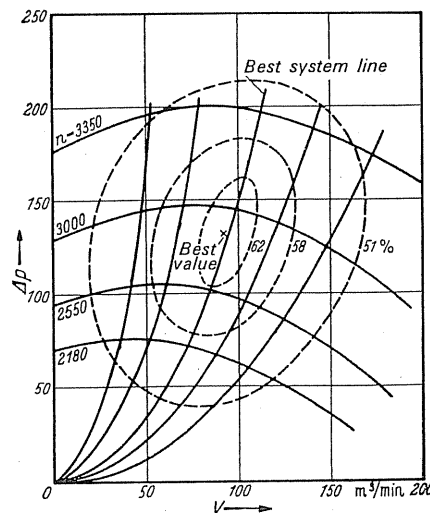


FIG. 341. Fan characteristics at various speeds; including system curves for different resistances and efficiency curves.

of the fan. It is often observed that the ellipsoidal curves remain open at the top which often shows up very prominently in the analysis. The course of these curves depends greatly on the rules according to which the losses vary with the variation of the speed. At the moment it is not possible to express the curves in Fig. 341 by precise mathematical expressions.

The power of the fan which is proportional to the driving power can be represented by $N = V \Delta p / 75$ (hp). Since V varies with the first power of the speed and Δp with the square of the speed, then N must vary with the cube of the speed.

$$\frac{N_I}{N_{II}} = \left(\frac{n_I}{n_{II}} \right)^3. \quad (237)$$

If, for instance, the speed varies by 2%, then the driving power varies by 6%. Due to the large increase of driving power with speed, it is, on the one hand, impossible to achieve excessive speeds when the machine is driven through a series wound motor. On the other hand, at low speeds the power will be extremely small, thus presenting very favourable conditions for the prime movers of the fan.

For the torque the following formula applies:

$$\frac{M_I}{M_{II}} = \left(\frac{n_I}{n_{II}} \right)^2. \quad (238)$$

126. LOGARITHMIC REPRESENTATION OF THE CHARACTERISTICS

Different auxiliary curves which are essential for assessing the fan characteristics have power functions. For instance, the throttling curves are simple parabolas, the curves for shaft power are parabolas of the third order. If the characteristics are plotted on log-log graph paper, the throttling characteristics appear as straight lines of gradient 2:1, whereas the power curves are straight lines of gradient 3:1. The characteristics for different speeds are now, however, identical curves, which only must be shifted along the lines of the equivalent throttling state in the direction of these straight lines, i.e. 2:1. The whole effective range of the fan can thus be embraced in a single curve as otherwise only straight lines

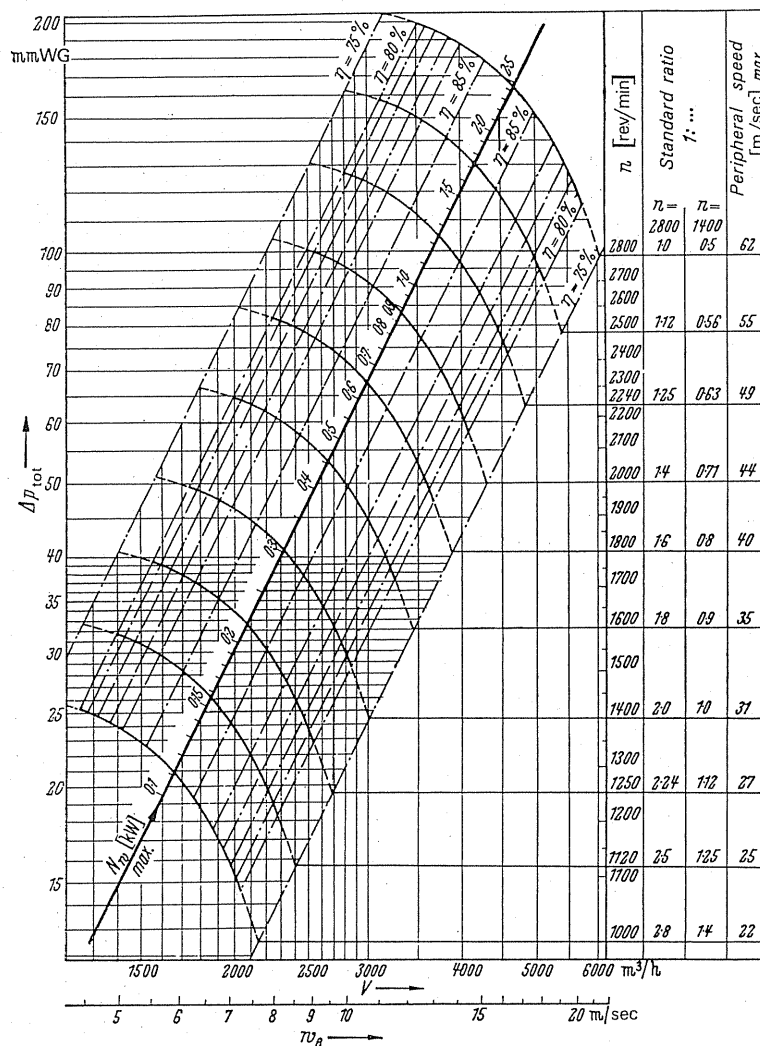


FIG. 342. Performance curves of fans. P. Pollrich-Werke, Mönchen-Gladbach.

would arise. Here it is unimportant that in a logarithmic representation zero values are infinite. If, furthermore, the highest shaft power lies in the region of the optimum efficiency, which should be the aim for efficient fans, the plotting of this curve can be dispensed with altogether. On a straight line along the shock state of the optimum efficiency only the shaft powers need be stated in figures. In this way the relatively smaller variations of efficiency along the curves of equivalent shock state are dispensed with. This gives us a fan chart which really contains all values of importance for any range of speed. Figure 342 is a chart of this kind. Apart from the suction volume V a scale for inlet velocity is available. The standard speeds, the standard gear ratios, and the peripheral velocities are included as ordinates along with the total pressure.

Standard values for practical use in dividing up ranges of types can be found in Rüttschi's⁽⁷⁾ work.

⁷ Rüttschi, K., Standardisation of turbine machines, *Schweiz. Bauztg.*, 1947, No.4.

CHAPTER XVI

FANS AND DRIVING MACHINES

127. GENERAL PRINCIPLES

In all previous investigations it has always been assumed that *the speed of the blower remains constant*. The characteristics are based on this condition and represent the simplest and most practical representation of the characteristics of a fan. However, in practice, the condition of equal speeds has never been quite fulfilled, for, strictly speaking, no prime mover exists which retains exactly the identical speed at varying loads nor even when it is a matter of slight deviations of 1–2% from a given speed. According to the character of the prime mover, speed fluctuations are extremely varied. In particular, *prime movers are desirable whose speed can be adjusted within wide limits* in order to take into account any call for regulation of an installation. Of course, variations which arise in the characteristics are significant if the speed of the prime mover varies. The effects on the fan characteristics are often so profound that it is inevitable that attention is given to these factors.

General rules. In order to make accurate calculations in every case, the relations between fan and prime mover must be considered.

The two main rules:

(1) *The torque of the prime mover in every case is exactly identical with the torque of the fan.* The state and the speed at which this condition is fulfilled is set automatically. The torque of the fan is easily obtained from the power consumption curve at constant speed.

Since $L = M\pi n/30$, the torque M at constant n is always proportional to the power L . By varying the scale therefore, curve $M = f(V)$ can easily be obtained.

What pressure and what delivery volume will be set? If—as is assumed at present—the throttling state of the duct system remains unchanged, the relationship Δp proportional to V^2 , the case can be represented easily by means of a parabola. Previously we had found that the point of intersection of this parabola with the characteristic represents the operating point. Since any other measures on the fan or on the prime mover have no effect on the throttling condition of the ducting, the following law applies.

(2) For all alterations on the prime mover (for instance by engaging the resistance) or the fan (for instance guide or impeller blade adjustment) the throttling parabola remains unaltered and one point of this parabola (or the necessary band) is *always* retained as the operating point.

Equations (234)–(238) demonstrate how volume, pressure, power, and torque vary with change of speed.

128. DRIVE BY ELECTRIC MOTORS

There are two important questions:

- (1) Which characteristic applies if the prime mover alters its speed automatically at load and the unit is left to itself?
- (2) What characteristics arise if some sort of regulation is undertaken on the prime mover? How big in particular are the resultant savings compared to regulation by throttling alone?

In order to reply to these questions the curve $M = f(n)$ for different control settings must be known for each prime mover. For the main types of electric motor the following curves are given.⁽¹⁾ In Fig. 343 four different d.c. shunt motors with circuits are shown, and in Fig. 344 five different three-phase motors. The d.c. main series motor favoured for small units has almost the same characteristics as the three-phase motor with armature regulation (Fig. 344) and therefore does not need to be illustrated specially. The type illustrations contain the $M = f(n)$ curves for equivalent control setting. The blower torque is indicated in each illustration. The curve $M = f(n)$ (for equivalent throttling conditions) was accepted above as a parabola.

Two different heating limits are noted:

(1) **Heating limit for self-cooling.** Here a limit is quickly reached because at a lower speed the cooling fan of the motor is ultimately no longer up to its job as its delivery volume of course falls proportional to the speed.

(2) **Heating limit for outside cooling.** In this case the driving motor is cooled by a separate fan which is not driven by the prime mover. The fan power remains constant and can even be increased; thus at lower speeds the machine can take on an extended duty as will be observed from the curves.

At a mains frequency of 50 c/s standard values for slip asynchronous motors have the following speeds for different pole numbers (see Table 21).

TABLE 21

Pole pairs	1	2	3	4	5	6	7	8
Speed	2940	1470	980	730	580	485	418	360

The electric motor drive. What is important for economical running of a fan is that its operating point lies in the proximity of its optimum efficiency as well as in the proximity of the full load efficiency of the electric motor.

For the buyer of the fan unit it is highly important to know the precise electrical data of the driving motor. The fan efficiency can be reduced considerably by using an unsuitable driving motor.

¹ Taken from Schmidt, O., Fan drives by electric motor, *Arch. Wärmewirtsch.*, 1940, p.111. See also Müller, A., Projecting and operating performance of fans for steam boilers, Diss., Zürich, 1935.

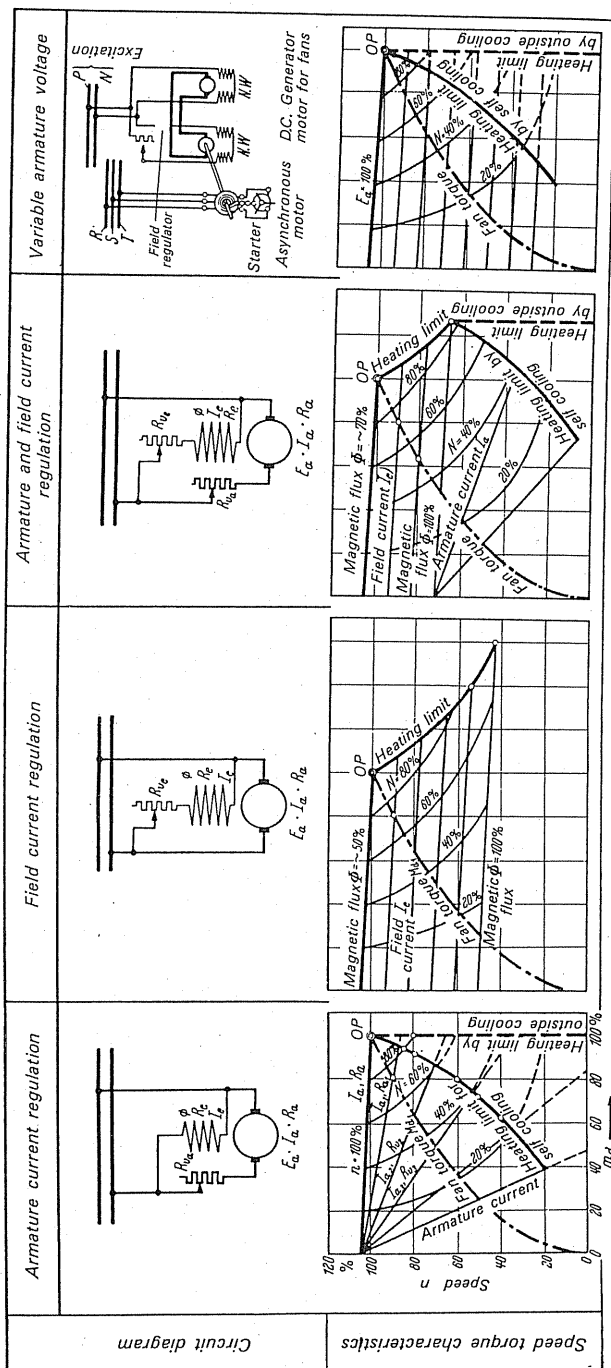


FIG. 343. Characteristics of d.c. shunt motors.

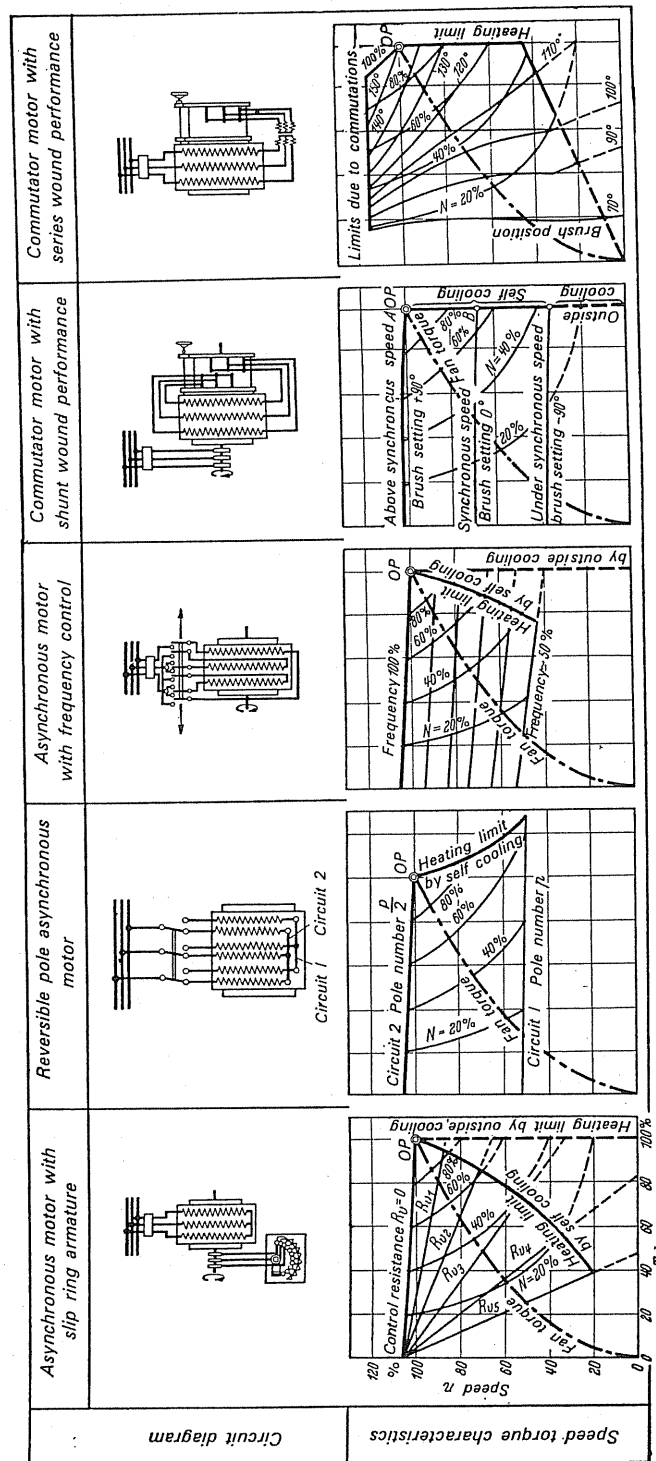


Fig. 344. Characteristics of three-phase induction motors.

The efficiency of a three-phase motor remains approximately constant over a wide range so that at half full load efficiency is still maintained. This is an advantage because the fan drive, for safety reasons, often cannot be fully loaded.

For the efficiency of the motors two typical divisions in respect of the course of the torque curve according to type are given.

Group 1. Motors where the current heat losses preponderate in the windings as a function of the load.

Group 2. Motors where the core, friction and air frictional losses preponderate as losses independent of load.

The torque curve of the two divisions will be observed from the diagram which follows.

With motors of group 1 the efficiency after initially falling below the nominal load still remains fairly constant or even rises a little (at about three-quarters load) and then drops again.

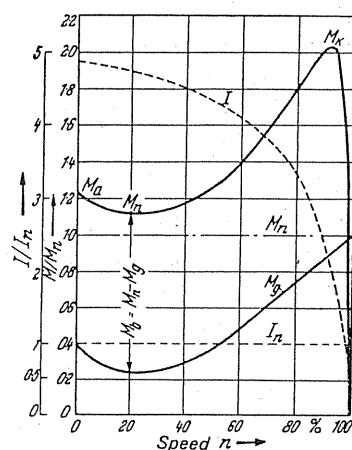


FIG. 345. Current and torque curves.

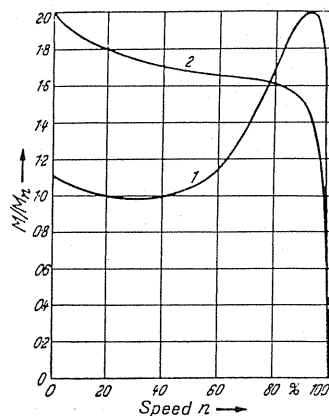


FIG. 346. Torque-speed curves of electric motors.

For motors of group 2, the efficiency curve drops steeply after falling below nominal load. The torque of commercial three-phase motors follows a course which meets the starting conditions occurring in operation. Blowers and fans require a rising torque towards the end of the starting period, whilst the starting torque may be small. Different types of torques emerge for the course of the torque curve.

Nominal torque	M_n (Motor torque)
Starting torque	M_a (Switching on torque)
High speed torque	M_h (Lowest "saddle" torque)
Breakdown torque	M_k (Maximum running torque)
Counter torque	M_g (The torque of the prime mover counteracting the motor)
Acceleration torque	M_b ($M_b = M_n - M_g$)

The current and torque curves are shown in Fig. 345.

The torque curve can be influenced by the type of motors: for bar-wound rotors, differentiation is made between motors with double-groove rotors and squirrel-cage rotors with double groove. In single-phase capacitance motors every increase of the starting torque at constant starting current is accompanied by diminishing of the breakdown torque and of the power factor.

Figure 346 shows in curve 1 the torque of a motor with a bar-wound rotor. If the starting torque according to curve 2 is raised to about double, the course of the torque alters very characteristically. The torque drops during the start-up, and thus the power factor also drops from $\cos \varphi = 0.90$ to $\cos \varphi = 0.86$.

Motors with a torque as shown in curve 2 are unsuitable for centrifugal machines where the counter-torque rises fully with the speed.

Asynchronous or synchronous motor? In fans, the asynchronous motor is mainly used. Its characteristic not to overload the network with too high a starting current, its capacity to accelerate under a very large working load, and its speed control capacity are very valuable characteristics. On the other hand, the synchronous motor was very late in being introduced in Europe; later than in the United States. The efficiency is better; there are almost no core losses in the rotor. It returns idle power back to the network and so can improve the overall power factor of the network. For powers of 1000 kW, which of course rarely occur in fan engineering, synchronous motors are preferable.

If possible, short-circuit rotors should be used for drives. If there is no need for speed regulation, which is available especially in slip-ring rotors, then the squirrel-cage rotor is *the standard drive of a fan*. Its efficiency is higher and its price is considerably lower than that of the adjustable motors. The worst starting properties formerly present have been alleviated considerably by the introduction of the *bar-wound rotor*, *high-bar rotor*, or the *double squirrel-cage rotor*. The efficiencies of the short circuit motors are about 5–10% above the values of other adjustable motors. A short circuit rotor of 7.5 kW, for example, has an efficiency of 86% at 1500 rev/min.

The following methods are available for varying the speed.

- (1) Engaging resistances in the rotor circuit (slip variation).
- (2) Pole reversal.

- (3) Alteration of mains frequency (squirrel-cage rotor is infinitely variable in speed by means of the frequency generator).
- (4) Combination of these methods.
- (5) Regulation with asynchronous coupling.

In variable-pole motors only specific speeds can be achieved as a function of frequency and pole number.

Slip-ring rotors are controlled in speed by means of control starters. In many cases slip-ring rotors present a useful solution.

Combinations for fan drives in particular have become interesting propositions.

Fan motors with squirrel-cage rotors, which can be regulated in several stages, are made by H. Buchele, Nürnberg. These fan motors, which are adjustable in stages compared to the full reversible or slip-ring rotor types, are of less in size and weight (weight saving up to 60%). When connecting up, the final speed is engaged in stages. These motors are available up to 20 kW.

In larger motors the desired speed variation can be achieved by sets of controls. The following methods are possible.

(a) **Krämer circuit.** Here a portion of the three-phase power is supplied to the main motor direct. The remainder, the proportion of which depends on the speed, passes via a rotor into a single-core transformer at reduced frequency and is then converted into d.c. This d.c. passes in an additional motor which is coupled to the main motor. In this way the speed can be varied within wide limits using the field regulator.

(b) Alternatively, this additional motor acts as a frequency converter which converts the rotor frequency into the mains frequency.

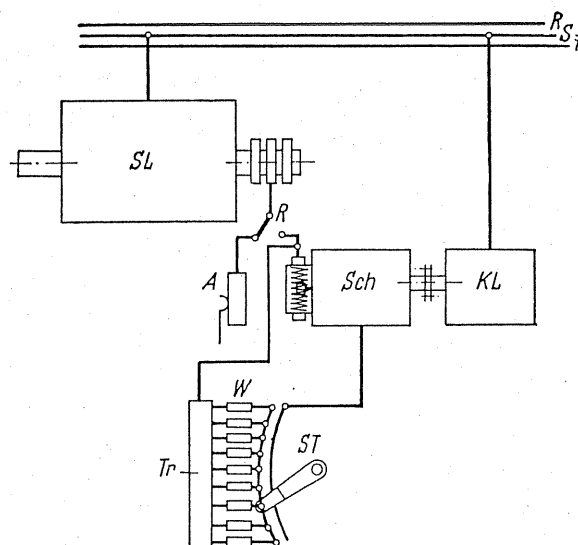


FIG. 347. Diagram of motor switch circuit according to Scherbius.

(c) **Scherbius motor by BBC.** By replacing the frequency convertor by a series machine the rotor power dissipated in regulation is transformed into mechanical power or returned to the network by a synchronous motor. This method has proved very satisfactory for some time when applied to control of high-duty mine fans.

The machines and appliances required for this purpose are illustrated in Fig. 347 (contributed by the kindness of Dipl. Ing. Reiss, BBC).

After the slip-ring rotor *SL* is started up in the usual manner with the starter *A*, the machine set consisting of Scherbius machine and squirrel-cage rotor motor *KL* acting as the driving motor is switched over by the rotor switch *R* to the rotor circuit of the slip-ring rotor. The speed is adjusted by means of the stepped switch *ST*. According to the position of the step-switch it is possible to vary the excitation of the Scherbius machine and in this way to supply a variable voltage with rotor frequency to the slip rings of the main motor. According to the magnitude of this control voltage and of the rotor voltage of the slip-ring rotor, a corresponding speed is achieved.

Speed controlled by asynchronous coupling. Recently success has been achieved in carrying out by electrical means the task which the Voith coupling does by hydraulic means. The firm O. Sager AG, Zürich, has developed electrical couplings without slip rings which are able to regulate down to zero, constructed for powers of up to 200 kW.

External rotor motors. For different applications of the Kelin fan design the external rotor motor has proved its worth. It has been found that a high power factor can be achieved by correct sizing and, moreover, the engaging current for star delta starting can be kept very low.⁽²⁾ The speed of these motors can be varied within wide limits by means of transformer, resistance, or step switch.

Shaded-pole motors. For driving miniature fans—below about 20 W—the shaded-pole gap motor is very useful. This is a single-phase motor working on the Ferraris principle. One or more blind short-circuit windings generate the necessary phase displacement for attaining the rotating field. They are wound round a portion of the pole. Disadvantages are the low efficiency and the low-power factor together with the dependency of the characteristic on the accuracy in manufacture. Nevertheless, its robust construction, low price, and safety in working has won for it the market for miniature fans.

129. STEAM-TURBINE DRIVE

Steam turbines are often used as prime movers. In the simplest case of a single-stage pressure turbine a speed characteristic is shown in Fig. 348.⁽³⁾

If the control is by shut-down the steam throughput remains constant. Figure 348 shows the curves for various control positions. In the range of higher steam throughput volumes the torque increases considerably at low speeds, so accordingly in coupling to a fan profound alterations may be expected.

² Axial-flow fans with outside rotor motor, *Heizung-Lüftung-Haustechnik*, 1956, p. 89.

³ From Gramberg, *Maschinenuntersuchungen*, 3rd edn., Berlin, Springer, 1924.

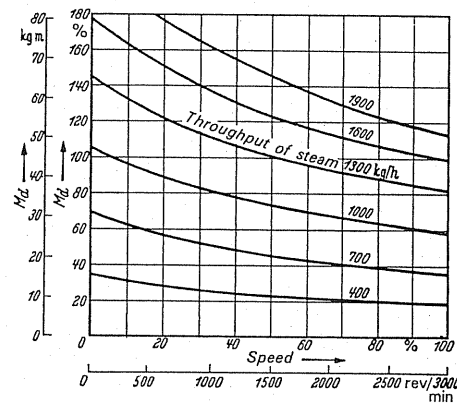
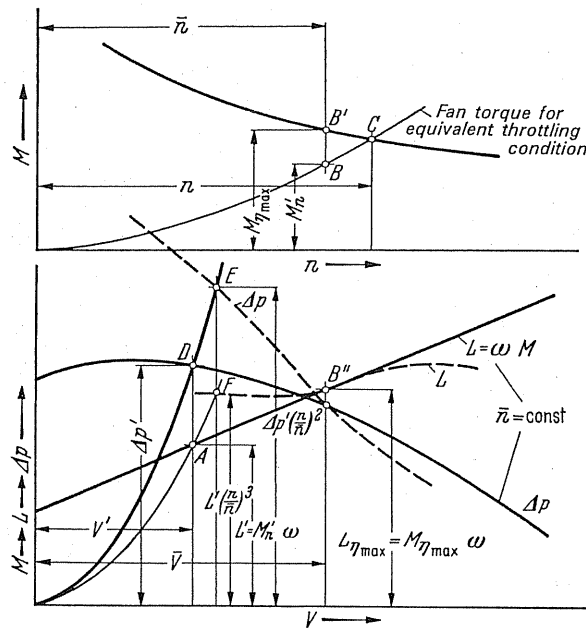


FIG.348. Torque curves for impulse steam-turbine.

130. DETERMINATION OF CHARACTERISTIC AT CONSTANT SETTING OF THE PRIME MOVER

It is intended to show by a few practical examples how in a given case the altered characteristic can be plotted. In the bottom portion of Fig.349 we have the characteristic and power requirement for $n = \text{const}$. Above this for one position of the driving motor the $M = f(n)$ curve is plotted. At \bar{n} and \bar{V} we have the point of optimum efficiency and therefore the point B' corresponds to point B'' . The torque for the point of optimum efficiency

FIG.349. Graphical method for determining the blower characteristic of the prime mover at a given M/n curve.

is proportional to the distance lying below B'' and corresponds to the torque at B' . For points A or D we shall follow up the reconstruction. The torque in B' is reduced in the ratio $M'_n/M_{n\max}$. Thus we obtain the point B . The parabola of equivalent throttling condition is drawn through B and meets the torque line in C . The speed available at C corresponds to the new speed of the former operating point A , thus we obtain a new power $L' (n/\bar{n})^3$ and a new pressure $\Delta p' (n/\bar{n})^2$. The levels of these quantities are cut by a parabola passing through D or by a cubic parabola passing through A at points E and F . E is a point of the new characteristic and F a new point of the power-demand curve. This method is followed for numerous points, and the new characteristics are thus obtained.

In the second example shown in Fig. 350 a characteristic with an S-loop was selected such as is present for example in inclined blade blowers. The method compared to Fig. 349 is simplified by the fact that the torque curve of the motor is plotted into the chart directly and the starting point of its coordinates is moved right into the centre of the field. Since

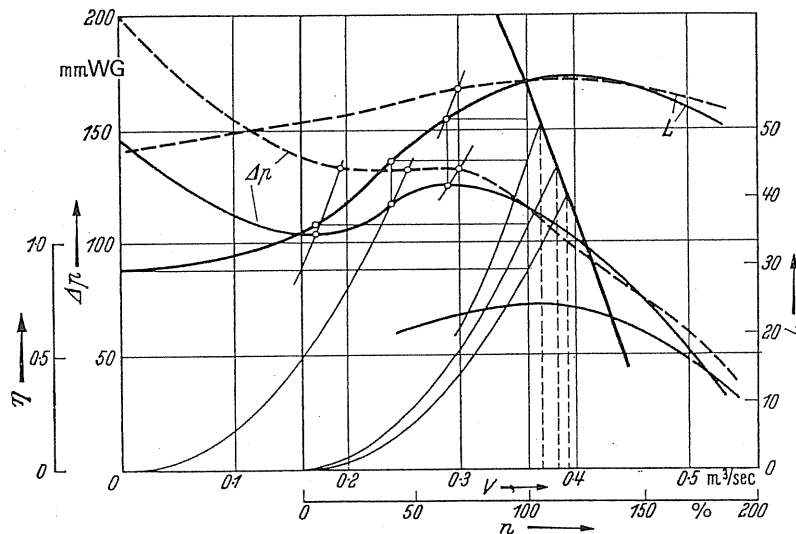


FIG. 350. The effects of the motor on a blower with S-shaped characteristics.

there is no obligation to have the two abscissa-zero points coincide, it is possible to use this freedom for obtaining some conveniences in drawing. Otherwise the plotting of the graph is analogous to the above example.

In both cases the maximum of the characteristic has disappeared altogether. With the steep power-demand curve of the first case (for instance in radial-tipped blades) the modification is more profound than in the second. Where the power demand alters less, right down to zero delivery volume, the overall modifications are so far-reaching in both cases that an accurate construction of the new characteristic may be essential for a given application.

Typical test results are shown in Fig. 351. This refers to a small starting blower which is driven by a universally used motor with main current characteristics. When the speed rises

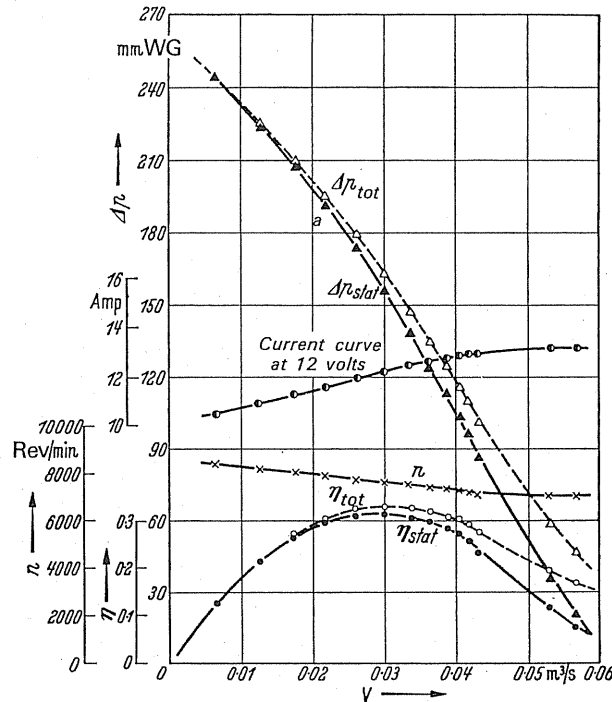


FIG.351. Characteristic for blowers driven by universal motors at various speeds (η_{stat} should be replaced by ϵ_{stat}).

as the volume diminishes, we obtain a characteristic of extreme steepness as may be seen in the graph. In this case the speed increase only comes within the order of magnitude of about 15%.

131. STARTING AN ELECTRIC MOTOR FOR DIRECT DRIVE

When starting an electric motor the demand is made that the motor should run up to full power within a certain starting period t_a , i.e. a maximum value of t_a should not be exceeded in order to avoid undesirable overheating. The motor in this period must be able to accelerate or overcome its own inertia, the inertia of the prime mover as well as its counter torque due to the air delivery.

The existing motor characteristic $M_d = f(n)$ represents the acceleration torque M_{bm1} actually available, the area below the characteristic being the corresponding acceleration power. In the same diagram the torque characteristic of the prime mover increases from the point $n = 0$, $M_d = M_R$ (M_R represents the frictional allowance of $x\%$) quadratically and intersects the motor characteristic at the operating point. Similarly, the area below the latter-named curve represents the acceleration power required by the prime mover. The difference between both areas thus gives the acceleration power available for overcoming the motor and the prime mover masses.

From the areas of the rectangles of the width n_0 (synchronous speed) and of height M_{bm1} , M_{bm2} and $M_{bm} = M_{bm1} - M_{bm2}$ can be obtained. The mean acceleration torque M_{bm} defined thus is the basis for the calculation, i.e. of the time required for accelerating the inertial masses (Fig. 352).

The mathematical procedure is as follows.

(1) **Rough determination of motor size. Power of prime mover**

$$N_{n2} = \frac{V_h \Delta p_t}{102 \times 3600}; \quad N_w = \frac{N_{n2}}{\eta_{tot} \eta_K}.$$

Choice of motor size.

(2) **Determination of nominal torque of motor.**

$$M_{dnom} = 974 \frac{N_{n1}}{n_n}.$$

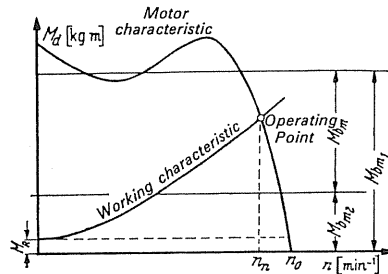


FIG. 352. Determination of power consumption of a motor during acceleration.

(3) **Calculation of prime mover characteristic.** By graphical methods between points

$$n = n_{nom}; \quad M_d = M_{dnom} \quad \text{and} \quad n = 0; \quad M_d = M_R.$$

(4) **Determination of M_{bm1} .** The overall area below the motor characteristic is determined by Simpson's rule, and from this a rectangle of equivalent area is formed with the base line $n = n_0$ and the height M_{bm1} .

(5) **Determination of M_{bm2} .** Determination of the overall area below the prime mover characteristic and determination of M_{bm2} analogous to remarks under (4).

(6) **Determination of M_{bm} .** $M_{bm} = M_{bm1} - M_{bm2}$.

(7) **Reduction of the masses of the prime mover on the motor shaft.**

$$J_m 4g = GD^2$$

$$GD_{II}^2 \text{ related to shaft I} = GD_{IIaI}^2$$

$$GD_{IIaI}^2 = GD_{II}^2 \left(\frac{n_{II}}{n_I} \right)^2.$$

(8) **Determination of the overall masses.** GD^2 = motor plus work machine related to motor shaft.

$$GD^2 = GD_1^2 + GD_2^2 \left(\frac{n_{II}}{n_I} \right)^2.$$

(9) **Checking the starting period.** The starting time is calculated according to the formula

$$t_a = \frac{GD^2 n_n}{375 \times M_{bm}}.$$

The value thus calculated must not exceed a given maximums; if it does, the motor selected at direct engagement cannot be used as a drive.

Designations:

Symbol I.1: Drive motor

N_{n1} [kW] Nominal power

n_n [min^{-1}] Nominal speed

M_{bm1} [kgm] Mean acceleration torque

GD^2 [kgm^2] Moment of inertia

t_a [sec] Starting time

Symbol II.2: Work machine

N_m [kW] Theor. power work machine

N_w [kW] Shaft power of work machine

V_h [m^3/h] Delivery volume

Δp_t [mm WG] Total pressure

η_{tot} Overall efficiency

η_K V-belt efficiency

M_{bm1} [kgm] Mean drive torque

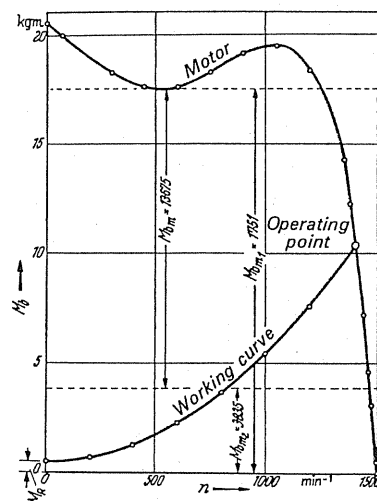


FIG. 353. Numerical example of accelerating torque of electric motor.

Example: Fan type 26090 (Fig. 353).

$V_h = 55,000 \text{ m}^3/\text{h}$, $\Delta p_t = 80 \text{ mm WG}$, $J_m = 8 \text{ kg m sec}^2$.

From test: $\eta_{tot} = 0.85$, $\eta_K = 0.95$, $n_{II} = 700 \text{ min}^{-1}$.

(1) Fan power. $N_{n2} = \frac{55,000 \times 80}{102 \times 3600} = 11.98 \text{ kW}.$

$$N_w = \frac{11.98}{0.85 \times 0.95} = 14.84 \text{ kW}.$$

Motor selected: $Nn_1 = 15 \text{ kW}$; $n_n = 1410 \text{ min}^{-1}$; $GD^2 = 0.57 \text{ kg m}^2.$

(2) Motor nominal torque.

$$M_{d \text{ nom}} = 974 \frac{15}{1410} = 10.36 \text{ kg m}.$$

(3) Fan characteristic. $M_d = f(n).$

(4) M_{bm1} : with Simpson rule. $M_{b1} = 17.51 \text{ kg m}.$

(5) M_{bm2} : with Simpson rule. $M_{bm2} = 3.835 \text{ kg m}.$

(6) $M_{bm} \cdot M_{bm} = M_{bm1} - M_{bm2} = 13.675.$

(7) Reduction of $(GD^2)_{\text{fan}}$ on motor shaft:

$$GD_{II}^2 = J_m \times 4g = 8 \times 4g = 314 \text{ kg m}^2.$$

$$GD_{IIaI}^2 = 314 \times \left(\frac{700}{1410} \right)^2; \quad GD_{IIaI}^2 = 77.4 \text{ kg m}^2.$$

(8) Overall GD^2 :

$$GD^2 = GD_I^2 + GD_{IIaI}^2 = 0.57 + 77.4 = 77.97 \text{ kg m}^2.$$

(9) Starting period:

$$t_a = \frac{77.97 \times 1410}{375 \times 13.675} = 21.41 \text{ sec}.$$

The starting period required comes within permissible limits.

Determination of Mean Acceleration Torque M_{bm} .

$$\text{Simpson's rule: } F = \frac{h}{3} [y_0 + 4y_1 + 2y_2 + \dots + 4y_{2n-1} + y_{2n}]$$

$$F = \frac{h}{3} \sum_{i=0}^{2n} c_i y_i \quad \begin{matrix} c_{2n} = 2 \\ c_{2n-1} = 4 \end{matrix}$$

1. M_{bm1}

	Area F_2		Area F_1		Area F_3		
x_i	y_i	$c_i y_i$	y_i	$c_i y_i$	y_i	$c_i y_i$	
0	19.6	19.6	20.5	20.5	10.9	10.9	$F' = F_1 + F_2 + F_3$ $F' = 262.75$ $x = 15$ $M_{bm1} = F'/x = 17.51$
1	18.7	74.8	20.4	81.6	10.1	40.4	
2	17.98	35.96	20.3	40.6	9.2	18.4	
3	17.55	70.2	20.2	80.8	8.2	32.8	
4	17.72	35.44	20.12	40.24	7.0	14.0	
5	18.35	73.4	20.04	80.16	5.8	23.2	
6	19.05	38.1	19.96	39.92	4.6	9.2	
7	19.5	78.0	19.88	79.58	3.4	13.6	
8	19.0	38.0	19.79	39.52	2.2	4.4	
9	18.1	72.4	19.7	78.8	1.1	4.4	
10	10.8	10.8	18.6	19.6	0	0	
$h = 1.3$		546.70	$h = 0.1$		601.22	$h = 0.1$	171.3
$F_2 = \frac{1.3}{3} 546.7$			$F_1 = \frac{0.1}{3} 601.22$			$F_3 = \frac{0.1}{3} 171.3$	
$F_2 = 237$			$F_1 = 20.04$			$F_3 = 5.71$	

2. M_{bm2}

	Area F_2		Area F_1		Area F_3	
x_i	y_i	$c_i y_i$	y_i	$c_i y_i$	y_i	$c_i y_i$
0	0.56	0.56	10.15	10.15		
1	0.75	3.00	10.2	40.8		
2	1.1	2.2	9.2	18.4		
3	1.65	6.6	8.1	32.4		
4	2.4	4.8	7.0	14.0		
5	3.3	13.2	5.7	22.8		
6	4.3	8.6	4.6	9.2		
7	5.5	22.0	3.4	13.6		
8	6.85	13.7	2.2	4.4		
9	8.4	33.6	1.0	4.0		
10	10.15	10.15	0	0		
$h = 1.3$ 118.41			$h = 0.1$ 169.75			
$F_2 = \frac{1.3}{3} 118.41 = 51.3$			$F_1 = \frac{0.1}{3} 169.75$			
$F_2 = 51.3$			$F_1 = 5.658$		$F_3 = 0.50$	
$M_{bm} = 17.51 - 3.831 = 13.679$						

$$F' = F_1 + F_2 + F_3$$

$$F' = 57.46$$

$$x = 15$$

$$M_{bm2} = F'/x = 3.831$$

CHAPTER XVII

OPERATING BEHAVIOUR OF A FAN

132. THE OPERATING POINT OF THE FAN

At what point of the characteristic will the fan operate if it is connected up to any sort of ducting system? Obviously the output of the fan must be just as high as the quantity forced through the ducting system. Furthermore, the pressure rise created by the fan must be identical with the pressure drop of the whole ducting. If coincidence of this nature is not immediately fulfilled, there would be an acceleration or deceleration due to high pressure or low pressure in the ducting but eventually equilibrium will be achieved. The fan characteristic \bar{a} and the ducting characteristic a , however, have only one point at which the pressure and the quantity coincide, namely the point of intersection OP (Fig. 354). This point thus becomes the operating point OP . Independent of whether the exact curves \bar{a} and a are known or not, this point of equilibrium automatically enters into the operation.

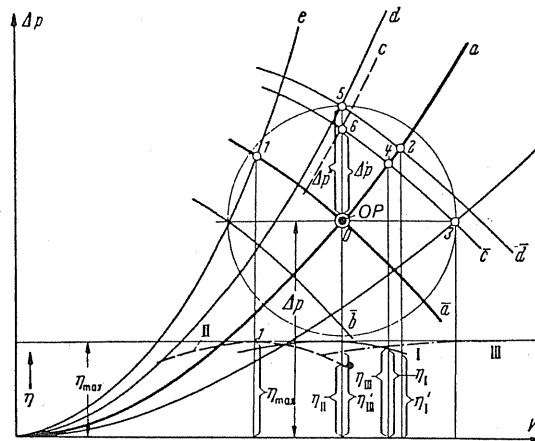


FIG. 354. The operating point OP of a fan.

Theoretically speaking there are various possibilities according to the physical character of the resistance. These cases which have already been represented diagrammatically in Fig. 307 are the following:

- (1) $\Delta p = \text{const}$ (for instance, blowing air through a bath of liquid): pure static resistance.
- (2) $\Delta p = C_1 + C_2 V^2$: liquid bath with primary or secondary turbulent frictional resistance.
- (3) $\Delta p = C' V^n$: polytropic resistance.

- (4) $\Delta p = \bar{C} V$: pure laminar friction, for instance when blowing through a filter.
- (5) $\Delta p = \bar{C} V^2$: pure turbulent friction or resistance (most frequent case).

The operating point OP of the fan characteristic. In line with these, practically all intermediate positions occur; for instance, a resistance which lies between laminar and the turbulent flow. It may also occur that certain changes of pressure occur, for instance, if some critical characteristics of the resistance are exceeded. In practice, however, in most cases there is turbulent flow and therefore Δp is proportional to V^2 . This is taken as the basis for the following considerations.

The fan should be designed in such a way that OP coincides with the point of the optimum efficiency. This obvious requirement cannot be fulfilled easily in every case because the determination of the system characteristic often causes difficulties.

SAFETY ALLOWANCES IN FAN DESIGN

In most cases engineers hope to deal with this factor in design by providing sufficiently large safety allowances to the original estimated values, thus enabling the fan to be dimensioned amply. We shall now investigate how allowances of this kind are worked out.

In Fig. 354 let OP be the actual operating point, the exact position of which is unknown to us. Let \bar{a} be the fan characteristic and a the system characteristic unknown to us or not accurately known. The allowances for deviations from the actual operating point OP are to be taken into account by designing the fan for points which lie in the neighbourhood of OP , i.e. at the selected safety allowances in different directions from OP .

(1) Let the design point lie on the correct characteristic \bar{a} but at 1 so that the throttling line e passes through this point. At point 1 the fan gives the optimum efficiency η_{\max} . In spite of wrong design, \bar{a} intersects the actual throttling line at the correct point OP . At this point, however, the fan has a lower efficiency which is shown by the bottom efficiency line II. The wrong design therefore is "only" noticeable as long as the fan works with the lower efficiency η_{II} instead of with η_{\max} . For the better understanding of the following considerations let the reader look at the different efficiency curves which are shown in Fig. 354. The points of all characteristics situated above the efficiency maximum work at this efficiency if the fan is designed for this volume. The efficiency curve drops towards the left and right. Therefore if the fan is operating at a distance from this maximum, the efficiency will drop all the more the further the distance from the optimum. In Fig. 354 three efficiency curves of equal magnitude are plotted which corresponds to a rating for point 1: OP or 6 or 5 and 3.

(2) Let the design point lie on the correct throttling line a but outside OP for instance at 2. Pressure and quantity are too high. The constant η_{\max} of point OP can be achieved by *speed reduction* without sacrificing any efficiency. *This is the only case where by speed variation a satisfactory correction of the wrongly plotted points can be achieved.* If, instead, the correction were imposed by throttling, the pressure loss, $\Delta p''$, would result.

(3) Let the pressure be correctly chosen but V too large for instance at 3. For the throttling line b passing through 3, the fan now has the highest efficiency. The characteristic \bar{C}

passing through 3 intersects the throttling line actually available at 4, and this operating point adjusts itself. Pressure and volume therefore are too great. The point 4 can be moved towards *OP* by speed reduction. Here, however, the efficiency, which the fan provides at the throttling line *a* at point 4, is retained, i.e. η_{III} (see bottom dotted efficiency line III). The "price" which has to be paid for this correction is that the fan operates with the lower η_{III} instead of with η_{max} .

(4) Let the volume *V* be correctly chosen (often accurately indicated in chemical processes, combustion, etc.), whereas the "careful" design engineer, to be on the safe side, has chosen a considerably higher pressure point 5. The fan characteristic \bar{d} passing through 5 intersects the system characteristic *a* at point 2. Therefore if nothing else is done, the fan will work at this point. Pressure and volume are therefore too high. In order to achieve *OP* the point 2 at *a* can be moved towards *OP* by speed reduction. In this displacement there is little, if any, change in efficiency. The fan operates at *OP*, therefore with the same efficiency which was available previously at 2, i.e. η'_I (see lower drawn out η curve) instead of with η_{max} . By direct throttling from 5 towards *OP*, i.e. by $\Delta p''$, the same result can be achieved.

133. SPEED CONTROL OR THROTTLE CONTROL?

The question may be asked: Is there any difference in carrying out the corrections indicated previously by speed variations or by simply operating a throttling damper? The loss through speed regulation is due to the fact that afterwards the fan assumes a lower efficiency in *OP* than in the wrongly selected design point. For instance, in case 4 the power absorbed in *OP* is greater by the factor η_{max}/η'_I than that relating to correct design.

If, for instance, case 3 were to be corrected by throttling, the fan would operate at point 6. This is easy to appreciate. Throttling alters the system curve available formerly. The greater resistance now present in the ducting becomes obvious by the fact that the former throttling curve *a* rises towards *c*, so that actually 6 is the operating point. What power should now be generated? Now the fan operates at a great distance from its design point 6 and with the worse efficiency η'_{III} , i.e. with power increased by the factor η_{max}/η'_{III} . Of the power raised the portion $\Delta p'$ is simply destroyed and the power is increased by

$$\frac{\Delta p + \Delta p' \eta_{max}}{\Delta p \eta'_{III}}.$$

A reduction thus takes place which throttles back the delivery volume from V_3 to $V_6 = V_{OP}$.

The total power therefore has altered by the factor

$$\frac{\Delta p + \Delta p' \eta_{max}}{\Delta p \eta'_{III}} \frac{V_3}{V_6}.$$

To what extent it has increased or reduced depends solely on the characteristic of the existing fan. In each case the throttling control is tantamount to a deterioration compared with speed regulation.

Throttling control acts more favourably in the case where we start from point 5 because at this point the fan has its optimum efficiency. The loss on the correction, hence, comes

out at the down throttled pressure $\Delta p''$ alone, and therefore a power increased by the factor $(\Delta p + \Delta p'')/\Delta p$ is present at OP , whereas in speed regulation a power increase by the factor η_{\max}/η'_1 occurs. This is always considerably smaller than the factor $(\Delta p + \Delta p'')/\Delta p$.

The result of this is that the speed control is better and in most cases even considerably better than throttling control.

Summarising, it may be stated that *so-called safety allowances are always dangerous. There is only one safety measure: namely, accurate determination of the throttling characteristic.*

In view of the preceding facts, let us consider the most favourable case where the incorrectly sized fan operates at a point on the correct throttling curve—a process which can also be checked mathematically. In doing so we only want to select the “proximity” of the operating point which is still an assumption, to be so far away from the actual operating point that the *throttling curve* can be replaced by its *tangents* at OP . The most favourable case, then, is the one where we move along the tangent; the most unfavourable case lies on the normals to the tangent. If V_0 and Δp_0 define the operating point, the equation of the throttling line is $\Delta p = \Delta p_0 (V/V_0)^2$; from this we obtain

$$\frac{d[\Delta p]}{dV} = 2\Delta p_0 \frac{V}{V_0^2}; \quad \frac{(d\Delta p/\Delta p_0)}{(dV/V_0)} = 2 \left(\frac{V}{V_0} \right).$$

For the reference point $V = V_0$ we then have

$$\frac{d[\Delta p]/\Delta p_0}{dV/V} \approx \frac{\Delta[\Delta p]/\Delta p}{\Delta V/V} = 2 \text{ in the case of the most favourable estimate,}$$

or

$$\frac{\Delta[\Delta p]/\Delta p}{\Delta V/V} = \frac{1}{2} \text{ in the case of the most unfavourable estimate.}$$

From this we obtain the following rule. *If we try to aim at the least amount of over-sizing for safety reasons, the allowance for pressure must be twice as great as allowance for volume.* The most unfavourable case is the converse.

134. UNSTABLE OPERATING PARTS OF THE INDIVIDUAL BLOWER

Most characteristics rise to a maximum value and then drop steadily. The drop from maximum pressure to zero delivery volume may be unstable in certain circumstances. There is a very simple explanation for this. Let us imagine that a fan delivers into a compressed air vessel. When filling up this vessel the fan starts working on its characteristic upward from A (Fig. 355). The pressure rises until point B is reached, from which point as much air is extracted from the vessel as is delivered to it. Let us now consider a small disturbance. Suddenly a volume greater by ΔV than the delivered volume is extracted from the vessel. The consequence is that the pressure in the vessel begins to drop. On the characteristic the pressure drops at the greater delivery volume. At a reverse disturbance the fan works according to requirements, i.e. a stable process.

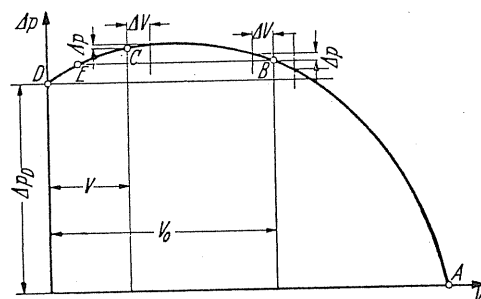


FIG. 355. Unsteady operation of a fan near the maximum of its characteristic.

We will now examine a similar disturbance if the fan works at point C. Let the delivery volume increase at C also by ΔV . The blower must adapt itself to the falling vessel pressure. According to the characteristic, however, this is only possible if the delivery volume drops still further. At the same time, however, the fan pressure also decreases and point D will be reached very shortly, which is the point when the fan does not deliver at all. The vessel evacuates itself further until the pressure drops below point D. Then the fan starts to work on the section AB. The delivery volume is too large; therefore the pressure commences to rise again until point C is reached. The whole process then repeats itself. At higher pressures this swing can lead to very dangerous shocks which are well known under the term “surging”, particularly in turbo compressors.

135. SATISFACTORY AND UNSATISFACTORY OPERATIONS AT UNSTABLE RANGE

The so-called “unsteady characteristic”, i.e. a characteristic with peaks requires more detailed explanation. Primarily it will be seen from Fig. 356 that instability occurs at a constant working pressure $\Delta p'$ which has to be overcome since the constant pressure line intersects the characteristic twice in p_1 and p_2 . This case occurs very seldom in fans—for instance, when forcing a volume of air through a water-bath without any other resistance. In most other

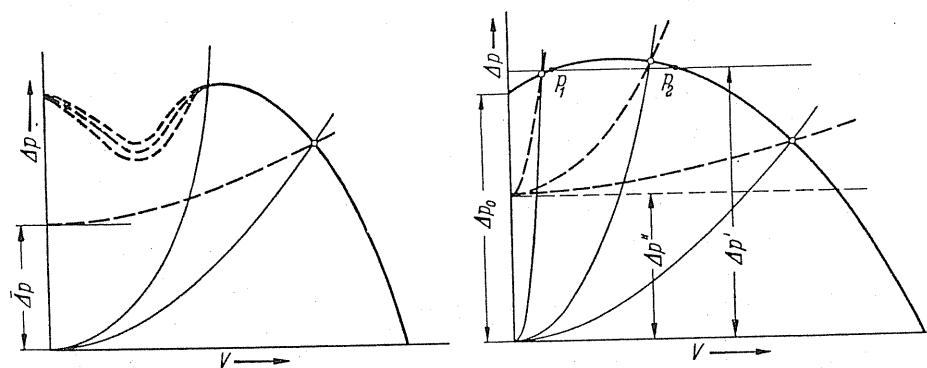


FIG. 356.

cases the so-called unsteady part of the characteristic can be maintained absolutely stable because always only *one* point of intersection with the characteristic occurs. If, for instance, such a characteristic as shown in Fig. 356 intersects three different resistance parabolas in front of and behind the peak, then these operating points are absolutely stable and do not give rise to any disturbance. There will even be no disturbance if a constant pressure $\Delta p''$ is added to the resistance parabola, the additional pressure being smaller than Δp_0 . Only when several fans are arranged in parallel does the unsteady part of the characteristic—as shown above—become worse.

There are, however, fans with so-called unsteady characteristic which cannot be run in the steady part. In axial-flow fans of high pressure, this is the case. The characteristic of fans such as these as shown in Fig. 356 on the left, has a stable part which is practically incapable of adjustment because by doing so, large fluctuations within the fan begin to show themselves. There are already oscillations occurring in the fan which sometimes make it impossible to determine these points accurately. If a fan in these ranges, for instance, were coupled to a boiler, there would be operational disturbances such as fluctuating combustion and vibrations and so on arising immediately.

Therefore differentiation should be made between *operable* and *non-operable* unsteady parts. All radial-flow fans even the drum impeller are only provided with operable unstable parts so that radial-flow fans are more foolproof in this direction.

136. SEVERAL FANS WORKING TOGETHER

Very remarkable working conditions, often difficult to visualise, arise if several identical or non-identical fans are arranged in parallel or in series. Particularly in ventilation, very complicated problems arise in this connection. On the one hand, seasonally affected alterations of the resistance—for instance, running up and running down in a mine according to outside temperature—can rarely be anticipated with sufficient accuracy. Hence alterations to mine ventilation occur which could not be assessed originally. The result is that owing to all these factors one is never certain about the outcome if suddenly it is necessary to arrange fans in parallel or in series. Such disadvantages might be overcome by providing a centralised installation, but there are objections to this. For instance, it may lead to an unnecessarily high power cost if in a system of ventilation in a mine instead of extracting from several shafts, extraction occurred at one point only. In doing so there may be considerably higher frictional losses in certain circumstances.

The undesirable consequences of permitting several fans to work together are:

- (a) Back-flow through an impeller.
- (b) Reduction of overall delivery volume when switching the fans on collectively.
- (c) Unsteadiness in the form of an oscillation of the delivery volume, overflow of a fan.

We will deal with these consequences as follows. The problem can be satisfactorily resolved in the case where the characteristic of a system of ducts is known and an accurate answer may be obtained.

(a) DETERMINATION OF THE RESULTANT CHARACTERISTIC IN A PARALLEL ARRANGEMENT

In a parallel arrangement a definite state of equilibrium will occur *if the positive pressure of both fans is identical*. Therefore by drawing the characteristic curves of both fans next to each other the possible operating points occur through the lines $\Delta p = \text{const}$.

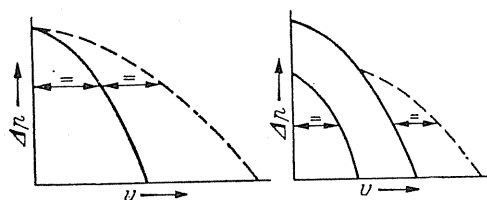


FIG. 357. Resultant characteristic shown in dotted lines for two fans running in parallel. *Left:* identical fans. *Right:* different fans.

The case of the characteristic without a maximum is very simple. The two characteristics are simply added. Figure 357 (left hand) shows the case of two identical fans, whilst Fig. 357 (right hand) shows two different fans working together.

Complications begin when the characteristics have one maximum close to other maximum. Two points of intersection for the same pressure are found at *A* and *B* (see Fig. 358). By placing the characteristics of two identical fans with maximum together, various branches occur according to Fig. 358. By doubling *B* the point *BB* is obtained, and doubling point *A* gives point *AA*. The combination of *A* and *B* gives the point *AB*. Furthermore it should be noted that the fans have a negative characteristic to the left for $V < 0$. In Fig. 358

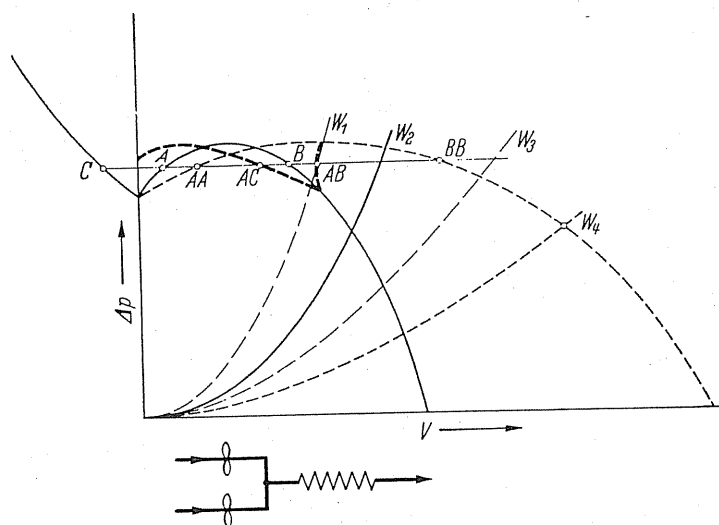


FIG. 358. Various characteristics obtainable when two identical fans are arranged in parallel.

continuation of this via $V = 0$ is drawn in. In this way we obtain another combination from C and B in the point AC . It will be realised that in the present case there are six different operating points. According to the system characteristic, complications can only occur due to these system lines intersecting the characteristic *several times*. This is the case for W_1 . This characteristic has three points of intersection with the resultant characteristics. The fans can oscillate between these three points and one fan can even be overblown. At system characteristics W_2, W_3, W_4 there are distinct points of intersection and no oscillation.

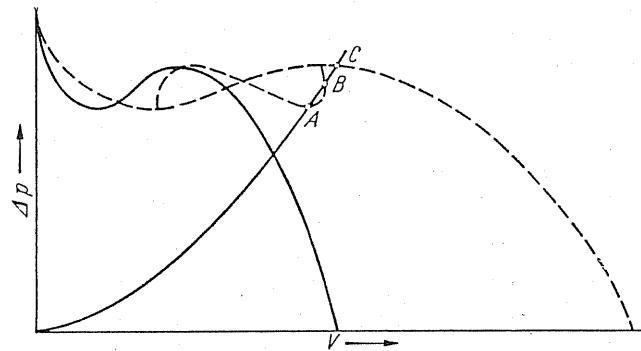


FIG.359. Characteristic of two identical fans working in parallel loops due to various combinations in the characteristics of the individual fans.

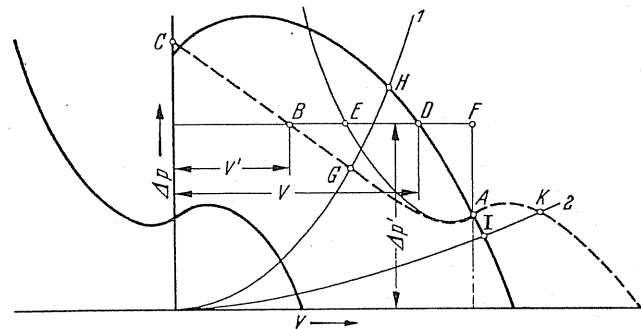


FIG.360. Two entirely different fans working in parallel showing a maximum in the characteristic of the two fans. The characteristics of the individual fans are also shown.

Conditions become more involved if the fans differ and characteristics with points of inflection are present, as is the case, for instance, with axial-flow fans. If the characteristics have a point of inflection apart from a maximum, the conditions shown in Fig.359 are created. In the vicinity of the peaks at identical pressure, *three* different delivery volumes are found. The combined characteristics have a notable loop.

If the fans differ and if one fan is smaller in respect of delivery quantity and delivery pressure, conditions occur which have been plotted in Fig.360. As before, the smaller characteristic is simply displaced to the right and brought up against the other. How does the overall installation behave, however, if a deficient delivery volume occurs at point A ? Since the pressure of the larger fan is greater than the pressure of the smaller where the delivery

volume is zero, obviously air is being *forced back* through the small fan. This fan now works solely as a *flow resistance*. For this purpose the extension of the characteristic for negative volumes must be known. This negative characteristic is indicated in Fig. 360. If we now carry this negative characteristic upwards from point *A* it is easy to visualise the conditions. At pressure $\Delta p'$ the larger fan delivers quantity *V*. Of this the amount *EF* is blown back through the small fan and therefore a point *B* arises on the new characteristic which can easily be found through $BD = EF$. It is worth noting that the zero point of the new characteristic *C* lies above the zero point at single delivery. The new common characteristic (dotted) shows the following remarkable behaviour. If, for instance, we consider two different duct characteristics 1 and 2 we obtain at 1 a reduction of delivery volume from *H* to *G* whilst at 2 there is an increase from *I* to *K*.

(b) FANS ARRANGED IN SERIES

When fans are arranged in series the air volume delivered must be identical. Points belonging together are obtained accordingly through the condition $V = \text{const}$. The pressures are simply added. If the fans are not identical, as for instance, in Fig. 361, the continuation to such delivery volumes must be known for the smaller fan, at which a pressure drop is required in order to continue to deliver. According to the duct characteristic, the delivery volume can be increased (from *A* to *B* at 1) or reduced (from *C* to *D* at 2) by adding a second blower.

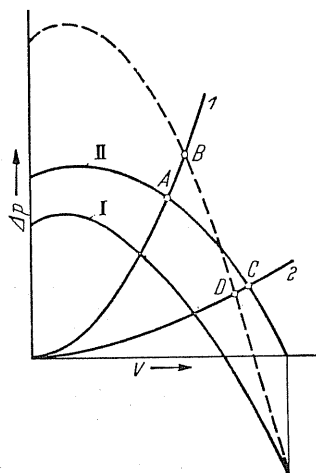


FIG. 361. Two fans in series.

(c) INSTABILITY, OSCILLATION

When several fans are working in parallel as indicated when one or a number of them deliver air, instability will always arise where the duct characteristic possesses several

points of intersection with the resultant characteristics. In Fig. 359 there are three possible points— A , B , C .

Of these, the points which are situated on the descending characteristic, i.e. A and C are stable. If these points are close together, which often happens, then even small pressure fluctuations might initiate oscillation. Once oscillation has been initiated for whatever reason, additional uncontrollable displacements of the characteristic will occur due to continuous accelerations and delays of the individual air columns. To prevent this, care must be taken that the operating point is at some distance from the critical range.

The conditions can be studied without plotting the resultant characteristic. Thus, in accordance with Fig. 362, the two characteristics are plotted perhaps after deducting the

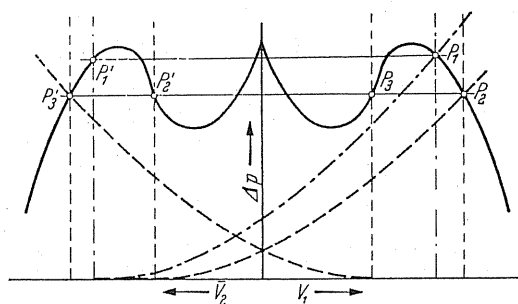


FIG. 362. Graphical method for determining unstable working conditions in two fans running in parallel.

resistance characteristic in the individual ducts to the left and to the right of the Δp axis. Then a system characteristic is plotted on transparent paper, i.e. mostly one parabola. This sheet is pushed along until both points are found at which the intersection with the V_0 axis and with the fan characteristic presents equivalent Δp . In the actual example, thus pairs of points $P_1'P_1$, $P_2'P_2$, $P_3'P_3$ will be found. It will be easily realised that of these three possibilities, only $P_1'P_1$ is stable.

What is interesting is that oscillations on fans having a characteristic according to Fig. 362 can be eliminated if this fan is provided with upstream adjustable guide blades. Situations such as these arise in meridionally accelerated axial-flow fans. In reality the characteristics are varied by means of the inlet guide blades.

(d) TWO IDENTICAL CIRCUITS WORKING IN PARALLEL AND JOINED BY CROSS-CONNECTION

An important special case of two fans working in parallel arises if the two fans serve independent sets of ducts and are coupled together by a cross-connection. As an example larger boiler units are often fitted with two fans on the forced draught end, which also work individually and are intended to serve the whole "network", when very small boiler outputs are called for. The diagram is shown at the bottom of Fig. 363. By means of the

cross-connection AB , which is possibly controlled by a throttling damper, excess flow arises which, as when starting up a fan, can be eliminated by means of a further damper. The layout is represented in Fig. 363.

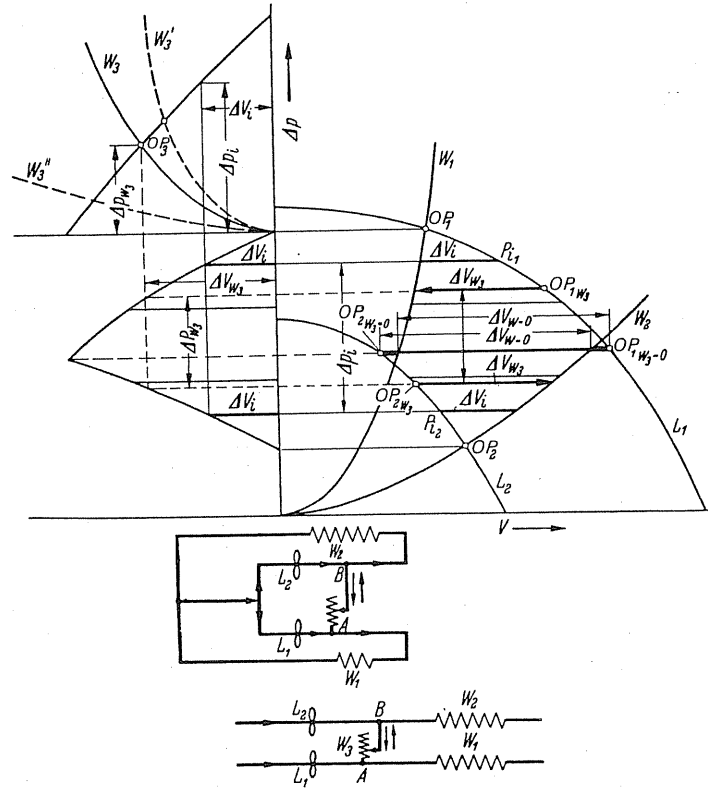


FIG. 363. Two fans working in parallel on two similar circuits with a cross-connection.

Let us assume generally that fan L_1 is working on the resistance W_1 and the fan L_2 on the resistance network W_2 , all being different. When the slide damper between A and B is closed the two fans operate on the operating points OP_1 and OP_2 . What condition will occur if the intermediate duct is fully or partly open? Let us select a random intermediate point P_{i1} on the characteristic L_1 between the points OP_1 and OP_2 . Contrary to the position on the system characteristic on W_1 at the same pressure, a volume greater by ΔV_i occurs. If we assume that this excess quantity ΔV_i flows from A to B , then the network W_2 must absorb this quantity exactly. For this purpose we must look for a point at which difference between L_2 and W_2 is exactly equal to ΔV_i . This is the case at point P_{i2} . Between two fans or between point A and B there is a pressure difference Δp_i . Let us move these two points to the left-hand side of the Δp axis. We carry out the same design only for all points between OP_1 and OP_2 . Thus we have two curved lines with a definite peak. This is indicated by the fact that at this point there is no pressure difference between A and B . Then the two points $OP_{1W_3=0}$ and $OP_{2W_3=0}$ would result. This is the working state when resistance is present between A and B , i.e. the throttling slide is fully open. In this

case the volume $\Delta V_{W=0}$ flows from A to B . In order to obtain the operating point for an arbitrary intermediate resistance we draw the two curved parts on the left-hand side of the diagram in such a way that the actual Δp_i is always entered above ΔV_i . This corresponds to A to B for the ducting in approximately one replacement fan characteristic. According to the setting of the throttling damper, various resistance characteristics arise between A and B as, for example, W_3 , W'_3 , W''_3 . For $W_3 = 0$ we obtain the abscissae which were mentioned previously. Let us select, for instance, the characteristic W_3 . We then obtain a point of intersection at OP_3 . This is the operating point of the intermediate section AB . Let us now transfer this point back into the original diagram. Thus we obtain the operating points OP_{1W_3} and OP_{2W_3} . The pressure difference in the intermediate section is Δp_{W_3} . Here the volume ΔV_{W_3} flows between A and B .

In this way for any random point of the throttling damper it is possible to calculate the correct network load. Richter⁽¹⁾ has published a paper on this subject. The present solution is a simplification compared to the one which he has discussed.

The last case is particularly important in practice if both fans and both resistance characteristics are the same. Disturbances and backflows may arise if the characteristics of the fan are unstable. This problem receives special attention because of the practical importance of axial-flow fans.

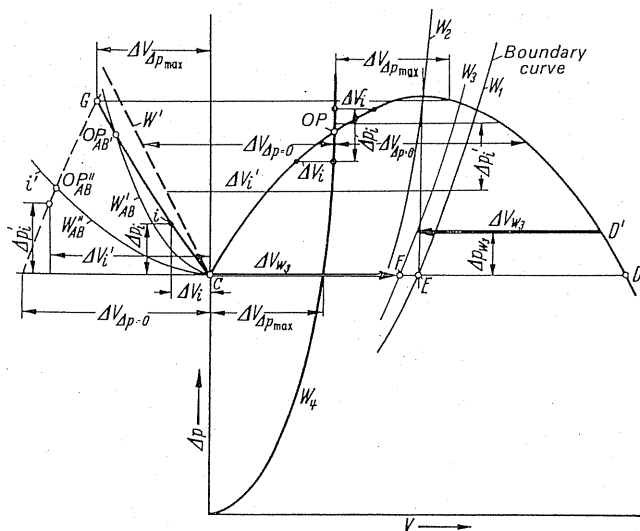


FIG. 364. Two identical fans working in parallel with maxima, having a cross-connection and a throttling damper.

The characteristics of these fans according to Fig. 364 have a large peak. Let this be the characteristic for both fans. Furthermore, let the arrangement be as shown in Fig. 363 at the bottom. Moreover, let the characteristic for negative V be known, a state which has been described as "over blowing". Since the working conditions for stable

¹ Richter, W., Twin fan operation with cross connection, *Heizung-Lüftung-Haustechnik*, 1959, No. 6, p. 149.

characteristics are stable and no oscillations can arise, we only meet these conditions which arise if operating points come in the proximity of the peak of the characteristic. First we will deal with the question if, and under what conditions, an overflow between A and B occurs without resistance. According to the existing resistance characteristic of the ducting system, this question has to be answered in different ways. The boundary position is particularly interesting, i.e. from what point onwards will such a kind of overflow occur for the first time? Previous studies of this problem are not sufficiently precise. Throughout, the opinion is given that this risk only occurs if the resistance characteristic passes straight through the peak of the fan characteristic, namely for characteristic W_2 . The investigations of Richter, however, have shown that even for points of intersection which lie somewhat to the right of it, possibilities of this kind are feasible. Actually this question can be answered precisely. To this end we will examine the boundary position first. The last possibility is then available if the chord of the peak with points C and D are considered as operating points. If the network, for instance, has a system characteristic W_3 , the two points D and C will still be allied working points if there were a pressure difference Δp_{W_3} in the intermediate ducting AB . Then the volume ΔV_{W_3} would overflow between points A and B . To what maximum value can this volume ΔV_{W_3} attain, if there is no pressure difference present between A and B ? It will be obvious from Fig. 364 that this occurs only if the characteristic passes through point E , i.e. for a system characteristic W_1 . In this case the volume $CE = DE$ would overflow between A and B . The decisive condition for this is that for all operating characteristics which lie to the right of the centre point E of the chord of the peaks, stable working positions are present. For all characteristics to the left this is not the case. The decisive role is taken over by the *centre point of the chord* and not by the peak of the characteristic. This is of importance because in certain axial blowers the point of optimum efficiency lies only a little to the left of the peak. Therefore it will suffice if we restrict ourselves to the system characteristics which lie to the left of point E . As an example, let us consider the characteristic W_4 . The operating point for closed duct AB lies at OP . When opening the throttling damper various possibilities occur. Possible operating points arise from the condition that the ΔV which flows across AB must be positive for the one fan and negative for the other. We will consider for instance two points at which an ΔV_i is available. Here there is a pressure difference Δp_i available between the two branches. This point we will plot according to the construction of Fig. 364 to the left of the diagram from point C to the left. Thus we obtain point i . The highest volume ΔV with a maximum pressure difference Δp_{\max} is obtained from point G . The volume is indicated with the symbol $\Delta V_{\Delta p_{\max}}$. There is still the possibility, however, that a fan will overblow. The characteristic W' , entered to the left (dotted), represents this case. For example, point i' arises from the fact that an overflow volume $\Delta V'_i$ occurs with pressure difference $\Delta p'_i$. Thus we obtain a second characteristic part which is shown as a dotted line up to G and is only applicable for the working condition of the overblow. According to the position of the throttling damper for the intermediate power AB , different operating points will take effect. Let us mark out different resistance parabolas W'_{AB} and W''_{AB} to the left starting from C , and having points of intersection OP'_{AB} and OP''_{AB} . The first points to establish are those at which both fans are operating in the same direction but with considerably varying volumes whereas in the second case overblow of a fan takes effect. In

principle, working conditions such as these can only be prevented if the throttling damper is fully closed between *A* and *B*.

The example is intended to demonstrate that, when using fans with unstable characteristics in parallel, extraordinary difficulties may arise. They can be studied accurately if the characteristic is accurately known.

(e) DOUBLE-INLET FANS

In double-inlet fans two fans work in parallel so it is necessary to know when unstable behaviour may be expected. Since the air flows meet directly behind the impeller, the static pressure should be investigated at this point. Therefore the *gap characteristic* previously considered must be taken into account in this investigation. The former investigation, however, shows that this gap characteristic was practically without peak with backward-curved and forward-curved blades. Only at $\beta_2 = 90^\circ$ or blade angles which are in this vicinity, are maxima obtained. This means that danger arises only in these cases and therefore the rule can be recommended *not to use blades with $\beta_2 \approx 90^\circ$ for double-acting fans*.

137. PERFORMANCE OF ONE OR SEVERAL FANS CONNECTED TO ANY DUCT SYSTEM

In practice fans are often connected to complicated duct systems. On the one hand, several fans can be coupled up in parallel or in series, and alongside there are often ducting systems or arrangements of equipment so complicated that the overall assessment and the selection of the correct fans presents a difficult problem to the engineer. Hitherto no one appeared to trouble about this—apart from mining perhaps, but this situation is no longer tolerable today. It is, of course, senseless to specify maximum efficiency fans and not to have any reliable data on the system. Many fans in practice do not work at the point of the optimum efficiency and no one appears to bother about it or is aware of the immense waste of energy. Industry alone has to bear the cost of this inefficiency. In order to give the practical engineer some assistance, the following important factors will be dealt with.

(a) SYSTEM CHARACTERISTIC IN DUCT BRANCHES

The fan often has to move air through a network of ducts, mountings, etc., and the air therefore has often to follow very complicated paths, and the designer does not know the velocity at which the air flows through different portions of the duct work. It is not always easy to lay down the actual working characteristics of such systems satisfactorily. In ventilating a mine with a number of shafts, galleries, cross-cuts, ventilating ducts, etc., such problems arise on a small scale but also in a quite similar way in equipment for the most varied applications. The diagram of the ventilation of a ship, as shown in Fig. 365, demonstrates what a complicated line of ducts is often present. The accurate mathematical

solution of such problems is usually impossible. The engineer is forced to make do with other methods. A fairly satisfactory solution of these problems must be found, otherwise design errors will become inevitable and these will have an adverse effect on the best of

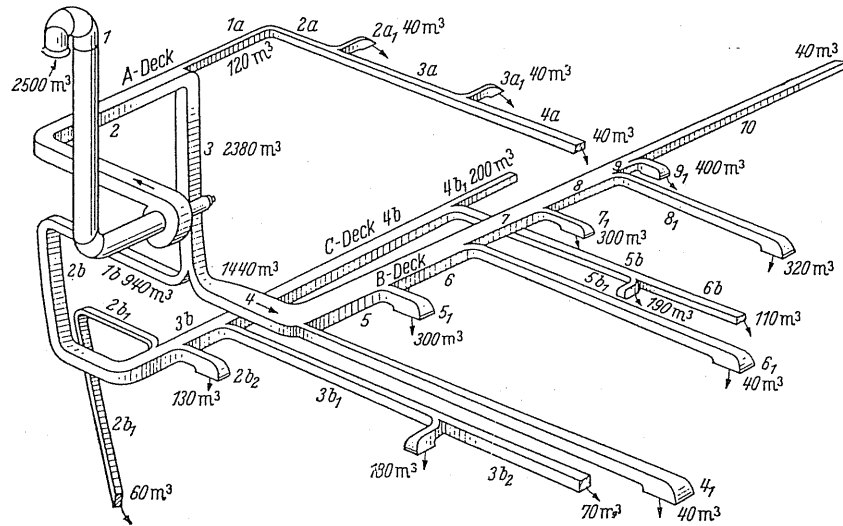


FIG. 365. Diagram of a ship's ventilation system.

fans. In the following discussion some graphical aids will be developed which will satisfy most cases.

In the following considerations it is useful to introduce a simple evaluation of the resistance of a duct. Since, owing to turbulent flow, resistance occurs by which the pressure losses Δp are proportional to the square of the volume flow V , it can be stated that $\Delta p = RV^2$, according to whether an individual resistance $\Delta p = \zeta (\varrho/2) c^2$ or pipe friction

$$\Delta p = \lambda \frac{l}{4(F/U)} \frac{\varrho}{2} c^2$$

occurs; because of $V = Fc$ it becomes

$$R = \zeta \frac{\varrho/2}{F^2} \quad \text{or} \quad R = \lambda \frac{l(\varrho/2)}{4(F/U)F^2}. \quad (239)$$

There is thus an analogy with electrical resistances where the resistance value is known to be proportional to the driving force which, in this instance, is a potential difference.

Resistances in series. In a pipeline the resistances R_1, R_2, R_3 follow each other. How is the resultant resistance obtained? The individual resistances are shown in Fig. 366. In all three resistances the volume flow must be the same in each case. At a constant volume V

obviously the three resistances must be added together. This has been done in Fig.366; hence we have the resultant resistance R .

For $V = \text{const}$ we have $\Delta p = \Delta p_1 + \Delta p_2 + \Delta p_3$.

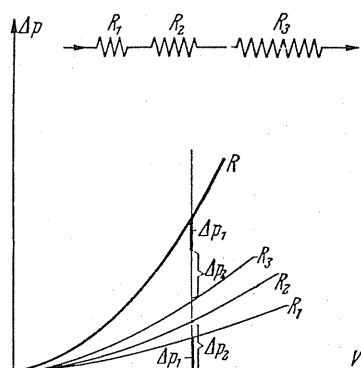


FIG.366. Resistances in series.

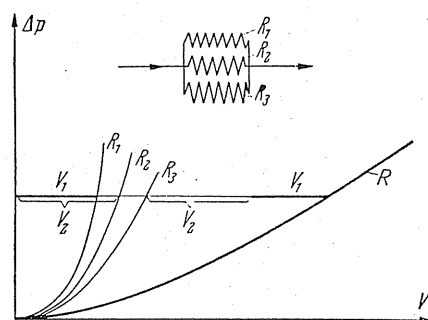


FIG.367. Resistances in parallel.

The following calculation also shows how the equivalent orifice behaves; if we express

$$\Delta p = (\rho/2) (V^2/F^2), \quad \Delta p_1 = (\rho/2) (V^2/F_1^2), \dots \quad \text{in} \quad \Delta p = \Delta p_1 + \Delta p_2 + \Delta p_3,$$

we obtain

$$\frac{\rho}{2} \frac{V^2}{F^2} = \frac{\rho}{2} V^2 \left[\frac{1}{F_1^2} + \frac{1}{F_2^2} + \frac{1}{F_3^2} \right],$$

i.e.

$$\frac{1}{F^2} = \frac{1}{F_1^2} + \frac{1}{F_2^2} + \frac{1}{F_3^2}. \quad (240)$$

Resistances arranged in parallel. The resistances are now to be arranged in parallel as shown in Fig.367. The individual resistances are shown in Fig.367. In parallel arrangement the pressure differences obviously must be identical, as otherwise no equilibrium is possible. At constant-pressure differences the volumes flowing in each branch of a duct are added, i.e. these volumes are simply added together. Thus we obtain the resultant characteristic, since according to Fig.367 the V values are simply added for a curve $\Delta p = \text{const}$.

For the R values the following applies:

$$\Delta p = \text{const}; \quad V = V_1 + V_2 + V_3.$$

From $\Delta p = R V^2$ we express $V = \sqrt{(\Delta p/R)}$ in

$$\sqrt{\frac{\Delta p}{R}} = \sqrt{\frac{\Delta p}{R_1}} + \sqrt{\frac{\Delta p}{R_2}} + \sqrt{\frac{\Delta p}{R_3}}; \quad \frac{1}{\sqrt{R}} = \frac{1}{\sqrt{R_1}} + \frac{1}{\sqrt{R_2}} + \frac{1}{\sqrt{R_3}}. \quad (241)$$

For the equivalent resistance this means that the reciprocal values of the square root are added from the R values.

The same also results from $V = V_1 + V_2 + V_3$ for the equivalent orifice $F = F_1 + F_2 + F_3$.

Arbitrary combination of parallel and series arrangements. The relation derived previously can be transferred to any combination of parallel and series resistances. According to Fig. 368 the case will be treated where primarily two resistances R_1 and R_2 operate in parallel, following on with R_3 , and then there are still four resistances in parallel available, mainly R_4, R_5, R_6, R_7 .

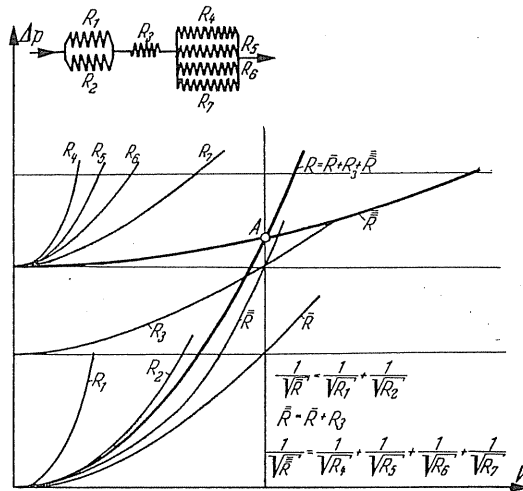


FIG. 368. Combination of parallel and series resistances.

First let us add R_1 and R_2 by adding the volumes for a curve $\Delta p = \text{const}$. Thus we obtain the resultant resistance \bar{R} for the first two resistances. The next resistance R_3 is arranged in series so that at $V = \text{const}$ the value of R_3 is to be added. Thus we obtain the resultant resistance $\bar{\bar{R}}$. At the end limit of R_3 we draw a parallel to the V axis and on this new axis we show the resistances R_4 to R_7 working in parallel. We draw a line $\Delta p = \text{const}$ at any *random* point and add together in the method known, so that a resultant characteristic $\bar{\bar{\bar{R}}}$ for R_4 to R_7 becomes apparent. At point A this curve intersects the straight line $V = \text{const}$ used previously for the addition of the resistances. The parabola passing

through A is then the resultant resistance. The process in no way is bound by any square law of resistance. It can even still be applied if, for example, each individual characteristic is to be determined only by testing. In this case, however, it will not suffice to determine an individual point. So many individual points of the ultimate resultants then have to be determined that these could be shown by a line drawn with a French curve. The process can be carried out in a fairly short time and always leads to the required result in any number of individual resistances.

(b) CHARACTERISTIC FIELD OF THE EQUIVALENT ORIFICE

The application of the term of equivalent orifice often used is closely related to the problem of how the characteristic field of the curve thus arising should be plotted and numbered.

First let us consider, according to equation $\Delta p = (\rho/2) (V^2/F_D^2)$, the relationship between Δp and V . Obviously this is a parabola with its minimum at zero. So we have a family of parabolas. Let us draw a straight line parallel to the V axis, i.e. let us consider the condition $\Delta p = \text{const}$ and then we obtain, for instance, for three different parabolas,

$$\Delta p = \frac{\rho}{2} \left(\frac{V_1}{F_{D_1}} \right)^2 = \frac{\rho}{2} \left(\frac{V_2}{F_{D_2}} \right)^2 = \frac{\rho}{2} \left(\frac{V_3}{F_{D_3}} \right)^2 = \text{const},$$

i.e.

$$V_1 : V_2 : V_3 = F_{D_1} : F_{D_2} : F_{D_3}.$$

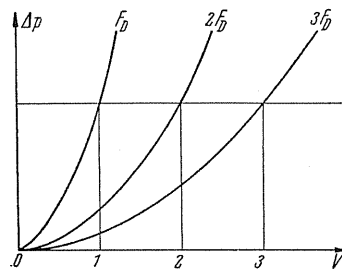


FIG.369. Family of characteristics of the equivalent orifice.

However, this means that the points of intersection limit the V values of this parabola which are proportional to the actual value of the equivalent orifice. Thus the family of parabolas according to Fig.369 is easy to evaluate.

(c) VARIATION OF THE FAN CHARACTERISTICS BY THROTTLING

It will now be asked what practical importance a fixed combination of fan and throttle can have. A case of this type can arise if heated air passes into a duct. The heating of this air is effected by means of a heat resistance, i.e. a throttle.

According to Fig. 370 the values of various throttling lines, namely 1, 2, 3, 4, 5, are deducted from the values of original characteristic. Thus we obtain new characteristics I, II, III, IV, and V. The distinctive feature of this diagram is that, in this combination, the characteristics become steeper, the greater the additional resistance.

(In the following illustration the parabolas are marked by the sign R in accordance with $\Delta p = RV^2$.)

In place of a throttle any kind of resistance can be considered in association with the fan. This method of examination could be beneficial in different applications.

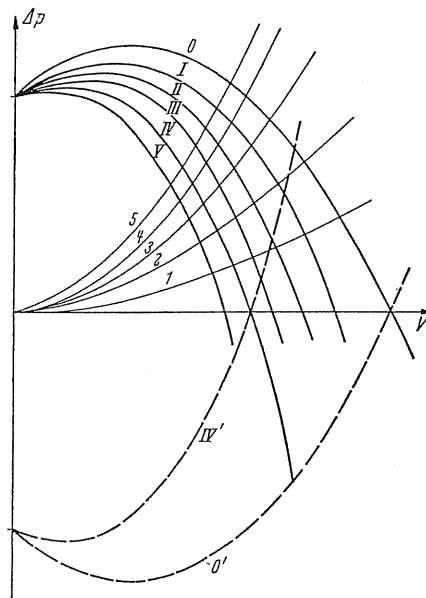


FIG. 370. Variation of characteristics of a fan by a damper.

It should be emphasised that the problem may be considered in reverse. If, for instance, we do not start off from the fan but from the resistance, it may be asked how the problem of resistance alters if there is still a fan working in the duct. Therefore the fan itself can be assumed to represent an *apparent resistance*. This way of looking at the problem is sensible in the case where several fans for any reason are working in a duct system. Then it is often advantageous to consider a fan as a delivery link and the others as the *resistances* with pressure gain. The resistances need only be plotted positively upwards and the fan pressure be deducted therefrom, but this means that the top illustration of Fig. 370 is reversed. The dotted lines show approximately how this appears if the throttling line 4 is taken as basis.

It is purely a question of practicability as to the method used. In the following discussion both methods will be applied to suit various requirements.

(d) RESISTANCE AND FAN AS PARTS OF A SYSTEM OF DUCTS

Hitherto only resistances in different arrangements have been examined. The case where a fan is fitted somewhere in a branched duct is important. For instance, it may be a supply fan in a mine, but it can also be a very highly branched ventilating installation of another type, where for some reason a stand-by fan is working somewhere within the system. In these cases the fans affect the overall throttling curves considerably, whereas

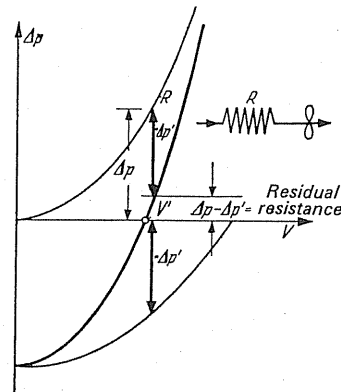


FIG. 371. Resistance and fan in a circuit.

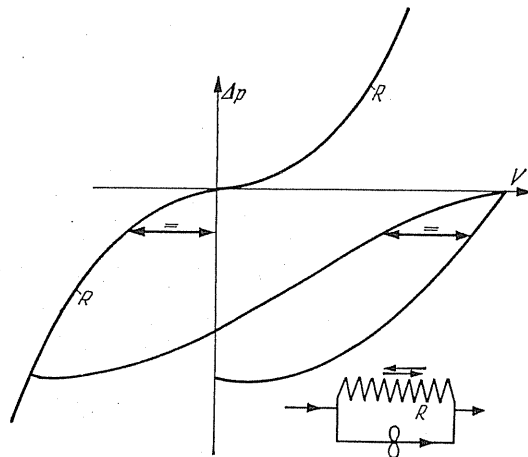


FIG. 372. Fan and resistance arranged in parallel.

resistances bring about a *pressure drop in the direction of the flow*. A built-in fan brings about an increase in pressure. The sudden change of pressure is in either direction. Designating RV^2 as the pressure drop of the resistance and $\Delta p'$ the *pressure increase* of the fan, the pressure drop then is the combination $RV^2 - \Delta p'$ arranged in series. Figure 371 shows how the common throttling curve is obtained. The fan characteristic must be plotted on the negative Δp axis. The resultant characteristic arises from the fact

that for the vertical lines, i.e. $V = \text{const}$, the algebraic sum of the ordinates is formed. It is worth noting here that up to a delivery volume V' a positive pressure is created, i.e. an excess of pressure in the direction of flow. Above V' there is a pressure drop the same as with resistances. It should be remembered that in such cases the resultant throttling curve is no longer a parabola and in connection with the previous examples the resultant curves cannot be obtained any more by deriving a point but by building up point by point.

Particularly in mines and skyscraper hot-gas ducting systems, the case may still arise that the natural ascent of the gases plays a part. In these cases a third member is derived so that the equation reads as

$$RV^2 - \Delta p' = \pm \Sigma(\Delta h \gamma).$$

Special conditions arise if a resistance and the fan are arranged in *parallel*. In this case it could be that air flows back through the resistance. Figure 372 shows a graphical derivation of the throttling curve which now appears on the negative Δp axis.

A further example (Fig. 373) deals with the combination of these two cases.

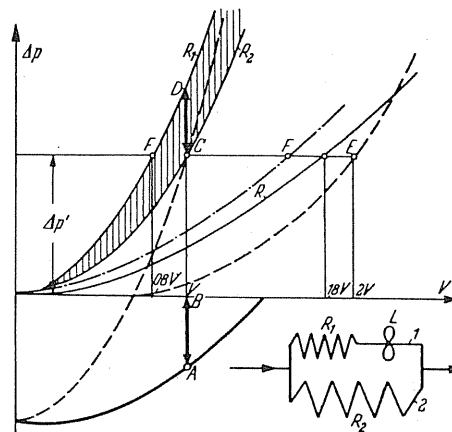


FIG. 373. Combination of Figs. 371 and 372.

In both duct lines arranged in parallel there are two resistances R_1 and R_2 . According to former derivations the resultant throttling curve is obtained by adding the volumes for curves $\Delta p = \text{const}$. Thus the characteristic R occurs where

$$\frac{1}{\sqrt{R}} = \frac{1}{\sqrt{R_1}} + \frac{1}{\sqrt{R_2}}.$$

Since the resistance is $R_1 > R_2$ the flow through system 1 is less than through system 2. From Fig. 373 it will be observed, for instance, that only 80% of the volume flowing through system 2 is passing through system 1. It is now intended to use a higher duty fan in system 1 to enable the volume flowing through the two systems to be identical. The problem can easily be resolved by means of the graph in Fig. 373. If system 1 were also able to deliver the volume V , a pressure drop increased by CD would have to be included for this. The lack of pressure must be covered in some way or other. This means that a

fan must be used which gives a pressure of the order of magnitude $CD = AB$ for a delivery volume V . The important factor for selecting the fan, therefore, is solely the point A . The further construction is shown in Fig. 373. With the auxiliary fan a resultant throttling line passing through E is obtained and therefore a volume $2V$ is delivered exactly at E . The resultant characteristic (dotted line) then is no longer a parabola.

It may still be asked what conditions arise if the adjustment is made by simple *throttling*. For this purpose a throttling damper or a similar appliance would have to be fitted in the system 2 in order to increase the resistance correspondingly. Let us start from the equivalent pressure $\Delta p'$. Then the throttling in the system 2 must be so great as to bring point C to F . The throttling line R_2 must therefore be moved towards R_1 . For the volume V , therefore, a pressure drop CD must be provided for in the throttling position. Thus the degree of throttling is fixed. The throttling region is indicated by shading in Fig. 373. In this way we obtain a throttling line passing through F . A quantity $1.6V$ compared to $1.8V$ is achieved without auxiliary measures and $2.0V$ when using an additional rotor.

(e) BYPASS DUCT FOR STARTING AND CONTROLLING FANS

The above-stated fault of certain axial-flow fans, that the unsuitable part of the characteristic cannot be used, can be partly improved by connecting up a bypass duct. The arrangement used is shown diagrammatically in Fig. 374. Before and after the fan L a bypass

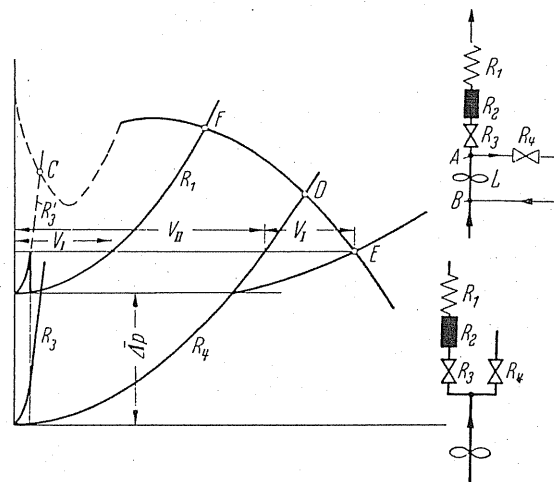


FIG. 374.

duct branches off at A and B in which an adjustable slide or a throttling damper with a variable resistance R_4 is fitted. Following B there is a sliding damper with resistance R_3 of the ducting system. It is composed of the constant pressure resistance R_2 (e.g. a liquid bath or of the constant pressure in a tank or in a boiler system) and of the resistance R_1 , based on the square law.

The question arises as to how the fan can be connected without making use of the part

of the fan characteristics which cannot usually be operated. The first idea would be to start up the fan with the slide R_3 closed and then to open this slide slowly. Thus the resistances R_1 , R_2 , R_3 would be arranged one after the other and all would have to be added together; thus, for example, R_3 would be obtained which would intersect the non-operative characteristic at C . This means that this starting process is impossible to operate. The picture is quite different if the slide damper R_3 is fully closed first and return flow takes place via R_4 . The fan would then operate at point D . If we now slowly open R_3 we obtain a point E in which the volume V_I flows through the main network and V_{II} flows back

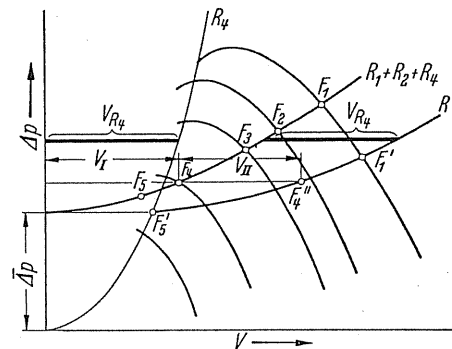


FIG. 375.

through the bypass duct. If we then close the slide damper R_4 , the operating point migrates from E to F . By using the bypass duct, therefore, satisfactory starting is readily obtained. It should be mentioned further that the diagram can be simplified by as much as the point B can be separated since there is no resistance present at the suction end. The simplified diagram thus demonstrates the most important conditions exactly (Fig. 374).

When regulating this fan one should be aware of some difficulties. In many cases an inlet guide equipment is used for regulating. This brings about fan characteristics according to Fig. 375. If, on the other hand, to take a general case, a constant *over-pressure* Δp (originating from R_2) and a parabola resistance R_1 are used in calculation, then the operating point for maximum delivery volume (i.e. inlet adjustment) becomes F_1 . Regulating downwards to F_2, F_3, F_4 , can now be carried out with the *adjustable guide device*. One point F_5 , however, would already fall in the range of the characteristic which cannot be operated. If the bypass duct is opened at a specified slide damper setting, the resistance characteristic with the succeeding resistances R_1, R_2, R_3 is arranged in parallel with R_4 . Thus we obtain the characteristic R . In opening the guide device of point F further, the point F'_1 would be set. Along this resistance curve regulation down to F'_5 can then take place undisturbed. For point F_4 , for instance, there would be a point of intersection F''_4 on the characteristic R . In this case the volume V_I would be delivered into the duct network and the volume V_{II} into the bypass duct. If the slide damper R_4 is steadily opened from about F_3 onwards, smaller volume through bypass would result. Operation of the slide damper R_4 can also be made fully automatic by using the adjustable guide device. Moving forward steadily in operating the slide damper R_4 to point F_5 can then be set as

the ultimate point. In this case the delivery into the duct system is equivalent to zero, i.e. it can be adjusted down to zero through the bypass duct. Richter⁽²⁾ was the first one to deal with the question of bypass ducts.

(f) FANS AND RESISTANCES IN VARIOUS COMBINATIONS

After having become acquainted with the different methods and ways of analysis, various combinations of fans and resistance can be dealt with. To suit conditions a fan will be considered as an "apparent resistance" to the resistances or conversely the resistances will be deducted directly from the fan characteristics. A certain freedom exists as to how the main throttling curve should be viewed ultimately. According to the situations which arise, the different viewpoints dealt with previously will be applied.

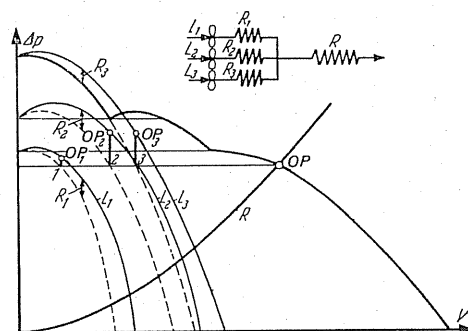


FIG. 376. Arrangement of three fans in parallel with resistances connected to one resistance.

In Fig. 376 we have a case of three different fans, L_1 , L_2 , and L_3 , behind which there are the resistances R_1 , R_2 , and R_3 arranged in series, the fan being connected up in a row to the resistance R . First we will draw the different fan characteristics shown in the diagram as L_1 , L_2 , and L_3 and deduct from this the three throttling lines R_1 , R_2 , and R_3 . Thus we get the dotted line characteristics which now act as the resultant characteristics of the individual branches. The parallel arrangement of these three characteristics is carried out and shows a thick drawn-out characteristic which possesses two points of instability owing to the variable level of the zero points of the three individual characteristics. The point of intersection with the throttling curve R leads to the operating point at OP . It is very interesting to ascertain at which points the individual fans actually operate. If we draw a parallel line through OP this intersects the three dotted curves in 1, 2, 3. If we go upwards from these points right up to the fully drawn-out characteristic, the actual operating points of the individual fans are found at points OP_1 , OP_2 , and OP_3 , so that the pressure and delivery volume of each individual fan can easily be read.

In accordance with Fig. 377 three fans are now expected to operate in such a way that there is a resistance R_1 and R_2 between fans L_1 and L_2 as well as L_2 and L_3 . All fans then blow commonly through R_3 . Let us start with L_1 since we designate the appropriate fan

² Richter, W., Concerning the problem of bypass ducts for fans, *Maschinenmarkt*, 1958, p.13.

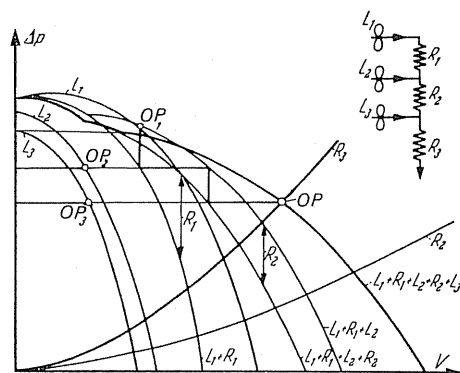


FIG. 377. Three fans with intermediate resistances.

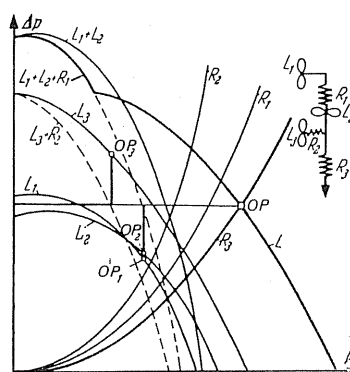


FIG. 378.

characteristic in the diagram with this letter and therefrom we deduct the resistance R_1 arranged in series. Thus we obtain the characteristic shown as $L_1 + R_1$. L_2 is now arranged in parallel with this characteristic since the characteristic displaced in the direction of V is added to the characteristic $L_1 + R_1$. Thus the characteristic designated $L_1 + R_1 + L_2$ is obtained. The throttling line R_2 is now deducted from this combination, since the resistance for the previous combination is arranged in series. Thus we obtain the characteristic designated as $L_1 + R_1 + L_2 + R_2$. The fan L_3 is now added at this point operating in parallel, so that the characteristic of L_3 in parallel displacement must be added. Thus we obtain the full characteristic designated at $L_1 + R_1 + L_2 + R_2 + L_3$. If we examine a spare fan at this point together with the total characteristic derived above, this fan would have to work together with the resistance R_3 . This characteristic intersects this throttling curve R_3 at the actual operating point OP . If we return from this point taking into consideration all operations carried out previously, we very quickly obtain the operating point of the individual fans at points OP_1 , OP_2 , and OP_3 . The pressure and delivery volume of each fan can then be read from these points.

In a further example (Fig. 378) a resistance R_1 is connected up between the fans L_1 and L_2 arranged in series. This is followed by a further fan L_3 arranged in parallel which is connected up in series with the resistance R_2 . Following the parallel arrangement there is

a further resistance R_3 . First we add the characteristics L_1 and L_2 in vertical direction and obtain characteristics designated $L_1 + L_2$ as well as $L_1 + L_2 + R_1$.

We then deduct from the characteristic L_3 first the resistance R_2 and thus we obtain the characteristic $L_3 + R_2$ (dotted). The addition of the latter two characteristics in parallel gives us the overall characteristic designated as L thickly drawn. The point of intersection with the throttling line R_3 is obtained from the operating point OP . If we draw a horizontal through OP and retrace the individual steps, again we obtain the actual operating points of the individual fans at OP_1 , OP_2 , and OP_3 .

(g) DUCTING SYSTEMS WITH CROSS-CONNECTIONS

If any cross-section is present between ducts arranged in parallel, it is possible that the volume flows in these cross-connections are in different directions. If no pressure drop happens to be present, then there is no flow. These part-flows naturally affect the pressure distribution in the main branches indirectly, and a state of equilibrium is obtained which is difficult to visualise. Certain special cases are available, however, for calculation,⁽³⁾ but, in general, graphical or experimental methods will have to suffice.

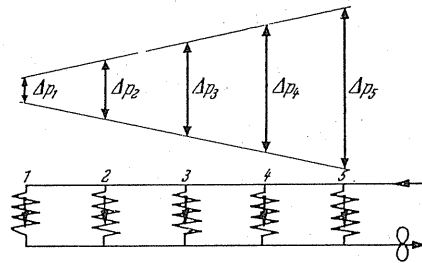


FIG. 379.

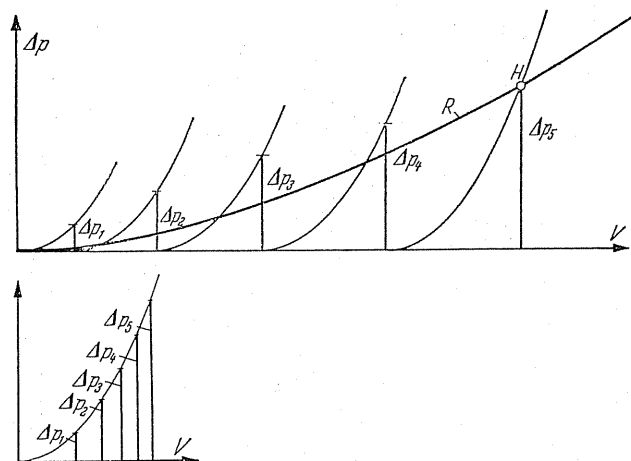


FIG. 380.

³ Richter, W., Solution of a problem on flow in duct systems, *Ing.-Arch.*, 1951, p. 143.

In Fig. 379 there are five cross-connections with equivalent throttling curves between two parallel ducts. We will take the exceptional case where the total pressure drop Δp_s is given (Fig. 380). From there onwards let it be assumed that the pressure drop decreases linearly in the main duct approximately as shown in Fig. 379. In this way we find out the pressure drop in each cross-connection and therefore this actual pressure drop can be transferred to the throttling curve. This gives us the actual volume flow. By arranging these volumes in a line and then vertically entering the last one, i.e. the maximum pressure drop, we obtain a point H of the resultant characteristic (Fig. 380). This procedure can only be applied if the pressure distribution has been obtained by measurement.

Graphical solutions at any combination of cross-connections. In view of the great and almost insuperable difficulties of a purely mathematical treatment, graphical methods are important, since by these means the problem of cross-connections can be resolved.

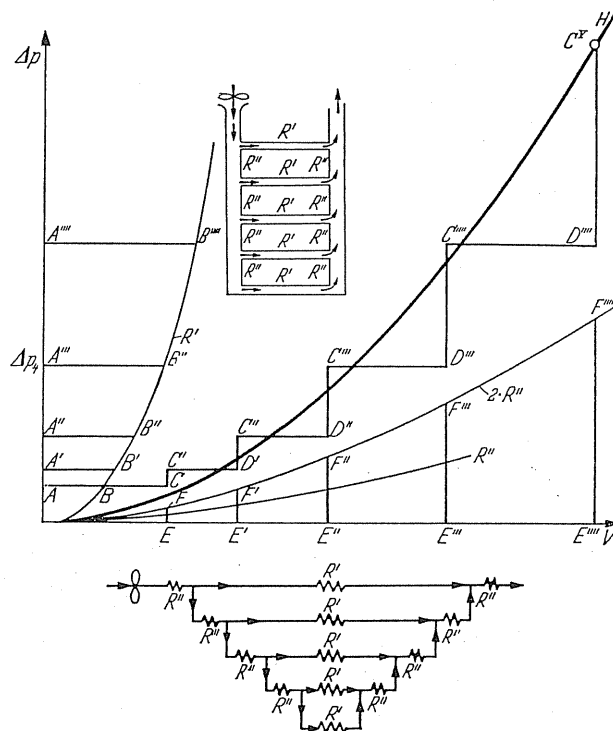


FIG. 381. Shaft ventilation. Combination of resistances.

According to Fig. 381 a fan blows into a shaft from which five cross-connections lead to the upcast shaft (diagram at the top of Fig. 381). The resistance of the cross-connections is designated R' and the resistance of the part of the main shaft situated between the branching off point is designated as R'' . Thus we obtain an idealised resistance shown diagrammatically in Fig. 381 (bottom). This system is examined in such a way that, approximately with the two last cross-cuts—individual parts of the overall plant in parallel are

considered. This idea will be better understood if we consider the resistance of the system shown diagrammatically in Fig. 381 as being broken down. If we start right from the bottom, primarily two resistances R' work in parallel.⁽⁴⁾ To this we enter the throttling curve R' and draw a horizontal line through an arbitrary point A and duplicate the strip AB up to point C . The parabola passing through C would accordingly be the overall characteristic for the bottom two cross-connections arranged in parallel. If we now move higher up to the next cross-connection, the resistance R'' will be added to both sides of the main shaft, but these will lie in the bottom system in series. The throttling parabola R'' , which is duplicated in the direction Δp , must be added towards the top. At C the portion EF will be drawn upwards to C' . Now let us examine the very lowest portion with two cross-connections R' and twice R'' in series as one duct unit, which works in parallel with the succeeding cross-connections. For this purpose a portion $A'B'$ of the parabola R' situated at height C' must be moved from C' to D' . Here again the piece $E'F'$ is moved perpendicularly up to C'' and so on for the succeeding part of the main shaft. Ultimately we obtain H as the extreme limit, and a parabola drawn through H portrays the overall throttling line of the whole system. The method also can be carried out if the resistances of the cross-connections and of the shaft sections vary. In each case a stepped line drawn ascending right up to the end limit is obtained.

(h) THE LEAKING DUCT

In long ducts the useful flow volume can be reduced considerably due to leakages of the most varied kind. In mining such leakages brought about by the permeability of the earth can have very unpleasant effects. Often only about 50% of the effective output can be expected. The problem can, however, also arise in another form. If, for instance, a duct—

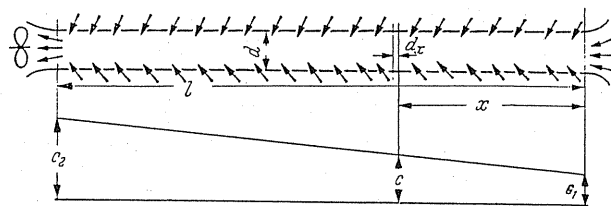


FIG. 382. The leaking duct.

possibly by taking in air from several individual points—is being fed steadily, or, conversely, when many blow-off points come off a main duct, similar flow problems arise. A typical example is given below.

Figure 382 shows a duct of length l and constant diameter d in which air is drawn steadily

⁴ The resistances R'' in between which actually are arranged with the lower R' in series have been ignored because an over-small correction would arise which would be difficult to illustrate. This would have to be taken into consideration if the resistances R'' and R' were approximately identical with respect to magnitude.

through the walls. In order to visualise a simple case it will be assumed that owing to the lateral flow the speed rises linearly from c_1 and c_2 giving the following formula for c .

$$c = x \frac{c_2 - c_1}{l} + c_1.$$

For a small length dx according to Fig. 382 we have a pressure loss

$$d[\Delta p] = \lambda \frac{\rho}{2} c^2 \frac{dx}{d} = \lambda \frac{\rho}{2} \left(x \frac{c_2 - c_1}{l} + c_1 \right)^2 \frac{dx}{d}.$$

Integration gives us

$$\begin{aligned} \Delta p &= \frac{\lambda (\rho/2) l}{d} \frac{1}{3} (c_1^2 - c_2^2 + c_1 c_2); \\ \Delta p &= \lambda \frac{l}{d} \frac{\rho}{2} c_2^2 \frac{1}{3} \left[-1 + \frac{c_1}{c_2} + \left(\frac{c_1}{c_2} \right)^2 \right] \\ &= \lambda \frac{l}{d} \frac{\rho}{2} c_1^2 \frac{1}{3} \left[1 + \frac{c_2}{c_1} - \left(\frac{c_2}{c_1} \right)^2 \right] = \lambda \frac{l}{d} \frac{\rho}{2} c_1^2 n. \end{aligned} \quad (242)$$

For different ratios c_2/c_1 we obtain the following n values which indicate by what factor the pressure loss increases due to the fact that at a constant inlet velocity c_1 , the leakages or side infiltrations assume different values.

c_2/c_1	1	1.1	1.5	2	2.5	3
n	1.0	1.105	1.585	2.33	3.25	4.33

(i) ADDITIONAL LOAD OF A DUCT SYSTEM BY CONSTANT POSITIVE PRESSURE OR NEGATIVE PRESSURE

Up to now two main groups of duct loadings have been dealt with, i.e. resistances of different types and fitted fans. Apart from these possibilities excessive or reduced pressures can be present at the intake or the outlet of the duct. An everyday case is the blowing of a volume of gas through a bath of liquid. Loads having such constant liquid columns are the normal case in centrifugal pumps, whereas they occur more rarely in fans. Cases are of greater importance where by thermal lift or descent unaffected by liquids a more or less constant pressure difference is superimposed on a system. Natural draught in a chimney is an example. In this case, at a height H and at outside and inside temperatures T_1 and T_2 , a "static" pressure difference of the magnitude

$$\Delta p = H(\gamma_2 - \gamma_1) = H \left(\frac{p}{RT_2} - \frac{p}{RT_1} \right) = H \frac{p}{R} \left(\frac{1}{T_2} - \frac{1}{T_1} \right) \quad (243)$$

is present.

According to the actual temperatures it may be a question of negative or positive pressures. Apart from this known example, which plays an important part in induced-draught fans, many other cases can be cited. When ventilating and air conditioning a skyscraper and in ventilating mines, for instance, very considerable static pressure differences arise.

In the following cases the constant positive and negative pressure is charted in reference to the intake flow in a boiler. Five typical examples all taken from practice are given to show how the operating point OP is obtained in such cases.

(a) **Flow into a pressurised space.** A straight line running parallel to the V axis at a distance $\Delta p'$ forms the throttle line which intersects the fan characteristic at OP (Fig. 383). The same situation prevails if the fan exhausts a space which is below atmospheric pressure

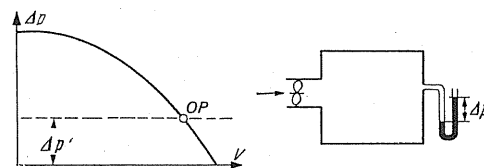


FIG. 383. Blowing into a pressurised space.

in which case the diagram can be turned down around the V axis in order the better to illustrate reduced pressures in this way. (The graphical illustration of these cases leaves open the purely technical solution of the negative pressure or positive pressure space.)

(b) In order to prevent confusion the case is illustrated where a fan forces air into a space at below atmospheric pressure. In this case the sub-atmospheric pressure will be recorded at the bottom so that the fan shows a *greater* delivery volume at OP than at the zero pressure (Fig. 384).

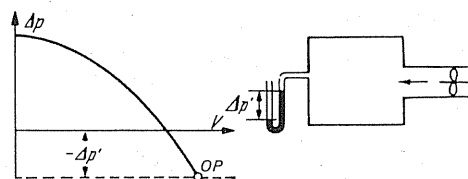


FIG. 384. Blowing into a room below atmospheric pressure.

(c) **Exhausting from a space below atmospheric pressure with a connected resistance due to turbulent flow.** Resistance and negative pressure now act in the same direction. Adding them together gives us R , the characteristic raised by $\Delta p'$ and the point OP (Fig. 385).

(d) **Delivery into a space below atmospheric pressure is to be effected through the resistance R_2 ,** in which shortly before R_2 a ducting branches off with resistance R_1 . The parabolas for R_1 and R_2 are taken from the zero point. R_2 is moved parallel downwards up to the dotted straight line which represents the negative pressure $\Delta p'$. Horizontally the R_2 parabola is added to this displaced R_1 parabola. The drawn-out curve is the resultant throttling line. It intersects the fan characteristic (Fig. 386) at OP .

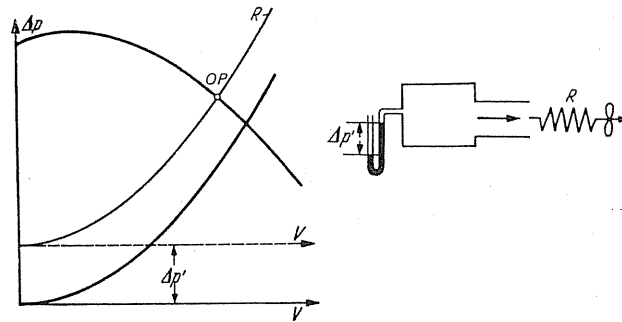
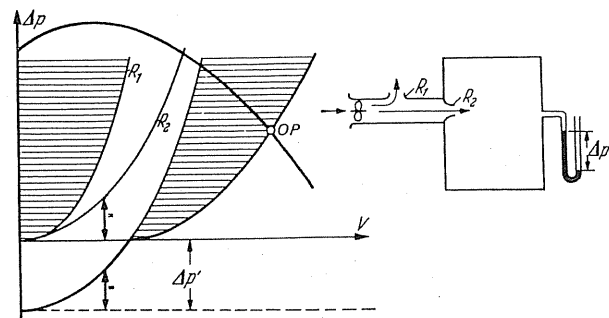
FIG. 385. Exhausting from a room below atmospheric pressure with resistance R .

FIG. 386. Partial flow with resistance entering into a room below atmospheric pressure.

(e) In contrast to (d) there is only the difference that delivery is effected into a pressurised space. The positive pressure line which is chain dotted is now situated on the positive Δp axis. The parabolas R_1 and R_2 are recorded as before. R_2 is raised by the amount $\Delta p'$ and added to R_1 in horizontal direction. This curve is the resultant throttling line (Fig. 387) which intersects the fan characteristic at OP .

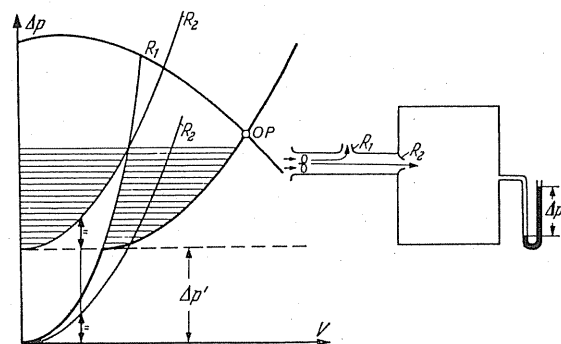


FIG. 387. Partial flow with resistance entering a pressurised room.

(k) VENTILATING A SPACE WITH RETURN AIR

A further example is given to show how in the individual case a plant can be sketched to allow a graphical construction of characteristics.

According to Fig. 388 (top) a space is ventilated by a fan possibly when using an air conditioning plant. A portion of the air is blown out to atmosphere through an adjustable throt-

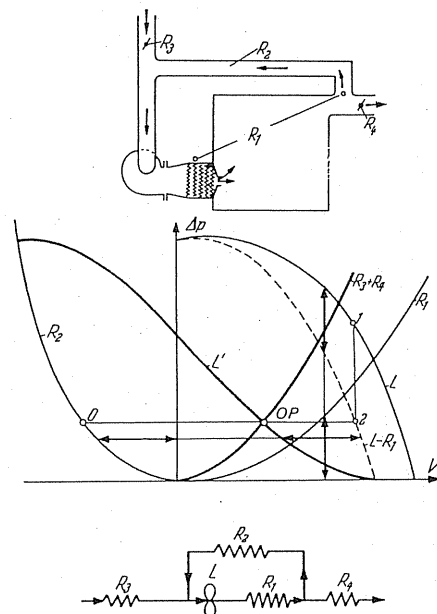


FIG. 388. Ventilating a space by an air conditioning plant.

ting damper R_4 whilst the rest is recirculated by the fan through a special duct. The fresh air is taken in beforehand through an adjustable throttling damper R_3 . The essential layout is shown in Fig. 388. It is therefore a case similar to that of a feeder fan. The analysis can easily be carried out. The resistance R_1 is deducted from the fan characteristic L . Thus a new characteristic $L - R_1$ is formed. Since air flows back through resistance R_2 , the throttling line for R_2 must be plotted to the left on the negative V axis. The arrangement in parallel of R_2 and $L - R_1$ signifies that the same pressure is present at the branch junctions. The two characteristics are thus combined in such a way that the volumes are deducted for lines $\Delta p = \text{constant}$. Thus we obtain the actual "fan characteristic" L' . Most remarkable characteristics are obtained which appear to have no relationship at all with the original fan characteristic. This "ventilating system" now operates on resistances R_3 and R_4 . The characteristic of these two resistances designated $R_2 + R_4$ intersects L' at the operating point OP . If a parallel line to V axis is drawn through OP , the volumes of air which are delivered through the individual ducts will be found at points 0 and 2. Point 1 is the point on which the fan is actually working.

(I) TWO FANS WITH VARIABLE RESISTANCE WORKING TOGETHER

Two fans L_1 and L_2 working in parallel are to supply air jointly through a resistance R , whilst following the fan assembly L_1 a variable resistance R_1 is connected in series (Fig. 389).

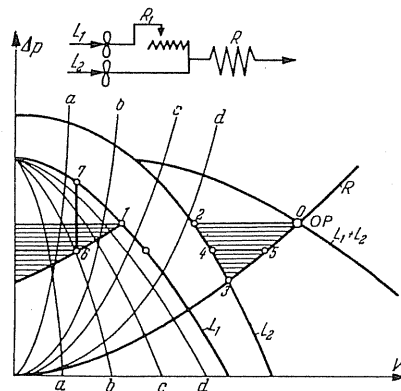


FIG. 389. Two fans working together at variable resistance.

If primarily R_1 is cut out, the common characteristic $L_1 + L_2$ is obtained by addition of L_1 and L_2 . The point of intersection with the throttling line R gives us the operating point OP at point O . If now we first take the resistance R_1 as infinitely great for instance if we fully close the throttling damper acting as the resistance, the fan L_2 operates alone and will operate at a point which is obtained by causing the characteristic L_2 to be intersected by R . Point 3 therefore is this operating point. By a steady opening of the throttling damper R_1 , therefore, the operating point will move on the throttling line from 3 to 0. Let us look, for instance, at a medium operating point, approximately 5. A parallel line with the V axis intersects the characteristic L_2 at 4, so that this fan therefore has its operating point at 4 and delivers a volume which corresponds to point 4. It will be realised that the throttled fan L_1 delivers the volume between points 4 and 5. If we move this section up to the Δp axis we obtain point 6. The fan L_1 therefore must operate at this point. This will be readily appreciated if we remind ourselves of the combination fan and throttling damper previously discussed. Parabolas were obtained for the individual throttling damper positions shown as faint lines in Fig. 389. The working method of the fan L_1 is now understandable. It works at point 6 on the characteristic passing through 6, so that the pressure has been throttled down from 7 to 6. This means that the fan viewed on its own operates at point 7 of its characteristics. If we now ask what additional volume does the full combination deliver if the throttling damper is steadily opened from the closed state until it is fully open, the zone shaded in the triangle $O23$ is obtained which is delivered by fan L_1 . To comprehend the situation better this shaded range was moved up to the Δp axis, which can be taken as the substitute characteristic of the auxiliary arrangement.

(m) DESIGN WITH FLUCTUATING RESISTANCES

In many cases the resistance of a ducting system fluctuates more or less during the run. This means that there is no definite throttling line available but a range in which the throttling line can fluctuate. In an induced-draught fan this situation occurs if the fuel bed has different levels, the fouling rate of the boiler increases or similar contingencies are present.

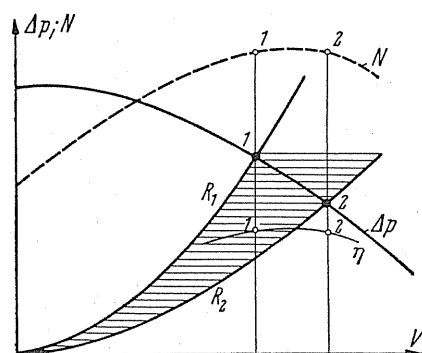


FIG. 390. Performance of a fan with variable resistances when the power curve has a maximum value.

In pneumatic handling installations there are obvious differences according to whether material is being handled or the plant is being run with clean air at intervals. Many such examples of application could be cited.

In such cases one is primarily inclined to select the mean throttling line of the given range as the guide line and to use the point of intersection with the fan characteristic for designing. Moreover, the power required by the shaft must also be considered. It could easily occur that in spite of this layout the power demand would rise considerably at the centre of the range and, therefore, a larger motor would be necessary. The aim in such cases should be for the power-demand curve in the centre of the range to have a maximum value as shown in Fig. 390. Nowadays fans with these features are being sold. They have the convenient feature that in spite of a very wide operating range the power requirement remains practically constant. This point of view is often more important than a high-peak efficiency. The maxima of the efficiency and of the power demand, of course, do not always coincide, as shown in Fig. 390. In such cases it is often advisable to design to suit the maximum power demand and not to go by the maximum efficiency. In many cases fans will be aimed at which have a power-demand curve with a maximum limit. In the high-duty fan as shown in Fig. 102 this is the case whereas in most other fans this kind of maximum does not occur. The great practical importance of fans with a power-demand maximum is clearly apparent from these remarks.

(n) CLOSED DUCTING SYSTEM

Many cases arise where a ducting system is fully closed and circulation only takes place on the inside. Figure 391 shows one of these cases. Two fans are coupled up to a closed ducting system and provided with six different resistances. In cases such as these, the graphical method derived previously can be applied by a simple expedient. In these cases the

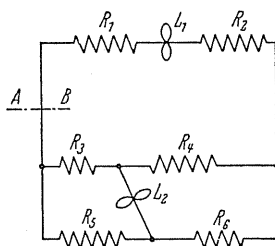


FIG. 391. Closed ducting system.

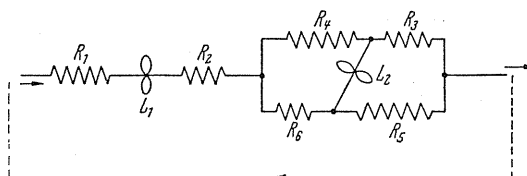


FIG. 392. Opening the ducting system of Fig. 391.

duct system is opened up. The ducting is cut open at any point *AB* and it is assumed that the gases discharge here and afterwards re-enter without resistance. Obviously by this method, characteristics of such a system remain unchanged. Figure 392 shows how the case can be shown diagrammatically as an open system. It can then be dealt with according to former methods.

(o) FAN CHARACTERISTIC AT VARIOUS DENSITIES

The densities of the media to be handled can vary very much for different reasons. There may be temperature variations and there may also be marked variation in levels. In both cases, in accordance with the main gas equation $\gamma = 1/v = p/(RT)$, an alteration can be easily calculated. The fan pressure now is $\Delta p = \gamma \Delta H$, so that at different temperatures the pressures vary according to

$$\frac{\Delta p_{t_1}}{\Delta p_{t_2}} = \frac{T_2}{T_1} = \frac{273 + t_2}{273 + t_1},$$

whereas for alteration of atmospheric pressures

$$\frac{\Delta p_1}{\Delta p_2} = \frac{p_1}{p_2}$$

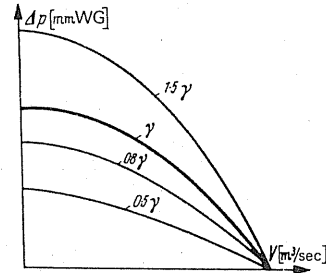


FIG. 393.

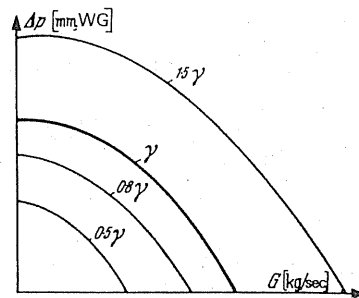


FIG. 394.

applies. If Δp and V are taken for the characteristic, Δp varies proportionately with the density in accordance with Fig. 393. In each case the volume remains constant at the fan, since this is only governed by the velocity triangle of the impeller as well as by the size of the impeller. If the weight of the gas delivered is plotted on the abscissa instead of the volume, here again, since $G = V\gamma$, a variation proportional to the density is available. At different values of γ we then obtain the result as shown in Fig. 394. Often, however, it is desirable to obtain a characteristic independent of the actual variation of the density. For this purpose only the amount of pressure height ΔH need be plotted in place of $\Delta p = \gamma \Delta H$. In the same way as the volume, this quantity is constant and does not even alter if the impeller moves water instead of air. Thus we have an independent characteristic (Fig. 395) which is obtained in applying the dimensionless values ψ and ϕ . The relationship between p in mm WG and H in metres is approximated for the case $\gamma/g = 1/8$ at

$$100 \text{ m} \cong 123 \text{ mm WG} \quad (244)$$

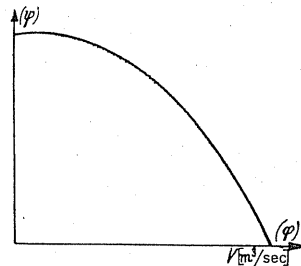


FIG. 395.

(p) THE EFFECT OF DENSITY VARIATION ON THE SYSTEM LINE

Whereas the fan used locally operates in a pressure and temperature range which can be defined exactly, this is certainly not the case with ducting.

On the one hand, large barometric pressure differences can arise, for instance in skyscrapers, chimneystacks, or mineshafts, which will give rise also to temperature differences of considerable magnitude if, for example, a hot gas is delivered through one branch of ducts and cold gas through another. These variations in state bring about greatly variable volumes and pressure losses of variable size. The method outlined previously for determining the common operating characteristic cannot be used any more without alteration.

First of all it is necessary to ascertain what absolute pressures are to be introduced if marked variations of levels are present. Let us take from the whole height H the small differential height dH and so that $dH = dP/\gamma = v dP$. By integrating we obtain

$$H = \int_1^2 v dP.$$

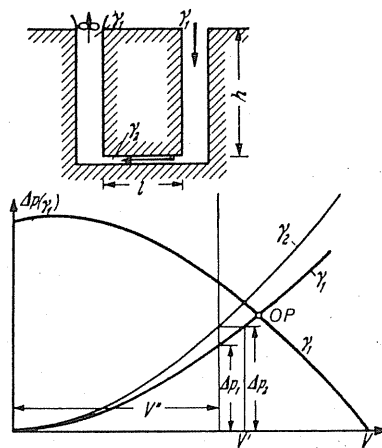


FIG. 396. Air at various densities extracted from a duct system.

When carrying out the integration, the variation of state must be known. Experience shows that neither isotropic nor isothermal behaviour come into question because they set other temperatures on the average. In order to embrace all possible seasonally affected cases we generally use the formulae

$$H = \lg(p_1/p_2) [18.4 + 0.067t_m + 0.085\varphi_m e_m], \quad (245)$$

$$\lg p_1 = \lg p_2 + \frac{H}{18.4 + 0.067t_m + 0.085\varphi_m e_m}, \quad (246)$$

where H is the difference in height (km),

p_1 is the absolute pressure at the top (kg/m^2),

p_2 is the absolute pressures at the bottom (kg/m^2),

t_m is the mean dry temperature ($^{\circ}\text{C}$),

φ_m is the mean relative humidity, and

e_m is the saturated pressure of water vapour present at t_m (kg/m^2).

Where the difference in height up to about 200 m is not too great it will be better to substitute the integral by a mean value $\int (dp/\gamma) = \Delta p/\gamma_m = H$.

$$\Delta p = \gamma_m H = \frac{\gamma_1 + \gamma_2}{2} H. \quad (247)$$

Calculating the pressures b (owing to measurement with barometers) in torr (mm Hg) we obtain for the mean density

$$\Delta p = H \frac{13.6}{2} \left(\frac{b_1}{R_1 T_1} + \frac{b_2}{R_2 T_2} \right). \quad (248)$$

How is the working characteristic to be realised at a sectional system where the temperatures and perhaps the heights vary noticeably, i.e. where the densities alter appreciably in the network? In the former investigations the basis taken was

$$\Delta p = \lambda \frac{l}{d} \frac{\gamma}{2g} c^2 = \left(\lambda \frac{l}{d} \frac{\gamma}{2g F^2} \right) V^2 = R V^2.$$

The value of R defined here is directly proportional to the density γ , whereas the volume flowing through is subject likewise to considerable fluctuations with the variation of γ . All values will have to be converted at some particular state. Here the problem is solely at what point the reference state should be selected. Since the fan only responds to volume and not to weight, it might be advisable to *select the state immediately in front of the fan as a basis* of comparison and reference point.

In accordance with Fig. 396 a fan is expected to overcome the resistance of a gallery of length l deep down in a pit. Downcast and upcast shafts are to be assumed as free of resistance. Let γ_2 be the density in the pit, whilst at the top there is a value γ_1 available at the fan. The characteristic plotted in the diagram refers to the conditions in the pit. What substitute characteristic is now to be expressed in the diagram? Comparison will be made for a volume V . If the index 1 refers to the upper state and 2 to the bottom state, then the formula

$$V = \text{const}, \quad \Delta p_1 = R_1 V^2, \quad \Delta p_2 = R_2 V^2$$

which gives

$$\Delta p_1/\Delta p_2 = R_1/R_2 = \gamma_1/\gamma_2, \quad (249)$$

i.e. the pressures $\Delta p_1/\Delta p_2$ behave like the densities. In this way the characteristic related to state 1 can be obtained immediately. It may be necessary to know the values of volumes at constant resistances. The calculation shows at

$$\Delta p = \text{const}, \quad \Delta p = R_1 V'^2, \quad \Delta p = R_2 V''^2$$

which gives

$$\frac{V'}{V''} = \sqrt{\frac{R_2}{R_1}} = \sqrt{\frac{\gamma_2}{\gamma_1}}. \quad (250)$$

The volumes therefore must be modified in the inverse ratio of the square roots of the densities.

First of all, one resistance network after the other must be converted in this way on the same reference state.

The position is quite different if, instead of the pressure-volume characteristic, the pressure level H is recorded as a function of the flow volume V . By defining a resistance value \bar{R} in a similar manner it is found that this no longer is a function of the density

$$\Delta H = \lambda \frac{l}{d} \frac{c^2}{2g} = \left(\lambda \frac{l}{d} \frac{1}{2gF^2} \right) V^2 = \bar{R} V^2. \quad (251)$$

The conversions referred to previously in Fig. 396 are then unnecessary. In all cases, therefore, it pays to derive the system characteristics in H - V charts where marked variations of the density occur.

(q) EXPERIMENTAL DETERMINATION OF THE DUCT CHARACTERISTIC

In many, probably the majority of cases, a safe mathematical prediction of the system characteristic is impossible. In such cases all that is left to us is a purely experimental analysis. Often conditions are such that there is uncertainty present only at individual fittings in the ducts whereas the remaining duct parts are accessible for calculations. Then it will be sufficient to determine the resistance of these parts.

A fortunate circumstance is that in the majority of cases, resistance laws are available which obey a *power function*. This fact facilitates the assessment very much. The relationship between Δp and V is then obtained according to the following law:

$$\Delta p = C V^n.$$

For determining this function the values for C and n have to be found. For this purpose a measurement at two points will suffice. In the case $n = 2$, which is generally valid and points to purely turbulent flow resistances, mostly a parabola $\Delta p = C' V^2$ is obtained, one point only being required for its determination. Figure 397a shows two different throttling curves a and b . The latter is a parabola. The operating point OP , which is obtained from the intersection of the fan characteristic a , is of no account for measurement. It is essential that curve a or b be ascertained in some way. As an example two test points 1 and 2 can be selected which give a considerably smaller volume V_1 and V_2 in contrast to V_{OP} . For determining the exponent n the log-log plot according to Fig. 397b is advisable because then the throttling characteristic results in a straight line whose gradient is n . This gives us

$$n = \tan \alpha = \frac{\lg \Delta p_2 - \lg \Delta p_1}{\lg V_2 - \lg V_1}. \quad (252)$$

For a parabolic throttling line a straight line with a gradient 2:1 is obtained.

It is of great importance for practical application that such measurements must not be carried out with the often very high power which is available at the operating point OP . Often considerably lower volumes will do. Let us assume, for instance, that the fan at the operating point has a power of about 125 kW. We carry out the measurement at one-fifth of the volume present at V_{OP} and, as is known, the driving power reduces with the third power, i.e. $1:5^3 = 1:125$. The test blower therefore only requires a power of 1 kW. This means, however, that a measurement of this kind can be carried out with a small auxiliary

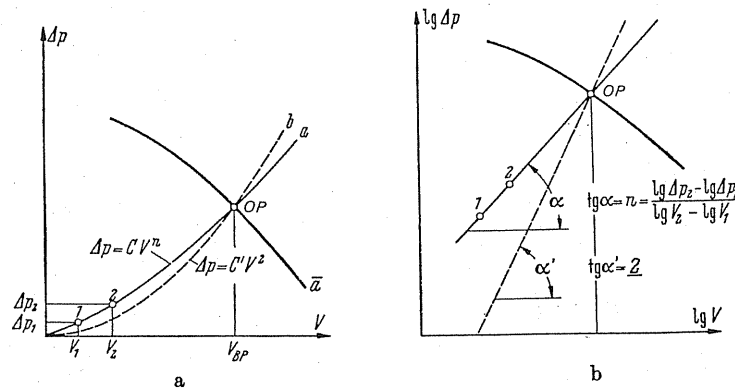


FIG. 397. (a and b) Fan characteristics at different values of the exponent of the volume function.

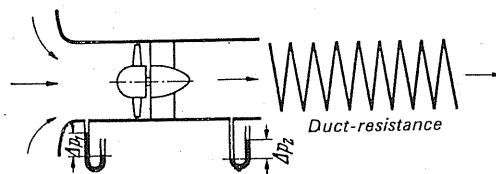


FIG. 398. Test fan for measurements of operating characteristics.

blower. As an example a small wind tunnel is shown in Fig. 398 commonly used for testing purposes. If this kind of blower is arranged in front of the duct resistance by finding the recorded pressures Δp_1 (negative pressure) and Δp_2 (positive pressure), a test point can be determined for each. It will be appreciated that it is possible to check the duct characteristics in this way with very little expense. The expenditure on this account only amounts to a fraction of the cost of the damage which would have occurred due to wrong designing. Even if such measurements actually do not supply any exact values and only those above certain Re values are possible, these test methods are often to be preferred to the very uncertain methods of calculation. In many cases, testing on models will also lead to success. The costs, of course, are only permissible in uncomplicated installations. For this purpose a geometrically similar scale modification is essential in all details.

Experimental stipulations. It is only possible to carry out the tests indicated above if the appropriate instruments are available. On the one hand, instruments must be available which are able to measure air velocities of 1 m/sec; whilst static pressure differences can still be readily determined from a fraction of 1 mm WG upwards. Are there portable

instruments available? Actually the first task can be fulfilled with the available instruments. An air velocity below 1 m/sec can be easily and immediately read from an anemometer made by W. Lambrecht (Göttingen), without any conversions being necessary. An instrument by Reichardt (Göttingen) measure air velocities of 1 cm/sec. They are both very convenient as *working instruments*.

Unfortunately for the measurement of minimum static pressures no suitable instrument is yet available. It would have to be as sensitive as the Betz manometer but be foolproof and a convenient instrument possibly without the use of fluid. A suitable diaphragm instrument is lacking.

Not only could the whole of the field of ventilation but also the complete application of fans be placed on a safe basis if it were easy in practice to carry out accurate measurements in this way for determining the system characteristics.

138. ELECTRICAL METHODS FOR DETERMINING THE SYSTEM CHARACTERISTICS

The resistance law for pressure losses $\Delta p = R V^2$ in some ways is similar to the ohmic law $U = WJ$ and gives rise to the idea that the resistance characteristic can be determined by electric analogue measurements. Feith was the first to deal with the problem of network models in 1940-1. Unfortunately in the first case a quadratic function of the volume and in the second case a linear function of the flow is obtained. On the other hand, there is accurate agreement between Kirchhoff's law of duct junctions and the similar behaviour in the hydraulic case. If it is desired to use electrical methods, care should be taken in some way or other that a quadratic function of the flow is obtained. For this purpose there are different possibilities. Wolfram filament lamps,⁽⁵⁾ due to the dependency of the electrical resistance on the temperature between 27 and 115 V, have a very accurate quadratic relationship between voltage and current $U = W J^2$. Hence these types of lamps can be used directly as substitutes of hydraulic resistances. Indeed, this method is the most popular. Figure 399

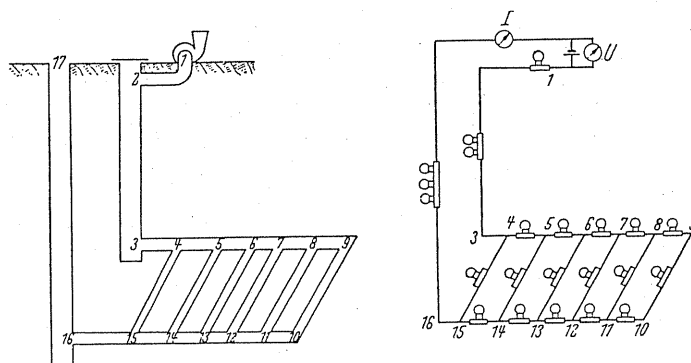


FIG. 399. Electrical analogue of a system of mine ventilation, with various resistances represented by special electric lamps.

⁵ Unfortunately, easy burning out of the lamps and the alteration of their characteristics through ageing limit their use.

shows how the resistances in a pit are replaced by suitable filament lamps. In a similar manner heated resistances can also be used. This term covers resistances which are wound round an insulating element and which have a heating wire inside the insulating element. The whole is enclosed in a gas-filled glass bulb.

Normal resistances can also be used if some effort is made to alter the resistance in such a way that it will result in a quadratic law. If, for instance, the ohms is expressed in the form $U = WJ = (W/J) J^2 = W' J^2$, then we have available the same mathematical relationship as in the hydraulic procedure. The expression $W/J = W'$ must be kept constant by some way or other. This can, for instance, be obtained by means of two resistances which can be adjusted by hand. A new method, brought out by the Institut d'Hygiène des Mines in Belgium, is much simpler. Here, apart from the ohms resistances, electronic tubes are used and manual adjustment is always possible.

A step forward would be to make the whole process automatic. This is effected with the so-called resistance box consisting of various resistances, a servo motor, and a measuring instrument. Here the re-setting of the optionally adjustable resistances is controlled automatically. Figure 400 shows a resistance box of this type supplied by Montanforschung GmbH, Düsseldorf.

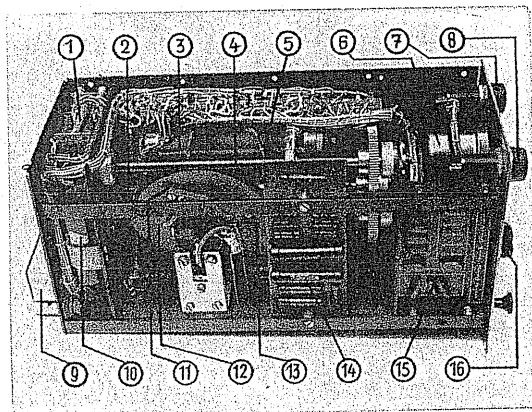


FIG. 400. Resistance box manufactured by Messrs. Montanforschung GmbH, Düsseldorf.

The basic principle of the assembly of the simple filament lamp unit is shown in Fig. 401. The resistance of each individual part is substituted by a filament lamp or a group of filament lamps. The supply source is represented by the "fan"; voltage and ammeter correspond to pressure and volumetric measurements.

In the main these rather costly electrical models serve the purpose of controlling visually the effect of any alterations taking place in an existing installation. If, for instance, in any part of the mine faulty ventilation is found, investigations can immediately be undertaken on a ventilation model as to the measures which can be applied for improving the conditions. A gallery can be widened in the cross-section, and this causes the resistance to drop. For this purpose, in the ventilation model only one resistance need be substituted by a correspondingly smaller one. It is, however, possible to remedy the fault by an appropriately mounted additional fan. To this end in the ventilation model a d.c. current source with the

voltage and supply would be fitted in the place provided to supply the desired ventilation at the point in question.

The cost would be the lowest if rotary resistances by Hiramatsu⁽⁶⁾ were used and the resistances determined by an iterative process. Pohle⁽⁷⁾ has reported fully on the methods used in practice.

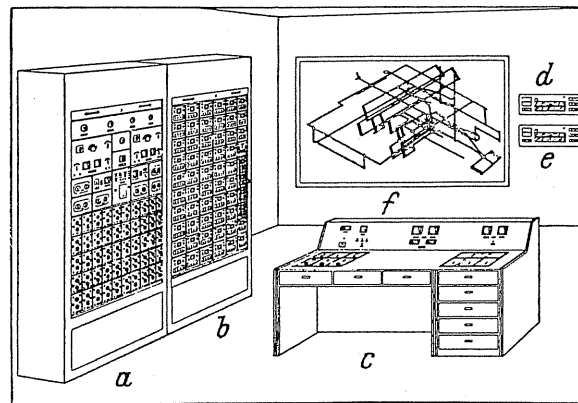


FIG. 401. Special electric lamp for determining the system characteristics. *a* and *b*, filament lamp cabinets; *c*, control and service desk; *d* and *e*, wiring diagram.

By this method working shifts of a few hours for trained personnel are required to carry out the iterative process. The cost for example of the ducting system of a large steam generator with a mill fed furnace accordingly amounts to DM 1500 including the electrical instruments used. It is hoped that the purchaser of large fans which are destined for a complicated duct system will make more use of these possibilities. The costs of such preliminary investigations only come to a small fraction of the cost of the immense damage produced by a wrongly designed fan.

A field of application where such pains are taken to determine accurately the resistances and the duct characteristics is in mining. In many other cases the state of affairs is almost the same as in mining, e.g. the complicated ventilation system of an ocean liner, the labyrinth of ducting of ventilating and air conditioning of large buildings, skyscrapers, etc. The only "excuse" which some engineers give for almost *completely ignoring these problems* is that relatively small outputs are involved which are of no great interest. Such engineers should remember although "so-called experiences" enable him to work by "rule of thumb", *the pressure loss necessary in each case will become greater*. If, therefore, the fan is designed for a completely superfluous higher pressure difference, *excessive noise will be generated*. For this reason alone good designing is essential. The ventilation engineer is unlikely to use costly electrical ventilation models in order to facilitate design but great head-

⁶ Hiramatsu, Y., Determination of strengths of ventilation flows in mine ventilating ducts according to formulae for electric current, *Glückauf*, 1953, p. 355.

⁷ Pohle, R., Firing techniques: Notes on the solution of the problem of volume flow and pressure distribution in controlled air duct systems of steam generators, using an electrical network model, Diss., Freiburg, 1958.

way will be made if he becomes acquainted with graphical methods which will enable him to arrive at *an almost accurate solution*. For this reason the methods mentioned above will have to be explained in detail. The author bases his views on many observations in practice. Design methods and the determination of ducting characteristics are, of course, governing factors in ordering fans and it is no exaggeration to say that they, remain the most neglected fields in the whole industry.

PART D

SPECIAL PROBLEMS, SPECIAL USES

CHAPTER XVIII

MINE VENTILATION AND BOILER FANS

139. BLOWERS FOR MINE VENTILATION

If a great deal of stress is laid on mine ventilation, this is because it is a major field of application for fans and also because part of the development of fans is identical with the development of mine fans. The excellent book by Fritzsche⁽¹⁾ is very informative. The state of affairs prevailing up to 1935 is given in a paper⁽²⁾ by the same author.

Here the main task of the fans is to supply the whole gallery and shaft system with ample fresh air.

Since every man requires about 6 m³/min of air for each day he works underground, large fan ratings are obtained. In the Ruhr region there are 454 main and standby fans in operation. The pressures to be overcome range mainly from 100 to 350 mm WG. The maximum pressure is approximately 580 mm WG. The highest delivery volume is approximately 28,500 m³/min. The highest driving power is 2300 kW. The proportion of radial flow fans used is $\approx 70\%$ of which 43.3% have no regulation. Axial-flow fans amount to 30% of which 2% are without regulation. The mean fan efficiency for the German mining industry is stated at 0.49 by Linsel⁽³⁾. For the German mining industry for the same period in the year 1953 the same source stated the optimum efficiency to be 0.83. These values in the meantime have risen to about 90% by fitting the high-duty blower.

For a long period the radial-flow fan held the field. The rather immense constructions of their spiral housing assemblies, often with tower structures, are well known and dotted about mining regions. The explanation for these oversize constructions was that, at the time, hardly satisfactory efficiencies could only be achieved to some extent with small diameter ratios. A considerable improvement was achieved when axial-flow fans were introduced: efficiency rose and sizes became considerably smaller. This development in recent times has been interrupted again by the improvements of radial-flow fans. At the moment the situation is such that almost equally efficient axial-flow and radial-flow fans can be fitted. All former disadvantages which could be rightly attributed to radial-flow fans are no longer present today.

The design of the main fans is associated with large basic difficulties. On the one hand, it should be considered that for a given mine extension the development is continuous and is

¹ Fritzsche, C.H., *Lehrbuch der Bergbaukunde*, Vol.1, 9th edn., Berlin/Göttingen/Heidelberg, Springer, 1955.

² Fritzsche, C.H., Development, efficiency and possibilities of application of modern propellor fans for mines ventilation, *Glückauf*, 2 (1953) 1045.

³ Linsel, E., Mine ventilation, *VDI-Z*, 1953, p.429; and Position and trend of development of mine ventilation, *Habilitationsschrift TH Aschen*, 1949.

always altering. According to the advance of the working, new shafts and galleries are added so that the air volume as well as the necessary pressure loss is altering steadily. The problem now is to design in such a way that these unknown developments can be accommodated approximately. Even the calculation of the resistance of an accurately established widely

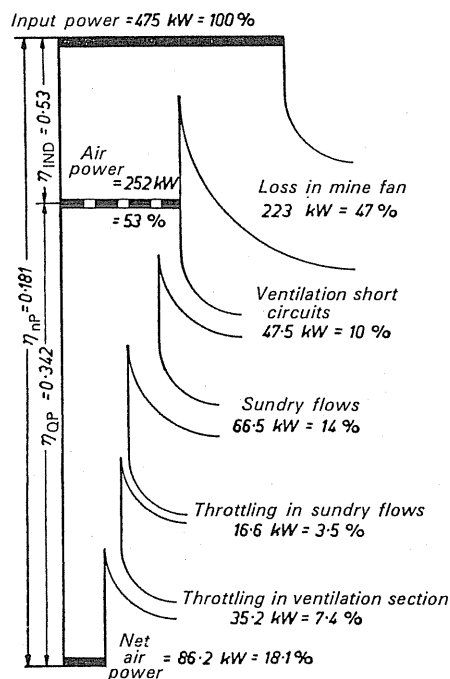


FIG.402. Diagram of flow losses in mine ventilation systems according to Linsell.

branched ducting system is still a problem. An added complication is that in the mine between the shafts and the gallery intermediate streams flow through the beds according to the composition of the geological formations. Therefore a considerable leakage of air occurs. On the average about 45% for the so-called short circuiting can be expected. All these aspects bring out the fact that in mining considerable value is laid on determining the resistance. To this end newer experimental methods are being used as for instance the electrical model.

An interesting diagram by Linsell (Fig.402) shows the magnitude of the losses under ground.

To get an outline of the overall situation we will first look at Fig.403. Air from the outside enters through the shaft *A*, flows through all workings which end in shaft *B*. At the top end of this covered shaft we have the mine fan which exhausts the air to atmosphere through a diffuser. Alongside this problem there is the one of steadily ventilating the new workings obtained in advancing. Figure 404 shows the basic solution of this problem. For this purpose there is generally a fan at the inlet to the new gallery which sucks air from the main gallery and forces it through a duct to the end of the working. This air then flows back into

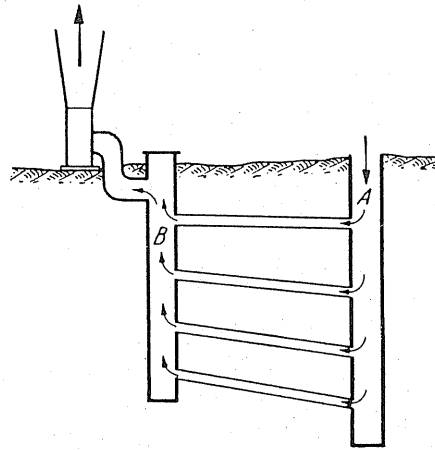


FIG.403. Diagram of a mine ventilation system.

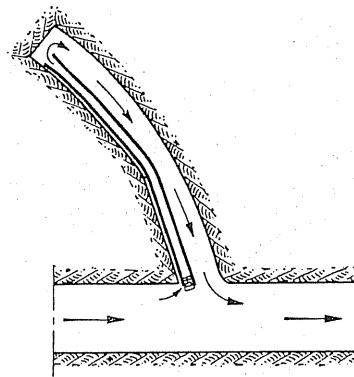


FIG.404. Ventilation of a blind gallery.

the main working. As the working is extended, the duct called the ventilating duct is extended. The fans necessary for this job are called auxiliary fans.

For correcting the ventilation of individual parts of a mine the procedure formerly was that, e.g. in parallel trunks, one trunk would be throttled by means of a so-called ventilating door. In this way the other trunk would be ventilated better. This, of course, leads to great losses. In recent times the special *booster fan* carried out the adjustment. This booster fan, as shown in Fig. 405, is positioned in the ventilating doors, which were previously used for throttling.⁽⁴⁾ As opposed to the simple throttling this is a considerable improvement. This particular case has already been dealt with basically in former examples, thus three particular types of fans emerge which are used in mining.

The main fans. As quite a number of former fan designs are operating even today for different applications and their construction formed the background of later developments, they should be mentioned here. In order of importance, i.e. the numbers which have been

⁴ Batzel, Improvement of air circulation by means of booster fan, *Glückauf*, 1953, p.20.

installed, the following types are involved: Capell, Rateau, Pelzer, Geisler, Winter. The design by Rateau is worthy of interest because certain features have to some extent been taken up again. This refers to the somewhat inclined position of the blades and also the projection of the blades into the axial suction space (Fig. 406).

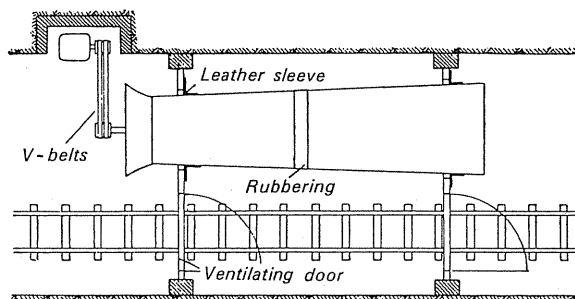


FIG. 405. Booster fan in the ventilating door of a mine.

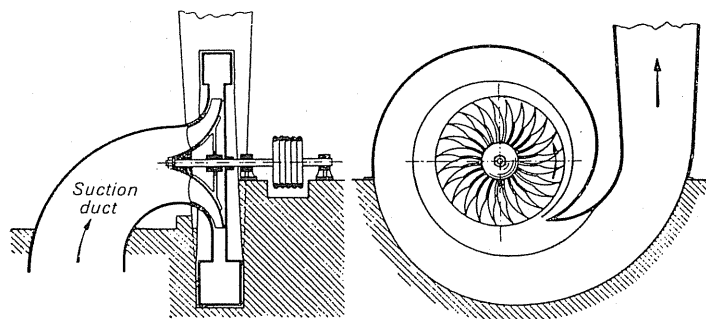


FIG. 406. Mine fan with the blades projecting into the suction space. (Design by Rateau.)

Typical of the development has been the retention of radial impellers of fairly small diameter ratios. This development is explained by the fact that for these types of impellers the widest experience was available. A further contribution may have been the circumstance that almost all research work particularly in the field of centrifugal pumps has been concentrated on this type of impeller. Hence mine fans, some of them with enormous dimensions, were manufactured. Figure 407 shows one of these enormous constructions which at that particular time was considered the best design. It is rather enlightening that this giant design became obsolescent when the axial-flow fans of much smaller size, considerably higher efficiencies, and better regulation facilities became available.

The situation with mine fans as a whole can be assessed as follows. Axial-flow fans and radial-flow fans are both being used. The advantage of the axial-flow fan is the better regulation due to the possibility of blade adjustment, whilst radial-flow fans have a higher efficiency and generate less noise. The following factors speak for and against both types.

Owing to the operationally safe clearance required between outside wall and impeller, the efficiency of the axial-flow fan dropped quite considerably. Therefore, the mean for optimum designs can be taken at about 85–86%. In modern radial-flow fans a value greater

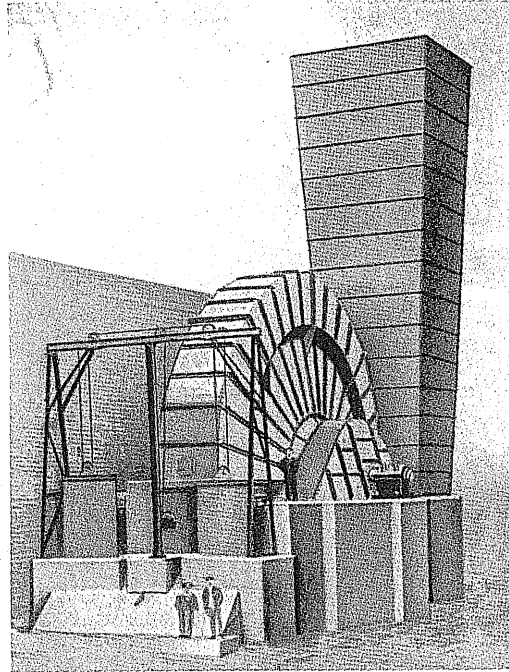


FIG.407. Mine fan with radial impeller of Messrs. Westfalia-Dinnendahl-Gröppel in Bochum.

than 90% can be achieved. In axial-flow fans without blade adjustment it is impossible to obtain peak characteristics. With blade adjustment the envelope of all curves for individual blade adjustments is obtained as the efficiency curve. In Fig. 408 this is represented with the envelope shown. The curve has been obtained from the comparison of a large number of the best axial-flow fans. The thick lines are the curve corresponding to the later radial-flow

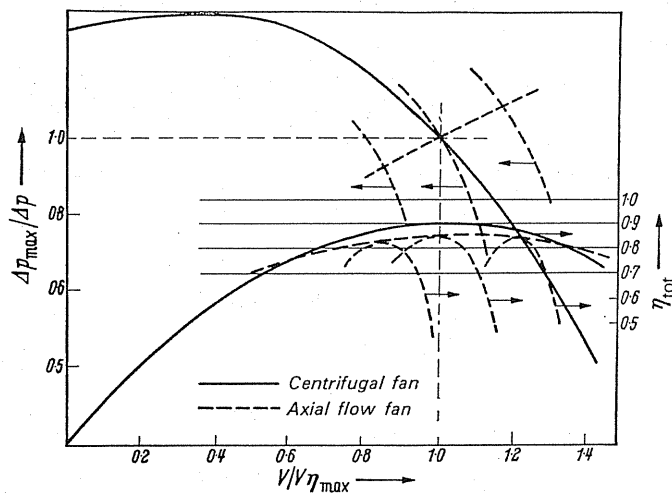


FIG.408. Efficiencies and pressure characteristics for centrifugal fans (solid lines) and axial-flow fans with adjustable blades (dashed line).

fans. Without any adjustment the range above $\eta = 0.8$ is still somewhat larger than for axial-flow fans.

Only below 80% is the efficiency curve of axial-flow fans superior. The curve for radial fans has been raised in the meantime (Fig. 102).

The overall picture, however, alters due to the fact that the axial-flow fan requires mostly a further bend. The losses arising on this account as shown in tests by Voith are significant (Fig. 409). Furthermore, in most cases of axial-flow fans a silencer is required on the diffuser

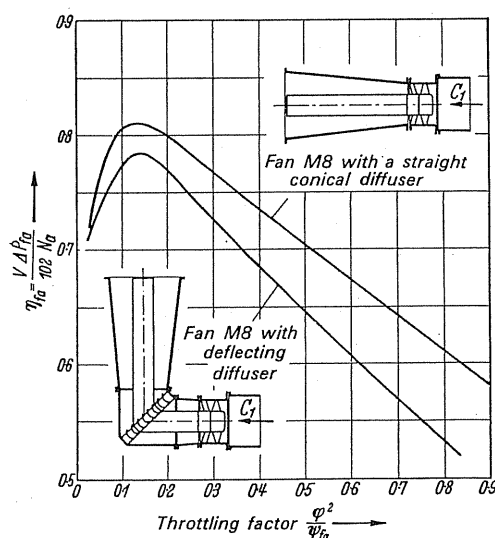


FIG. 409. Losses in bends downstream of an axial-flow fan according to Voith.

which again is associated with losses. In addition the cost of this silencer which necessitates strengthening the diffuser are considerable; sometimes they may amount to 30% of the whole installation.

The control chart must also be watched continuously. The operating point of the mine fan alters in the course of time. If, for example, steady advancing is being carried out, over a period a range of operating points arises which have to be adjusted over the years. The delivery volume rises throughout and the mine extension can also alter. When purchasing a new mine fan, therefore, a time chart must be plotted containing the demands over a period of about 10–20 years.

Modern time charts such as these demand such a wide range of essential operating points that even the blade adjustment of axial-flow fans will not meet the case. Therefore the choice of velocity adjustment offers itself automatically as a control. Since the operating points of the time chart are situated throughout to the left and right of a throttling curve, i.e. a curve of constant mine extension, the efficiency hardly alters at all in velocity adjustment. In radial-flow fans, therefore, the unique possibility exists of always being able to run at *peak efficiency*. By employing gears where the sets of gears can be changed, this method of regulation is being applied in large numbers today.

A set of gears is simply replaced at intervals of about 5 years. A still better speed adjust-

ment is by means of the *Scherbius motor*. This frequency regulated motor has the singular feature that the efficiency of the motor remains constant at speed regulation.

A practical example, where over a period of 15 years four different speeds were operated, is shown in Fig. 410. The thick lines are the operating points which result from the extensions to the mine in the course of time. It will be observed that the main points can almost always be run at maximum efficiency.

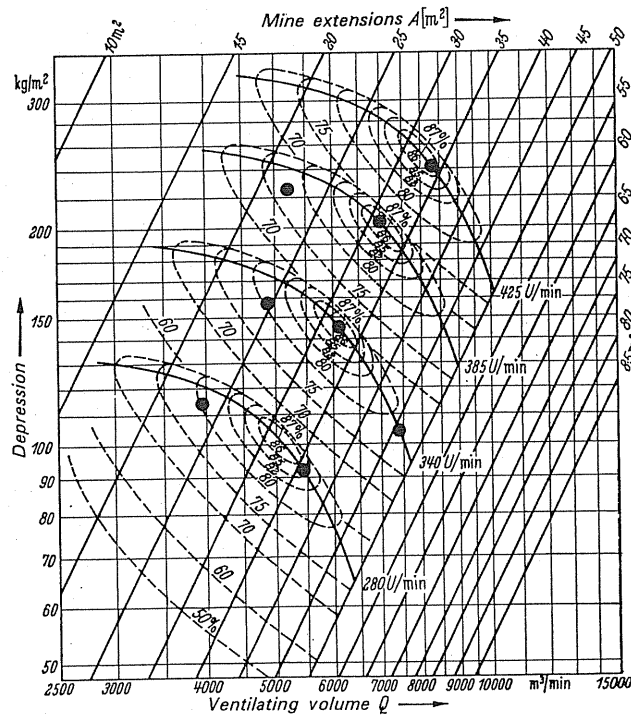


FIG.410. Characteristics of a centrifugal fan with speed adjustment. Black dots = operating points over extended development period of a mine.

If the controllability of centrifugal and axial-flow fans is compared, a characteristic difference is found. In Fig. 411 the ellipsoidal curves for both types are plotted, from which a type of axial-flow fan was selected which no doubt offers the widest range of regulation. The typical difference is that axial-flow fans can be regulated well above the normal characteristic whereas radial-flow fans hardly respond to counter rotation of inlet-guide vanes. On this account, hitherto, there were notable differences to be found in the controllability of both types.

The author has dealt with these defects for a long time and has looked for other methods of regulation. It has now been found that the improvement can be made by an absolutely new aerodynamic design of the radial impellers. Figure 412 shows the result obtained on the first model. The illustration shows a new regulation method for the case of upward regulation. Accordingly, the pressure can be increased by 45%, i.e. by the equivalent amount as in the axial-flow fan. A much steeper regulation is obtained going downward. Thus

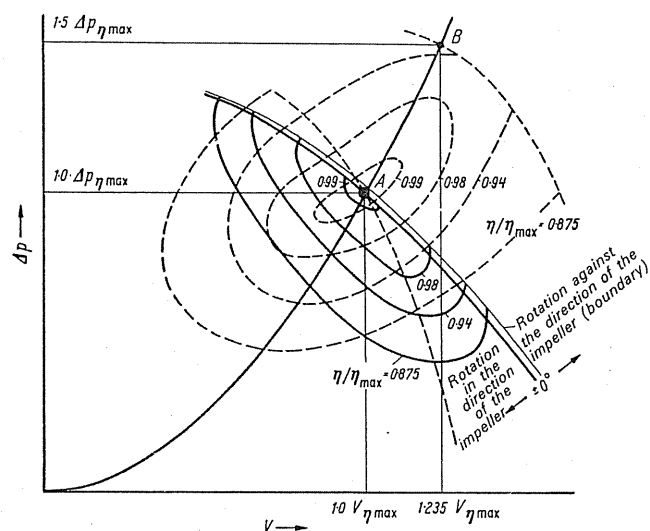


FIG.411. The effects of varying the blade angle on the performance of centrifugal fans (solid line) and axial-flow fans (dashed line).

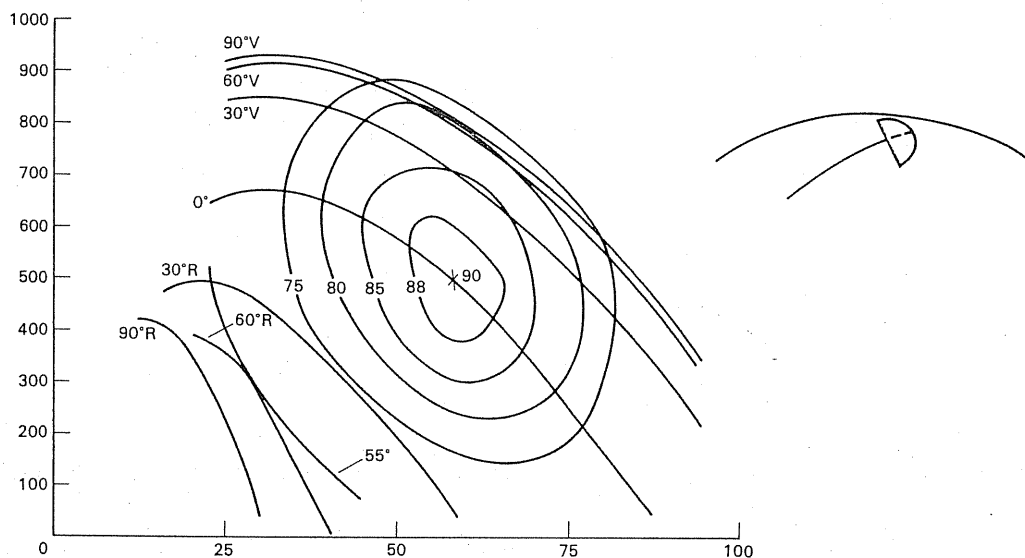


FIG.412. Flap regulation of radial-flow fans.

it is to be hoped that the radial flow fan will shortly no longer lag behind the axial-flow fan on account of regulation.

Figure 413 shows a modern centrifugal mine fan and Fig.414 shows an axial-flow mine fan.

Auxiliary fans. Auxiliary fans are designed throughout as single or multistage axial-flow fans. The auxiliary fans used in mining have diameters of 300, 400, 500, 600 mm. Figure 415 shows a typical arrangement by the firm Korfmann, Witten, Ruhr.

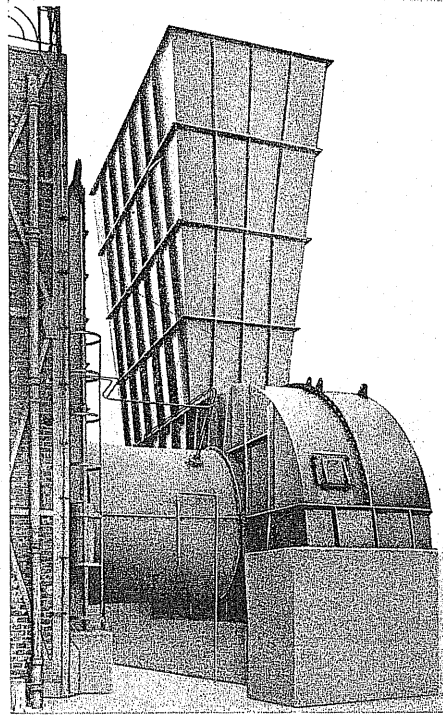


FIG.413. Mine fan designed by Eck and manufactured by Messrs. Büttner-Werke AG, Krefeld-Uerdingen.

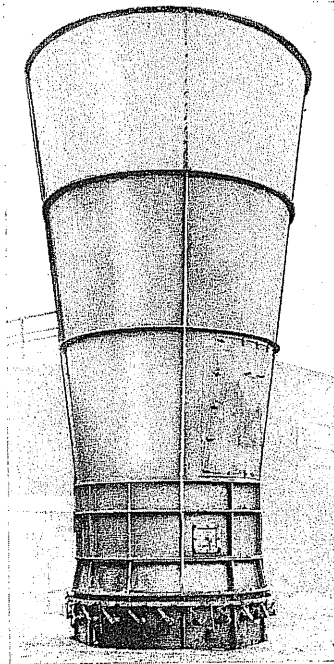


FIG.414. Vertical constant pressure fan designed by Schicht.

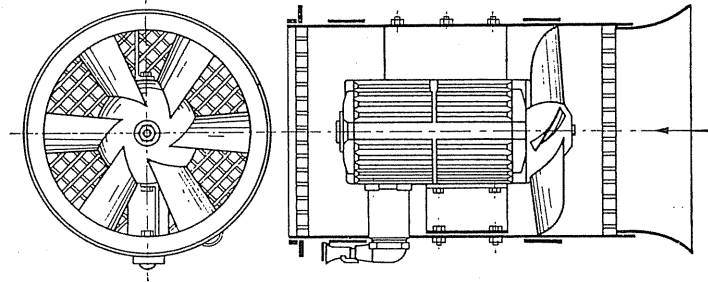


FIG.415. Ventilating fan manufactured by Korfmann, Witten/Ruhr.

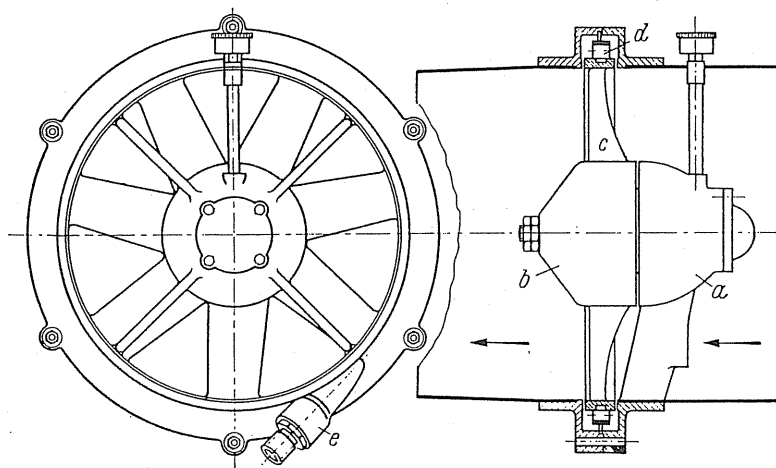
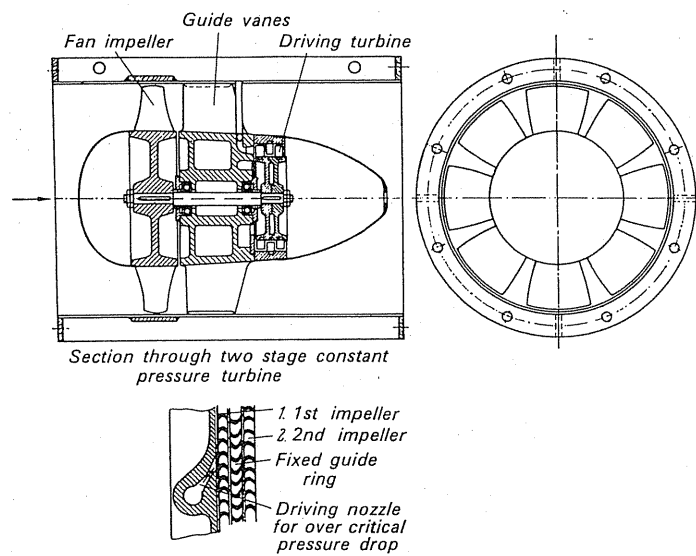
FIG.416. Effect of blading outside the aerofoil (Korfmann). *a*, hub retainer; *b*, fan hub; *c*, axial blade; *d*, turbine blades; *e*, compressed-air nozzle.

FIG.417. Multistage action impeller with driving turbine in the hub (Korfmann).

Apart from being driven by electric motor, compressed-air drive is also included either as a compressed-air motor in the hub or the compressed air acting on an action blading, which is fitted outside the aerofoil (Fig. 416). An improvement has been made by a multi-stage action wheel being accommodated in the hub as shown in Fig. 417. In spite of the

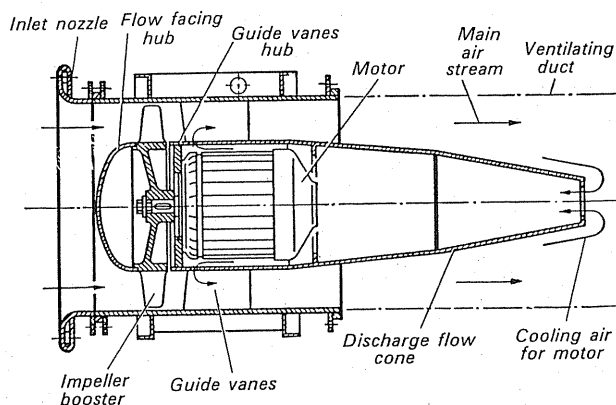


FIG. 418. Booster fan with motor, cooled by air.

inferior overall efficiency ($\eta \approx 25\text{--}30\%$) these types are still being recommended. Apart from fire-damp safety they still have the advantage that very desirable cooling effects are brought about through the expanding compressed air.

Booster fan. This is a somewhat larger fan which often has to overcome a pressure of 100–200 mm WG. This fan in its assembly is no different from a normal axial-flow fan. Designs as shown, for example, in Fig. 418 are being installed according to Fig. 405. Hitherto auxiliary fans and booster fans were exclusively of the axial type. Here, the mounting of radial impellers of a special type might be in many cases an attractive proposition.

140. BOILER FANS

In modern high-output boilers the fans are of great importance and represent an important field of application for fans. For achieving improved boiler efficiency the hot gases are cooled as much as possible in passing through a bank of heat exchangers. Today it is a matter of course that as much dust as possible is removed from the exhaust gases. These tasks can only be carried out with a high-pressure loss. Even the high chimney stacks do not provide the draught which would be required for the purpose. Hence it is essential to make up the lack of draught artificially by fans arranged in front of or following the boiler. For this purpose forced-draught fans and induced-draught fans are required. From the fan engineering angle it would be the simplest to provide the additional draught required by positive pressure using blowing fans, so called, forced-draught fans blowing cold but dust-free air (in the case of pre-heating the combustion air). This, however, will not do because a positive pressure in the boiler will lead to an unavoidable discharge of gas into the boiler

house, since even with the best workmanship sufficient air tightness and pressure tightness of the walls are impossible to achieve. The pressure generated by forced-draught fans therefore can only be limited. It would be restricted more or less to overcoming the resistance in the fuel bed. In addition even if equivalent pressure is present above the fuel beds to that in the boiler house, a lower positive pressure may arise at the higher boiler levels owing to the rising highly heated combustion gases. Therefore with leaking walls gas may penetrate to atmosphere. Therefore in practice *exhausting the whole* combustion gases is unavoidable, and so-called *induced-draught fans* must be fitted.

Induced-draught fans alone will not do the job. Exhausting on its own would mean that the resistances in the grate, the velocity heads, the fresh air nozzles, etc., have to be overcome by the induced-draught fan. This would lead to a relatively high negative pressure in the combustion chamber, and the furnace walls of the usually enormous combustion chambers would be highly stressed. Apart from this, unavoidable and uncontrollable quantities of leaking air would flow in. For this reason it is essential in large installations to fit a so-called forced draught fan in front to create approximate pressure equilibrium with the outside atmosphere. The pressures to be overcome therefore may be great. On the average they range between 300 and 700 mm WG, whereas in induced draughts pressures occur between 200 and 750 mm WG. The exhaust gas temperatures work out at about 170–340°C. Air consumption and output are shown in the following table.

	Forced-draught fan	Induced-draught fan
Air demand in kg/sec { brown coal for 100 t/h { bit. coal	40–60 30–40	60–80 40–60

The installed power in kW for each 100 t/h for forced-draught and induced-draught fans combined works out at:

for brown coal	500–600
for bituminous coal	250–300.

The following example shows the power consumed in modern power stations for this purpose. A power station with an installed capacity of 200,000 kW requires 5200 kW alone for driving the boiler fans. The installed power of boiler fans installed in Germany might be in the region of 350,000 kW.

In assessing the pressure loss it should be taken into account that, *inter alia*, the resistance can rise by 10–20% through dirt deposit. With dirt deposit there is a most remarkable phenomenon. It has been found that as the rate of deposit increases, the resistance first declines. This is explained by the fact that dirt accumulates *behind* the numerous tubes which forms a sort of discharge flow element. With further deposits the resistance then starts to rise at a high rate. The resistance on the air side of the fuel bed is difficult to assess. Grain sizes, bed thicknesses, slag deposits, charred grate bars fluctuate considerably. Hence the situation for *forced-draught fans* is almost contrary to that for induced-draught fans. Whilst in forced-draught fans the delivery volume is known very accurately, the resistances of the grate bed fluctuate a great deal in operation. In induced-draught fans the resistance as such

can be assessed some way or other, whereas the delivery volumes can be extremely variable. Since present-day high furnace chambers cause a furnace gas lift up to 10 mm WG the negative pressure should be amply estimated to allow negative pressure to be available with certainty everywhere in the furnace chamber.

If the quantity of coal to be burnt remains constant and as scheduled, conditions can be controlled accurately. If the fuel weight remains constant, then the weight of exhaust gas will remain constant subject to controlled combustion. The volume then can be easily ascertained from the exhaust gas temperature as follows:

$$G_{\text{gas}} = \gamma V = \frac{P}{RT} V. \quad (253)$$

In order easily to check the performance of the fan, we select fan characteristics which are invariable. In accordance with previous practice we plot the *pressure heads* H as a function of the *delivery volume* V and we obtain a fan performance curve for constant temperature (Fig. 419).

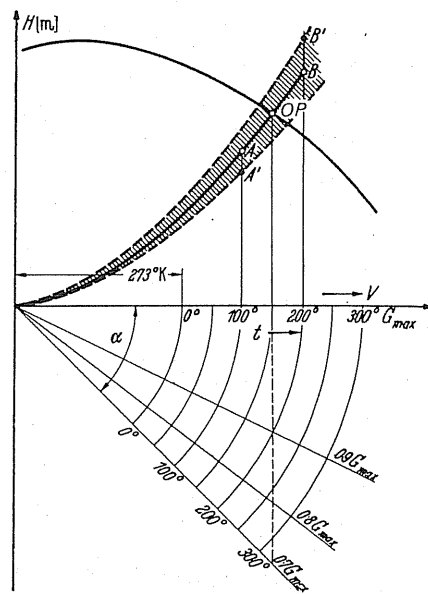


FIG. 419. The effects of air temperature on fan characteristics.

In the same way if we check not the pressure loss but the pressure head loss H of the gas paths, we obtain a system characteristic which is also independent of the temperature, and this leads to an equation of the following type:

$$H = \zeta \frac{V}{2g F^2},$$

where F is the typical area of an orifice. The alteration of resistance through dirt deposits will result in various ζ values. If we look at the lowest and highest values of ζ we obtain the two dotted line resistance parabolas as shown in the diagram. The mean position is shown

by thick lines. The fan characteristic independent of the temperature intersects the throttling curve at OP . However, at $G = \text{const}$, in accordance with eqn. (253), V is proportional to T ; the abscissa for the volume in the suitable scale also applies to the absolute temperature.

Let us look at different gas weights (i.e. also different coal quantities); then for the equivalent volume we obtain the following relationship:

$$\begin{aligned} G_1 &= \frac{p}{R} \frac{V}{T_1}; \\ G_2 &= \frac{p}{R} \frac{V}{T_2}; \\ \frac{G_2}{G_1} &= \frac{T_1}{T_2} = \cos \alpha, \end{aligned} \quad (254)$$

if G_1 is the maximum delivery weight.

This signifies, however, that different gas weights can be taken into account in such a way that the temperature scales can be plotted on the equivalent scale under the angle α in accordance with Fig. 419 with the abscissa applicable for the highest gas weight. By following a constant volume, i.e. a vertical line, it will soon be realised that higher temperatures are essential to smaller gas weights. The possible fluctuations in volume, and accordingly the different points of the characteristic, which occur in practice, can easily be determined from this diagram. If, for instance, at a medium gas temperature of 150°C the temperatures fluctuate by 50° , points of intersection will occur on the throttling line A' and B' since, at the lower temperature which is obtained in clean gas passes, the bottom throttling line applies and vice versa. This signifies, however, that the difference in pressure head from A' to the characteristic would have to be throttled down. The steeper the characteristic the greater the amount of throttling necessary, if no fan regulation is available.

The numerical alteration of the volume with the gas temperature to

$$\frac{\Delta V}{V} = \frac{\Delta t}{273 + t}$$

is easily obtained from $V = \text{const}$. If, for example, at a mean exhaust gas temperature of 100°C there are fluctuations of 50° , then fluctuations in volume of 13.5% will occur whereas with 100° the fluctuations in volume will be 27%.

The state of the pressure compensation in the furnace. The forced-draught fan of the furnace only produces *positive pressure* and the induced-draught fan only *negative pressure*. Therefore, of necessity, there must be somewhere in the furnace a zone where the same pressure prevails as that outside the furnace. This zone should, as far as possible, still be in the fire bed, to give at least a little negative pressure above it. In this way gases are prevented from discharging when the furnace door is opened. This "neutral" zone will, however, only be located at this point if the pressures laid down for the two fans actually agree, which is seldom the case. A separate calculation of the two fans therefore is possible

because the forced-draught fan cannot make any contribution to the negative pressure of the induced-draught fan. The only problem is the accurate predetermination of the actual pressures up to the neutral equivalent pressure zone.

WEAR

In fans, wear by entrained ash particles is a very important problem. Even when an electro-static precipitator is used it may be expected that if this equipment fails, ash particles acting on the blower for a short time will pass through. The relative velocity along the blade surfaces and perpendicular to these governs the rate of wear, i.e. the shock components of the relative velocity. Equipment of this kind, therefore, is interesting, in which the relative velocities are as low as possible. The dependency of the life of impellers on the relative velocity was determined by Kohler.⁽⁵⁾ According to his theory, hyperbolic curves are created for this dependency. Local velocities with concentrated dust ratios can often be corrected by special guide vanes.

Differentiation should also be made between frontal wear by direct impact of the dust particles on the front surface of the blades and flank wear. Pointed facets are often sufficient to reduce the frontal wear. Thus pointed, forward, blade edges which can furthermore be reinforced by welding on harder material are designed. The shapes are contrary to the requirements based on flow principles.

Radial-flow fans have positively smaller relative velocities and are not open to the same dangers as axial-flow fans. In radial-flow fans, moreover, the maximum relative velocity can still be reduced by choosing smaller diameter ratios. However, this is at the cost of the dimensions, i.e. of the price, since the suction capacity of these impellers is small.

Apart from the relative velocity the deflection of the positive streamlines plays an important part because in this way the velocities at which the particles can impinge perpendicularly on a blade area are determined to a greater or lesser extent. The greater the deflection the greater does this effect take place.

As the maximum relative velocity stands in a fixed ratio to the peripheral velocity in axial impellers a dependency on the pressure coefficient ψ is obtained. In the first approximation the following rule can be stated: *The greater the pressure coefficient the less the wear.* Since meridionally accelerated axial impellers always have twice the pressure coefficient of the normal axial impeller, the wear in the latter is considerably less. For this reason, these types of blower have proved very successful in induced-draught plants.

The problem then arises of having a form sensitivity. In meridionally accelerated impellers with sheet-metal blades this sensitivity is not present, but it is available in high-grade blowers with aerofoil blades. These aerofoils are extremely sensitive to alterations of section. If it is realised that, under certain circumstances, the fly ash can alter the aerofoil section considerably within a few hours, the advantage of designs which are without this sensitivity will be appreciated.

Another important factor is that lower efficiency fans wear quicker than higher grade fans. The material collects in the separation spaces. A very strong milling effect is the result.

⁵ Kohler, W., Boiler fans, *Österr. Ing.-Z.*, 1958, p.193.

Hübner⁽⁶⁾ initiated tests on wear. The difference between axial-flow and radial-flow fans is very clearly demonstrated in these tests. At almost identical dust content the radial-flow fan had running time of 30,000 h and the axial flow fan only 5000 h. Throughout, the running periods of the radial impellers were 5 times as large as those of the axial-flow fans.

The latest investigations are those undertaken by Trenkler who thoroughly investigated the wear in meridionally accelerated axial-flow fans at the Rhein, Braunkohlenwerken, Cologne on a scientific basis. The remarkable result of this investigation was that a surprisingly large high rate of wear takes place if appreciable shock components arise perpendicular to the intake relative velocity. Figures 420 and 421 are photographs taken by Hübner and

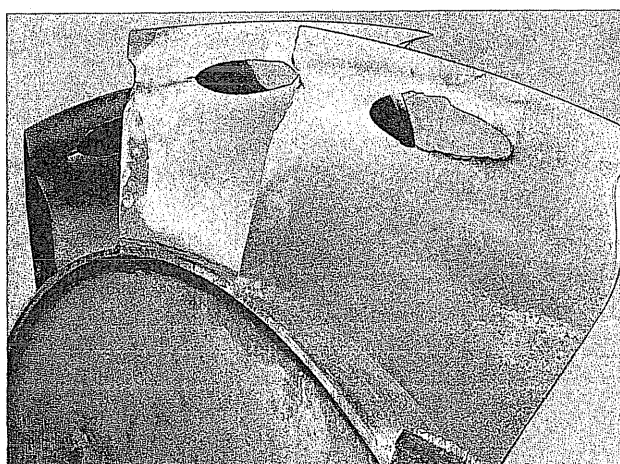


FIG.420. Erosion of blades of an axial-flow fan by coal ashes.

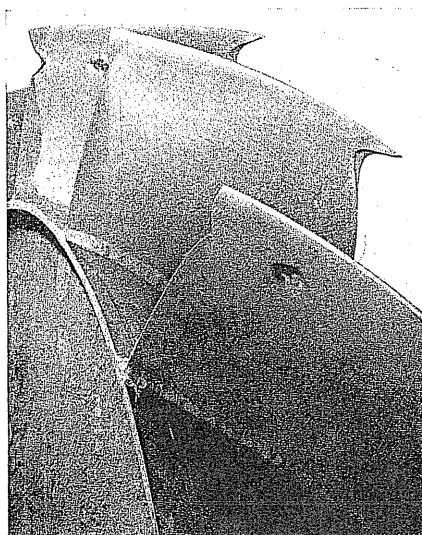


FIG.421. Erosion of blades in an axial-flow fan, visible pitting at the inlet.

⁶ Hübner, M., *Experiences in Operation with Radial and Axial Induced-draught Fans*, Report of VGB, 1958, p.274.

Trenkler showing wear in various stages. Two points of attack are characteristic of this type of wear. First of all, there is the inlet cone just in front of the outside diameter, and then there are characteristic holes at about one-third of the height of the blade from the outside diameter in the centre of the blade to the end.

The shock components indicated are characteristic for design faults which are particularly typical of boiler fans. In these cases the fan, as considered in Fig. 354 and section 132, works well away from the optimum efficiency parabola, and throughout on the steep fall of the characteristic in axial-flow fans. The very high wear feature of axial-flow fans using brown coal *if certain design faults are exceeded* is very apparent from the very comprehensive tests by Trenkler.

DESIGN AND REGULATION OF BOILER FANS

In the boiler fan layout there are a few complications which will now be explained briefly. Taking as a basis a known quantity of coal which is to be burnt, the amount of air required for combustion can be obtained with sufficient accuracy from the combustion formulae. This means that for the forced-draught fan the delivery volume is fairly accurately known. The case, however, is quite different for the exhaust gas volume which has to be obtained for calculating the induced-draught fan. For this a significant but unknown factor comes into the problem, namely the *exhaust gas temperature*. The heat transfer inside the furnace, the radiation of solid coal, the radiation of bright flames, the almost incalculable influence of the dirt deposits on heat transfer are very important factors. It is quite impossible to carry out in advance an accurate calculation of the heat transfer.

Hence if the delivery volume required for the fan calculation is not even known accurately, then a further unknown factor comes into the picture and this is the pressure loss which has to be overcome. Air temperature, moisture, and barometric pressure are subject to annual fluctuations. Therefore the draught in the chimney fluctuates as well. These seasonal variations could easily amount to 20 mm WG. The flow losses on the inside of the gas flues are likewise almost impossible to determine mathematically; nevertheless an assessment should be made of this uncertainty apart from the unknown exhaust gas temperature. *However, this uncertainty can be reduced by experiments.* For this purpose all that needs to be measured is the pressure which has to be overcome by the induced-draught fan in practice for a specified exhaust gas volume. This means, of course, that, first of all, a fan must be available. Owing to the high importance of knowing this detail accurately, the idea might occur that, first of all, a test impeller be fitted for determining the resistance and, consequent upon this the final impeller designed. Recently, the method used has been to determine the resistance by means of an electrical model.⁽⁷⁾

The variable rate of dirt deposit and atmospheric fluctuations due to the varied coal composition do not lead to a definite operating point but rather to an operating area. In view of these uncertainties which are increased by the fact that the resistances which are to be

⁷ Pohle, R., A contribution to the solution of the question of volume flow and pressure distribution in regulated air duct systems of steam generators by using an electrical network model, *Freiberger Forschungsheft*, 133 (1959).

specified are scarcely reliable, the customer will be inclined to add safety margins. According to experience with larger units there are numerous contingencies governing the problem, and therefore it often occurs that a safety margin is added at each point and *the fans are hopelessly miscalculated*. It is no exaggeration to state that half the induced-draught fans in use are wrongly estimated.

Independent of this uncertainty in the fundamental design it is necessary to regulate the different delivery volumes during operation to suit the steam demand of the boiler. Owing to the relatively low water capacity of modern boilers, control demands must be met *rapidly*. What are the operational characteristics for boilers? Generally these are square laws which produce the well-known parabola as the characteristic. An exception is the oil-fired boiler where a more or less constant pressure is expected to be present in front of the burners. In this way a line parallel to the V axis is obtained which is succeeded by a flat parabola for the remaining flow resistances. Regulation in this case is extremely simple. Simple throttling will do, because by approaching the regulating instruments to the flat parabola hardly anything is to be gained in percentage.

For furnaces burning coal and pulverised fuel a parabola or a parabolic strip according to Fig. 419 is obtained in which also the variations through dirt deposit and other factors can be accounted for. The fans operate in the point of intersection of this strip with the fan characteristic. If we assume a 10% increase and reduction of the delivery volume which generally is too low, this gives us a maximum displacement from A' to B' . Whereas the lower points can be set by throttling, there is no possibility without control measures to obtain the higher pressure at B' . This fault can be remedied in simple installations by designing the fan for point B' and to run it with a little throttling in the normal state. In larger installations, however, such measures involving high losses are intolerable.

For a long time it was considered a great advantage of the meridionally accelerated axial-flow fan, that these control requirements could be fulfilled by means of a simple control of rotation operating with and against the rotation, whereas the counter rotation only has a small effect in radial-flow fans and is not sufficient for regulation. Unfortunately, these axial-flow fans have approximately a five fold rate of wear in comparison to radial-flow fans and wear out too rapidly, when strong shock components occur. In addition, new dust blowers of the radial type have been designed which are much smaller than former types and have been improved considerably not only in efficiency but also in the controllability.

In the meantime requirements have become more stringent since overloads of almost 20% must be expected. If in such cases every possible source of loss is to be prevented in regulation, there is nothing left but to use an electric motor with several available speeds or one with an adjustable speed. An outline of the losses involved in different possibilities of this kind due to Kohler⁽⁸⁾ is illustrated in Fig. 422.

Since speed regulation owing to the high fly-wheel masses is not able to comply with the actual control requirements in boiler operation, efforts have been made recently to combine speed variation for the long period of fluctuation and the guide vane adjustment free of inertia for the short period fluctuations. Installing the induced-draught fan is often difficult because the position of the boiler, chimney stack, and ducting vary a great deal on account of local conditions.

⁸ Kohler, W., Boiler fans, *Österr. Ing.-Z.*, 1958, p.183.

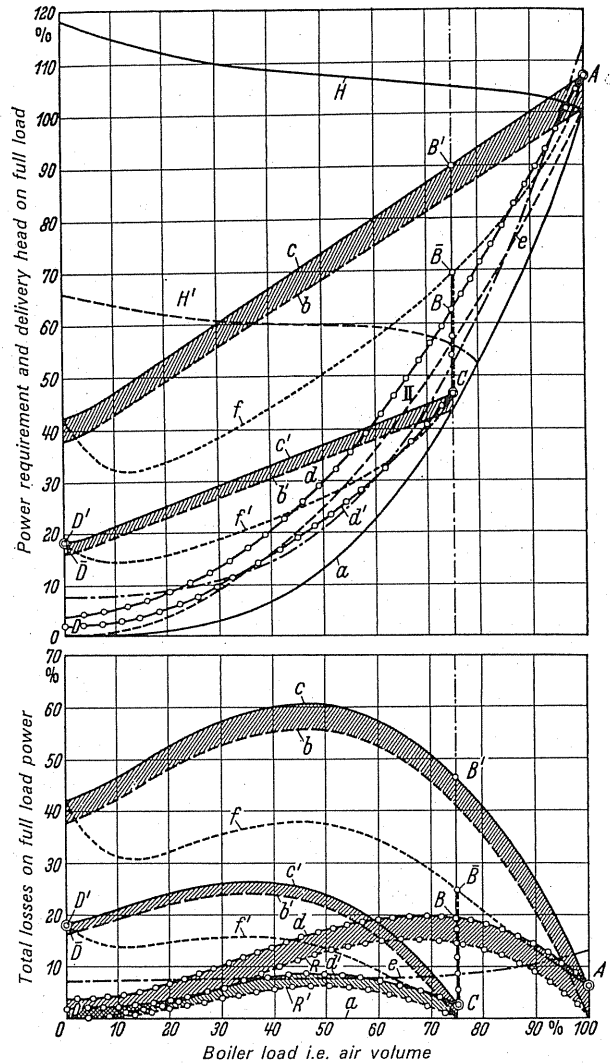


FIG.422. Variable control of a centrifugal fan on constant opening according to Kohler. *Top*: Power demand as a function of speed and air volume. *Bottom*: Power loss as a function of speed and air volume. The values appearing in the diagram having ' refer to $n = 75\%$, the corresponding value without ' refer to full speed $n = 100\%$. a , fan shaft power only due to speed control; b , fan shaft power only due to throttling control at constant speed; c , input power to a squirrel cage motor only due to throttling control at constant speed; d , input power of a slip ring motor with speed control by means of resistances, in the rotor circuit. The overall losses d or d' are made up of the internal motor losses and the losses R or R' in the control resistance. e , input power of an a.c. commutator motor; f , regulation of volume flow by inlet guide vanes where the fan is driven by a constant speed squirrel cage motor; H , pressure head of a fan. Π , manometric pressure head at constant opening. $ABCD$ pole reversible slip ring motor, speed variation between the stages by means of adjustable resistances in the rotor circuit; $AB'CD'$ poles reversible squirrel-cage motors with speed ratio 3:4 and intermediate adjustment by throttling; $\overline{AB}\overline{C}\overline{D}$ pole reversible squirrel-cage motors with speed ratio 3:4 (730:970 rev/min) and intermediate adjustment by means of inlet guide vanes.

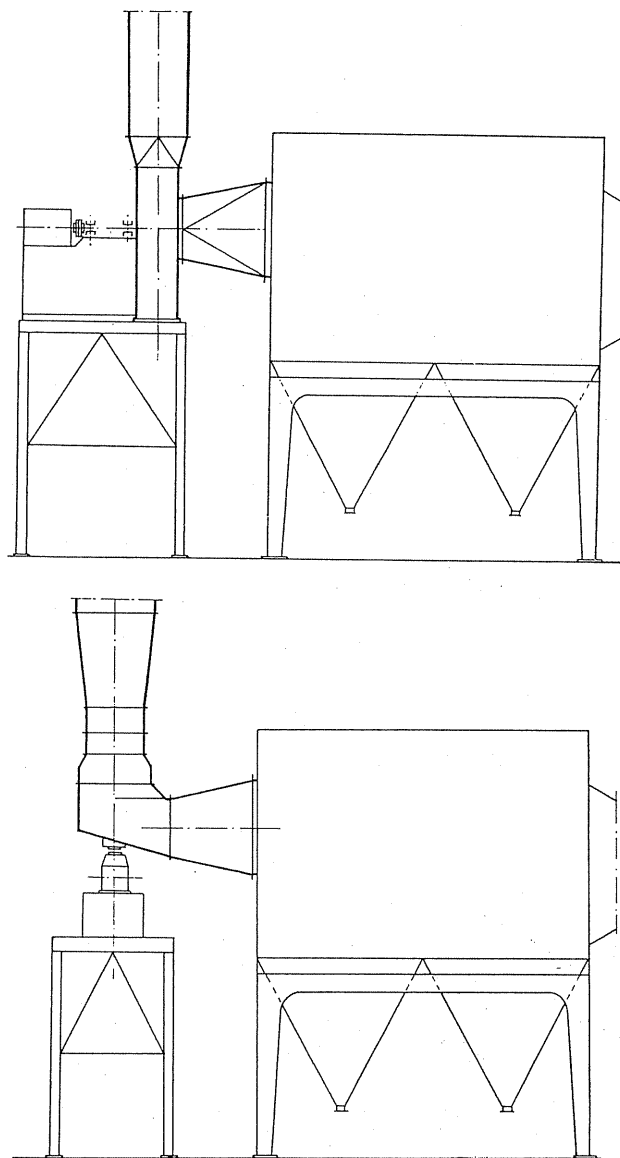


FIG.423. Comparison of installations of induced draught fans. *Top*: Installation of centrifugal fan. *Bottom*: Installation of axial-flow fan.

The induced-draught fan must be skillfully installed in the overall plan. According to circumstances, an axial-flow fan (Fig.423; below) or a radial flow fan (Fig.423; at the top) would be the right solution.

Figure 424 shows an induced-draught fan of the Büttner-Werke immediately in front of the chimney stack.

An interesting special design is one by Henschel (Kassel) for locomotives. Induced-draught fans are required here when running on the condenser, and the usual exhaust pipe

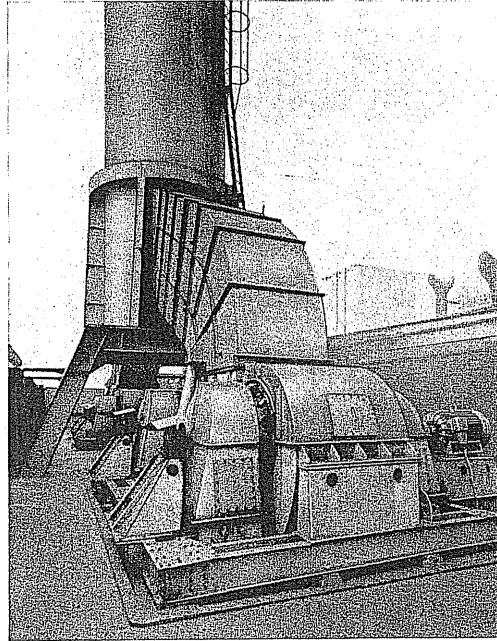


FIG.424. Induced-draught fan manufactured by Messrs. Büttner-Werke AG.

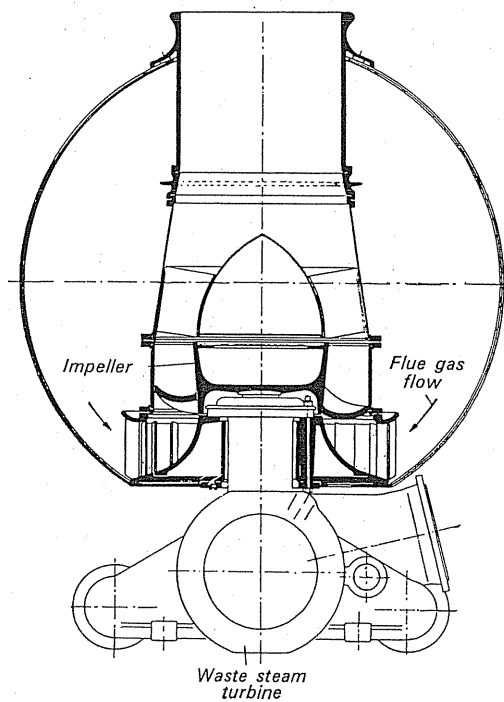


FIG.425. Induced-draught fan for locomotives manufactured by Herschel. Reg. Patent.

of the combustion gases is not available. In dry areas, for instance in South Africa, this type of locomotive is in use. A fan with a high-pressure factor of the axial-flow fan type was used and, owing to the unavoidable wear, special measures had to be taken. The fan produces a pressure difference of approximately 150 mm WG (Figs. 425 and 426).

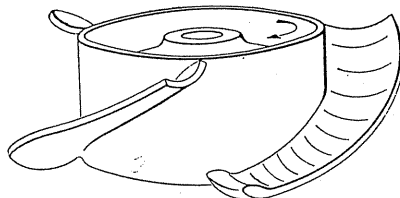


FIG. 426. Wear-resistant blade of the fan impeller as shown in Fig. 425 Pat. Reg.

Jet nozzle as induced-draught fan. There are many instances where it is impossible to use an induced-draught fan either because the temperatures are too high or there are some excess energies of expanded gases or vapours present, or simplicity and foolproof considerations are paramount. In such cases the gases can be delivered through a jet nozzle as shown in Fig. 427. The locomotive exhaust pipe is a classical example of this. Even if the

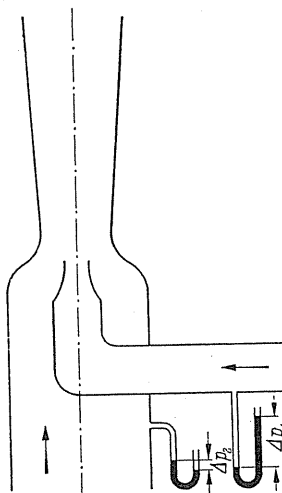


FIG. 427. Ejector arrangement acting as an induced-draught fan.

efficiencies of this type of delivery are fairly small, there are various cases in industry where the spray nozzle is absolutely appropriate. By appropriate designing a tolerable energy conversion can often be achieved. The calculation of this process has been developed by Flügel⁽⁹⁾ and in recent times extended by Jung⁽¹⁰⁾.

⁹ Flügel, Calculation of spraying units, *VDI-ForschHft.*, 395 (1951), 2nd edn.

¹⁰ Jung, R., Calculation and employment of spray blower, *VDI-ForschHft.*, 479.

CHAPTER XIX

TYPICAL APPLICATIONS

141. IMPELLER FOR AIR CIRCULATION

There are many fields of application where impellers are fitted only for circulating air or gas in tanks or equipment for specific applications. These tasks arise for instance in centrifugal sieves, electric furnaces, drying equipment, etc. Such applications are of considerable importance in industry. Therefore it pays to study the constructional principles of the impellers used in these cases because it is possible to obtain an almost exact mathematical solution of the problem.

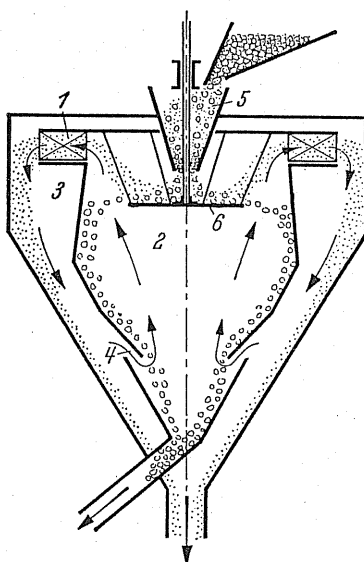


FIG. 428. Centrifugal separator.

A centrifugal sieve (Fig. 428) will be taken as an example for investigation. The impeller 1 sucks air from space 2, forces this into 3 and then back into the space 2 through openings 4. Granular material is simultaneously fed through the hopper 5 on to the entrained disc 6 and from there led into the ascending air current. The device is intended to grade the material. The problem itself demonstrates fairly clearly that the outlet rotation of the air discharging from the impeller is lost. Therefore it is only a matter of gap pressure. The pressure loss in the rotation and centrifugal injection of the particles depends on the speed at which the mixture is rotated. The rotary cycle assumes the highest speed shortly before the entry into

the impeller. This is an absolute inlet speed designated by c_1 . Therefore it is appropriate to express the pressure loss as the multiple n of the pressure head of this velocity:

$$\Delta p_{\text{loss}} = n (\rho/2) c_{1m}^2.$$

The two more or less sharp deflections lead to the assumption that according to the order of magnitude a double amount of this pressure head may be expected, i.e. $n = 2$.

If it is desirable to obtain the best conditions in the impeller, a deceleration in the impeller channels must be avoided. This means that $w_1 = w_2$. With this assumption the amount left for the static pressure in the gap of the impeller is

$$\Delta p_{\text{stat}} = \frac{\rho}{2} (u_2^2 - u_1^2) = \frac{\rho}{2} u_2^2 \left[1 - \left(\frac{r_1}{r_2} \right)^2 \right].$$

Since we have the expression $\Delta p_{\text{loss}} = \Delta p_{\text{stat}}$, we obtain

$$n \frac{\rho}{2} c_{1m}^2 = \frac{\rho}{2} u_2^2 \left[1 - \left(\frac{r_1}{r_2} \right)^2 \right],$$

and from this

$$c_{1m}^2 = \frac{u_2^2}{n} \left[1 - \left(\frac{r_1}{r_2} \right)^2 \right].$$

If by reason of the former considerations for avoiding deflection losses on entering the impeller we select $b = r_1/2.4$, then the amount of air spun per second can be calculated as

$$V = c_{1m} b 2r_1 \pi.$$

In this formula we enter the values for b and c_m and obtain

$$V = \frac{u_2}{\sqrt{n}} \sqrt{1 - \left(\frac{r_1}{r_2} \right)^2} \frac{2r_1^2 \pi}{2.4} = \frac{u_2 2\pi}{2.4 \sqrt{n}} \sqrt{r_1^4 - \frac{r_1^6}{r_2^2}}.$$

For a specified value of r_1 the volume of air spun reaches its maximum. By a simple differentiation $dV/dr_1 = 0$ we obtain

$$r_1 = \frac{r_2}{\sqrt{1.5}} = 0.817r_2, \quad (255)$$

which means that the optimum value of r_1 is independent of n and also of the intake acceleration.

If we express the value of r_1 found in c_{1m}^2 , we obtain

$$c_{1m}^2 = \frac{u_2^2}{3n} = \frac{u_1^2 (r_2/r_1)^2}{3n} = \frac{u_1^2}{2n}.$$

From above,

$$\frac{c_{1m}}{u_1} = \tan \beta_1 = \frac{1}{\sqrt{2}} \frac{1}{\sqrt{n}}. \quad (256)$$

Accordingly, in the final solution we obtain a specified inlet blade angle which is dependent on n . Besides the interest in a simple impeller, if we assume a constant width, then the outlet angle β_2 is easy to calculate:

$$\sin \beta_2 = \frac{\sin \beta_1}{\sqrt{1.5}}.$$

For possible values of n , the angles shown in Table 22 are obtained. The characteristics φ and ψ are still interesting. We obtain: $\psi = 2 (c_u/u_2) \varepsilon \eta$; with $c_u \approx u_2 - u_1 = u_2 \times 0.183$ and $\varepsilon = 0.8$ as well as $\eta \approx 0.8$ gives $\psi = 0.234$.

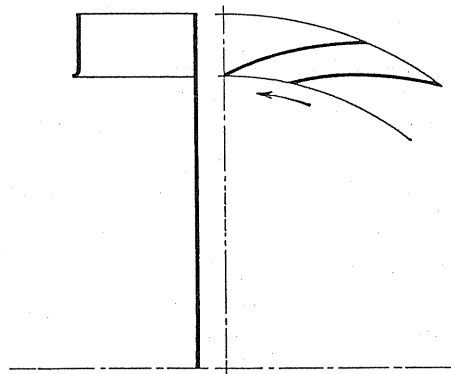
TABLE 22

n	1	2	3	4	5
β_1	35.3	26.5	22	19.5	17.5
β_2	28.2	21.5	17.8	15.8	14.3

$$\varphi = 4 \frac{b_2}{d_2} \frac{c_{2m}}{u_2} = \left(\frac{d_1}{d_2} \right)^3 \frac{1}{1.2 \sqrt{2} \sqrt{n}};$$

for $n = 2$ we have $\varphi = 0.225$. Figure 429 shows the representation of this case to scale.

The information shows that in the present case whose feed position is given for many practical applications, there is in all cases an optimum diameter ratio $d_1/d_2 = r_1/r_2$, whereas the blade design will incorporate certain angles which can be calculated accurately to suit the pressure differences.

FIG.429. Scale example for $n = 2$.

142. FREE-RUNNING RADIAL IMPELLERS WITHOUT CASING

Radial impellers without casing are used for a number of special applications. The best-known example is the so-called Savonius fan which has become very popular. The impeller (Fig.430) is powered by a wind-driven vertical turbine. The impeller situated underneath

has mainly backward-curved blades. The Savonius rotor extracts about 30 % of the energy⁽¹⁾ from the wind. The blower impeller therefore develops 1.6 times the pressure head of the wind below atmospheric pressure. The illustration shows a special design supplied by F. Schillbach, Stettin, for a boiler-house in Gumbinnen. For ventilating purposes many open impellers are often to be found. Applications such as these are occasionally suitable in equipment where the efficiency has no distinguishing role, and it is very desirable to utilize the feature of the radial impeller that a deflection by 90° is obtained, i.e. the impeller simultaneously acts as a bend. The former gap characteristic (Fig. 87) already discussed gives information on the suitability of radial impellers for such purposes. Figure 431 shows

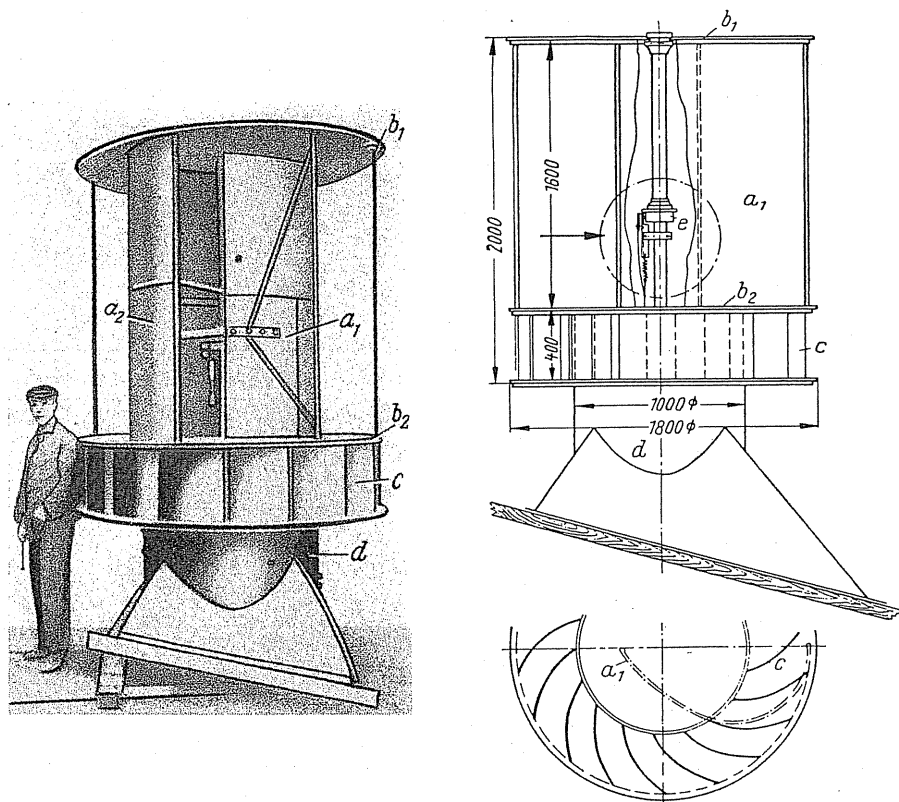


FIG. 430. Savonius impeller manufactured by F. Schillbach: a_1 and a_2 , air turbine blades; b_1 and b_2 shroud plates; c , fan blades; d , cylindrical transition to roof.

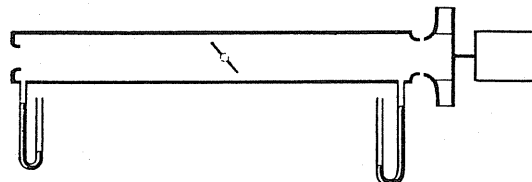


FIG. 431. Measurement of gap pressure characteristic (measured at suction end).

¹ Bach, Concerning flow tests on Savonius rotors, *Forschung*, 1931, p. 218.

how a gap characteristic of this sort has been obtained by experiment. For this purpose the impeller is allowed to run open and the metering tube is connected up to the suction end. The static depression before the impeller indicates the useful pressure. Figure 432 shows the measurements at the suction end. Previously we had found that backward-curved blades

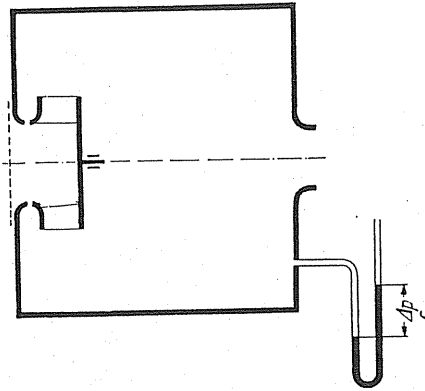


FIG. 432. Test rig for measuring gap pressure characteristic (measured at pressure side).

result in the highest reaction effect, which in this case, also is a criterion for the efficiency which can be achieved. In the problem where for a given peripheral velocity a negative pressure as high as possible is to be achieved, then, according to former tests, only blade outlet angles of 90° can be envisaged.

143. LOAD RELIEF OF A FAN BY RISING HOT AIR, EFFECT OF WIND, EFFECT OF TRAVEL DRIVE

If heated air or gas is carried upwards there is natural draught by which the fan load is relieved. What is meant is the well-known stack effect which at times can assume appreciable values. The draught is equivalent to the difference in weight between the hot gas and the cold environment. Per unit of surface there is a pressure difference

$$\Delta p = H(\gamma_1 - \gamma_2) = H \left[\frac{p_1}{R_1 T_1} - \frac{p_2}{R_2 T_2} \right]. \quad (257)$$

Taken at 0° and 760 mm Hg the mean values are equivalent to:

$$\gamma = 1.325 \text{ gases from hard coal,}$$

$$\gamma = 1.27 \text{ gases from brown coal.}$$

As the differences compared to air are relatively slight, mean values can be used for calculation as a first approximation. Hence we have

$$\Delta p = H \gamma_m \frac{\Delta T}{T_m}. \quad (258)$$

Example

The chimney stack of a brown-coal-fired boiler plant which is 100 m high emits waste gases at a super-temperature 170°C and the specific gravity and the temperature of outside air are 1.226 and 12°C respectively. The mean value of γ works out at $\gamma_m \approx 1.0$. $T_m = (443 + 285)/2 = 364^\circ\text{K}$.

Thus we obtain $\Delta p = 100 \times 1.0 (158/364) = 43.5 \text{ mm WG}$.

If, for instance, to name a mean value the pressure difference of the boiler plant to be overcome is 220 mm WG, then the chimney stack is responsible for 20% and relieves the blower considerably.

Considered on its own the chimney stack is a fan of unsurpassed simplicity. Now let us determine the efficiency. The output is $L = V \Delta p$. The weight of gas handled, which in this investigation we can express without any risk, as equivalent to a weight of air heated by ΔT with respect to the environment. This means a thermal difference of the amount $Q = c_p G \Delta T$. For the efficiency therefore, we have

$$\eta = \frac{GH}{Q} = \frac{H}{427 c_p \Delta T}$$

In the above example, $\eta = 0.62\%$. The efficiency thus is very small and mostly below 1%.

The draught by movement of *cold* air often has to be taken into account, for instance in mine ventilation during the summer. If the wind is blowing on the stack, the flow around the stack outlet creates a wake with stagnant pressure equal to the velocity pressure of the wind provided the chimney is not discharging. As soon as gas discharges, however, this wake is destroyed.

COOLING TOWERS

For cooling the very large quantities of water from power stations and other industrial installations, cooling towers with or without fans are used. Figure 433 shows one of these constructions. In this case axial fans with aerofoil blades up to 20 m diam. are used. One of

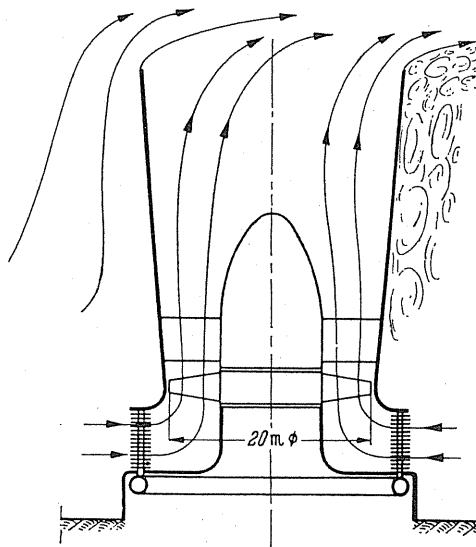


FIG. 433. Cooling tower for condensed water in a large aircooled power station.

these units just about accommodates a steam turbine power of 25,000 kW. Although the fan adds a third to the cost of a cooling tower, it often shows advantages. On the one hand, there is the possibility that a considerably better cooling can be achieved. Furthermore, the cold water temperature is independent of atmospheric conditions due to the adjustability of the fan. For the individual case only an accurate investigation of prevailing conditions will decide whether it is better to install a stack cooler or a fan cooler.⁽²⁾

The largest cooling towers with large axial impellers of 20 m diam. in use at the present time were taken into commission a short time ago at the Goldenbergkraftwerk at Cologne.⁽³⁾ It handles 2840 m³/sec at a speed of 76 rev/min and a pressure difference of 12 mm WG.

The problem is also very important for motor vehicles. Here cooling fans are supported by the stagnant pressure of the wind velocity. According to Fig. 434 it is best to allow the air to enter in the vicinity of the stagnant point and to discharge at some point at the top or at the side, where the wind pressure is as low as possible. When the intake and outlet are correctly arranged it is easy to make use of a pressure of half of the stagnant pressure of the wind velocity. At high driving speeds the fan would be completely free of load, and in certain circumstances would operate as a turbine, i.e. would speed up the motor somewhat.⁽⁴⁾

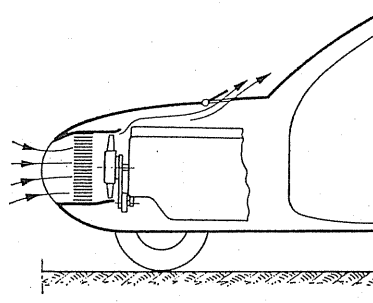


FIG. 434. Utilisation of pressure head due to the driving speed in cooling fans for motor vehicles.

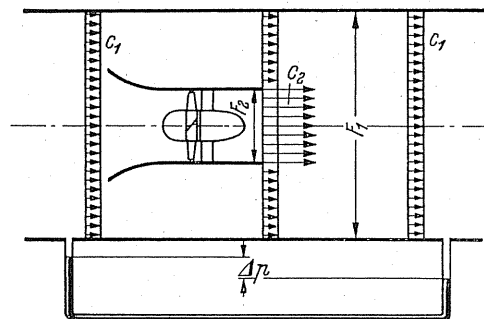


FIG. 435. Booster action using an axial-flow fan.

² Döpel, W., and Kattanek, S., Aspects of the economical and application fields of chimney and fan cooling towers, *Energietechnik*, 1958, Nos. 6 and 8.

³ Schmiederer, B., Fan with aerofoil blades for large cooling towers, *VDI-Nachr.*, 1960, No. 35.

⁴ Eckert, B., The cooling fan of motor trucks and its behaviour in operation, Diss., Stuttgart, 1940.

Suction nozzles in ships are also worthy of mention; they enable the load of the very comprehensive blower and fan installations of ships to be relieved considerably (Fig. 446, No. 6).

144. VENTILATION BY MOMENTUM DRIVE, TUNNEL VENTILATION

In many cases it is impossible for a fan to cover a duct cross-section completely, maybe because the duct should remain passable or only an occasional ventilation is necessary or for some other reason. In such cases a simple air movement can be achieved by allowing smaller fans to blow freely into this cross-section. The momentum pressure of the outgoing stream imparts a slight positive pressure over the whole cross-section by turbulent mixing and thus ensures a small air movement. Figure 435 is given as a typical example of the many practical cases of application.

Using the symbols in Fig. 435 we obtain, according to the momentum principle, an excess pressure Δp by the following equation:

$$\Delta p = \rho/2 \, c_2^2 \, 2 \left[F_2/F_1 + \frac{1}{1 - F_2/F_1} \left(\frac{c_1}{c_2} - \frac{F_2}{F_1} \right)^2 - \left(\frac{c_1}{c_2} \right)^2 \right]. \quad (259)$$

Example

Let $F = 5 \, \text{m}^2$; $F_2 = 0.5 \, \text{m}^2$; $c_1 = 4 \, \text{m/sec}$; $c_2 = 20 \, \text{m/sec}$; $\gamma/g = 1/8$. $\Delta p = 0.1422 (\rho/2) c_2^2 = 0.1422 \times 25 = 3.55 \, \text{mm WG}$. This means that at a 25 mm WG pressure of the fan a pressure of 3.55 mm WG is transmitted to the 10 times greater cross-section.

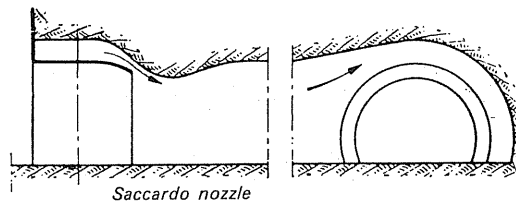


FIG. 436. Longitudinal section and cross-section of a Saccardo nozzle at a tunnel entry.

If the duty of the fan is to generate velocity only in the large cross-section, probably for small duct lengths at which an excess pressure is not required for overcoming the frictional resistances, then the excess pressure calculated above is used for producing the pressure head of the velocity c_1 . Accordingly, eqn. (259) is expressed as $\Delta p = (\rho/2) c_1^2$ and the ratio c_1/c_2 calculated. For this we obtain a quadratic equation.

For the above example worked out at $c_1/c_2 \approx 0.38$, $c_1 = 7.6 \, \text{m/sec}$ at $c_2 = 20 \, \text{m/sec}$.

If the free duct cross-section for installations according to Fig. 435 is not available, for instance in tunnel ventilation, the momentum must be generated through slots which are mounted on the walls. Thus the so-called Saccardo nozzles (Fig. 436) have been developed which are fitted at the inlet of a tunnel. The fans force the air into an annular compartment space provided in front of the annular slot. Föttinger⁽⁵⁾ was the originator of an interesting

⁵ Heuschke, H., Investigation on improved jet blowers for tunnel ventilation, Diss., Berlin, 1930.

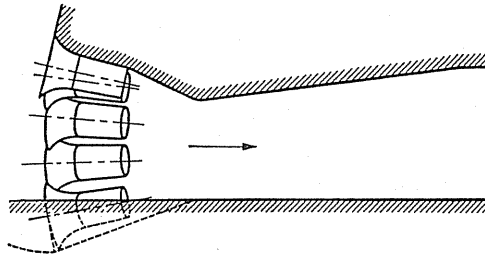


FIG.437. Tunnel ventilation by jet blowers designed by Föttinger.

solution of this problem. This, according to Fig. 437, comprises a row of jet fans arranged in front of the narrowest tunnel cross-section at an angle of 10–20°.

Special conditions arise if jet blowers discontinue to suck air owing to injector effect. This takes place if the resistance in the tunnel becomes too great, for instance in long tunnels or where there is interference from high wind. It may happen that the injected air flows right

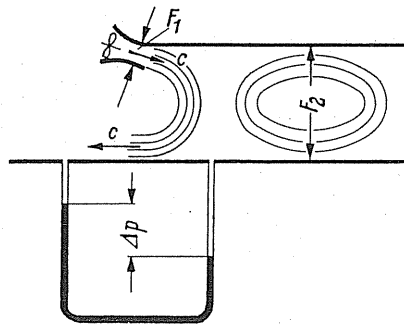


FIG.438. Return flow of an impulse jet when the reverse pressure is too high.

back again. The flow thus obtained is shown in Fig. 438, where a fan blows into a closed tube. In this case the intake momentum is vqc whereas at the outlet the same momentum vqc discharges in the opposite direction. The change of momentum therefore is $2vqc$. On the inside of the tube a uniform excess pressure is produced which acts on the area F_2 . Thus we have

$$\Delta p F_2 = 2vqc = 4 (\varrho/2) c^2 F_1,$$

and from this

$$\Delta p = (\varrho/2) c^2 4 F_1 / F_2.$$

In the tunnel shown in Fig. 437, i.e. the Cochemer Kaiser Wilhelm tunnel, the author was able to make some accurate measurements. It was found that when operating with 1–8 jet blowers air was entrained from the outside by way of injection, whilst when operating ten jet blowers a portion of the injected air flowed back. The fans had a pressure head of 25 mm WG. Under certain working condition in the tunnel, positive pressures up to 20 mm were measured.

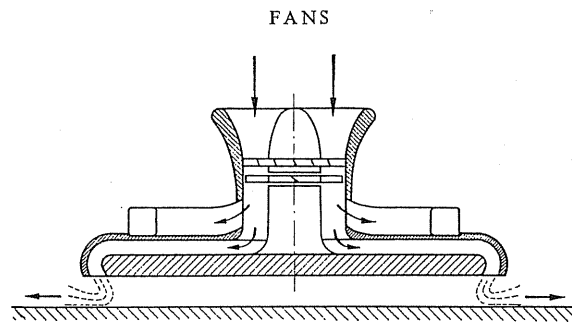


FIG.439. Diagrammatic sketch of a hovercraft.

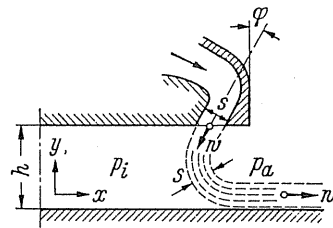


FIG.440. Diagram showing the flow and pressure conditions at the rim of a hovercraft.

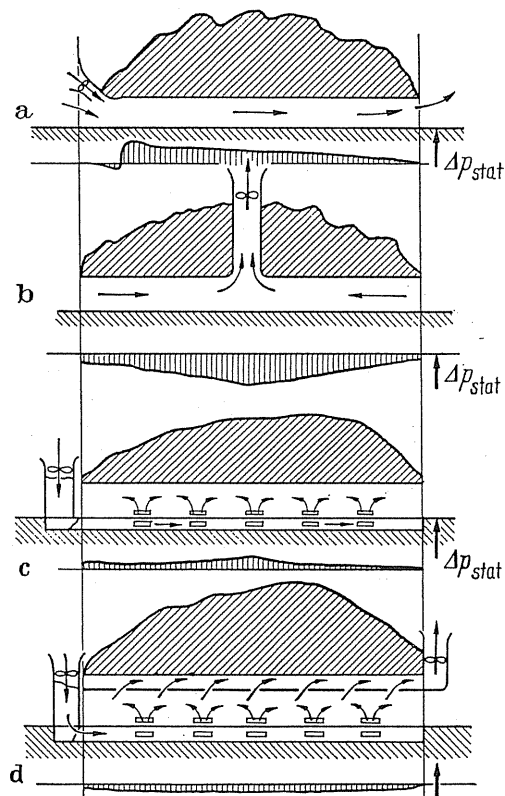


FIG.441. (a-d) Various systems in tunnel ventilation. (a) Longitudinal ventilation. (b) Longitudinal ventilation with shaft fan. (c) Semi-cross-ventilation. (d) Cross-ventilation.

Similar interesting combined effects have been obtained in the latest development in hovercraft⁽⁶⁾ (Fig.439). In Fig.440 the discharge conditions at the boundary of the base plate will be recognised. Here, under the plate, a pressure is created of magnitude

$$\Delta p = (\rho/2) w^2 2 \frac{s}{h} (1 + \sin \varphi).$$

Survey of the possibilities offered in *tunnel ventilation* are shown in Fig.441.

(a) *Longitudinal ventilation*: very susceptible to adverse pressure, for instance wind interference; can be remedied possibly by jet blowers at both openings for reversing the ventilation. If correctly designed, it can overcome considerable back pressures.

(b) *Longitudinal ventilation with shaft fan*: only useful in a tunnel of limited length because, owing to the one-sided pressure effects, a portion of the tunnel will remain unventilated.

(c) *Semi-cross-ventilation*: direct fresh-air supply to each point. Longitudinal discharge to both sides.

(d) *Cross-ventilation*: complete cross-ventilation gives a complete independence of each longitudinal flow. It is the best and the most expensive type. Haerter⁽⁷⁾ has provided a comprehensive illustration.

145. SUCTION EFFECT OF WIND PASSING DUCT OPENINGS (ROOF VENTILATORS AND SIMILAR)

If the open end of a duct is brought into an air current, there is a negative pressure in the duct. This negative pressure can be used for exhausting gas or air through the duct. This, for instance, is what happens in the chimney which is swept by wind. Within various equipment, however, this suction effect is often used in order to obtain an ordinary "ventilator".

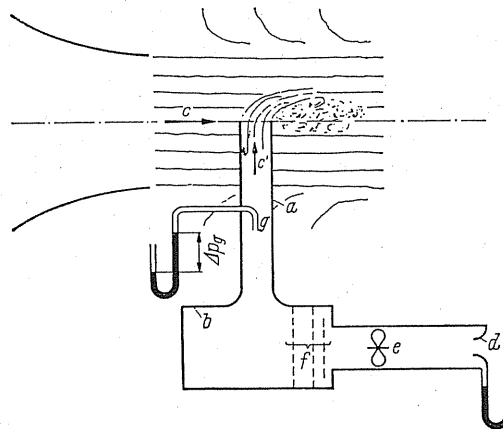


FIG.442. Measurement of the suction effect of a duct in the air stream.

⁶ Ackeret and Baumann, Concerning hovercraft, *Schweiz. Bauztg.*, 1960, p.137.

⁷ Haerter, A., Tunnel ventilation, Diss., Zürich, 1961.

What basic properties, i.e. what characteristic does this type of "blower" possess, and what possibilities are there of influencing this effect?

Figure 442, first of all, shows how an investigation can be carried out. The duct *a* is inserted in the centre of the free stream of a wind tunnel. *a* is connected to a reservoir *b* into which air is freely drawn in from the outside by means of an inlet nozzle *d*. An additional fan *e* is mounted to ensure that the characteristic can be used on full range. By alteration of the resistances, e.g. screens *f*, the resistance of the ducting system is varied in such a manner that all operating points from delivery volume zero to the largest volume can be obtained.

The overall pressure in the exhaust duct measured by means of a pitot tube facing the flow is the criterion for the negative pressure obtained. The measured quantity Δp_T indicates the amounts by which this total pressure is below the atmospheric pressure. The delivery volume can be measured satisfactorily through the inlet nozzle *d*. Thus also the speed c' is obtained. It is best to express Δp_T as dimensionless since the pressure head $(\rho/2) c^2$ is always divided in the free stream. Thus we obtain two dimensionless values, which are to be used below:

$$\eta = \frac{\Delta p_T}{(\rho/2) c^2}; \quad \lambda = \frac{c'}{c}.$$

Open ducts. The most important is the case of the round duct. Besides this, square sections also are important. In these cases it is likely that the inlet-flow direction will play a part, such that, above all, the two salient directions (parallel to the edge and in the direction of the diagonals) are important.

For these three cases the characteristic obtained from tests by the author have been plotted in Fig. 443. The relationship $\lambda = f(\eta)$ is represented by a slightly bent curve which

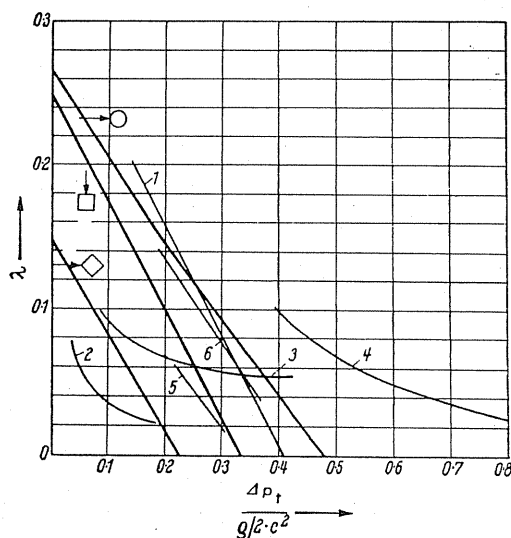


FIG. 443. Analysis of nominal values for duct openings and roof fans swept by air.
The figures refer to the details in Fig. 446.

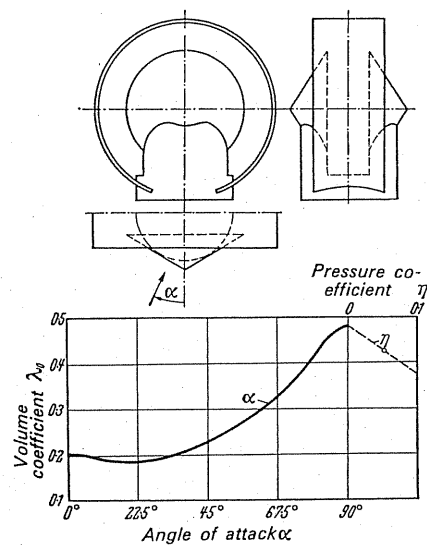
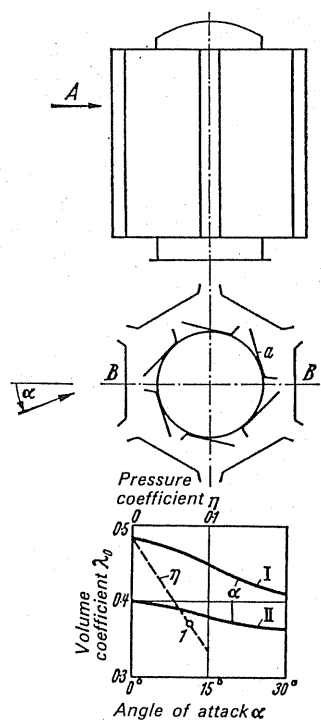


FIG. 444. Chimney mounting.

FIG. 445. Chimney mounting. a , inside guide; I and II, curves for α values to the left and to the right of the symmetrical axis BB respectively.

in the first approximation can be taken as a straight line. The round cross-section accordingly is far the best. The square cross-section is very sensitive to direction. It is striking that in the intake flow in the direction of the diagonals the delivery head drops down to about half; this is rather interesting because all house chimneys have a square cross-section.

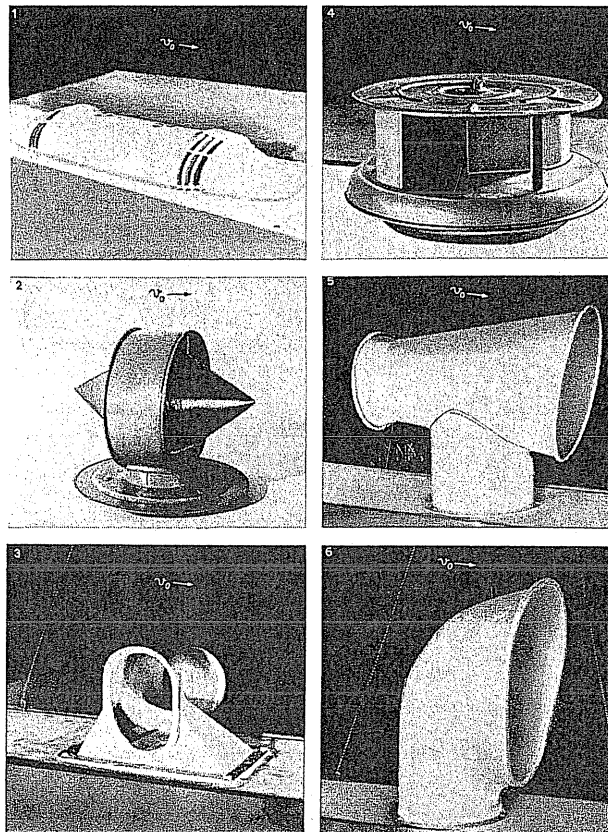


FIG. 446. Views of different fan shapes according to Marcinowski. (Test results in Fig. 443.)

It may be asked how far the effect can be improved by special fittings, i.e. the so-called chimney mountings.⁽⁸⁾ The number of constructions and patents of this type has become so large that it is impossible to mention even a fraction here. In principle it may be stressed that such constructions are only useful which are able to give better results than open cross-sections. It must occur to everyone that this necessary comparison is completely overlooked in chimney mountings. What is the sense of any of these figures if they do not give in *quantitative terms the improvement the chimney with the mounting will give as opposed to the chimney without mounting*? Since most mountings cannot stand up to such comparisons, it will suffice to give a few examples where there is a clear superiority over the free discharge. Figures 444 and 445 show two mountings which O. Conrad⁽⁹⁾ examined in detail. The maximum volumes are considerably greater than in Fig. 443.

⁸ Schrenk, O., Investigation of roof ventilators, *AVG*, No. 4.

⁹ Conrad, O., Natural space ventilation by means of single and surface ventilators, *VDI Z.*, 1953, p. 497.

New investigations of roof ventilators used in practice have been provided by Marcinowski.⁽¹⁰⁾ The results of these investigations have been plotted in Fig. 443. Figure 446 shows the views of these fans. In these fans there is to be found also a rotary fan (Flettner fan) of the Savonius model. The remarkable thing about this is the considerably greater pressure effect of this rotary fan. The reference surface for designating the fan size was the area of the fan which is obtained by projecting on a surface, situated perpendicular to the blowing and driving direction. This must be taken into account when comparing with the curves of ordinary ducts.

146. ELEVATOR BLOWERS, BLOWERS FOR PNEUMATIC TRANSPORT OF MATERIAL

For granular and fibrous stock, pneumatic transport is applied to a very large extent. Long pipelines used for this purpose require pressures up to 3000 mm WG. At the highest pressures the material is dropped into bucket wheels. Low-pressure blowers with a simple

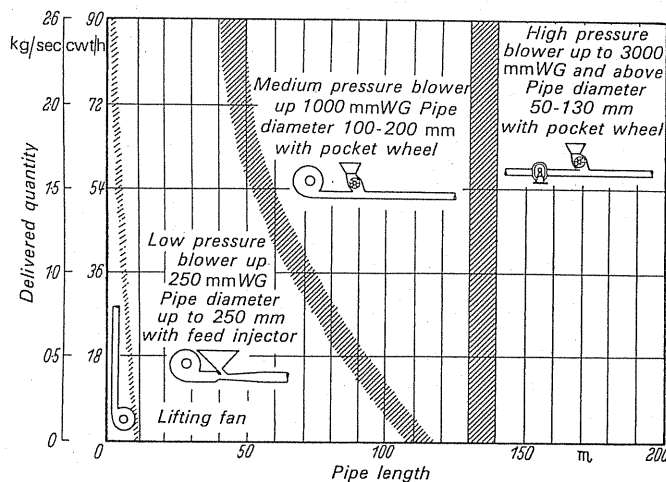


FIG. 447. Pneumatic handling by injectors, pocket wheels and high pressure blower.

injection feed will do for conveying up to 100 m. Simple elevating blowers can be applied to advantage for small and for preference vertical handling tracks. Figure 447 is a diagrammatic survey.

The development and the theoretical treatment of blowers has mainly been taken care of by Segler.⁽¹¹⁻¹⁴⁾ These blowers operate in such a way that the material is handled directly

¹⁰ Marcinowski, H., Experimental investigations in the air flow department, *Voith-Forschung u. Konstruktion*, 1958, No. 4.

¹¹ Segler, G., Accurate construction of conveying blowers, *Landwirtsch. Forschung*, 1 (1951) 2-10.

¹² Kampf, G., Investigations on elevator blowers, *Landwirtsch. Forschung*, 6 (1957).

¹³ Kampf, G., Theoretical and experimental tests on elevator blowers, *VDI-Forsch.-Hft.*, 466 (1958).

¹⁴ Segler, G., Investigations on grain blowers and basis for calculation, Diss., Munich, 1934.

by the impeller and subsequently is spun into a vertical discharge tube. Because of special supply cylinders which are fitted into the suction space of the impeller as shown in Fig. 448 and the provision of a small inlet orifice, very little air is entrained. Thus the impeller is operated in the air practically without load. The material is spun at about 15–20 m/sec peripheral speed in the discharge tube. In this way a head $H = u_2^2/2g$ was achieved without losses. At $u_2 = 20$ m/sec, for example $H = 20$ m, was obtained. Owing to the pipe friction

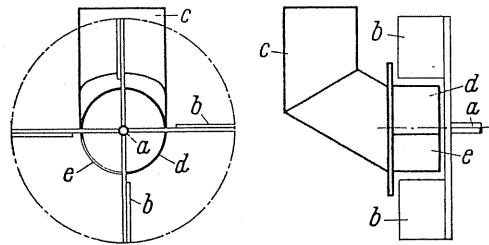


FIG. 448. *a*, fan shaft; *b*, impeller blades; *c*, inlet bend; *d*, division wall in intake cylinder; *e*, free intake.

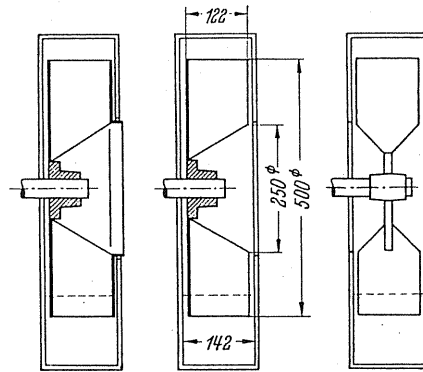


FIG. 449. Approved design of fans for conveyance of materials.

and the unavoidable air resistances, actually about 6–7 m delivery head was achieved. In spite of these unavoidable losses, the procedure is more favourable and simpler than for pneumatic handling, because the losses are considerably greater in the latter.

As the considerable air power in these fans becomes lowest at radially and forward-curved blades, these impellers will now be discussed. It has, however, been found that according to the structure of the material, backward-curved blades are better under certain circumstances. For instance, this is the case when handling granular material.

For handling granular material the impeller profiles shown in Fig. 449 are appropriate, and designs open and closed at one end have given satisfaction. Figure 449 shows an open design where 4–6 blades are used. In straw and chaff blowers, wheels open only at one end or open at both ends are the only types used. The side gap between impeller and inside wall of the housing should not be too large. Six blades will do for spiral housings and four blades for concentric housings.

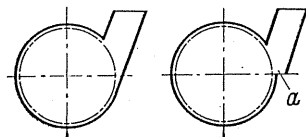


FIG.450. Blower design for lifting fan. *Left*: Tangential discharge. *Right*: Improved design with opening *a*.

Of outstanding importance in elevator fans is the shape of the spirals. For grain blowers concentric housing are still the most convenient, as shown in Fig.450, but for bulky material special measures are required to obviate the material sticking. On the one hand, the blade wheel should have a profile, as shown in Fig.449, from which the fibres can slide off at any point, whilst the housing can be profiled in different ways to suit the condition of the material and also take into consideration the moisture content.

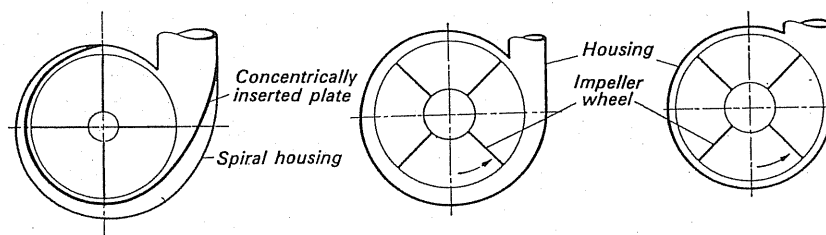


FIG.451. Housing shapes for different applications. *Left*: Housing for green stuff which tends to be sticky. *Centre*: Housing for dry chopped straw. *Right*: Housing for green chopped straw.

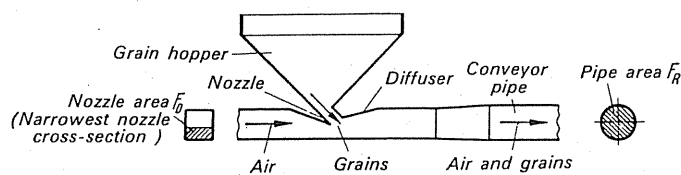


FIG.452. Injector for grain handling.

Figure 451 in the centre shows the housing for dry straws. Figure 451 at the right shows the design for wet straw, whilst a special configuration as Fig.451 at the left is essential for green stock which has a tendency to adhere.

The design of grain injectors is shown in Fig.452. The efficiencies which can be achieved for different types of jets are shown in Fig.453 as a function of the surface ratio.

When designing these fans, figures taken from practice are indispensable and must be used. The data for fans used for grain conveyance are given by Kampf.⁽¹⁵⁾ To give the reader an idea one example will be given. For conveying grain at the rate of 1 kg/sec an impeller of 600 mm diam with four blades will be required. At $n = 600$ rev/min a delivery head of 5 m is achieved. For handling green stock the same fan requires a speed of 900 rev/min. The elevating power demand is 0.7 hp for a vacuum power requirement of 0.5 hp.

Another special problem arises in pneumatic exhausting. If material is sucked directly

¹⁵ Kampf, G., *VDI-Forsch.-Hft.*, 466.

from a heap the problem is to separate the air from the material at the end of conveyance and to blow it to atmosphere again by means of a fan. For this purpose in association with a set test arrangement, the author developed a design as shown in Fig. 454. Here the impeller intake is formed by means of a semi-spherical screen⁽¹⁶⁾ which rotates along with the impeller. The material impinging on the screens is swept off and collects in an annular space b from whence it flows into a bin.

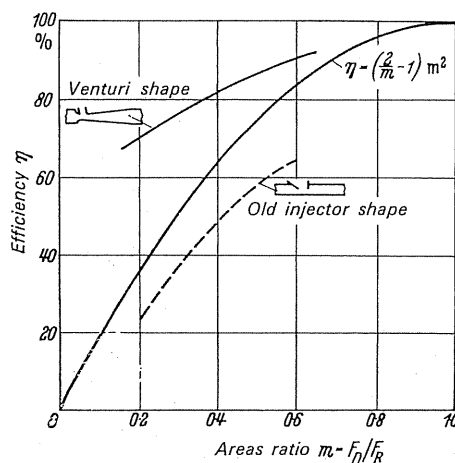


FIG. 453.

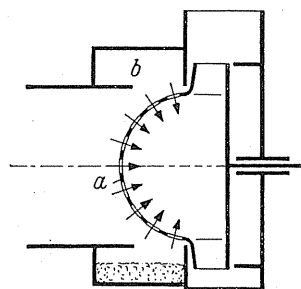


FIG. 454. Fan with rotating screen basket for separating material in pneumatic handling.

FANS FOR HIGHLY CORROSIVE MATERIALS

When handling coal, sand, etc., and similar materials, there is often considerable wear on the impeller. Therefore the impellers should be estimated with an accurate ψ value to enable the lowest possible peripheral speeds to be obtained. For this purpose blade angles β_2 above 45° are necessary in order to prevent the material sticking at the back of the blades. Designs are desirable in which the wear becomes uniformly distributed.

According to one suggestion by the author the opposite view can be taken so that the

¹⁶ *Cylindrical Rotating Screen used by G. Segler: Pneumatic Grain Conveying*, National Institute of Agricultural Engineering, 1951.

wear be deflected intentionally to certain parts of the impeller which can be changed readily. Figure 455 is a sketch of this suggestion. Inlet, by means of an open and shutting louvre screen through which the material causing wear, is shifted towards the centre, separated from the main air, and is conducted by a special duct to the centre of the impeller. Here the material is separated with very little conveying air and led into a radial duct which is secured to the impeller plate. The material is then separated from the remaining air in this special replaceable duct, accelerated, and united again with the other air in the housing. The replaceable radial duct can be shorter than the impeller, because with radial direction higher pressures are obtained than with other types of blading. Special care, however, must be taken so that the material leaving the radial portion is not caught up in the succeeding blades.

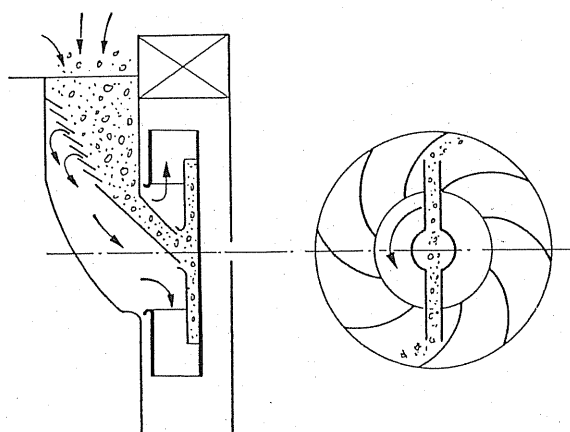


FIG. 455. Fan for separation of corrosive material in a special replaceable blade strip.

147. MINIATURE FANS

No field in fan engineering is so undeveloped as that of miniature fans. These are, of course, the smallest size fans which are often fitted anywhere as unimportant mountings and only become noticed if their air capacity is inadequate. There has been an increasing vogue for these fans for about 10 years, but they are not so popular today. Certain practical experience can lead to new developments in larger units permitting the design of improved small radial-flow fans with higher suction capacity and higher efficiency. Moreover, new designs of drum impellers may lead to a new breakthrough in many fields of application. In this connection, no doubt, drum impellers will be used with normal flow as well as being used as cross-flow fans. The failure of the axial-flow impeller in the field of miniature fans is due to the fact that at small Re values with the unavoidable high losses in flowing through blade ducts the pressure contributions $(\rho/2)(c_2^2 - c_1^2)$ as well as $(\rho/2)(w_1^2 - w_2^2)$ are very much involved, whilst the contribution by centrifugal forces $(\rho/2)(w_1^2 - w_2^2)$ is not affected by the Re value. Therefore it is clear that axial-flow fans are no use at all.

Despite recent successful developments, it is not practicable to discuss miniature fans extensively. It will suffice—in this edition—to deal with a typical field of application, namely vacuum cleaners.

Vacuum cleaners. This group of miniature fans occurs in one of the most useful and most popular of household appliances. There are about 6–7 million vacuum cleaners in use in the Federal Republic and the number used all over the world could come to more than 100 million. The first useful form of vacuum cleaner was brought out by Hubert Cecil Booth in 1901. Mass production, however, only started in 1914 because as a prerequisite a fractional

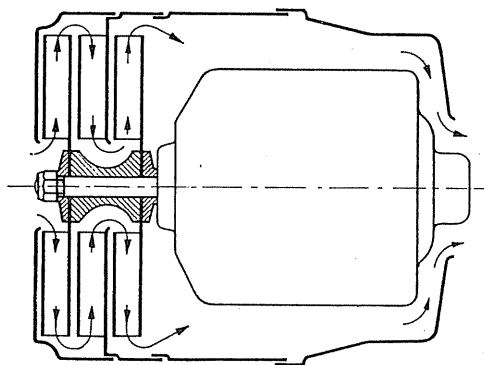


FIG.456. Sketch of a vacuum cleaner with two-stage fan.

horse-power motor had to be provided for safe operation. The negative pressures obtained in vacuum cleaners, according to type of application, are $150 < \Delta p < 1300$, whilst the air delivery fluctuates within the limits of $0.3 < V < 3 \text{ m}^3/\text{min}$. Speeds fluctuate between $8000 < n < 20,000$. The power consumed in domestic cleaners is from 100 to 300 W, and industrial vacuum cleaners consume 1–2 kW. Two types are available—small domestic ones and the larger so-called industrial vacuum cleaners. Steep characteristics are obtained in the first type which are suitable for the manifold uses of the cleaner. They are created easily due to the motor characteristics because the universal motor with the mains characteristic used for these appliances accelerates when the load is relieved. Because of this, an otherwise flat characteristic can become very steep. In industrial vacuum cleaners conditions are different. These are designed to handle large volumes of air and smaller pressures. The characteristics are fairly flat.

The model is governed by the arrangement of dust removal and, as a rule, a filter bag is used. According to whether this filter bag is arranged in front of or behind the fan, the fan

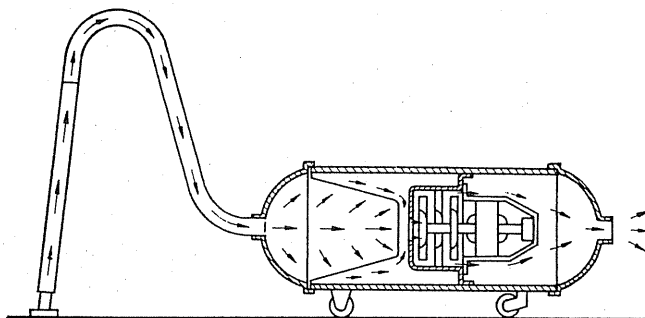


FIG.457. Suction of clean air by two-stage fan.

impeller is swept by clean or dust-laden air. Apart from this aspect a factor—which might appear irrelevant at first glance—which governs the size and model is whether a long hose or only a short tubular handle is used. When using a longer hose a large part—sometimes

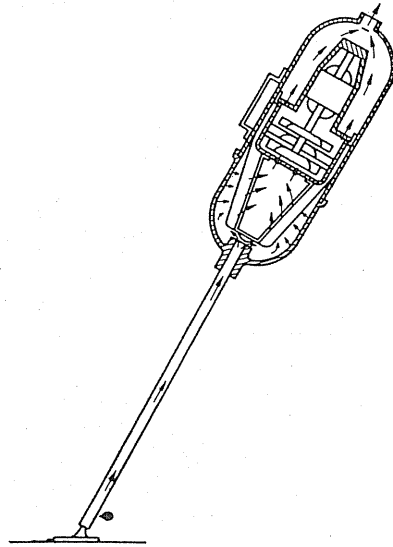


FIG.458. Air suction without hose; dust separation at suction end.

the major portion—of the blower power is lost in the hose. Therefore it is essential to provide a multistage fan. It is necessary to make these multistage fans easily accessible in relation to a confined space, and this is shown in Fig. 456. Figure 457 shows the overall arrangement. The dust-laden air flows first into the filter bag and leaves this in a clean condition for entering the fan. It then flows, subsequently cools the motor, and is discharged from the appliance. There are, of course, other arrangements if it is decided to pass the dust-laden air uncleaned

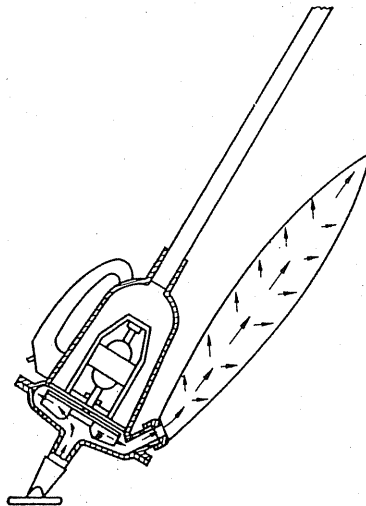


FIG.459. Single-stage vacuum cleaner fan with dust bag.

through the fan. In this case, however, there has to be a compromise in choosing the fan impeller. The impeller must not choke even if fibres are sucked in. These requirements lead to impeller and blade design which have very poor efficiencies. One creditable advantage is that the filter bag is situated in the positive pressure field, and since it is freely suspended it is of a large size and hence associated with very low-pressure loss. By dispensing with the hose, as with many new appliances, and by developing a column and hand-operating device, very light and small appliances are obtained such as are portrayed diagrammatically in Fig. 458. The single-stage appliance with dust-bag (Fig. 459) in respect of power and weight has the advantage over dust separation at the suction end in multistage fans with short, fixed, suction pipe.

Lately an advance in vacuum cleaning has been made possible by using cross-flow fans and drum impellers.

148. SUPERCHARGERS

In order to maintain the power of aero-engines at greater heights, air fed to the engine is pre-compressed by special fans. In one stage positive pressures of 1 atm are then

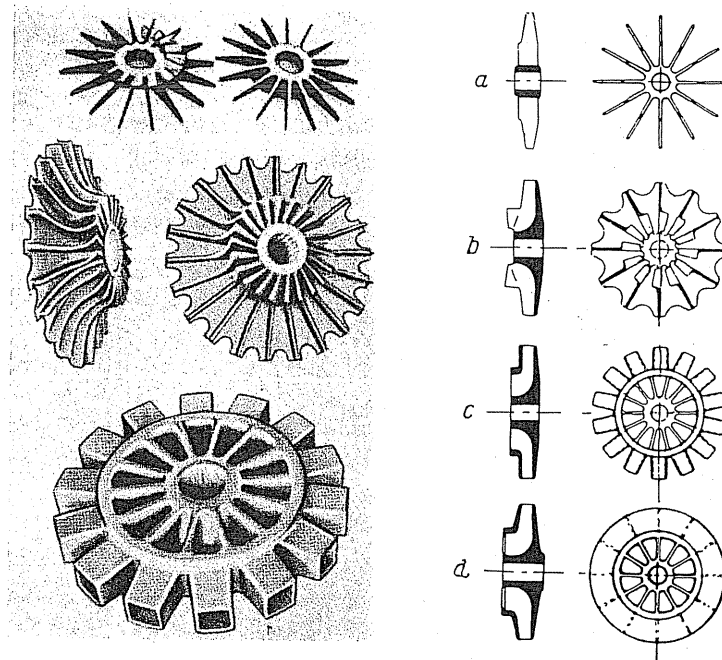


FIG. 460. Different forms of superchargers.

achieved. For this purpose, peripheral speeds of 300–400 m/sec are essential which can only be developed by using special designs. Solid-forged impellers with outwardly reducing cross-sections, blade stars fixed to the hub, and similar designs have been developed for this

purpose. Figure 460⁽¹⁷⁾ shows a typical model. The forward-curved blades are characteristic of the component. Another advance in this direction is by placing special axial impellers in front of the radial impeller. Figure 461 shows an interesting construction where the enlarged diameter axial impeller is arranged opposite the intake suction component. The enlarged axial impeller runs at a higher speed in order to achieve an appreciable precompression even

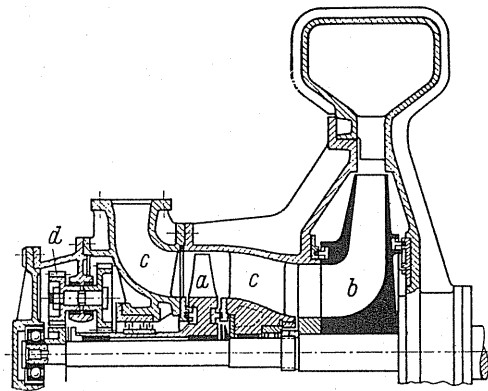


FIG.461. Supercharger with higher speed axial forerunner designed by von der Nüll. *a*, axial pre-runner; *b*, radial impeller; *c*, intermediate guide vanes; *d*, gear.

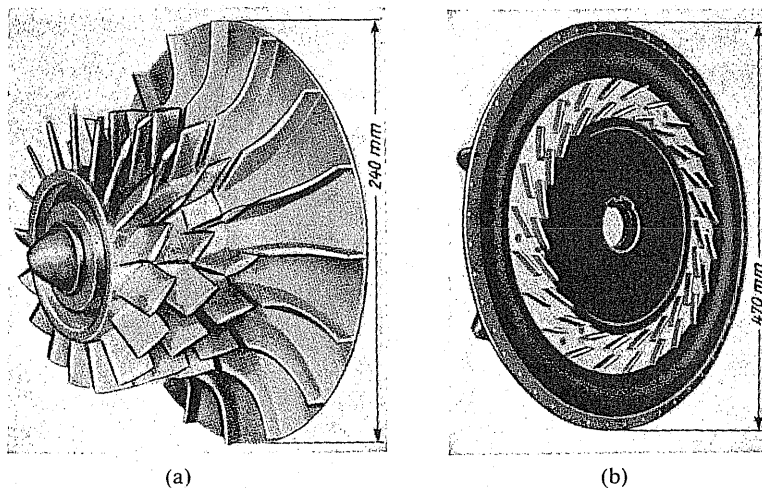


FIG.462. (a and b) Supercharger by Sydlowski-Plariol with subdivided aerofoil impellers and subdivided guide vanes.

before entering the radial impeller. The same effect is intended with a French design (see Fig. 462) which has three differently set axial impellers. Since these impellers are very *finely machined and polished on all sides*, the construction is costly.

¹⁷ von der Nüll, W., *Luftfahrtforschung*, **14** (1937) 244; *ATZ*, 1938, pp.282-95; *Luftwissen*, 1937, pp.169-86; *Jahrb. der deutschen Luftfahrtforschung*, 1938; *Z VDI*, 1941, pp.763, 905, 981; *Automobiltechn. Handb.*, 1942, pp.1149-1213.

What distinguishes this fan is that it is the most widely used impeller with a spiral housing. Subdivided impellers are even found in these applications. Figure 462 at the right shows the guide wheel of the French impeller mentioned above.

Efficiencies of 70–80 % are achieved with these fans.

The same fan is mass produced today as small superchargers for heavy goods vehicles.

PART E

CONSTRUCTIONAL SHAPES
AND
CONSTRUCTIONAL FEATURES OF FANS

CHAPTER XX

SURVEY

149. GENERAL ASPECTS FOR SHAPING OF RADIAL-FLOW FANS

The assembly of an ordinary radial-flow fan is extremely simple and offers few constructional difficulties. Taking the common design (Fig. 463), the essential features will be stressed. The example is a low-pressure fan by Sulzer with forward-curved blades. The impeller is

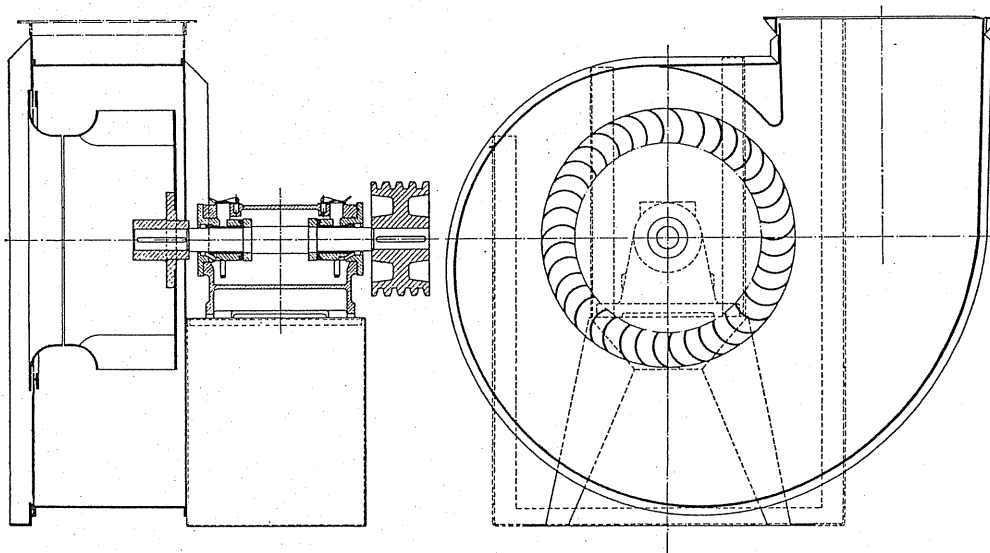


FIG. 463. Low-pressure fan manufactured by Sulzer.

free-running. The two outside bearings are connected to the spiral housing by means of a pedestal block. The bearings used are ring-lubricated bearings and ball-bearings. The rear wall of the impeller very often seals with the spiral wall. Since the spiral housing, which is generally of a rectangular cross-section in low-pressure fans, possesses a larger width than the impeller, it is necessary to fit a nozzle or even a tapered piece to connect to the circular duct. The seal between impeller and housing is formed by keeping the intermediate space as narrow as possible. The spiral housing is mainly made of steel sheet which is riveted or welded. The straight surfaces are stiffened by angle-iron. From the standard shape a rectangular air discharge cross-section has evolved, and special transition pieces are necessary if round ducts are to be connected up. Figure 464 is the outside view. Figure 465

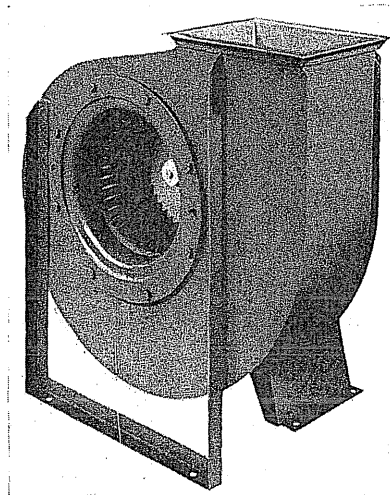


FIG.464. Low-pressure fan manufactured by Sulzer.

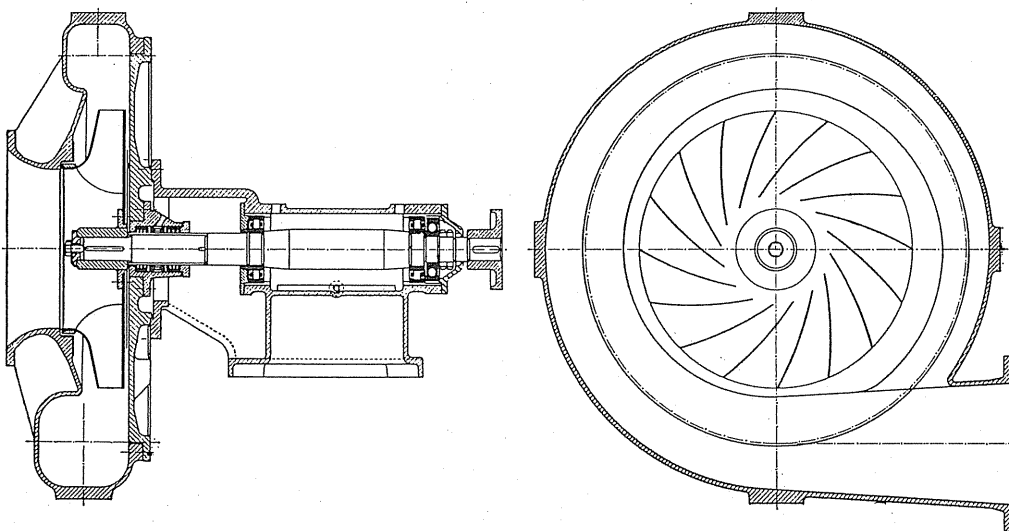


FIG.465. Medium-pressure fan manufactured by Sulzer.

shows the section of a medium pressure fan made by casting. This is a design equipped with shaft seal and which can be used for gases.

Coupling the motor with the fan can also be accomplished without using plate pedestals if an integral connection shown in Fig.466 is made by using the tubular construction. This is a fan by Sulzer with acid-protective coating.

In order to improve fans with high suction capacity the firm Sulzer has transferred the appropriate designs from centrifugal machines with double-curved blades to fans. Thus we have blades which are extremely similar to Francis turbine runners (Fig.467). The

impellers are stamped and welded together with disc and ring.⁽¹⁾ Figure 468 shows a double-groove runner of this type.

In double-groove fans the design of the housing creates some difficulty. Figure 469 shows an ingenious solution of this problem by Messrs. Sulzer.

The use of external rotor motors with fans in various cases leads to considerable simplification of the overall assembly. The firm Zeil-Abegg is occupied entirely with this field. A very interesting type, for example, is the installation of a motor of this type in a double-ended suction drum impeller as shown in Fig. 470.

A new housing design with many applications has been brought out by Messrs. P. Pollrich (Fig. 471). The housing for the drum impeller is connected up to the base plate and is

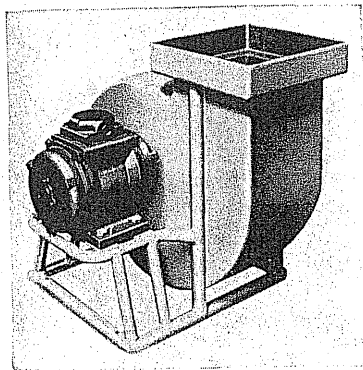


FIG. 466. Fan with tubular steel pedestal.

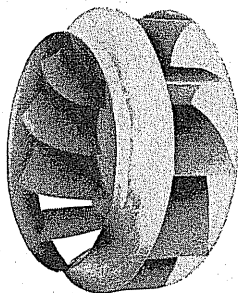


FIG. 467. Impeller with double-curved blades manufactured by Sulzer.

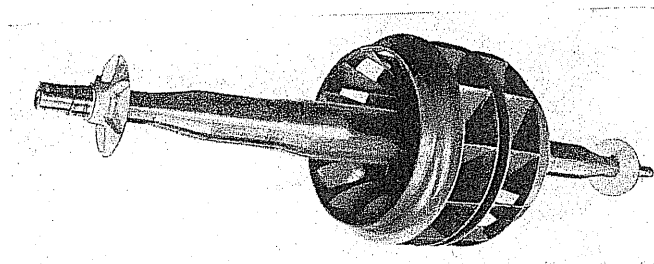


FIG. 468. Double-entry suction impeller with double-curved blades made by Sulzer.

¹ New developments in fan engineering, *Schweiz. Bauztg.*, 1950, No. 16.

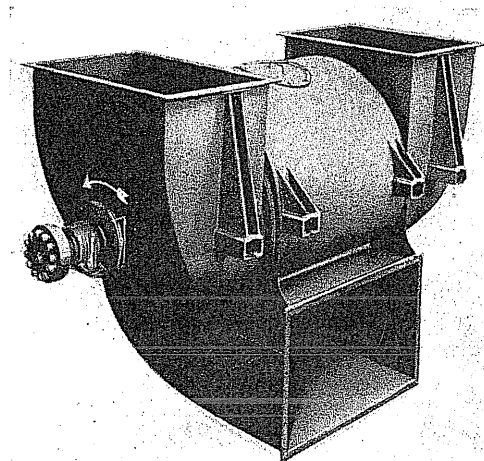


FIG.469. Fan with suction at both ends and discharge branch below.

adjustable, so that in this way any required discharge opening angle can be obtained. Another feature is that the drum impeller can be replaced by a high-duty impeller which creates a higher pressure and reduces the delivery volume.⁽²⁾

Single-stage fans for high pressures incorporate many features of turbo-compressors. The features of a few examples of this type will be discussed. Heavy rings reinforce

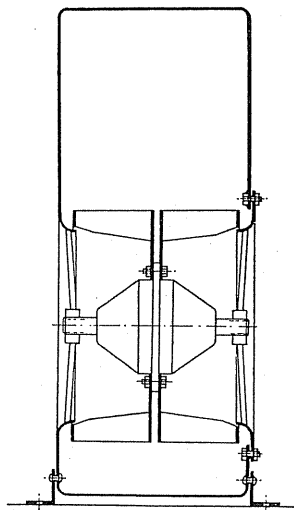


FIG.470. Multivane impeller with external electric rotor fitted inside the hub.

the cover plate on the internal diameter. They are useful at the same time for receiving special labyrinth seals. One of the features is that with gases through the shaft is sealed by means of carbon stuffing boxes, but these will not be adequate with very dangerous gases. An absolute seal, however, is obtained by using a fluid stuffing box.

² This design was created by Beiten on the unit principle.

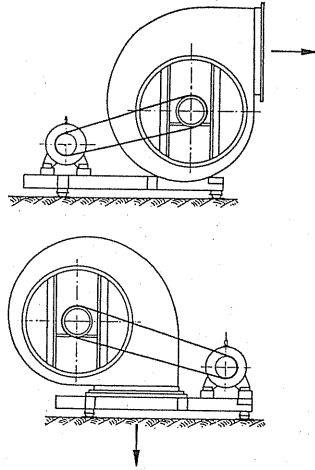


FIG.471. Multivane impeller made by Messrs. P. Pollrich with possibilities of orientation in any direction and exchanging impellers.

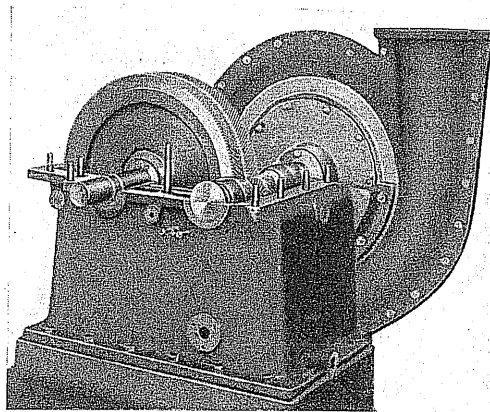


FIG.472. Small spiral housing by Demag for 0.6 atm pressure.

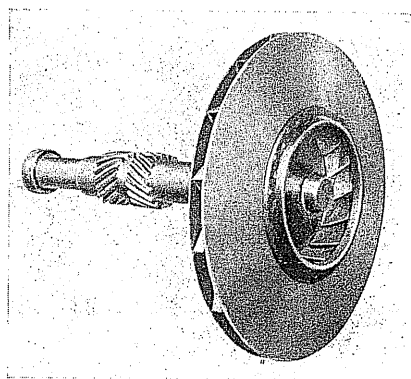


FIG.473. Impeller with pinion shaft for Fig.472.

Figure 472 shows a small spiral housing for pressures of approx. 0.6 atm. The fan shaft, which is made in one piece solid with the pinion, is driven by a gear. The peripheral speed of the impeller is about 240 m/sec. Figure 473 shows the impeller, which looks like a turbo-compressor wheel.

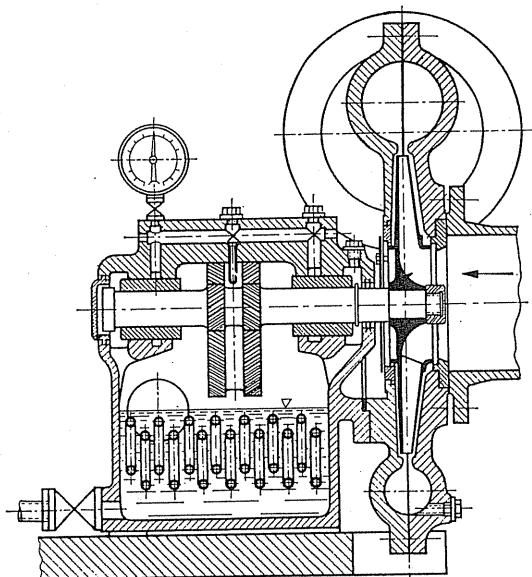


FIG.474. Cross-section through high-duty fan made by Demag. Cooling of the oil bath by water-cooling pipes.

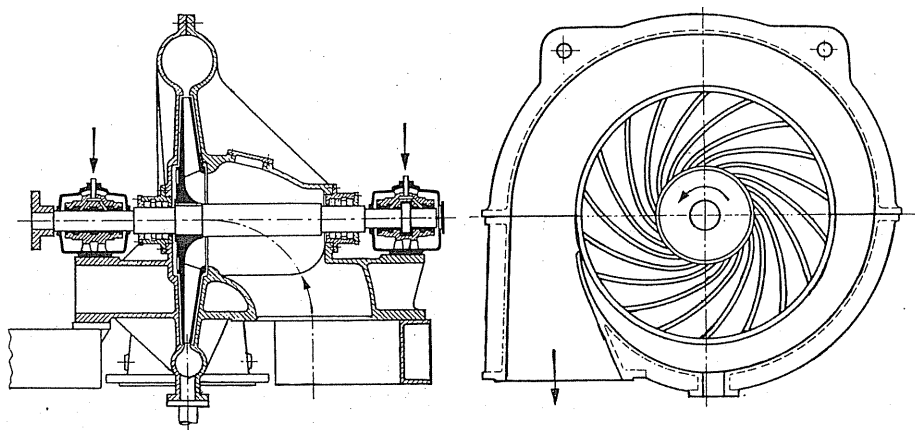


FIG.475. Gas blower for high pressure (Demag).

The important point in this design is the gear form. The oil used for gears and the bearings has to be cooled artificially. For this purpose Messrs. Demag and other firms use water-cooled tube coils which are immersed in the oil bath. The efficiencies obtained with these fans are in the region of 80%.

Figure 475 shows a gas fan designed by Messrs. Demag for high pressures.

Recently Messrs. Demag have been constructing impellers with radial-tipped blades

which have an axial intake. These impellers, which were originally developed for superchargers, have proved eminently suitable for general application in high-pressure installations. Figure 476 shows an impeller of this type. This is a remarkable new method of construction. The blades are at first welded to the shroud plate (Fig. 477) and then to the impeller disc.

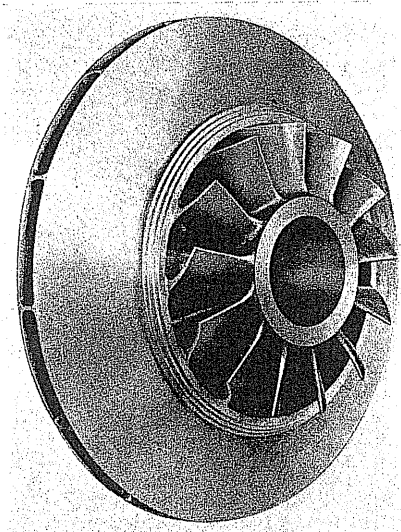


FIG. 476. Impeller with fixed blades on the shroud (Demag).

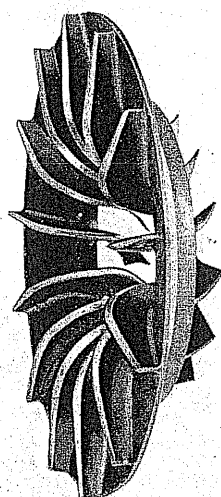


FIG. 477. Shroud with blades.

Still higher pressures can be achieved if the disc design of the impeller is ignored in principle and only the blades retained. Figure 478 shows one of these impellers by Messrs. Rateau of Paris, a firm which has made great efforts in the development. Figure 479 shows a fan of this design with suction at both ends: the fan is mounted in an open housing.

Great demands are often made on the materials used for fans according to the gases which pass through. Processes in the chemical industry involve gases which would rapidly attack steel. In this industry there are fans made of wood (for use with chloride vapours), lead, stoneware, silicon, and other materials. Figure 480 shows a fan made by Messrs. Sulzer built entirely of wood.

The high-duty fan made by Messrs. Schnackenberg (Wuppertal) was constructed wholly in PVC. In this way advantage is taken of the properties of new materials.

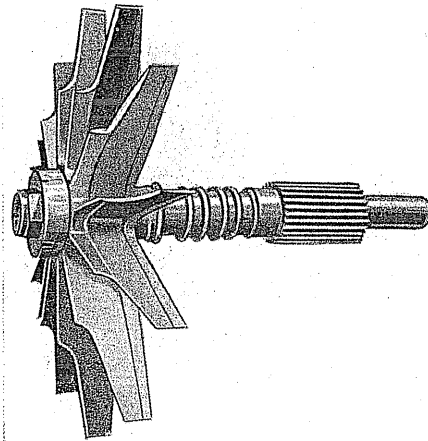


FIG.478. Fan impeller for maximum peripheral speed according to Rateau.

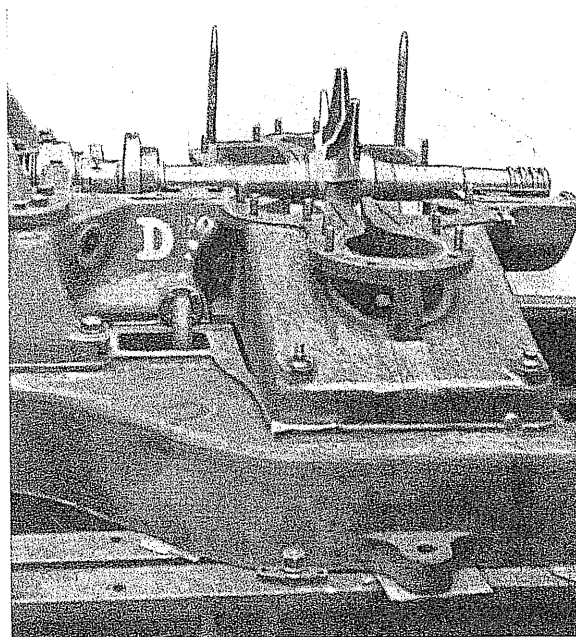


FIG.479. Fan designed by Rateau with double entry of air.

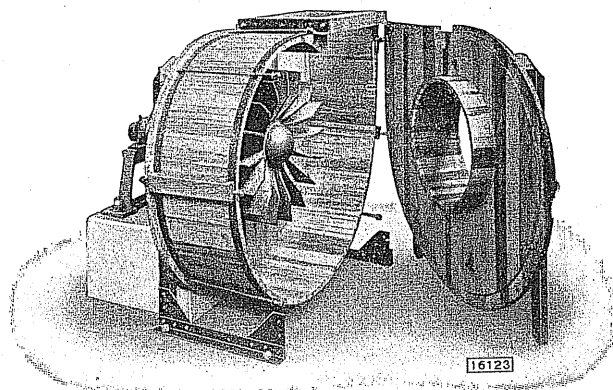


FIG.480. Fan constructed wholly of wood made by Sulzer.

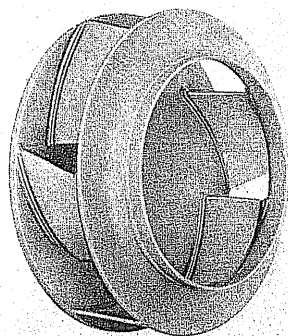


FIG.481. High-duty fan constructed of plastic material made by Messrs. Schnackenberg.

The *air-cooling of Otto and Diesel engines* has opened up a new field of application for fans. As the flow resistance, brought about mainly by cooling fins, can now be accurately determined by tests on models, it is possible to create a precise design which allows high grade axial-flow fans to be utilised to advantage. As a guide it may be stated that the temperature of air flowing through the cooling fins is raised by about 50°C . The loss of pressure is about 150–200 mm WG. With a repeatedly varying load the delivery volume of the fan must be carefully adjusted. Owing to their flatter characteristic, centrifugal fans are generally the most suitable, since with axial-flow fans speed regulation or blade adjustment has to be accepted. The interesting solution shown in Fig.482 was utilised in the Volkswagen engine. Here a centrifugal impeller with backward-curved blades, i.e. a high reaction rate, was chosen. By means of inserts and guide vanes the air stream in the housing was divided to feed the two cylinders, and a fitted oil cooler was added before the division of flow. In spite of its flat characteristics, the fan is still interesting from the point of view of regulation. In the suction space of the impeller a tubular component is inserted which ensures only partial loading of the impeller. The movement of this component is controlled automatically by a temperature sensitive device. Eckert⁽³⁾ has given detailed information on the use of axial-flow fans in motor vehicles.

³ Eckert, Motor vehicle cooling fan and its operational behaviour, Diss., Stuttgart, 1940; and Cooling fans for air-cooled motor vehicle engines, *Deutsche Kraftfahrtforschung*, 67 (1942).

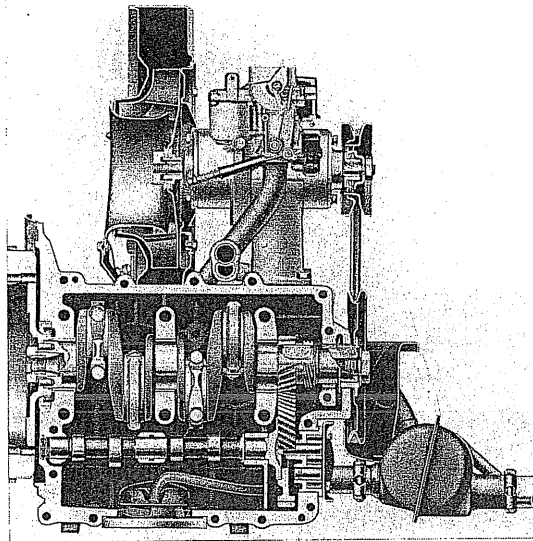


FIG.482. Centre line section through cooling fan of Volkswagen engine.

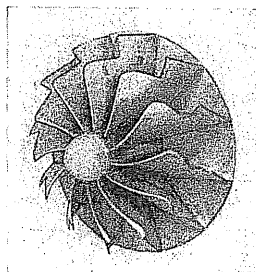


FIG.483. High-duty fan designed by Eck.

Special impellers are used for circulating air in furnaces, where the problem is to circulate air at high temperatures ($500\text{--}600^{\circ}\text{C}$) at any speed. In large industrial furnaces this gives rise to considerable pressure differences when starting up with cold air: the impeller stresses are considerable and it is imperative that the peripheral speed should be the lowest possible. The stipulation that bearings should be kept out of the hot zone is a further complication. In addition, the presence of *cold* air when starting the furnace calls for three to four times the normal motor power other conditions being equal. In this case it is important for the blower to have the lowest possible driving power at zero delivery so that overloading of the motor may be avoided by throttling when starting up. No conventional impeller satisfies all the above stated criteria; neither an axial-flow fan nor a centrifugal fan have been found suitable. At the instigation of the firm of Junker the author undertook investigations into this problem and developed a special impeller⁽⁴⁾ for this purpose. Figure 483 is a view and Fig. 484 is a typical installation in a large bolt-butting oven rated at 1500 kW.

⁴ Eck, B., Technical flow problems in the circulation of electrically heated air through furnaces, *Elektrowärme-Technik*, 1951.

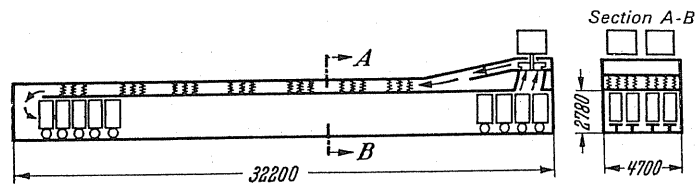


FIG. 484. Section through a large furnace with air supplied by fans.
(Otto Junker in Lammersdorf.)

150. FORM OF AXIAL-FLOW FANS

In axial-flow fans the form of the impeller is of primary interest. The outside housing is of simple construction and need not be discussed at length.

The simplest form of an axial impeller is to be found in fans whose main task is the delivery of large volumes of air. Curved blades preponderate here. With correct sizing and observation of the basic principles previously outlined, it is possible to achieve good efficiency.

For greater requirements aerofoil profiles will be called for throughout as the basic form for the propeller blades. Aluminium is the most suitable material for low peripheral speeds, e.g. $u < 50$ m/sec. At higher speeds, aluminium alloys, like Dural, Lantal, Elektron, etc., are appropriate. High efficiencies can only be achieved, however, if the *blades are precisely machined and polished after casting*. For the individual sections, templates of the aerofoil profiles have to be used to enable the designed form to be reproduced. The need for this extremely difficult finishing work is the reason for the high prices of the rather simple aero-

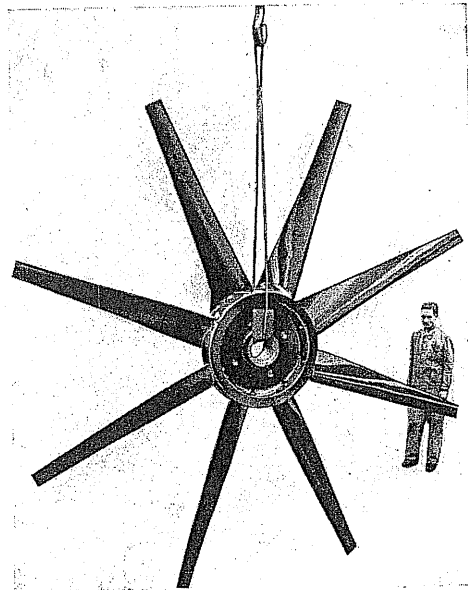


FIG. 485. Axial-flow fan made by Messrs. Escher-Wyss for $\varphi = 0.193$, $\psi = 0.045$; $D = 3000$ mm dia.

foils. The efficiencies indicated in section 108 can only be reached if great care is taken in manufacture. As machining and polishing are simpler and cheaper when wood is used in the construction material, very good results can also be obtained with wooden aerofoils.

Escher-Wyss developed a design with a relatively small hub for low pressure factor and high delivery rate (Fig.485).

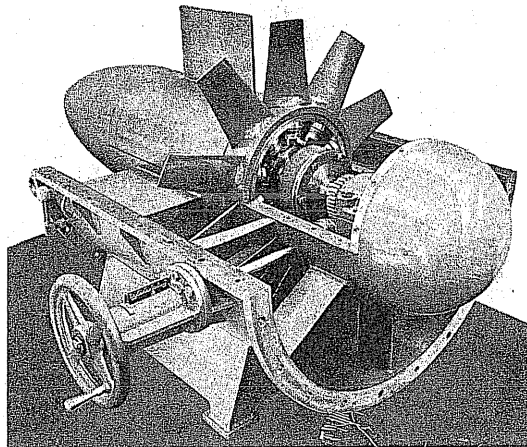


FIG.486. Axial-flow fan with blades adjustable from outside.

The fields of application of axial-flow fans are often such that the resistances to be overcome cannot be stated beforehand. Therefore the customer is often left with the problem of adapting the fan later to the conditions which exist. Adjustable impeller blades are very convenient in this case. The firm Escher-Wyss, Zürich, have been responsible for initiating the development of adjustable impeller vanes.

Even for multistage fans, impellers with vanes which could be adjusted during operation were developed by Escher-Wyss. A notable design is shown in Fig.486. Here the blades are

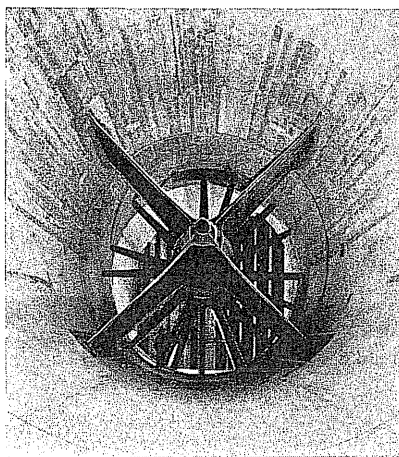


FIG.487. Wind tunnel fan made by Messrs. Escher-Wyss.

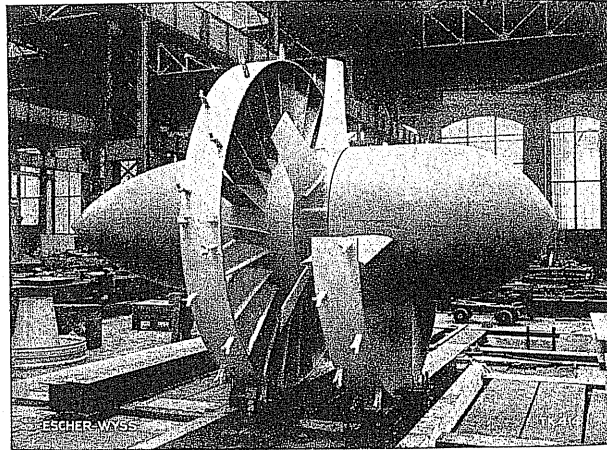


FIG.488. Axial-flow fan for large delivery volumes made by Messrs. Escher-Wyss.

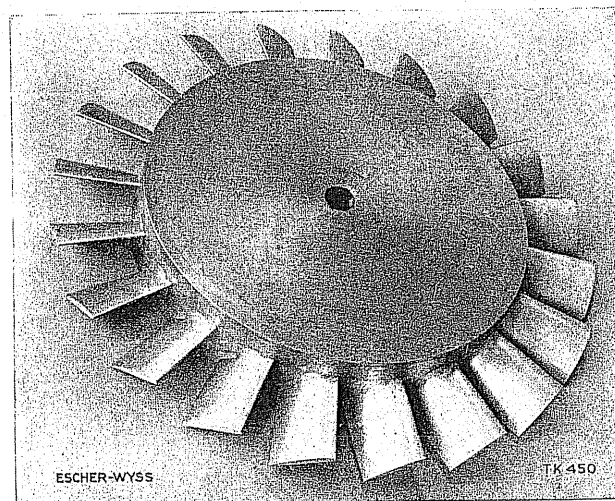


FIG.489. High-pressure impeller made by Messrs. Escher-Wyss.

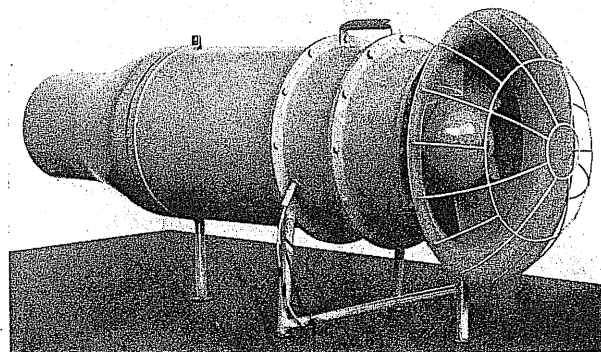


FIG.490. Wind tunnel with axial-flow fan.

adjustable from the outside by means of the hand-wheel shown in Fig. 486. The top part of the housing has been removed and the guide vanes situated in front of the impeller are uncovered.

Figure 487 shows a wind tunnel fan by Escher-Wyss.

Figure 488 shows a standard model by Escher-Wyss with guide vanes and outside ring. The illustration portrays practically the whole of the fan which has been changed into what may be regarded as a fitting for a pipeline. At higher pressures the hub diameter must increase considerably. A higher pressure impeller of this type where ψ values of 0.6 were achieved is shown in Fig. 489. A very large unit in course of erection is shown in Fig. 488. The blades of the divided ring, which is grouted into a concrete duct, serve the purpose of bracing the hub of the impeller.

Figure 490 shows the installation of an axial-flow fan in a small wind tunnel. Axial-flow fans are able to achieve considerable outputs at low peripheral speeds and also with very little noise. The small appliance with a driving power of 1.5 kW produces a wind velocity of approximately 40 m/sec.

For handling large volumes of air at moderate pressures, the axial fan appears to be an ideal solution. A propeller fan for a cooling tower delivering 60 m³/sec at about 9 mm WG, installed by the firm Sulzer, is shown in Fig. 491. The axial-flow fan solves this problem with an effective power consumption of only 11 hp.

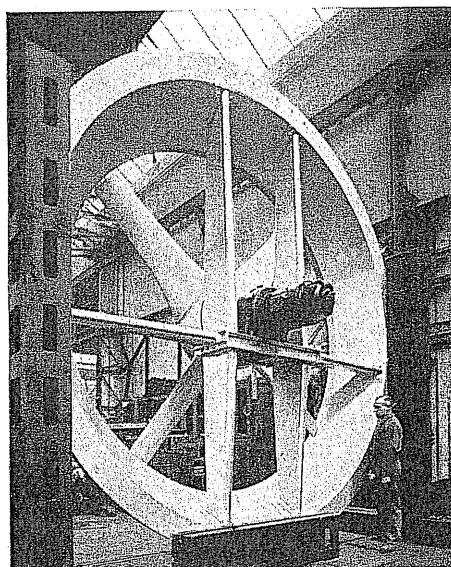


FIG. 491. Axial-flow fan made by Messrs. Sulzer for 60 m³/sec and 9 mm WG.

Mechanical speed adjustment is advisable for many special tasks, e.g. in the cooling fans of motor vehicles. Figure 492 shows how this problem was solved by means of a friction wheel gear developed by FKFS adjustable from the outside.

There is probably no fan so widely used as the well-known *table fan*. The low driving power and the satisfaction of being able to obtain results even with simple designs may contribute to the fact that this application has received little scientific attention. It is therefore

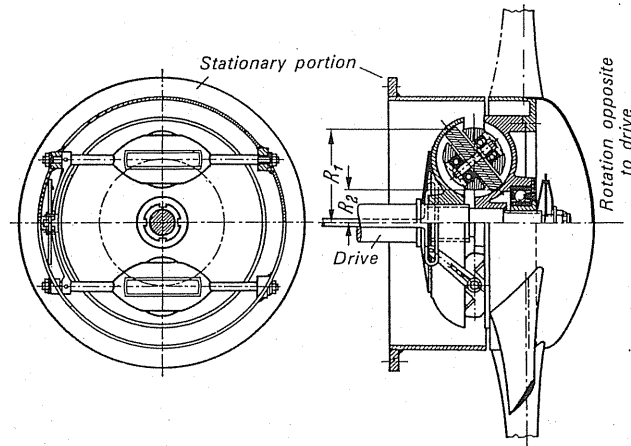


FIG.492. Friction wheel drive for speed control in axial-flow fans designed by FKFS.

to be welcomed that certain firms are attempting to market technically up-to-date designs in this respect. Figure 493 is an interesting design by the Samson United Corporation in Rochester, USA (DRP 699 902). The blades, which have a twisted circular section, are made of rubber sheets thickened at the hub end. These blades are inserted into grooves of a hub in the shape of a bell. From the aerodynamic aspect the shape is fairly satisfactory and the use of rubber eliminates danger so that the fan can be used without a guard. Owing to the higher efficiency these impellers can be run at low peripheral speeds.

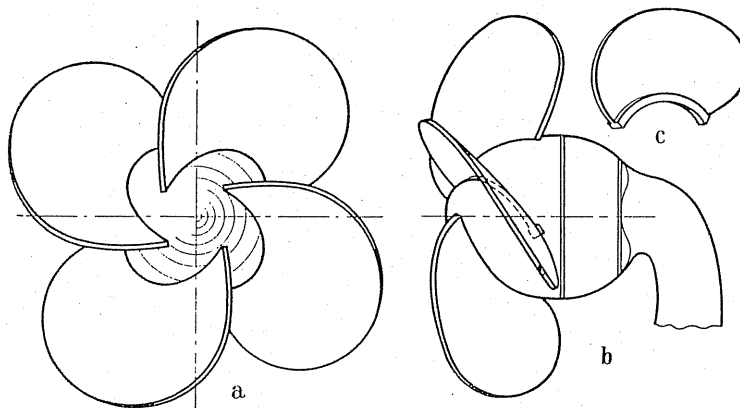


FIG.493. (a-c) Axial-flow fans with rubber aerofoils and hub discharge.

For an impeller of this type the author measured $\varphi = 0.16$, $\psi = 0.135$. This shape of blade has already been used previously in the United States⁽⁵⁾ for table fans.

Recently, very small cross-flow fans have been produced as table fans.

An interesting special design by Messrs. P.H.Fröhlich⁽⁶⁾ for generating small pressure differences is shown in Fig.494. This is a propeller fan design projecting at a slope into a

⁵ Baumeister, *Fans*, New York, McGraw-Hill, 1935, p.23.

⁶ DRP 473 579.

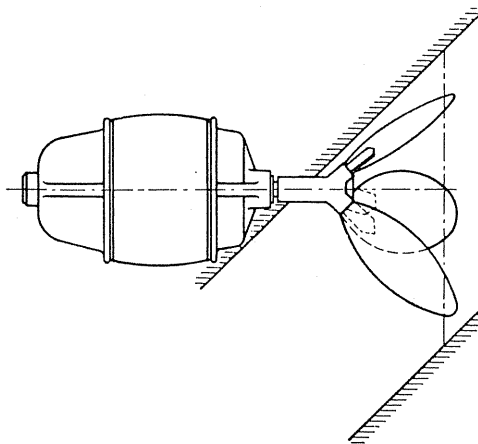


FIG.494. Axial-flow fan designed by Fröhlich.

duct so that there is always a portion of the blade actively effecting the flow. Drive and bearings are located outside the duct. Designs of this kind may be interesting for small gas flues where it is often required to boost the chimney draught which may not be adequate. In such cases the power consumption of the drive is readily acceptable.

In the chemical industry, owing to the use of corrosive gases, many special designs are called for. Plastic fans are very popular and, having fairly good mechanical strength, they present no difficulties. In special instances, however, stoneware is the only material which

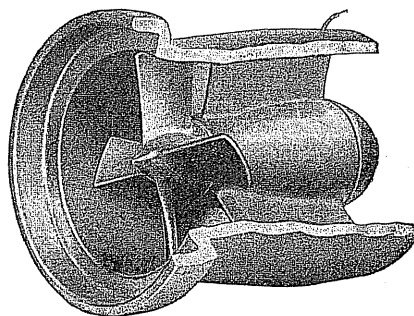


FIG.495. Propeller fan made of stoneware.

can be used. Figure 495 shows a propeller fan where the impeller and the housing are made exclusively of stoneware. This type of fan is produced for volumes of 10–20 m³/min and pressures up to 12 mm WG.

151. IMPORTANT CONSTRUCTIONAL DETAILS

The construction of *impellers* is governed by the peripheral speed. At very high peripheral speeds, as in superchargers, star blade configurations are used which are all based on the original design by Rateau (Fig.478). Highly stressed impellers with side walls call for

forged plates in alloy steel. The blades are riveted on. U- or Z-shaped blade profiles, as shown in Fig. 496b and c, are used in these designs (Demag design). However, blades with rivet heads which are machined (Fig. 497) (type BBC) are used alternatively. The opened-up impeller (Figs. 497 and 498) portrays the difference. Welding is not suitable for the high-alloy discs which are required in this design. For the smaller peripheral speeds commonly

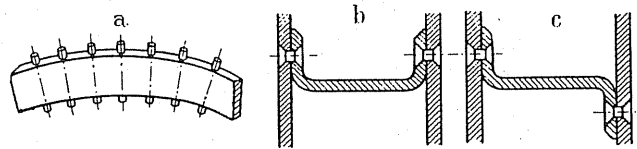


FIG. 496. (a) Blade with fixed rivets. (b) and (c) Typical riveting layout.

occurring in fan engineering, welded designs are usual. The distortion which was formerly a frequent source of complaint can be eliminated entirely by using modern welding devices and modern welding machines. Semi-automatic butt welding is a rather important feature in this construction. Figure 499 shows a very large construction by MAN which is completely welded. It will be observed that the impeller has blades of double curvature.

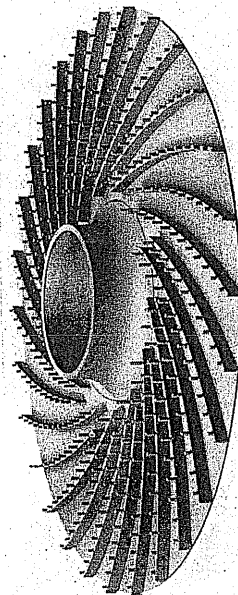


FIG. 497. Impeller opened up to show milled rivets (BBC).

With wide blades these are inserted at various depths in the plate and the whole is then welded together as shown in Fig. 500.

Hollow air-screw blades made from steel⁽⁷⁾ are being used lately for axial-flow fans.

Adjustable guide vanes of radial-flow fans have been developed by the firm BBC. Figures 501 and 502 show typical components of this design.

⁷ *Konstruktion*, 1954, p.114.

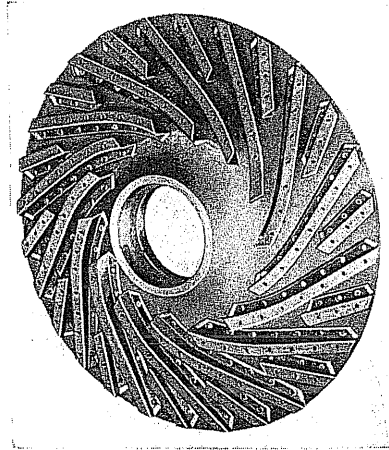


Fig. 498. Impeller opened up to show riveted blades (Demag).

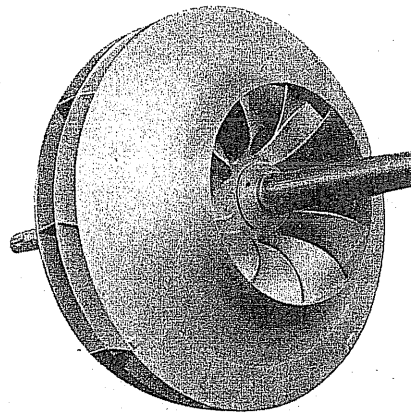


FIG. 499. Fully welded impeller designed by MAN.

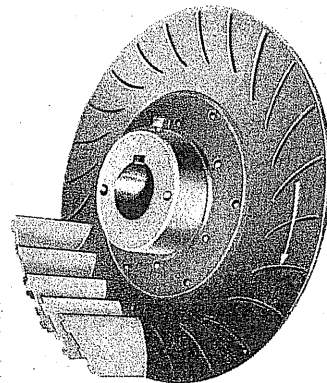


FIG. 500. Blades inserted in shroud recesses.



FIG. 501. Guide blade ring with adjustable guide blades according to BBC.

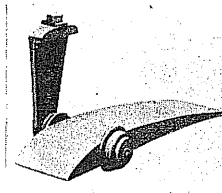


FIG. 502. Adjustable guide blades according to BBC.

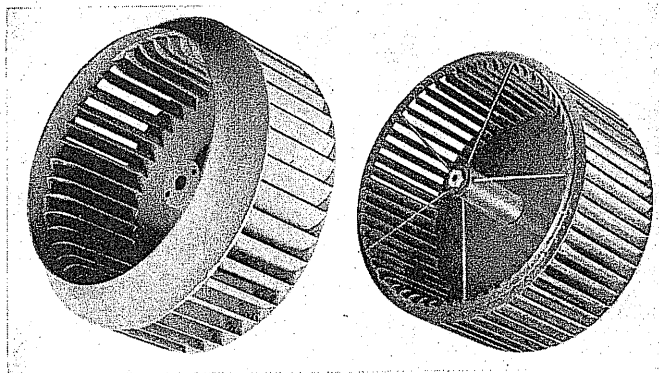


FIG. 503.

FIG. 504.

FIG. 503. Drum impeller with open ring.

FIG. 504. Bracing by struts in drum impeller.

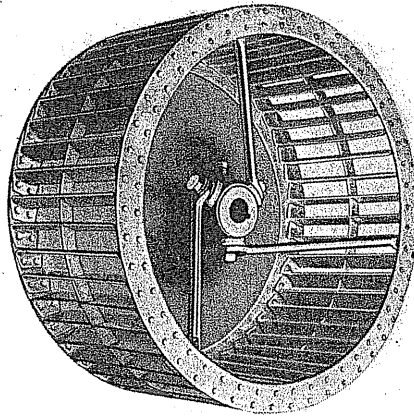


FIG. 505.

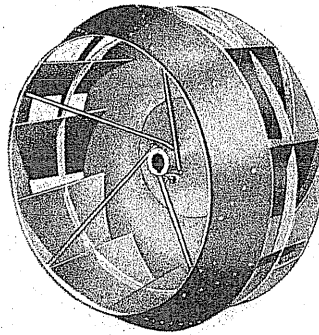


FIG. 506. Bracing by means of a ring.

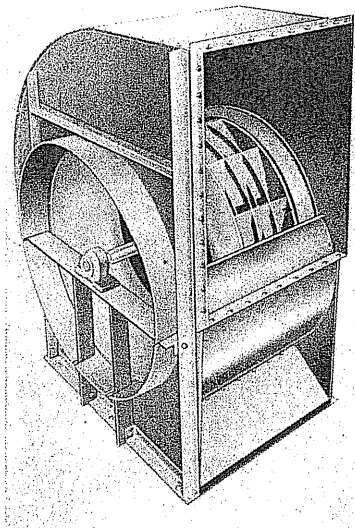


FIG. 507. Bracing by means of several rings.

The main constructional problem in wide blades such as are used for drum impellers is the strength of the drum impeller union. A thick intake ring as shown in Fig. 503, for instance, will meet this requirement provided there is an adequately small diameters ratio. Bracing offers further possibilities. This method can be observed in the designs shown in Figs. 504, 505, and 506. Finally, the blades can be relieved by intermediate rings. Figure 506 shows a single ring and Fig. 507 several rings. In order to provide relief to the hub and simultaneously self-adjustment of the impeller without bending stresses, BBC suggest that for highly stressed impellers the wheel be fastened by a resilient annular spring, a design which clearly points to the influence of steam-turbine engineering (Fig. 508).

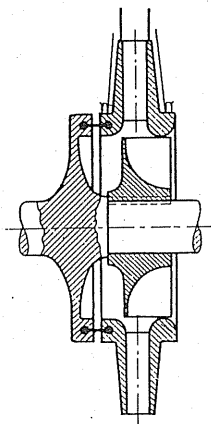


FIG. 508. Spring-mounted impeller according to BBC.

In the construction of the fan housing it is often important that the housing can be easily turned in any direction. For this purpose the scroll housing can be mounted on a pedestal which accommodates the driving motor on the inside (Fig. 509). In the manufacture of low-cost impellers, each blade may be connected to the hub by a bracket. Figure 510 shows examples.

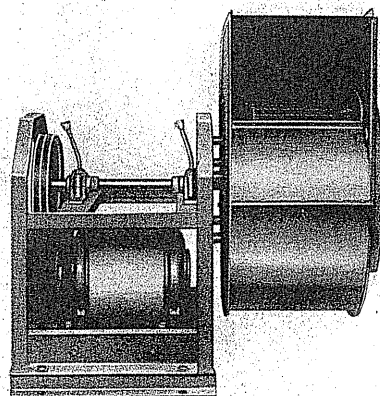


FIG. 509. Spiral housing mounted on a pedestal.

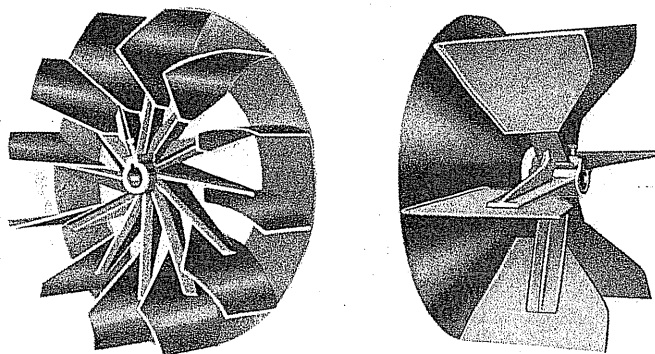


FIG. 510. Impeller with each blade supported separately.

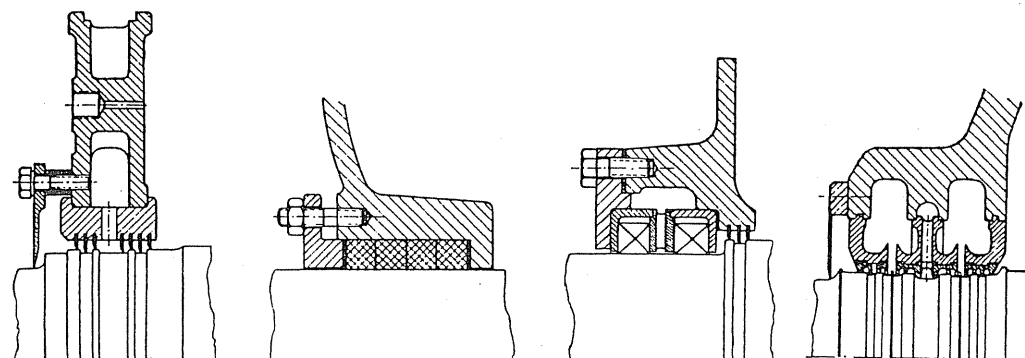


FIG. 511. Various shaft seals: labyrinth-seal, soft packing, carbon packing.

In gas-blowers *shaft seals* are of great importance. The toxicity of the gases may call for absolute tightness of the shaft entry. Figure 511 shows four typical designs which have been developed⁽⁸⁾ by Messrs. Demag.

152. AIR-COOLED BEARINGS FOR HOT-GAS BLOWERS

In hot-gas blowers one of the *most* important applications for fans, the safe cooling of the bearings during operation, is the major factor. If it is not possible or convenient to provide water cooling, artificial auxiliary air currents can be arranged for cooling the bearings. Figure 512⁽⁹⁾ shows an arrangement in which a small radial-flow impeller is situated behind the main impeller providing air for cooling. Both bearings are encased in steel sheet and the air exhausted by the auxiliary impeller first has to pass over the outer surfaces of the bearings. It is then sucked through the hollow shaft which is provided with radial openings at intake points adjoining the bearings. The air then passes through further radial openings in the hollow shaft into the blades of the auxiliary impeller which are also hollow.

⁸ Details of new labyrinth seals are found in Eck, B., *Technische Strömungslehre*, 6th edn., Berlin/Göttingen/Heidelberg, Springer, 1961.

⁹ Air-cooled bearings for radial- and axial-flow fans, used for a hot gas, VDI-Z, 1953.

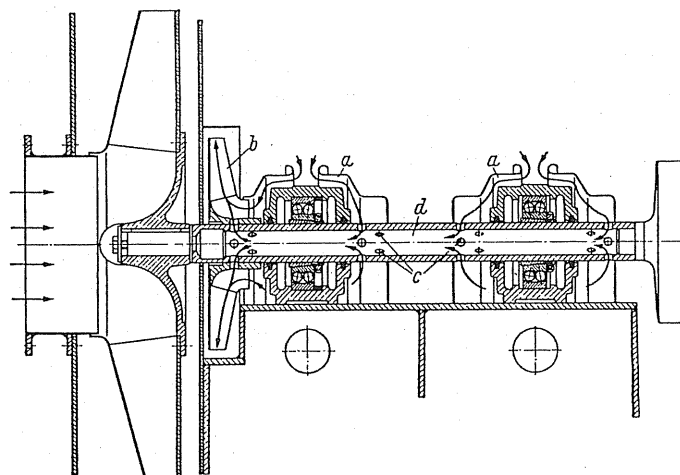


FIG. 512. Air-cooled bearings for fan handling hot gases (Mabag, Sulzbach). *a*, bearing covers; *b*, cooling impeller; *c*, openings in a hollow shaft for sucking air for cooling purposes; *d*, hollow shaft.

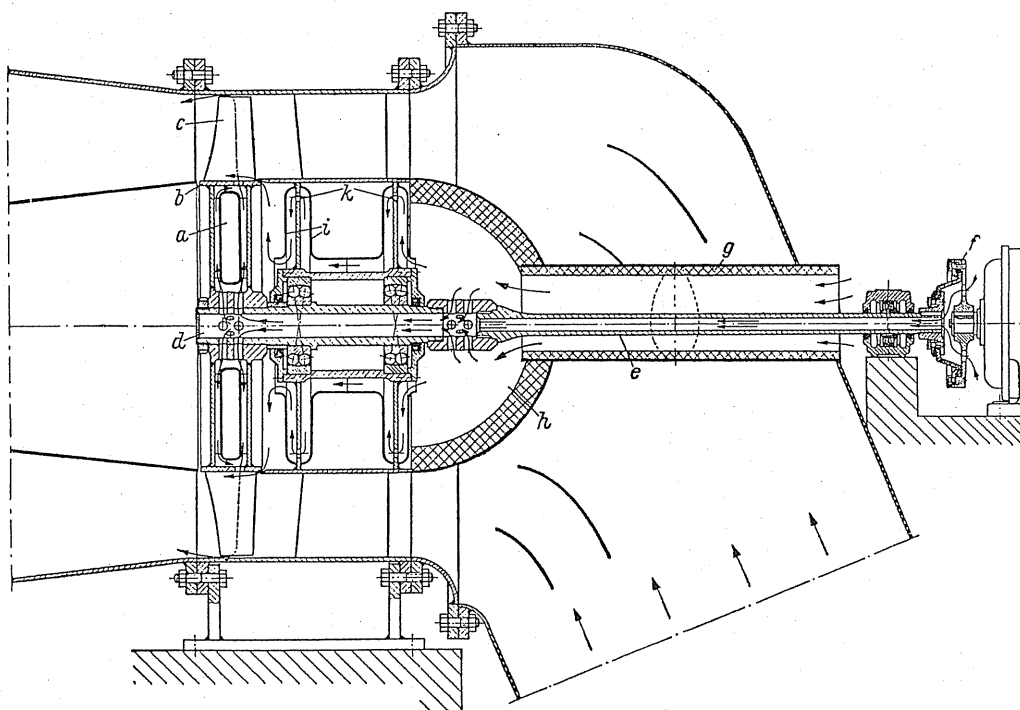


FIG. 513. Cooling bearings in the hub of an axial-flow fan (Mabag, Sulzbach). *a*, displacing member, dividing cooling impeller in two parts; *b*, hub cylinder of the axial-flow impeller; *c*, axial-flow fan blades; *d*, hollow space in shaft through which the cooling air is sucked; *e*, hollow supply shaft; *f*, coupling; *g*, shaft cover; *h*, hub cover; *i* and *k*, passage walls.

A more difficult problem is that of cooling a bearing built into the hub of an axial-flow fan. Such an arrangement is shown in Fig. 513. Incorporated in the hub of the axial-flow fan is a centrifugal impeller which is divided by means of a displacer *a* into two narrow parts. Air is again exhausted through radial openings in the hollow shaft. The air exhausted by the radial blades then passes into the axial-flow fan blades which are hollow and is discharged at their open ends. A second current of air for cooling the bearings is branched off at previous stage. This partial air current is conducted to the point which has the lowest negative pressure. This is the gap between the impeller and the guide wheel.

A remarkable design is shown in Fig. 514. Here cooling air is forced into the motor from the pressure end of an axial-flow fan through the hollow wall bracket which supports it. As shown by the arrows, the cooling air is then directed back to the axial impeller.

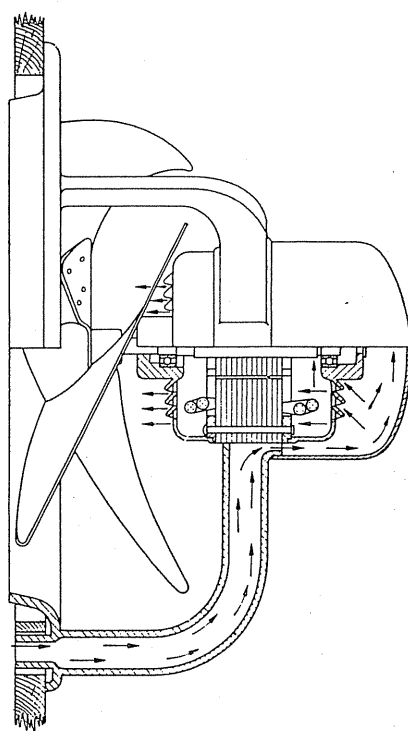


FIG. 514. Cooling of motor from the pressure side of an axial-flow fan.

As relatively small air volumes are involved, the efficiency of the cooling fan is unimportant. Therefore a drum impeller can be used without any disadvantage thus making for compactness. Figure 515 shows an instance where a miniature drum impeller is arranged adjoining the fan housing wall and right next to the bearing. Guide blades enforce the circulation round the bearing.

The most effective cooling is by water. For this purpose generally a bearing bush, i.e. the top bearing bush, is provided with a water-cooling passage. Figure 516 shows an example of this arrangement. The water enters through branch *a* and leaves through branch *b*.

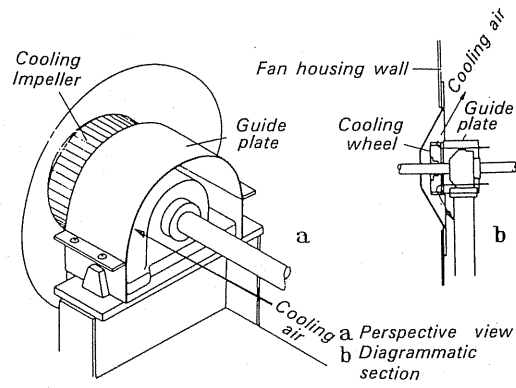


FIG. 515. (a and b) Bearings cooled by means of a special drum impeller.

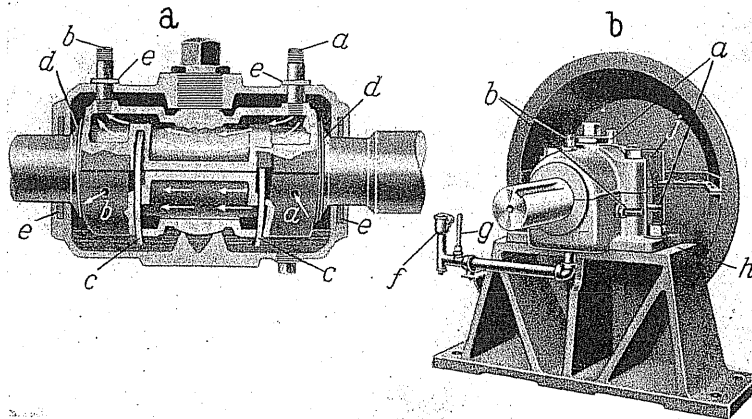


FIG. 516. Water-cooled bearing. *a, b*, water circulation connection; *c*, oil sump; *d*, spray ring; *e*, seal; *f*, oil supply branch.

PART F

SOUND GENERATION AND SOUND
ATTENUATION OF FAN INSTALLATIONS

CHAPTER XXI

SOUND GENERATION BY FANS

(Treatise by B. REGENSCHEIT)

THE following remarks only concern sound which arises from air flow in the fan. There will be no discussion of noise arising from bearings, drives or motors.

Nowadays investigations into fan noise are of extreme importance due to the advance of air conditioning and ventilation techniques. They form the basis for assessing silencers. They can also lead to the improvement of fans as it is by no means justified to assume that the present levels of noise radiated from fans are unalterable.

A large number of investigations on sound have been carried out. The total sound intensity as well as the frequency spectrum of noise have been investigated for axial-flow and for centrifugal fans. The most important investigations are mentioned in the footnotes.

Very few theoretical investigations are encountered: the work of Peschka⁽¹⁾ on the axial-flow fan as a source of sound is one of them.

153. DEPENDENCY OF RADIATED SOUND POWER ON THE PERIPHERAL SPEED

For sound level measurements on fans which are connected up to a given ducting system Stang and Zeller⁽²⁾ found the sound level to be a function of the fifth power of the peripheral speed of the impeller. (The throttling factor τ is kept constant.) Zeller⁽³⁾ states that the power is a function of the frequency itself. By plotting power against frequency, we obtain Fig. 517. The actual mean frequencies can be correlated by a straight line if the log of the power is plotted against the log of the frequency. Hübner⁽⁴⁾ finds the 5.5 power in the range of the peripheral speed up to 50 m/sec. From 50 to 100 m/sec the value is 6.7. Measurements of Holle and Lübke⁽⁵⁾ indicate a seventh-power law in the range from 30 to 160 m/sec, i.e. in the total range covered by the measurements by Zeller, Stang, and Hübner. For

¹ Peschka, W., The axial compressor as a source of sound, *Öst. Ing.-Arch.*, **10** (1956), No. 1.

² Zeller, W., and Stang, H., Predetermination of the axial-flow fans, *Heizung-Lüftung-Haustechnik*, **9** (1957), No. 12.

³ Zeller, W., Concerning mathematical treatment of noise behaviour in fans for air conditioning plants, *VDI-Berichte*, 1959, No. 38.

⁴ Hübner, G., Noise generated by centrifugal fans, *Siemens-Z.*, 1959, No. 8.

⁵ Holle, W., and Lübke, E., Concerning measurement of sound intensity of sound generated by rapidly moving profiles, *Luftfahrtforschung*, **17** (1940).

technical purposes the fifth power is used for calculation in America. The 4.6 power was indicated by von Riollot.⁽⁶⁾

We must conclude from the diversity of results that there is no universally valid dependency of sound power on peripheral speeds. It is probable that the dependency is affected by the construction of the fan. (A few unpublished test results show that this may be so. In these tests the power was altered from 5 to 4 by means of slight changes in construction.)

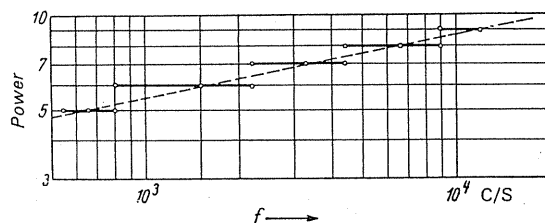


FIG. 517. The power with which the sound level increases as a function of the frequency according to Zeller.

154. DEPENDENCY OF SOUND LEVEL ON THE AERO-DYNAMIC FACTORS OF THE FAN

(a) DEPENDENCY ON EFFICIENCY

It is found in many cases that the sound level has the lowest value in the range of maximum efficiency. In some cases the maximum efficiency and the lowest sound level even coincide.⁽⁷⁾ Measurements by Hübner⁽⁸⁾ are the exception, and he lays stress upon this point.

(b) DEPENDENCY ON FLOW VOLUME AND PRESSURE

Measurements made by Hübner were carried out at constant value $\tau = \varphi^2/\psi$. Alteration of this value (pressure and volume were altered) caused a distinct alteration to the sound level. With the increase in τ (increasing volume, decreasing pressure, i.e. according to Hübner, decreasing ζ) the sound level rises. In the working range of the fan the difference amounts to about 5 dB. Measurements made by Riollot⁽⁹⁾ on Rateau fans led to the sound level being found to be a function of the volume coefficient φ . Variation from the optimum volume coefficient, either an increase or decrease in volume, results in an increase in sound level.

⁶ Riollot, G., Laws of sound emission of a fan obtained by dimensional analysis, *9th International Congress of Applied Mechanics, Brussels*, Part II.

⁷ Zeller, W., and Stang, H., Prediction of the sound intensity of axial-flow fans, *Heizung-Lüftung-Haustech-nik*, 8 (1957), No. 12. Schubert, E., Axial- and radial-flow mine fan noises, *VDI-Berichte*, 35 (1959). Allen, C. H., Noise from air-conditioning fans, *Noise Control*, 3 (1957). Madison, D., and Graham, J. B., HPAC fan noise variation with changing fan operation, *Transactions American Society of Heating and Air Condition-ing Engineers*, 64 (1958).

⁸ Hübner, G., Noise generation by centrifugal fans, *Siemens-Z.*, 1959, No. 8.

⁹ Riollot, G., Law of sound emission of a fan taken from the dimensional analysis, *Ninth International Congress of Applied Mechanics, Brussels*, Part II.

Works by Stang and Zeller⁽¹⁰⁾ and Zeller⁽¹¹⁾ show the sound level to be clearly a function of the throttling condition of the fans. In addition to the curves for the sound level, they also give a graph of the dimensionless characteristic of the fans ψ against φ (pressure coefficient $\psi = \Delta p_t / (\rho/2) u^2$, volume coefficient $\varphi = V/Fu$). The sound level is entered above φ . Unfortunately, Hübner and Zeller failed to indicate the efficiency of the fans investigated. It is, however, essential to know this for a comparative assessment of the fan noise, since measurements show that the minimum level occurs in the proximity of maximum efficiency.

155. FAN NOISE AS A FUNCTION OF FREQUENCY

This function depends very much on the design of the fan. All fans where the blades are in alternating action with static or moving counterblades display this in the frequency spectrum. In axial-flow fans the counter blades can be guide units or a contra-rotating impeller or even only the supporting structure situated before or following the impeller. In centrifugal fans the impeller blade is affected by the spiral housing. The greatest effect occurs at the tongue of the housing, i.e. at the narrowest point between impeller and housing wall. The effect becomes distinguished by peaks in the frequency spectrum. The typical frequency is explained by the number of disturbances per impeller rotation. Centrifugal fans without spiral housing, such as occur in cooling fans for electrical machinery or axial-flow fans which are fitted to specially pulled-out shafts, do not show these distinct peaks in the frequency distribution. This was demonstrated by Hübner,⁽¹²⁾ particularly for centrifugal fans.

In a centrifugal fan with spiral housing of the usual type, the interruption only occurs at one point in the housing. For Z blades the frequency of interruption is obtained from the relationship

$$f = \frac{an}{60} Z, \quad (260)$$

n being the rev/min, Z being the number of blades.

In this equation a is an integer ($a = 1, 2, 3, \dots$) which indicates the order of the oscillation. With $a = 1$ the basic frequency is obtained. In centrifugal fans with several spiral housings or several housing tongues, the frequency increases according to the interruptions. In an axial-flow fan, where the number of blades in the impeller would be equal to those in the guide wheel, the interruption appears simultaneously in all Z blades. The sound level caused by the interruption is considerable. If this simultaneous disturbance is eliminated there is a reduction of radiated sound intensity. It can be assessed on the basis that two equal sound sources emitting simultaneously raise the level by 3 dB. The following table gives the decrement in sound level in dB if the simultaneous disturbance is avoided. For

¹⁰ Zeller, W., and Stang, H., Predetermination of the sound intensity amplitude of axial-flow fans, *Heizung-Lüftung-Haustechnik*, 8 (1957), No. 12.

¹¹ Zeller, W., Concerning mathematical treatment of noise behaviour in fans for air conditioning plants, *VDI-Berichte*, 1959, No. 38.

¹² Hübner, G., Sound generation in centrifugal fans, *Siemens-Z.*, 1959, No. 8.

example, in a fan with sixteen impeller blades it may be expected that the sound level will drop by 12 dB if the sixteen guide vane blades are arranged in such a way that not all the blades coincide simultaneously. This is obtained by unequal blade pitch of the guide vane blades. More often the number of guide vane blades is made unequal to that of the impeller blade.

Number of blades on impeller	1	2	4	8	16
Decrease of sound level (dB)	0	3	6	9	12

It is an advantage to vary the number of blades in such a way that the timing between the interruptions reaches a maximum.

The angle between two impeller blades amounts to

$$\Delta\varphi_1 = \frac{360}{Z_{\text{imp}}}, \quad Z_{\text{imp}} = \text{number of blades.}$$

This angle is divided into Z parts and we obtain

$$\Delta\varphi_2 = \frac{360}{Z_{\text{imp}}^2} = \frac{\Delta\varphi_1}{Z_{\text{imp}}}.$$

The angle between the blades of the guide vane unit is

$$\Delta\varphi_1 \pm \Delta\varphi_2 = 360 \left(\frac{1}{Z_{\text{imp}}} \pm \frac{1}{Z_{\text{imp}}^2} \right);$$

from this we obtain the number of guide vanes:

$$Z_{\text{guide}} = \frac{360}{\Delta\varphi_1 \pm \Delta\varphi_2} = \frac{Z_{\text{imp}}}{1 \pm 1/Z_{\text{imp}}}.$$

The following table shows the analysis if total number of blades are specified:

Impeller blades	4	8	12	16
Guide blades (min.)	3	7	11	15
Guide blades (max.)	5	9	13	17

It will be appreciated that it is correct to allow a tolerance of ± 1 in the difference in the number of guide vanes to impeller blades.

In axial-flow fans with guide vanes three special sound frequencies arise. Each impeller blade interacts with each guide vane to produce the frequency

$$f_1 = \frac{an}{60} Z_{\text{guide}}. \quad (261)$$

Each guide vane interacts with the impeller blades to produce the frequency

$$f_2 = \frac{an}{60} Z_{\text{imp}}. \quad (262)$$

Between the periods of each blade induction the neighbouring blades will slip past each other. Thus the frequency obtained is

$$f_3 = \frac{an}{60} Z_{\text{imp}} Z_{\text{guide}}. \quad (263)$$

The difference between the frequencies is approximately the beat frequencies. An important beat frequency is

$$f_3 - f_1 \approx f_3 - f_2 = f_s = \frac{an}{60} Z_{\text{imp}} (Z_{\text{guide}} - 1) \approx \frac{an}{60} Z_{\text{guide}} (Z_{\text{imp}} - 1),$$

which is audible.

From this follow a number of assumptions used in assessing the frequency spectrum. The interruption frequencies which result from the geometry of the fan increase proportionately with the speed. If an axial-flow fan is compared with a centrifugal fan, the low frequencies are approximately equal for equivalent number of blades on the impeller and for equivalent speeds. In axial-flow fans a high frequency is approached which is obtained from the product $Z_{\text{guide}} \times Z_{\text{imp}}$. However, if a centrifugal fan has to supply the same volume at the same pressure as an axial-flow fan, it usually has larger impeller blade diameters. It runs at a lower speed; therefore it has a lower fundamental frequency than the axial-flow fan.

Generally sound spectra with predominantly low frequencies are more pleasant than those with a considerable proportion of high frequencies. This is clearly shown in the investigations by Schubert.⁽¹³⁾ The disturbance occurred in the vicinity when operating axial-flow and centrifugal mine fans was examined. The complaints about the axial-flow fans were very considerable, but they were very few for the centrifugal fans. The loudness measured in phons was approximately the same for both. The centrifugal fan had the maximum noise at lower frequencies, unlike the axial-flow fan. Noises with considerable proportions at high frequencies can, however, be readily reduced by means of simple silencers.

Noises where low frequencies predominate require a higher outlay for silencers. If a noise has very low frequency components, which is the case with slow-running centrifugal fans with a small number of blades, the danger of resonance in the building arises. If, for instance, one of these fans blows into an air distribution duct made of concrete which is not insulated against sound, resonance of considerable intensity may occur. The frequencies arising in ducts closed at both ends are expressed by the relationship

$$f = \frac{ac}{2l}. \quad (264)$$

For a duct open at one end we have

$$f = \frac{(2a - 1)c}{4l}, \quad (265)$$

¹³ Schubert, E., Noises in mine fans of the axial- and radial-flow type, *VDI-Berichte*, 1959, No. 35.

where c is the speed of sound (343 m/sec at 20°C), l is the length of duct, a is the multiple of the fundamental frequency, $c = 20\sqrt{T}$, and T = absolute temp. (°K).

Therefore a duct closed at both ends 5 m long has a natural frequency ($a = 1$) of

$$f = \frac{343}{10} = 34.3 \text{ c/s;}$$

closed at one end

$$f = \frac{343}{20} = 17.15 \text{ c/s.}$$

A centrifugal fan with six blades and a spiral has this fundamental frequency:
closed at both ends:

$$n = \frac{f \times 60}{Z} = \frac{34.3 \times 60}{6} = 343 \text{ rev/min;}$$

closed at one end:

$$n = 171.5 \text{ rev/min.}$$

The numerical example shows that resonance frequencies are likely to occur with ducts: they must be carefully watched.

For correct application of a fan, a knowledge of the frequency spectrum is just as important as the value of the sound level in dB. It is impossible to assess the size of a silencer correctly without knowing the frequency spectrum.

156. SOME REMARKS ON SOUND GENERATION

The sound radiating from the fan has been created by flow processes along the blades and along the housing, i.e. by interaction between blades and housing.

Sound does not arise only from the effect of friction in the flow. Considerable contributions of sound can arise without friction.

Let us now examine an impeller without guide vanes and without housing. With an axial impeller particularly, generation of sound may be expected. This has been explained by Ernsthausen⁽¹⁴⁾ and Billing⁽¹⁵⁾ for air screw. Here the sound is generated by the rotating pressure field around the impeller aerofoil (rotary tone). If the impeller is surrounded by a housing, the noise radiated radially (where it is generated by sweeping round the blade tips) is avoided. The remainder is reflected by the housing and is suitably absorbed appropriately by the housing material. The housing also can be excited to natural vibrations and even radiate sound.

If before or after the impeller a guide wheel is fitted, a source of sound is created by the interaction of one with the other. The conditions in an axial-flow fan with upstream guide vanes will now be described in detail. Extension to other arrangements is difficult.

¹⁴ Ernsthausen, W., The influence of aerodynamic characteristics on the field of sound and the radiation power of an air screw, *Zeitschrift für Luftfahrtforschung*, 1941, p.284.

¹⁵ Billing, H., *Moving Sources of Sound, Modern Flight Acoustics, Monographs, Advances in Flight Research*, Report of Aerodynamic Testing Establishment, Göttingen. See also Natural science and medicine in Germany from 1939 to 1946, *Fiat*, Vol.11, and *Z. angew. Math. Mech.*, 29, p.268.

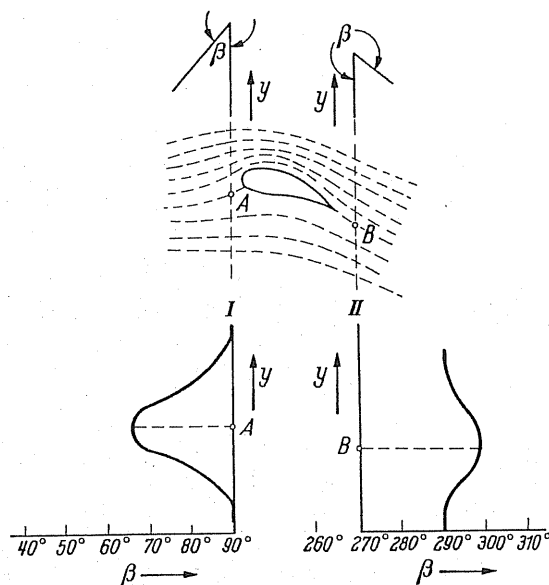


FIG. 518. Flow at leading and trailing edges of the aerofoil in planes I and II.

The field of flow around a simple aerofoil is shown in Fig. 518. We will examine the flow direction at a certain distance from the leading and from the trailing edge of the aerofoil. If we are far removed from both the leading and trailing edges of the aerofoil, the flow direction in the plane perpendicular to that of the initial flow is constant. Close to the aerofoil the direction of the streamlines alter in the direction of y . The flow angle before the aerofoil is $\beta < 90^\circ$ and after the aerofoil $\beta > 270^\circ$. The directions of flow are diagrammatically represented; they represent extreme values.

If we now examine a pure potential flow we find that there is a similar field of flow present at the impeller blades and guide vanes. By moving from one guide vane blade to the other and measuring the direction of flow after the guide vanes, we find that these vary from a maximum value of the deflecting angle β after the blade down to a minimum value between the blades. As the distance from the plane of the guide vane blade trailing edge increases, this fluctuation in angle decreases. This variation has completely disappeared at an infinite distance, i.e. β is constant. The impeller, however, can be arranged at a finite distance after the guide vanes. The alteration of direction of the flow in the plane behind the guide vanes appears in the impeller as a periodic fluctuation of the inlet direction. This leads to alterations in circulation on the aerofoil of the impeller and thus to pressure fluctuations which are audible as noise.

The process has been represented in a very simplified manner. In reality, the impeller also alters the flow on the guide vanes and thus causes fluctuation in pressure to occur at that point. It is very difficult to estimate mathematically the reciprocal effects and the pressure fluctuations thus caused, since the length of the impeller and the guide vane aerofoils cannot be ignored. The angle deviation longitudinal to the aerofoil depth still has to be considered, even if the effects at the trailing edge of the guide vane wheel and at the leading edge of the impeller are the major factors.

The same processes can be assumed to occur in an axial-flow fan with downstream guide vanes or for the reciprocal action of aerofoil design and impeller.

In the centrifugal fan the inlet direction of the tongue fluctuates periodically; it then releases an audible periodic pressure fluctuation.

By means of the observations on the fan without friction it is possible to get some estimate of the inevitable noise of the fan. Research, however, has not advanced so far that results can be discussed.

In the example we have examined a potential flow. Actually a boundary layer forms on the guide blade and on the impeller, and this we find again as a downstream of the aerofoil. The development of the boundary layer on the aerofoil already generates noise. The frequency of this sound is obtained from the Strouhal number

$$S = \frac{fD}{v}, \quad (266)$$

where D is the sectional thickness (m), f is the frequency (c/s), and v is the inlet velocity (m/sec).

The Strouhal number amounts to about 0.21 for Reynolds number $Re = (vD)/\nu$ above 10^3 (references Blenk, Fuchs, Lievers⁽¹⁶⁾). No measurements are yet available regarding the sound level of this interference noise as a function of the velocity. It may be assumed, however, that the contribution to the overall fan noise is slight.

A much greater contribution to the overall noise is due to the influence of the wake (which contains the aerofoil boundary layer) of the impeller.

In a paper by Schlichting⁽¹⁷⁾ we find the sketch shown in Figure 519. Immediately

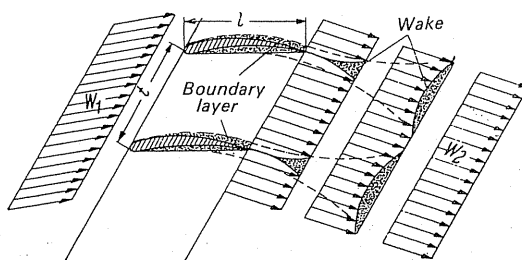


FIG. 519. Flow through a plane cascade of blades (flow with friction) according to Schlichting.

behind the guide-wheel trailing edges the velocity in the wake core is zero owing to the fluid being in contact at the guide vane surface. The flow velocity is undisturbed outside this wake. The aerofoil of the impeller must pass through this wake, and in doing so it suffers considerable fluctuations due to inlet velocity. These flows are modified considerably if the impeller leading edge is moved away from the guide wheel trailing edge. By selecting as distance about 20–30 displacement thicknesses (displacement thickness δ^* is expressed

¹⁶ Blenk, Fuchs, and Lievers, Concerning measurements of vortex frequencies, *Luftfahrtforschung*, 12 (1935) 38–41. See also Schlichting, *Grenzschichttheorie*, 3rd edn., p.29.

¹⁷ Schlichting, H., Application of the boundary layer theory to flow problems of turbo machines, *Siemens-Z.*, 33 (1959) No.7.

by the term⁽¹⁸⁾

$$\delta^* = \int_0^\infty \left(1 - \frac{u}{\bar{u}}\right) dy,$$

where u is the velocity at y in the boundary layer and \bar{u} is the velocity outside the boundary layer).

We are sufficiently far away to enable the velocity in the wake to rise to more than half the mean flow velocity. At the same time, the wake flow has become broader and the fluctuations are less. In the radial-flow fan also it has been found that a distance $>0.05D$ is necessary between tongue and wheel in order to minimise fan noise. If this distance is reduced, a very high increase of noise can certainly be anticipated.

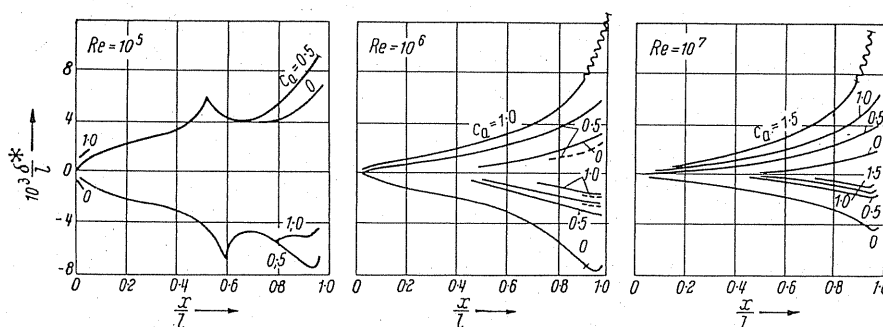


FIG. 520. Curve of boundary layer displacement thickness at NACA, section 64-109, for different Re numbers and Ca values. Transition point at $Re = 10^5$ in the laminar separation point, at $Re = 10^6$ in the laminar separation point (dashed lines) and in minimum pressure (solid lines), at $Re = 10^7$ in the minimum pressure (turbulent separation zone; expressed by wavy lines). $\delta^*/l > 0$ top end. $\delta^*/l < 0$ bottom end. (According to Riegels.⁽¹⁹⁾)

The displacement thicknesses of the suction and pressure side of the guide-wheel aerofoil due to the boundary layer development can be determined, for instance, by the Truckenbrodt⁽²⁰⁾ method. In this connection it is also important to note that the boundary-layer development along with the width of the wake is a quantity dependent on the lift coefficient. Figure 520 is obtained from Riegels.⁽²¹⁾ The displacement thickness of the boundary layer for suction and pressure side is taken as 95% of the aerofoil depth (Fig. 521). It will be seen that the sum which then forms the wake has a minimum value at a lift coefficient $C_A \approx 0.5$. If an axial-flow fan were fitted with this profile and arranged in such a way that it is stressed in all sections, then at this value of C_A it will be the least noisy at that state. At a deviation through altering the throttling rate in both directions, it should become noisier.

Thus we have the basis for the experimental finding of minimum sound level in the zone of the maximum efficiency. We can still estimate the approximate frequency of the wake

¹⁸ See, for example, Schlichting, *Grenzschichttheorie*, Karlsruhe, Braun.

¹⁹ Riegels, F. W., Latest results of the aerofoil profile theory, *Z. f. Flugwiss.*, 1958, Nos. 1 and 2.

²⁰ Truckenbrodt, E., A quadrature method for calculating the laminar and turbulent friction layer at plane and rotation-symmetrical flow, *Ing.-Arch.*, 20 (1952) 221-8.

²¹ See footnote 19, Chapter XXI.

noise. We assume that the wake width B is a multiple value of the sum of the displacement thicknesses of the boundary layer. Thus we have

$$B = m (\delta_D^* + \delta_S^*).$$

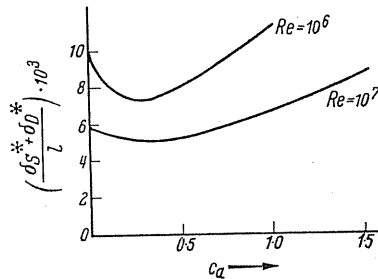


FIG. 521. Sum of the displacement thicknesses of pressure side and suction side at $x/l = 0.95$ for the profile NACA 64-409 (l = depth of profile).

The impeller blade moves at the peripheral speed $(2\pi n r)/60$ if we consider a radius $r < R$. The time during which the impeller leading edge is available in the wake flow of the guide wheel then amounts to

$$t = \frac{B}{u} = \frac{m (\delta_D^* + \delta_S^*) \times 60}{2\pi n r} \quad (\text{sec}),$$

which gives a frequency

$$f = \frac{2\pi n r}{60m (\delta_D^* + \delta_S^*)} \quad (\text{c/s}),$$

where δ^* is the displacement thickness of boundary layer (m), $m = 1$ at the trailing edge of the guide unit, $m > 1$ increases with the distance from the guide unit, r is the radius of point examined at impeller (m), D is the pressure side (index), S is the suction (index), B is the width of wake (m), and n is the speed of impeller (min^{-1}).

Example

$$\frac{\delta_D^* + \delta_S^*}{l} = 6 \times 10^{-3}.$$

$n = 500 \text{ rev/min}$, $m = 15$, $r = 0.5 \text{ m}$, $l = 0.3 \text{ m}$.

$$f = \frac{2\pi \times 500 \times 0.5}{60 \times 15 \times 0.3 \times 6 \times 10^3} = 970 \text{ c/s}.$$

In well-profiled blades, where δ^* is small, the frequency of this sound is higher than at less well-profiled blades. The frequencies which arise are lower at the hub than at the blade tips. As m increases, i.e. as the distance from the guide unit increases, the frequencies become lower.

The boundary layer generated at the impeller blade is dominated by the centrifugal force. The boundary layer therefore will migrate along the blade surface to the larger

radius. This effect from a noise point of view is less disturbing in upstream guide vanes but in downstream guide vanes this might be more disturbing due to the boundary layer growing outwards.

A further source of noise may be found at the blade tips of the impeller. The blade cannot be of such a length that the gap between housing and blade tip is infinitely small. There is a position intermediate between the finite and the infinite aerofoil. The blades have an infinite length when the value of the gap is zero because we then are able to compare then with blades having infinitely large end plates. The end plate is the side wall. For finite blades it is known that there is an induced resistance operating because boundary vortices can be shed from the end of the blade. The thickness of this vortex shedding from the end of the blade is a function of the gap between impeller and housing wall.

Measurements by Marcinowski⁽²²⁾ on freely exhausting axial-flow fans without guide vanes demonstrate a notable increase of the sound pressure in a wide frequency range as the gap between housing and impeller increases. The gap longitudinal to the periphery was constant.

If the gap along the periphery is not constant, the thickness of the discharging vortex alters periodically. The sound level produced thereby depends on the quality of manufacture. Very stringent requirements are laid down for this, because in a fan of 1 m diam. the gap is about 2–3 mm. Any variation in diameter of a housing wall within ± 1 mm creates a considerable variation in the gap. For reasons of cost, smaller tolerances are not likely to be found in fan engineering.

The sizes of vortices on the periphery of the impeller are, furthermore, affected by the boundary layer growth on the housing wall. The boundary layers on the housing wall in a freely aspirating fan are approximately of the order of magnitude of the gap. It fluctuates, however, if the free suction is not amply safeguarded along the periphery. If the blade tips run tangentially for instance along the periphery of the wall, the air flows undisturbed at that point with the thicker boundary layer in the guide and impeller planes. This fluctuation in the boundary layer along the periphery produces periodic fluctuations in the aerodynamic values of the impeller blade especially at the extreme radii of these. Essentially the thickness of the discharging edge vortex and its locality will steadily vary.

Apart from this boundary-layer effect, a unilateral pre-rotation will develop due to walls and floors, and this, as shown by Marcinowski,⁽²³⁾ can give rise to sound generation. These concepts can be transferred partly to the centrifugal fan. The boundary layer on the impeller blade creates inlet-flow fluctuations at the tongue of the spiral housing. In the centrifugal fan, in addition, the air present in the blade passages flows at a lower rate through the tongue and the following part of the spiral housing compared to the speed before the tongue. Due to the delay, periodic separations can arise in the blade passage. As a rule it has been found that centrifugal fans with many blades, i.e. 18–20, run more silently than those with a few blades (5–6). Moreover, in centrifugal fans with a small number of blades, which are, of course, much cheaper to manufacture, there is the danger of resonance with portions of buildings.

²² Marcinowski, H., Effect of impeller gap in freely exhausting axial-flow fans without guide vanes, *Voith-Forschung u. Konstruktion*, 1958, No.3.

²³ Marcinowski, H., Single-stage turbo-compressor, *Chemie-Ingenieur-Technik*, 1959, No.4.

In the centrifugal fan the gap between impeller and housing is a source of noise, but it cannot be designed to be free of fluctuation if manufacturing costs have to be kept within reasonable limits.

The boundary-layer thickness of the inlet air at free suction depends on its accompanying limitations. One gets the impression, however, that the centrifugal fan is rather less sensitive to such influences than the axial-flow fan.

Badly designed protective screens at the fan intake may be the sources of unpleasant noises.

157. DERIVATION OF A REFERENCE QUANTITY FOR THE SOUND POWER

The former discussion has shown that the sound level of a fan is a function of the peripheral speed, the delivery volume, the pressure, and the efficiency. The most important influence for a given fan is the peripheral speed. The potential at which it enters, however, is a function of the design of the fan. In order to compare fans of different types for their sound power, a reference quantity is desirable which will indicate immediately what can be expected for the sound level.

In a paper by Grünewald⁽²⁴⁾ an effort has been made to find a characteristic quantity of this kind by means of a dimensional analysis. Like the author formerly, he started up from relating the sound intensity to the delivery of the fan and develops

$$\frac{I D^2}{\Delta p V}.$$

The author suggested a relationship of

$$\frac{I D^2}{\Delta p V [(1/\eta) - 1]},$$

i.e. to the power loss of the fan and not to the effective power. It can be concluded from Grünewald that combinations of dimensionless values may also be formed. For instance, he multiplies with a dimensionless pressure $\Delta p / (\rho c^2)$, (where c is the velocity of sound and ρ the air density) and so obtains the expression

$$\frac{I D^2}{\Delta p V} \frac{\rho c^2}{\Delta p} = \frac{I_0 c^2 D^2}{\Delta p^2 V}.$$

Since with $\Delta p^2 \sim u^4$ and $V \sim u$ repeatedly the fifth power is found for the expression $\Delta p^2 V$.

We do not wish to follow this idea since experiments have shown that the fifth power is not universally valid.

²⁴ Grünewald, W., Proposal for a uniform noise measurement on fans, *Heizung-Lüftung-Haustechnik*, 1959, No. 10.

In order to satisfy various power laws it would have to be stated, for instance, that this expression

$$\frac{I D^2}{\Delta p V} \frac{\rho c^2}{\Delta p} \frac{\rho c^2}{\Delta p} = \frac{I D^2 \rho^2 c^4}{\Delta p^3 V}$$

must also be valid with $\Delta p^3 V \sim u^7$. By this method every power can be satisfied without having to conclude that, for instance, $\Delta p^3 V$ is a really characteristic reference quantity.

Riollet⁽²⁵⁾ suggests for the reference quantity the expression

$$\rho a^3 R^2,$$

where ρ is the air density, a is the speed of sound, and R is the impeller radius. This expression has no relationship to the aerodynamic characteristics of the fan.

Let us take the expression

$$\Delta p V \left(\frac{1}{\eta} - 1 \right) = \varphi \psi \left(\frac{1}{\eta} - 1 \right) \frac{\rho}{2} u^3 F = \varphi \psi \left(\frac{1}{\eta} - 1 \right) \frac{\rho}{2} u^3 D^2 \frac{\pi}{4} \quad (267)$$

$$F = D^2 \pi/4$$

as the reference quantity. If we relate the overall radiated sound power to a spherical surface it is useful to select a multiple of the impeller surface. The sound power emitted per unit surface will then be

$$I_r = K_1 \varphi \psi \left(\frac{1}{\eta} - 1 \right) \frac{\rho}{2} u^3,$$

where K_1 includes the numerical factors for surface conversion. In order to be able to take the influence of the peripheral speed into account, we extend the power of u by the term n and obtain the expression

$$I_r = K_2 \varphi \psi \left(\frac{1}{\eta} - 1 \right) \frac{\rho}{2} u^{3+n}.$$

The K_2 has the dimension of $(\text{sec/m})^n$.

Still relating to the sound power per unit surface area at the stimulus threshold level of the human ear I_R , this gives

$$\frac{I_r}{I_R} = K \varphi \psi \left(\frac{1}{\eta} - 1 \right) \frac{\rho}{2} u^{3+n},$$

and K has the dimension $(\text{sec}^{n+1}/\text{kg m}^{n-1})$. In this expression all constants are included. The sound intensity level in dB by the usual method works out at

$$L = 10 \log K \varphi \psi \left(\frac{1}{\eta} - 1 \right) \frac{\rho}{2} u^{3+n}. \quad (268)$$

²⁵ Riollet, G., The laws of sound emission of a fan shown by a dimensional analysis, *Ninth International Congress of Applied Mechanics, Brussels, Part II*.

The power is $n = 1.5-4$. It is much more important than the factor K . Both factors have to be determined by measurement for a given fan. If K fluctuates by a factor 2, this means that the sound level varies by 3 dB.

Since the dimensionless accuracy of sound level measuring devices is within ± 1 dB, K cannot be determined more accurately than in the ratio 1:1.26.

A definite measuring method should be agreed upon. Work by Zeller⁽²⁶⁾ and Grünewald⁽²⁷⁾ contain very useful hints.

The above choice of relative quantity is similar to the representation chosen by Lighthill⁽²⁸⁾ for air jets of subsonic velocity. According to Lighthill the radiated sound power of a jet is

$$N = K_s \rho_0 A V^3 \left(\frac{V}{a_0} \right)^5 = K_s \rho_0 A \frac{V^{3+n}}{a_0^n}, \quad (269)$$

where N is the radiated sound power, K_s is the constant of sound radiation of an air jet, ρ_0 is the air density of the medium surrounding the jet, A is the cross-sectional area of nozzle, V is the mean discharge velocity of jet, and a_0 is the sound velocity of medium surrounding the jet.

In the jet the power amounts to $n = 5$ which was derived mathematically by Lighthill.⁽²⁹⁾ From a lecture by Dryden⁽³⁰⁾ we obtained Fig. 522 which shows the sound power radiated from air jets as a function of Lighthill's factor. Factor K_s is calculated as a constant from Fig. 522 at: $K_s = 0.22 \cdot 10^{-4}$.

In fans other numerical values are obtained.

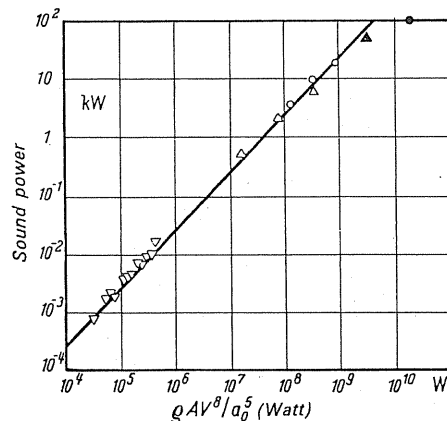


FIG. 522. Sound power of a jet engine according to Dryden. ○ Drive gear 10,000 lb thrust. ● Similar to ○, after combustion. △ Drive gear 5000 lb thrust. ▲ Similar to △, after combustion. ▽ Air jets with 3-5 in. diameters.

²⁶ Zeller, W., Concerning mathematical treatments of noise behaviour in fans for comfort and ventilating installation, *VDI-Berichte*, 1959, No. 38.

²⁷ Grünewald, W., Suggestion for a uniform noise measurement on fans, *Heizung-Lüftung-Haustechnik*, 1959, No. 10.

²⁸ Lighthill, M.I., On sound generated aerodynamically, I: General theory, *Proc. Roy. Soc. London*, **211** (1952).

²⁹ See previous footnote.

³⁰ Dryden, H.C., Present-day problems in flight research, *Z. f. Flugwiss.*, 1958, No. 8.

CHAPTER XXII

SOUND INSULATION OF FANS AND AIR-HANDLING INSTALLATIONS

(By E. GOEHLICH, Dipl.-Ing., Dortmund)

158. BASIC CONCEPTS

Frequency f is the number of oscillations per second denoted as c/s. Sound propagates in gases in longitudinal waves.

Sound velocity a is the velocity with which a sound travels:

$$a = \sqrt{\kappa p / \rho}. \quad (270)$$

For the atmospheric pressures we have the expression

$$a_{\text{air}} = 331.8 \sqrt{\frac{T}{T_0}} \text{ m/sec} \quad (271)$$

(approximations: $a_{\text{air}} = 330 + 0.5 t$ m/sec).

NUMERICAL VALUES OF VELOCITY OF SOUND

Medium	Temperature (°C)	Velocity of sound (m/sec)
Air	20	343.8
Water	4	1399
Aluminium	18	5104
Iron	18	5124
Glass		5191
Pine wood		4179
Concrete		1700

The relation between frequency f and wavelength λ is derived from the formula

$$f\lambda = a. \quad (272)$$

The range limit for the human ear is 16,000–20,000 (c/s) (upper limit for the age group 40–50 years drops to approximately 16,000 c/s).

WAVELENGTH IN AIR FOR DIFFERENT FREQUENCIES AT 20°C

f (c/s)	20	100	500	1000	10,000
λ (m)	17.2	3.438	0.688	0.3438	0.03438

Sound pressure. The dynamic pressure fluctuations arising in a sound process give rise to sound pressure.

Units:

$$\mu\text{bar} = 1 \cdot 10^{-6} \text{ b} \approx \frac{1}{100} \text{ mm WG}$$

$$(1 \text{ bar} \approx 1 \text{ kg/cm}^2 = 10,000 \text{ mm WG}).$$

Lowest audible sound pressure (called *stimulus threshold*) at 1000 c/s:

$$p = 2 \times 10^{-4} \mu\text{bar} \approx 2 \times 10^{-6} \text{ mm WG}.$$

(Comparison: pressure fluctuation in Brownian motion, which our ear is no longer able to hear, is $10^{-5} \mu\text{bar}$.)

Sound power. The power J in W/cm^2 flowing through 1 cm^2 perpendicular to the direction of propagation is designated as sound intensity.

$$J = pv \quad (v \text{ is the sound velocity in m/sec}).$$

This gives the following formulae:

$$p = vZ.$$

$$Z = \rho a \quad (Z \text{ is the sound wave impedance analogous to electrical resistance}).$$

$$J = p^2/z = v^2 z.$$

$$J_1/J_2 = (p_1/p_2)^2.$$

The sound intensity in the audibility threshold $J_0 = 10^{-16} \text{ W/cm}^2$.

Example

Sound pressure of $200 \mu\text{bar}$ corresponds to a sound intensity of $J = 10^{-4} \text{ W/cm}^2$, i.e. for a surface of 10 m^2 a transmitted sound power of $N = 10^{-4} \times 10^5 = 10 \text{ W}$ is obtained.

Range of audibility threshold to threshold of feeling $P_0/P_{\text{feeling}} = 1/10^6$; $J_0/J_{\text{feeling}} = 1/10^{12}$.

159. LOGARITHMIC RATIO NUMBER. SOUND LEVEL

Based on the large range indicated previously, the comparison of variable sound pressures or sound intensities give rise to high numerical ratios, which cannot be controlled. In order to arrive at reasonable values in such cases the decibel (dB) has been introduced in electronics as a useful scale. The common logarithm of ratio of sound intensity is calculated and this ratio multiplied by 10 in order to arrive at the final figures. Since two sound intensities behave like the squares of the corresponding sound pressures, the equation can also be written as

$$L = 10 \log \frac{J_2}{J_1} = 10 \log \frac{p_2^2}{p_1^2} = 20 \log \frac{p_2}{p_1} \quad (\text{dB}). \quad (273)$$

In this case we have a dimensionless quantity which only expresses the ratio of two sound intensities or sound pressures.

By introducing the reference sound intensity $J_0 = 1 \times 10^{-16} \text{ W/cm}^2$ and the reference sound pressure $p_0 = 2 \times 10^{-4} \text{ } \mu\text{bar}$ at 1000 c/s at the audibility threshold, according to

$$L = 10 \log \frac{J}{J_0} = 20 \log \frac{p}{p_0} \quad (\text{dB}) \quad (274)$$

it is possible to obtain absolute values of the sound intensity or of the sound pressure. These values in decibel are called sound levels.

Sound levels occurring in practice range between $L = 0 \text{ dB}$ corresponding to the sound intensity at the audibility threshold at 1000 c/s and approximately $L = 130 \text{ dB}$. In the whole frequency range in this case, the threshold of feeling has already been exceeded. Higher sound levels are no longer found to be louder but only increase the sensation of pain. The highest theoretical sound intensity which can be imagined corresponding to a pressure fluctuation between absolute vacuum and double atmospheric pressure is $L = 194 \text{ dB}$ which no longer is physically possible with a pure sinusoidal type of tone.⁽¹⁾

The sound intensity. With the characteristics stated for the field of sound these are purely physical quantities which can be measured with suitable instruments. It is usual to measure the wide band sound level in decibels as the overall sound level over the whole audibility range or to measure the sound level in separate frequency band. Investigations have shown that there is a more complicated association between measured sound levels of variable frequency and human subjective sensitivity.

In the range of small and medium sound levels between 0 and 60 dB, for instance, a 100 c/s tone at 50 dB appears as loud as a 1000 c/s tone of 20 dB.

At sound levels above 80 dB the subjective sound intensity difference between a deep tone and a high tone of the same sound level is only slight.

From tests carried out on a large number of people between the age groups 18 and 25 with normal hearing, curves of equivalent sound intensity were plotted for pure tones.

In this case a tone with the normal frequency of 1000 c/s was transmitted alternately with a tone of the frequency to be assessed. The 1000 c/s tone was varied in intensity until it became as loud as the tone to be assessed. The sound level of the tone was measured in dB and the measuring point supplied entered into a system of coordinates. By connecting up by means of a curve the tones of variable frequencies found to be of equal loudness, curves of equivalent sound intensity are produced and are called phon curves. They are given the numerical value which was measured in dB at the appropriate standard frequency of 1000 c/s. The value of the sound intensity in phon and the value of the sound level in dB at a frequency of 1000 c/s always have the same numerical value. These curves of equivalent sound intensity have been drawn by Fletcher and Munson and are shown in Fig. 523. Investigations by Robinson and Dadson produced the curves as shown in Fig. 524.

The lowest curve designated 0 phon represents the stimulus threshold at this level. A person with normal hearing receives the very minimum audibility pressure here. The

¹ Bürck, W., *Die Schallmeßfibel für die Lärmbekämpfung*, published by Rhode & Schwarz, Mindelheim Sachon, 1955.

topmost curve with 120 phon represents the threshold of pain. Higher sound levels only become negligibly louder but are more painful.

These results were obtained in tests with pure tones. They can only be roughly approximated to sound processes, where several or a very large number of tones are present at the same time.

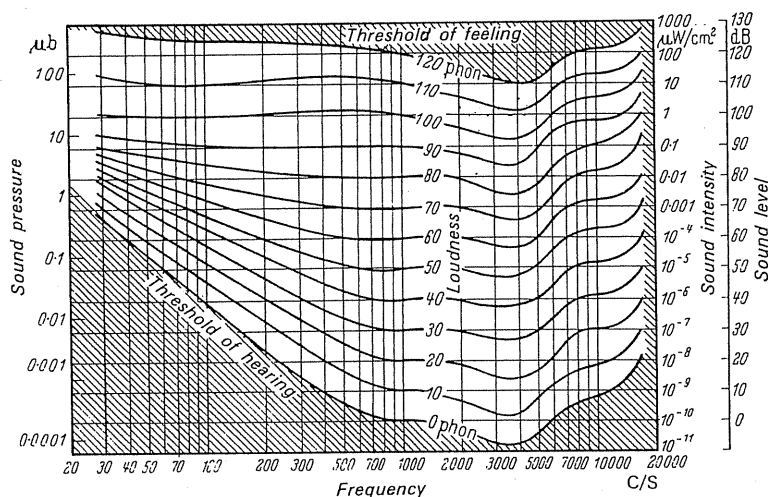


FIG. 523. Curves of equal loudness for pure tones (phon curves) according to Fletcher and Munson.

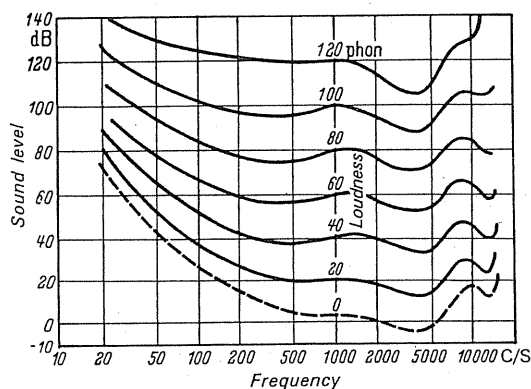


FIG. 524. Curves of equal loudness for pure tones (phon curves) according to Robinson and Dadson.

DIN-phon value. For direct measurement of sound intensity there must be a network of filters connected to the amplifier of the measuring instrument. The outputs from the filters are plotted as curves of equal loudness, and hence the sensitivity curves of the human ear. In order to obtain in this case a practical arrangement the curves of equal loudness have been simplified diagrammatically. To this end in the DIN standard 5045, a curve was fixed for the range between 0 and 30 dB (curve 3), a further curve somewhat flatter for the range between 30 and 60 dB (curve 2) and a still flatter curve for the range 60–130 dB (curve 1). Measurements made with instruments of this kind are designated as DIN-phon.

International assessment according to A, B, C. In the United States a similar chart of curves of equivalent sound intensity as in Germany according to DIN 5045 was laid down in the ASA Z 24.3 Standards. A frequency curve for the range from 20 to 55 dB designated *A*, a curve for the range 55–85 dB designated *B*, and a curve over 85 dB with a linear frequency path designated *C* were laid down as a standard.

The corresponding measured values are listed as dB *A*, dB *B*, and dB *C*.

In the ISO recommendations the curves according to DIN standard 5045 and the ASA curves *ABC* are compared together. The DIN curve 3 range 0–30 dB is cancelled. The ASA curve *A* is altered corresponding to the DIN curve 2 range 30–60 dB, the ASA curve *B* altered to suit the DIN curve 1 range 60–130 dB. The ASA curve *C* is given a very curved path at very low and very high frequencies in order to keep out inaudible signals from the infra and supersonic range.

Loudness. Considerable difficulties occur in the addition of variable sound intensities according to the frequency composition of the noises.

Two individual tones of equal loudness and equal frequency each of 70 phon, for example, produce together 73 phon (and not approximately 140 phon). Two equally loud noises with equivalent noise spectrum of 70 phon each for example are measured at about 73 overall sound intensity. If the two noises are of a considerably variable frequency composition, the overall sound intensity up to 10 phon can be at a higher level than that of the two sources of sound⁽²⁾ of equivalent loudness.

Investigations have shown that an increase of about 10 phon corresponds to a doubling of the subjective sensitivity.

Fletcher in the United States derived a loudness function which indicates the association between phon values and the values of loudness which goes by the name of “son”.

This function is shown in Fig. 525.

Forty phon was given the value 1 arbitrarily.

Fifty phon (i.e. twice as loud) take the value 2 son and therefore an addition of the son values corresponds to a subjectively accurate increase of the loudness sensitivity. In

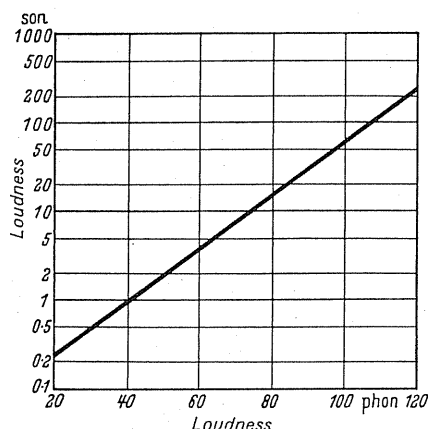


FIG. 525. Relationship between loudness in phon and the loudness in son (according to Geigy).

² Furrer, W., Noise and noise-protection, from the series “Man and Environment”, Vol. 3, *Documenta Geigy*, Basle, J.R. Geigy, 1958.

measured wide band noises the addition of the son values is only justified if the noises possess a considerably varying frequency composition; at equivalent frequency composition the resultant phon value is mostly considerably lower.

These differences are based on the fact that in sound intensity measurements the masking effect of the human ear is not taken into consideration in respect of the neighbouring frequencies; wide band noises produce a value which is too high.

In order to obtain more accurate results, various methods have been worked out by which the frequency spectrum of the noise can be divided up into bands. The individual bands are measured in phon and the son values determined accordingly, the son values are then added and the resultant phon value found by applying the function in Fig. 525.

This method, however, has not yet been adopted in Germany.

Frequency analysis. Efforts have been made to distinguish the subjective effect of a sound process with a single measured quantity. The DIN phon value, the international evaluation *ABC*, and the loudness value son are quantities of this kind.

From the previous section it will be realised that these quantities do not lead to satisfactory results in sound processes of variable frequency composition.

A much clearer picture of a sound phenomenon is shown in the plot of its spectrum.

By this is understood the plotting of the sound level in dB as a function of the frequency. The frequency band to be investigated which is mostly the overall audible range from 50 to 16,000 c/s is measured in stages by means of an electrical reversible filter which only allows a narrow frequency band through and cuts off the other ranges. Here filters having a pass band width of an octave or the pass band width of a third octave, also called tierce are used. The individual ranges have the same relative bandwidth in common. There are filters where the ranges are continuous or overlap. Moreover, it is possible to measure the sound level of individual tones with the aid of an analyser which has a particularly narrow bandwidth. The measured values are plotted on a system of coordinates in which the ordinates for the sound level in dB have a linear scale and the abscissae for the frequency have a logarithmic scale.

A frequency analysis using a tierce filter gives a clearer picture of a sound phenomenon than a frequency analysis with an octave filter. However, it is time-consuming and expensive on instrumentation when plotting tierce analysis than when plotting an octave band analysis.

160. DAMAGE THROUGH NOISE

Noise deafness can arise through exposure to intense noise. This deafness is recognised as an industrial disease subject to compensation in the metalwork industry, the textile industry, and on test rigs. Impact noises can lead to mechanical damage to the eardrum and thus to deafness.

According to the latest knowledge, based particularly on the work by Prof. Dr. med. G. Lehmann, Max-Planck Institute for Industrial Physiology, Dortmund, the whole organism is affected by noise. In this connection it does not matter whether the person in question feels distressed by noise or not. Noise brings about disturbances of various organs of the

body through the autonomic nerve system which can lead to cardiac and circulatory illness and to stomach and bowel disorders.

According to the investigations by Prof. Lehmann a reduction in the heart-stroke volume and variations in the ECG occur between 65–90 DIN phon. Long-term effects include neurotic effects followed by organic damage. Moreover, with continuous noise, the capacity to think and concentrate, together with vigilance, are adversely affected, and therefore efficiency deteriorates markedly. The level of noise which can be described as endurable depends on the type of the work to be carried out.

In very great noise, moreover, signals or warning signals may fail to be heard, and this may lead to accidents.

Different authorities have endeavoured to issue regulations and criteria curves about the permissible level of noise.

161. NOISE ABATEMENT REGULATIONS, CRITERIA CURVES

Recommendation for maximum loudness in workrooms:

Offices and similar premises: max. 65 DIN-phon

Workshops max. 90 DIN-phon but where possible not above 85 DIN-phon.

In work which requires a moderate amount of concentration such as ordinary office work, typewriting, 60–70 DIN-phon. For work which requires no special concentration, for instance on standard work machines, 80–85 DIN-phon is allowed.

Recommendations for maximum permissible sound intensities have been worked out by the Abatement Technical Committee on Vibration of the Verein Deutscher Ingenieure and have been published in the VDI Regulations, VDI 2058 July 1960, *Assessing and Combatting Industrial Noise*.

EFFECT OF NOISE ON HUMAN BEINGS

Stage	Sound intensities (DIN-phon)	Effects
0	0–30	None
1	30–65	A person, due to psychological defensive attitude, might regard a certain noise as a burden. Therefore the noise at this stage is a purely psychological problem
2	65–90	Nervous stress, independent of the personal attitude of the person to noise. Reduction of heartstroke volume and variation in the electrocardiograph may in the long run lead to neurotic, and, as a result of this, to organic damage, e.g. stomach ulcers
3	90–120	Permanent damage to hearing. Recession of temporary deafness at a duration of action of 2 h, only takes effect after about 2 days, therefore testing for permanent deafness can only be carried out after a long period of rest
4	above 120	Damage to the body by injury and disturbances to the central nerve system which may be fatal in extreme cases

1. Workshops

In work demanding continuous intensive concentration	50 DIN-phon
For office and similar work	70 DIN-phon
For work	90 DIN-phon

Above these levels noise protecting devices should be worn.

2. Dwellings according to DIN 4109, sound insulation (in blocks of flats).

By day	7-22 hours	45 DIN-phon
By night	22- 7 hours	30 DIN-phon

3. Effect of industrial noise on the neighbourhood. On outside walls of houses

	Purely industrial zones	Mixed zones	Purely residential zones
By day (7-22 h)	65 DIN-phon	60 DIN-phon	50 DIN phon
By night (22-7 h)	50 DIN-phon	45 DIN-phon	35 DIN-phon

The difference from 2 and 3 between the phon values must be obtained by corresponding insulation of dwellings.

The values stated refer to continuous noise. Peaks of brief duration may have higher value than the levels.

Criteria values without any indication of the permissible frequency distribution of the disturbance noise will not meet increased demands.

Curves of equal loudness, criteria curves. Experience has shown that sound with a preponderance of low-frequency components is less annoying than sound of the same intensity which is composed mainly of high frequencies. This effect of sounds with high-frequency components does not depend only on the fact that they seem to be louder but on the fact that the subject consciously or unconsciously can locate the direction from which the sound is coming due to the shorter wavelength of the high-frequency vibrations. At low frequencies the wavelength is very much greater than the distance between the two ears of a human subject. A directional effect therefore does not arise.

Individual tones are considered as much more disturbing than a wide band noise of the same overall sound level. The sensory nerve appropriate to this tone is stimulated by the individual tone according to its sound energy, whereas with wide-band noise the sound energy is distributed over many sensory nerves, each of them being affected by a lower sound energy.

Various investigators have attempted to establish curves of equal loudness with fairly satisfactory results.⁽³⁾

³ Lübke, E., Noise measurement, *Frequenz*, 12 (1958), No. 7.

L. Cremer and E. Lubke have suggested curves which at a slope of 3 dB per octave band lead to high frequencies. In the system of coordinates described previously, these curves are shown in Fig. 526. They are designated by the Bel value which they possess at the standard frequency of 1000 c/s and are called noise rating curves. The criteria curve 10, for instance, is a curve which connects the three points 100 c/s—110 dB, 1000 c/s—100 dB, 10,000 c/s—90 dB. These curves can be introduced in the coordinate system very easily; furthermore, the frequency analysis to be assessed is also entered in the coordinate system and a clear assessment can be made by how many dB and in what frequency range of the curve of the frequency analysis a criteria curve is excessive or deficient.

By introducing these criteria curves considerably more details can be given about an existing or noise level target to be aimed at than by other methods which do not take into account the frequency distribution.

The criteria curve 9 wherever possible should not be exceeded by a curve of a tierce analysis at 1 m distance from a large machine. The criteria curve 9 corresponds approximately to the boundary values found by F. J. Meister, Med. Akademie, Düsseldorf, where the damage to hearing arises at continuous exposures. In exceeding the criteria curve 8, the person who is subject to these noises is expected to be adversely affected psychologically. Therefore the request is made to many machine operators that the machine noise should not exceed the criteria curve 8.^(4,5)

The following table lists the effects at a number of criteria curves.

Criteria curve in Bel	Damage brought about by daily work	
	8 h	1 h
10	100% damage certainly occurs	25%
9	Approximately 50%	Very slight
8	0%	0%

When observing a frequency analysis of wide band noise with an octave band filter, value increases by 4.8 dB are measured compared to tests with a one-third octave band filter, since a greater proportion of energy is allocated to the energy portion corresponding to the greater band width of the octave band filter. Therefore when making tests with octave filters, based on the same scale, values greater by 5 dB are obtained than when using a frequency analysis carried out with a tierce filter.

The criteria curve 9 or 8 when carrying out tests with a tierce filter would correspond to the criteria curve 9.5 or 8.5 when carrying out tests with an octave band filter.

Where, however, frequency spectra with individual tones have the higher values than the overall level are concerned, there is no difference between a tierce or an octave band analysis in regard to height of the maximum sound levels.

The criteria curves by L. Cremer and E. Lubke have been successfully used for the

⁴ Köhler, R., The state of noise abatement in mining, *Glückauf!*, (1960), No. 13, pp. 785, 793.

⁵ Köhler, R., Combating industrial noise with due regard to the noise spectrum, *Stahl u. Eisen*, 79 (1959), No. 1, pp. 37-41.

evaluation of industrial noise in particular in the mining region of the Ruhr and in the Ruhr steelworks.

Criteria curves were also drawn up in the United States which have a slightly curved course and which are rated by their dB value at 1000 c/s. Internationally accepted criteria curves are shown in Fig. 526.

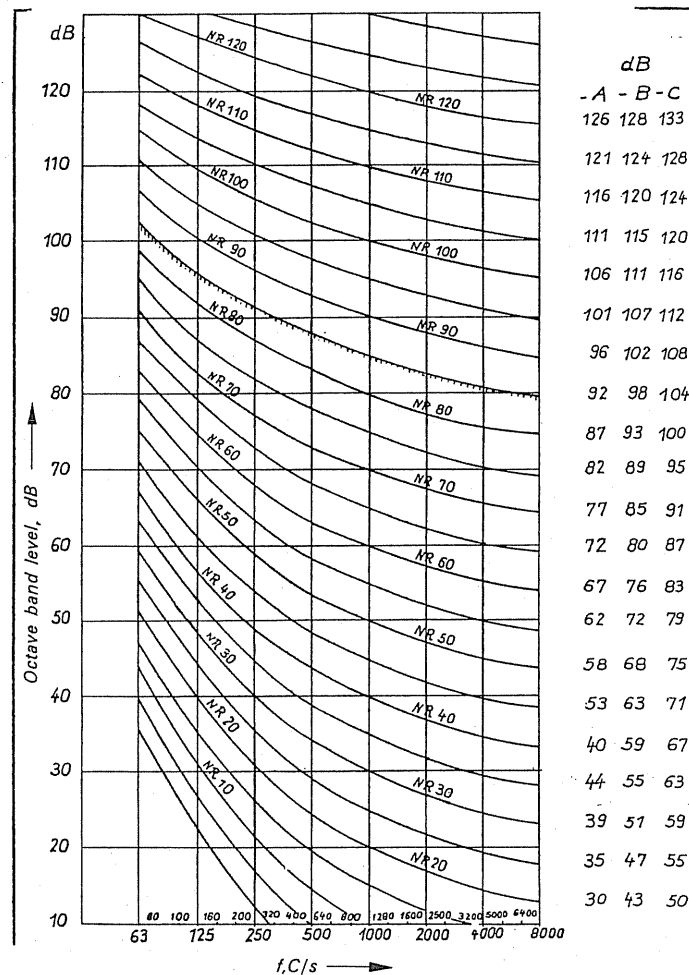


FIG. 526. Noise rating curves. Overall values of noise rating curves in dB for A, B, and C scales.

Criteria for ventilation plants. According to the VDI ventilation rules, DIN 1946, the following sound intensities are laid down as the upper limits of the noises caused by a ventilating plant:

Radio and broadcasting studios	20 DIN-phon
Concert halls, theatres, cinemas with high requirements	25 DIN-phon
Audition rooms, meeting halls, cinemas where demands are low	30 DIN-phon
Public halls	35 DIN-phon
Hotels	40 DIN-phon; 45–50 DIN-phon

Rules for sound absorption in ventilation plants were issued by Dr. Ing. Walter Kuhl of the Radio Institute, Nuremberg.⁽⁶⁾ These criteria curves are shown in Fig. 527.

It may be assumed that the different committees are also working out recommendations in the form of criteria curves for other fields where continuous very annoying tones would have to be specially evaluated.

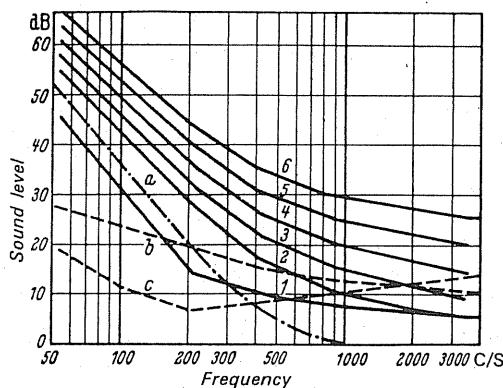


FIG. 527. Criteria curves by Kuhl for maximum permissible sound level per octave at continuous noises as, for instance, in ventilation plants. *a*, audibility threshold; *b*, noise from condenser microphones M 59/M 60; *c*, noise (mains hum) dynamic microphone D.20; 1, broadcasting studios, control rooms; 2, sound absorption spaces; 3, concert halls, theatre; 4, churches, lecture halls, etc.; 5, cinemas, small offices; 6, large offices, restaurants, etc.

162. A FEW THEORETICAL BASIC PRINCIPLES

The law of addition. The overall sound intensity of a number of sources of sound available simultaneously can be calculated by adding the sound intensity of the individual sources of sound.

$$J_T = J_1 + J_2 + J_3 + \dots \quad (275)$$

The overall sound level can be expressed, moreover, by taking into account the fact that two sound intensities behave like the square of the appropriate sound pressures.

$$L_T = 10 \log \frac{J_1 + J_2 + J_3 \dots}{J_0} = 10 \log \left(\frac{\sqrt{p_1^2 + p_2^2 + p_3^2 + \dots}}{p_0} \right)^2 \quad (\text{dB}) \quad (276)$$

$$J_0 = 1 \times 10^{-16} \text{ (W/cm}^2\text{)}, \quad p_0 = 2 \times 10^{-4} \text{ (}\mu\text{bar)}.$$

If two equally loud sound levels are added an increase of 3 dB is obtained corresponding to doubling the sound power. When adding several sound sources of variable loudness, the loudest of them always decides the issue.

⁶ Kuhl, W., Rules for sound absorption of ventilation plants, Internal memorandum of the Radio Institute, Nuremberg.

Propagation of sound. A spherical wave with unobstructed propagation of sound corresponding to the decrease of its energy density diminishes by 6 dB on doubling the distance from the source of sound.

Where an earth floor is present for all practical cases a decrease by 5 dB can be roughly estimated when the distance from the source of sound is doubled. Obstructions which are small compared with the wavelengths which are not too close together and have no absorption, have practically no effect on sound. If the obstructions are large compared with the wavelength, the sound is reflected or deflected by them. The propagation of sound is highly dependent on wind and weather. The source of sound is heard much better in the direction of wind than against the wind. This, however, is not at all connected with the fact that the sound is damped by opposing wind. In almost all practical cases the velocity of propagation of sound is much greater than the wind velocity. Moreover, in opposition to the wind, sound is deviated upwards whereas in the direction of the wind it is deviated downwards to the ground.⁽⁷⁾ Rain and fog have a damping effect on sound since the high frequencies are more highly absorbed than the low and medium frequencies. High frequencies, even in clear weather, are damped more strongly by the absorption of the air than low and medium frequencies.

Layers of air, layers of vapour, or clouds, act like a reflector. A number of cases are known where the fan noises in induced-draught installations issuing from high brickwork chimneys were reflected by air and cloud layers and could be heard very clearly several miles away and acted as interference.

The reduction of sound intensity with increasing distance acts in the case of sound intensities above 70 DIN-phon and medium frequencies in a similar way as the reduction of the sound level. Low frequencies of low sound intensities diminish more quickly at increasing distance, but equal sound intensities corresponding to the curves (Fig. 524) damp out considerably more rapidly than their appropriate sound level.

Figure 528 was plotted⁽⁸⁾ on the basis of measurements by the Berggewerkschaftskasse in Bochum relating to the reduction of generated noises from mine fans as a function of the distance. Here a reduction by approximately 7 DIN-phon was found when the distance was doubled, since mostly low frequencies of small and medium sound intensity were concerned.

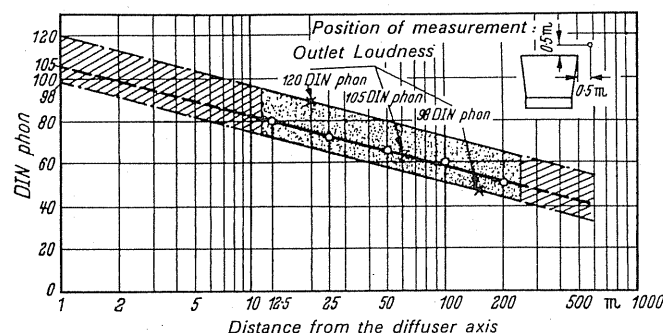


FIG. 528. Mean loudness as a function of a distance from mine fans.

⁷ Zeller, W., *Technische Lärmabwehr*, Stuttgart, Kroner, 1950.

⁸ Schubert, E., Noises from mine fans of axial and centrifugal type, *VDI-Berichte*, 1959, No. 35.

163. DIRECT AND REVERBERANT SOUND FIELDS

If a source of sound is introduced into a closed space a certain amount of time goes by until a constant sound level is produced in the space. During this stationary state the sound power absorbed by surrounding walls or passed through them is equal to that of the sound power released by the sound source if the absorption by air is ignored. This process is known as direct sound field.

It is clear that after cutting out the sound source the sound does not suddenly disappear but the sound energy stored in the space gradually decays. This process again is known as the reverberant sound field. For physiological reasons the reverberation comes into evidence more strongly than the direct sound and therefore is better known.⁽⁹⁾

The first investigations on reverberation processes were carried out by static methods by Sabine who also has indicated the relationships which he found empirically and which today are still used in calculation. He also defined the reverberation time as the time required for the sound energy density to decay to 60 dB (i.e. to 10^{-6} of its original value). According to Sabine's theory the direct and the reverberant sound field are represented by exponential curves. With a recorder which plots the sound level logarithmically, the reverberation process is illustrated by means of a straight line, and its slope gives the reverberation time. It is obvious that the reverberation time is longer for the large volume of the space and is shorter when surrounding walls of the space absorb or transmit the sound. By increasing the absorption of the surrounding walls, the time can also be reduced. In this way, even in the stationary state, in the space a lower sound energy density results, i.e. with reduction of the reverberation time the sound level in the space diminishes.

$$T = \frac{0.163V}{A_T} \quad (\text{sec}) \quad (277)$$

$$A_T = A_1 + A_2 + A_3 + \dots = \alpha_1 F_1 + \alpha_2 F_2 + \dots$$

$$A = \alpha F \quad (\text{m}^2)$$

$$\alpha = \frac{\text{sound power absorbed or filtered through}}{\text{incident sound power}} \quad (278)$$

Reduction of sound level at decrease of reverberation time

$$\Delta L = 10 \log \frac{T_1}{T_2} = 10 \log \frac{A_{T2}}{A_{T1}} \quad (\text{dB}), \quad (279)$$

where T is the reverberation time (sec), V is the space volume (m^3), A_T is the absorption capacity of space (m^2), α is the sound absorption coefficient, and F sound absorbing areas (m^2).

The same sound level is always measured independent of the room reverberation in direct proximity to a constant source of sound surrounded by sound absorbing walls a good distance away. However, at some distance from the source of sound the level measured depends essentially on the reverberation field of the space.

⁹ Furrer, W., *Raum- und Bauakustik für Architekten*, Basle/Stuttgart, Birkhäuser, 1956.

Special attention should be paid to this phenomenon when erecting machines which generate a lot of noise.

Later investigations of energy and wave theories were improved and show that during reverberation the decay does not follow the frequency of forced oscillations at the stationary state, but it follows the natural frequencies of the space.⁽¹⁰⁾ These variable reverberation processes superimpose on one another and therefore it is no longer a question of individual reverberation times. Moreover, the tests show that the Sabine relationship for heavily damped spaces no longer applies, because the reverberation time would then become zero, which obviously it does not according to the previous formula. For a rough assessment within the framework of noise abatement problems the Sabine relationships will suffice.

164. SOUND INSULATION ELEMENTS

The single wall. By assuming the single wall to be an inert mass we find that at constant surface weight the higher frequencies are damped more than the low frequencies. Figure 529 shows this relationship. R. Berger was the first to carry out tests on this problem, and therefore this law is also called the Berger law of masses.

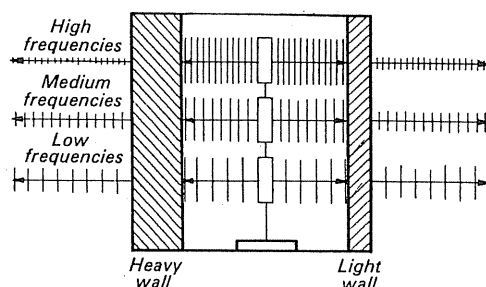


FIG. 529. Damping by heavy and light wall at various frequencies.

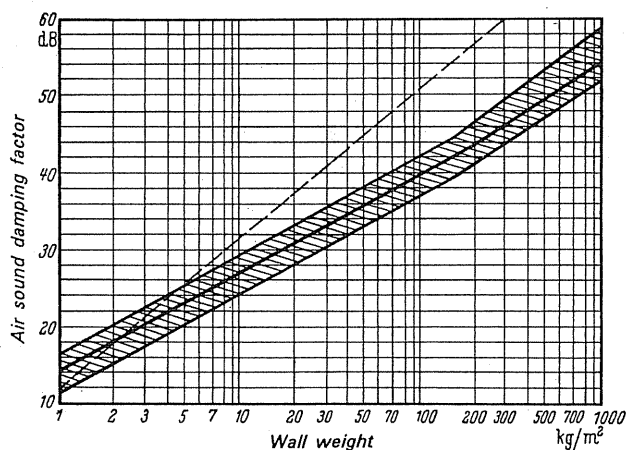


FIG. 530. Air sound damping factor as a function of the weight of the wall.

¹⁰ Cremer, L., *Die wissenschaftlichen Grundlagen der Raumakustik*, Vol. III, *Wellentheoretische Raumakustik*, Leipzig, S. Hirzel, 1950.

In practice, however, tests have shown that the insulation is not so good as might be expected from the simple law of masses. For a large number of walls measured by Schoch on a logarithmic frequency scale, insulation between 100–3000 c/s was plotted and the planimetric mean values were taken from this frequency curve. These values were plotted in the new system of coordinates as a function of the area weight. Figure 530 shows this relationship. The values were called mean sound absorption coefficients and apply approximately at a frequency of 550 c/s. In the same graph the mean sound absorption coefficient is plotted in dashed lines according to the simple theory of masses.

Taking 550 c/s as a basis, an amount of 4–5 dB can be respectively added or deducted when the basis frequency is doubled or halved.

According to L. Cremer the curve shown in Fig. 530 can be substituted in the first approximation by a straight line which is represented by the simple formula.

$$R = 14 \times \lg G + 14 \text{ (dB)},$$

where R is the mean sound absorption coefficient (dB) and G is the weight of wall (kg/m^2).

When a sound wave impinges on a wall at a slope the wall is excited into its own natural frequency in bending. In the wall the velocity of propagation of the bending wave is dependent on frequency. Low frequencies travel slower than high frequencies. Investigations by L. Cremer have shown that the mass reactance and the stiffness reactance of a wall are equal when the exciting wave velocity is in phase with the velocity of the bending wave.

This causes a change in the absorption effect. At a given frequency this effect is a function of the angle of the incident wave. Incident velocity is understood as the velocity at which the incident wavelength when projected on the wall gives the bending wavelength. This effect is called wave coincidence or coincidence effect.

On this basis a critical frequency can be defined above which changes in the nature of insulation may be expected, through the wave coincidence effect. At about one octave above the critical frequency the insulation rate starts to rise again, heavy rigid walls have a low critical frequency, light flexible walls have a high critical frequency.

This fact explains why heavy rigid walls should always insulate above their critical frequency and therefore do not achieve the insulation according to the law of masses whereas light flexible walls insulate below their critical frequency and their insulation effect therefore corresponds to the law of masses. There is a special risk attached to walls with an area weight of 30–100 kg/m^2 , since in this case the critical frequency lies in the most interesting frequency range between 300 and 3000 c/s.⁽¹¹⁾ In order to achieve the highest possible sound insulation in the frequency range between 100 and 3000 c/s, heavy walls with an area weight above 100 kg/m^2 should be stiffened as much as possible in order to reduce their critical frequency well below 100 c/s. Light walls with an area weight below 30 kg/m^2 should be as flexible as possible to raise their critical frequency above 3000 c/s.

The double wall. It is well known that by arranging two walls one behind the other a higher absorption effect is achieved at the same area weight than with a single heavy wall of the equivalent weight. Moreover, the absorption effect of an existing heavy single wall can

¹¹ Eichler, F., *Sound in Multi-storey Buildings*, Berlin, Verlag Technik, 1952.

be improved by erecting a panel in front of it. A few rules have to be followed for correct sizing. A light panel erected in front of a heavy wall is then to be considered as a mass and the intermediate space between these two walls filled with air to be treated as a spring. According to a rule of thumb a resonance frequency for the sound wave incident at right angle is obtained by the formula

$$f_{\text{res}} = \frac{600}{\sqrt{Gd}} \quad (\text{c/s}), \quad (280)$$

where G is the area weight of the light wall (kg/m^2) and d is the distance between the two walls (cm).

For a double wall made of two panels which are of equal weight, the formula applies as follows:

$$f_{\text{res}} = \frac{850}{\sqrt{Gd}} \quad (\text{c/s})$$

where G is the area weight on a wall (kg/m^2) and d the distance between the two walls (cm).

If the two walls have a variable area weight but if one of the walls is not heavier by a multiple than the other wall, the resonance frequency can be calculated according to formula

$$f_{\text{res}} = 600 \sqrt{\frac{G_1 G_2}{G_1 + G_2}} d \quad (\text{c/s}), \quad (281)$$

where G_1 , G_2 are the area weights of each (kg/m^2) and d the distance between the two walls (cm).

At this resonance frequency the absorption of the double wall is changed. By appropriate selection of the area weight and of the distance, this resonance frequency is reduced to the lowest possible frequencies. Basing on a resonance frequency of 75 c/s and applying a rough formula for a double wall consisting of two heavy panels of equal weight, the minimum distance between walls can be calculated by the formula

$$d_{\text{min}} = \frac{140}{G} \quad (\text{cm}), \quad (282)$$

where G is the area weight of one wall (kg/m^2).

For a double wall consisting of one very heavy panel with a light panel in front of it, we obtain

$$d_{\text{min}} = \frac{70}{G_1} \quad (\text{cm}), \quad (283)$$

where G_1 is the area weight of the light wall (kg/m^2).

For a light wall consisting of two panels, the area weight and the elasticity of the two panels should differ so that both panels obtain a variable critical frequency of the wave coincidence effect. Figure 531 is a chart of the absorption effect where a sound wave impinges obliquely on a single wall, for a double wall made up of two identical panels and for a double wall made up of two different panels.

The air space between the two panels should be insulated by inserting fibre matting. When erecting a double panel wall it is not essential to separate the sub-structure of the two panels completely. It is, however, important that securing to the sub-structure is not carried out by rigid clamps to enable the free bending waves to develop. The sub-structure

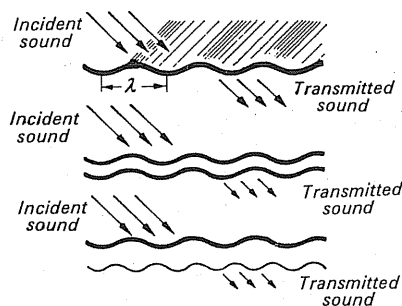


FIG. 531. Diagram of the damping of oblique sound waves by a light single and double wall showing refraction of sound waves according to Eichler.

itself should be of the heaviest possible material. The success of double walls depends quite a lot on the care taken in erection and the special attention which is paid to having perfectly sealed connections between the individual wall elements and at the surrounding walls.

The mean sound absorption coefficient of a double wall can be calculated roughly by the formula:

Mean sound absorption coefficient at overall area weight of both panels according to Fig. 530 + 10 to 15 dB.

The sound absorption coefficient of an existing single wall with bad absorption can be improved up to 20 dB by fitting a flexible panel. This additional panel should be fitted at the wall side of the space to be insulated, since the elastic panel has a smaller reflecting effect than the existing rigid wall.

Sound transmission through small openings. In large openings the ratio of incident sound power to the transmitted power is proportional to the ratio of the corresponding areas. The appropriate absorption is defined by

$$D = 10 \lg \frac{J_1}{J_2} = 10 \lg \frac{F_1}{F_2} \quad (\text{dB}) \quad (F_2 < F_1), \quad (284)$$

where J_1 is the incident sound intensity impinging on F_1 and J_2 is the sound intensity transmitted through F_2 .

At small openings this geometrical method of observation no longer applies, since more sound power passes through small holes than would be expected according to the area ratios.

For small round holes using a derivation by L. Cremer we obtained the formula

$$D = 10 \lg \frac{J_1}{J_2} = 10 \lg \frac{F_1}{4F_2} \quad (\text{dB}) \quad (F_2 \ll F_1), \quad (285)$$

where J_1 is the sound intensity incident on F_1 and J_2 is the sound intensity transmitted through F_2 . In this case, therefore, the effective acoustic aperture is four times as large as the geometrical one.

The same applies also for narrow slots or cracks which should be avoided. When building sound-absorbing division walls, sound-absorbing doors or windows, special attention must be paid to absolute tightness. For sound-absorbing doors with a high power of absorption even a keyhole can affect the absorption adversely. The material, used for sound-absorbing walls or doors, should not be porous since on this account the absorption effect drops considerably. On the other hand, for thick walls hair-cracks are less dangerous than is generally assumed, since the sound energy on passing through this very narrow slot is absorbed by friction.

165. SOUND ABSORPTION

If a sound wave impinges on a wall, part of the incident sound power is transmitted through or absorbed by the wall and the rest is reflected. Accordingly, the sound absorption coefficient α can be defined as

$$\alpha = \frac{J_2}{J_1}, \quad (286)$$

where J_1 is the incident sound intensity and J_2 is the absorbed or transmitted sound intensity. At total reflection the sound absorption rate = 0, at total absorption = 1.

In the same way as in electronics, the definition of a wall impedance is

$$W = \frac{p}{v}, \quad (287)$$

where p is the sound pressure and v is the sound velocity. Wall impedance is considered complex in general since the sound pressure reaches the wall before the velocity.

Furthermore, the wall resistance is a function of frequency and a function of the incidence angle of the impinging sound wave. The sound absorption coefficient α is at its highest when the wall impedance W is equal to the sound wave impedance Z of the air. This phenomenon is called matching because, due to the coincidence of the two impedances, the overall incident sound power is absorbed by the wall.

The magnitude of the wall impedance is a function of the angle of the incident sound wave, and therefore the attenuation of sound also varies with the angle of incidence. Attenuation is not always at its highest when the angle of incidence is perpendicular. There are cases when corresponding to the incident angle the wall impedance is approximately equivalent to the sound wave resistance of the air, i.e. when good matching prevails. There is, therefore, an optimum angle of incidence. The sound attenuation decreases very considerably when this optimum angle is exceeded. At a grazing incidence its value amounts to 0.

Sound absorption by porous materials. When a sound wave impinges on a very thick porous layer, the major portion of the sound energy penetrates and is converted into heat by friction, and a very small portion is reflected by the surface of the layer. The absorbed portion of the energy increases with porosity of the layer (porosity is understood as the ratio of the voids volume to total volume) and the smaller the flow resistance of the layer. Flow resistance is understood as the pressure difference through a porous layer divided by the flow velocity.

Every finite porous layer is bounded by a rigid wall from which the sound energy which has transmitted into the layer is reflected and returns to the outside. To avoid this, the flow resistance of the layer should be as large as possible. In practice, there must be a compromise which essentially depends on the thickness of layer chosen. With a thick layer a small flow resistance can be selected in order to achieve good matching and also adequate absorption on the inside. In a thin layer the flow resistance should be larger, but then the matching becomes worse.

In representing a complex wall resistance of a porous layer, the layer thickness is associated with the frequency and the wavelength of the sound. To achieve good absorption the layer should be thicker in order to suit the lower absorbing frequency. Furthermore, a "structural factor" must be taken into consideration which not only takes into account pores running parallel to the direction of the propagation of sound in practical sound-absorbing materials, but also those running at a slope and transversely to the direction of propagation of sound. A detailed elaboration of this complex theory which has been described fully by Cremer⁽¹²⁾ is outside the scope of this work.

In sound-absorbing materials used in practice there are no great fluctuations in porosity. The ratio of voids to volume lies between 0.6 and 1. The flow resistance, however, is of the order of 0.1. Furthermore, the total flow resistance is always a function of the thickness of the layer. It is obvious from this that the correct choice of the layer thickness and the flow resistance is the criterion for the best possible attenuation of a given frequency.

A sound absorption rate of about unity when the frequency to be damped is achieved by a layer thickness equal to $\lambda/4$. The flow resistance should in this case amount to about $2Z$, where Z is the wave impedance of air. From this frequency onwards the sound absorption rate oscillates between 0.9 and 1. At equivalent flow resistance and a layer thickness of $\lambda/16$ the absorption rate amounts to approximately 0.5 and for a layer thickness of $\lambda/8$ the absorption rate is approximately 0.75.

The greater the density of a sound-absorbing material the higher is its flow resistance. Amongst various fibrous materials used as sound absorbers, a density ranging from 30 to 120 kg/m³ according to layer thickness is used.

The frequency response of the sound absorption rate of a porous layer can be considerably affected by arrangement of sound-absorbing material having variable flow resistance in layers. Pressed-fibre boards are also used which, moreover, act as resonators in the absorption of low frequencies. Very thin dense foil can also be laid in front of the absorbent layer. Due to their very low masses the foils are acoustically transparent to sound of low frequencies. Due to their low mass they form a resonator with the air enclosed behind acting as a spring in medium frequencies. For higher frequencies they are, however, no longer

¹² Cremer, L., see footnote 10 on p. 512.

acoustically transparent and the absorption rate diminishes. When building anechoic chambers, where a sound-absorption rate is called for down to very low frequencies, all surrounding walls are lined with very thick wedge-shaped fibrous material of a specified flow resistance. The wedge-shaped arrangement gives very good acoustic matching and, owing to the flow resistance, a high absorption of sound energy which has penetrated. The overall layer is increasingly thicker if the very low frequencies are to be damped.

The porous layers should be protected against damage by covering them with a solid acoustically transparent sheet. For this purpose perforated panels of wood, plastic, plaster, or steel can be used. In all panels the acoustic transparency diminishes as the frequency increases, but for a perforated panel there is a limiting frequency at

$$f_T = \frac{3500e}{d^2} \quad (\text{c/s}), \quad (288)$$

where e is the diameter of perforation (cm) and d is the number of holes per unit length (cm).

In this limiting frequency approximately 90 % of the incident sound power passes through the panel, i.e. the sound absorption coefficient is 0.9. The formula applies to perforated panels up to approximately 5 mm thick.

Sound absorption through resonating surfaces. In the section referring to double walls we gave for the resonance frequency of a first layer in front of a rigid wall the formula

$$f_{\text{res}} = \frac{600}{\sqrt{Gd}} \quad (\text{c/s}), \quad (289)$$

where G is the area weight (kg/m^2) and d is the distance between the two walls (cm).

A first layer oscillating in its resonant frequency acts as a sound-absorbing surface for this frequency. By suspending a fibre mat in the intermediate space the frequency range of the absorption is extended. In rooms with plywood covered surfaces, hard fibre or plaster boards are used for absorption of low frequencies and the boards are arranged at a slight slope with a variable distance in front of the rigid wall and thus a wide frequency band is covered. If a plate is excited in its natural bending frequencies it abstracts energy from the incident sound and acts as an absorbent surface for this frequency, with the highest absorption occurring at the lowest natural bending oscillation. For a firmly secured homogeneous panel with a constant thickness the lowest natural frequency is given by

$$f = 1.03 \frac{d}{e^2} c \quad (\text{c/s}),$$

where d is the panel thickness (cm), e is the panel width (cm), and $c = \sqrt{E/\rho}$ is the sound velocity of the material used (cm/sec).

Sound absorption, by resonators. Figure 532 is a sketch of an air resonator. The air in the whole of the panel acts as a mass and the air behind as a spring. The resonance frequency works out at

$$f_{\text{res}} = \frac{a}{2\pi} \sqrt{\frac{F}{Ve(e + 2\Delta e)}} \quad (\text{c/s}), \quad (290)$$

where a is the sound velocity (cm/sec), F is the area of panel (cm²), V is the air volume (cm³), e is the panel thickness (cm), and $2\Delta e$ is the correction coefficient.

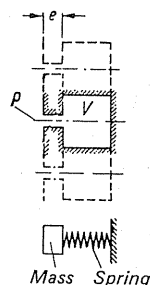


FIG. 532. Helmholtz resonator.

If the resonator is loaded with sound energy of a frequency which is equal to its natural frequency, the air volume in phase oscillates with this frequency in the whole of the panel and extracts the energy from the incident sound. Figure 533 shows a diagram of a perforated resonator and its resonance frequency is given by

$$f_{\text{res}} = \frac{a}{2\pi} \sqrt{\frac{F_2}{F_1} \frac{1}{(e + 2\Delta e)b}} \quad (291)$$

$$2\Delta e = \frac{\pi r}{2},$$

where r is the perforated radius (cm), a is the sound velocity (cm/sec), F_1 and F_2 are the areas corresponding to Fig. 533 (cm²), e is the panel thickness (cm), and b is the distance of the panel from the rigid wall (cm).

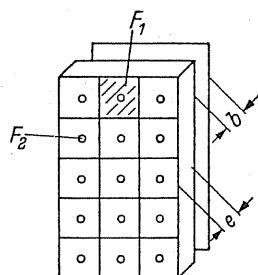


FIG. 533. Perforated Helmholtz resonator.

The sound-absorption rate equals 1 at the resonance frequency. Close to the resonance frequency it is also still considerable but diminishes considerably at both ends as the frequency moves further away from the resonance frequency. By suitable choice of panel thickness e and the distance b , the width of the absorption curve can be varied. Furthermore, the width of the absorption curve can be increased by fitting a fibre panel before or after the perforated panel.

Sound absorption in pipes and ducts. Fan noises are conducted through supply and discharge ducts connected to the fans and transmitted in a manner similar to a speaking tube. The same applies to suction and blow-off piping of all kinds.

If the absorption of the walls of the ducts is inadequate the sound energy is radiated from the walls of the duct or radiates at the open ends of the duct. Therefore silencers are required which should be inserted as tightly as possible behind the sources of noise in the duct walls in order to eliminate radiation of noise in the duct walls. If there is not inconvenience or the duct walls are sufficiently sound absorbent, the silencers can also be placed at the ends of the ducts.

When selecting suitable silencers, aspects of flow must be taken into consideration along with acoustical requirements. The free cross-section in the silencers is essentially governed by these factors.

Absorption silencer. The absorption silencer in its simplest form consists of a duct, the walls of which are lined on the inside with a porous sound absorbent layer. Piening obtained an empirical formula for silencers which was later confirmed and improved by L. Cremer as a result of theoretical investigations:

$$D = 1.5 \frac{U}{F} L \alpha \quad (\text{dB}) \quad (\text{Piening}), \quad (292)$$

$$D = 1.1 \frac{U}{F} L \left(\alpha + \frac{\alpha^2}{2} \right) \quad (\text{dB}) \quad (\text{Cremer}), \quad (293)$$

where U is the extent of sound absorbent lining (m), F is the free cross-sectional area (m^2), L is the length of damping path (m), and α is the sound absorption coefficient.

For a high-sound absorption coefficient both formulae give practically the same damping value. For low-sound absorption coefficients the formula by Piening gives a damping value somewhat too high. As shown by the formulae, the absorption rises with increasing ratio U/F . For this reason the free cross-sectional area desired is constructed in the form of one or several narrow ducts. Sound absorption in a round pipe is least efficient because in this form the ratio of circumference to area is at its lowest. The thickness of the sound absorbent layer is governed by the lowest frequency to be absorbed. If a limited length of silencing path is available for a specified sound absorption, the sound absorption coefficient should be as close as possible to one at the lowest frequency to be absorbed. The layer thickness as shown above must be approximately equal to $\lambda/4$. If a greater length is available for the silencing path the layer thickness may also be thinner. This gives a smaller sound absorption coefficient for the lowest frequency to be absorbed. To achieve the same absorption as before the absorption path must then be longer.

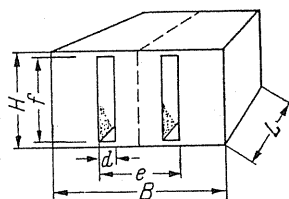


FIG. 534. Silencer for a ventilating plant.

Figure 534 shows an absorption silencer with a free cross-section made up of two narrow sound-absorbing ducts used mainly for air conditioning and ventilation plant.

To save space, the sound absorbent layers have variable layer thicknesses at both ends of the ducts. For absorbing the low frequencies only one end is lined with a thick layer.

Figure 535 shows an absorption silencer circular in shape which is often fitted to round ducts: The diameter of the actual silencer element is somewhat greater than that of the

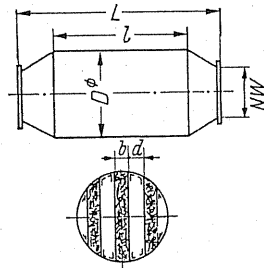


FIG. 535. Silencer for fitting into a pressure ducting of Messrs. Oskar Gerber.

existing duct, since by fitting the sound-absorbent splitters which divide the free cross-section into narrow silenced channels there is a loss in cross-sectional area. Due to the wide frequency band of the sound absorption coefficient, absorption silencers have a very wide bandwidth right up to very high frequencies. Here the absorption decreases again because the perforated panels covering the porous layers lose their acoustic transparency or the wavelengths of the high frequencies are short compared to the duct widths. Hence the waves sweep through the ducts without contacting the sound absorbent surfaces. Therefore for adequate absorption of high frequencies the duct width should be as small as possible or the ducts should be constructed at an angle as shown in Fig. 536 for a suction silencer.

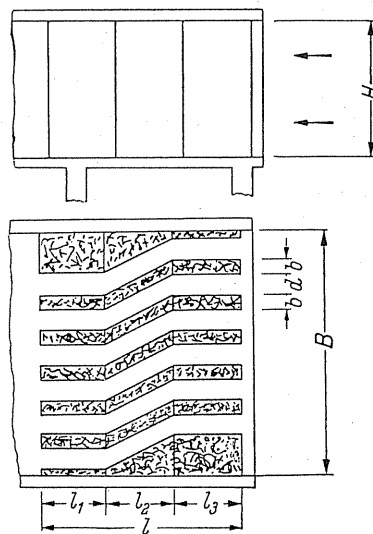


FIG. 536. Coulisse muffler for suction silencer at high frequencies made by Messrs. Oskar Gerber.

For improving the absorption silencer at low frequencies Professor L. Cremer studied the theory, and the experimental tests for this were conducted by Dipl. Ing. O. Gerber, Stuttgart.⁽¹³⁾ The aim was to find the wall resistance of a narrow duct at which maximum absorption occurs. Very complicated theoretical considerations and calculations led to the course of the complex wall resistance which provides maximum absorption at all frequencies. Theoretically, absorptions of 380 dB can be obtained for a silencing path 1 m long and a channel width of 10 cm for low frequencies. The absorption would still be 300 dB at 1000 c/s. Experiments were made to obtain these wall resistances. Unfortunately, this was not possible for a wide band but only for a narrow frequency range. In the channel width and length mentioned before, an absorption of 200 dB was measured at 500 c/s. The sound absorbent layer thickness for obtaining the wall impedance must lie between $\lambda/4$ and $\lambda/5$ to suit the channel width. The layer must consist of very loose sound-absorbent substances, and for eliminating the longitudinal spread of sound energy, transverse walls must be arranged on the inside of the layer at a distance of a few centimetres only. In this way we arrive practically at $\lambda/4$ long duct sections filled with absorbent materials which can be connected up laterally to the ducts to be silenced.

By varying the layer thicknesses by using a somewhat closer packing than called for in theory, the frequency range of the absorption can be enlarged even if the absolute limit of absorption is considerably increased thereby. This method of absorption offers advantages mainly for absorbing narrower frequency bands below 500 c/s provided that ample space is available for layer thicknesses of $\lambda/4$.

The advantages of the absorption silencer are as follows:

- (i) wide band absorption;
- (ii) raising of specified frequency ranges by corresponding build up of sound absorbent layers;
- (iii) possibility of larger cross-sectional area and smaller pressure losses; and
- (iv) simpler and safer assembly.

For these reasons this attenuation principle is used increasingly for designing silencers for industrial installations. The silencers can be made of suitable sheet material such as wood, cement, and asbestos, and plastic or steel sheeting, to suit the purpose. For practical reasons the silencers of today are mainly fabricated from steel sheeting.

166. THE RESONANCE SILENCER

It is built up like the absorption silencer except that the absorbent layer is replaced by a perforated or a slotted resonator as shown in Fig. 533. Mainly narrow frequency bands of low frequency are absorbed by this silencer. Compared to the standard absorption silencer, the advantage is that the layer thickness is thinner than in the absorption silencer of otherwise similar arrangement and equal absorption. Basing on the corresponding absorption coefficients, the same absorption formula as those for the simple absorption silencer apply.

¹³ Gerber, O., Improved silencing and its application in blow-off and ventilation ducts, *Konstruktion*, 5 (1953), No. 2, pp. 363-8.

167. REFLECTION SILENCER

If the cross-sections are constricted successively in a duct, the air volumes in the constrictions act as masses and the intermediate volumes between the constrictions act as springs. Taking the geometrical dimensions as a basis, a limiting frequency can be calculated up to which the frequencies can be allowed to pass through, but above which they are damped out. This arrangement therefore represents a low-pass filter such as is known in electronics. Corresponding to the analogy between acoustics and electricity, the same formula can be used for calculating acoustical low-pass filters. These silencers are therefore called reflection silencers because above the limiting frequency there is such a large mis-matching of the acoustic wall impedance that the incident sound wave is reflected at this point. The absorption diminishes at high frequencies because the geometrical dimensions of the silencer are no longer small in proportion to the wavelength and the air volumes no longer act as masses and springs. The reflection silencer is suitable mainly for absorbing low frequencies below 500 c/s on fitting into thinner ducts. It is used particularly for absorbing exhaust noises from combustion engines.

168. INTERFERENCE SILENCERS

If an existing duct is provided with a bypass duct, the length of which differs from the existing duct there is sound absorption for all frequencies for which the difference in the run of the two ducts equals $\lambda/2$ and multiples thereof. The diameters of the duct should also be equal and must be small compared with the wavelength of the frequency to be absorbed. The interference occurs only at a specified frequency and its multiples. Therefore the principle may only be applied for absorbing available constant individual tones. Since the bypass duct can be varied in length (similar to the tube of a trumpet), the optimum absorption can be accurately set for a specified frequency.

169. NOISE ABSORPTION

Sheet metals possess a low natural absorption. Therefore when the vibrational energy is supplied to them by propagation of sound, only a small proportion of the energy is converted into heat during the process. The major portion is transferred to the surrounding air by radiation or removed by the sound structures. Radiation is very great, particularly if the sheet is excited within the range of its bending natural frequencies. By mounting sound absorbing media on the sheets, absorption is increased considerably and consequently its radiation capacity reduced. Comprehensive tests have shown that the lagging material apart from a high absorption coefficient should also possess a high degree of stiffness—in other words, a high modulus of elasticity. The sound-absorbing media can be sprayed on to the sheets and thick layers can be obtained. According to the sound-absorbing material used and the absorption required, the thickness of the layer should be between 0.5 and 1.5 times

the thickness of the sheet. When coating with sound-absorbing media thinner panels are best and very effective.

For thicker sheets from 3 to 4 mm thickness the layers to be deposited become too thick and therefore are uneconomic.

The weight of a given surface area of the steel sheets is only negligibly increased by depositing sound-absorbing media and therefore the air silencing by the sheets is not improved.

170. SOUND-ABSORBING HOOD

If the surface of a machine-housing radiates disturbing noise, the machine should be placed under a silencing hood for absorbing the noise.

The walls of the silencing hood should be of heavy but flexible plating; they can be of single sheets or double sheets according to the required absorption. When using steel sheets for external wall casing these should be treated for sound absorption or, better still, provided with a heavy and flexible layer in order to get a higher weight per unit area and therefore a greater absorption. The internal space must be lined completely with high-grade sound-absorbing material, and the choice of the sound-absorbing lining should be governed by the frequencies. If the sound-absorbing lining were to be dispensed with, the sound level inside the hood would rise owing to reverberation, and thus the effectiveness of the hood would be reduced.

Frequently the hood has to be ventilated to discharge heat and the ventilation must be provided through sound-absorbing ducts which are arranged in the walls of the hood, or separate inlet and discharge silencers must be provided. Corrugated passages or other moving parts should be connected through the sound-absorbing ducts. Observation windows, flaps, or doors may be fitted. For high sound absorption, however, tight sealing is essential in the mounting. The hood should rest on the floor on a rubber pad which gives a satisfactory insulation, and at the same time it isolates the vibrations existing in the floor.

171. SOUND-ABSORBING LAGGING OF PIPES AND DUCTS

The sound-absorbing lagging of pipes and ducts is assembled in a manner similar to normal heat insulation and is frequently combined with this. Acoustically it consists of one or two very heavy, but very flexible compact outside shells which are arranged at an appropriate distance in front of the noise radiating wall. The distance is governed by the frequency range to be absorbed so as to avoid interference due to resonance on the basis of eqns. (280)–(283). The intermediate space between the noise radiating wall and the outside shells is filled up with a fibre matting. For damping low frequencies the single-shell lining is preferred in which the outside lining can be of fairly heavy construction. The distance from the noise-radiating wall should be taken fairly large (approximately 8–10 cm). For absorbing distressingly high frequencies the double lining construction should be used. The individual linings are easier to construct and the distances to the noise-radiating wall and to each other can be shorter.

For practical purposes the piping is lagged by a fibre mat on to which the hard casing is attached. In the double-lining construction another fibre mat is mounted on to hard casing and this is attached to the second hard casing. The external covering may be of steel, with the outside lining being composed of semi-sheet steel linings. The heavy hard layer is attached directly on to steel casing. It is important that the outside linings have no structural connection with the noise-radiating walls, and they are supported by noise insulators. Similar noise damping casings can be developed also for noise radiating machine housing or mountings.

172. SOUND-ABSORBING ROOM LINING

In machine shops generally there is no sound-absorbing material. The floor and a part of the side walls are tiled or consist of various non-absorbing materials. Therefore these rooms have a long reverberation time, and the noise of the machines installed inside is very disturbing. By lining the ceiling and a portion of the side walls with a sound-absorbing layer, the reverberation time can be shortened and in this way the mean sound level reduced. In direct proximity to the noise-radiating machines this reduction is hardly noticeable since here the directly radiated sound level predominates. The reduction associated with it has been found to be very desirable at some distance from the source of noise.

Sound-absorbing wall insulation can be carried out in many different ways according to the frequency range to be absorbed. A selection can be made amongst the manifold acoustic panels which are on the market. Certain frequency ranges are readily absorbed by fitting very thick perforated sheets with small holes, and sound attenuation is augmented owing to the resonator effect. A lining acting on a wide band for medium and high frequencies consists of a fibre mat 3–4 cm thick which is mounted in a frame. The external acoustically transparent covering is effected by means of a perforated plate. Movable lightweight division walls can be fitted around machines which are highly noise radiating, and the walls can be insulated in the direction of the source of noise.

173. FLEXIBLE MOUNTING OF MACHINES

When machines are rigidly mounted, the out-of-balance forces and the structural vibrations are transmitted through the supporting area straight to the foundation which, together with the boundary walls, are made to vibrate. For reducing this transmission the machine acting as a mass is placed on a flexible support. In this way a mass with the natural frequency f_0 (also called fundamental frequency) is produced. If the frequency of the out-of-balance force P_e is below the fundamental frequency f_0 (in the sub-critical range), the forces P_f transmitted by the spring are equal to the out-of-balance force transmitted to the foundation when the structure is rigid. If the frequency at which the out-of-balance force is acting, however, lies above the fundamental frequency (in the supercritical range), the forces P_f transmitted by the springs are considerably less than the out-of-balance force. If the driving frequency of the out-of-balance force is quite close to the fundamental frequency, considerably higher

forces than the out-of-balance force are transmitted by the springs to the foundation. The machine is then operating in resonance, a situation which should be avoided at all costs. This relation, which is obtained from the solution of the differential equation for forced vibration,⁽¹⁴⁾ is illustrated in Fig. 537. The frequency ratio $A = f/f_0 = \omega/\omega_0$ ($\omega = 2\pi f$ = angular frequency) is plotted as the abscissa. Insulating efficiency without considering absorption D can be defined as

$$\eta = \frac{A^2 - 2}{A^2 - 1} \times 100 \quad (\%) \quad (294)$$

which indicates by the proportion the out-of-balance force which does not act on the foundation. The frequency range of the efficiency is also shown in Fig. 537. It will be

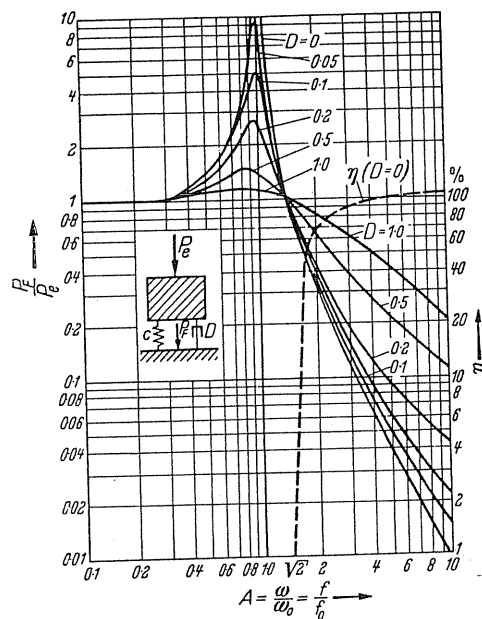


FIG. 537. Power ratio P_e/P as a function of frequencies ratio f/f_0 taking damping into account.⁽¹⁵⁾

observed that the efficiency increases as the difference between the operating and fundamental frequency increases. Efficiencies of more than 90% can be achieved immediately, and therefore only a small proportion of the out-of-balance force is transmitted through the springs to the foundation. The frequency ratio A should be selected approximately at 4. This gives an insulating efficiency of approximately 94%. The curves for additional absorption are plotted in Fig. 537. It will be appreciated from this that through the absorption the storage effect is diminished. When the frequency is above resonance, transmitted forces are reduced. This process, however, occurs so quickly in all relevant cases that no amplification arises. In purely rotating machines, therefore, additional silencing can be dispensed with. In shock-excited machines silencing, however, is beneficial.

¹⁴ Lürenbaum, K., Contribution to dynamics of flexible machine foundations, *VDI-Z*, 98 (1956), No. 18, pp. 976-80.

¹⁵ *VDI-Berichte*, 8 (1956) 82-85.

From the dynamic point of view a flexibly mounted machine becomes free-floating in the room well above the fundamental frequency. It is then excited to forced vibration for floating on the springs only due to out-of-balance forces. The amplitude thus arising can be calculated by the formula

$$a_f = \frac{P_e 25 A^2}{G f^2 (A^2 - 1)} \quad (\text{cm}), \quad (295)$$

where a_f is the amplitude (cm), f is the forced frequency (c/s), A is the frequency ratio f/f_0 , P_e is the out-of-balance force (kg), f_0 is the natural frequency (c/s), and G is the total weight (kg). From this it is obvious that at constant operating conditions the amplitude can only be reduced by increasing the total weight. An increase of the frequency ratio has only a very small effect.

At constant frequency ratio the efficiency of the flexible mounting is unaffected by increasing the total weight.

The above analysis must be applied to all six degrees of freedom. In very many cases, however, the exact calculation will have to be carried out only for vibrations in a vertical direction, the vibration amplitudes being assessed in the remaining degrees of freedom.

When machines have a flexible mounting for absorbing the out-of-balance forces, vibrations in solids are isolated and will not be transmitted back to the machine.

Flexible mounting of fans. Well-balanced fans should also be flexibly mounted if they are to be erected on a concrete base. In fans which are subject to heavy wear or where foreign particles could adhere to rotating parts, flexible mounting is indispensable. It has the further advantage that by observing the vibration amplitude it is possible to control the increase in the out-of-balance forces.

In slow running or very heavy fans, spiral isolating steel springs are arranged below the base frame symmetrical to the centre of gravity. For high-speed fans rubber-bonded metal plates have proved excellent.

Fans where considerable out-of-balance forces may be anticipated are placed on elastically mounted concrete blocks or their base frame is grouted in with concrete.

It is not necessary to secure the spring-mounted insulators or rubber-bonded metal plates on to the foundation, and it is quite in order to provide the bearing surfaces with a ribbed rubber plate or similar device, since no dynamic forces are transmitted by the springs.

174. ISOLATION OF FAN VIBRATION

Well-balanced fans with low out-of-balance forces, where no vibration excitation may be feared, frequently have to be mounted with vibration isolation in order to attenuate sounds generated by the drive, bearing friction, rotation, or other factors. For this purpose the best appliances are mountings made of rubber, cork, or felt or even composite flexible products with high internal absorption which are laid below the resting surfaces of the fans in the form of plates. Figure 538 shows the range of frequency of the damping vibration for various

elastic materials at longitudinal excitation and the loads used in practice.⁽¹⁶⁾ Even with composite mountings the absorption effect only starts above the fundamental frequency (f_k). In the range of the fundamental frequency the curves show negative values of damping, i.e. the forces generated by these vibrations are transmitted more intensely and consequently

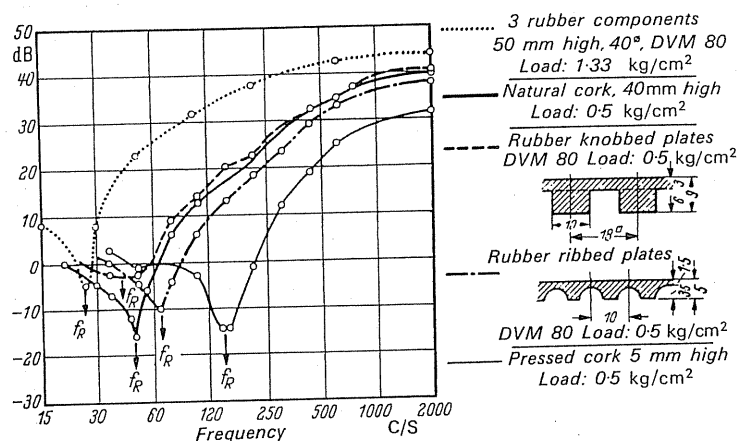


FIG. 538. Isolation of vibration by elastic materials.

the elastic material with the loaded mass will fall in resonance. This contingency must be avoided at all costs. It may occur that the rotational frequency of a high-speed fan might coincide with the fundamental frequency of the damping vibration.

When erecting fans having a speed range from 1000 to 1500 rev/min, care must be taken with the design of the concrete bases. The natural frequencies of concrete bases often come within this range, and are also strongly excited even with well-balanced fans. Preference should be given to flexible mountings on spring isolators.

With spring isolators, as already mentioned, good damping through solids is achieved, but the internal damping of the springs also plays an important role. In steel springs it is insufficient to damp out the natural frequencies of the springs which arise in the vibration of solids. Therefore, where it is a matter of damping a very high vibration of solid, panels of vibration damping material should be inserted below the spring isolators.

The ducts also should be protected from vibration either by lining or suspending the ducts. It is not enough to connect the ducts to the fan with a flexible canvas sleeve or similar flexible material, since the duct walls are excited to vibrations by the sound in air.

175. NOISE REDUCTION DEVICES IN FANS

Constructional measures in the layout of housings and ducts. In the construction of housings and ducts, aspects of vibration and sound must be taken into account in order to prevent excessive vibration in the housing and duct walls so that excessive noise is not

¹⁶ Gerber, O., Practical aspects for mounting of machines for isolation of vibration, *VDI-Berichte*, 8 (1956) 82-85.

generated. One must know the probable main interference frequencies in which the fundamental frequency has the greatest proportion of energy. The housing diameter, the housing width, and the dimensions of the ducts should not be equal to the $\lambda/2$ or multiples thereof in order to prevent excitation of space resonances. The fundamental frequencies of natural vibrations of flat steel plates fall to a large extent in the field round about 100 c/s. The fundamental frequency of rotary noise of radial-flow fans with a small number of blades often occurs in this frequency range. There have been cases where flat duct walls have been excited to such high vibrations that the welding seams have burst. At the same time these vibrations are associated with a very high radiation of noise. By means of strong stiffener with a very close mesh, the natural frequencies of the panels can be raised to very high frequencies. In long lengths of ducting, therefore, it is often easier to replace the impeller with a small number of blades by an impeller with more blades. With centrifugal fans of the double entry type the blades arranged at the two sides should be staggered since the basic rotary noise disappears almost completely owing to a 180° phase lag. This aspect has been confirmed by means of alterations to the impeller in different fans.

If two identical fans are run in parallel, then, due to the slight variable slip of the driving motor, the rotary noise produces beats, in which case the maximum sound intensity at maximum beat is about 6 dB higher than the sound intensity of the individual fan. In the maximum beat the sound pressure doubles itself, which is tantamount to the radiation of fourfold sound power, i.e. an increase by 6 dB. In order to eliminate disturbing beats the speed and the number of blades should be varied.

In many cases it is an advantage to have round ducts since with these the vibrations and therefore the noise radiation which arise are less. In ducting for air conditioning and ventilation installations, however, rectangular ducts should have preference. The vibrations of the duct walls consume sound energy. For this reason in long ducts there is, in addition, very considerable absorption of low frequencies.

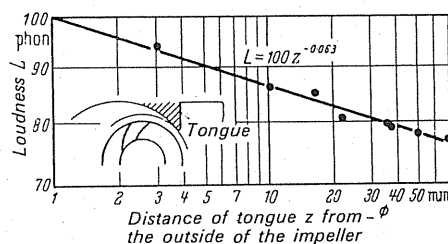


FIG. 539. Loudness as a function of the distance of the tongue in centrifugal fans.

In centrifugal fans the distance of the tongue from the fan impeller has a considerable effect on the intensity of sound. Figure 539 shows an example of this effect. Similar results were found for the distance of guide vanes from the impeller in axial-flow fans.

Profiled blades or other hollow members should be stuffed tightly with wool fibre or with fine-grained dry sand and sealed.

176. ASSESSING THE NECESSARY ATTENUATION OF NOISE

To obtain an objective representation of the reduction of sound requires very exact knowledge of the frequency spectrum of the source of sound and of the direction of propagation. This knowledge is best gained from existing installations by measurements at various salient points of the path of sound propagation. In prospective installations the frequency analysis of fan noise on a test rig or on a similar plant should be measured. (The siting of the microphone must be stated.) The attenuation of noise in the direction of propagation must then be assessed taking into account the frequency spectrum.

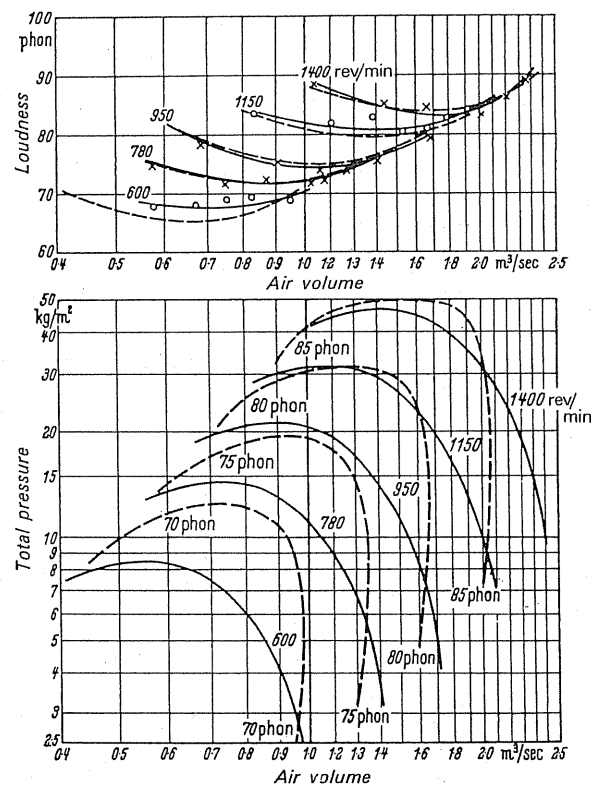


FIG. 540. Loudness as a function of quantity of air and of the characteristic of a Pollrich axial-flow fan of 450 mm dia. according to measurements by W. Zeller.

Variation of loudness by altering the operating point of a fan must be taken into consideration. Figure 540 shows the result of measurements of loudness on an axial-flow fan, the operating point, and the speed of which were varied. These measurements were carried out by Dr. Ing. habil. W. Zeller, Essen.

Generally, however, it is not just a matter of a single source of sound but of several simultaneous sources. For instance, sound is radiated from the motor, from the gear, from the inlet opening, from the fan housing, and from the pressure piping. Owing to matching effects

the loudest source of sound manifests itself subjectively and in measurement. The reduction in the level of the loudest source of sound by means of noise reduction devices is often disappointing. This is because another noise source only slightly below the loudest source of sound now appears to be the dominant source. By measuring in direct proximity to individual sources of sound an approximate picture of the magnitude of their levels can be obtained, but it is not only a question of the absolute magnitude of the individual sound level but also of the area from which it is radiated, since ultimately the radiated sound power is a criterion for the noise level at a greater distance.

After having obtained some idea of the existing or anticipated sound field, the sound-insulating components for reducing the existing sources of noise can be defined after fixing the desired noise level (for instance, the measurements by an octave or tierce band spectrum should not exceed the values of noise criteria curve at any specific measuring point). From the point of view of economics the effect of the noise-insulating components must be synchronised in such a way that the residual sounds have approximately the same level. Due to the uncertainty of prediction of the necessary sound reduction, the sound-insulating components should be oversized rather than undersized. For this reason, under complex conditions it is advisable to mount the individual sound insulating components in stages starting from the loudest source of sound and to check the actual performance by measurements.

CHOICE AND LAYOUT OF SOUND-ATTENUATING COMPONENTS

The enclosure. The surrounding walls of an enclosure in which the fans are to be mounted constitute a sound-damping capsule for the noise from the acoustic point of view. Therefore they should satisfy high damping requirements and should consist of solid stone- and brickwork plastered on both sides or of concrete walls of approximately identical density (approximately 350 kg/m^2). Existing walls with inadequate absorption should be provided with an outer panel, and for very stringent requirements double-panel designs should be provided. Wherever possible, the reverberation time of the room should be reduced by sound-absorption lining of the ceiling and parts of the walls.

For stringent requirements openable windows must be replaced by thick, glass slabs for instance. The doors (or ports) should be designed as double doors or single doors in sound-absorbing construction. For removal of any incidental operating heat and for venting the space, artificial ventilation should be provided with equipment fitted with silencers. In this case the fan motor or the fans themselves can provide the air throughput called for, by extracting a portion of their delivery volume. The fans along with their driving units should be supported on flexible mountings and damped against sound propagation through solids. Ducting and piping should be arranged in suspension for isolation against sound transmission through solids. Particularly noisy surfaces should be encapsulated with a sound-damping casing.

The silencers. When designing the silencer the frequency spectrum and the level of damping desired must be taken as a basis. The free cross-section should be chosen in such a way

that there is no undesirably high pressure loss in the passage of the gas volume delivered or that excessive flow velocity arises in the ducting.

A high flow velocity generates new noises, which in certain circumstances could adversely affect the action of the silencer.

Loudness as a function of the flow velocity⁽¹⁷⁾ is shown in Fig. 541.

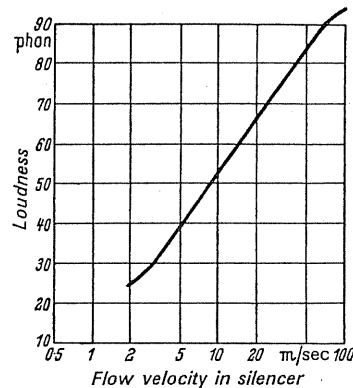


FIG. 541. The relation between flow velocity in silencer and loudness.

In exhaust silencers a pressure loss of a few hundred mm WG can invariably be allowed. The free cross-sectional area in the silencer and the exhaust aperture must be governed by the flow velocity which may be set so high that the flow noise thus brought about lies somewhat below the sound level leaving the silencer. For this reason exhaust silencers must frequently be placed at the end of the exhaust duct and cannot be inserted inside the duct because, owing to the high flow velocity in the duct following the silencer, an intolerably loud noise in flow would occur.

In ventilation and air-conditioning plants, noises in flow also decide the final level in the space. In low-pressure plants the velocity in the ducts and silencers is recommended at about 6 m/sec. The inlet velocity in the spaces should be at about 2–3 m/sec. In air-conditioning plants with particularly noisy delivery, such as radio and television studios, secondary silencers therefore must be provided in front of the exhaust openings (the primary silencers are arranged immediately behind the fans) in order also to reduce noises in the flow.

If high-pressure installations are to be built also for low final levels in which the ducts have higher velocities, secondary silencers will also be required. The layout of the ducts should be such that flow noises are avoided at bends, branches, edges, or slots.

In many silencers the free cross-sectional area is determined by the demand for minimal pressure loss. As stated above, damping by an absorption silencer rises with the increasing ratio of circumference to free area. The frictional loss also increases with increase in ratios of perimeter to free area. Therefore at a constant free cross-section and a given length of silencer the call for high-absorption and low-pressure loss contradicts itself. Hence the free cross-section and length of silencer must be increased in order to satisfy the demand for ample absorption and low-pressure loss.

¹⁷ Gerber, O., Noise generation and its damping in ventilators, *Lärmbekämpfung*, 1 (1957), Nos. 5–6, pp. 93–101.

This leads to the following economical aspect.

If with damping remaining constant the free cross-section of a silencer is halved, then the cost would approximately halve itself. By halving the free cross-section the flow velocity doubles itself and the pressure loss quadruples itself, since it is proportional to the square of the velocity. The operating costs required for overcoming the pressure loss, therefore, are increased fourfold. Taken over one year, these additional operating costs in very large fans come to considerable amounts which generally far exceed the extra cost of a large silencer.

Absorption silencers for insulating low frequencies must be equipped with very thick sound-absorbent packing. They are therefore more wasteful and dearer than silencers for damping medium and high frequencies for which thinner packing will do.

With a silencer a maximum attenuation of approximately 45–50 dB can be achieved. Extra length of silencing does not give any further benefits, since the sound energy which is transported through the longitudinal duct into the silencer walls manifests itself and prevents a further rise in the attenuation effect. If a still higher attenuation is required, two silencers must be arranged to follow each other, and distance between them should be large enough by comparison with the wavelength of the lowest frequencies to be damped.

According to the frequency range and the attenuation required, the free cross-section and the location of the installation, silencers can be arranged in many different ways. Figure 536 shows a suction silencer for high frequencies fitted in the shape of coulisses in a concrete ducting.

Figure 542 shows a suction silencer with the silencer in the shape of coulisses for medium frequencies and a follow-on silencer with deep side attenuating ducts for absorbing low frequencies.

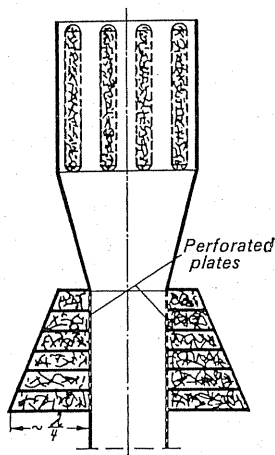


FIG. 542. Suction or exhaust silencer for absorption of low and medium frequencies. Silencer for low frequencies and a coulisse silencer for high frequencies.

Figure 543 is a suction silencer of a double-entry centrifugal fan. The sound-absorbent coulisses are arranged as panels. The connection of the two internal panels with the sound-absorbent plate simultaneously provides the encapsulation for the fan housing.

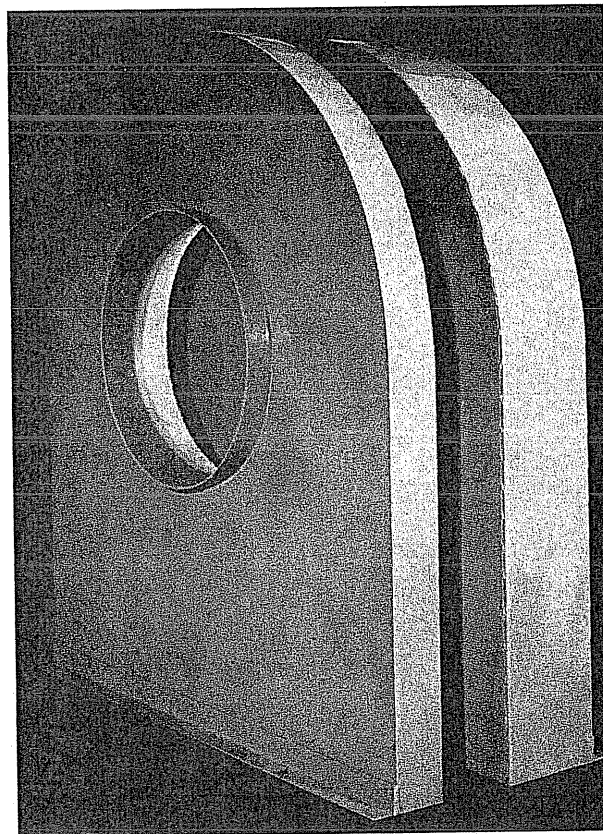
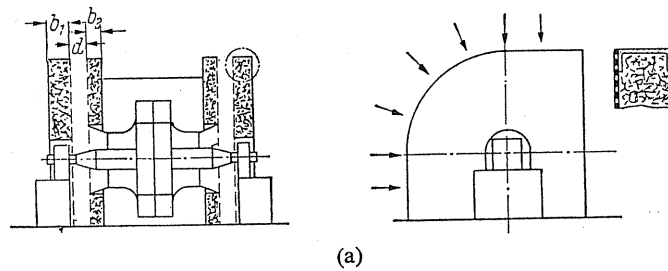


FIG. 543. Suction silencer of a double-entry suction centrifugal fan.

Suction silencers in wing form can be arranged in concrete ducts in such a way that they can be withdrawn through the ducts for the transport of machinery or pushed together sideways by a crank drive.

The attenuation of noise due to pulsating flow may be achieved by the installation of suitable screens in the duct.

The absorption of sound by duct walls in ventilation and air-conditioning fans with rectangular ducts plays a significant part in low frequencies because of the exciting natural frequencies of the ducts. This should be taken into account in an economical estimate when

calculating the design of a silencer. Investigations in this connection were carried out by Dr. Ing. W. Kuhl, Radio Institute, Nuremberg. For ducts made of 1-mm-thick steel sheet and 4-mm-thick hard fibre-board panels with free dimensions of 250×250 and 300×300 mm respectively, peak values of 7 and 10 dB per metre were measured in the range round about 100 c/s. Here also the attenuation increases with increasing ratio of circumference to area. At either end of the frequency at which these peak values occur the attenuation, however, diminishes very greatly, as it is very difficult to carry out a preliminary calculation. The attenuation values have to be ascertained by measurement. For rough calculation a safety margin in the range round about 100 c/s of approximately 0.5 dB per metre should be allowed for attenuation.

If this additional attenuation is required, the steel ducts should not have their natural metallic noise removed because this will be at the cost of radiation from the duct walls. Round ducts do not show this effect. Therefore for these the silencer must have an ample attenuation effect even of low frequencies. They radiate noise much less strongly than rectangular ducts and can be installed advantageously where radiation of sound is a nuisance and sound-absorbing lining is omitted.

Noise attenuation by outside lining of housings, ducts, and silencers. The noise radiation of ducts can be reduced either by fitting a silencer or by means of a sound-absorbing lining. Whichever method is chosen depends primarily on operational and economical aspects; practically the same effect can be achieved with both methods. Where only a short length of duct is concerned, the most economical solution is lining of the duct. Where a very long duct is concerned it would be more advantageous to fit a silencer. For stringent requirements or for very noisy fans, the fans themselves, the duct up to the silencers, and the silencers up to half their length must be provided with sound-absorption linings, since noise is still strongly radiated from the extreme front end of the external walls of the silencer.

Anechoic chamber for testing. More accurate sound investigations on fans and other equipment will have to be carried out in anechoic chambers. All walls and all floors of such spaces must absorb all the sound waves impinging on them from a very low fundamental frequency (upwards of 70–150 c/s) to reduce the reverberation time of the space to zero. This is achieved by lining the walls with long wedge-shaped sound absorbers of a porous nature (mostly wool fibre) which must have a specified flow resistance. The length of the absorber is a function of the fundamental frequency involved. Solid surrounding walls of the room must have a particularly high sound-absorption coefficient. The walking floor should consist of a grid or a net.

177. EXAMPLES OF DESIGN

Mine fans. Noise investigations on mine fans were carried out by the establishment of the mining research in Bochum and published by Dipl.-Ing. Schubert. For this purpose axial- and radial-flow fans were used. Generally the speeds and flow velocities in axial-flow fans are higher than in centrifugal fans. Their frequency spectra also differ correspondingly.

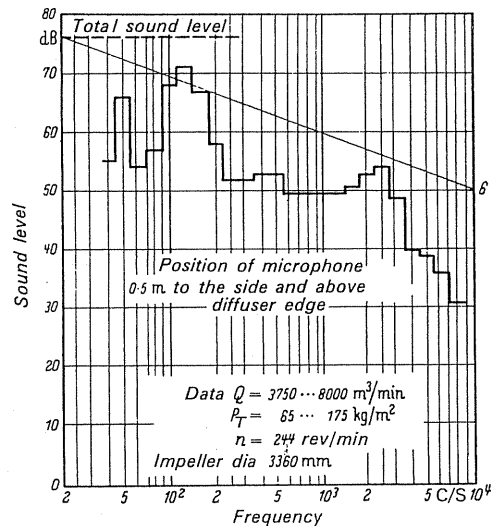


FIG. 544. Frequency spectrum of a mine fan, centrifugal type, designed by Eck. Microphone 0.5 m to the side and above diffuser edge according to Schuberth.

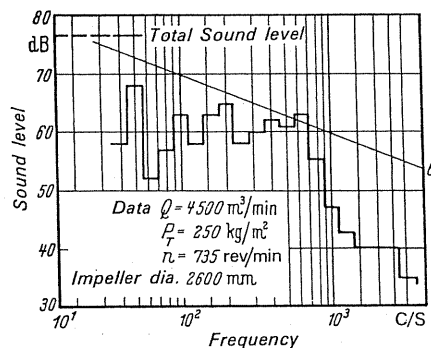


FIG. 545. Frequency spectrum of a mine fan axial-flow type. Microphone 12 m distance from the diffuser axis according to Schuberth.

Figures 544 and 545 show the frequency spectra of two comparable fans. Figure 544 shows the spectrum of the centrifugal fan when the microphone is mounted 0.5 m to the side and above the diffuser edge. Figure 545 shows the spectrum of the axial-flow fan when mounting the microphone at a distance of 12 m from the axis of the diffuser.

If this axial-flow fan were measured at the same position as the radial-flow fan, i.e. directly behind the diffuser, an overall sound level would be approximately 12 dB higher. Independent of this it is shown by the assessment with the criteria curve that axial-flow fans with higher frequencies cause more disturbance. In axial-flow fans, therefore, a great deal of noise damping measures are required while in centrifugal fans (Fig. 546) they can be dispensed with as a rule.

Figure 546 shows the drawing of an absorption silencer for mounting on the diffuser of a mine fan. Figure 547 shows a main mine fan axial-flow type with mounted absorption silencer. To reduce pressure losses, the free cross-section in the silencer should be chosen

just as large as the free cross-section at the diffuser outlet. Mathematically, additional pressure losses of 2–3 mm WG then occur which are practically of little consequence since the modification of the silencer wings cause a smoother flow in the diffuser and its efficiency is thus increased.

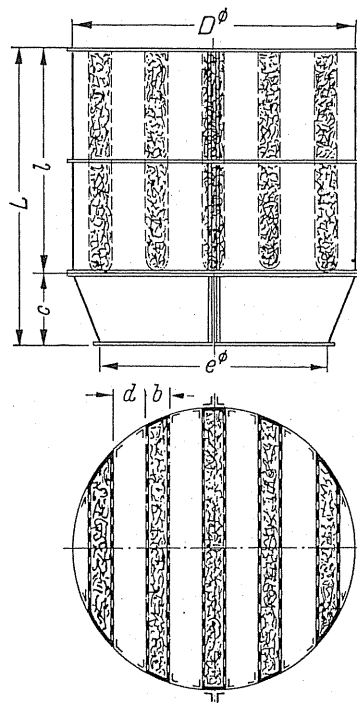


FIG. 546. Absorption silencers for mounting on the diffuser of a mine fan made by Messrs. Oskar Gerber.

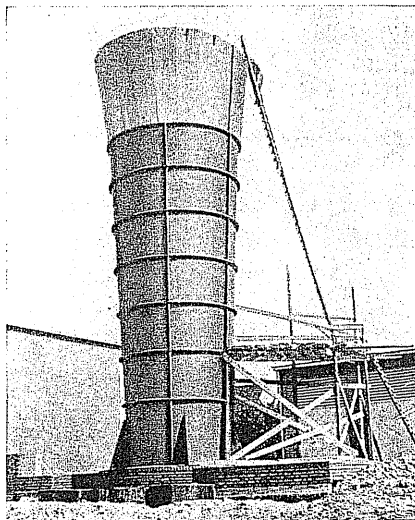


FIG. 547. Mine fan, axial-flow type with absorption silencer.

Attention should be paid also to the noise radiation from driving motors, gears, and fan and diffuser external casing.

In a new installation the motor, the gear, and the actual portion of the fan in a building which has noise-attenuation arrangements should be mounted above or below the ground level.

A concrete diffuser radiates the noise less than a steel-plate diffuser. The latter should be provided with noise-damping linting.

For assisting the damping of the mounted silencer the hub and the deflection blades should be made in sound-absorbent materials. These noise attenuation measures fulfil the requirements of the mining authorities for 50 DIN-phon at 50 m distance.

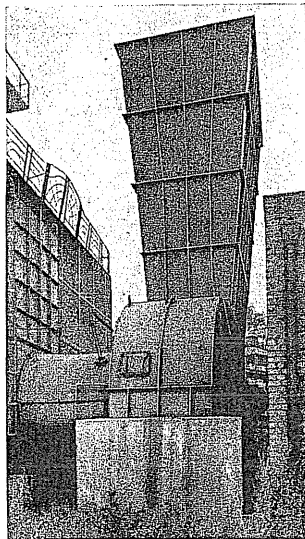


FIG. 548. Mine fan, centrifugal type, Eck-Büttner design; no silencer required.

178. GAS TURBINES, BLAST FURNACE BLOWERS, TURBO-COMPRESSORS, HIGH-PRESSURE BLOWERS

All four machines show similar very loud and high frequency spectra. A sound level of 110–120 dB is to be anticipated before the suction opening. Therefore a suction silencer is fitted in the suction duct before or after the air filter, usually in angular wing form.

The free cross-section should be of adequate dimensions to achieve a low-pressure loss which is important for good efficiency.

If a low residuary sound level is called for, exhaust-gas silencers should be provided in gas turbines.

The starting and the discharge ducts of blast furnace blowers and turbo-compressors are fitted with discharge silencers which, however, should not show a very high-pressure loss, as during the starting process—according to the characteristic—a large volume delivery takes place against a small pressure. The pressure lines should be provided with pressure

silencers since they are generally run over long distances and, owing to their large pipe surface and the high sound level, they radiate a large sound power.

Inside a machine room a high sound level is generated through radiation in particular by the pipelines located in the cellar. The pipelines should be lined with sound-absorbing material and the lining must be designed as thermal insulation with which many pipelines, particularly for gas turbines, are fitted as a matter of course.

The cellar should be separated from the machine-room floor by a thick ceiling cover passing right through. The passage through the foundations should be sealed. Break-ins with gratings are to be avoided. For high duties parts of machines which are particularly noisy should be encapsulated or the whole machine should be placed underneath a hood. For fitting out the machine room the measures described in section 163 apply.

179. INDUCED DRAUGHT BY INJECTION

Figure 549 shows a diagrammatic representation of sound attenuation measures carried out on a plant installed for induced draught by injection. The axial blower and the motor are erected in a building with solid walls. The roof is sealed by a sound-absorbent steel casing which can be taken apart to enable parts of the machines to be dismantled and removed

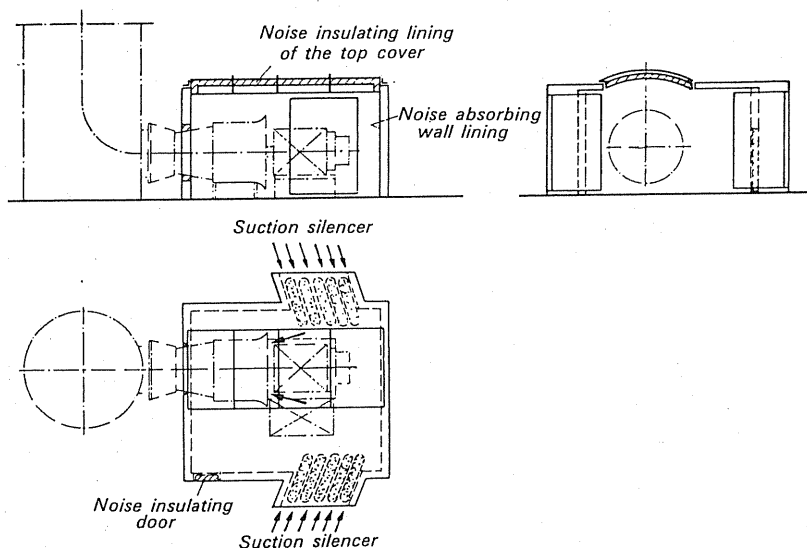


FIG. 549. Noise control in induced-draught fan made by Messrs. Oskar Gerber.

for repair. Duct sections are connected up to both longitudinal walls, and in these the sound-absorbing wings are fitted to act as silencers. They were arranged at a slope in order to sweep the driving motor with fresh air for cooling and to prevent direct incidence of sound waves emitted from the suction opening. The rear wall of the building is lined with sound-absorbent material in order to reduce the reflection emitted from it. A sound insulated metal door is provided for entering the room.

180. FUTURE PROSPECTS

At the present state of knowledge almost every requirement for noise attenuation remains to be solved. Extra fitting of sound-absorbing components which had not been anticipated frequently raises difficulties due to conditions of space or is quite impossible to carry out. Therefore, when designing new installations the necessary noise-attenuation measures should be included or envisaged for fitting later.

PART G

CALCULATIONS OF STRENGTH

CHAPTER XXIII

SHORT REVIEW

181. BASIC PRINCIPLES

When working out sizes, some attention should be paid to the stressing of impellers by centrifugal forces. In this respect we are in the fortunate position of being able to make fairly reliable calculations which measure up to a number of demands. In the following discussion a brief outline is given which stresses the most important and essential factors to be considered by the engineer.

The freely rotating ring. In Fig. 550 we see a thin ring which rotates at a peripheral speed u and we investigate the stresses which are caused by the centrifugal forces. For this purpose

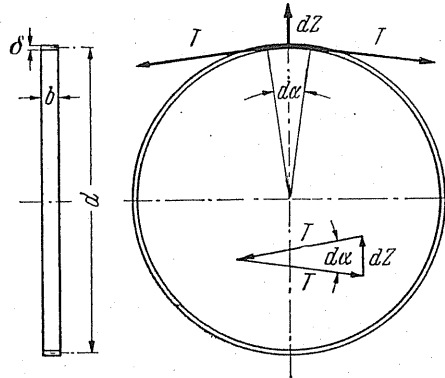


FIG. 550. Freely rotating ring.

consider a sector having the angle $d\alpha$ and examine the forces on this element. The acting forces are:

- (1) Tangential forces T which bring about an evenly divided tensile stress σ on a ring which is sufficiently thin are expressed by the equation $T = \sigma f = \sigma b \delta$.
- (2) The centrifugal force acting outwards is

$$dZ = \frac{d}{2} (d\alpha) b \delta \frac{\gamma}{g} \frac{d}{2} \omega^2.$$

The equilibrium of these forces is represented in Fig. 550 as a triangle of forces. Thus we have $dZ = T d\alpha$ or $T = dZ/d\alpha$.

$$\sigma = \frac{\gamma}{g} u^2. \quad (296)$$

The freely rotating bar. According to Fig. 551 we allow a bar of constant cross-section f to rotate at the peripheral speed u . We consider a small element of radius dr and calculate the centrifugal forces acting at this section:

$$dZ = dr f \frac{\gamma}{g} r \omega^2.$$

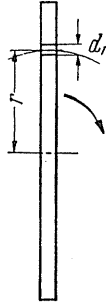


FIG. 551. Freely rotating bar.

The integration is easy to carry out and it yields

$$Z = \int_{r_1}^{r_2} dr f \frac{\gamma}{g} r \omega^2 = f \frac{\gamma}{g} \omega^2 \int_{r_1}^{r_2} r dr = f \frac{\gamma}{g} \frac{u_2^2 - u_1^2}{2}.$$

The stress is the highest in the middle of the bar, i.e. for $r = 0$. In cross-section f a stress σ will be generated by Z according to the equation $Z = f\sigma$, from which

$$\sigma = \frac{Z}{f} = \frac{1}{2} \frac{\gamma}{g} u_2^2 \left[1 - \left(\frac{r_1}{r_2} \right)^2 \right]; \quad \sigma = \frac{1}{2} \frac{\gamma}{g} u_2^2 \quad \text{for } r_1 = 0.$$

These results are of fundamental importance and deserve some attention. First of all it is noteworthy that the stresses are only a function of the peripheral speed u . This means that, for example, the speed and the diameter are of equal importance at the same peripheral speed. A minutely small ring would be stressed just as much as a giant ring if, in both cases, the peripheral speed is the same. Although the freely rotating ring and the rotating bar hardly ever occur as constructional elements, it is strongly advisable to use the stresses arising in this test as a comparative scale for all other cases occurring in fan engineering. Thus we arrive at dimensionless quantities of an impeller design which indicates how great is the largest stress occurring in an impeller compared to a ring or a bar. The ring is used for comparison in disc-type configurations whereas all bar or spoke-shaped configurations (for instance, all blades of axial-flow fans) can be compared to the rotating bar. The characteristics can be regarded as *geometrical* phenomenon of a design. Thus we obtain two characteristic quantities:

$$k = \frac{\sigma_{\max}}{(\gamma/g) u^2}, \quad (297)$$

$$k' = \frac{\sigma_{\max}}{\frac{1}{2} (\gamma/g) u^2}. \quad (298)$$

By applying these coefficients we obtain for the largest stress the relationships:

$$\sigma_{\max \text{ ring}} = k \frac{\gamma}{g} u^2, \quad (299)$$

$$\sigma_{\max \text{ bar}} = k' \frac{1}{2} \frac{\gamma}{g} u^2. \quad (300)$$

The advantage of this method of observation is that *the knowledge of a single quantity will suffice to verify the quality and applicability of a design.*

As mentioned initially the stresses arising from the centrifugal forces can be calculated or graphically determined with sufficient accuracy in most designs. The methods are, of course, rather time-consuming but offer no fundamental difficulties. The methods were developed by Heller,⁽¹⁾ Donath,⁽²⁾ Stodola,⁽³⁾ Honegger,⁽⁴⁾ Keller,⁽⁵⁾ Grammel⁽⁶⁾ and Baer.⁽⁷⁾ Within the scope of this work the author cannot give an exhaustive description of these methods and would refer the reader, when the case arises, to the literature. In most cases, of course, it is sufficient to know the relationship shown below and to apply it appropriately. Thus Fig. 552 has twelve different sectors of disc-shaped configuration which provides an assortment and an average survey of designs which occur. For each design the coefficient k is shown. If any design differs from the illustrations, then we look for two configurations between which the design envisaged lies. Then the higher coefficient is chosen as safety margin for the calculation of stress. So we have a rapid process which, from the purely scientific point of view, has many flaws but meets the requirements in practice, where accurate calculation is not always absolutely necessary.

The value of $k = 0.157$ in the conical solid disc shows clearly the essential load relief which can be achieved by a suitable sizing as compared with the free ring. The rule which applies can also be read from Fig. 552. By accumulation of material towards the rotating axis, a noticeable reduction of the highest stresses can be achieved. Stiffening a smooth disc by means of a ring (see Fig. 552) is typical of how very strong discs can be built by simple means.

Considering the blades, it is possible that the stress on the disc attached to the blade is tantamount in practice to the specific weight of the disc being increased in the ratio

$$\frac{\text{Disc weight} + \text{blade weight}}{\text{Disc weight}}.$$

According to the above definition a simple method of calculation will be given which should suffice as an approximation (approximately 20–25% accuracy). The method consists in the mean value of the tangential stresses being used for comparison. This mean value can

¹ Heller, *Schweiz. Bauztg.*, 1909, p. 307.

² Donath, *Die Berechnung rotierender Scheiben und Ringe nach einem neuen Verfahren*, 2nd edn., Berlin, Springer, 1912.

³ Stodola, *Dampf- und Gasturbinen*, 6th edn., Berlin, Springer, 1924.

⁴ Honegger, *ZAM*, 1927, No. 2.

⁵ Keller, Contribution to analytical calculation of highly loaded impeller discs, memorial lecture, Stodola.

⁶ Biezeno-Grammel, *Technische Dynamik*, 2nd edn., Berlin/Göttingen/Heidelberg, Springer, 1953.

⁷ Baer, *Z VDI*, 1940, p. 359.

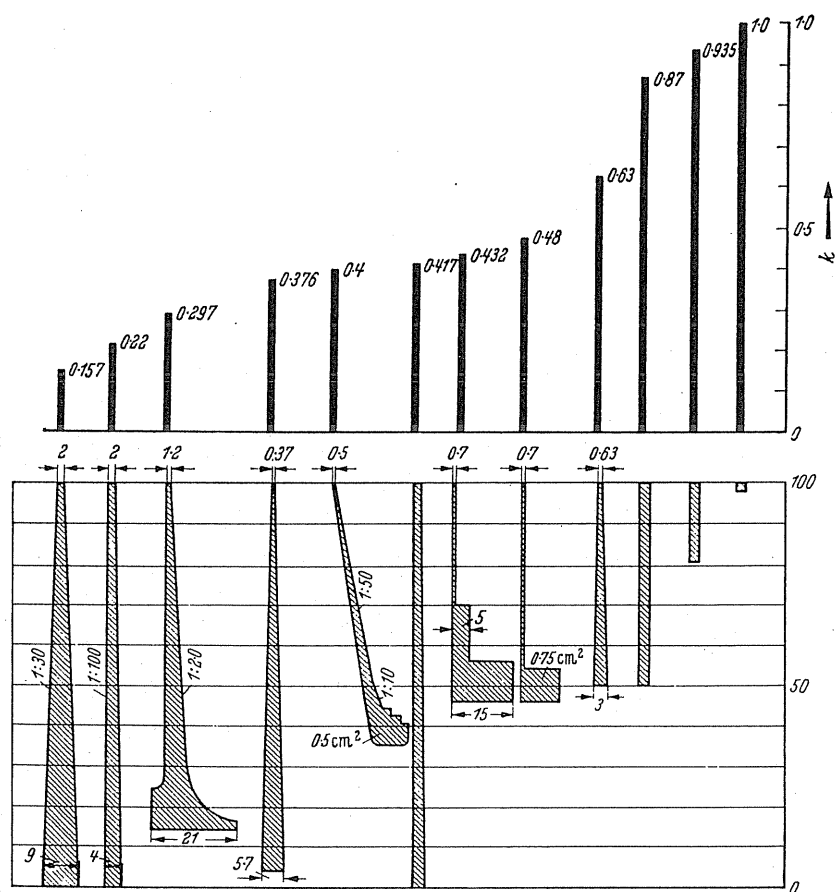


FIG. 552. Stress properties of typical impellers shown as dimensionless ratios.

be rapidly and accurately determined for any design of disc whatever. Let us imagine the disc being cut up into individual thin rings. Then each ring in its rotation would be unaffected by the others which show the ring stress $(\gamma/g) u^2$ corresponding to its mean velocity. In the solid disc these ring elements affect each other reciprocally. The effect is such that the above-mentioned free ring stresses are displaced. In each case, however, the total sum of these stresses still remains available for reasons of equilibrium. This means that the mean value of the tangential stresses is determined accurately if the stresses of all elementary rings are added together. Applicable for each portion of the ring we have:

$$dT = b dr \sigma \quad b = \text{width at radius } r$$

$$T = \int b dr \sigma \quad \sigma = (\gamma/g) u^2 = (\gamma/g) r^2 \omega^2.$$

The overall tangential force which acts perpendicularly on a radial section of the disc we imagine as having arisen through a mean stress σ_m which acts on the cross-sectional area F :

$$T = F \sigma_m.$$

Thus we have

$$\sigma_m = \int \frac{1}{F} b \, dr \, \sigma = \frac{1}{F} \int b \frac{\gamma}{g} r^2 \omega^2 \, dr = \frac{(\gamma/g) u_a^2}{F} \int_r^{r_a} b \left(\frac{r}{r_a} \right)^2 \, dr,$$

from which we obtain

$$k = \frac{\sigma_m}{(\gamma/g) u_a^2} = \frac{1}{F} \int_r^{r_a} b \left(\frac{r}{r_a} \right)^2 \, dr.$$

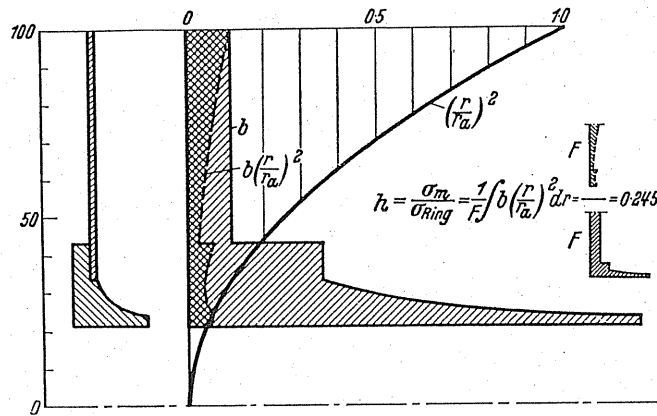


FIG. 553. First approximation of the graphical method of estimating stresses in discs.

Figure 553 shows the graphical evaluation of this formula on an example of an impeller disc where a smooth disc is secured to the hub (welded or riveted). Firstly, the width b of the disc in appropriate enlargement is plotted. The parabola $(r/r_a)^2$ also plotted above r indicates the values by which b has to be elongated. Thus we obtain the cross-hatched area, the content of which is equivalent to the value of the integral $\int b (r/r_a)^2 \, dr$. The ratio of the two areas gives the coefficient k .

Calculations give $k = 0.245$.

If coefficient k has been determined by first approximation with one of the methods stated, then the maximum stress is known immediately. At greater radial expansion, deviations occur.

Example

For the previous example let us take the case where $u_a = 246$ m/sec.
For σ we obtain

$$\sigma = k \frac{\gamma}{g} u_a^2 = 0.245 \times \frac{7850}{9.81} \times 246^2 \times 10^{-4} = 1200 \text{ kg/cm}^2.$$

With aerofoil configuration, for which the straight bar was recommended as comparatively simple, now an accurate method can be given. The small element of the radius dr generates the centrifugal force

$$dZ = dr F \frac{\gamma}{g} r \omega^2,$$

from which we have

$$Z = \frac{\gamma}{g} \omega^2 \int_r^{r_a} F r \, dr.$$

The largest force, and mostly also the largest stress, is to be expected at the blade root because here the centrifugal force is transferred to the whole blade. If at this point the area is F_1 and the tensile stress σ_1 , then it gives

$$Z = F_1 \sigma_1.$$

If the area represented by the integral is designated \bar{F} , then it becomes

$$\sigma_1 = \frac{\gamma}{g} \omega^2 \int_r^{r_a} \frac{F}{F_1} r \, dr = \frac{(\gamma/g) u_a^2}{r_a^2} \int_r^{r_a} \frac{F}{F_1} r \, dr = \frac{(\gamma/g) u_a^2}{r_a^2} \bar{F},$$

so we obtain for the characteristic

$$k = \frac{\bar{F}}{r_a^2}. \quad (301)$$

Taking an axial blade as an example, Fig. 554 shows the graphical evaluation. First, the blade cross-sectional area F is plotted as a function of radius r . The radius r , i.e. a straight line sloping at 45° , is multiplied by the ratio F/F_1 . The area \bar{F} under the curve $(F/F_1) r$ which arises therefrom is determined. In the example we obtain

$$k = \frac{53.6}{225} = 0.239; \quad k' = 2k = 0.478.$$

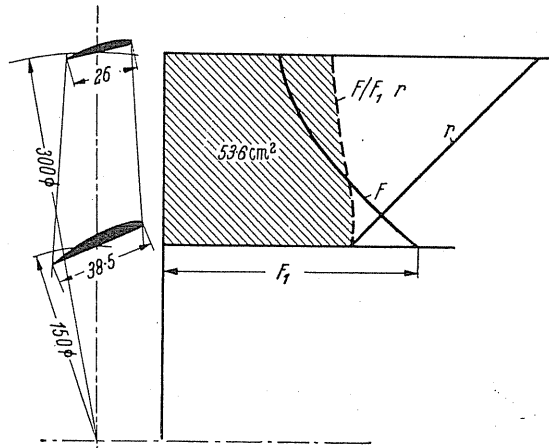


FIG. 554. First approximation of the graphical method of estimating stresses in blades.

Choice of material. It can easily be derived from the basic equation (297) that the attainable peripheral speed is dependent on the characteristic of the material. When resolving for u we obtain

$$u = \sqrt{\frac{g\sigma}{k\gamma}}.$$

The magnitude of the value σ/γ thus is decisive. The importance of this value is very clear. Let us imagine a cylindrical bar of material having cross-sectional area F freely suspended and of such length that it just about tears at the top end. At a specified length R this will be the case. Since the load is only given by the weight $G = RF\gamma$, we obtain the following equation:

$$RF\gamma = F\sigma,$$

which gives us

$$R = \frac{\sigma}{\gamma} \quad (302)$$

The length R is appropriately described as the *tearing length*. The material used for fan construction has these properties. The maximum peripheral speeds can therefore only be obtained with materials where the greatest tearing lengths occur.

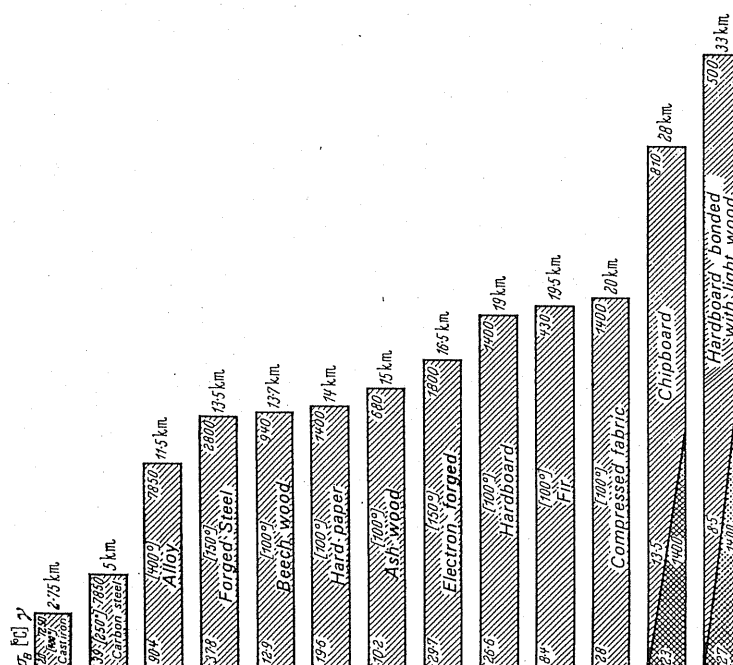


FIG. 555. Tearing length, temperature limit, ultimate tensile stress, specific gravity for various materials.

Thus we can have a graded range of materials. A diagrammatic outline is given in Fig. 555. It is surprising that not steel or alloyed light metals, but wood and hardboard take first place. With these materials tearing lengths of 22–25 km are achieved. The fact that these materials cannot be used more frequently is due mainly to other reasons, for instance low resistance to deterioration and susceptibility to moisture and high temperature. Figure 555 also shows the temperatures at which a marked irregular decrease of the tearing length may be expected.

The maximum values can be obtained with bonded materials. This is understood to be a type where the portion close to the hub is made of heavier material with a high strength and then followed by lighter materials with a higher tearing length. Combinations such as steel + wood, compressed carbon + wood or light metal, steel + compressed wood + light wood, etc., are quite feasible. Figure 555 shows two combinations of bonded wood. In this case a tearing length of 33 km was even achieved.

New plastics stiffened with glass-fibre insertions are also being considered in fans.

Safety. If the coefficient k and therefore the stresses are known, the question arises as to the safety margin which can be recommended for fans and blowers. Since it is a matter of static loading, small values, approximately $\mathfrak{S} = 2.5$ will do if the material characteristics are accurately known and accurate calculation has been made. Otherwise the value 3 would be chosen related to the elastic limit.

PART H

EXPERIMENTAL TESTING OF FANS

EXPERIMENTAL TESTING OF FANS ⁽¹⁾

For testing fans on the test rig for verifying manufacturers' guarantees in operation, etc., tests are required which sometimes may be very difficult. Fitting fans with any kind of instruments in a more or less compact overall arrangement often gives unreliable measurements or involves extremely difficult technical problems. The errors observed in industrial tests of this kind are more numerous and more risky than is generally assumed. This is frequently the case when the application of flow rules is simply impossible, and measuring methods to suit the character of the case have to be evolved. It is easy but very cheap to criticise the engineer for using apparently unscientific methods. The desire of the engineer to find some kind of solution is misunderstood.

The following is a statement of a few typical problems which have occurred in practical tests.

Problem

For assessing a fan the delivery volume V (m³/sec), the pressure rise ΔP (mm WG) and the power N (hp) absorbed at the shaft must be known. In order to appreciate the overall operational behaviour, furthermore the characteristic $\Delta p = f(V)$ as well as $N = g(V)$ must be known. Acceptance tests will be limited throughout to the verification of the guaranteed items whilst the characteristic can be plotted from the measurements on the test rig.

In the following discussion all problems of air measurement and also any possible electrical measurement which must be observed, are listed. All details of methods will also be shown numerically as obtained from examples of acceptance tests carried out.

¹ See also Rules of performance testing on fans and compressors, *VDI-Verlag*, 1966, as well as *VDI-Durchfluß-Meßregeln*, 6th edn., Düsseldorf, Deutscher Ingenieur-Verlag.

CHAPTER XXIV

GENERAL ASPECTS

182. OUTLINE OF TEST CIRCUIT FOR FAN TESTINGS

According to whether the measurements take place wholly or partly in the suction side or the pressure side and according to whether the fan is operating as an exhaustor or compressed-air blower or mixed operation is involved, many different kinds of circuit are possible. If, at the same time, the necessary prerequisites have been met such as are laid down for volume measurement in flow-measurement regulations, ample accuracy is obtained in these measurements.

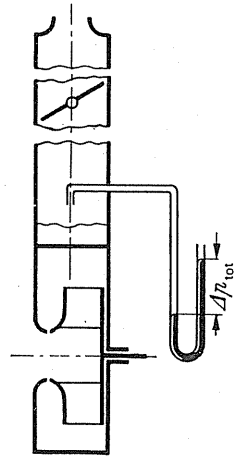


FIG. 556. Total pressure measured at the blowing end of an impeller.

The total pressure which the fan develops is determined by means of the difference in energy between outlet and inlet:

$$\begin{aligned} \Delta p_{\text{tot}} &= [p_2 + (\rho/2) c_2^2] - [p_1 + (\rho/2) c_1^2] = p_2 - p_1 + \rho/2 [c_2^2 - c_1^2] \\ &= \Delta p_{\text{stat}} + \Delta p_{\text{dyn}}. \end{aligned} \quad (303)$$

Hence a purely static and a dynamic proportion is created. If this blower only sucks and discharges freely into atmosphere, the total pressure can be obtained directly by means of the differential pressure measurement with pitot tubes indicated in Fig. 556. In other cases the total pressure difference in accordance with Fig. 557 can be measured. First it may be assumed that in the measuring cross-section mean overall pressure is present everywhere. Since this is seldom the case, the total energy present in a cross-section is determined by the

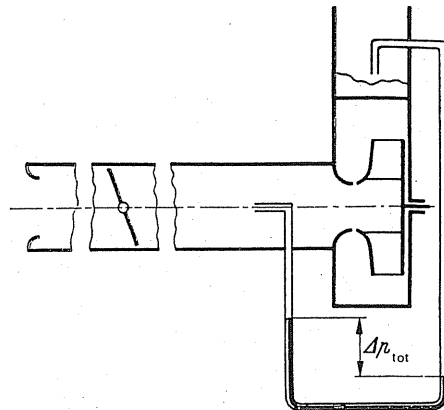


FIG.557. Total pressure measured between the outlet and the inlet.

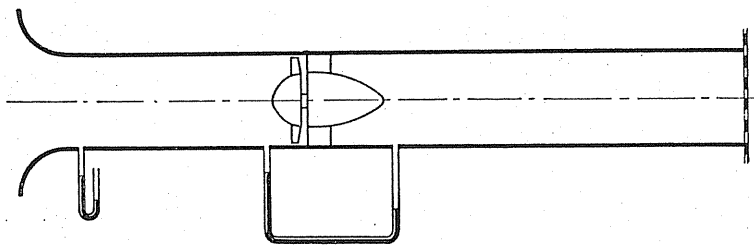


FIG.558. Measuring section for axial-flow fan.

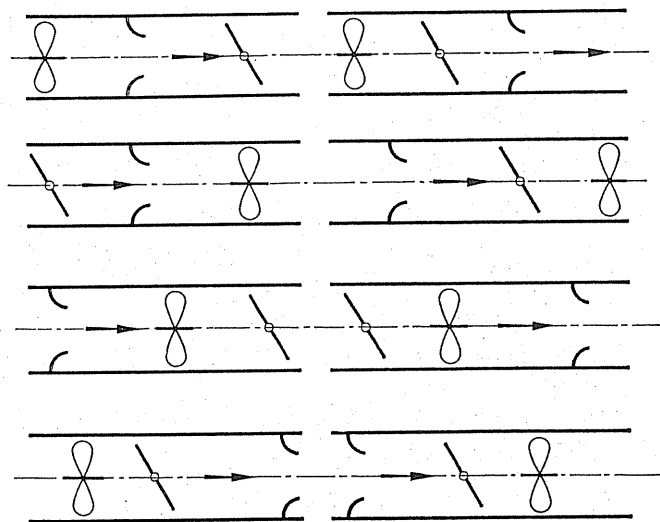


FIG.559. Eight circuit arrangements of throttling devices and nozzles.

fact that the static pressure is obtained by means of a hole drilled in the wall and the dynamic pressure head p_{dyn} is calculated by substituting a mean velocity c obtained from the average volume flow.

Thus, for instance, for an axial-flow fan (Fig. 558) a measurement is obtained by using the negative pressure measured at the front of the intake nozzle for obtaining the quantities whilst the pressure difference measured is determined at the hole drilled in the wall before and after the fan. If these cross-sections are equal, then no conversion is necessary because now the static pressure difference agrees with the difference of the total pressure. It may, however, arise that the blow-off cross-sectional area is greater than the suction cross-

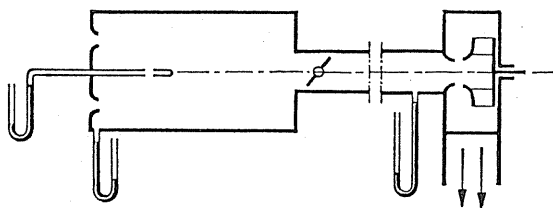


FIG. 560. Part of test-rig mounted on the suction side of an impeller.

sectional area (Fig. 592). Since $c_1 > c_2$ we now have $\Delta p_{st} > \Delta p_T$, i.e. the measured static pressure difference is greater than the difference of the total pressure. This leads to irregularities which have already been discussed at another place.

For test-rig measurements, quantity measuring devices are required, mainly in the form of nozzles or orifice plates, as well as throttling appliances in the form of throttle valves or screens, to be able to plot the whole characteristic. According to whether these devices are arranged before or after the fan, eight different circuit possibilities emerge which are sketched in Fig. 559. Measuring sections with intake or outlet nozzles for orifice plates arranged before or after the fan (Figs. 560 and 561) are of special importance. In these cases there is the convenience of having several nozzles which can be switched off and a large number of quantity ranges can be covered without any great modification. Measuring sections are indispensable in cases of fans which operate in the open without housing.

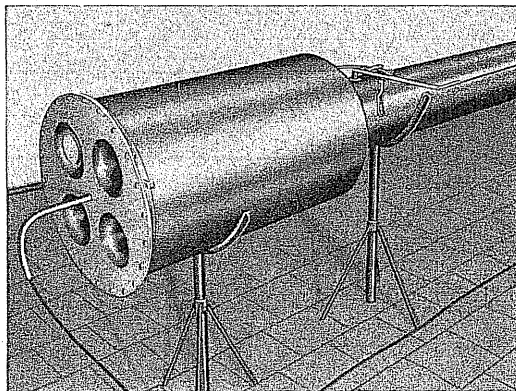


FIG. 561. Test-rig with four standard nozzles cut out by rubber seals, adjustable throttling damper.

In many cases it is difficult to produce the characteristic completely on the test rig, because the resistance remaining in the nozzle or the orifice plate sets the limit for the maximum quantity. This can be overcome by using a secondary auxiliary blower either before or after the fan, and this provides the excess pressure for extending. One of these auxiliary blowers, for instance, is shown in Fig. 562 at the end of the test run.

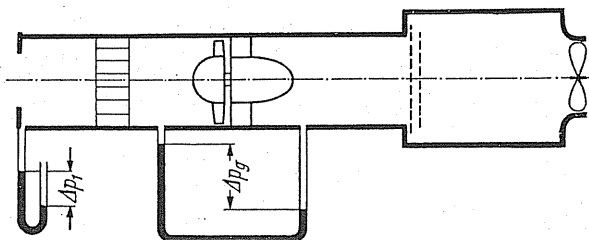


FIG. 562. Test-rig with suction fan on the delivery side of the main fan.

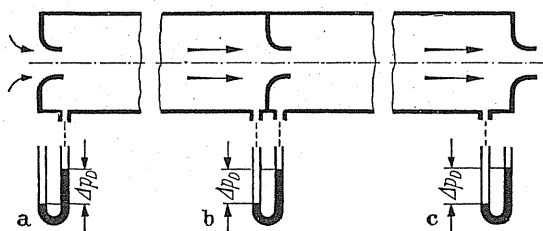


FIG. 563. (a-c) Various arrangements of nozzle.

The data required for measuring quantities are listed fully in the VDI flow measurement regulation. It may be pointed out in this connection that intake and outlet orifice plates in particular according to arrangement Fig. 563 occur just as often as the simple orifice plates. Delivery weight or volume is obtained from the pressure differences measured on the basis of the following formulae:

$$\begin{aligned} G_{\text{sec}} &= \alpha \varepsilon F \sqrt{2g} \sqrt{\gamma} \sqrt{\Delta p_D} \quad (\text{kg/sec}), \\ V_{\text{sec}} &= \alpha \varepsilon F \sqrt{2g} \sqrt{\frac{\Delta p_D}{\gamma}} \quad (\text{m}^3/\text{sec}). \end{aligned} \quad (304)$$

The coefficients α and ε are contained in the flow measurement regulation.

Quantity measurements are more difficult if it is impossible to carry out an orifice plate or nozzle measurement. Often it is impossible to fit a volume-throttling device in view of the low pressures of fans, because then the total volume flow would be altered decisively and the flow quantity might be considerably reduced. In cases like these only such measurements can be carried out which possess no resistance worthy of mentioning. For this purpose, for instance, a cross-section can be probed by means of a Prandtl-static tube. If a circular cross-section is involved, the cross-section is divided up into equal circular rings and the measurement is made in the centre of these annular elements. If the velocity is w in a ring of radial length r , then the quantity flowing through this ring is $dV = w 2\pi r dr$.

Hence the flow through the whole cross-section is

$$V = w_m r_a^2 \pi = 2\pi \int w r dr,$$

and here w_m is the mean velocity:

$$w_m = \frac{2}{r_a^2} \int w r dr = \frac{1}{r_a^2} \int w d(r^2). \quad (305)$$

The amount rw can either be plotted against r and the area under this curve is obtained or w plotted against r^2 . Both methods are shown in Fig. 564 according to Gramberg.

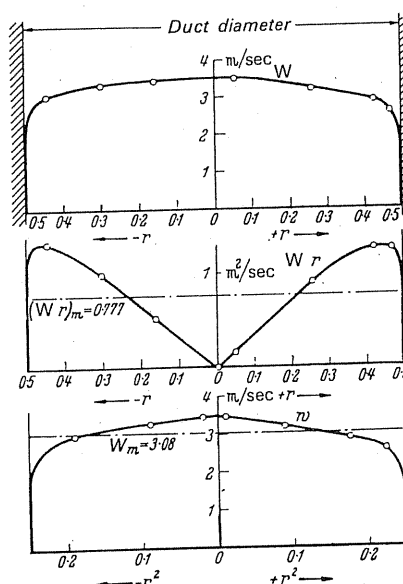


FIG. 564. Graphical determination of flow quantity from velocity distribution.

The method is convenient for two radii at right angles to each other and the mean value of a number of these measurements is obtained. In other cross-sections the area is subdivided into an equal number of areas and in the centre of each area a measurement is taken (Fig. 565). A problem in all these measurements is that a certain amount of time is taken up in probing the whole area with any kind of velocity gauge. During this time it is possible, due to operational causes, that the flow quantity may have altered. Fluctuations in flow will give wrong readings. The accuracy of the measurement due to this contingency is adversely affected.

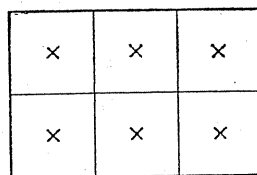


FIG. 565. Arrangement of measuring points in a rectangular duct.

The following simple method may be helpful. An anemometer is fastened to a bar and traverses the whole measuring cross-section for approximately a period of 2 min. Surprisingly good mean values are obtained by this method. For larger cross-sections the method can be improved still more by fitting anemometers at different places in the given cross-section of the duct.

Thermal method of quantity measurement. A very simple method of measurement, which is seldom used in practice, is a purely thermal method. It consists in supplying electrical thermal energy to a point through resistance wires which are laid transverse to the flow. A little downstream the temperature rise which has taken place in the meantime is then measured. If Δt is the temperature rise observed and Q the quantity of heat supplied in calories, G_L being the gas weight per second in kg this gives

$$Q = c_p G_L \Delta t; \quad G_L = \frac{Q}{c_p \Delta t}. \quad (306)$$

183. SOURCES OF ERROR IN PRESSURE MEASUREMENTS

Even the determination of the static pressure of a duct before or after a fan presents a large number of basic fundamental difficulties which are given below.

(a) UNEQUAL PRESSURE DISTRIBUTION IN THE DUCT CROSS-SECTION

A uniform static pressure distribution only takes place in a straight duct if the streamlines are straight as shown in Fig. 566. Medium turbulent fluctuations have no effect and also the velocity distribution can be ideal. The *essential* condition is that the flow streams be straight.

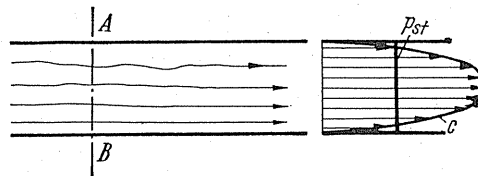


FIG. 566. Pressure and velocity distribution at steady flow.

With a strong one-sided velocity distribution it is always found that the static pressures vary throughout the cross-sectional area. This can only be explained by the fact that the streamlines are *curved* and thus *centrifugal forces* perpendicular to the flow alter the pressure. At a throttling point as shown in Fig. 567 the curvature of the streamlines is obvious in cross-section AB. To have an approximate guide it can be assumed that in Fig. 567 the streamlines have a mean radius of curvature $R = 2.5d$. Under this assumption the pressure

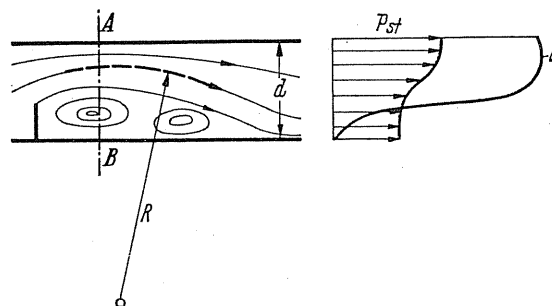


FIG. 567. Pressure and velocity distribution with non-steady flow. In cross-section AB the pressure and velocity distribution are shown on the right.

differences in the cross-section can be approximated. The pressure gradients due to centrifugal forces is

$$\frac{\Delta p}{\Delta r} = \rho \frac{c^2}{R}.$$

Thus we have

$$\Delta p = \Delta r \rho \frac{c^2}{R} = \Delta r \rho \frac{c^2}{2.5d};$$

substituting $\Delta r \approx d/2$,

$$\Delta p = \rho \frac{d}{2} \frac{c^2}{2.5d} = \frac{1}{2.5} \frac{\rho}{2} c^2 = 0.4 \frac{\rho}{2} c^2. \quad (307)$$

This means, however, that in the most unfavourable case in a cross-section static pressure variations of 40% of the velocity pressure can arise.

Similar conditions prevail if, according to Fig. 568, there are strong one-sided velocity differences possibly generated by a screen fitted at one side.

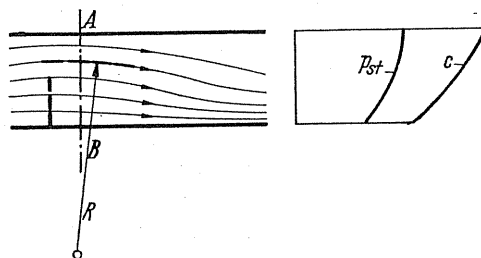


FIG. 568. Flow affected by screen (pressure and velocity distribution in cross-section AB on the right).

By turbulent mixing, equilibrium will occur in the flow subsequently. This, however, brings about a curvature in the flow as shown in Fig. 567. Owing to this curvature, the above-mentioned centrifugal forces with static pressure differences are generated.

Another case is one where the flow passing through experiences rotation. As long as the cross-section is round, no pressure differences can be found on the edges for reasons of symmetry. Towards the interior, however, the static pressure becomes lower since the

peripheral components of the velocities alter according to the rotational principle $rc_u = \text{const.}$ Where the cross-section, however, is not round but almost square as shown in Fig. 569, pressure difference may also be found along the sides according to whether the measurement is taken in the centre or more to one side. Figure 569 shows the pressure difference thus obtained.

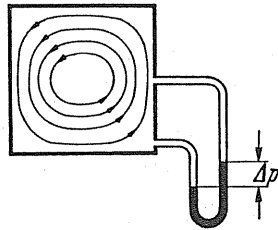


FIG. 569. Rotational flow in duct.

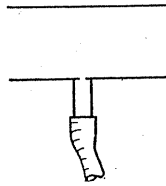


FIG. 570.

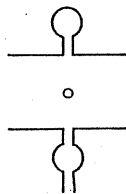


FIG. 571.

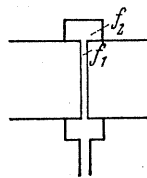


FIG. 572.

FIGS. 570–572. Static pressure measurements.

If the pressure measurement at one point through a test hole does not always ensure that a static pressure will be found which corresponds to the mean value, then by means of certain measurements a good mean value can be measured, nevertheless, in the cross-section at pressure differences which are not too high. For this purpose, in accordance with Fig. 571 holes are drilled at several points at the same cross-section and the pressure taken from these

points into a hollow ring which is then bled off at one point for the measurement of the pressure. In these cases an annular chamber in accordance with Fig. 572 is a better proposition. This, however, is only reliable if $f_1 < f_2$.

(b) UNEQUAL PRESSURE DISTRIBUTION ALONG THE DUCT WITHOUT LONGITUDINAL VORTICES

When choosing a measuring point for pressure, the problem often arises at what point of the duct the measuring point shall be set. For pressure measurements before or after the fan, opinion tends to the measuring point being sited as close as possible to the fan, because any resultant frictional losses justifiably are not wanted to be attributed to the fan. However, these frictional losses actually play a lesser part than other manifestations, which are usually ignored.

In front of and behind the fan there are unstable velocity distributions which are more or less irregular. Unstable velocity distributions are understood to be those which deviate from the ultimate turbulent velocity distributions. Owing to bends in front or owing to uneven energy distribution, for instance, very often heavily one-sided velocity distributions are present in the outlet throat of a spiral housing. In such cases it has been found that the uneven velocity distribution straightens itself slowly downstream and the static pressure *rises*, more or less rapidly. Only when equilibrium has been reached does the static pressure drop slowly—again due to the effect of wall friction. In certain cases in the duct the pressure first rises and then drops.

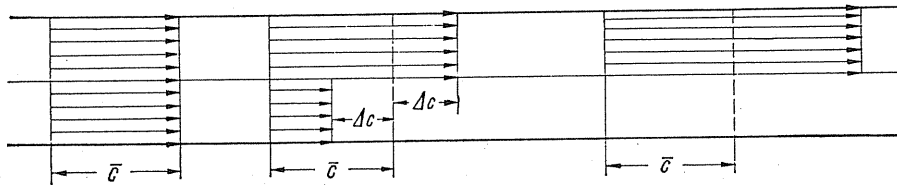


FIG. 573. Pressure distribution on periphery of the duct.

In order to obtain a fundamental simple outline of the problem we will assume in accordance with Fig. 573 that in a rectangular duct the flow through one half of the cross-section is such that a velocity $c + \Delta c$ is present, and in the other half of the cross-section there is a velocity lower by Δc . The kinetic energy flowing through the total cross-section in the unit of time then amounts to

$$E = \sum \Delta V \frac{\rho}{2} c^2 = \frac{V}{2} \frac{\rho}{2} (\bar{c} + \Delta c)^2 + \frac{V}{2} \frac{\rho}{2} (\bar{c} - \Delta c)^2 = V \frac{\rho}{2} \bar{c}^2 + V \frac{\rho}{2} \Delta c^2.$$

Hence, with $\bar{E} = V(\rho/2) \bar{c}^2$, gives a positive

$$\begin{aligned} \Delta E &= V \frac{\rho}{2} \Delta c^2 \\ \frac{\Delta E}{\bar{E}} &= \left(\frac{\Delta c}{\bar{c}} \right)^2. \end{aligned} \quad (308)$$

Therefore, through the irregularity of flow compared to uniform flow there is a kinetic energy increased by $V (\varrho/2) \bar{c}^2$. If, for instance, $(\Delta c)/2 = \frac{1}{2}$ we have a $(\Delta E)/E = (\frac{1}{2})^2 = \frac{1}{4}$, i.e. a 25% variation in velocity pressure. With any irregularity, no matter how it appears individually, an increase of kinetic energy of this kind is available. If in the further course of the flow, equilibrium is again reached, then the maximum of this increase of energy *can be recovered as an increase in static pressure*. This means, however, that the static pressure must rise in these cases. Under such circumstances it would therefore be improper to measure the pressure directly after the fan. The measuring point must be set further downstream.

When measuring after the fan a pressure *lower* by $(\varrho/2) \Delta c^2$ is measured. *The reverse is the case for measurements in the suction side of duct, and too large a value is measured* because pressure below atmosphere is present at that point. The errors in differential pressure measurements between suction and pressure sides *may be reduced* and in the most favourable case can be cancelled. In order to avoid uncertainties such as these the pressures should be measured at a little distance away from the fan.

There is still the problem as to how far downstream or how far upstream of the suction opening the measuring point for pressure should be sited. According to measurements carried out for similar problems, the maximum pressure rise is only reached at about 8 times the duct diameter. In practice, for taking into account the main effect distances of 2–4 duct diameters are ample. There is a lower limit to this because in the case of uniform velocity distribution, such as is present, for example, in high class fans in the vicinity of the outlet, the best efficiency is available. The pressure drop by duct friction would constitute a counteracting source of error. According to the formula for losses in a pipe,

$$\Delta p = \lambda (l/d) (\varrho/2) \bar{c}^2,$$

a pressure drop of the magnitude $\Delta p \approx 0.1 (\varrho/2) \bar{c}^2$ is found for instance for $l = 3d$ and $\lambda = 0.03$. In other words it is one-tenth of the velocity head which is obtained from the average velocity in the pipe.

These considerations show what care has to be taken in pressure measurements for fans. Not taking account of these facts could lead to inaccuracy of efficiency calculation by 5–10%.

(c) PRESSURE MEASUREMENT OF ROTATIONAL FLOW

In many cases the flow is rotational with the vortex axis in the centre of the pipe. Axial-flow fans have this type of flow. Therefore, we will have to deal with it. This is all the more necessary since if the following aspects are not taken into consideration a completely erroneous assessment of an axial flow fan is obtained. The danger is that the calculated efficiency would be too high and would have no practical meaning. Even if the discharge flow from an axial-flow fan is free of rotation from the design points, a rotation would still remain in cases of variable delivery volume, i.e. smaller or larger volumes, since guide arrangement can be designed completely free of rotation for a specified throughput only. This is the reason why almost *in every case* a certain swirl remains in the flow.

By considering the flow after the guide vanes of an axial-flow fan, we find the conditions represented in Fig. 574. If there is rotation present the c_u components increase from the outside to the inside, the meridional velocity c_m is generally constant or approximately constant, whilst the static pressure increases towards the outside. Although all streamlines have the same flow energies, this horizontal pressure increase is helped by the centrifugal forces of the c_u component. If this component is c_{iu} on the inside and c_{au} on the outside, then the pressure difference is $\rho/2 [c_{iu}^2 - c_{au}^2]$. If the static pressure is now obtained through a pressure tapping in the wall of the duct the *increase in pressure mentioned before is measured simultaneously*. By traversing the cross-section with a probe, a static pressure distribution approximately as shown in Fig. 575 is obtained. In the centre there is clearly a "depression". The mean static pressure resulting from this type of measurement is variably assessed as the actual pressure level. This method, however, is not very accurate as the equalisation can vary according to the shape of the following duct.

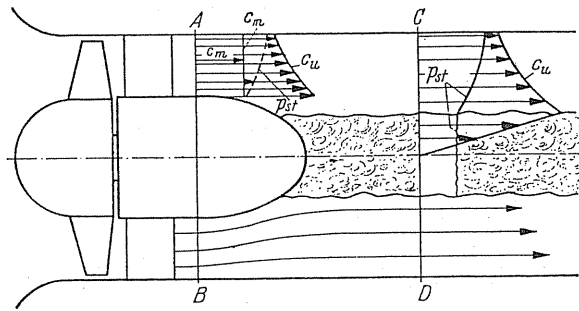


FIG. 574. Pattern of flow after downstream guide vanes of an axial-flow fan.

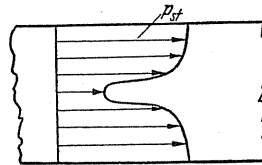


FIG. 575. Static pressure distribution due to rotational flow.

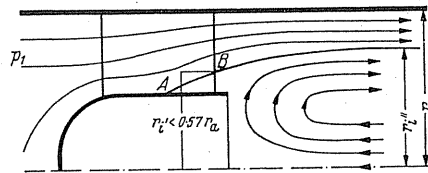


FIG. 576. Velocity distribution after guide vanes.

Flow separation from the central core as shown in Fig. 576 is also observed in fixed guide vanes.

The practical question then arises as to whether the pressure thus measured, which is greater than the internal pressure, has any real significance or remains constant downstream, independent of the wall friction. For this reason we have to deal with this problem

or at least endeavour to obtain an answer which is useful for practical purposes. *How important this question is can be gathered from the fact that for axial-flow fans differences in efficiency of 10% or more may be involved if this condition is taken into account or not.* This is particularly the case if—as always occurs with fans—the dynamic part of the total pressure energy is not ignored. Moreover, here we have the crucial point where the scientist differs from the practical man. The former is justified in pointing out that the total energy after the fan can be attributed to the fan whilst the practical man contends that the customer is deceived thereby, since he cannot make any more use of the rotational energy he has accepted, and “apparent efficiency” of this kind in the axial-flow fan is only interesting from a theoretical point of view.

It would now appear that according to later observations a portion of the rotational energy is recovered whilst the major portion probably will have to be regarded as lost. Indirectly the rotation can still be of benefit as the efficiency of a following diffuser can be improved. The phenomena of vortex core formation and reversal of rotational flow have already been mentioned.

(d) MAGNITUDE OF ERROR

When investigating fans and particularly when assessing the efficiency, considerable error may occur due to the measuring methods and the choice of instruments used. In the common types of pressure gauges approximately the following accuracy of readings can be assumed.

Pressure gauge type	Reading accuracy (mm)
Single U-tube	1
Sloping tube manometer	0.5
Betz or Debro manometer	0.1

The air power $L = V \Delta p_{\text{tot}}$ is made up of the products of two quantities V and Δp_{tot} which are both determined by means of pressure gauge measurement. To determine the inaccuracy in a measurement we examine the alteration of power if small alterations of V and Δp_{tot} occur through measuring faults. For this we have the expression

$$\Delta L = \Delta p_{\text{tot}} \Delta V + V \Delta \Delta p_{\text{tot}}.$$

The percentage variation therefore is

$$\frac{\Delta L}{L} = \frac{\Delta V}{V} + \frac{\Delta \Delta p_{\text{tot}}}{\Delta p_{\text{tot}}}.$$

This formula means that the errors in measuring the volume and the pressure are additive.

As the volume throughout is determined by means of nozzles, orifice plates and similar appliances according to the relationship

$$V = \alpha \varepsilon F \sqrt{\frac{\Delta p_{\text{nozzle}}}{\rho/2}} = C \sqrt{\Delta p_{\text{nozzle}}},$$

we then obtain

$$\frac{\Delta V}{V} = \frac{1}{2} \frac{\Delta p_{\text{nozzle}}}{\Delta p_{\text{nozzle}}}$$

The final formula is expressed as

$$\frac{\Delta L}{L} = \frac{1}{2} \frac{\Delta p_{\text{nozzle}}}{\Delta p_{\text{nozzle}}} + \frac{\Delta p_{\text{tot}}}{\Delta p_{\text{tot}}} \quad (309)$$

(the individual error calculation for the nozzle and overall pressure calculation was tabulated by Ing. Bommer). In order to ascertain average condition let us assume that the effective pressure of the nozzle is half as great as the total pressure, i.e. $\Delta p_{\text{nozzle}} = 0.5 \Delta p_{\text{tot}}$. Furthermore, it will be defined that $\Delta p_{\text{tot}} = \Delta p_{\text{stat}}$, and if a dynamic part is present, this part must be determined through the nozzle measurement where there is a small deviation which is not so important for the overall picture.

Using these assumptions the following situation for different total pressures emerges:

ERROR IN PERCENT OF POWER MEASUREMENT

Pressure to be measured in mm WG	40	80	200	400
U-tube	5	2.5	1	0.5
Sloping manometer	2.5	1.25	0.5	0.25
Betz or Debro manometer	0.5	0.25	0.1	0.05

This table is instructive. If the measuring accuracy of 0.5% is called for, this can only be achieved by means of the Betz manometer at pressures of 50 mm WG. Simple U-tubes only provide this accuracy at a pressure of 400 mm WG. It follows, therefore, that with almost all fans a satisfactory accuracy can only be achieved if measurements are taken with Betz or Debro manometers. This finding opens up problems in many industrial measurements.

It is obvious from the above formula that volumetric measurements and pressure measurements in themselves are not very reliable. In measurements of volume the errors are half those in measurement of pressure. Therefore in the measurement of power, since two pressures have to be measured, accuracy would have to be greater than when a single volume measurement is made in order to achieve equivalent accuracy. These values are substituted in the last formulae for the values

$$\Delta [\Delta p_{\text{nozzle}}] \quad \text{and} \quad \Delta [\Delta p_{\text{stat}}].$$

184. REASSESSMENT

By enlarging the dimensions and increasing the *Re*-number there is an improvement in efficiency. Since tests on large unit installations seldom can be carried out with accuracy, tests on models are carried out initially and the rise in efficiency when developing the proto-

type must be determined or estimated. The mathematical relationships of this so-called reassessment, therefore, are extremely important in fan engineering.

Hitherto usually the reassessing formulae by Pfeleiderer and Ackeret were used in calculations:

$$\frac{1 - \eta_2}{1 - \eta_1} = \left(\frac{Re_1}{Re_2} \right)^\alpha \text{ Pfeleiderer; } \frac{1 - \eta_2}{1 - \eta_1} = \frac{1}{2} + \frac{1}{2} \left(\frac{Re_1}{Re_2} \right)^{2\alpha} \text{ Ackeret,} \quad (310)$$

generally making use of $\alpha = 0.1$. It has, however, been found that a considerably lower value of exponent α than $\alpha = 0.1$ is obtained with higher Re numbers. This extreme variation of the exponents point to the fact that the true mathematical relationship cannot be correctly assessed with the formulae mentioned above.

Rütschi⁽²⁾ pointed out that the reference of the Re number to the outlet diameter cannot be correct because without doubt the pressure head but not the volume flow is a function of the outlet diameter. The inlet diameter of the impeller D_s detects the volume flow better. This is obvious from an illustration by Rütschi in which first the outlet diameter and then the inlet diameter have been taken as the abscissae of the efficiencies. Whereas for the first case (Fig. 577) curves are obtained, in Fig. 578 all data fall on one curve which shows that the inlet diameter is the correct parameter.

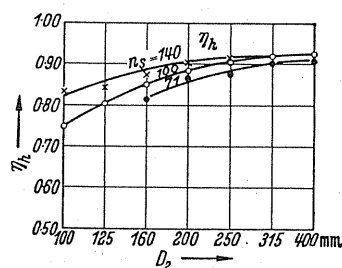


FIG. 577. η_h as a function of the outlet diameter D_2 .

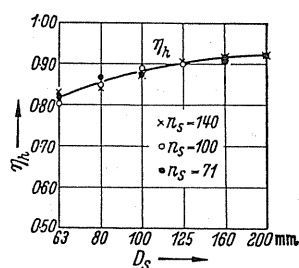


FIG. 578. η_h as a function of the inlet diameter D_s .

Rütschi also found there are two kinds of reassessment. The less accurate one occurs if the same machine is operated with different Re numbers, for instance by varying the pressure of the flow medium while the more accurate reassessment is observed when various

² Rütschi, K., Reassessment of efficiency of flow machines. Behaviour of an individual machine and a range of machines of different sizes, *Schweiz. Bauztg.*, 1958, p. 603.

sizes of machines are compared with each other. In the first case a maximum is rapidly achieved whilst the second form of reassessment displays a significantly larger values. Figure 579 shows this very clearly. This leads us to the realisation that the former viewpoint is incorrect and air pressure alterations on the same model, i.e. geometrically similar machines, give the same results as in increasing the impeller diameter.

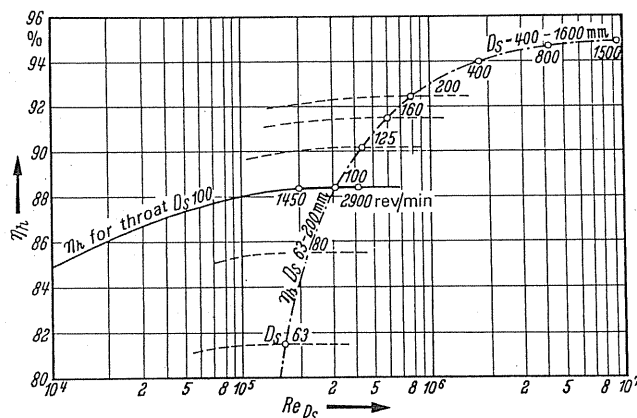


FIG. 579. Evaluation of efficiencies of a particular machine and a series of geometrically similar machines.

Whilst comprehensive test data are available on centrifugal pump and hydraulic machines by means of which the latest viewpoint can be expressed by formulae, there is at present in fan engineering still no possibility of obtaining similar absolutely reliable data. Unfortunately it is not possible simply to calculate without accurate tests. This is due to the fact that the surface structure of most welded constructions shows different friction factors in the transitional field of the Coolebrock's curve than the cast-iron surfaces in centrifugal pumps.

185. TEST EQUIPMENT

Pressure measurements. The accurate measurement of pressure governs all air measurements on fans. According to requirements simple U-tubes, water-filled, can be used in this case, with the glass tube diameter not less than 12–15 mm, or also an Askania-type water-level meter, a measuring device by Reichardt for smaller pressures, an immersion pointer, and, in particular, the Betz manometer or Debro miniscope for routine test plant measurements.

Spot-check speedometers are particularly suitable for speed measurements; also stroboscope instruments with electronic flash lighting are coming more and more into favour.

By dynamometer is probably the best method for measuring power. Figure 580 shows a dynamometer developed by the author in which the outer bearing housings supporting the motor can be moved in opposing directions. In this way a sensitivity of bearings similar to that of the knife-edge bearings is achieved. This device is very convenient particularly for zero

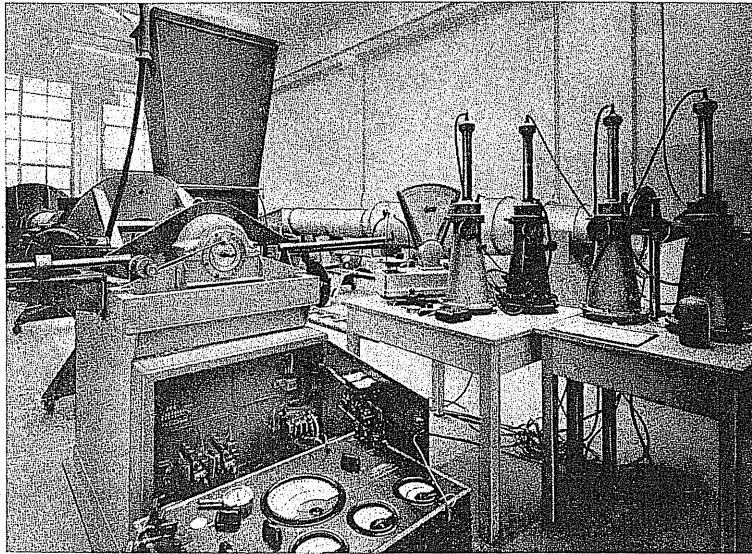


FIG. 580. Dynamometer designed by Eck. Test-rig of Messrs. Büttner-Werke AG.

setting. A direct indication can also be obtained if, for example, the dynamometer as shown in Fig. 581 is designed as a pendulum and the deflection is shown by means of a suitable pointer.

The test rig. When it is possible to carry out accurate measurements on the test rig it is absolutely essential to apply the flow measurement rules accurately. By observing every rule an accuracy of 1–2% can be achieved. Whether extracting or blowing operations or

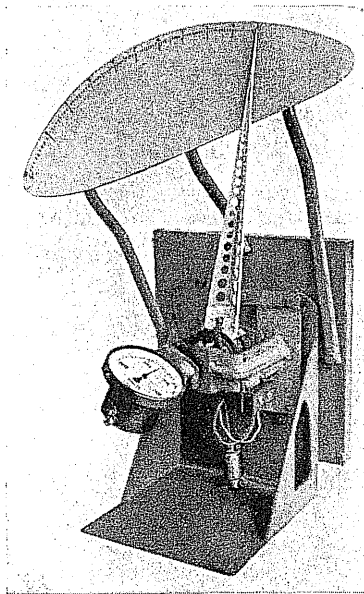


FIG. 581. Small fan test-rig with directly indicating dynamometer.

mixed operation are selected on the test rig is immaterial. The free suction (blowing operation) or free discharge (extracting operation) is a practical advantage since the blower is not situated in between but *at the end* of the measuring lines, and alterations to the fan or changing of impeller can be carried out without dismantling the duct. In addition, the open side is very convenient for observing flow with streamers or suitable probes. Throttling dampers and screens are used for altering the resistance. If the throttling device is situated at the end of the pressure duct a movable "valve plate" or even an iris diaphragm can be provided. These *symmetrically* acting throttling devices are known to require smaller free duct lengths if, for instance, influence on the previous nozzle or orifice is to be avoided.

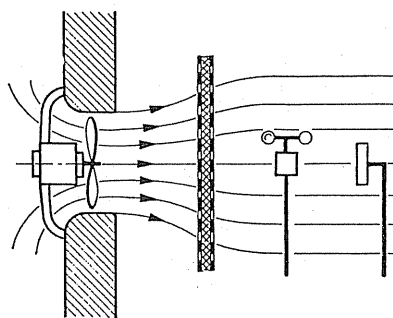


FIG. 582. Measurement of the flow from the fan.

Conditions are difficult if the free stream has a rotation for instance in free discharging axial-flow fans. Figure 582 shows some streamlines at some distance behind the fan where there is a light filter, the duty of which is to eliminate the rotation and to make the flow smooth. The elimination of the rotation can be still improved perhaps by means of one or two plates in front of the filter. A number of screens can be used, or a light packing made of slag wool which is held between wide mesh screens. The low speeds available after the filter is fitted are best measured by means of anemometers. The lateral expansion of the stream extended through the filter has to be probed. Freedom of rotation is best tested by means of rotation gauges, for instance small surfaces of thin plate or drawing paper revolving in the centre of their plane.

The term much used in practice of equivalent diameter would encourage the idea of using the outlet cross-section of a fan adjustable by means of an end plate, for provisional volume measurement, as shown in Fig. 583 (top). This is not feasible, however, because the contraction of the stream alters it fundamentally. If, in accordance with Fig. 583 (bottom) a movable bent plate in the shape of a nozzle is used, then a fairly useful measuring nozzle is obtained.

Often the question is asked whether the failure of a fan can be attributed to the impeller or the housing. For establishing such faults a measuring tube⁽³⁾ provided with a small bore, as shown in Fig. 584, can be arranged to move around the periphery behind the impeller. The measuring tube connected to a manometer must be moved until the maximum value

³ This total pressure measurement directly behind the impeller gives a mean value which will differ from the correct value if the blade channels contain separation and dead spaces, which periodically affect the observation, not insignificantly, i.e. wheels with a poor efficiency.

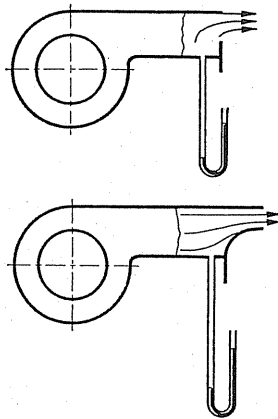


FIG.583. Experimental outlet nozzles.

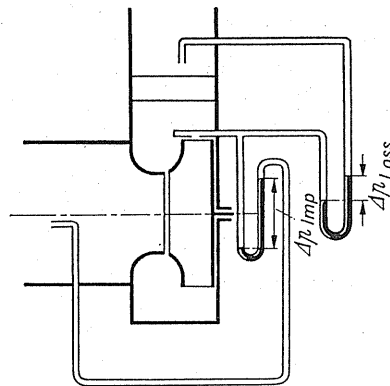


FIG.584. Total pressure measurement after impeller.

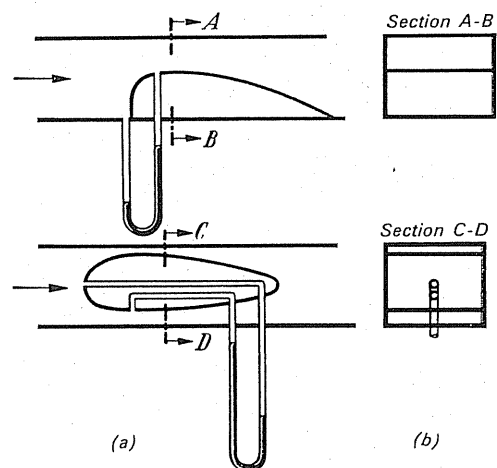


FIG.585. (a and b) Experimental venturi measurements in duct.

is observed. The pressure thus measured represents the total pressure after the impeller, exclusive of diffuser losses. If the measurement is associated with a pitot tube measurement in front of the fan, and another similar measurement at the pressure side of the fan, as shown in Fig. 584, the guide vanes and the spiral housing loss can be read immediately.

In rectangular ducts it is possible to provide a simple *venturi measurement* if, according to Fig. 585a, a plate bent to shape is attached at one side to a wall. By inserting a profiled filling element as shown in Fig. 585b (bottom), a symmetrical configuration can also be achieved. With adequately large effective pressure, i.e. at large contraction, measured values are obtained which are only a few per cent behind standard measurements.

CHAPTER XXV

MEASUREMENTS AND THEIR SOURCES OF ERROR

186. PRESSURE CURVE FOR THE DIFFERENT MEASURING METHODS

There are various possibilities of mounting fans. Fans are used for exhausting, for blowing, and for exhausting and blowing. They are also used as auxiliary delivery appliances at pressures either above or below atmospheric pressure. Besides these, there are the open suction and open discharging arrangements, for instance, for ventilating spaces. The diversity of arrangements for the fan assembly can cause some confusion. Therefore it would appear essential to give some distinct rules for eliminating erroneous measurements.

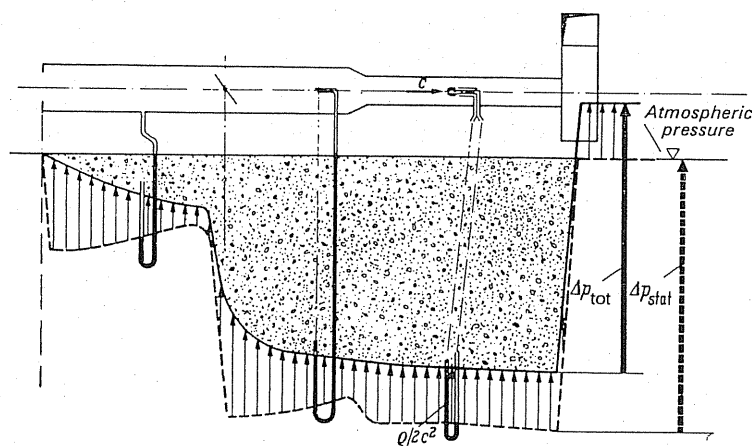


FIG. 586. Static and dynamic pressures and losses when measuring at the suction side of the fan.

The measurement at the suction side (Fig. 586) will be explained by a practical example. The pressures are plotted diagrammatically below the datum line which represents atmospheric pressure. Let us assume that the pressure will be traversed in the whole length of the duct by using a tube facing the flow, i.e. a pitot tube. The pressure thus obtained is, in every case, identical with the total pressure, i.e. the total energy content at this point. The indication of the instrument as a result of this traverse will be indicated by a thick line. Thus we have the total pressure curve. The losses which arise through friction and throttling are represented by the region between this line and the datum line. After this first measurement

we shall allow another instrument to traverse the duct which will indicate the static pressure measured through the hole drilled in the wall. For this purpose a simple pressure probe may be used. In this way we obtain the thick dotted line which lies below the total pressure line. Finally, a third traverse will be carried out by means of a Prandtl pressure tube. This instrument shows a pressure difference at every point which corresponds exactly to the distance between the full and dotted lines. This theoretical argument makes everything clear. The thick arrow represents the total pressure difference which the fan produces, whilst the dotted arrow gives the static pressure difference of the fan. Since there is still some velocity energy present at a free discharge, the arrow of the total pressure lies above the atmospheric pressure by this amount.

In every case the procedure is similar. For measurements in a blowing system all pressure measurements are shown above the datum line. The losses reappear in the same form. For this case the following rules can be given as follows. If a parallel line is drawn in the highest total pressure, the distance up to the total pressure line is the actual loss.

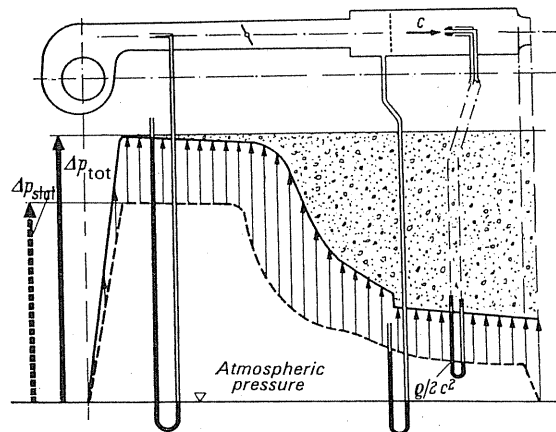


FIG. 587. Pressure curve for measurement on the blowing side of a fan.

The second case shows a fan with free suction and only loaded at the pressure side (Fig. 587).

The third case in which the fan is situated between the suction and the pressure measuring duct is shown in Fig. 588. This case enables the rule to be defined for determining the losses. The position of highest total pressure shall be sought across the fan. Therefore, a horizontal line is drawn on the outlet and the actual loss is obtained by the distance from this horizontal line to the total pressure line. The remaining rules are exactly the same as before.

To enable the pressure conditions to appear clearly the case will be dealt with where the fan is working in a network of ducts where overall pressure is below atmospheric (Fig. 589). Here, again, using our three measuring instruments the same traverses are carried out and we obtain a full line (total pressure) and a dotted line (static pressure curve). Subsequently we obtain the total pressure maximum across the fan and it appears between two horizontal lines. The difference between these represents the actual loss. The line representing the considerably higher atmospheric pressure appears very clearly here incidentally as a datum

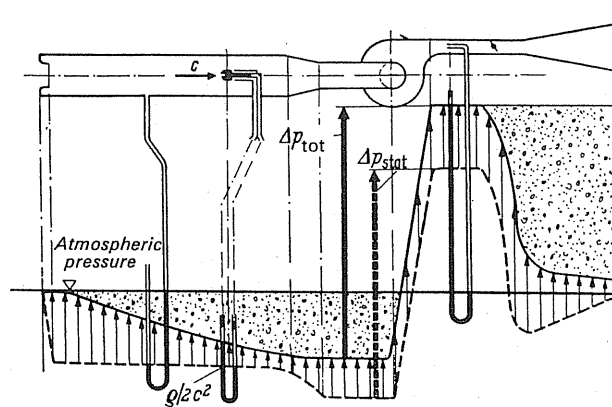


FIG. 588. Pressure curve for measurement on the suction and the blowing sides of a fan.

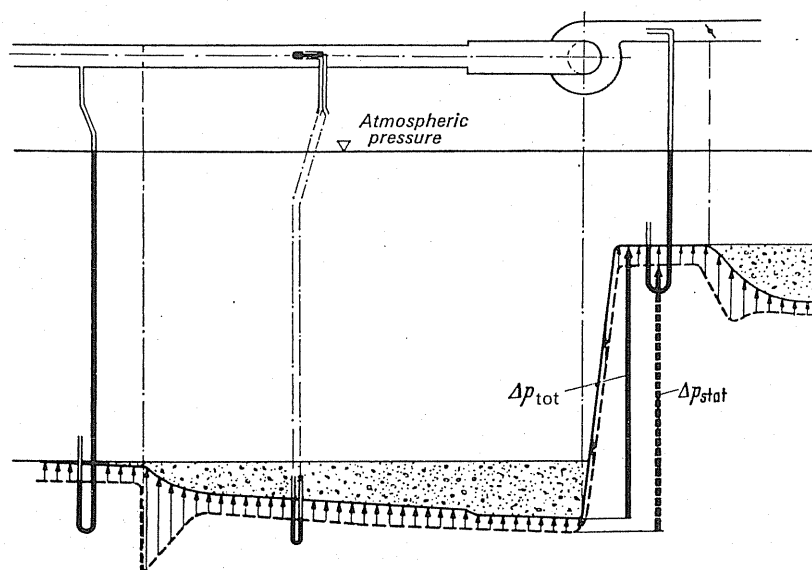


FIG. 589. Pressure curve for measurement on the suction and the blowing sides, when the duct system is below atmospheric pressure.

line. If the fan were only working in a pressure above atmospheric the lines would only run upwards. We, therefore, maintain that the pressure curves of the fan are independent of the position of the datum line. The significance of pressure above and below atmospheric will be clearly appreciated from the illustrations.

In Figs. 590 and 591 all measurements for the two cases are shown again separately. In one of them there is a pressure below atmospheric and the other pressure above atmospheric in the ducting tested. These illustrations should explain clearly the significance and the method used for these pressure measurements without specifying pressures in every case which might be confusing.

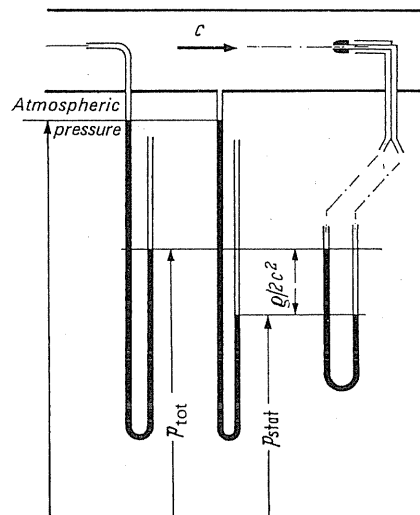


FIG. 590. Total pressure, static pressure, and dynamic pressure, when the duct system is below atmospheric pressure.

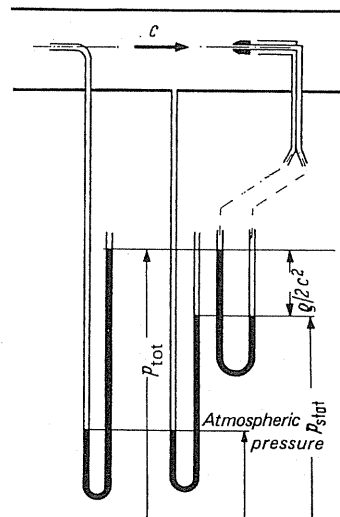


FIG. 591. Total pressure, static pressure, and dynamic pressure, when the duct system is above atmospheric pressure.

Particular reference should be made to the distinct difference between total pressure and the purely static pressure difference in fans. Figure 592 illustrates the possible instances. According to whether the discharge cross-section of a fan is greater, equivalent or smaller than the inlet diameter, the static pressure difference produced by the fan may be smaller, identical, or larger than the total pressure. This demonstrates clearly that the static pressure need not be identical to the total pressure. This should be taken into account when preparing specifications.

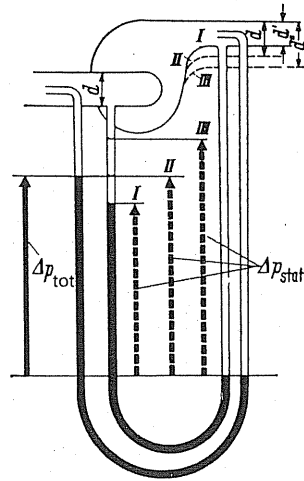


FIG. 592. Total pressure and static pressure difference of a fan at varying cross-sections of outlet.

187. MECHANICAL POWER MEASUREMENTS

Usually the shaft power is obtained from the following formula:

$$L_w = M_d \omega \text{ (kgm/sec),} \quad (311)$$

it will be observed from Fig. 593 that $M_d = Gl$.

$\omega = (\pi n)/30$ is a well-known formula.

Equation (311) may then be expressed as

$$L_w = Gl \frac{\pi n}{30} = \frac{\pi}{30} l n G.$$

$$L_w = KnG \text{ (kgm/sec).} \quad (312)$$

It is obvious from eqn. (312) that the speed n and the weight G at the balance need only be measured. The value of K is given from the design of the dynamometer.

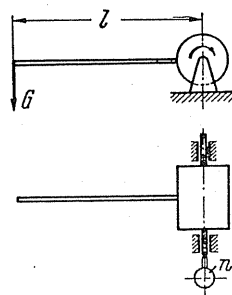


FIG. 593. Dynamometer.

188. ELECTRICAL POWER MEASUREMENT

Various methods are available for this and are summarised in Rules, VDE 0530.

The indirect measuring method for asynchronous motors is described below because in fan-engineering motors of this kind are mainly used.

The efficiency of the motor is found by determining individual losses. It is obtained from the ratio of the dissipated power N_w to power N_A absorbed.

$$\eta_{\text{mot}} = \frac{N_w}{N_A}. \quad (313)$$

N_A is measured in watts and is best achieved by means of the two-watt-meter method. According to this method we have

$$N_A = N_1 + N_2 = C_1 \alpha_1 + C_2 \alpha_2 \quad (\text{W}). \quad (314)$$

α_1 and α_2 are the indicated values of the instruments. C_1 and C_2 are the actual conversion factors, also called instrument coefficients.

The absorbed power N_A is fairly easy to determine but the shaft power N_w is more difficult and is lower than the sum of the individual losses by

$$N_w = N_A - \Sigma \text{loss} \quad (\text{W}). \quad (315)$$

Hence these losses have to be determined.

For this we require (a) a no-load test, and (b) a load test.

The no-load test. The iron and friction losses are determined by means of this test and these are independent of the load.

Let

$$N_0 = V_{\text{Fe}} + V_R + V_{\text{Cu1}} \quad (\text{W}), \quad (316)$$

where N_0 is the total loss at no-load, V_{Fe} is the iron losses, V_R is the friction and fan losses, and V_{Cu1} is the copper losses in the stator.

Equation (316) can be rearranged to give

$$V_{\text{Fe}} + V_R = N_0 - V_{\text{Cu1}} \quad (\text{W}). \quad (317)$$

The friction losses (V_R) are very small and in the first approximation can be grouped along with the iron losses.

Hence

$$V_{\text{Fe}+R} = N_0 - V_{\text{Cu1}} \quad (\text{W}). \quad (318)$$

The copper losses in the stator V_{Cu1} are obtained from the phase current and phase resistance. Using Ohm's law this gives

$$U = JR \quad (\text{V}). \quad (319)$$

The power loss is

$$N = UJ \quad (\text{W}). \quad (320)$$

Equation (319) substituted in (320) gives

$$N = J^2 R \quad (\text{W}). \quad (321)$$

Two different cases emerge:

(a) The motor is connected in star. Then the measured phase current J is expressed by J_φ and the phase resistance R by R_φ .

For all three phases the power loss is then expressed as

$$V_{\text{Cu1}} = 3J_\varphi^2 R_\varphi \quad (\text{W}). \quad (322)$$

(b) The motor is connected in delta. For J we have to substitute $(J_\varphi/\sqrt{3})$, and thus we obtain

$$V_{\text{Cu1}} = 3 \left(\frac{J_\varphi}{\sqrt{3}} \right)^2 R_\varphi = J_\varphi^2 R_\varphi \quad (\text{W}). \quad (323)$$

R_φ is best measured after the no-load using a Wheatstone bridge.

The copper losses in the rotor are equal to zero because there is practically no slip present in no load.

According to eqn. (318) only the sum of the iron and the friction losses is obtained from the no-load test. It should be observed that the friction losses can also be separated from the iron losses. This is obtained by measuring the no-load power at constant speed with variable

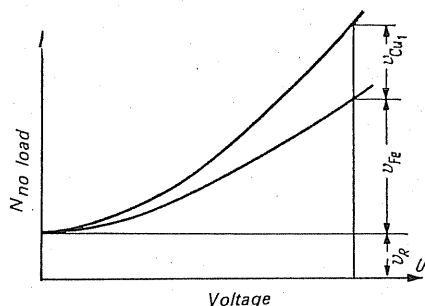


FIG. 594. Losses in conditions of no-load at variable voltages.

voltage and recording the voltage (Fig. 594). At the point of intersection with the ordinates the loss portion of the friction can then be read independently of the voltage.

The iron losses act similarly to the squares of the voltages (Fig. 594).

$$\frac{V_{\text{Fe1}}}{V_{\text{Fe2}}} = \left(\frac{U_1}{U_2} \right)^2. \quad (324)$$

The load test. In motors under load the iron and friction losses are of the same magnitude as in no load. The copper losses in the stator V_{Cu1} due to the higher phase current J , however, are considerably higher. In this case as in the no-load test they are calculated according to eqn. (322) or (323).

In addition to the losses previously described there are the copper losses in the rotor V_{Cu2} and the auxiliary losses V_Z .

In the load test due to the slip present the copper losses V_{Cu_2} are no longer equal to zero. In general the formula

$$V_{Cu_2} = s N_\delta \quad (W) \quad (325)$$

applies where N_δ is the air-gap power and s the motor slip.

The air-gap power is determined by subtracting the copper, iron, and friction losses from the power N_A supplied:

$$N_\delta = N_A - (V_{Fe+R} + V_{Cu_1}) \quad (W). \quad (326)$$

The motor slip s can be determined from the ratio of the so-called slip speed to synchronous speed:

$$s = \frac{n_0 - n}{n_0}. \quad (327)$$

Here n_0 is the synchronous speed (3000, 1500, etc.), i.e. the speed of the rotating field divided by the number of pairs of poles, and n the measured speed of the motor. By substituting eqns. (326) and (327) in eqn. (325) we obtain

$$V_{Cu_2} = \frac{n_0 - n}{n_0} [N_A - (V_{Fe+R} + V_{Cu_1})] \quad (W). \quad (328)$$

Equation (328) gives us the copper losses in the rotor. The auxiliary losses V_z individually are undetectable and as a rule are assumed at 0.5% of the power N_A absorbed:

$$V_z = 0.005 N_A \quad (W). \quad (329)$$

By grouping all losses together we obtain for eqn. (315)

$$N_w = N_A - (V_{Fe+R} + V_{Cu_1} + V_{Cu_2} + V_z) \quad (W). \quad (330)$$

N_w is the shaft power dissipated by the motor which is identical to the shaft power of the fan if the motor is coupled directly to the rotor of the fan.

THE EFFICIENCY

The reader will have noticed that in dynamometer measurements the shaft power is designated by L_w and in the electrical measurement by N_w .

This is explained by the fact that within the scope of this section L is always understood to be the power in kgm/sec, and N the power in watts.

The relationship between L and N is the following:

$$1 \text{ kgm/sec corresponds to } 9.81 \text{ W.}$$

This should be observed in determining the efficiency of a fan.

$$\eta = \frac{L_n}{L_w} = \frac{N_n}{N_w} = \frac{9.81 L_n}{N_w} = \frac{N_n}{9.81 L_w},$$

where L_n is the output power in kgm/sec, N_n is the output power in watt, L_w is the input power in kgm/sec, and N_w is the input power in watt.

189. EXAMPLES OF AN ACCEPTANCE TEST

Verifying the technical data of a fan as guaranteed by the manufacturer:

$$V_h = 4500 \text{ m}^3/\text{h at } n = 2600 \text{ rev/min,}$$

$$\Delta P_T = 130 \text{ mm WG, } \gamma = 1.2 \text{ kg/m}^3, \eta_T = 83.0\%,$$

and determining a blower characteristic for two different speeds. (The $\Delta p - V$ curves for $n_1 = 2770 \text{ rev/min}$ and $n_2 = 1860 \text{ rev/min}$ were applied.)

(a) TEST ARRANGEMENT

The arrangement of the measurements is according to the "VDI flow regulations DIN 1952" and the "Rules for power tests on fans".

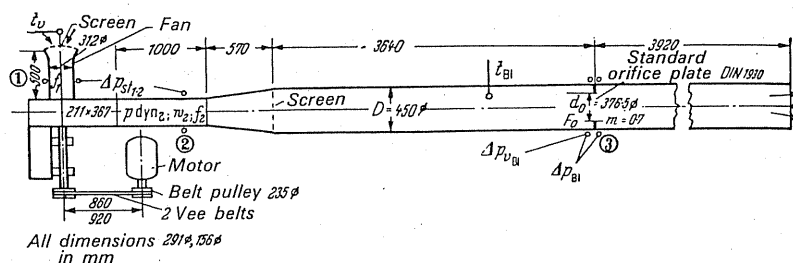


FIG. 595. Sketch of test arrangement.

(b) DESCRIPTION OF MEASUREMENTS CARRIED OUT AND THEIR EVALUATION

Determination of effective power. Let

$$L = G_{(\text{sec})} H_{(\text{kgm/sec})} \text{ or } N_n = 9.81 G_{(\text{sec})} H \text{ (W).}$$

1. Volume delivered at inlet and outlet.

$$G_{\text{sec}} = \alpha \varepsilon F_0 \sqrt{2g} \sqrt{\gamma_{B1}} \sqrt{\Delta p_{B1}} \text{ (kg/sec).}$$

$\alpha = 0.802 = \text{const}$ for $Re > 300,000$ and $m = d_0^2/D^2 = 0.7$. Since for all flow measurements of this test $Re < 300,000$, α is below the constant value. $\alpha = f(Re)$ was determined periodically

$$\varepsilon \approx 1 \text{ for } \Delta p_{B1} < 100 \text{ mm WG.}$$

$$F_0 = 0.1112 \text{ m}^2.$$

Hence we have

$$G_{\text{sec}} = \alpha \times 0.4923 \sqrt{\gamma_{B1}} \sqrt{\Delta p_{B1}} \quad (\text{kgm/sec}).$$

$$\gamma_{B1} = \frac{P_0 + \Delta p_{vB1}}{R_\varphi T_{B1}} \quad (\text{kg/m}^3)$$

$$\gamma_1 = \frac{P_0}{R_\varphi T_1} \quad (\text{kg/m}^3); \quad \gamma_2 = \frac{P_0 + \Delta p_{st2}}{R_\varphi T_2} \quad (\text{kg/m}^3),$$

$P_0 = B_a \times 13.6$ atmospheric pressure in mm WG.

Δp_{vB1} gauge pressure before the orifice plate.

R_φ gas constant for moist air.

T_{B1} absolute temperature before orifice plate.

T_1 absolute temperature at measuring point 1.

T_2 absolute temperature at measuring point 2.

Δp_{B1} effective pressure of orifice plate.

Δp_{st2} static pressure at measuring point 2.

Δp_{st1} static pressure at measuring point 1.

This gives

$V_1 = G_{(\text{sec})}/\gamma_1$ volume at measuring point 1.

$V_2 = G_{(\text{sec})}/\gamma_2$ volume at measuring point 2.

2. Delivery head or total pressure. According to eqn. (8) we have

$$H = \alpha \frac{\Delta p_t}{\gamma_1}$$

$$\Delta p_t = p_{t2} - p_{t1} = \Delta p_{st1,2} + \Delta p_{dyn}.$$

$$\Delta p_{dyn} = p_{dyn2} - p_{dyn1}.$$

From the values of the weight throughput ascertained and the delivery head the effective power $G_{(\text{sec})} H$ works out at

$$N = 9.81 G_{(\text{sec})} \frac{\Delta p_g}{\gamma_1} \alpha \times 10^{-3} \quad (\text{kW}).$$

Determination of shaft power. A three-phase motor made by Zimmermann Type DM 4000/4 No. 831392 was used for the test.

Motor plate.

$$U = 220/380 \text{ V}, \quad I = 15.2/8.8 \text{ A}, \quad N = 4.0 \text{ kW}, \quad \cos \varphi = 0.84,$$

$$n = 1420 \text{ rev/min.}$$

The power absorbed by the motor was measured by means of two wattmeters (double wattmeter method: see Hütte, *Electrical Measuring Methods*, vol. II).

The motor losses were determined according to VDE 0530/2.51, para. 58 III. For determining all the driving losses the following were essential:

- (a) A no-load test according to VDE 0539, para. 59 (without V-belts).
- (b) The different load tests according to VDE 0530 (paras. 61 and 63).
- (c) A no-load test as stated under (a) (with V-belts).

The shaft power is then expressed as:

$$N_w = N_A - \Sigma \text{ loss} = N_A - [V_{\text{Fe}+R} + V_{\text{Cu1}} + V_{\text{Cu2}} + V_Z + V_k]$$

$$V_{(\text{Fe}+R) \text{ no load}} = N_0 - V_{\text{Cu1 no load}} \quad V_{\text{Cu1}} = 3R_\varphi J_\varphi^2 \quad \text{for } \Delta \text{ star connection.}$$

$$V_{\text{Cu2}} = s N_\delta = \frac{n_0 - n}{n_0} [N_A - (V_{\text{Cu1}} + V_{(\text{Fe}+R)})].$$

$$V_{(\text{Fe}+R) \text{ load}} = \left(\frac{U_{\text{load}}}{U_{\text{no load}}} \right)^2 V_{(\text{Fe}+R) \text{ no load}}.$$

$$N_{\text{ab}} = N_\delta - (V_{\text{Cu2}} + V_Z)$$

$$\eta_{\text{mot}} = \frac{N_{\text{ab}}}{N_A}.$$

$$N_w = N_{\text{ab}} - V_k$$

$$\eta_{\text{v-belt}} = \frac{N_w}{N_{\text{ab}}} = \frac{N_{\text{ab}} - V_k}{N_{\text{ab}}} = 1 - \frac{V_k}{N_{\text{ab}}}.$$

Designation of individual losses.

- V_{Cu1} copper losses in stator.
- $V_{(\text{Fe}+R)}$ iron and friction losses.
- V_{Cu2} copper losses in rotor.
- V_Z supplementary losses ($0.005N_A$).
- V_k V-belt losses $= N_{0k} - [V_{\text{Cu1}} + V_{(\text{Fe}+R)}]$.
- N_{0k} no-load power with V-belts.
- N_0 no-load power without V-belts.
(Motor measurement on no-load.)
- R_φ phase resistance.
- s slip.
- N_δ Air-gap power.

The efficiency of the fan is

$$\eta_t = \frac{N_n}{N_w} = \frac{N_n}{N_{\text{ab}} - V_k}.$$

(c) TEST EQUIPMENT USED

For determining the effective power the following measuring equipment was used:

- 1 stationary barometer by Lambrecht.
- 1 aspiration Assmann psychrometer by Lambrecht.
- 3 Betz micro manometers with $\frac{1}{10}$ mm graduation.
- 2 thermometers with $\frac{2}{10}$ graduation.
- 1 spot check tachometer by Hasler, Switzerland.

For electrical measurement there were available:

- 1 three-phase current measuring board (circuit for two wattmeter method with current transformer) containing:

- | | |
|------------------------|--------------------------------------|
| 2 wattmeters | } quality grade manufacturer Gossen. |
| 2 current transformers | |
| 3 ammeters | |
| 2 voltmeters | |

- 1 Wheatstone measuring bridge by Hartmann and Braun.

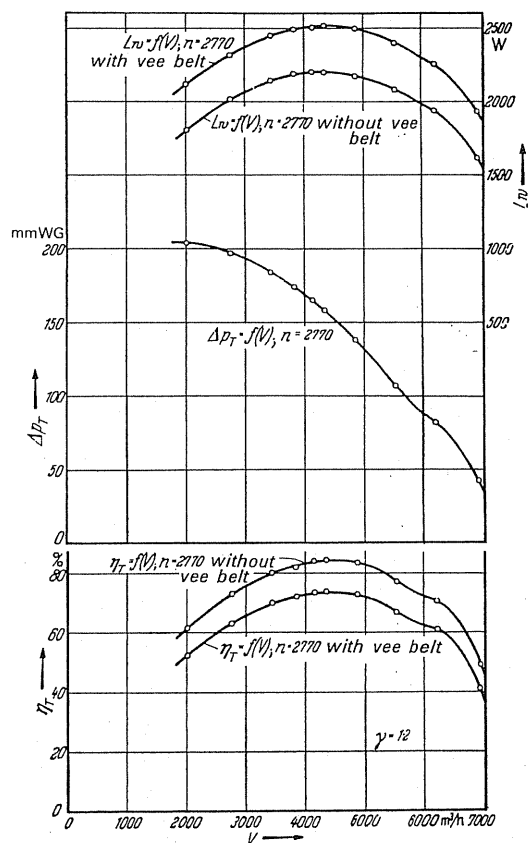


FIG. 596. Test results for $n = 2770$ rev/min.

The test was carried out with the best available instruments. Unfortunately for reasons of bearing support, with the motor and V-belt drive shaft unduly heavy, at the lower speeds this is evident through the very bad motor and V-belt efficiency (see Figs. 596 and 597). The determination of motor losses at part load is just as exact as at full load. The V-belt losses were determined in no load for the actual speed. They can with sufficient accuracy be placed at the same level as the losses on load.

Statement of test results from Figs. 596 to 598.

It will be observed from Fig. 598 that the deviation from the guaranteed values is very slight. The efficiency is even a little better than indicated.

As demonstrated by the test, it is important that motor and V-belt drive are exactly matched to the shaft power of the fan otherwise the losses in relation to the shaft power will be too great, and the overall efficiency of the installation is poor, although the fan efficiency might achieve the guaranteed figure.

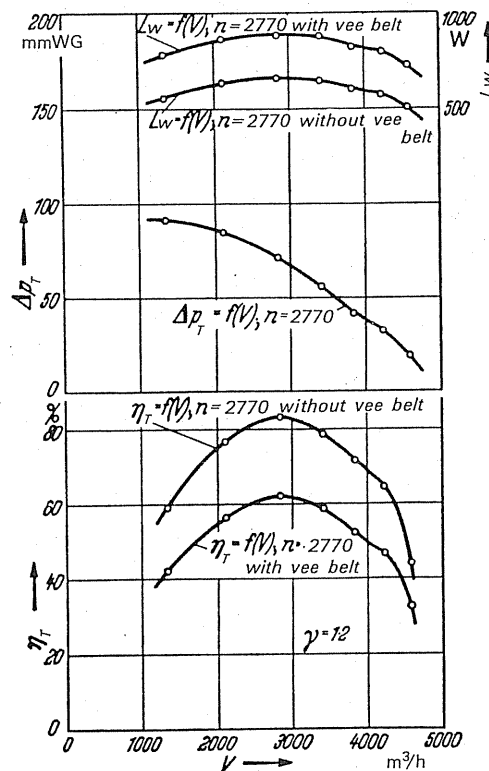


FIG. 597. Test results for $n = 1860$ rev/min.

In fans like those investigated here the optimum efficiency cannot be achieved for the following reasons:

- (1) A cheap and light design has to be put forward for reasons of price. (This entails higher clearances and therefore higher gap losses.)

- (2) The laws of assessment apply particularly for high duty fans. (In this case a drop in efficiency is positively associated with the size and the lower power.)
- (3) The roughness of surfaces of blades and spiral is higher.

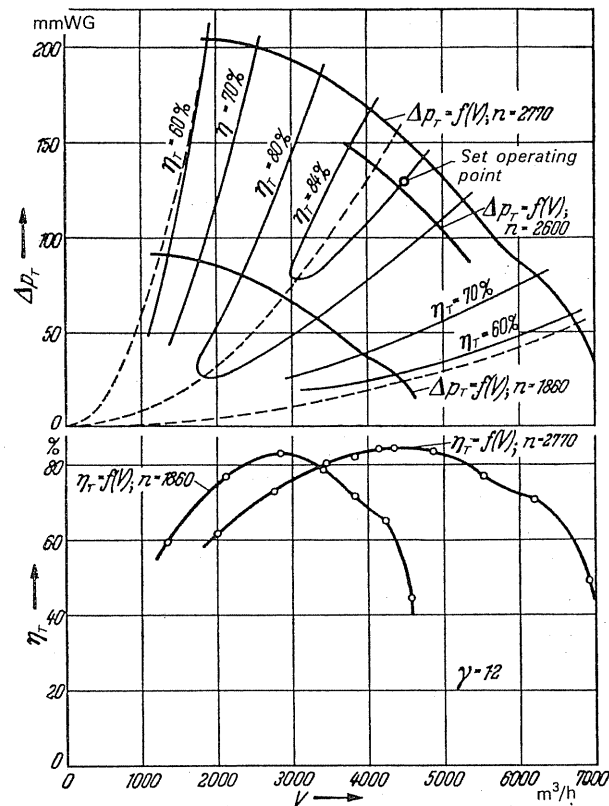


FIG. 598. Field characteristic of the tested fans.

AUTHOR INDEX

Ackeret 157, 441
Albring 127
Allen 486
Andritzky 117, 133

Bach 434
Baer 545
Bammert 266
Batzel 411
Bauersfeld 118, 239, 261
Baumann 441
Baumeister 471
Berlage 319
Biezeno-Grammel 545
Billing 490
Blashuus 60
Bommes 112
Briling 261
Broecker 218
Broer 210, 215
Bühning 250
Bürk 501

Canaan 268
Charwat 124
Coester 165
Conrad 444
Cordier 60
Cremer 512

Darrieus 220
De Fries 157
De Haller 266
Döpel 437
Donath 545
Dryden 498

Eck 20, 57, 60, 78, 82, 92, 108, 133, 158, 166, 173,
181, 182, 220, 277, 306, 314, 333, 466, 478
Eckert 237, 283, 298, 306, 437, 465
Eichler 513
Ernsthausen 490
Euler 7

Fette 43
Fickert 271
Fischer 43
Flügel 78, 123, 127, 430
Föttinger 439
Frietsch 43
Fritzsche 315, 409
Fröhlich 472
Furrer 503, 511

Gerber 522, 528, 532
Graham 486
Gramberg 354, 558
Grünagel 43
Grun 29
Grunewald 496, 498
Gutsche 240

Haerter 441
Hansen 78
Hasselgruber 106
Heller 545
Heuschke 438
Himmelskamp 124, 240
Hiramatsu 404
Hoffmann 111, 112
Holle 485
Honegger 545
Howell 263
Hübner 485, 486, 487
Hutton 269

Ibering 156
Iserland 267

Jung 430
Jungclaus 46, 126

Kampf 445, 447
Kármán 72
Karrer 203
Kattanek 437
Kearton 33, 48, 82, 115
Keller 60, 240, 250, 545

- Kisters 123
 Köhler 507
 König 240
 Kohler 423, 426, 427
 Kranz 210
 Kucharski 27, 118
 Kuhl 509
- Laing 173
 Lewinsky-Kesslitz 41, 44
 Lighthill 498
 Linsel 117, 133, 409
 Lübke 485, 506
 Lürenbaum 526
 Lyons 306
- Madison 486
 Marcinowski 250, 254, 268, 269, 272, 290, 306, 445, 495
 Meldu 266
 Mortier 156
 Moser 217
 Müller 348
 Muesmann 124, 237
 Mulsow 62, 123
- Naumann 75
 Numachi 240
- Oberländer 106
 Oertli 43
 Oesterlen 210
- Palin 169
 Pantell 101
 Peschka 485
 Pfeiderer 42, 213
 Pohle 404, 425
 Pollmann 228, 333
 Prian 43
- Quantz 100
- Rannie 242
 Rateau 117, 156, 412, 464
- Regenscheit 336
 Reichardt 46, 126
 Richter 373, 385, 387
 Riegels 493
 Riollot 486, 497
 Roy 146, 316
 Ruden 240, 292, 295
 Rüttschi 59, 346, 567
- Scheer 290
 Schicht 313
 Schilhansl 240
 Schlichting 264, 492, 493
 Schlünkes 267
 Schmarje 157
 Schmidt 348
 Schmiederer 343, 347
 Schmitz 124
 Scholz 264
 Schrader 188
 Schrenk 444
 Schubert 486, 489, 510
 Schultz 108
 Schultz-Grunow 72
 Segler 445, 448
 Shemoyama 23
 Sörensen 312
 Sprenger 156, 171
 Stepanoff 18
 Stiess 43
 Stodola 36, 240, 545
 Strassacher 204, 217
 Straszacker 215
 Strscheletzky 267
- Traupel 41, 82, 283
 Trenkler 424
 Truckenbrodt 493
- von der Nüll 453
- Weber 325
 Weinig 240, 263
 Widmar 325
- Zeller 485, 486, 487, 498, 510, 530
 Zweifel 261

SUBJECT INDEX

- Absorption 516, 523
- Absorption silencer 520, 536
- Acceleration torque 360
- Acceptance test 581
- Action 187
- Adjustable blade tips 333
- Adjustable disc 333
- Adjustable guide blades 475
- Adjustment 339
- Aerofoil friction 242
- Aerofoil theory 234
- Air 393, 435
- Air heater 175
- Air sound damping factor 512
- Allowance 363
- Angle 149, 259
- Arc profile 238
- Arranged in series 370
- Arrangement 368
- Attenuation of noise 530
- Auxiliary fans 416
- Axial-flow fans 225, 240, 251, 308
- Axial impeller 276

- Baffles 330
- Bar 544
- Bearing losses 83
- Bends 414
- Bernoulli's equation 10, 39, 148
- Blade 15, 31, 51, 52, 55, 100, 120, 143, 182, 185, 220, 257, 271, 272, 331, 333, 458, 475
- Blade angle 92, 95
- Blade passage 22, 108
- Blade setting 293
- Blower 323, 383, 445, 478
- Boiler fan 412, 419, 425
- Booster fan 412, 419
- Boundary layer 250
 - effects 256
 - in axial-flow fans 240
- Breadth 89
- Breadth/diameter ratio 111

- Calculation of strength 551
- Casing 219
- Ceiling fan 304, 315
- Centrifugal fan 107
- Centrifugal separator 431
- Change in static pressure 10
- Characteristics 57, 107, 113, 289, 400, 435
 - in the case of infinite number of blades 15
 - of static pressure developed in the impeller gap 18
- Chimney mounting 443
- Circuit 554
- Circular arc blade 100, 143, 257
- Circulation 26, 36
- Clearance 268
- Clearance losses 80
- Coefficients 15, 57, 58, 60, 64, 66, 243
 - of diameter 61
 - of performance 64
- Compensation 422
- Compression 6, 20
- Conditions 299
- Constant-pressure fan 312
- Constructional feature 455
- Contra-rotating axial-flow fans 308
- Control 166, 364
 - of rotation 337
- Cooling 176
- Cooling towers 436
- Coriolis force 23
- Counter 161
- Counter rotation 171
- Coupling 341
- Criteria curves 506
- Cross-connections 387
- Cross-flow fan 156
- Cross-flow multivane impeller 178
- Cross-ventilation 441
- Curve 62, 254, 255
 - blade 458
- Cylindrical blade 272

- Dead space 266
- Decrease 149
- Design 425
- Determination 400
- Devices 336
- Diameter 61, 92, 111
- Difference 577
- Diffuser 170, 219, 279
- Diffuser loss 79, 83, 276
- Dimension of the lip 216

- Dimensionless characteristics 51
- Direct sound field 511
- Disc 333
- Discharge filters 220
- Discharging 251
- Distribution 276
- Double-curved blades 458
- Drag 234, 251
- Draught 539
- Driving machine 361
- Duct 400
- Dust-laden gases 132
- Dynamometer 569

- Eddies 46
- Effect
 - of boundary layer 256
 - of free jets 267
 - of travel drive 435
 - of wind 435
- Efficiency 84, 85, 248
- Electric motor 357
 - cooling 176
- Electrical power measurements 579
- Element 512
- Elevator blowers 445
- Energy 10, 24
- Entry blade angle 92
- Entry breadth 89
- Entry rotation 11
- Equivalent orifice 64, 379
- Error 559, 573
- Exhaust diffusers 280
- Experimental determination of duct characteristic 400
- External rotor motors 354

- Fairing 298
- Fan 61, 107, 225, 304, 311, 312, 315, 383, 409, 412, 416, 419, 420, 425, 449, 466
 - and driving machines 362
- Fan noise 487
- Fan vibration 527
- Field 511
- Filament lamp 403
- Filter 220
- Finite number of blades 31
- Flexible mounting 525
- Flow 24, 46, 211
- Fluctuating resistance 395
- Force 22, 23
- Formation 266
- Free jets 267
- Freely discharging axial-flow fans 433
- Free-running radial impeller 433
- Friction 72, 242
 - in the blade passage 108
 - in volutes 208
- Friction wheel gear 470
- Function of frequency 487
- Furnace 422

- Gap pressure characteristic 113, 434, 435
- Gases 132
- Gear 342, 470
- Generation 490
- Guide blade gap 271
- Guide blades 185, 220, 475
- Guide devices 336
- Guide vanes 325
- Guide wheel 269

- Heater 175
- Height of lift 3
- Helix volute 197
- High-duty fan 466
- High-performance fan 117
- Hood (sound-absorbing) 524
- Hot-gas blowers 478
- Hovercraft 421, 440
- Hub dead space 266
- Hub diameter 265
- Hub diffuser 280
- Hub ratio 298

- Imparting rotation 330
- Impeller 18, 139, 161, 182, 276, 433
- Impeller friction losses 72
- Impeller losses 75
- Impeller shrouds 98
- Inactive blade 52
- Inclined blade fan 311
- Induced draught 539
- Induced draught fan 420
 - by injection 539
- Infinite number of blades 15
- Injection 445, 447
- Inlet diameter 92
- Inlet-flow condition 299
- Inlet guide vanes 325
- Inner volute 196
- Insulation element 512
- Interchange action 187
- Interference silencers 523
- Investigation on sound 485
- Isolation of fan vibration 527
- Isotachs 45

- Jets 267

- Kinetic energy 10

- Labyrinth-seal 478
- Lamp 403

- Law 402
Leaking duct 389
Level 500
Lift 3
Lift-drag ratio 251
Load test 579
Longitudinal ventilation 441
Loss 75, 78, 79, 80, 83, 109, 276
 in bends 414
 in volute casing 217
Loudness 503
- Machine 354, 362, 561
Main equation 8
Measurements 559, 573, 578
Measuring section 555
Mechanical efficiency 84
Mechanical power measurement 577
Mechanical speed adjustment 339
Meridionally accelerated axial-flow fans 308
Mine fans 409
Mine ventilation 409
Miniature fans 449
Model fans 61
Momentum 149
 moments of 3
Momentum drive 438
Motor 354, 357
Mounting 443, 525
Multivane impeller 139
- Narrow blade passage 22
Noise absorption 523
No-load test 578
Nose fairing 298
Nozzle 438
Number
 of blades 15, 31, 51
 of baffles 330
- Operating characteristics of centrifugal fans 107
Operating parts 365
Operating point 362
Optimum blade angle 95
Optimum curves 62, 254, 255
Oscillating blade impeller 182
Oscillation 370
Outlet angle 259
- Parallel arrangements 368
Part-characteristic 290, 291
Partial volutes 204
Passage 108
Performance 64
Phon value 502
- Potential vortex 164
Power measurements 577
Pre-rotation 97, 154, 160
 counter to impeller 161
Pressure coefficient 57, 243
Pressure compensation in the furnace 422
Pressure difference 577
Pressure distribution in axial impeller 276
Pressure fan 312
Pressure head 4
Pressure measurement 561
Pressure side 574
Problem 407
Profiling 265
- Quantity measurement 559
- Radial entry 10
Radial impeller 433
Reaction effect 10, 14, 42, 143, 163, 230, 233, 310
Reassessment 566
Reduction
 in output 32, 33
 of rotational flow due to friction 211
Reflection silencer 523
Regulation of blowers 323, 383
Relative circulation 26, 36
Relative eddies 46
Relative flow 24
Relative velocity 3
Removal of the boundary layer 250
Resistance box 403
Resistance law 402
Resonance silencer 522
Resonator 518, 519
Return air 393
Reverberant sound field 511
Reynolds number 237
Ring guide blades 220
Rising hot air 435
Roof ventilator 441
Rotating bar 544
Rotating ring 543
Rotation 11, 171, 330
Rotational effect of free jets 267
Rotor motor 354
Rubber aerofoil 471
- Saccardio nozzle 438
Safety allowance 363
Savonius rotor 434
Scherbius machine 354
Self-adjustment 338
Separator 431
Series 370
Shaft seals 478

- Shear flow 46
Shock losses 78, 109
Shrouds 98
Silencer
 absorption 520, 536
 interference 523
 reflection 523
 resonance 522
Sirocco runner 139
Sound absorption 516
Sound damping factor 512
Sound field 511
Sound generation 490
Sound insulation 499
 elements 512
Sound level 500
Sound pressure 500
Sound transmission through small opening 515
Sound velocity 20, 499
Source 189
Sources of error 559, 573
Special problem 407
Speed 45
Speed adjustment 339
Speed coefficient 60
Speed control 364
Spin dryer 176
Spiral housing 189
Stabilising characteristics 289
Starting an electric motor 357
Starting fans 383
Static pressure 10, 18
 measurement 561
Stream momentum 149
Strength 551
Suction side 573
Superchargers 452

Tearing length 549
Test 581
Test circuit 554
Test rig 556, 557

Thermal method of quantity measurement 559
Throttle control 364
Throttling coefficient 64
Tip clearance 268
Tongue 529
Torque 360
Total efficiency 85
Total pressure 5, 13, 576
Total reaction effect 14
Transmission 515
Travel drive 435
Triangle 13, 15, 158
Tunnel ventilation 438
Twisted blade 120

Unstable operating parts 365

Vacuum cleaners 450
Variable resistance 394
Velocity 3, 20, 499
Velocity coefficient 66
Velocity pressure 13
Velocity triangle 13, 15, 158
Ventilating doors 412
Ventilation 409, 438, 441
Ventilator 441
Vibration 527
Volume coefficient 58, 243
Volumetric efficiency 84
Volute 196, 204, 208, 217
Vortex control 166
Vortex core formation 266
Vortex source 189

Wear 423
Wheel 269, 470
Wind 435
Working together 367